Proceedings of the U.S. Nuclear Regulatory Commission

Twelfth Water Reactor Safety Research Information Meeting

Volume 5
- Mechanical Engineering
- Structural Engineering
- Seismic Research
- Process Control
- Instrumentation and Control Program
- Equipment Qualification and Nuclear Plant Aging

Held at
National Bureau of Standards
Gaithersburg, Maryland
October 22-26, 1984

U.S. Nuclear Regulatory Commission

Office of Nuclear Regulatory Research

Proceedings of the U.S. Nuclear Regulatory Commission

Twelfth Water Reactor Safety Research Information Meeting

Volume 5
- Mechanical Engineering
- Structural Engineering
- Seismic Research
- Process Control
- Instrumentation and Control Program
- Equipment Qualification and Nuclear Plant Aging

Held at
National Bureau of Standards
Gaithersburg, Maryland
October 22-26, 1984

ABSTRACT

The papers published in this six volume report were presented at
the Twelfth Water Reactor Safety Research Information Meeting held
at the National Bureau of Standards, Gaithersburg, Maryland during
the week of October 22-26, 1984. The papers describe progress and
results of programs in nuclear safety research conducted in this
country and abroad. Foreign participation in the meeting included
twenty-six different papers presented by researchers from seven
European countries, Japan, and Canada.

PROCEEDINGS OF THE
TWELFTH WATER REACTOR SAFETY RESEARCH
INFORMATION MEETING

October 22-26, 1984

Published in Six Volumes

GENERAL INDEX

PROCEEDINGS OF THE
TWELFTH WATER REACTOR SAFETY RESEARCH
INFORMATION MEETING

held at the

NATIONAL BUREAU OF STANDARDS
Gaithersburg, Maryland
October 22-26, 1984

TABLE OF CONTENTS - VOLUME 5

SEISMIC RESEARCH (Cont'd)

PROCESS CONTROL
Chairman: K. G. Steyer, NRC

INSTRUMENTATION AND CONTROL PROGRAM
Chairman: Bill M. Morris, NRC

EQUIPMENT QUALIFICATION AND
NUCLEAR PLANT AGING RESEARCH
Chairman: Bill M. Morris, NRC

PREFACE

This report, published in six volumes, contains 176 papers out of
the 205 that were presented at the Twelfth Water Reactor Safety Re-
search Information Meeting. The papers are printed in the order of
their presentation in each session. The titles of the papers and
the names of the authors have been updated and may differ from those
which appear in the final agenda for the meeting. The papers listed
under the session on Human Factors and Safeguards Research did not
appear in the agenda but were prepared for the panel discussions
that made up that session.

ENVIRONMENTAL/DYNAMIC MECHANICAL
EQUIPMENT QUALIFICATION AND DYNAMIC
ELECTRICAL EQUIPMENT QUALIFICATION
PROGRAM (EDQP)

J. A. Hunter

Idaho National Engineering Laboratory
EG&G Idaho

Equipment qualification research is being conducted by the Idaho National Engineering Laboratory to investigate acceptable criteria, requirements, and methodologies for the dynamic (including seismic) and environmental qualification of mechanical equipment and for the dynamic (including seismic) qualification of electrical equipment. The program is organized into three elements: (1) General Research, (2) Environmental Research, and (3) Dynamic Research. This paper presents the highlights of the results to date in these three elements of the program.

GENERAL RESEARCH

The activities being conducted within this element are in general applicable to electrical and mechanical equipment qualification.

Equipment Identification

Components that should be considered as candidates for qualification research have been identified. The method used to identify the components is based on a combination of domestic experience and probabilistic analyses completed by other NRC sponsored programs.

The purpose of the subject study documented in Reference 1 was to identify equipment and components which are predicted to be significant contributors to the dominant severe core damage accident sequences.

The NRC sponsored Accident Sequence Evaluation Program (ASEP) and Accident Sequence Precursor (ASP) study are the primary references used in the subject study. ASEP utilizes existing probabilistic risk assessments for various plants to determine the likelihood of severe core damage and evaluate the significant contributors for each dominant accident sequence on a plant specific basis. Approximately 10 to 14 dominant accident sequences were analyzed for each of the six pressurized water reactor plants and four boiling water reactor plants included in the study.

The ASP studies utilize the licensee event report as the basis for the accident initiating events. A series of subsequent events are then assumed, and an event tree is generated using the precursor as the initiating event. Those sequences resulting in predicted severe core damage are then used to identify the equipment and components contributing to each sequence.

A listing in Reference 1 of the equipment and components identified as pre-dicted significant contributors to severe core damage includes categories of valves, pumps, electrical equipment, instruments, systems maintenance and test, human error and weather. The non-equipment categories of maintenance and test, human error, and weather have been included to provide interface information on how equipment and component performance can be affected by such factors.

Because both the ASEP and ASP studies are limited to severe core damage, and because results of reference studies relating severe core damage to risk are not complete, certain equipment and components which would be identified between severe core damage and risk (release from containment), such as purge vent and containment isolation valves, have not been identified by this study. Additional work will be required on this study to include these types of equipment and components in updated versions of this report. This can be accomplished as soon as appropriate research is complete in such NRC sponsored programs as the Severe Accident Sequence Analysis and Severe Accident Risk Reduction Program. It is anticipated that as the probabilistic risk assessment matures, the techniques will become more accurate to the reactor system major component level and that they will characterize not only the normal operational loads but also the accident loads.

Equipment Qualification Standards

Since the ultimate use of the research products from EDQP will be the improvement of equipment qualification standards, the program has evaluated several standards in an effort to define uncertainties in these documents as they currently exist. This information will be used within EDQP to partially ensure that the program research activities address open technical issues associated with current domestic equipment qualification standards. Current equipment qualification standards either do not exist or do not totally reflect the effects of dynamic and environmental loads on equipment function. Specifically, the effects of some design basis accident conditions (dynamic cross coupling effects, non-linear vibration, pressure, and temperature) on equipment function are either not documented or are not adequately incorporated in qualification standards. Several domestic published and draft standards were evaluated by EDQP for open issues using a multidiscipline team. In particular, the evaluation assessed the applicability of the guidelines within Institute of Electrical and Electronic Engineers (IEEE) 323, 344, and 627 [References 2-4] to the qualification of safety-related mechanical equipment. The evaluation method was also applied to several draft standards for qualification of selected pump and valve assemblies. These standards documented in References 5-7 are currently under development or have recently been published by the American National Standards Institute (ANSI) and the American Society of Mechanical Engineers (ASME). These standards address the qualification of power operated valves, pump assemblies, and pump shaft seal assemblies.

The evaluation identified open issues in the categories of component equivalence, qualification maintenance, and qualification by test and/or analysis.

Qualification Using Existing Data

The qualification of equipment using existing experience data is recognized as a possible method to qualify equipment in several draft and published standards such as References 5 and 6. The issue to be addressed by the subject program involves the need for more definitive guidelines, that will assist in ensuring that the experience data is properly applied to the qualification process. As part of this effort, the program has completed a survey of a major domestic test laboratory to determine items such as the identification of equipment tested, seismic and environmental load characteristics utilized in the test methods and test plans used. The study examined 394 items of electrical equipment and 76 items of electromechanical and mechanical equipment. The results of this survey are currently under evaluation.

ENVIRONMENTAL RESEARCH

The research topics in this element of the program assess the effects of environmental loads on elastomer and organic materials. The data developed in this element of the program will be used to develop the technical basis, criteria, and acceptable methodologies for specifying the influence of environmental loads on elastomer and organic materials.

Reactor Coolant Pump Shaft Seals

The immediate issue addressed by this research is the characterization of the behavior of selected elastomer materials used in some pump shaft seal designs

3

when subjected to "station blackout conditions, loss of all AC power which produces a loss of cooling to the seal. The failure of the seal-elastomer O-rings can produce a small loss of coolant accident. The seal design considered utilizes a hydrostatic type seal which normally withstands a substantial portion of the seal pressure differential. A schematic of such a seal is depicted in Figure 1.

The long term issue to be partially resolved by this research is based on the fact that acceptance qualification criteria, requirements, and methodologies for reactor coolant pump shaft seals currently do not exist. The conditions used to simulate station blackout conditions ranged from 800 to 2400 psi and from 250 to 580 F. Two O-ring materials were tested: ethylene propylene E515-80 and ethylene propylene E740-75. The channel seal material was Tetralon 720. The O-ring test cell is depicted in Figure 2. The O-rings utilized in the experiments possess a cross section of 0.139 inch and outside diameter of 1.5 inch.

It must be remembered when interpreting the data from these tests that the tests are scoping tests. These tests included the influence of diametrical clearances, temperature, pressure and time on the O-ring and channel seal material. The possible effects of seal lubrication, of small movements of the seal components, of prior aging of the polymer materials, larger cross-section O-rings, and steam environment were not addressed in this study.

The main conclusion of the O-ring extrusion tests indicates that ethylene propylene E515-80 is not appropriate for high temperature water conditions likely to be encountered in station blackout conditions. The E515-80 material became soft within time durations as short as two hours at 550 F. Tests on the E740-75 compound showed superior resistance to high temperature extrusion.

Extrusion tests using the Tetralon 720 channel seals backed with E740-75 O-rings revealed severe extrusion of the Tetralon 720 channel seals. At small gaps this extruded material prevented subsequent sealing by the O-ring and consequently produced seal blowout. At large gaps, the Tetralon extrusion was sufficient to allow O-ring sealing. The results corresponded to those for E740-75 O-rings tested individually.

Blowdown tests were also conducted on two hydrostatic seals with seal face outer diameters of 2-7/8 inch and 4-3/4 inch. The test rig is schematically shown in Figure 3. The objective of these tests was to obtain qualitative estimates of leak rate and seal stability when leaking water flashes to steam across the seal. The main conclusion of these tests was that water flashing to steam between hydrostatic seal faces provides potential for unstable seal behavior.

Containment Penetration Elastomer Seal Tests

Scoping experiments were conducted to assess the behavior under accident conditions of two designs of seals and of the associated seal material used in containment penetrations. The failure of the seals in a reactor accident would potentially create a fission product release to the atmosphere.

The two designs tested were the O-ring configuration and the tongue-in-groove configuration shown in Figure 4.

The seals were tested in electrically heated 18 inch, 900 lb. flanges.

4

Pressurization was obtained with nitrogen. Temperatures used in the experiments ranged from 60 to 420°F for neoprene O-rings. The temperature range applied to the silicon tongue-in-groove seal ranged from 70 to 600°F. Pressure values utilized in the tests ranged up to 200 psig.

In general, the results of these tests indicate that the neoprene O-rings became brittle after being subjected to the test conditions. The silicone tongue-in-groove seal regained its soft state after experiencing the test conditions.

DYNAMIC RESEARCH

One of the objectives of the EDQP is to develop extrapolation guidelines that can be used to qualify mechanical equipment. With respect to the extrapolation of dynamic loads in the context of the EDQP, loads created by flow through a device are classified as dynamic loads. Consequently, the EDQP is conducting a major experimental program for containment purge/vent valves.

Purge/Vent Valve Experiments

The ability of the containment purge and vent valves to close against rising differential pressure resulting from a design basis accident loss of coolant accident was originally identified as a safety issue in Reference 8 and subsequently in Reference 9. Valve leak integrity was also included as part of the safety issue.

The objective of the dynamic flow tests was to establish guidelines that can be used to predict butterfly valve operability. The objective of the leak integrity testing was to obtain scoping data that can be ultimately used to develop and validate valve leakage models.

The purge valve flow experiments subjected three valves (two eight inch diameter valves and one twenty-four inch diameter valve) to valve inlet pressures ranging from 15 to 60 psig for valve position from fully open to fully closed. One eight inch valve and the twenty-four inch valve were the same basic design. During the flow tests, parameters such as valve torque, valve pressure differential, and valve inlet duct and outlet duct termperatures were measured. Valve orientation with respect to the flow and with respect to the test configuration (i.e., presence of duct elbows upstream of the test valve) was varied to assess the influence of these variables on valve performance.

Figures 5 and 6 schematically depict the two valve designs used in the experiment. Figure 7 schematically depicts the experimental apparatus with instrumentation locations designated.

Data obtained from the flow testing has been compiled and is currently under evaluation. The response of the valves to the test conditions has been characterized. The characterizations provide the information necessary to assess current techniques used to predict valve torque requirements. The assessment is currently in progress. It will compare experimental measurements with current torque prediction methods. The results of the comparison will be used to ultimately develop guidelines for valve performance extrapolation techniques.

As part of the program, scoping leak measurements were made for pressures

ranging from 3 to 125 psig and for temperatures ranging from ambient to 350°F. The objective of this scoping experiment was to obtain preliminary data that can be used to ultimately develop valve leakage models. The seal material used was ethylene propylene terepolymer. Measured leak rates varied from 0 to 505 standard cubic feet per hour. The leak rate was a strong function of pressure and valve orientation.

SUMMARY

This paper summarizes the results obtained to date in the EDQP. The program will continue in the future to perform research in the three elements of (1) General Research, (2) Environmental Research, and (3) Dynamic Research. Future research topics to be expanded include the dynamic response of equipment including pumps, valves, and electrical equipment; containment isolation valve performance; main coolant pump shaft seal research; fragility application to the equipment qualification process; and experience data application to equipment qualification.

REFERENCES

1. H. W. Heiselmann, Identification of Equipment and Components Predicted as Significant Contributors to Severe Core Damage, NUREG/CR-3762, May 1984.

2. IEEE-Standard 323-1974, IEEE Standard for Qualifying Class IE Equipment for Nuclear Power Generating Stations.

3. IEEE Standard 344-1975, IEEE Recommended Practices for Seismic Qualification of Class IE Equipment for Nuclear Power Generating Stations.

4. IEEE Standard 627-1980, IEEE Standard for Design Qualification of Safety System Equipment Used in Nuclear Power Generating Stations.

5. ANSI/ASME Standard N551.1, QNPE-1 Standard for Qualification of ASME Code Class 2 and 3 Pump Assemblies for Safety Systems Service-General Requirements (Draft).

6. ANSI/ASME Standard N551.2, QNPE-2 Standard for Qualification of ASME Code Class 2 and 3 Pumps for Safety Systems Service (Draft).

7. ANSI/ASME Standard N551.3, QNPE-3 Standard for Qualification of Shaft Seal Assemblies for ASME Code Class 2 and 3 Pumps for Safety Systems Service (Draft).

8. NRC Action Plan as a Result of the TMI-2 Accident, NUREG-0660, May 1980.

9. Clarification of TMI Action Plans Requirements, NUREG-0730, November 1980.
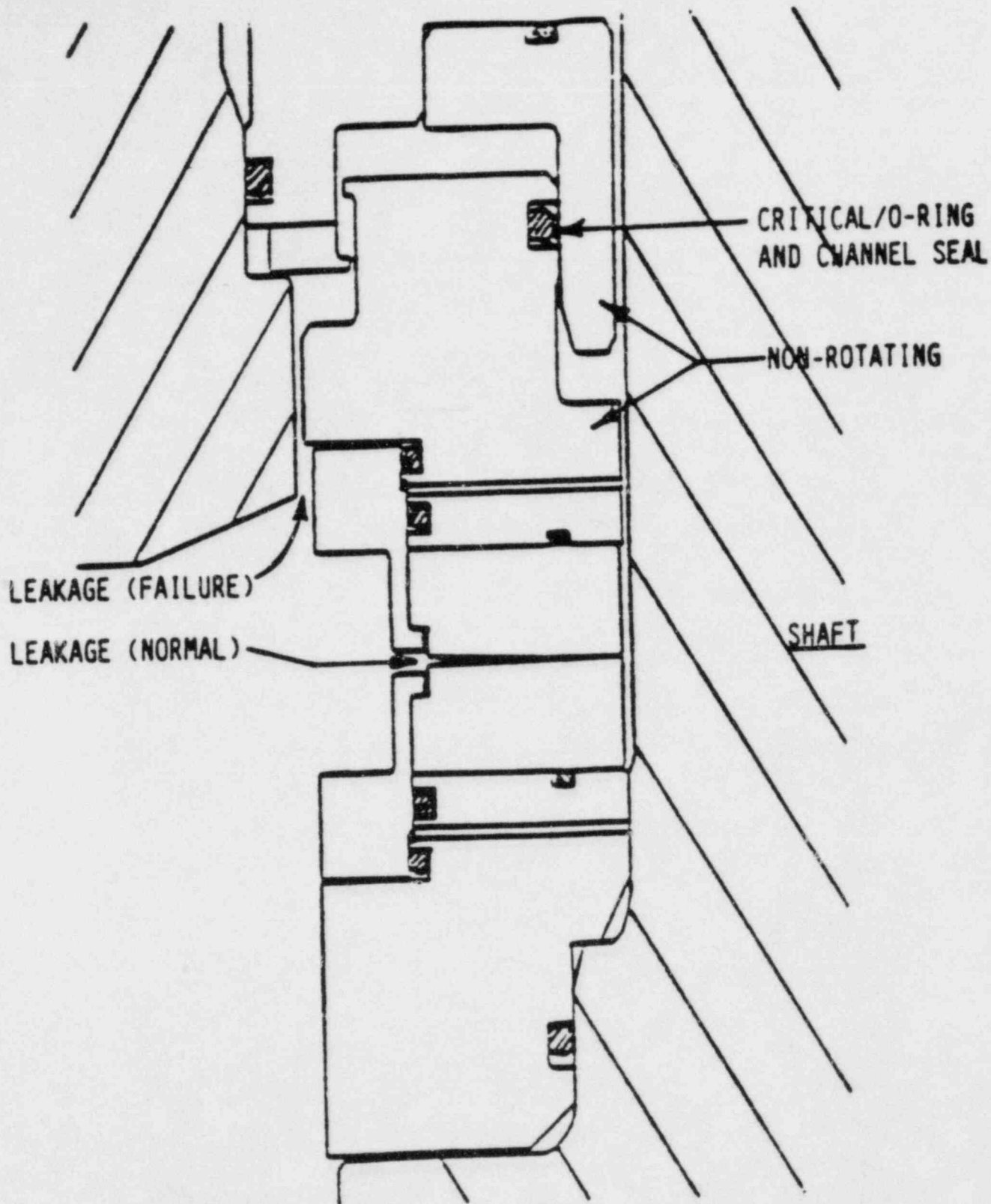
Figure 1. Pump Shaft Seal Schematic

8

CAP (304 SST)

1/8 TUBE
(300 SST)
2 PLCS

BODY (304 SST)
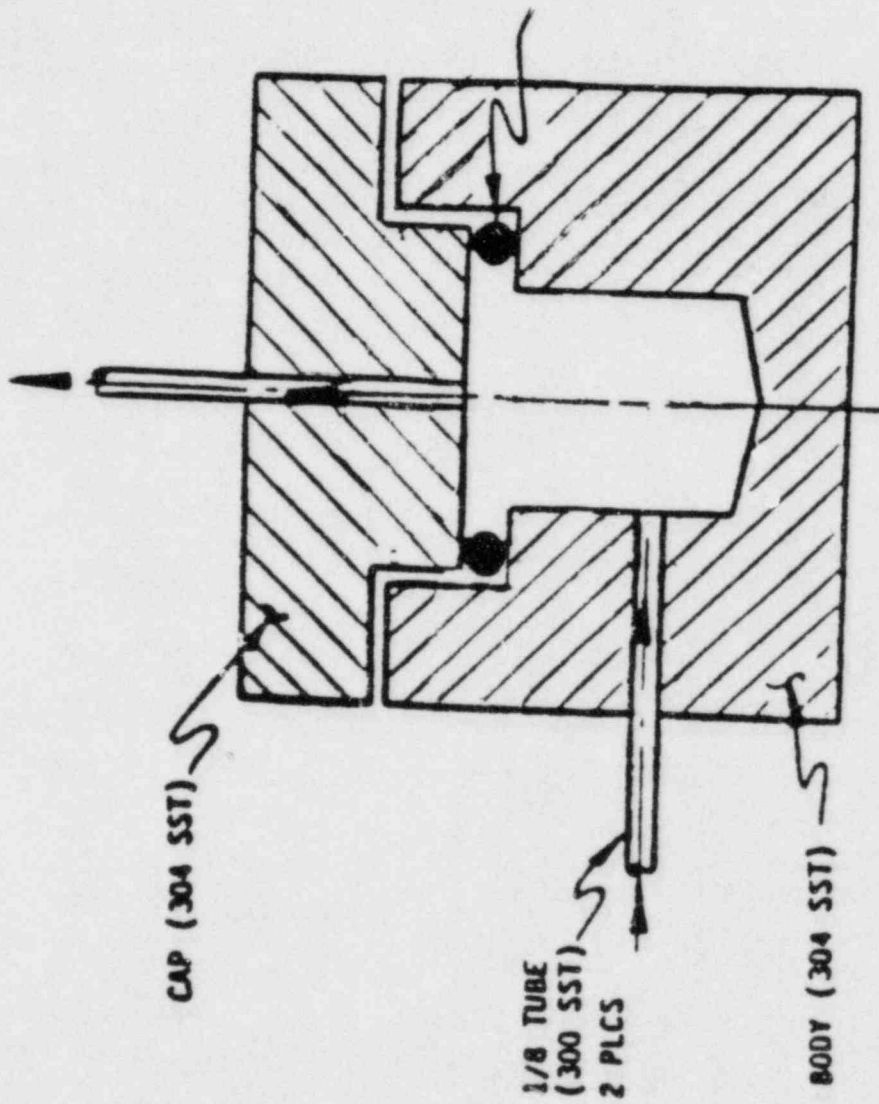
Figure 2.   O-Ring Test Fixture

9
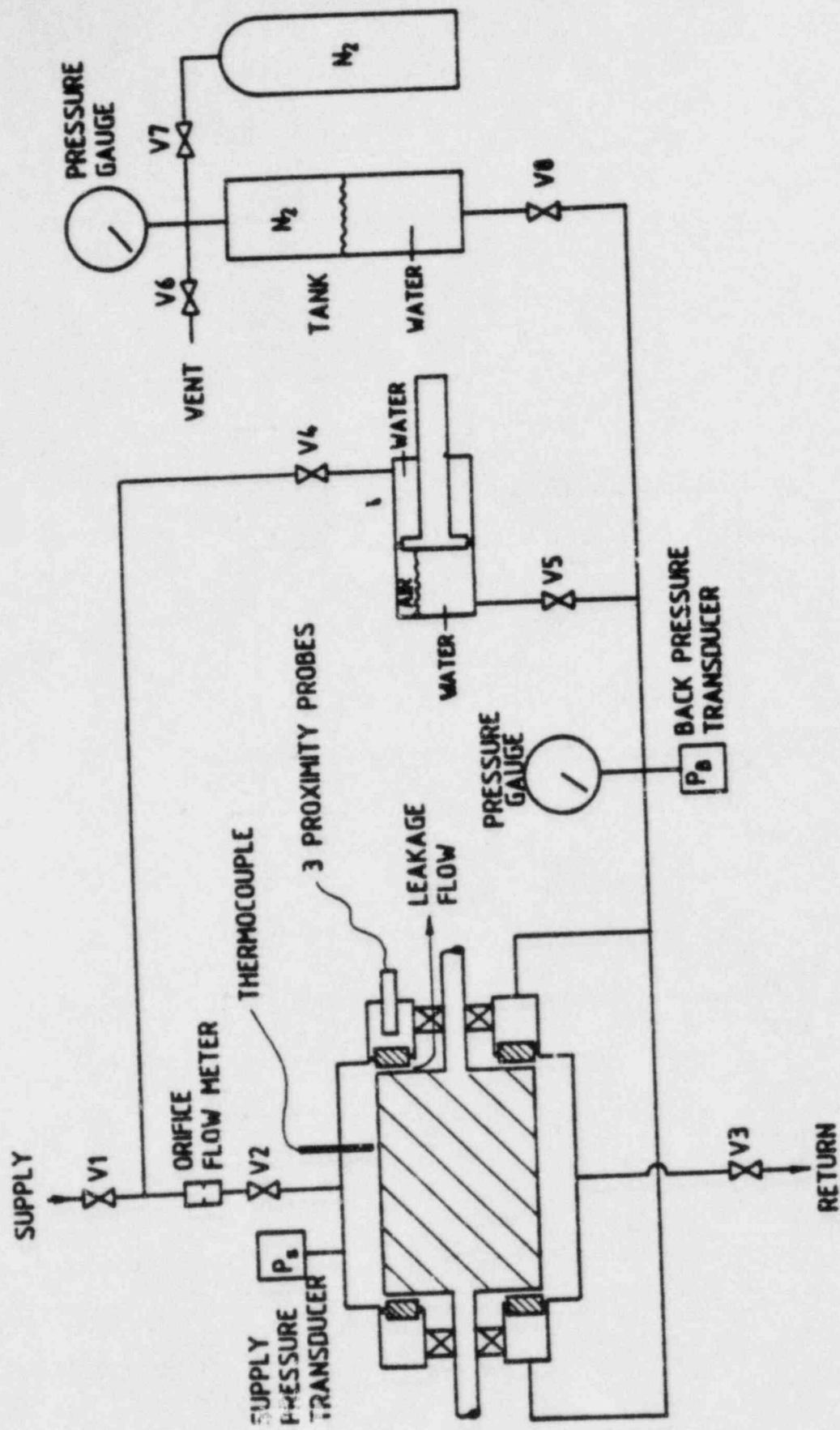
Figure 3. Shaft Seal Blowdown Apparatus

10
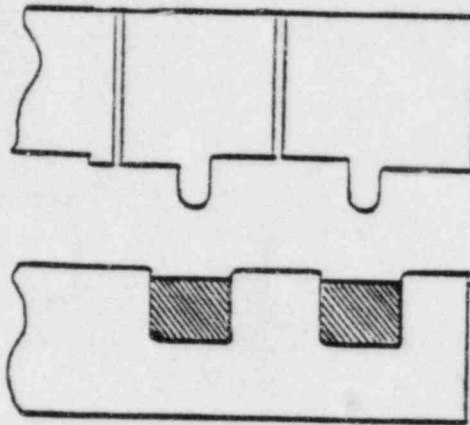
a. Tongue-In-Groove Seal
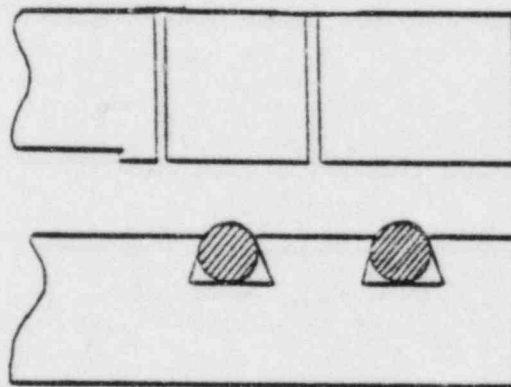
b. O-Ring Seal

Figure 4. Containment Flange
Seal Schematic

11
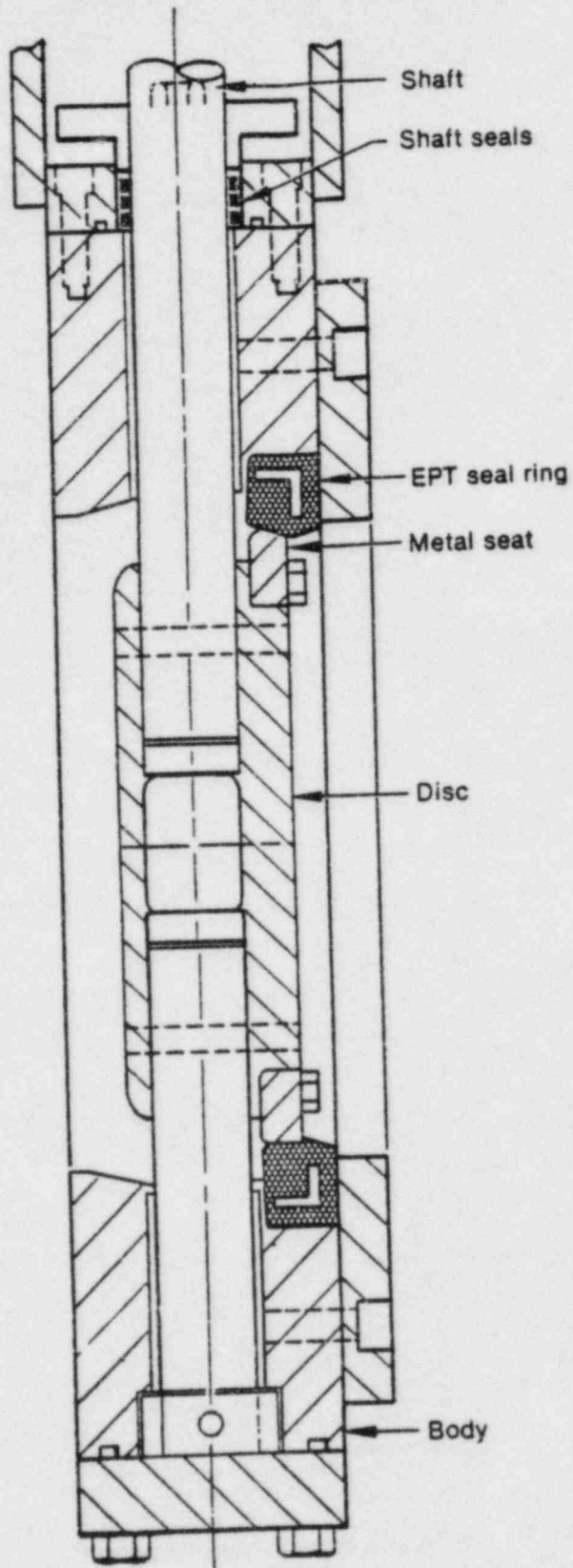
Figure 5. Purge Valve Number 1 Schematic

12
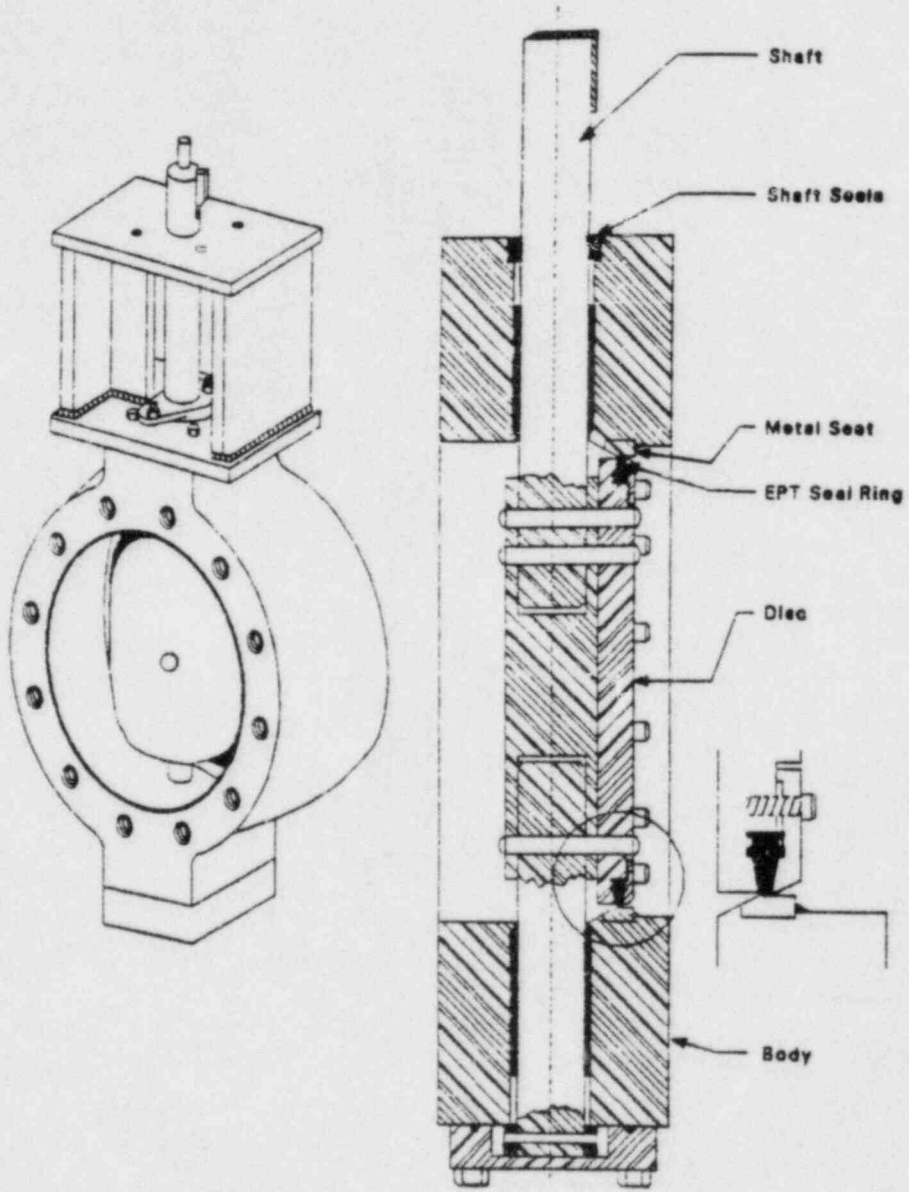
Figure 6. Purge Valves Number 2 and 3 Schematic
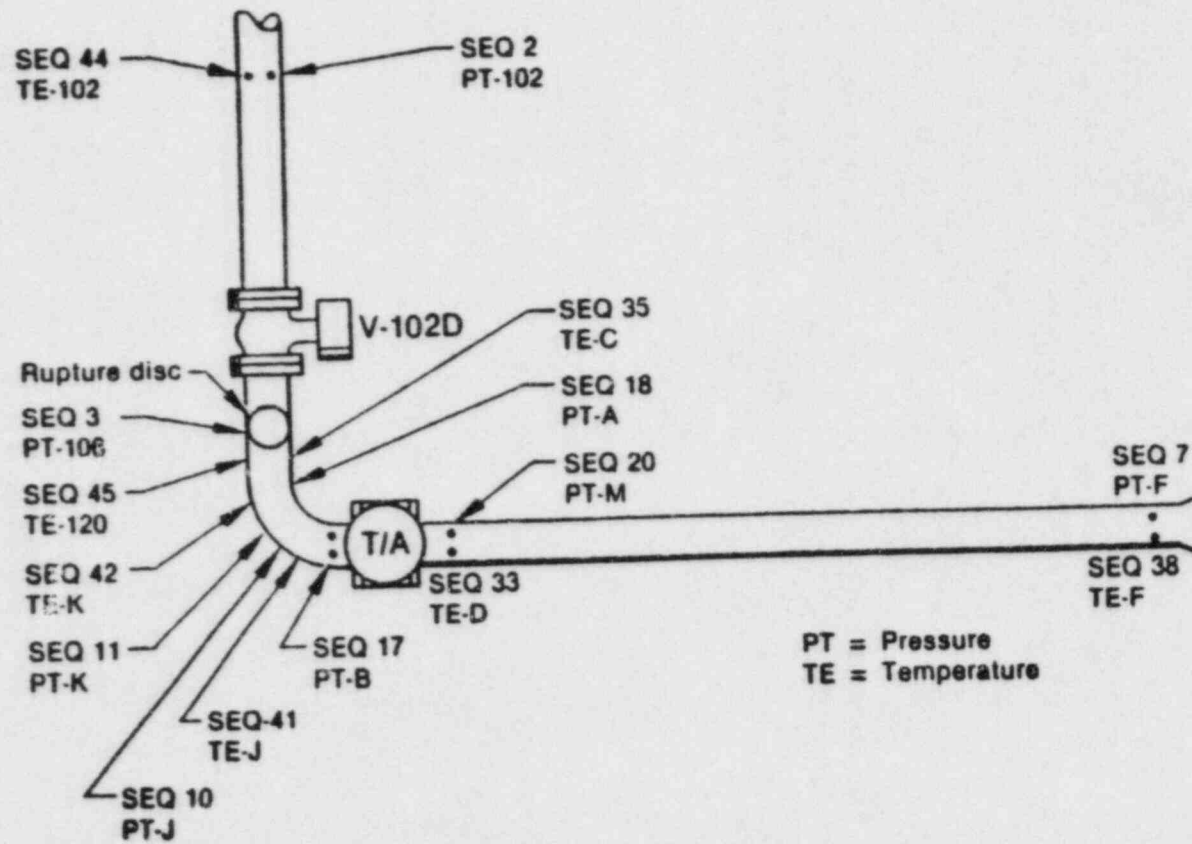
Figure 7. Purge Valve Test Apparatus Schematic

DOUBLE-ENDED BREAKS IN REACTOR PRIMARY PIPING

Garry S. Holman

Lawrence Livermore National Laboratory
University of California
P.O. Box 808, Livermore, California 94550

1. INTRODUCTION

The Lawrence Livermore National Laboratory (LLNL), through its Nuclear Systems Safety Program, is performing probabilistic reliability analyses of PWR and BWR reactor coolant piping for the NRC Office of Nuclear Regulatory Research. Specifically, LLNL is estimating the probability of a double-ended guillotine break (DEGB) in the reactor coolant loop piping in PWR plants, and in the main steam, feedwater, and recirculation piping of BWR plants. For these piping systems, the results of the LLNL investigations will provide NRC with one technical basis on which to:

(1) reevaluate the current general design requirement that DEGB be assumed in the design of nuclear power plant structures, systems, and components against the effects of a postulated pipe break.

(2) determine if an earthquake could induce a DEGB, and thus reevaluate the current design requirement that pipe break loads be combined with loads resulting from a safe shutdown earthquake (SSE).

(3) make licensing decisions concerning the replacement, upgrading, or redesign of piping systems, or addressing such issues as the need for pipe whip restraints on reactor coolant piping.

In estimating the probability of DEGB, LLNL considers two causes of pipe break: pipe fracture due to the growth of cracks at welded joints ("direct" DEGB), and pipe rupture indirectly caused by the seismically-induced failure of critical supports or equipment ("indirect" DEGB).

Although these investigations are limited to the reactor coolant piping noted above, the techniques used to assess reliability are sufficiently general that they could be conveniently applied to other piping systems not included in the present LLNL investigations.

2. APPROACH

To arrive at a general conclusion about the probability of DEGB in the reactor coolant loop piping of PWR plants, LLNL is taking a vendor-by-vendor approach. For each of the three PWR vendors (Westinghouse, Babcock & Wilcox, and Combustion Engineering) the principal tasks are to:

(1) estimate the probability of direct DEGB taking into account such contributing factors as initial crack size, pipe stresses due to normal operation and sudden extreme loads (such as earthquakes), the crack growth characteristics of pipe materials, and the capability to non-destructively detect cracks, or to detect a leak if a crack penetrates the pipe wall. To do this LLNL developed a Monte Carlo simulation methodology, implemented in the PRAISE computer code.

(2) estimate the probability of indirect DEGB by identifying critical component supports or equipment whose failure could result in pipe break, determining the seismic "fragility" (relationship between seismic response and probability of failure) of each, and combining this result with the probability that an earthquake occurs producing a certain level of excitation ("seismic hazard").

(3) for both causes of DEGB, perform sensitivity studies to identify key parameters contributing to the probability of pipe break.

(4) for both causes of DEGB, perform uncertainty studies to determine how uncertainties in input data affect the uncertainty in the final estimated probability of pipe break.

LLNL has completed generic evaluations of DEGB probability for plants with nuclear steam supply systems manufactured by Westinghouse (Fig. 1) and by Combustion Engineering (Fig. 2).[1,2,3] The results of these evaluations indicate that the probability of DEGB from either cause is very low. Therefore, this result suggests that the DEGB design requirement -- and with it related design issues such as coupling of DEGB and SSE loads, asymmetric blowdown, and the need to install pipe whip restraints -- warrants a reevaluation for PWR reactor coolant loop piping.

In the Westinghouse and Combustion Engineering evaluations, LLNL designated a single reference, or "pilot" plant, as a basis for methodology development as well as for extensive sensitivity studies to identify the influence that individual parameters have on DEGB probabilities. Thus, each pilot plant was used to develop and "shake down" the assessment methodology that was later applied in the corresponding generic study for each vendor.

In the generic study of reactor coolant piping manufactured by each of these vendors, LLNL evaluated individual plants, or groups of plants sharing certain common or similar characteristics, to arrive at an estimated DEGB

probability (including uncertainty bounds) characteristic of all plants. Thus, the generic evaluation represented a "production" application of the assessment methodology.

For Babcock & Wilcox PWR plants, LLNL has estimated the probability of indirect DEGB for each of two representative plants: one plant with the raised loop nuclear steam supply system, and one plant with the lowered loop configuration. LLNL has also obtained and reviewed information required for an evaluation of direct DEGB for the representative raised loop plant.

The objectives and approach of the BWR study are essentially the same. LLNL is currently limiting its investigation to Mark I plants, which have recirculation piping particularly susceptible to the effects of intergranular stress corrosion cracking (IGSCC), and is beginning with a pilot study based on the Brunswick plant operated by Carolina Power & Light. As part of the BWR investigation, LLNL has developed a probabilistic IGSCC model which considers crack initiation as well as the effect of stress corrosion on pre-existing cracks; a prototype has been completed and implemented in the PRAISE code. LLNL is also developing a PRAISE model to consider stress redistribution among weld joints due to the failure of intermediate pipe supports; this was unnecessary in the PWR evaluations because reactor coolant loop piping is supported solely by the loop components; preliminary results indicate that intermediate support failure is important only for earthquakes of twice the SSE or greater. The BWR pilot study is scheduled for completion in December 1984.

3. PROBABILISTIC FRACTURE MECHANICS MODELS

Over the past several years, probabilistic analysis techniques have gained increased acceptance as a method for evaluating the safety of nuclear power plants. One application has been through probabilistic risk assessment (PRA) of event sequences potentially leading to radioactive releases. A different application, which will be discussed here, probabilistically evaluates the adequacy of individual systems, structures, or components to resist failure when subjected to postulated loads.

In essence, a typical component evaluation compares some measure of its strength -- material yield stress, for example -- against the stress resulting from anticipated loads applied to it. If strength exceeds stress, the component is considered adequate for the postulated loads. Should stress exceed strength, however, the component is presumed to fail.

As illustrated schematically by Fig. 3, a deterministic calculation compares point estimates of stress and strength to evaluate component adequacy. Generally, these are nominal values established according to conservative load limits and material strength parameters such as those defined by the ASME Code.[4] In component design, the application of "safety

margins" provides an added measure of conservatism. The safety margin compenses for uncertainty associated with many factors, including:

o   variability in nominal material strength, that is, actual strength may be lower than that specified in the analysis.

o   degradation in material strength during plant operation, such as radiation embrittlement.

o   variations in postulated loading conditions such as pressure and temperature transients.

o   load conditions generally regarded as having secondary significance and which are therefore neglected in the evaluation.

o   unanticipated load conditions.

o   simplifications made in modeling a physical system.

o   approximation methods used to calculate stresses and resultant component response.

Stress and strength limits are generally set according to specific design considerations. It is not unusual that an evaluation based on "worst case" stress and strength values outside of the design scope will predict a negative safety margin, in other words, failure.

The deterministic approach embodies a significant degree of inherent conservatism, stemming from many sources:

o   the margin between code allowable limits and actual failure.

o   the margin between design conditions and code limits.

o   the particular analytic techniques used to predict component response to applied loads.

o   input conditions used in predicting component response.

These conservatisms generally add together; thus, the more parameters involved, the more conservative a deterministic evaluation tends to be.

The probabilistic approach replaces the fixed values with random variables, each of which has a statistical distribution. Thus, variations in strength and stress about their nominal (or "best-estimate") values are explicitly considered. When plotted together (see Fig. 4), the area where these distributions overlap represents the probability that stress exceeds strength, in other words, that the component will fail. Instead of setting

18

out to determine if a design is adequate and by what safety margin, a proba-
bilistic evaluation estimates the failure probability ("reliability") of the
design. The design is considered adequate ("safe") if the failure probability
is acceptably low. What constitutes "acceptably low" is subject to judgement,
usually taking into account the potential consequences of failure; the more
serious the consequences, the lower the tolerable failure probability.

By distributing each parameter statistically, a probabilistic evaluation
yields results that more closely reflect reality. Moreover, probabilistic
techniques can take event occurrence rate into account, and therefore more
realistically weight the relative effects of frequent vs infrequent load
events on overall reliability. Statistical uncertainties attached to each
distribution can be carried through the analysis to estimate the uncertainty
in the predicted reliability.

Because the simultaneous interaction of many individual -- and often
deterministically unrelated -- factors is reflected in a single result (i.e.,
failure probability), probabilistic techniques provide a convenient, yet
powerful basis for sensitivity studies. For example, the effect of material
property selection (strength, crack growth behavior) on piping reliability can
be weighed against that non-destructive examination (inspection interval,
crack non-detection probability).

The LLNL evaluations of DEGB in reactor coolant piping represent one
application of probabilistic fracture mechanics to the subject of pipe
failure. In these evaluations, the probability of pipe break or leak
resulting from crack growth at welded joints ("direct" DEGB) is estimated
using the procedure schematically illustrated in Fig. 4. The left column
represents the analytic procedure, the right column the input information and
analytical models used at each step of the simulation. The procedure,
implemented in the PRAISE (Piping Reliability Assessment Including Seismic
Events) computer code detailed in References 5 and 6, is summarized in the
following discussion.

For each weld joint of a piping system, the leak or break probability is
estimated using a Monte Carlo simulation technique. Each replication of the
simulation -- and a typical simulation includes several thousand -- begins
with a pre-existing flaw having initial length and depth randomly selected
from appropriate distributions. These distributions in turn relate the
conditional probability of crack existence. Fatigue crack growth is then
calculated using a Paris growth law model, to which are applied stresses
associated with normal operating conditions and postulated seismic events.
The influence of such factors as non-destructive examination (NDE) and leak
detection is also considered through the inclusion of appropriate statistical
distributions (e.g., probability of crack non-detection as a function of crack
depth). Leak occurs when a crack grows through the pipe wall, break when
failure criteria based on net section collapse or tearing instability are
exceeded.

Completing all replications for a single weld joint and tabulating those cracks that cause failure yields the failure probability as a function of time at that weld, conditioned on a crack existing at the joint and on an earthquake of given ground acceleration occurring. By combining the results for all welds in a particular piping system, and then performing a systems analysis incorporating crack existence probability (a function of the total volume of weld material) and seismic hazard (which relates the occurence rates of earthquakes as a function of peak ground acceleration), the non-conditional probabilities of leak and DEGB are obtained.

It is important to emphasize that this procedure is not a PRA utilizing event tree and fault tree analysis. Instead, the procedure incorporates deterministic (either empirical or analytic) models into a probabilistic "framework" that allows the results of deterministic growth calculations for literally thousands of individual cracks to be consolidated, along with the effects of other factors such as NDE intervals and earthquake occurrence rates, into a single convenient result, namely leak or break probability of a particular piping system. This result could, in turn, provide input for that part of a PRA event tree using the probability of pipe system failure.

4. DOUBLE-ENDED GUILLOTINE BREAK INDIRECTLY INDUCED BY EARTHQUAKES

4.1 General Approach

If earthquakes and large LOCAs are considered as purely random events, the probability of their simultaneous occurence is negligibly low. However, if an earthquake could cause DEGB, then the probability of simultaneous occurence would be significantly higher. Our study of direct DEGB in reactor coolant piping concluded that earthquakes were not a significant contributor to this failure mode. However, another way in which DEGB could occur would be for an earthquake to cause the failure of component supports or other equipment whose failure would in turn would cause a reactor coolant pipe to break. We refer to this scenario as "indirect" DEGB. Evaluating the probability of indirect DEGB involves the following steps:

o estimate the conservatism and the uncertainty in the calculated structural responses for various loading conditions, such as dead weight, thermal expansion, pressure, and seismic loads.

o identify critical components whose failure could induce a DEGB. For each component, identify failure modes and their corresponding fragility descriptions. Each fragility description represents the probability of structural failure conditioned on the occurrence of an earthquake of given peak ground acceleration.

o calculate the overall "plant level" fragility to account for all significant failure modes and the associated fragility descriptions.

20

o   calculate the non-conditional probability of indirect DEGB by convolving
     the plant level fragility with an appropriate description of seismic
     hazard. Seismic hazard relates the probability of occurrence of an
     earthquake exceeding a given level of peak ground acceleration.

Typical descriptions of seismic hazard and fragility are shown in Fig. 5.

4.2 Design and Construction Errors

The LLNL analyses of indirect DEGB probability assumed systems and
components that were free from design and construction errors. Because in
practice such errors are a real possibility, it is important to assess their
potential effect on the probability of pipe break. In principle, design and
construction errors could be treated probabilistically in the same way that
any other parameter is treated, if a distribution of errors could be
established. However, because actual NSSS heavy component support failures
are exceedingly rare, developing a meaningful distribution may not be
possible. Therefore, a limited sensitivity study was performed to determine
what degree of error would be required to significantly change the probability
of indirect DEGB.

In this study, plausible construction errors were first identified and
the corresponding reduction in the capacity of critical equipment estimated.
The indirect DEGB probability for Zion was then recomputed to determine the
resultant effect on the probability of indirect DEGB. This study indicated
that only very gross construction errors -- errors that would presumably be
detected by the stringent quality control measures applied to reactor coolant
piping -- could significantly increase the probability of indirect DEGB.

5. SUMMARY OF RESULTS

5.1 Probability of Direct DEGB in Reactor Coolant Loop Piping

We completed probabilistic analyses indicating that the probability of
direct DEGB in reactor coolant piping is very small for Westinghouse PWR
plants located east of the Rocky Mountains. These analyses calculated the
growth of as-fabricated surface flaws at welded joints, taking into account
loads on the piping due to normal operating conditions and seismic events.
Other factors, such as the capability to detect cracks by non-destructive
examination and the capability to detect pipe leaks, were also considered. In
this study, we performed "best estimate" calculations for each of 17 sample
plants (33 plant units), obtaining 17 point estimates of DEGB probability as
well as 17 point estimates of leak probability. These point estimates
described "best estimate" distributions of DEGB probability and leak
probability. The median values (50% confidence limit) of these distributions
provide generic point estimates of DEGB and leak probabilities characteristic
of all plants east of the Rocky Mountains.

The results of our evaluations indicate for Westinghouse plants east of
the Rocky Mountains that:

o   the "best estimate" probability of direct DEGB ranges from 1.1×10^{-12}
     to 6.3×10^{-12} events per plant-year, with a median value (50%
     confidence limit) of 4.4×10^{-12} events per plant-year.

21

o   the "best estimate" probability of leak (through-wall crack) ranges from 1.3×10^{-8} to 1.5×10^{-7} events per plant-year, with a median value of 1.1×10^{-7} events per plant-year. The significantly greater probability of break compared to DEGB supports the concept of "leak before break" in PWR reactor coolant loop piping.

o   uncertainty analyses indicated that the 90th percentile values of DEGB and leak probabilities for the sample plant with the highest probability of direct DEGB are 7.5×10^{-10} and 2.4×10^{-7} events per plant year, respectively.

Through sensitivity studies, we found that normal operating loads, such as stresses due to pressure and thermal expansion, were the dominant contributors to pipe failure; earthquakes had a negligibly small effect on the probability of failure.

Plant-specific evaluations were performed for reactor coolant loop piping at two west coast plants: Trojan and Diablo Canyon. For Trojan, the median probability of direct DEGB was 2.2×10^{-13} events per plant year, with 10th and 90th percentile values of 2.6×10^{-17} and 1.0×10^{-9} events per plant-year, respectively. The estimated median probability of leak was 5.9×10^{-8} events per plant year, with 10th and 90th percentile values of 2.0×10^{-8} and 1.5×10^{-7}, respectively. These values are comparable to corresponding generic DEGB and leak probabilities for plants east of the Rocky Mountains. As in our generic evaluations, we found that normal operating loads, such as stresses due to pressure and thermal expansion, were the dominant contributors to pipe failure; earthquakes had a negligibly small effect.

For Diablo Canyon, earthquakes contributed more significantly to the probability of direct DEGB. Using seismic hazard curves that we derived from three independent seismic hazard evaluations of the plant site, we estimated the median probability of direct DEGB to be 2.5×10^{-11} events per plant-year, about one order of magnitude higher than that for plants east of the Rocky Mountains. Although earthquakes less than about two times the SSE had only a negligible effect on DEGB probability, we found that the simultaneous occurrence of earthquake and DEGB dominated failure for earthquakes above this level. Furthermore, conditional probabilities of leak and DEGB (i.e., given that an earthquake of a given intensity occurs) were equal for earthquakes in this range, suggesting that pipe rupture, and not pipe fracture, became the mode of failure. This contrasted with our results for other plants, which showed that DEGB was typically several orders of magnitude less likely than leak.

Recognizing the increased importance of seismic effects, we performed an extensive series of sensitivity calculations in lieu of a detailed uncertainty analysis and investigated the effect that earthquakes had on the estimated probability of direct DEGB in the reactor coolant loop piping at Diablo Canyon. In particular, we repeated our best-estimate analyses for various values of maximum ground acceleration level as a check on our extrapolation of seismic hazard to five times the SSE. We also estimated the probability of direct DEGB using each of the three independent seismic hazard evaluations, both in extraplolated and unextrapolated form. The results of this sensitivity study indicated that the median probability of DEGB is relatively insensitive to the particular seismic hazard curve selected from among those used in our evaluation.

Our results for Westinghouse plants are presented in Table 2. The results of our generic study of Combustion Engineering PWR plants indicated that the probability of a direct DEGB in reactor coolant loop piping is similarly low (see Table 3). An interesting result here was that the probability of direct DEGB for the carbon steel piping used in these plants was typically higher than that for the more ductile stainless steel piping used in the Westinghouse plants, if the effects of non-destructive examination were neglected. However, the greater certainty of crack detection in carbon steel roughly equalizes the direct DEGB probabilities for the two types of reactor coolant loop systems, a clear illustration of the ability of probabilistic techniques to consider how the interaction of seemingly unrelated parameters can affect overall pipe reliability.

The results of this study also indicated that the probability of an earthquake causing a direct DEGB is as negligible for Combustion Engineering reactor coolant loop piping as it is for the eastern Westinghouse plants.

5.2 Probability of Indirect DEGB in Reactor Coolant Loop Piping

We completed probabilistic analyses for 46 Westinghouse plants located east of the Rocky Mountains indicating that the probability of indirect DEGB in reactor coolant loop piping is very small for these plants. In evaluating the probability of indirect DEGB for each plant, we first identified critical components and determined the seismic "fragility" of each. We then determined for each component the probability that its failure could lead to DEGB. Finally, we estimated the non-conditional probability of indirect DEGB by statistically combining generic seismic hazard curves for the eastern U.S. with a "plant level" fragility derived from the individual component fragilities.

The results of our analyses (see Table 4) indicated for Westinghouse plants east of the Rocky Mountains that:

o   the critical components whose failure would result in DEGB were the reactor pressure vessel supports, the reactor coolant pump supports, and the steam generator supports. For the Zion Unit 1 plant used in our pilot study, the overhead crane in the containment building was also a critical component due to its atypical design. More typical crane designs, supported on rails mounted to the containment structure near the dome, did not contribute significantly to the probability of indirect DEGB.

o   the best-estimate probability of indirect DEGB (50% confidence limit) is about 10^{-7} events per plant year, with an upper bound (90% confidence limit) of 7×10^{-6} events per plant year.

o   the best-estimate probability of indirect DEGB for one "lower bound" plant designed for the combination of safe shutdown earthquake (SSE) and DEGB loads was 3.3×10^{-6} events per plant year, with an upper bound (90% confidence limit) of 2.3×10^{-5} events per plant year.

23

o   the best-estimate probability of indirect DEGB for another lower bound
     plant designed for SSE alone (no DEGB loads) was 2.4×10^{-6} events per
     plant year, with an upper bound of 2×10^{-5} events per plant year.

     We also estimated the probabilities of DEGB for two west coast plants,
San Onofre Unit 1 and Diablo Canyon Units 1 and 2, using site-specific seismic
hazard curves derived from the results of several independent seismic hazard
evaluations. As in our evaluations of plants east of the Rocky Mountains, we
assumed that the RPV supports, reactor coolant pump supports, and steam
generator supports were the critical components whose failure would lead to
DEGB. The results of these analyses indicated that:

o   the median probability of DEGB in the Diablo Canyon reactor coolant loop
     piping is 1.7×10^{-6} events per plant-year, with a 90% confidence limit
     of 2.2×10^{-5} events per plant year. These values are about the same
     as those for the lowest seismic capacity plants east of the Rocky
     Mountains.

o   the median probability of DEGB in the San Onofre Unit 1 reactor coolant
     loop piping is 5.4×10^{-8} events per plant-year, with a 90% confidence
     limit of 9.5×10^{-7} events per plant year. These values, estimated
     using seismic hazard curves that asymptotically approached 1.05g maximum
     PGA (denoted as SONGS Set 1 in Table 4), are over one order of magnitude
     lower than those for the lowest seismic capacity plants east of the Rocky
     Mountains.

o   the probability of indirect DEGB is a strong function of seismic hazard.
     A sensitivity study performed for San Onofre Unit 1, for which we used a
     second set of seismic hazard curves extrapolated out to five times the
     SSE (denoted as SONGS Set 2 in Table 4), showed a two order of magnitude
     increase in indirect DEGB probability. This contrasts sharply with the
     results of our evaluations of direct DEGB probability, which was shown in
     general to be only weakly affected by earthquakes. Nevertheless, even
     when very large earthquakes are considered, the San Onofre results are
     still on the same order as those for the lowest seismic capacity plants
     east of the Rocky Mountains.

     The probability of DEGB due to crack growth at welded joints is typically
four to five orders of magnitude lower than that of DEGB indirectly caused by
the seismic failure of heavy component supports. Thus, our analyses clearly
point to indirect causes as the dominant mechanism leading to DEGB in reactor
coolant loop piping.

     We also performed a limited sensitivity study to determine what degree of
design or construction error would be required to significantly change the
probability of indirect DEGB. From this study, we concluded that only gross
design and construction errors of implausible magnitude could substantially
increase the probability of indirect DEGB beyond the values predicted.

     An evaluation of Combustion Engineering plants indicated the same general
results, with the probabilities of indirect DEGB in reactor coolant loop
piping typically lower than for the Westinghouse plants (see Table 5).

24

6. CONCLUSIONS

In general, the results of our evaluation indicate that the probability of DEGB in the reactor coolant loop piping of Westinghouse and Combustion Engineering plants is extremely low. Our results further indicate that:

o   indirect causes are clearly the dominant mechanism leading to DEGB in reactor coolant loop piping.

o   earthquakes have a negligible effect on the probability of direct DEGB. On the other hand, the probability of indirect DEGB is a strong function of seismic hazard, but is nevertheless low even when earthquakes significantly greater than the safe shutdown earthquake are considered.

o   only very large design and construction errors of implausible magnitude could significantly affect the probability of indirect DEGB in reactor coolant loop piping.

On the basis of these results, we recommend that the NRC seriously consider eliminating DEGB as a design basis event for reactor coolant loop piping in Westinghouse plants. Elimination of the DEGB requirement would accordingly allow pipe whip restraints on reactor coolant loop piping to be excluded or removed, and would eliminate the requirement to design supports to withstand asymmetric blowdown loads.

We also recommend that the current requirement to couple SSE and DEGB be eliminated. Recognizing however that seismically induced support failure is the weak link in the DEGB evaluation, we further recommend that the strength of component supports, currently designed for the combination of SSE plus DEGB, not be reduced. The support strength could be maintained in spite of a decoupling of DEGB and SSE by replacing the present combined load requirement with a factor applied to SSE load alone. This factor would be defined in such a way that the support strength would remain unchanged.

Our study indicates that the probability of DEGB in reactor coolant loop piping is sufficiently low under all plant conditions, including seismic events, to justify eliminating it entirely as a basis for plant design. This represents a fundamental change in design philosophy that has potential impact far beyond the single issue of SSE and DEGB coupling. Elimination of reactor coolant loop DEGB would require that replacement criteria be developed as a basis for various aspects of plant design, including, but not necessarily limited to:

o   blowdown loads on the reactor vessel and RPV internals
o   primary coolant discharge rate
o   containment pressurization
o   jet impingement loads
o   environmental effects
o   support loads
o   pipe whip

Any NRC rulemaking action defining general replacement criteria will have to be based on a comprehensive approach taking into account causes of pipe failure, break size and potential effects on plant design, acceptable levels of safety requirements, and criteria for regulating the postulation of pipe break. In the near term, however, the results of the evaluation reported here now provide NRC with one technical basis for making case-by-case licensing decisions applicable to reactor coolant loop pipng.

References

1. "Probability of Pipe Fracture in the Primary Coolant Loop of a PWR Plant", Lawrence Livermore National Laboratory, Livermore, California, Report UCID-18967, NUREG/CR-2189, Vols. 1-9 (September 1981).

> Vol. 1: Summary
> Vol. 2: Primary Coolant Loop Model
> Vol. 3: Non-Seismic Stress Analysis
> Vol. 4: Seismic Response Analysis
> Vol. 5: Probabilistic Fracture Mechanics Analysis
> Vol. 6: Failure Mode Analysis
> Vol. 7: System Failure Probability Analysis
> Vol. 8: Pipe Fracture Indirectly Induced by an Earthquake
> Vol. 9: PRAISE Computer Code User's Manual

2. NUREG/CR-3660, "Probability of Pipe Failure in the Reactor Coolant Loops of Westinghouse PWR Plants", Lawrence Livermore National Laboratory, Report UCID-19988, NUREG/CR-3660, in publication

> Vol. 1: Summary Report
> Vol. 2: Direct DEGB, Eastern Plants
> Vol. 3: Indirect DEGB
> Vol. 4: Direct DEGB, West Coast Plants

3. "Probability of Pipe Failure in the Reactor Coolant Loops of Combustion Engineering PWR Plants", Lawrence Livermore National Laboratory, Report UCRL-53500, NUREG/CR-3663, in publication

> Vol. 1: Summary Report
> Vol. 2: Direct DEGB
> Vol. 3: Indirect DEGB

4. Boiler and Pressure Vessel Code, American Society of Mechanical Engineers, New York, New York.

5. D.O. Harris and H.H. Woo, et al, "Fracture Mechanics Models Developed for Piping Reliability Assessment in Light Water Reactors", Lawrence Livermore National Laboratory, Report UCRL-15490, NUREG/CR-2310 (April 1982).

6. T.Y. Lo, et al, "Failure Probability of PWR Reactor Coolant Loop Piping", Lawrence Livermore National Laboratory, Report UCRL-86249 (February 1984). Presented at the ASME Pressure Vessel and Piping Conference, San Antonio, Texas, June 17-21, 1984.

7. R.D. Streit, "Probability of Pipe Fracture in the Primary Coolant Loop of a PWR Plant: Pipe Fracture Indirectly Induced by an Earthquake," Lawrence Livermore National Laboratory, Livermore, California, Report UCID-18967, NUREG/CR-2189, Vol. 7 (September 1981).

Table 1

Parameters Considered in Developing Component Fragilities

Structural Response

---

o   Ground spectrum used for design

o   Structural damping

o   Site characteristics (rock or soil, shear wave velocity, thicknesses
    of different strata)

o   Fundamental frequency of internal structure if uncoupled analysis was
    performed

o   Interface spectra for NSSS points of connection to structure if
    uncoupled analysis was conducted

o   Input ground spectra resulting from synthetic time history applied to
    structural model

NSSS Response

---

o   Method of analysis (time history or response spectrum, etc.)

o   Modeling of NSSS and structure (coupled or uncoupled)

o   NSSS system damping

o   NSSS fundamental frequency or frequency range

o   If uncoupled analysis was performed, whether envelope or
    multi-support spectra were used.

TABLE 2

Probabilities of Direct DEGB and Leak for Reactor Coolant Loop Piping in Westinghouse PWR Plants

(events per plant year)

	Confidence Limit[1]		
	10%	50%	90%
Plants East of the Rocky Mountains[2]			
DEGB	5.0×10^{-17}	4.4×10^{-12}	7.5×10^{-10}
Leak	5.6×10^{-10}	1.1×10^{-7}	2.4×10^{-7}
West Coast Plants[3]			
Trojan (DEGB)	2.6×10^{-17}	2.2×10^{-13}	1.0×10^{-9}
Trojan (Leak)	2.0×10^{-8}	5.5×10^{-8}	1.5×10^{-7}
Diablo Canyon (DEGB)	see text	2.5×10^{-11}	see text
Diablo Canyon (Leak)	see text	3.8×10^{-7}	see text

(1) A confidence limit of 90% implies that there is a 90% subjective probability (confidence) that the probability of leak or direct DEGB is less than the value indicated.

(2) Generic seismic hazard curves used.

(3) Plant-specific seismic hazard curves used.

TABLE 3

Best-Estimate Probabilities of Direct DEGB and Leak for Reactor Coolant Loop Piping in Combustion Engineering PWR Plants

(events per plant year)

	DEGB	Leak
Palo Verde 1,2,3	4.5×10^{-13}	1.5×10^{-8}
San Onofre 2,3	1.0×10^{-13}	2.2×10^{-8}
WPPSS 3	6.1×10^{-14}	1.8×10^{-8}
Waterford 3	9.0×10^{-14}	1.8×10^{-8}
Group A [1] Composite	5.5×10^{-14}	2.3×10^{-8}
Westinghouse[2]	6.3×10^{-12}	1.2×10^{-7}

(1) Composite plant enveloping data for Calvert Cliffs 1 & 2, Millstone 2, Palisades, and St. Lucie 1 & 2.

(2) Results for Westinghouse sample plant with highest probability of DEGB.

TABLE 4

Annual Probabilities of Indirect DEGB
for Westinghouse PWR Plants

(events per plant-year)

	Confidence Limit[1]		
	10%	50%	90%
Lowest Seismic Capacity Eastern Plants[2]			
Designed for SSE + DEGB	2.3×10^{-7}	3.3×10^{-6}	2.3×10^{-5}
Designed for SSE alone	1.0×10^{-7}	2.4×10^{-6}	2.0×10^{-5}
All 46 Eastern Plants[2]	2.0×10^{-9}	1.0×10^{-7}	7.0×10^{-6}
West Coast Plants[3]			
San Onofre Unit 1			
SONGS Set 1	3.1×10^{-10}	5.4×10^{-8}	9.5×10^{-7}
SONGS Set 2	1.3×10^{-7}	4.7×10^{-6}	4.9×10^{-5}
Diablo Canyon Units 1,2	4.0×10^{-7}	1.7×10^{-6}	2.2×10^{-5}
Median for West Coast Plants	2×10^{-7}	3×10^{-6}	5×10^{-5}

(1) A confidence limit of 90% implies that there is a 90% subjective probability (confidence) that the probability of indirect DEGB is less than the value indicated.

(2) Generic seismic hazard curves used in evaluation.

(3) Site-specific seismic hazard curves used in evaluation

31

TABLE 5

Annual Probabilities of Indirect DEGB for
Combustion Engineering PWR Plants

	Confidence Limit[1]		
	10%	50%	90%
Group A Plants			
Calvert Cliffs	2.3×10^{-8}	6.1×10^{-7}	6.1×10^{-6}
Millstone 2	9.0×10^{-10}	6.6×10^{-8}	1.2×10^{-6}
Palisades	5.0×10^{-7}	6.4×10^{-6}	5.2×10^{-5}
St. Lucie 1	1.2×10^{-8}	3.8×10^{-7}	4.1×10^{-6}
St. Lucie 2	6.6×10^{-8}	1.4×10^{-6}	1.1×10^{-5}
Westinghouse Lowest Capacity Plant	2.3×10^{-7}	3.3×10^{-6}	2.3×10^{-5}

(1) All probabilities are given as events per plant year. A confidence limit of 90% implies that there is a 90% subjective probability (confidence) that the probability of indirect DEGB is less than the value indicated.

(2) Generic seismic hazard curves used in evaluation.

TABLE 5 (cont.)

Annual Probabilities of Indirect DEGB for
Combustion Engineering PWR Plants

	Confidence Limit[1]		
	10%	50%	90%
Group C Plants			
Palo Verde 1,2,3 [2],[3]			
Site-Specific	4.0×10^{-19}	3.8×10^{-16}	1.0×10^{-13}
Generic	2.4×10^{-12}	5.4×10^{-10}	1.1×10^{-7}
San Onofre 2,3 [3]			
Site-Specific Set 1	3.5×10^{-18}	4.6×10^{-17}	3.2×10^{-14}
Site-Specific Set 2	5.0×10^{-17}	1.1×10^{-11}	2.1×10^{-9}
WPPSS 3 [2]	8.0×10^{-11}	2.9×10^{-9}	1.5×10^{-7}
Waterford 3 [2]	1.1×10^{-10}	1.3×10^{-8}	3.0×10^{-7}
Westinghouse Lowest Capacity Plant	2.3×10^{-7}	3.3×10^{-6}	2.3×10^{-5}

(1) All probabilities are given as events per plant year. A confidence limit of 90% implies that there is a 90% subjective probability (confidence) that the probability of indirect DEGB is less than the value indicated.

(2) Generic seismic hazard curves used in evaluation.

(3) Site-specific seismic hazard curves
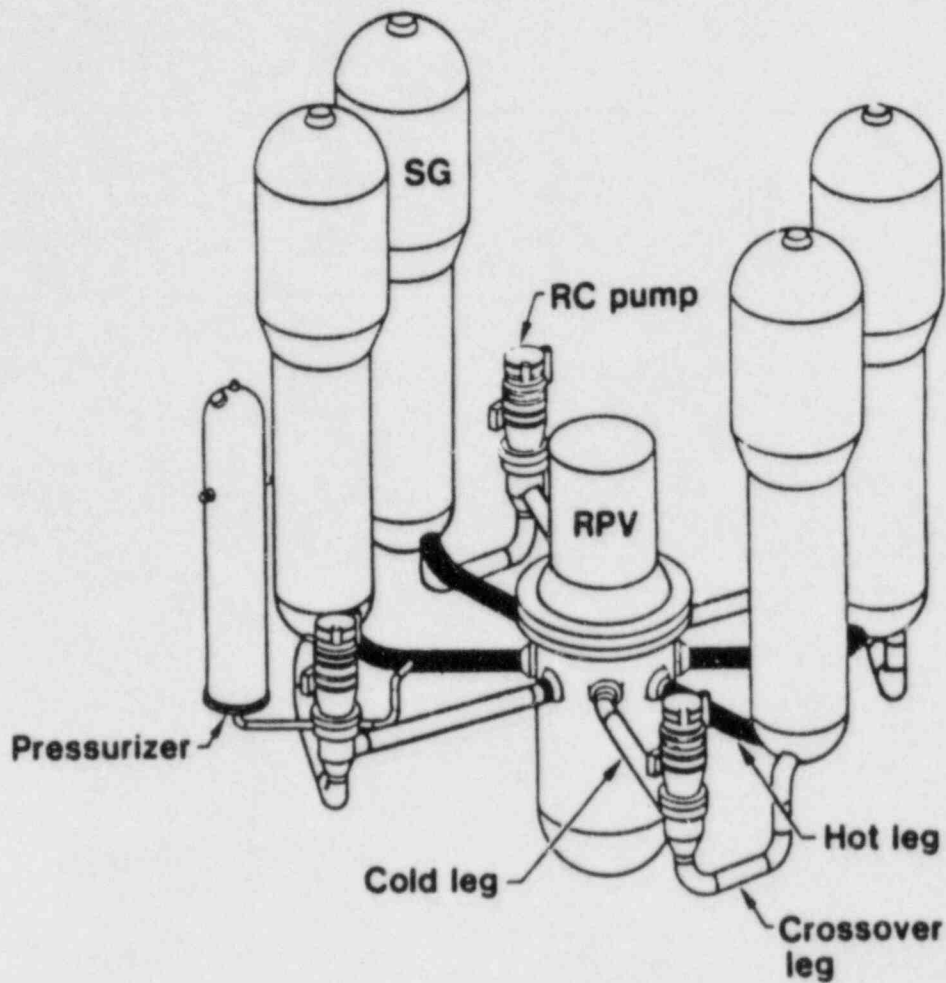
Fig. 1. Typical reactor coolant loop piping arrangement in a Westinghouse pressurized water reactor nuclear steam supply system.
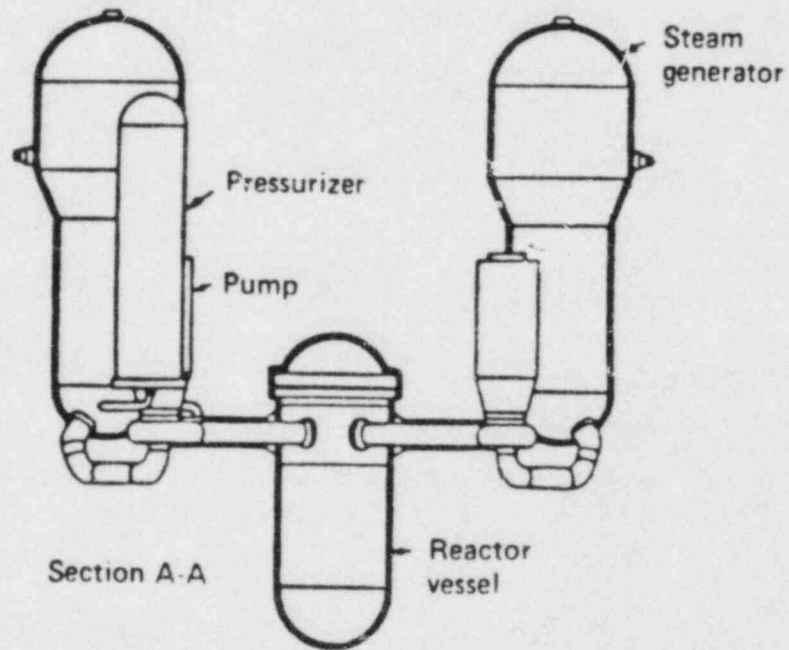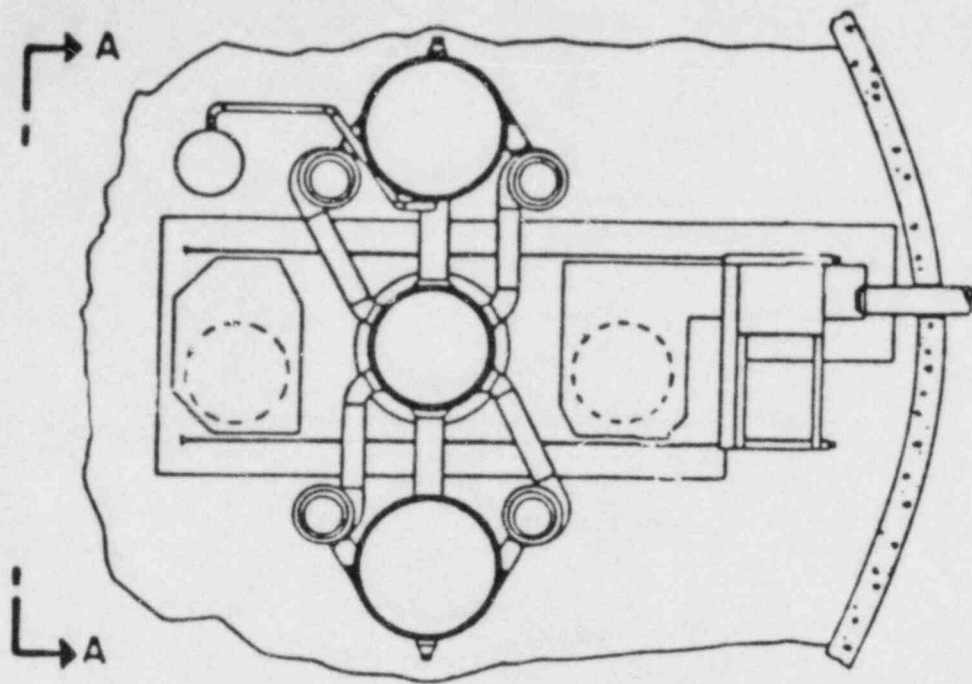
Fig. 2. Typical reactor coolant loop piping arrangement in a Combustion Engineering pressurized water reactor nuclear steam supply system.

Probabilistic Approach

Estimates failure probability

Stress (σ),
strength (S)

Applied stress
measure, σ

Strength
measure, S
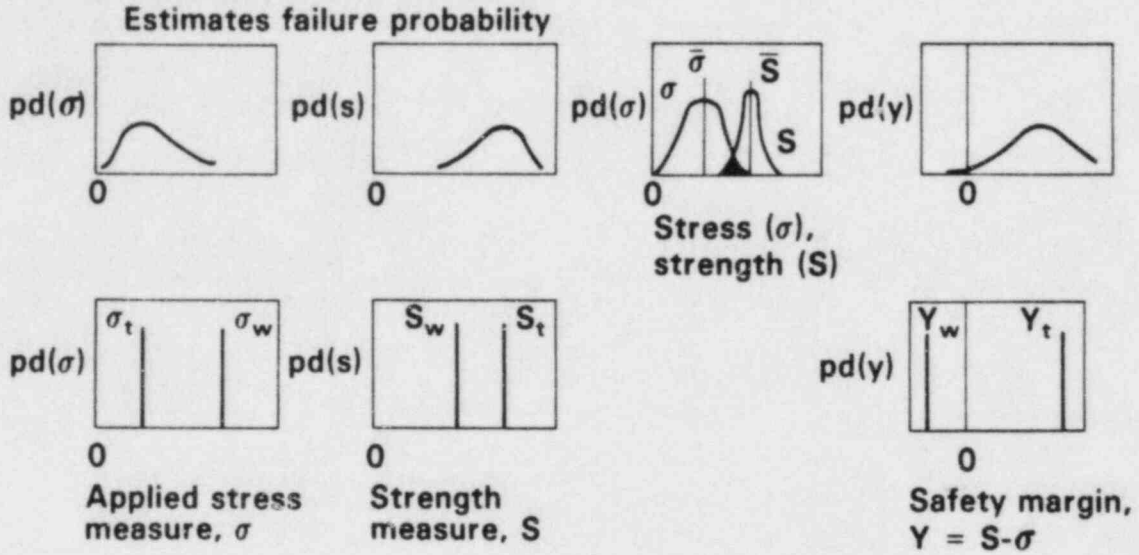
Safety margin,
Y = S-σ

Deterministic approach

"Typical" (t) analysis indicates adequate safety margin

"Worst-case" (w) analysis indicates negative safety margin or failure

Fig. 3. Schematic representation of deterministic and probabilistic
techniques for evaluating design adequacy. In the probabilistic
approach, failure is possible in the cross-hatched region.
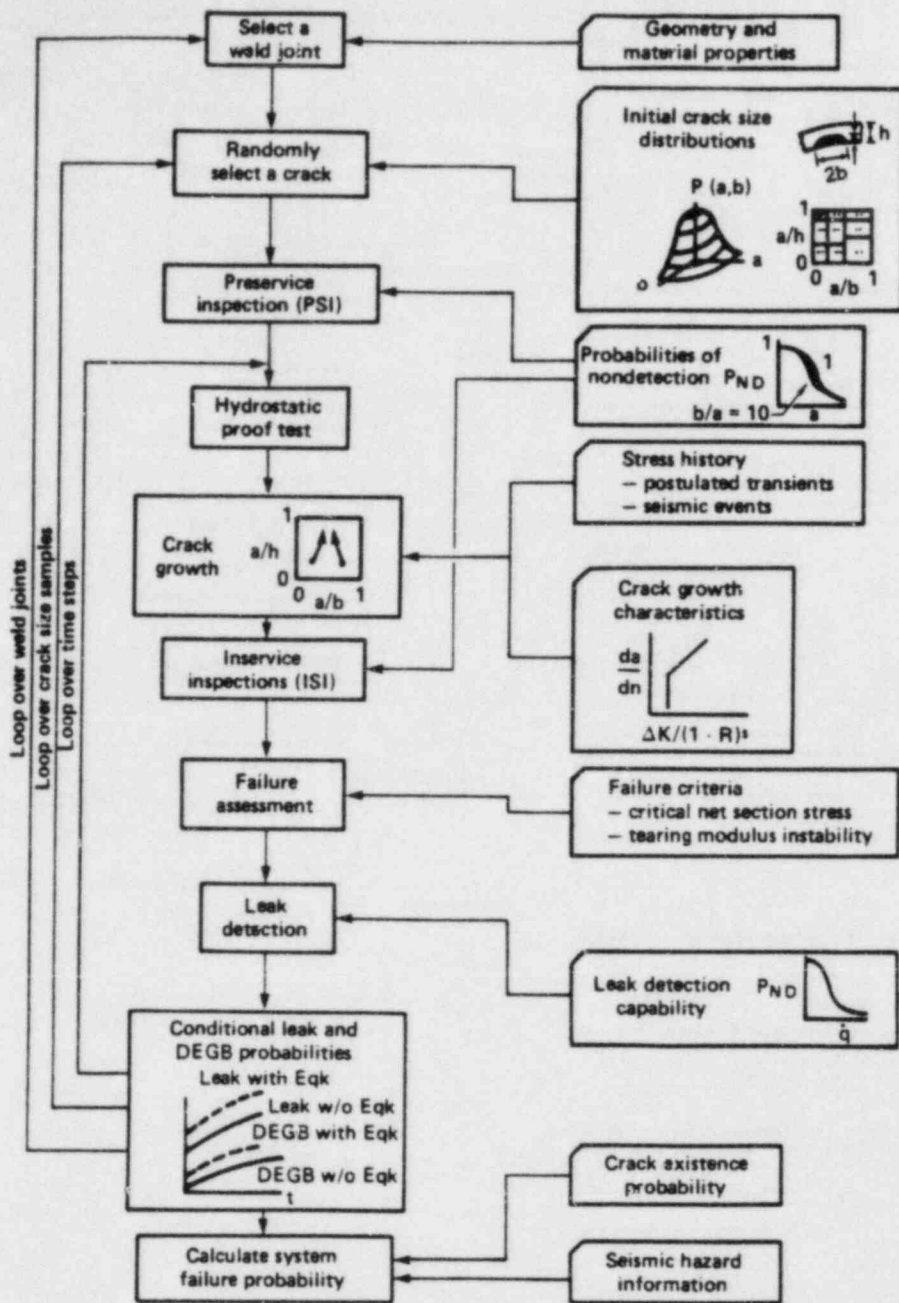
Fig. 4. Schematic representation of the probabilistic fracture mechanics simulation model implemented in the PRAISE computer code.
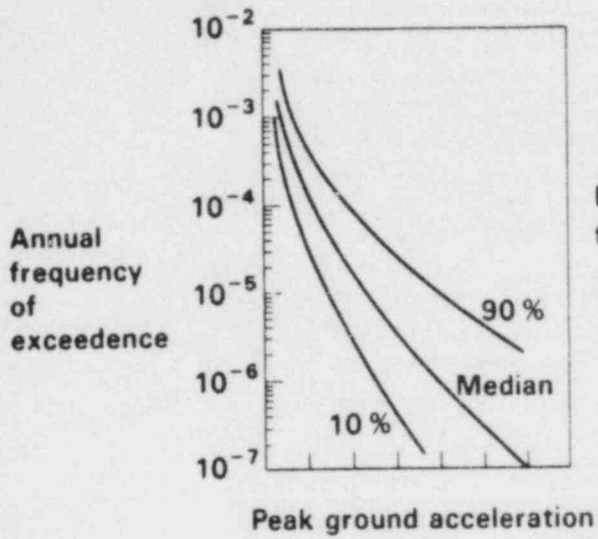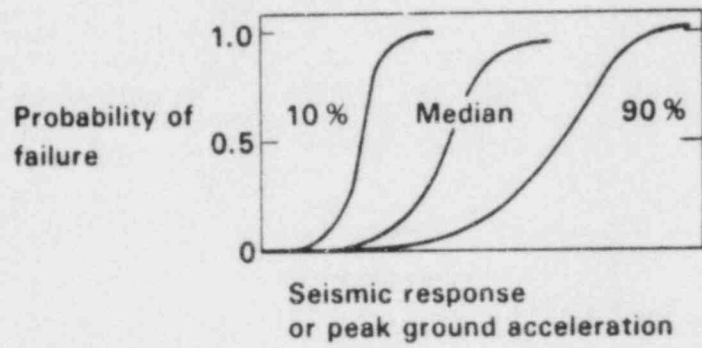
Fig. 5. Typical descriptions of seismic hazard (a) and fragility (b).

PIPE-TO-PIPE IMPACT

M. C. C. Bampton, J. M. Alzheimer, J. R. Friley, and F. A. Simonen

ABSTRACT

Existing licensing criteria express what damage shall be assumed for various pipe sizes as a consequence of a postulated break in a high energy system. The criteria are contained in Section 3.6.2 of the Standard Review Plan, and the purpose of the program described with this paper is to evaluate the impact criteria by means of a combined experimental and analytical approach.

A series of tests has been completed as part of the criteria evaluation program. Comparison of the test parameters with corresponding parameters from a SNUPPS plant model showed a deficiency in the range of pipes tested, and also in the extent of damage that might be feasible. The program has proceeded to remedy these deficiencies by implementing a second series of impact tests and with the aid of a more powerful, impact machine.

In parallel with the test program for evaluation of the pipe impact criteria, an analysis capability has been developed. This capability has been used to predict the damage resulting from the impacts of the first test series. Steps have been taken to improve the quality of prediction by the conduct of some tests that establish post-crush and bending relationships.

Upon completion of the test program and the corresponding analysis efforts, it is expected that two outputs will have been achieved:

. data that may, or may not, necessitate changes to the criteria after appropriate value impact evaluations

. an analytic capability for rapidly evaluating the potential for pipe whip damage after a postulated break.

These outputs are to be contained in a value-impact document and a program final report.

An additional study was undertaken to determine the possible existence of a plastic hinge forming in a pipe that was free to whip. Although very large displacements were generated, the concept of a hinge was not validated.

INTRODUCTION

The U.S. Nuclear Regulatory Commission (NRC) authorized the Pacific Northwest Laboratory (PNL) to investigate the behavior of piping during postulated pipe-to-pipe impact events. The Pipe-to-Pipe Impact (PTPI) Program is sponsored by the Mechanical and Structural Engineering Branch, Division of Engineering Technology of the NRC.

Justification for the PTPI Program stems from a need for data upon which to base licensing decisions. The current licensing criteria regarding PTPI, as contained in Standard Review Plan (SRP) Section 3.6.2, are stated as follows:

"An unrestrained whipping pipe should be considered capable of causing circumferential and longitudinal breaks, individually, in impacted pipes of smaller nominal pipe size, and developing through-wall cracks in equal or larger nominal pipe sizes with thinner wall thickness, except where analytical or experimental, or both, data for the expected range of impact energies demonstrates the capability to withstand the impact without rupture."

The current criteria define a readily usable set of conditions under which pipe-to-pipe impact events can be permitted or should be prevented. However, the criteria do not specifically address the available energies, piping arrangements, or other potentially significant parameters. Because data to validate the criteria are lacking, the conservatism cannot be assessed. Under certain circumstances, the current criteria may not be conservative. On the other hand, they may be overly conservative, thus adding unneeded restraints to power plants. The intent of the PTPI Program is to determine the range of parameters associated with postulated pipe-to-pipe impact events in typical nuclear power plants, conduct impact tests within the range of interest, evaluate current criteria in light of the test results, and, if appropriate, propose more realistic criteria.

This paper describes the reasoning behind the latest test series and the revised impact machine that was fabricated to accommodate the higher energy impacts. The developments to the impulse-momentum model that were performed in order to improve its correlation with the test results are also described. Finally, an analytical study to identify the feasibility of a plastic hinge developing in a whipping pipe is presented. The closing section of this paper discusses the items that are remaining in order for the program to be completed.

EXPERIMENTAL APPROACH

The experimental approach has been based upon the simulation of a pipe impact scenario using a special purpose machine designed and fabricated for the program. The sizes of the impacting and target pipes for an initial test matrix were selected on the basis of a range presumed to be typical of a nuclear plant piping system. Subsequent review of an actual plant (SNUPPS) model indicated that a different set of pipe dimensions would be more relevant. The initial test results also showed that insufficient energy was available to cause rupture damage in a significant number of tests (Two ruptures were observed in the tests).

The pipe whip configuration that was assumed to occur in the SNUPPS survey is shown in Figure 1. The two most critical assumptions were that the pipe whip restraints were absent, and that the pipe of concern experienced a guillotine break at the postulated locations. Note was then made of the pipe dimensions and proximities to other high energy pipes. These data are represented in Figure 2 and reveal that 67% of the pipes noted are 6 inches, or less, in diameter. For this reason, and also for considerations of economy, it was decided to limit the nominal sizes of the impacting pipes to within 6 inches. This decision not only offered a good coverage of the realistic range of possible pipe whip scenarios, but also assisted in maintaining an economic approach to a revised impact machine that was seen to be necessary to cause a significantly higher level of damage than had been achieved in the first series of tests.

In order that more damage could be achieved, it was evident that a machine with a higher capacity for delivering energy would have to be constructed. Since impact energy is directly related to the square of impact velocity a computer model of the existing impact machine's velocity, responses to various actuating pressure levels was exercised. A correlation of this computer model's predictive abilities is demonstrated in Figure 3 against some of the impact test results. These results show that the model could be used with a high degree of consistency in its predictions.

The computer model KATDYN was next applied to developing relationships between required actuating pressure and the desired velocities (impact energies). A target velocity of 400 feet per second (maximum) was identified as having a high probability for causing ruptures on the types of pipes under consideration. These relationships are shown in Figure 4 for various sizes of pipes being accelerated by the impact machine. From these data it was decided that an actuator with a pressure rating of 1500 psi would be required to perform the second series of impact tests in a manner that would provide sufficient damage data.

As a result of the significantly higher energies involved, a much stronger machine had to be designed and constructed. The resulting system is depicted in Figure 5 and it can be seen that it bears a strong resemblance to the earlier apparatus. The main distinction, apart from its enhanced strength, being that the mass of the catapult arm does not have to be decelerated by the compression side of the actuator. This relieves the actuator of some very large forces that would develop in the duration of the impact. The catapult arm is locked to the impacting pipe and has its kinetic energy absorbed by the impact.

41

The test matrix for the second series of tests is given in Table I below:

TABLE I. Test Matrix

Test Group #1: 3" schedule 160 impacting 6" schedule 160

Test Group #2: 4" schedule 160 impacting a 6" schedule 160

Test Group #3: 4" schedule 80 impacting a 4" schedule 80

Test Group #4: 4" schedule 160 impacting a 4" schedule 160

Test Group #5: 6" schedule 160 impacting a 4" schedule 160

Test Group #6: 6" schedule 160 impacting a 3" schedule 160

Test Group #7: 3" schedule 160 impacting a 6" schedule 40.

All groups will involve tests at various velocities in order to achieve a range of damage for each combination of impacting pipes.

ANALYSIS APPROACH

A simplied model was developed earlier to simulate the impact mechanics. The model used an impulse and a flexure phase as its basis for simulating the sequence of events during an impact. The separation of these two phenomena lends a very powerful simplicity to the simulation. Crush energy and flexure energy can be accounted for individually, and are determined by employing impulse momentum techniques for an infintesimal impact time. Crush energy has been treated empirically by means of static crush tests.

Evaluation of the energy attributed to crush during the impact provides a means for estimating the resultant change in diameters. Assessment of the corresponding flexure energy yields an estimate of the resulting bend angles. A comparison of diameter change estimates with the related test data has been carried out and is shown in Figure 6 for the various impact tests. The correlations are very mixed in terms of the quality of simulation. The comparison of bend angle estimates with the test data is shown in Figure 7 and reflects a much higher level of quality.

One avenue of development that has been pursued with a view to explaining, and remedying, the discrepancies is to evaluate the significance of the non-linear behavior associated with crushing due to bending. The current model not only separates the crushing and flexure behavior, but assumes that crushing energy has been fully absorbed prior to any transfer of energy to flexure deformation. One incentive towards believing that flexure is inducing further crushing is the marked association of large flexure angles in the results and poor agreement for the corresponding crush test data and estimates.

To establish the level of significance of such a coupling between flexure and additional crushing, a modest test program has been instituted. The essentials of this program are portrayed in Figure 8. A straight pipe specimen is held flat while an initial indentation is impressed upon it. A moment load is next applied gradually to the specimen such that it deflects relative to the center of the indentation. Step measurements of the flexure angle and the corresponding changes in the diameter at the section of interest are recorded.

Data for two such tests are shown in Figure 9 for 2 inch schedule 40 pipe specimens. One was given an initial indentation of 15% and the other was given an initial indentation of 29%. It can be seen from these results that a significant increment of diameter change can be caused. It has to be recognized that the data given in Figure 9 are applicable only to pipe specimens of diameter to thickness ratios close to that for the 2 inch schedule 40 pipes if a dimensionality relationship is to be maintained. Amongst the impact test specimens these data would be relevant to 6 inch schedule 80 pipes.

Referring back to Figure 7, test number 15 involves a 6 inch schedule 80 pipe. It can be seen that a flexure angle of about 25 degrees was developed after impact. From the crush-flexure data of Figure 9 it can be seen that a crush increment of approximately 10% could be achieved. The addition of this to the estimated diameter change given in Figure 6 for test number 15 would significantly improve its correlation with the test result.

In order to encompass the range of pipe specimens being used throughout the main test program, crush-flexure data for other pipe diameter to thickness ratios have been developed. These data will be incorporated into the existing model with appropriate dimensional theory considerations.

PIPE WHIP HINGE STUDY

A study was performed to investigate the large deformation behavior of whipping pipe. Due to the large jet forces, plastic deformation of the pipe is likely unless the postulated break occurs very near a restraint. The purpose of the hinge study was to determine the distance from the break to the point where a plastic hinge would form in the pipe. This information is the kind required for the design of pipe whip restraints and in the assessment of damage potential from the whipping pipe. A large displacement, transient dynamic finite element code was used for the analyses. Various parameters relevant to the motion of the whipping pipe were identified.

The pipe whipping model comprised elements that represented the beam behavior of a pipe that was experiencing very large displacements. In addition to the large motion characteristics it was also necessary to simulate the plastic strains associated with such motions. A further behavior of importance was the correct formulation of the dynamic loads arising out of a rapid transient phenomenon. The simplifying assumptions were that the activating forces remained perpendicular to the pipe tip and that cross sections did not change shape even under large plastic strain conditions.

All models were based upon 10 foot long pipes 6 inches in diameter. Two pipe thicknesses and two activating pressures were analyzed as variables. The pressures dictated the magnitude of the follower forces and were assumed to remain constant in magnitude throughout the time of the analyses. Figure 10 shows model components and an example of the deformed shape of one of the models after a lapsed time of 0.030 seconds since commencement of the whipping action.

The onset of yielding at various locations along the length of three models is depicted with respect to time in Figure 11. The middle curve (6 inch schedule 160, 2250 psi) shows that almost two-thirds of the overhanging pipe length indicates yielding very sharply, while the remainder of the pipe develops a yield condition in a more gradual manner. The upper curve displays a more gradual transition to yielding and the lower curve indicates that a dynamic effect can initiate yielding at an intermediate location other than the tip.

One limitation of the models was the assumption of a nonchanging cross section. Experimental data suggest that the pipe would probably ovalize which would reduce the moment resisting capability of the pipe. Under such conditions, the formation of an actual "hinge" may indeed be possible, but would be very difficult to predict without additional understanding of the large displacement behavior of the pipe wall due to combined bending and presence loads.

The conclusions to be drawn from these results are that the concept of a simple hinge may be unrealistic, although it may be convenient in developing a rapid assessment of pipe whip behavior. Also, very large motions could occur within the time frame of a pipe whip event. It appears reasonable to use simplified methods for determining hinge locations in assessing the distance of pipe swing. The energy available during an impact event is a function of the pipe swing distance and the amount absorbed by the plastic deformation of the whipping pipe. However, the use of plastic hinge models to predict whipping pipe motions and direction to any degree of accuracy is very questionable.

CONCLUDING DISCUSSION

- A revised test matrix will be completed in early FY1985. The data developed within this part of the pipe impact program, together with the previous results, should provide a sound basis for final evaluation of the pipe whip criteria expressed in the Standard Review Plan 3.6.2

- The impact machine developed for the latest series of tests will result in data that reflect more damage and rupture potential.

- A rationale has been formulated for incorporating the non-linear behavior associated with flexure induced crush.

- A study to evaluate the effect of plastic hinge development within the length of a whipping pipe indicated that the hinge concept was not realistic. The study also demonstrated that very large displacements could be developed within the time frame of pipe whip event.

FINAL ITEMS

The program will be completed in early FY1985 and the following items need to be addressed in order to fulfill the program objectives:

1) Complete the test program and assemble the total data set.

2) Perform the correlation analyses for the impact model in comparison with the total data set.

3) As the damage data evolves from the test program the failure rationale will be further developed to support the impact model in achieving a means of evaluating the S.R.P. criteria.

4) If the outcome of the above item is such as to indicate that a change to the criteria is necessary, a value impact evaluation will be performed.

5) A final report will be written that describes all aspects and findings of the pipe impact program.

ACKNOWLEDGEMENTS
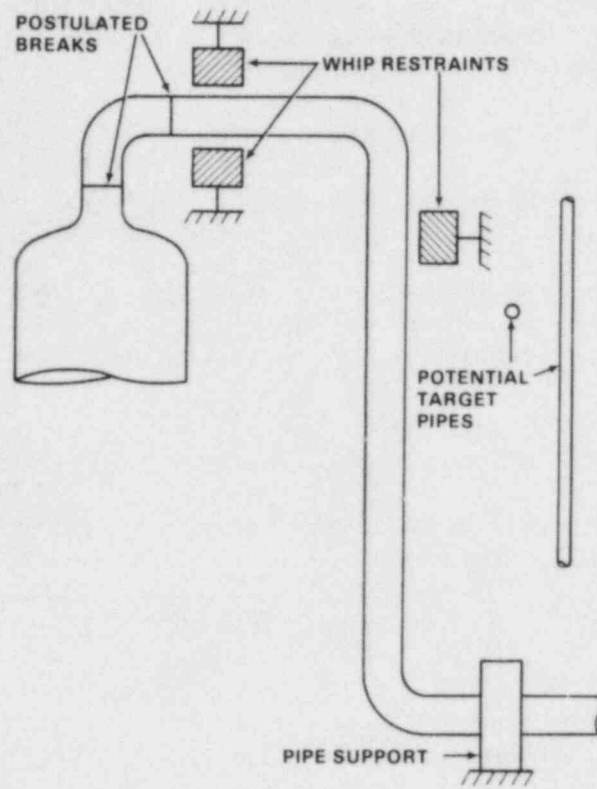
FIGURE 1. Typical Pipe Whip Configuration
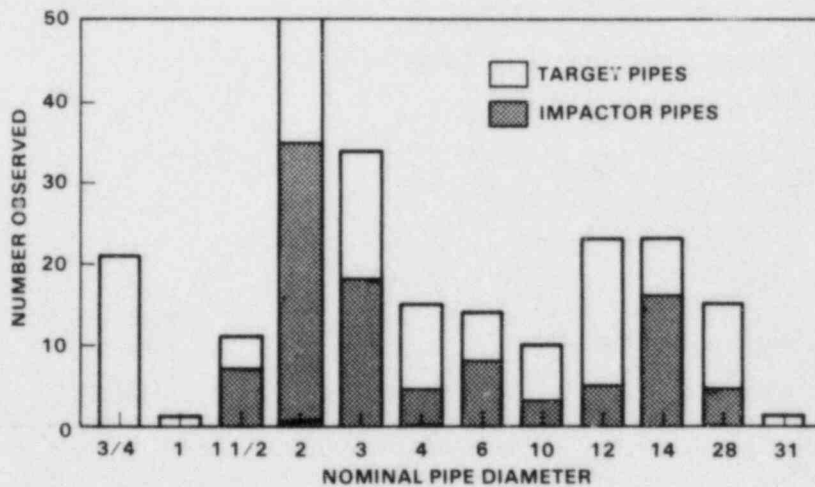
FIGURE 2. Histogram of Snupps Pipe Diameter Data
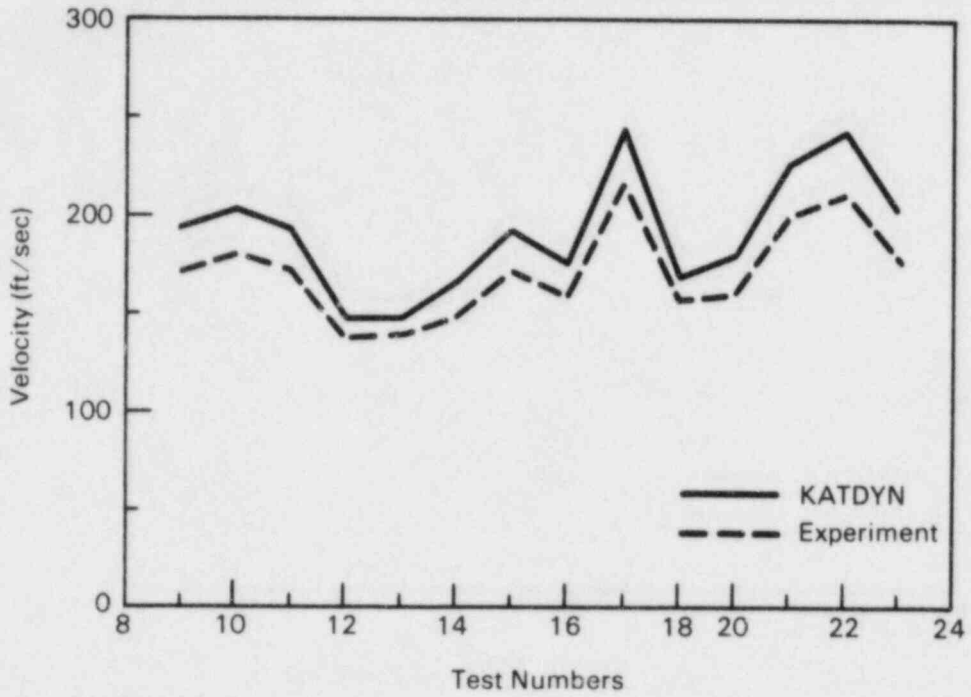
FIGURE 3. Correlation cf KATDYN with Impact Machine
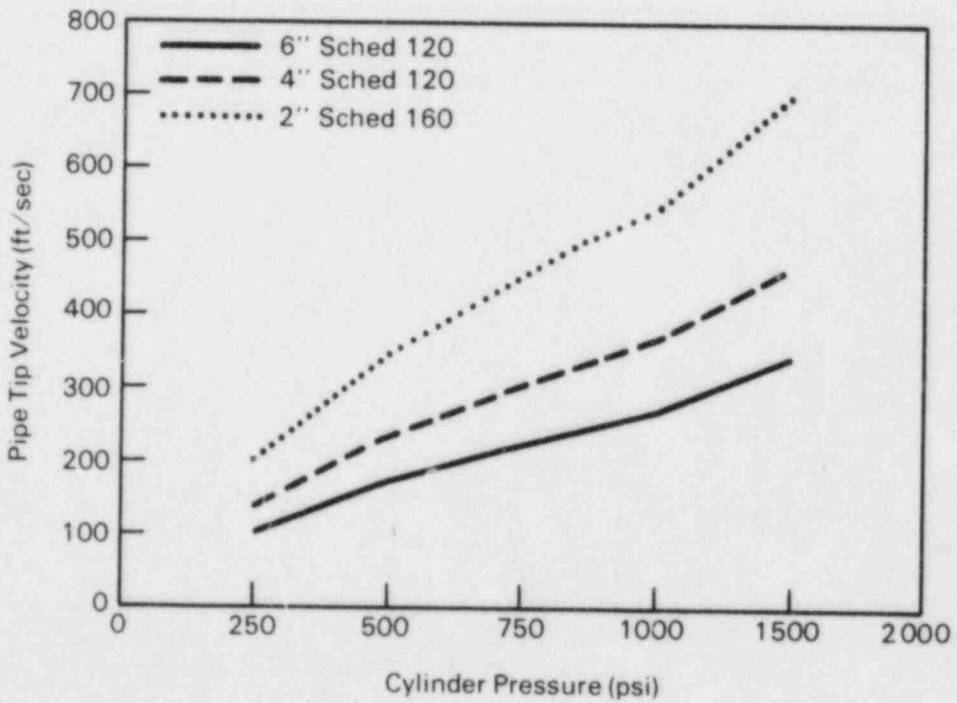
FIGURE 4. Application of KATDYN to Catapult Design

47
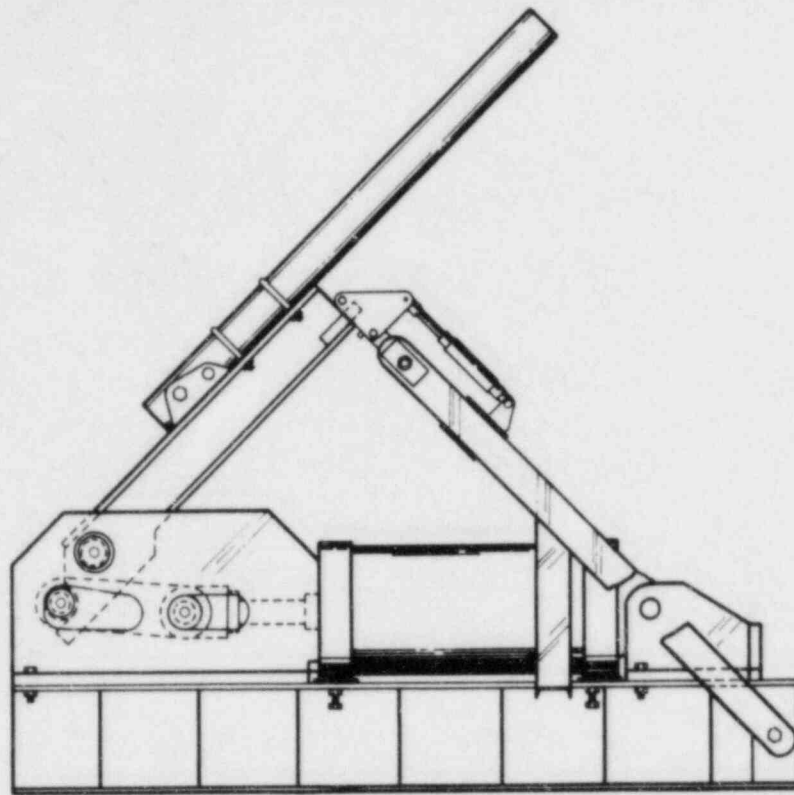
FIGURE 5. Revised Impact Machine
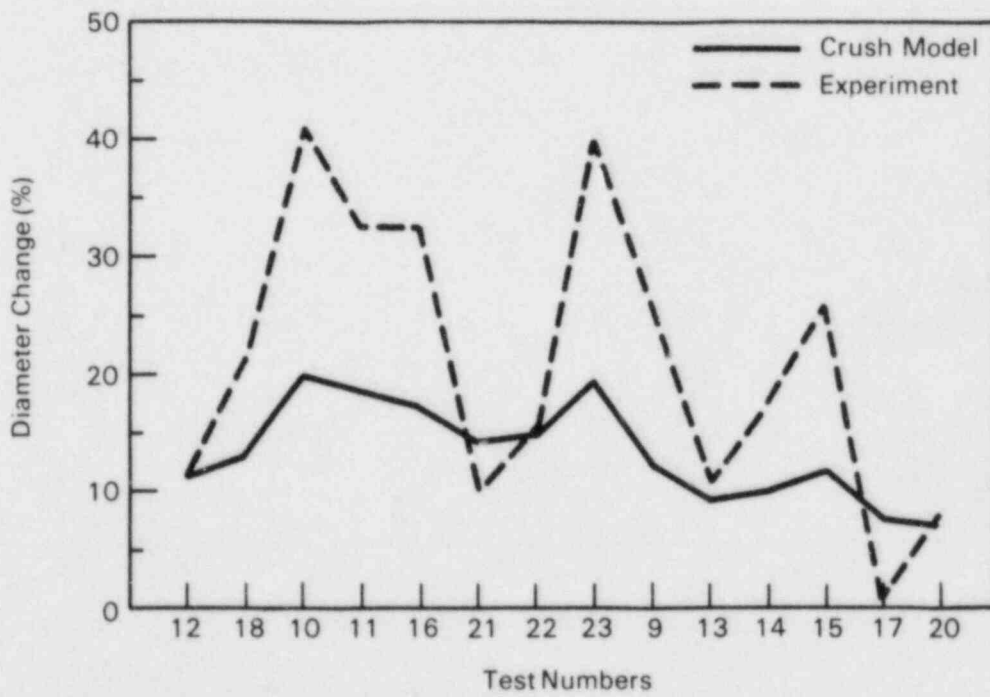
FIGURE 6. Correlation of Impact Analyses and Experimental - Diameter Changes
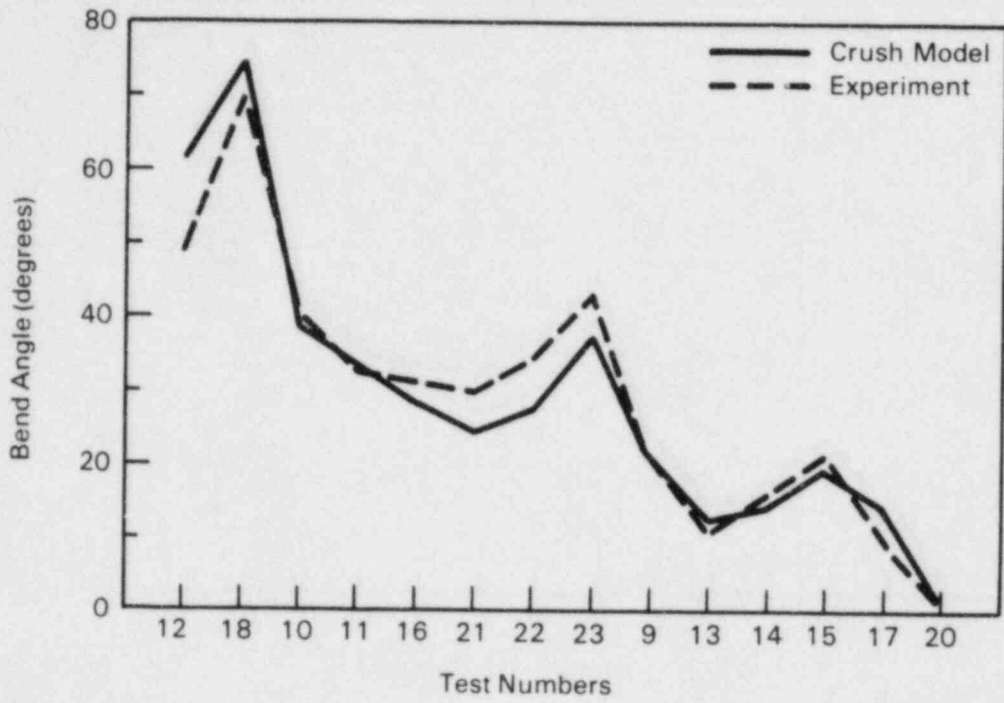
FIGURE 7. Correlation of Impact Analyses and Experimental - Bend Angles
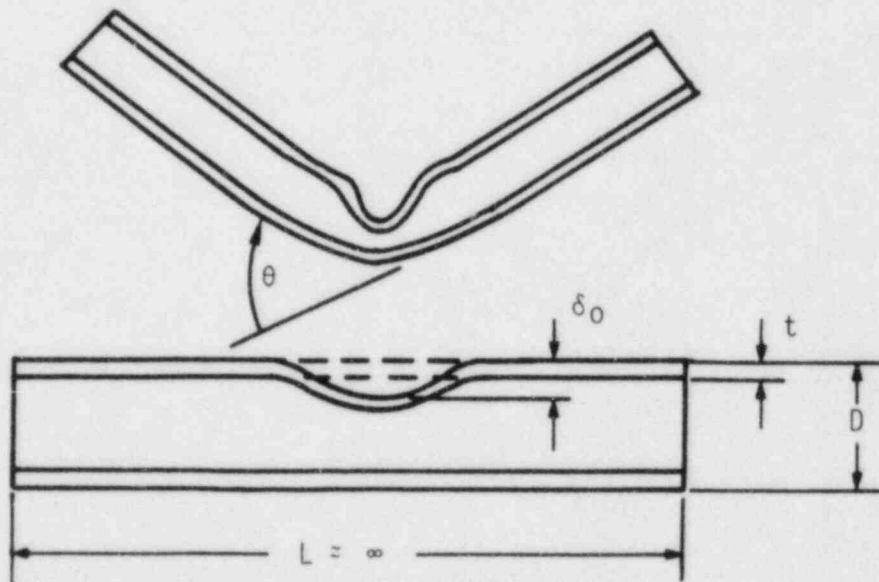
FIGURE 8. Ovalization Due to Flexure

49
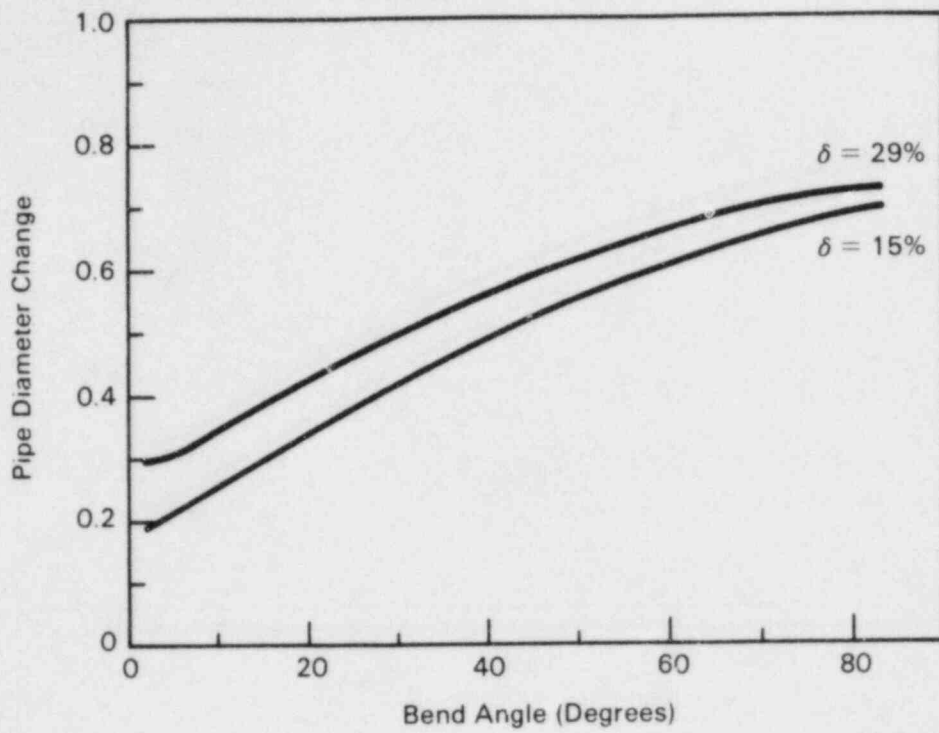
FIGURE 9. Bend Angle Effects Upon Diameter Changes
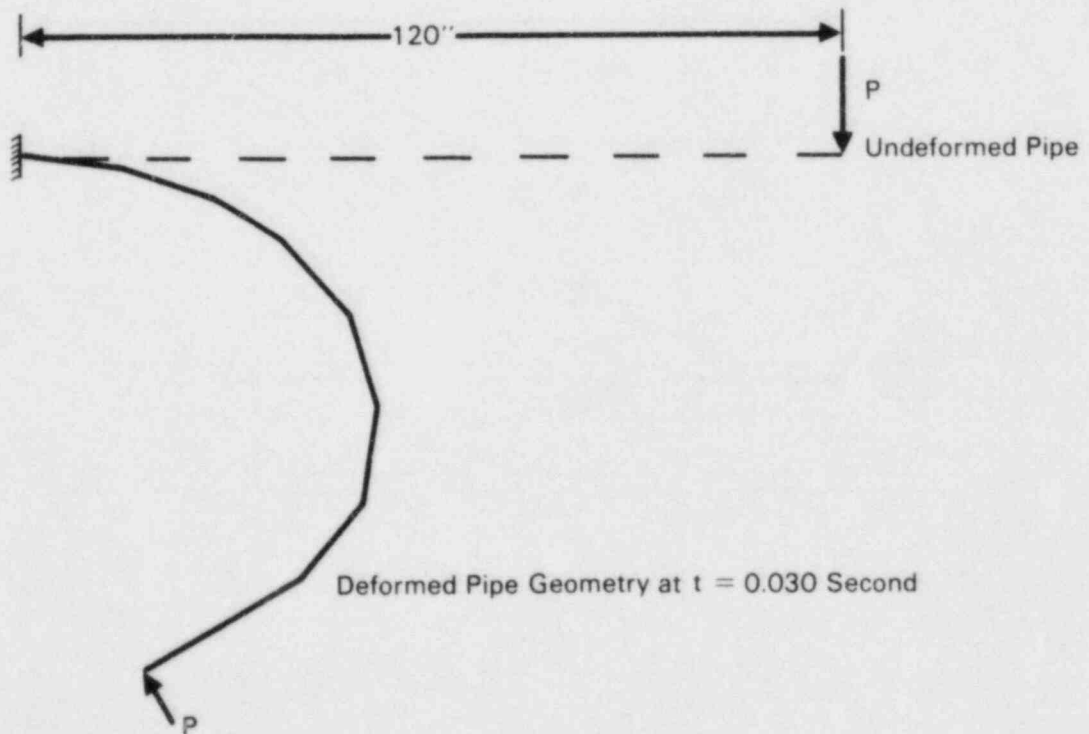
FIGURE 10. Plastic Bending of a Whipping Pipe
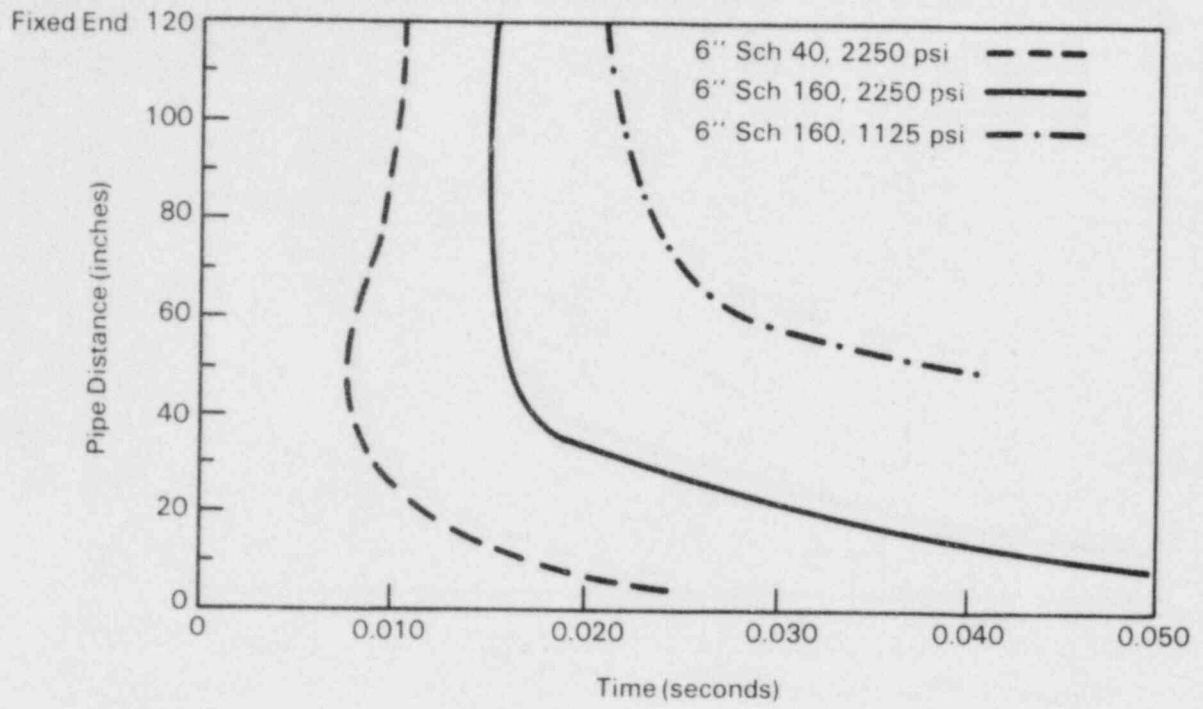
FIGURE 11. Whipping Pipe Yield Locations

51

PIPE DAMPING[a]

A. G. Ware
J. G. Arendts

EG&G Idaho, Inc.
Idaho National Engineering Laboratory (INEL)

INTRODUCTION

At present, studies are underway to determine whether an increase in the allowable damping values used in dynamic structural analyses of nuclear power plant piping systems, as stated in Regulatory Guide (R.G.) 1.61,[1] is justified. The Welding Research Council's Pressure Vessel Research Committee (PVRC) recently developed revised interim pipe damping recommendations (Figure 1) which have been approved for ad hoc use by the
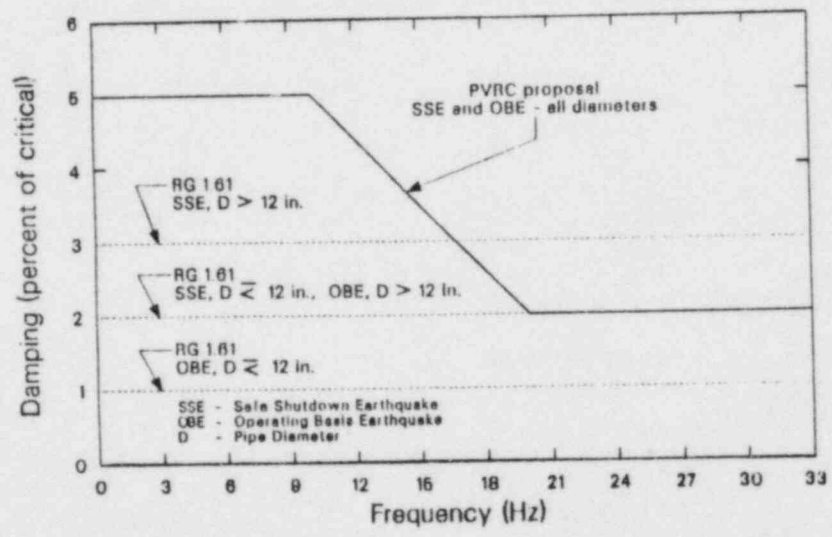
Figure 1. PVRC proposed pipe damping curve.

Nuclear Regulatory Commission (NRC). Increasing the allowable damping could lead to safer, more reliable, and less costly piping systems. A prevailing view is that conservative values for seismic design has led to overly stiff piping systems with excessive numbers of supports ill-suited to resisting thermal transients.

INEL PROGRAM (FY-81 to FY-83)

In support of evaluating changes to allowable damping values, the NRC and EG&G Idaho have been conducting programs to study structural damping in nuclear piping systems and provide data to support the final PVRC position. The program began in 1981 and has proceeded in phases. In the first phase, a literature survey of existing nuclear piping system damping data was conducted.[2] From this study, it was concluded that there were available data to support higher allowable damping values, particularly for certain sets of parameters. The results, containing data for the Heissdampfreaktor (HDR) project in the Federal Republic of Germany, the Kuosheng plant in Taiwan, and the LaSalle and Indian Point plants in the United States were used as some of the bases for the PVRC's interim position.

In the second phase, the parameters that appeared to have the greatest influence on damping were identified, and a test program was proposed to generate more damping data and investigate these parameters.[3] The most influential parameters were determined as type of supports, amplitude of excitation, frequency, and insulation. At the same time, a limited analytical investigation was conducted to determine whether an increase of the allowable damping from 2% of critical damping to a value of 5% of critical damping would indeed reduce the number of required seismic supports for piping systems.[4] The results demonstrated that, at least for a few typical systems, increasing the allowable damping would permit removal of supports while still meeting stress criteria.

In the third phase, the proposed test plan was carried out. In the initial phase of testing, a simple system consisting of straight sections

53

of 3-in. and 8-in. unpressurized piping was vibrated using various supports, amplitudes, and methods of excitation.[5] Constant-force hangers produced the highest damping of all the supports tested. Spring hangers and sway braces contributed little to damping except at very low vibration levels. Higher damping was induced by supports with gaps, such as snubbers and rod hangers with loose connections. While damping decreased with excitation level at low amplitudes, indicative of Coulomb friction, damping increased with excitation level at OBE and SSE stress levels. It was also found that modal damping is dependent on the position of the support with relation to the mode shape. There was no apparent trend to indicate that damping at frequencies of 33-50 Hz (above the seismic range) was different from damping values in the 20-33 Hz range.

INEL PROGRAM (FY-84)

The program has continued in FY-84 with a number of ongoing activities. An assessment was made of the difficulty involved in structural computer code implementation of the proposed PVRC damping curve in Figure 1.[6] The study showed that for response spectrum and time history modal superposition analyses, the most commonly used seismic techniques, the changes can easily be carried out with a few simple computer code changes. For the time history direct integration method of solution, developing an approximation for the PVRC curve in Figure 1 would be no more difficult than for the R.G. 1.61 curve.

A series of vibration tests was performed on the second configuration of the NRC/EPRI/ANCO piping system at the ANCO Engineers test facility to obtain piping system damping data using different supports and methods of excitation.[7] The 6-in. carbon steel piping system was approximately 50 ft long with two 3-in. branch lines (Figure 2). It was supported at five locations and excited using a single electro-hydraulic shaker. Both random and swept-sine methods were used for excitation. A variable support attached near the shaker location allowed four different configurations to be tested: a rigid strut, a mechanical snubber, a hydraulic snubber, and a rigid strut with a gap. Data were recorded for the lowest nine significant modes. Damping for the first three modes ranged from 1 to 3% of critical
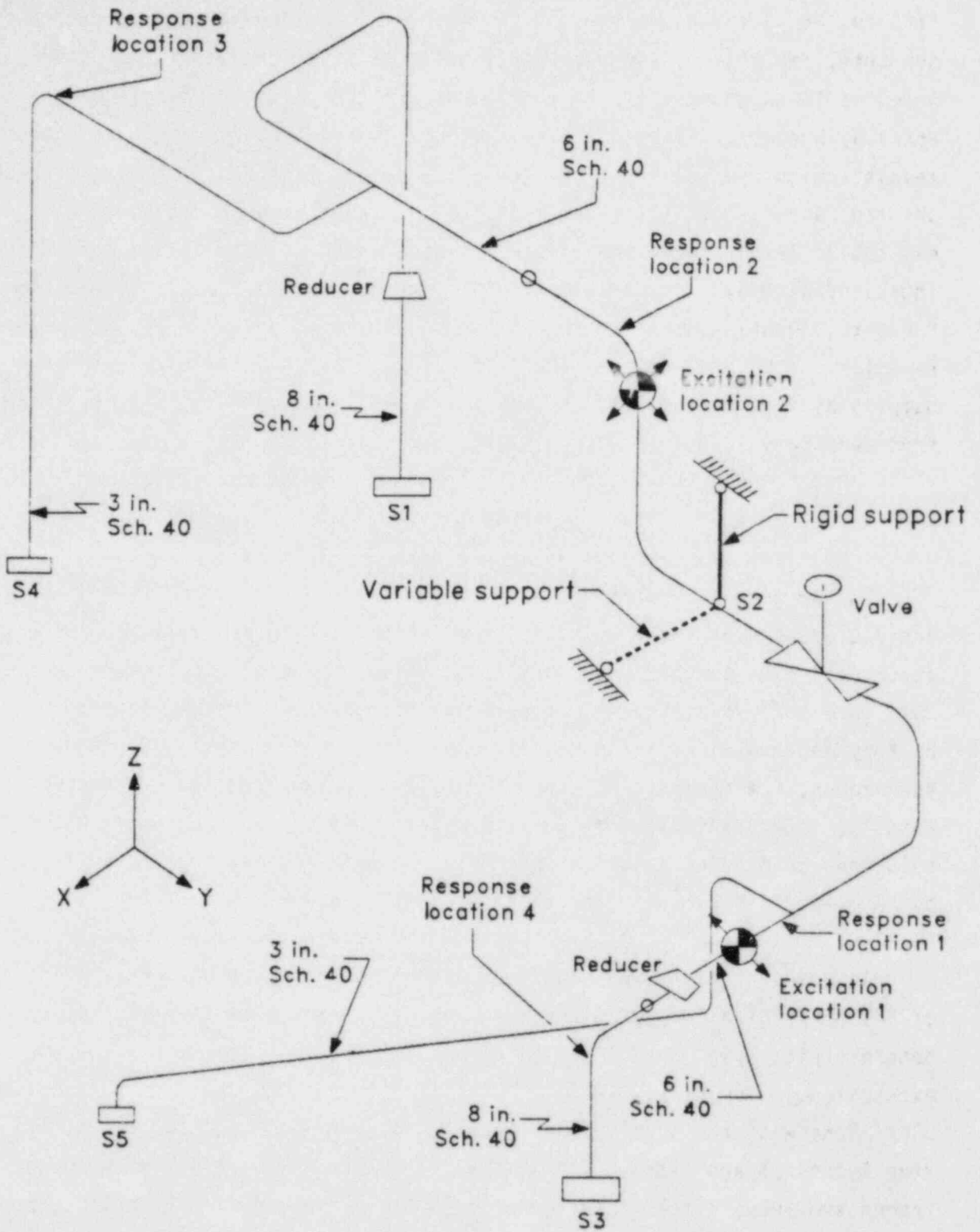
Figure 2. NRC/EPRI/ANCO piping system schematic diagram.

55

damping and decreased as frequency increased. The random excitation produced a slightly higher average overall damping than did the swept sine, but the effect did not appear significant (Figure 3). Changing the variable support also produced only a small change in the damping of the system (Figure 4). A metal fatigue crack in one of the branch lines, which occurred during test cycling, gives the warning that although higher damping levels may be appropriate for calculating primary stress levels, lower-level operational transients with damping levels of only 1 to 3% can produce fatigue failures.

Testing on a 5-in. small piping system at the INEL has been initiated (Figures 5, 6). This piping is being subjected to impact, hydraulic shaker (using both random and swept sine methods), and snapback excitation forces. The results will be used to further evaluate the effect of amplitude, frequency, pressure, supports, and insulation on damping.

In support of the PVRC position on damping, a multiple regression analysis has been conducted using the available data base to determine the effect of various postulated contributors to damping. Cases for each individual test and of all the data sets combined show that the dominant variable in the analysis is frequency. Further analyses were conducted with data normalized to 5 Hz to eliminate frequency as a variable, and for each mode individually. No other variables were clearly identified as being strong contributors to damping. This is at least partially attributable to the scarcity of data on the other important parameters. Grouping the data by mode number rather than frequency showed that mode number might also be considered as a substitute for frequency as the dominant variable.

In order to broaden the nuclear piping damping data base, and to allow future regression analyses to contain all the required information on the significant parameters, a worldwide data bank is being formed at the INEL. A standardized report form has been developed (Figure 7) and a request for data has been sent to 93 individuals in the U.S. and ten foreign nations who might have access to damping data.
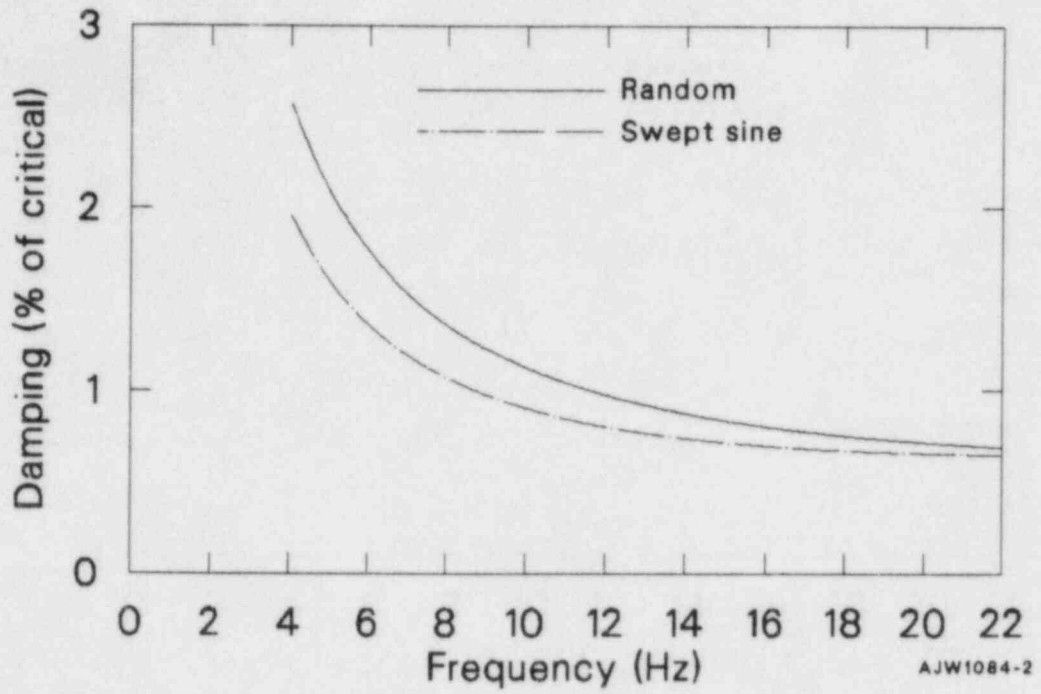
Figure 3. Excitation effect.
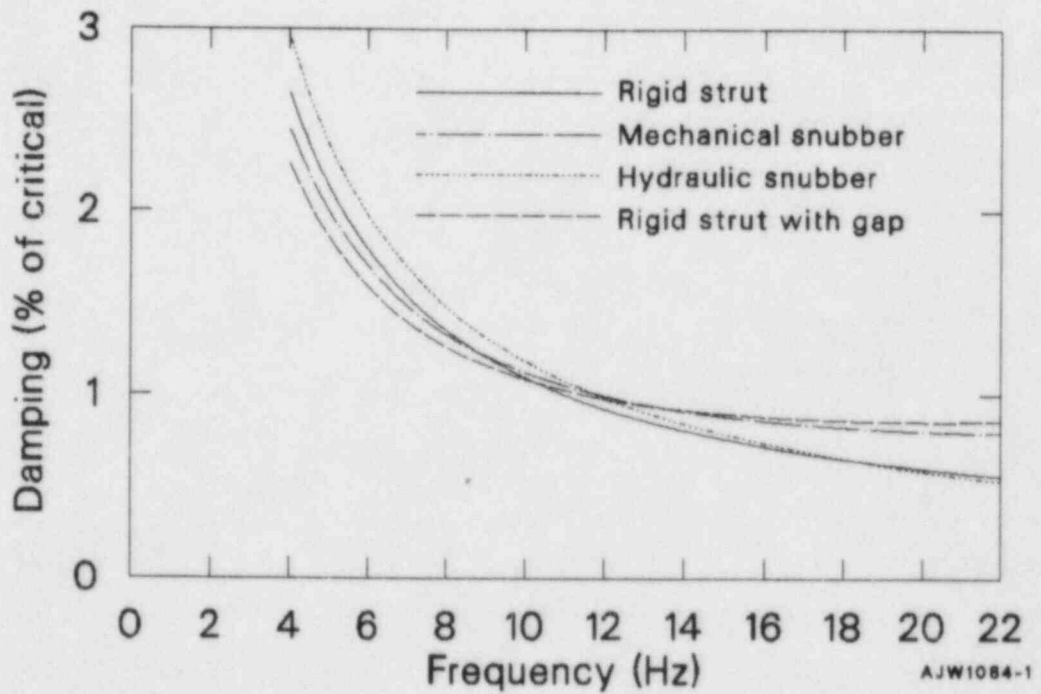
Figure 4. Support effect (swept-sine excitation).

57
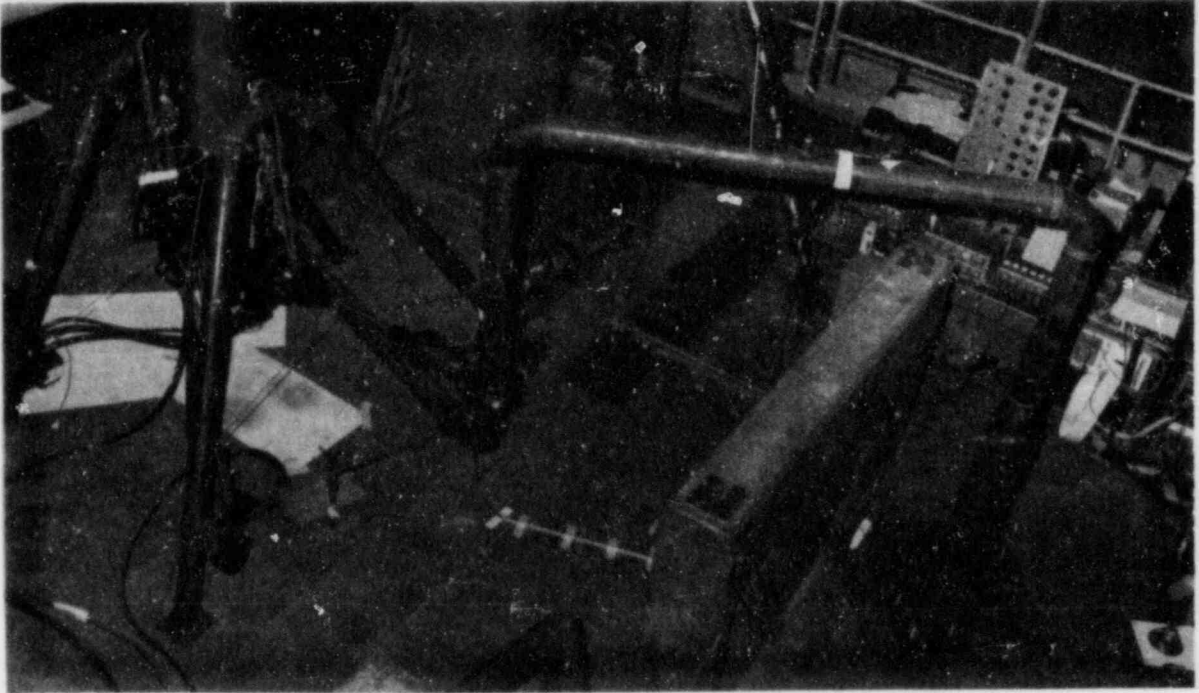
Figure 5. INEL test system (overhead view).
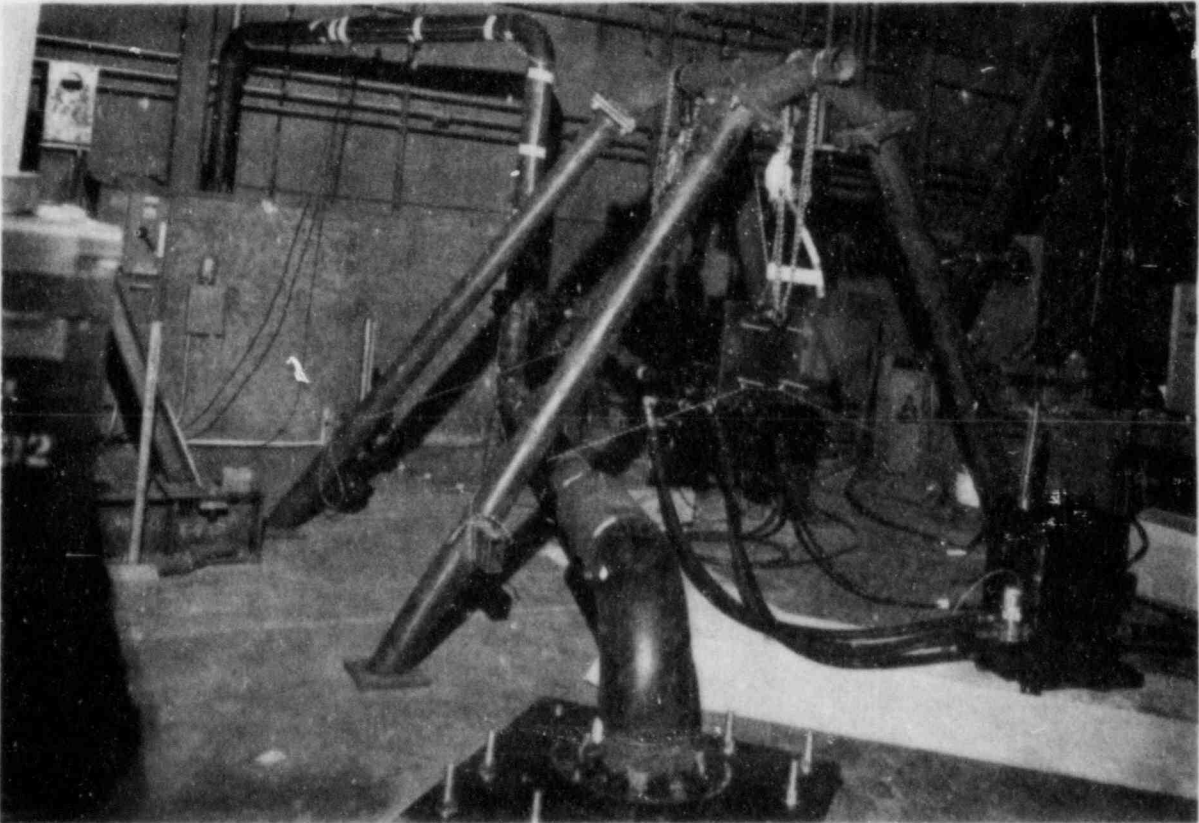
Figure 6. INEL test system (end view).

58

Nuclear Piping Damping Data Form

Data Base System Number _____   Sheet _____ of _____

I. General

1. Name of System/Plant (optional)
2. Type of System (laboratory, full scale, etc.)
3. Experimental Organization
4. Test Number / Date
5. Reference Document

II. System Description*

1. Diameter/Thickness or Schedule (units)   (   )
2. Piping Material
3. Total Length (units)**   (   )
4. Insulation Type
5. Full or Empty
6. Pressure (units)   (   )
7. Temperature (units)   (   )
8. Support Condition (normal, gapped, etc.)

9. Number of Supports
   a. Rigid Struts
   b. Mechanical Snubbers
   c. Hydraulic Snubbers
   d. Spring Hangers
   e. Constant Force Hangers
   f. Sway Braces
   g. Guide Restraints
   h. Anchors
   i. Other (specify in remarks)
   j. Total

III. Excitation

1. Source
2. Type of Motion
3. Direction/Location*
4. Input Level (units)   (   )

IV. Response

1. Maximum Overall Response
   a. Deflection (units)   (   )
   b. Stress/Strain (units)   (   )
   c. Acceleration (units)   (   )

2. Damping Calculation
   a. Method Used
   b. Transducer Used*
   c. Measurement Parameter (units)   (   )

3. Percent of Critical Viscous Damping by Mode or Response Level

a. Mode	1	2	3	4	5	6	7	8	9	10	11	12
b. Frequency (Hz)												
c. Damping (%)												
d. Response Level												

[Continuation of lines c and d (if required)]

Damping (%)												
Response Level												

V. Remarks (* please include system diagram)
(** Main line anchor to anchor, include branch lines in diagram)

Figure 7. Data form.

INEL PROGRAM (FY-85)

The damping study program will continue in FY-85 in support of the final PVRC position. Planned activities include:

1. Tests of a piping system at the Babcock & Wilcox (B&W) Alliance Research Center to determine the effect of pressure and temperature on system damping.

2. Conclusion of the INEL tests (Figures 5, 6) with insulation added to the system.

3. Final data reduction of the B&W and INEL tests, as well as data from the NRC/EPRI/ANCO system as shown in Figure 2 without branch lines, will be completed and results published.

4. Results of the multiple regression analysis will be summarized and published as part of a PVRC document.

5. The data bank of nuclear piping damping data is scheduled to be in place in March 1985.

6. The INEL is planning assistance to the Tennessee Valley Authority (TVA) and EPRI for vibration testing of a piping system in the cancelled Hartsville plant. System damping will be one of the parameters investigated as part of these tests.

CONCLUSION

A program has been developed to assess the available piping damping data, to generate additional data and conduct separate effects tests, and to establish a plan for reporting and storing future test results into a data bank. This effort is providing some of the basis for developing higher allowable damping values for piping seismic analyses, which will potentially permit removal of a considerable number of piping supports, particularly snubbers. This in turn will lead to more flexible piping

60

systems which will be less susceptible to thermal cracking, will be easier to maintain and inspect, as well as less costly.

REFERENCES

1. U.S. Atomic Energy Commission, "Damping Values for Seismic Design of Nuclear Power Plants," Regulatory Guide 1.61, October 1973.

2. A. G. Ware, "A Survey of Experimentally Determined Damping Values in Nuclear Power Plant Piping Systems," NUREG/CR-2406, EGG-2143, EG&G Idaho, Inc., November 1981.

3. A. G. Ware, "Parameters that Influence Damping in Nuclear Power Plant Piping Systems," NUREG/CR-3022, EGG-2232, EG&G Idaho, Inc., November 1982.

4. S. L. Busch, "A Comparison of Piping System Stresses Reflecting Support Optimization Based Upon Varying Response Spectra Damping Values," EG&G Report RE-A-83-008, February 1983.

5. A. G. Ware, and G. L. Thinnes, "Damping Results for Straight Sections of 3-in. and 8-in. Unpressurized Pipes," NUREG/CR-3722, EGG-2305, EG&G Idaho, Inc., April 1984.

6. A. G. Ware, "Assessment of Structural Computer Code Implementation of PVRC Recommended Piping Damping Values," EGG-EA-6550, Rev. 1, EG&G Idaho, Inc., March 1984.

7. J. G. Arendts, and A. G. Ware, "Tests to Determine How Support Type and Excitation Source Influence Pipe Damping," NUREG/CR-3942, EGG-2337, EG&G Idaho, Inc., September 1984.

RELIABILITY ANALYSIS OF STIFF VERSUS FLEXIBLE PIPING

S. C. Lu
Lawrence Livermore National Laboratory
Livermore, California   94550

ABSTRACT

The overall objective of this research project is to develop a technical basis for flexible piping designs which will improve piping reliability and minimize the use of pipe supports, snubbers, and pipe whip restraints. The current study was conducted to establish the necessary groundwork based on the piping reliability analysis.

A confirmatory piping reliability assessment indicated that removing rigid supports and snubbers tends to either improve or affect very little the piping reliability. We then investigated a couple of changes to be implemented in Regulatory Guide (RG) 1.61 and RG 1.122 aimed at more flexible piping design. We concluded that these changes substantially reduce calculated piping responses and allows piping redesigns with significant reduction in number of supports and snubbers without violating ASME code requirements. Furthermore, the more flexible piping redesigns are capable of exhibiting reliability levels equal to or higher than the original stiffer design.

An investigation of the malfunction of pipe whip restraints confirmed that the malfunction introduced higher thermal stresses and tended to reduce the overall piping reliablity. Finally, support and component reliabilities were evaluated based on available fragility data. Our result indicated that the support reliability usually exhibits a moderate decrease as the piping flexibility increases. Most on-line pumps and valves showed an insignificant reduction in reliablity for a more flexible piping design.

INTRODUCTION

Nuclear power plant components, including piping systems, are required by law to be designed to withstand the individual effects, as well as the appropriate combination of effects, due to normal operation, natural phenomena, and postulated accidents. The common practice in designing nuclear piping systems is to add support devices, such as rigid supports and snubbers, and pipe whip restraints to withstand effects of large dynamic loads caused by natural phenomena and postulated accidents. Events associated with natural phenomena and postulated accidents are random in nature and are often accompanied by great uncertainties. In order to accommodate these uncertainties, conservative design procedures have been adopted for nuclear piping systems and usually have resulted in stiff piping designs with excessive use of support devices. Excessive use of support devices, however, has created various problems:

A. Increased cost
B. Poor access for plant inspection and maintenance
C. Increased personnel exposure to radiation
D. Decreased piping reliability due to:
    a. higher thermal strtesses in stiff piping
    b. malfunction of snubbers
    c. malfunction of pipe whip restraints

Clearly, problems created by excessive use of support and restraint devices can be mitigated, if not completely eliminated, by adopting piping designs which include minimal use of support and restraint devices. Improved design requirements and criteria are needed in order to arrive at such piping designs.

The research project described in this report was initiated at Lawrence Livermore National Laboratory (LLNL) by the United States Nuclear Regulatory Commission (NRC). The objective of this project is to develop a technical basis for flexible piping designs that minimize the use of rigid pipe supports, snubbers, pipe whip restraints, etc.

APPROACH

A typical piping system usually consists of the piping, support devices (namely, rigid supports and snubbers), on-line components (such as, pumps and valves), and, in many cases, pipe whip restraints. The piping flexibility can be changed by adding or removing rigid supports and snubbers. Malfunctions of snubbers and pipe whip restraints can also affect the piping flexibility. We feel that a rational approach for developing a technical basis for flexible piping designs should be based on a reliability consideration. Accordingly, reliability analyses were conducted for a variety of piping systems.

Current design criteria for piping, which address specific load types individually, evolved under the presumption that higher seismic margins necessarily improve plant reliability. Conservative design against earthquake loads has relied increasingly on rigid supports, snubbers, and other types of seismic restraints to stiffen piping systems. The resultant decrease in flexibility, however, is likely to cause higher normal operating stresses because of the restraint of thermal expansion. Furthermore, because of the large uncertainty inherent in predicting seismic effects (compared to that in predicting themal effects), seismic loads dominate the design even though seismic loads occur very infrequently. As a results, stiffening a piping system to improve its resistance to seismic loads may actually decrease its overall reliablity during normal operation.

The first step undertaken by this research work was to assess the impact on the piping reliability due to the increased piping flexiblity for a number of piping systems. The goal is to confirm that a flexible piping design with reduced seismic restraints (both rigid supports and snubbers) can be more reliable than or as reliable as a stiff piping design. In this confirmatory study, we dealt only with the "piping" portion of a piping system. The reliabilities associated with pipe supports and on-line components as affected by the piping flexibility would be treated as separate tasks.

63

In order to quantify the piping reliability, pipe failure probabilities were computed. Pipe failure was assumed to be caused by fatigue crack growth at pipe weld joints. Two types of failure modes were considered, i.e., a through wall crack (leak) and a complete pipe severance (break). The pipe failure probability was estimated by applying a Monte Carlo method with a stratified-sampling scheme to simulate the life histories of the piping system.

Selected piping systems with related design data were collected from real nuclear power plant designs. Flexible piping designs were created from the existing designs by removing rigid supports and/or snubbers. Piping stresses for various designs were calculated for the reliability assessment.

This assessment recognizes the characteristic difference between regular pipe supports and snubbers. While removal of regular pipe supports changes both seismic stress and thermal expansion stress in a piping system, removal of snubbers affects only seismic stress. However, a piping system, including snubbers, may not exhibit the desired reliability because snubbers are known to have a high failure rate. The possibility of snubber malfunction is incorporated in this assessment.

We demonstrated in Step 1 the desirability of the flexible piping design based on the piping reliability consideration. In order to achieve more flexible and reliable piping designs, changes are needed with regard to current design requirements, criteria, and practices. In the next step, the current study investigated the impact on piping designs due to two changes to the NRC Regulatory Guides 1.61 and 1.122, dealing, respectively, with damping values and broadening floor response spectra for piping systems. These two regulatory guides introduce substantial conservatism in the seismic spectrum analysis and result in the excessive use of snubbers and rigid supports in nuclear power plant piping systems. Recently, the NRC has evaluated these changes which were initially proposed by the Steering and Technical Committees on Piping Systems of the Pressure Vessel Research Committee (PVRC) in order to reduce conservatism.

In this investigation, we quantified the reduction in calculated piping responses resulting from the changes. We showed that the potential benefit of the changes was to allow a redesign of the piping system where a substantial number of snubbers and rigid restraints could be removed without causing the calculated stresses in the pipe to exceed code allowables. We also showed that the more flexible redesign is acceptable based on a reliability analysis.

In the third step, we dealt with the malfunction of pipe whip restraints. We investigated in this step the situation where the pipe comes in contact with a restraint device during normal operation due to an imperfect installation. We calculated the actual stress distribution caused by the malfunction. We assessed the safety impact on the piping sytem by conducting a piping reliability analysis with and without the malfunction. The purpose was to confirm that the malfunction of pipe whip restraints introduces higher thermal stresses and reduces the overall piping reliability.

Having demonstrated the desirability of flexible piping design based on reliability consideration on the behavior of the piping itself, this study also evaluated changes in reliability for pipe supports as well as on-line

components as the piping design is made more flexible. Support and component reliabilities were evaluated based on available fragility data and were accomplished in Steps 4 and 5. The outcome of the support and component reliability evaluation was expected to identify precautions and restrictions that should be exercised in arriving at a flexible piping design.

CONCLUSIONS

Based on our observation, the change in piping reliability is not very sensitive to the change in piping flexibility for the cases we have studied. Consequently, the piping reliability is either improved or affected very little by the increased piping flexibility as a result of removing rigid pipe supports and/or snubbers. We have also observed that pipe failure probabilities are generally small, i.e., approximately 10^{-9} for "break" and 10^{-6} for "leak". We therefore conclude that the flexible piping design is desirably based on the reliability consideration although the flexible piping design also offers many other benefits.

An increase in piping reliability for a flexible piping design is generally attributed to relaxation of the thermal expansion stress for flexible piping, although the seismic stress may be increased by piping flexibility. The thermal stress is usually caused by plant operation and its cyclic effect is the major driving force for fatigue crack growth which may essentially cause the pipe to fail. On the other hand, seismic stress caused by an earthquake is a natural phenomenon with low probability of occurrence. Therefore, the contribution to pipe failure due to seismic loads is of secondary importance, since the event occurrence rate is considered in the piping reliability analysis.

Another reason why the flexible piping design may improve the piping reliablity is due to the fact that a flexible piping contains less snubbers. Snubbers are known to have a high rate of malfunctioning. The malfunction of snubbers tends to introduce unexpected and undesirable stresses in the pipe and increases the pipe failure probability.

In order to achieve more flexible and reliable piping designs changes are needed with regard to current design requirements, criteria, and practices. The current study investigated the impact on piping designs due to two changes proposed by the PVRC Steering and Technical Committees on Piping Systems with respect to the NRC Regulatory Guides 1.61 and 1.122. Our study has demonstrated that these changes can substantially reduce calculated piping response and, consequently, allow piping redesigns with significant reduction in the number of supports and snubbers without violating ASME code requirements. Furthermore, flexible piping redesigns are capable of exhibiting reliability levels equal to or higher than the original stiffer designs.

Although we have demonstrated that piping systems can be made more reliable by adopting flexible piping designs based on the piping reliablity analysis conducted in this study, we do caution that changes adopted in the piping design procedure to increase the piping flexiblity usually result in greater displacements. For this reason, the NRC may need to consider the implementation of certain displacement criteria or requirements to confine piping displacements.

As we discussed previously, pipe whip restraints, if not properly located or installed, can cause safety concerns as well as other problems. In this study, we examined the malfuncton of pipe whip restraints based on its impact on piping reliability. We confirmed that the malfunction introduced higher thermal stresses and tended to reduce the overall piping reliability. Our results provided additional support to other research efforts aimed at the elimination of the pipe break as a design requirement which leads to the need of pipe whip restraints.

Since pipe supports and on-line components (such as pumps and valves among others) are important parts of a piping system, the effects of increased piping flexibility on the reliability of supports and components were investigated. Our results indicated that the support reliablity usually exhibits a moderate decrease as the piping flexibility increases. We feel that the supports in a flexible piping design need to be either upgraded or subjected to further investigation.

For large components, such as steam generators, pressurizers, and large pumps, the global effect concerning the component support failure due to increased nozzle loads was evaluated. We found that in general the global effect is rather insignificant. We feel, however, the local effect at the vicinity of the nozzle may need to be further investigated. Without such an investigation, we suggest that removing pipe supports which are close to nozzles should be done with extreme care.

For self-supporting on-line valves, we discovered that the valve acceleration may or may not increase with the piping flexibility. Nevertheless, valves usually have sufficient design margins to accommodate the higher acceleration and are able to maintain the functionality. The problem in this case is the increased valve displacement usually associated with a flexible piping design. Specific design consideration may be needed in order to limit the valve displacement.

EXCESSIVE USE OF PIPE SUPPORT DEVICES CREATES VARIOUS PROBLEMS

- Icreased Cost

- Poor Access for Plant Inspection & Maintenance

- Increased Personnel Exposure to Radiation

- Decreased Piping Reliability
    - Higher Thermal Stresses in Stiff Piping
    - Malfunction of Snubbers
    - Malconstruction of Pipe Whip Restraints

OUR GOAL IS TO ESTABLISH A TECHNICAL BASIS FOR FLEXIBLE PIPING BY RELIABILITY ANALYSIS

- Confirm the Desirability of Flexible Piping Design
  Based on Reliability Analysis

- Identify and Evaluate Changes Resulting in
  Flexible Piping Design

- Evaluate Malfunction of Pipe Whip Restraints

- Evaluate Support Reliability due to Increased
  Piping Flexibility

- Evaluate Component Reliability due to Increased
  Piping Flexibility

WE COMPUTED PIPE FAILURE PROBABILITY TO ASSESS PIPING RELIABILITY

- Select Initial Crack Size in Weld According to an Appropriate Distribution

- Calculate Stress Histories due to Operating Conditions and Possible Seismic Events during the Life of the Plant

- Calculate Crack Growth due to Fatigue

- Determine whether the Expanded Crack Will Lead to Pipe Failure, i.e., a Through-Wall Leak or a Break

- Repeat the Previous Steps to Determine the Failure Probability at each Weld Joint

- Determine System Failure Probability

WE INVESTIGATED PIPING SYSTEMS FROM ACTUAL PLANT DESIGNS
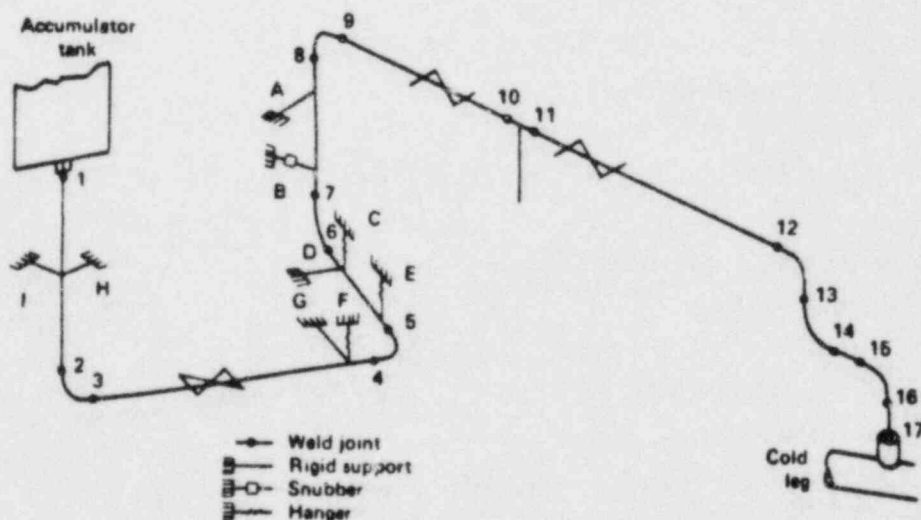
SAFETY INJECTION LINE FROM A PWR PLANT

FLEXIBLE DESIGN TENDS TO REDUCE THERMAL STRESS BUT INCREASE SEISMIC STRESS

	Piping Design		
	Existing	Flex 1	Flex 2
Thermal Expansion Stress (Ksi)	6.156	4.592	2.689
Seismic (OBE) Stress (Ksi)	1.485	2.780	35.050

MALFUNCTION OF SNUBBERS INTRODUCES UNEXPECTED PIPING STRESSES

	No Snubber Failure	Snubber Lock	Snubber Free
Thermal Expansion Stress (Ksi)	6.156	30.817	6.156
Seismic (OBE) Stress (Ksi)	1,485	1.485	3.705

PIPING RELIABILITY IS EITHER INCREASED OR AFFACTED VERY LITTLE DUE TO INCREASED PIPING FLEXIBILITY

Pipe Break Probability

Piping Design	No Snubber Failure	With Snubber Failure
1. Existing Design	1.143E-09	2.837E-08
2. Flex. Design 1	9.514E-10	----
3. The Snubber Removed	1.255E-09	1.255E-09
4. Flex. Design 2	6.645E-08	6.645E-08

CHANGES ARE REQUIRED IN ORDER TO ACHIEVE FLEXIBLE PIPING DESIGNS

- Changes Can Be in the Following Areas:
  - NRC Regulations
  - Current Practice (Design Philosophy, Methods of Analysis, Design Criteria, ect.)
  - ASME Code Requirements
  - New Restraining Devices

- The Current Study Evaluated only the Impact due to Changes to RG 1.61 and RG 1.122 with Regard to Damping Values and Floor Response Spectra

PROPOSED CHANGE TO RG1.61 INCREASES DAMPING SIGNIFICANTLY IN LOW FREQUENCY RANGE
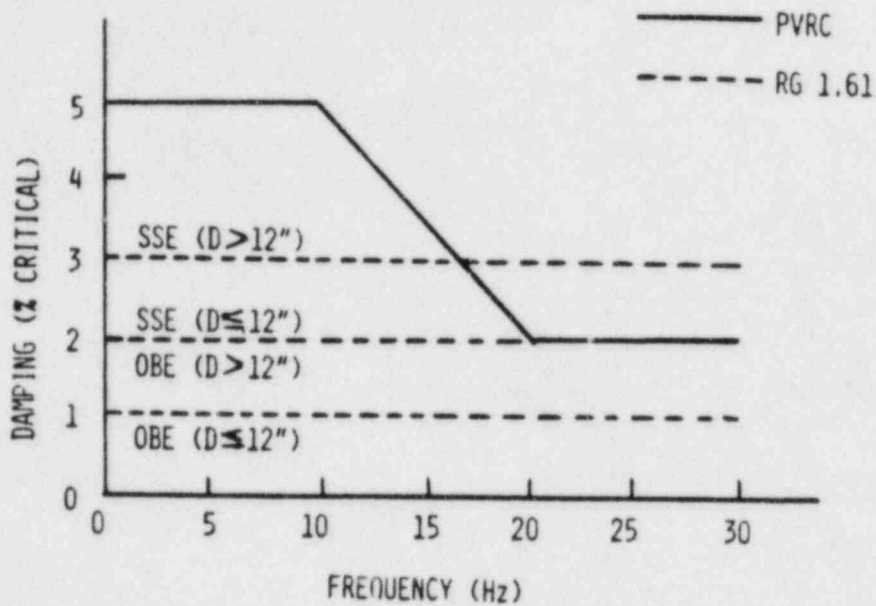
PROPOSED CHANGE TO RG1.122 SUGGESTS SHIFTING THE RAW SPECTRUM TO COUNT FOR UNCERTAINTY
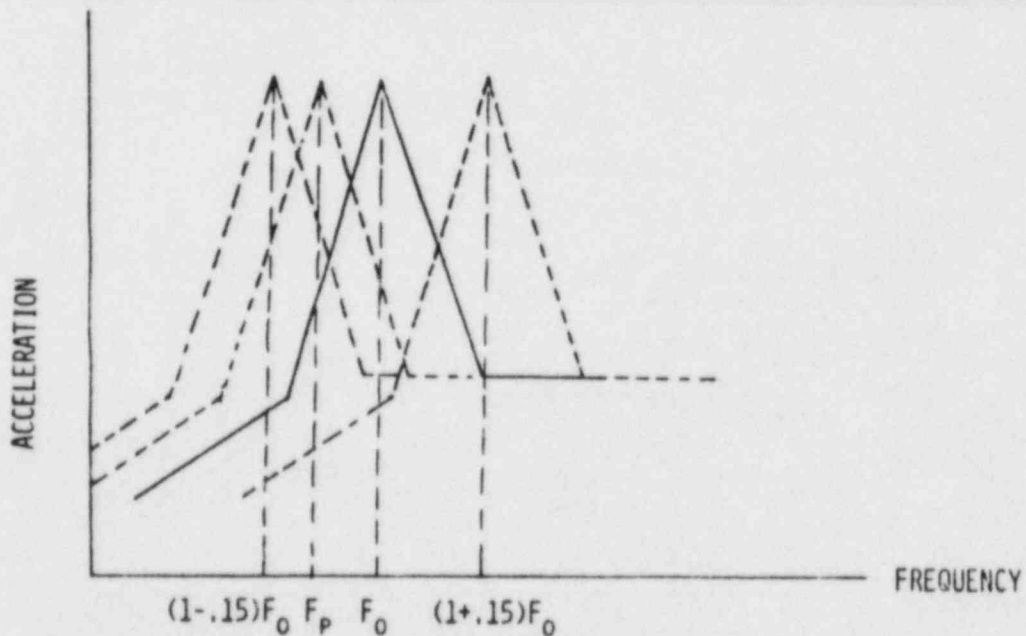
F_0 = THE PEAK FREQUENCY OF THE UNBROADENED SPECTRUM

F_p = ONE OF PIPING FREQUENCIES WITHIN ±15% RANGE OF F_0

71

PROPOSED CHANGES ALLOW A PIPING REDESIGN WITH A
SUBSTANTIAL REDUCTION IN NUMBER OF SUPPORTS

(PORTION OF AFW SYSTEM)
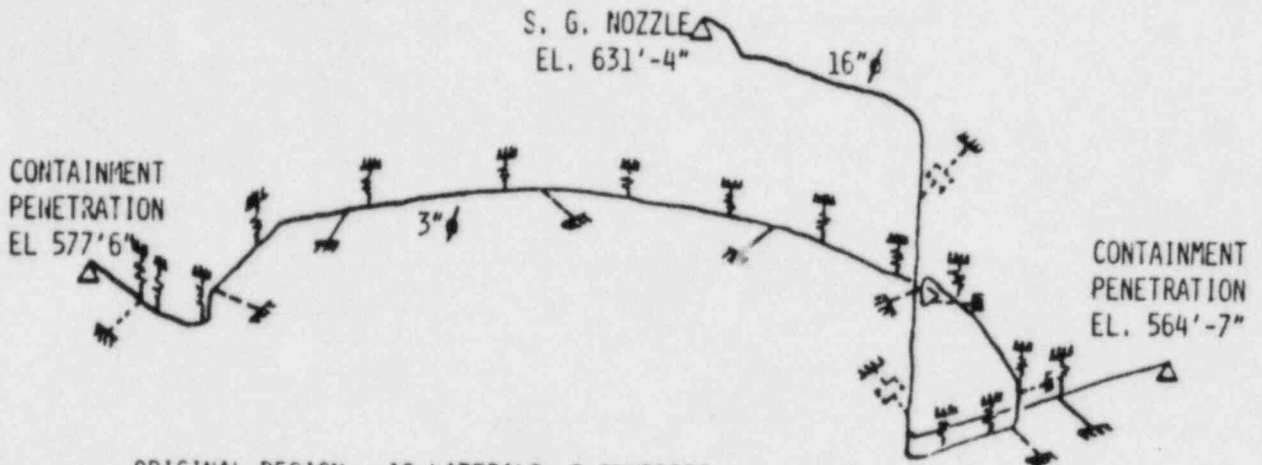
ORIGINAL DESIGN : 10 LATERALS, 2 SNUBBERS

REDESIGN : 3 LATERALS, 0 SNUBBERS

THE REDESIGN MEETS ASME CODE AS PROPOSED CHANGES
ARE ADOPTED
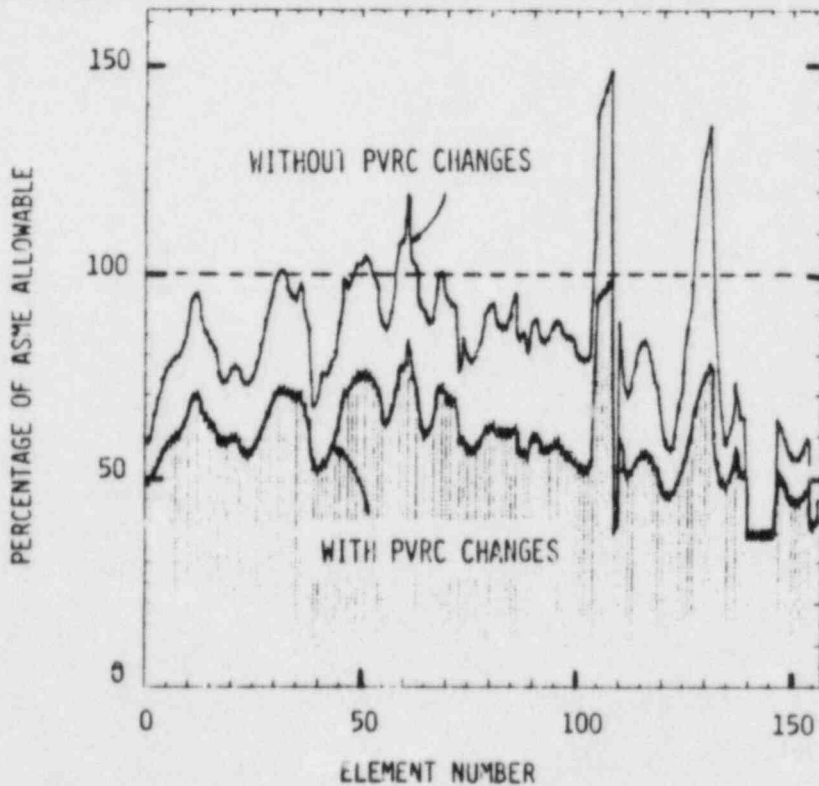
THE FLEXIBLE REDESIGN EXHIBITS SAME LEVEL OF RELIABILITY AS THE STIFF DESIGN

(PORTION OF AFW SYSTEM)

	ORIGINAL DESIGN[*]	REDESIGN
BREAK PROBABILITY	0.327×10^{-12}	0.616×10^{-12}
LEAK PROBABILITY	1.022×10^{-8}	0.836×10^{-8}

[*] A 10% PROBABILITY OF SNUBBER FAILURE IN EITHER LOCKED OR FREE MODE IS ASSUMED.

OUR RESULT CONFIRMED THAT PIPE WHIP RESTRAINTS ARE UNDESIRABLE
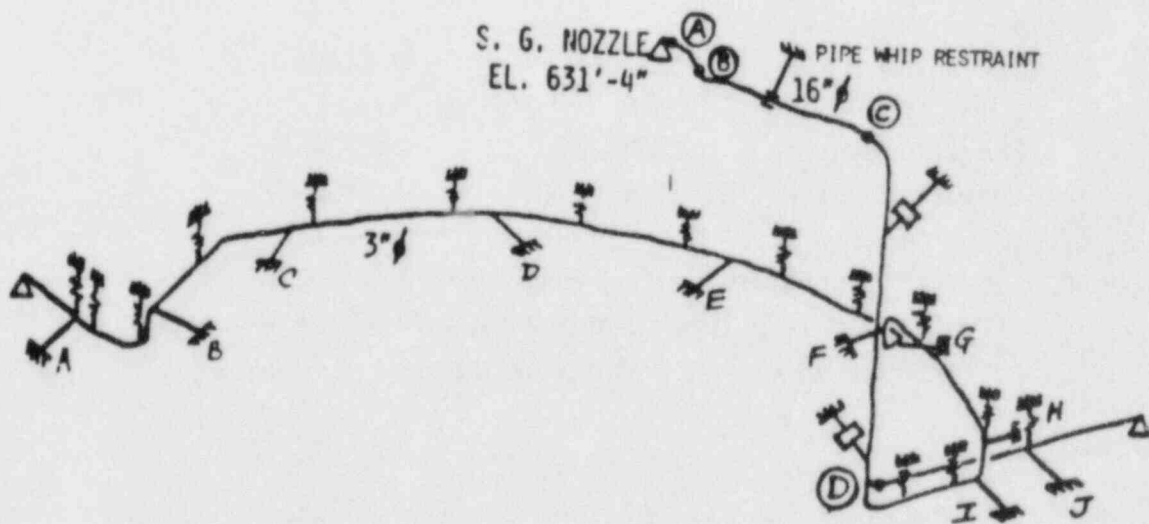
THE PIPE EXPERIENCES HIGHER THERMAL STRESSES DUE TO MALFUNCTION OF PIPE WHIP RESTRAINTS

	Thermal Expansion Stress (Ksi)	
Weld Joint	No Contact	In Contact
A	3.27	43.33
B	3.03	16.63
C	2.14	10.04
D	3.80	4.90

THE PIPING SYSTEM BECOMES LESS RELIABLE BECAUSE OF MALFUNCTION OF PIPE WHIP RESTRAINTS

- The Pipe Failure Probability Increases due to the Malfunction of the Pipe Whip Restraint

	No Contact	In Contact
Break Probability	0.327E-12	0.200E-11
Leak Probability	0.901E-08	0.239E-06

- Our Result Indicated that the Elimination of Pipe Whip Restraints is Beneficial but More Research is Needed to Limit the Use of Pipe Whip Restraints

SUPPORT FORCES IN GENERAL ARE HIGHER IN THE FLEXIBLE PIPING DESIGN

Support Forces (lbs.)
At One of the Supports of the AWF Line

	Stiff Design	Flexible Design
TH + DW	1,414	1,235
Seismic(OBE)	3,668	8,177
TH + DW + OBE	5,082	9,412

SUPPORT RELIABILITY EXHIBITS A MODERATE REDUCTION FOR THE FLEXIBLE DESIGN

- Example : Support Failure Probabilities
  (One of Supports in the AFW Line)

  2.55E-09(Stiff Design) 2.24E-07(Flex. Design)

  (Support Failure Probabilities Are Calculated Based
  on Generic Fragility Data)

- Supports may need to be Strengthened as less
  Supports are Used but Further Research may Suggest
  Weaker Support Design is Desirable.

75

GLOBAL EFFECT ON LARGE COMPONENTS DUE TO INCREASED PIPING FLEXIBILITY IS INSIGNIFICANT

● Nozzle Loads due to Earthquake may be Increased with Flexible Piping Design

Nozzle Loads at AFW S.G. Nozzle

	Stiff Design	Flexible Design
Thermal	50,170 ft-lbs	48,660 ft-lbs
OBE	7,230 ft-lbs	60,660 ft-lbs

● The Global Effect on Large Components was Found to be Insignificant Based on a Reliability Assessment on Component Supports.

● Without Further Research to Assess the Local Effect due to Increased Nozzle Loads, We Suggest not to Remove Supports which are Close to Nozzles.

ON-LINE VALVES USUALLY HAVE SUFFICIENT DESIGN MARGINS TO ACCOMMODATE HIGHER ACCELERATION IN FLEXIBLE PIPING

● Valve Accelerations may or may not Increase with Piping Flexibility.

● The Valve Acceleration Capacity is Based on Functionality.

● Specific Design Consideration May be Needed in Order to Limit Increased Valve Displacements Usually Associated with a Flexible Piping Design.

Standard Problems for Structural Computer Codes

C.A. Miller, C.J. Costantino, A.J. Philippacopoulos
M. Reich and M.T. Chang

Structural Analysis Division
Department of Nuclear Energy
Brookhaven National Laboratory
Upton, NY 11973

INTRODUCTION

This paper presents the latest results of the ongoing program entitled, "Standard Problems for Structural Computer Codes", currently being worked on at Brookhaven National Laboratory (BNL) for the Office of Nuclear Regulatory Research, U.S. Nuclear Regulatory Commission. During this year efforts were concentrated on verification of soil/structure interaction methods. The objective of the work is to verify the various methods used by the industry in performing soil/structure interaction analyses of nuclear power plant facilities. Verification is performed by comparing data. The overall goal of the study is to provide data which may be used by NRC in assessing the range of validity for each of the SSI methods.

Three type of SSI analyses methods are considered: lumped parameter; finite element; and substructuring. Each of the methods are reviewed so that the primary uncertainties in the methods may be established. A literature search is conducted to determine available sources of experimental data against which the SSI methods may be tested. Two sources of experimental data base habe been considered to date. The SIMQUAKE experiment was conducted in the southwest U.S. during 1977. Several model (1/24 to 1/8 scale) reactor containment structures were subjected to an earthquake like motion. The ground motion was induced by high explosive charges placed in the free field. These data are especially useful because of the extensive instrumentation placed in the free field and on the structures. The second data source is the data collected at the Fukushima Nuclear Power Station during a 7.4 magnitude earthquake. This data is valuable because it represents the full scale condition.

Analytic solutions using the three SSI methods are obtained for each of the data surces. A measured free field pulse is used as input and the analytic method used to compute structural motions and floor repsonse spectra. The spectra based on the analytic solutions are compared with spectra of the measured in-structure motion. Variations of the SSI models are made to assess the sensitivity of the results to changes in model characteristics.

The initial work on the program will be completed during the fall of 1984. The results of this work are discussed here. The work to be performed during later phases of the program is presented in the next section.

I. Identification of Uncertainties

As indicated above, three methods of performing SSI analyses are in common use. The first method, called "lumped parameter", is based on a spring/damper model of the interaction process. This spring/damper model is used to connect a model of the structure to the free field with the seismic disturbance input to the base of the spring/damper model. The parameters used to describe the spring/damper model represent the major uncertainty of this method. In particular, site conditions (such as layering, water table location, and nonlinear properties) would be expected to greatly affect the extent to which the standard interaction spring/damper model would be valid. This method also neglects any feedback from the structure to the free field; this assumption must be considered an uncertainty.

The second method is the finite element method. A finite element model of the soil is connected to the structural model with the seismic motion input to the base of the soil model. The major uncertainty of this method lies on the characteristics of the finite element mesh used to model the soil (mesh size, extent of mesh, transmitting boundaries, etc.). Another uncertainty arises in the details used to connect the soil mesh to the structural model. Typically a "welded" connection is used. However, any nonlinear effects such as liftoff or slippage at the interface make this connection invalid.

The substructuring method generates separate soil and structure solutions and then uses compatibility of soil and structural displacements to generate a solution. Most of the uncertainties which exist for the finite element method also apply here.

II. SSI Experimental Data Sources

A literature review was conducted to locate sources of experimental data which might be useful for resolving the uncertainties described above. This review included: data taken during actual earthquakes for both nuclear power plant facilities and related facilities; field experiments designed to simulate seismic loading acting on nuclear power plant facilities; laboratory studies of the SSI problem; and experimental programs conducted by the U.S. Department of Defense in support of weapon system design studies. Experimental data is only useful for this program if there are a sufficient number of gases located in both the free field and on the structure. This requirement eliminates most of the measurements taken during actual earthquakes since there are relatively few gages placed in the free field. Based on this review from the SIMQUAKE experiments and data from the Fukushima Nuclear Power Plant were selected for use on the study.

III. Correlation Studies

Correlation studies are made between the SIMQUAKE data and predictions made using the lumped parameter method and the substructuring method. All three of the SSI methods are used to perform the correlation studies using the Fukushima data. This section of the report contains a summary of the lumped parameter correlations. Results for the other methods will be available in the fall 1984.

A. Lumped Parameter Comparison with Fukushima Data

A general description of the site is shown on Fig. 1. The average properties of the mudstone are shown on this Figure. Free field measurements were m de at the indicated locations. SLAVE Code is used to generate free field pulses at the -4 M, -14 M, and -25 M elevations given the measured pulse at elevation -40 M. This is done for soil damping values ranging from 10% to 20%. Spectra are calculated for these pulses and comparisons are made with the spectra for the measured pulse at the -4 M elevation. These comparisons

are shown on Fig. 2. As may be seen the shape of the spectra of the computed pulses agree quite well with the spectra of the measured pulse. However, rather high soil damping is required to match the spectra amplitudes in the 3 cps region. This would indicate that the hysteretic soil damping model used in convolution analyses may underestimate damping effects.

Comparisons are next made between the measured responses in the structure and predicted responses using the lumped parameter method. Since all of the measured data is in the North-South direction, the model of interest is for structural displacements in the N-S direction and rotations about the E-W direction. A section through the center of the reactor building looking in the North direction is shown on Fig. 3a. The model used to represent the building is shown on Fig. 3b. Each of the elements is modeled as a beam including shear stiffness. The four vertical beams in the model represent the sections of the structure as shown on Fig. 3a. The interaction springs are attached to the base of the structure and to the sidewalls. If the structure is made rigid the coupled frequencies associated with the interaction springs are found to be 3.6 cps and 10.5 cps. When the structural flexibility is included, the first 12 modes of the system range from 2.5 cps through 20.o cps.

A comparison of the spectra from the predicted responses, using the measured pulse at -4 M as input, and the measured in-structure pulses are shown on Fig. 4. As may be seen the correlation between the two spectra is rather good.

B. Lumped Parameter Comparisons with SIMQUAKE Data

The SIMQUAKE II experiment was conducted on June 2, 1977 at the University of New Mexico's McCormick Ranch test site. Figure 5 shows a plan of the test bed. The loading was generated from the two planar arrays located about 150 feet from the area containing the structural models. Six structural scale models of containment structures were used with the scale factors varying form 1/8 to 1/24. About 150 channels of instrumentation was included in the free field and in the structures. The soil has shear wave velocites varying from 800 fps to 1100 fps in the top 90 feet.

81

Comparison between lumped parameter predicted responses and measured responses are made for the 1/8 scale model. The structure is a cylindrical structure having a diameter of 15 feet and a height of 22.5 feet. The walls of the cylinder are 1.51 feet thick and the base is 2.26 feet. The structure is embedded 25% into the ground. The structural frequencies are sufficiently high so that it is modeled as a rigid body. The interaction frequencies are 10.6 cps, 20.9 cps, and 25.5 cps respectively for rotational, vertical, and horizontal responses.

The response of the structure is generated using the standard interaction parametrs with the measured pulse taken as input. Horizontal spectra at the base and top of the structure are generated from the predicted and measured responses. Comparisons of the two are shown on Fig. 6. A reasonable comparison between the two is found at the base but there is poor correlation at the top of the structure. This occurred because the input had a sufficient amplitude to cause the base of the structure to separate (liftoff) from the sol. The effect of this was to significantly reduce the rocking frequency thereby transferring the energy in the spectra from the high to low frequency range.

The vertical response of the structure is also calculated and comparisons between the calculated and measured vertical in-structure vertical spectra are shown on Fig. 7. Once again liftoff effects result in poor correlation between the lumped parameter and measured spectra.

C. Finite Element Comparisons with Fukushima Data

A comparison of recorded vs. predicted data using the finite element method is in the process of being compelted. A detailed discussion of these results will appear in a forthcoming BNL/NUREG Report.

PLANNED FUTURE WORK

Two types of work are planned for the future. Other data sources from actual earthquakes will be analyzed. There is some data from the Humbolt Bay plant which is of interest because the facility is rather deeply embedded.

All of the data used to date is for facilities where embedment effects are not too significant. Therefore it has not been possible to draw conclusions regarding the adequacy of interaction modeling of embedment effects. Thre are dat sources from some of the more recent western U.S. earthquakes (e.g., Coalinga) which appear to of value and may be considered.

It appears that there is not a sufficiently broad data base to answer all of the uncertainties. Analytical studies can be made, however, which can test the significance of some of the uncertainties. It is planned to conduct such studies relating to the effect of layering, water table location, and nonlinear interface effects (liftoff and slip) on the interaction problem. These data will be useful in focusing any future experimental work in those areas that will be most beneficial and thus, we plan to persue the above during F.Y. 85.

REACTOR

ELEV. + 10 M

GAGE AH 12 ELEV. -4 M

GAGE AH 11 ELEV. -14 M

GAGE AH 8 ELEV. -25 M

GAGE AH 10 ELEV. -40 M

ELEV.- 160 M

MUDSTONE

V_P = 1700 m/s

SANDSTONE V_P = 1900 m/s
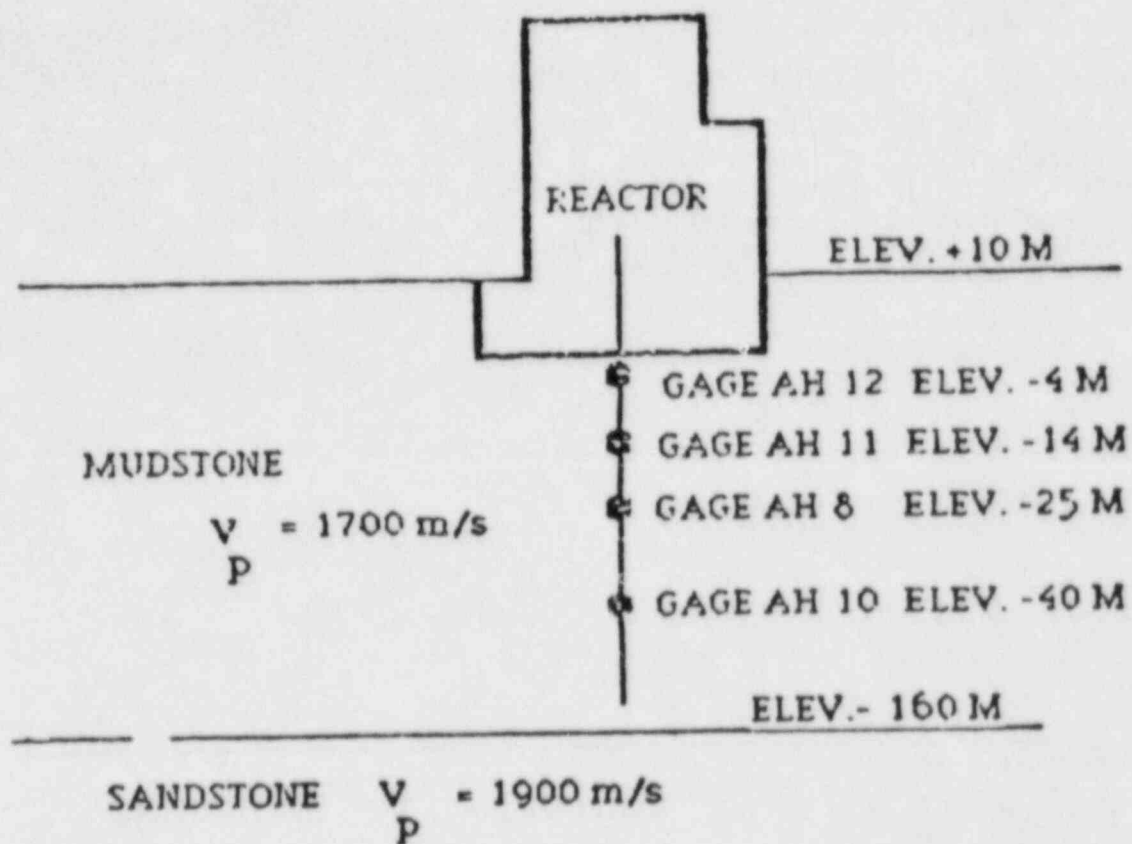
Fig. 1 SITE CONFIGURATION
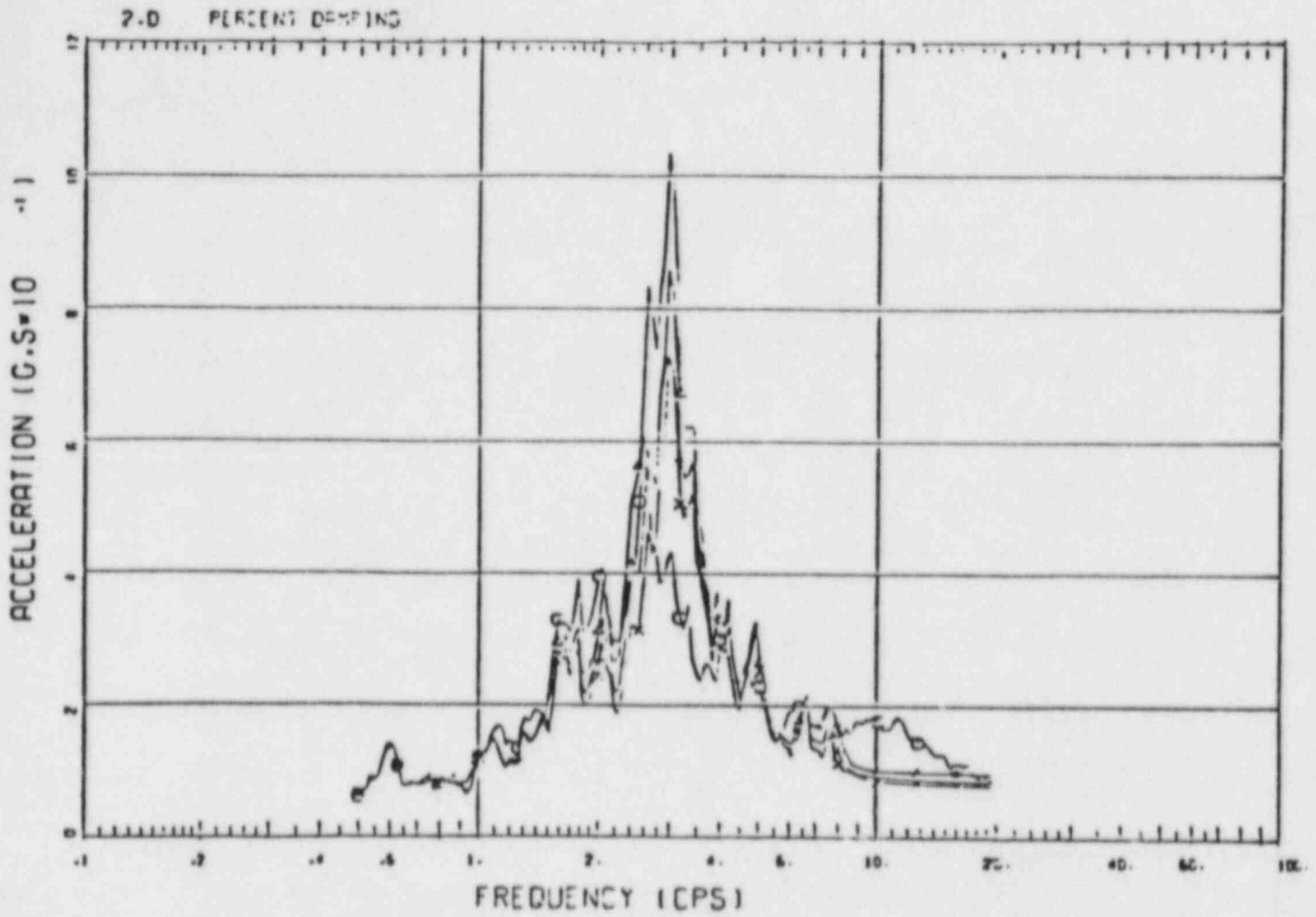
Fig. 2 SPECTRA CALCULATED AT - 4 M USING
PULSE AT - 40 M
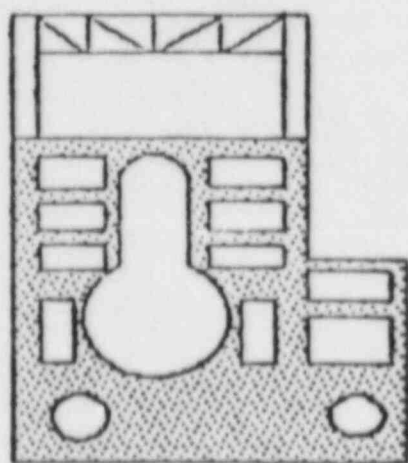
(a) Building Cross Section   (b) Model
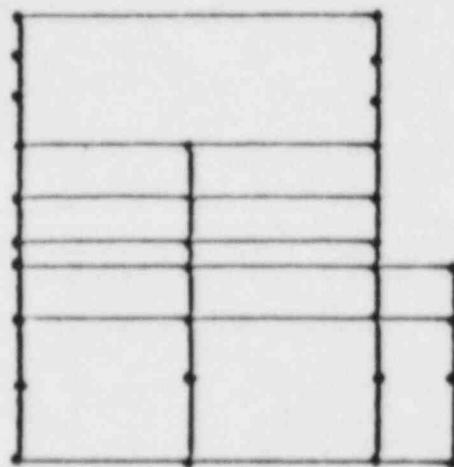
Fig. 3 FUKUSHIMA REACTOR CONTAINMENT MODEL
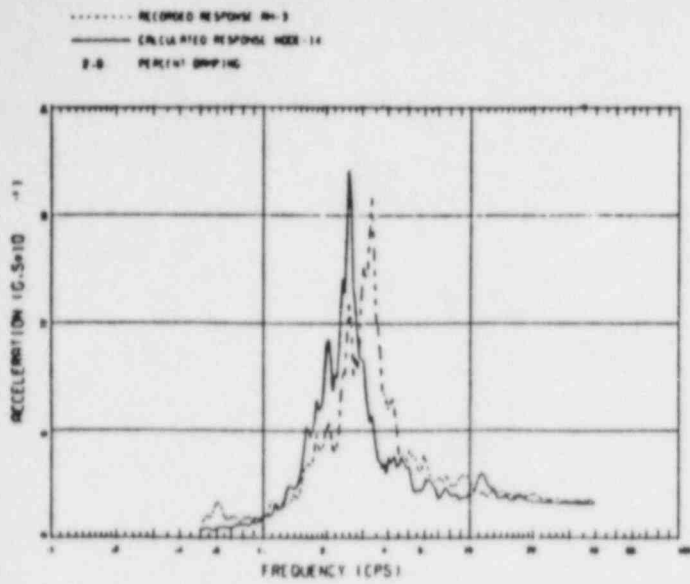
(c) Operating Floor
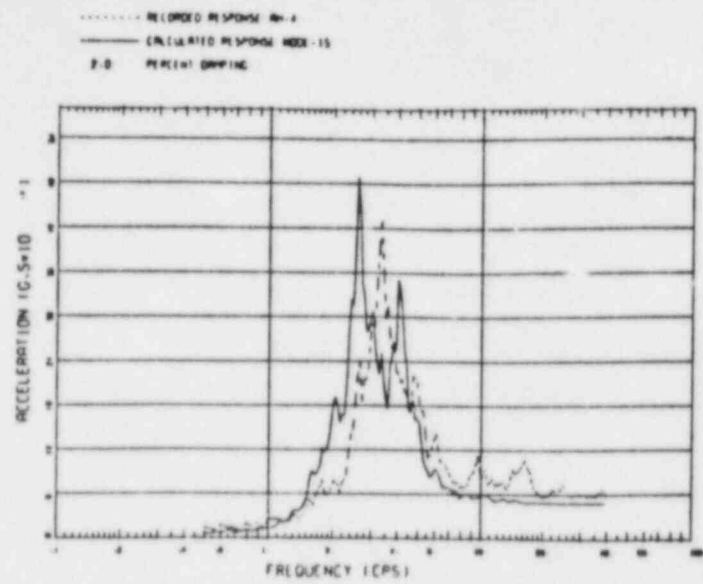
(d) Top of Structure
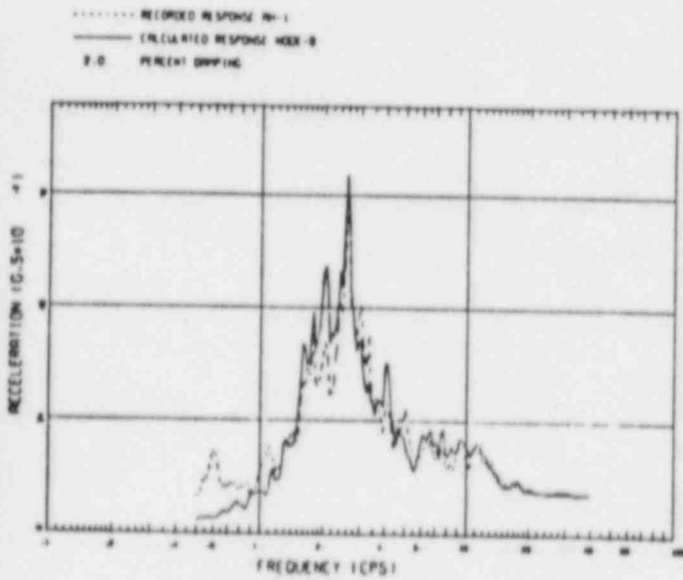
(a) Basemat
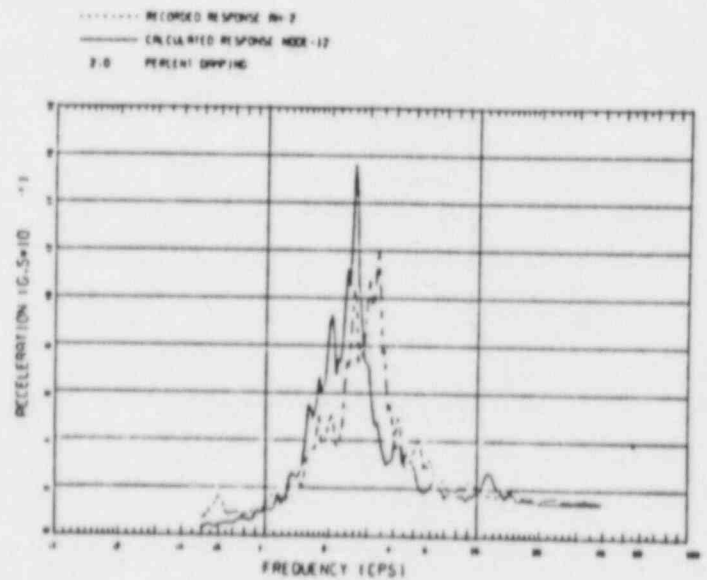
(b) Elev. 25.9 M

Fig. 4 - Comparison of Measured and Calculated Spectra
for Fukushima Using Measured Input Motion and
Standard Interaction Parameters.

EXPLOSIVE ARRAYS
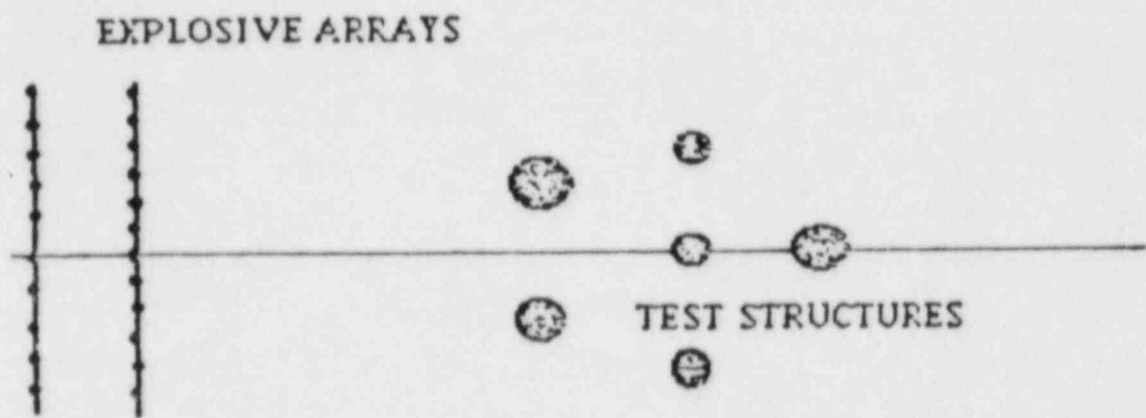
TEST STRUCTURES

Fig. 5 SIMQUAKE II TEST BED
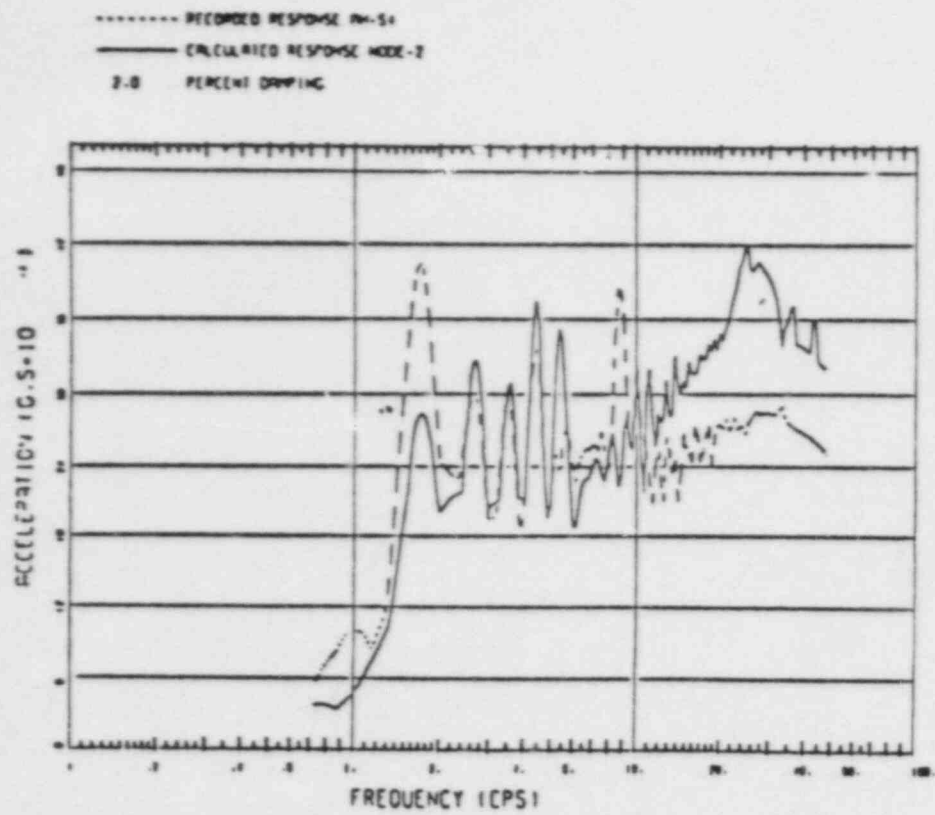
(a) Base of Structure
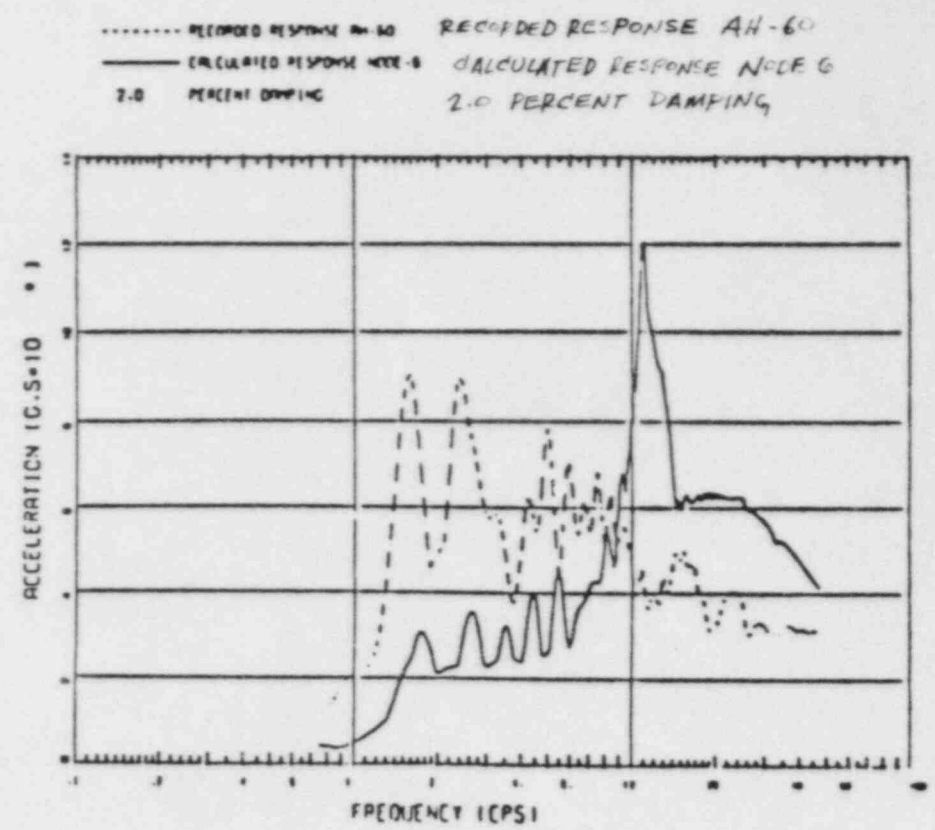
(b) Top of Structure

Fig. 6 - Comparison of Measured and Calculated Horizontal
Spectra for Simquake II Structure Using Standard
Interaction Parameters

89
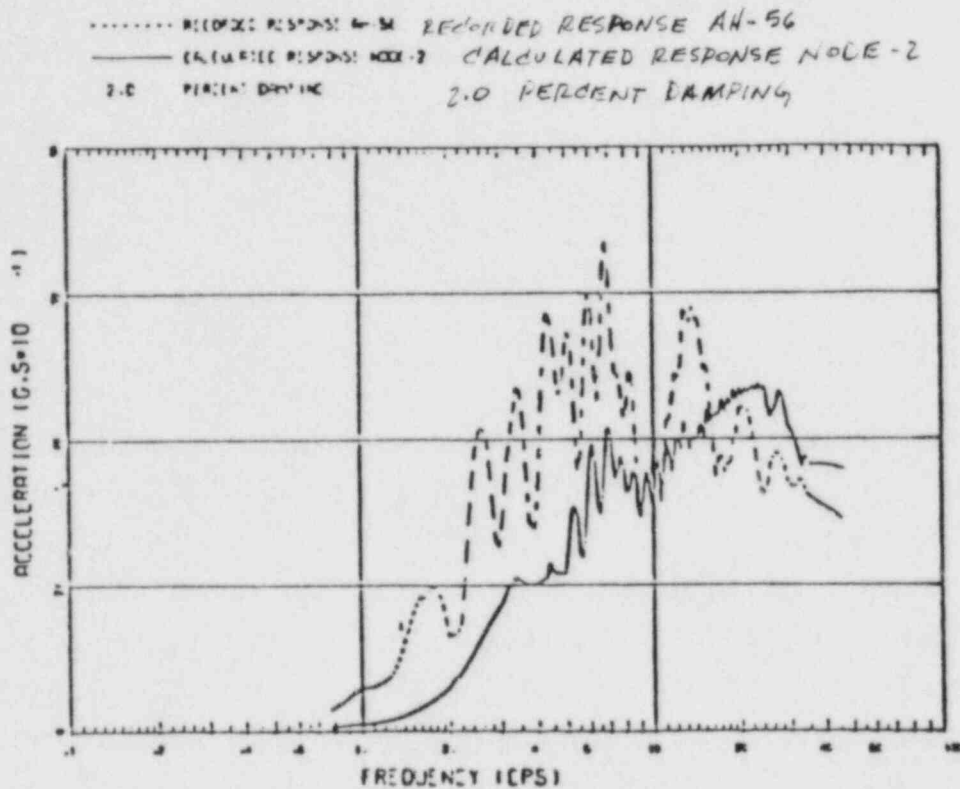
Fig. 7 - Comparison of Measured and Calculated
Vertical Spectra for Simquake II Structure
Using Standard Interaction Parameters.

PROBABILITY BASED LOAD COMBINATIONS

M. Reich and H. Hwang
Brookhaven National Laboratory
B. Ellingwood
National Bureau of Standards
M. Shinozuka
Columbia University

1. INTRODUCTION

The program entitled, "Probability Based Load Combinations for Design of Category I Structures", is currently being worked on at Brookhaven National Laboratory (BNL) for the Office of Nuclear Regulatory Research, U.S. Nuclear Regulatory Commission. The objective of this program is to develop a probabilistic approach for the safety evaluations of reactor containments and other seismic category I structures subjected to multiple static and dynamic loadings. Furthermore, based on the above developed probabilistic approach, load combination criteria for the design of seismic category I structures will also be established.

This paper presents the latest results of the program. Two major topics will be covered: the first describes the reliability analysis method for assessment of the safety margins of nuclear structures, while the second discusses the development of the probability-based load combination criteria for the design of concrete containments.

2. ASSESSMENT OF SAFETY MARGINS OF CATEGORY I STRUCTURES

The safety of nuclear power plant structures is of primary concern to the regulatory agencies, the nuclear industry and the general public because of the serious socioeconomic consequences that could result from structural failures. To ensure the structural safety, nuclear structures must be designed to

withstand all kinds of loads and load combinations that may be expected to occur during their lifetime. These loads include various static and dynamic loads, which are caused by operational, environmental and accidental conditions. It is recognized that the loads involve random and other uncertainties in nature. Similarly, the structural resistance also cannot be determined without uncertainties. The traditional methods of structural design attempt to account for the inevitable variability through the use of safety factors or load and resistance factors. These factors are specified in various codes such as ASME, ACI, AISC, etc., and the NRC Standard Review Plan (SRP). However, the subjective manner by which these safety factors have been determined may result in an unknown and nonuniform reliability. In view of randomness and uncertainty in loads, structural resistance etc., a probabilistic approach for assessment of structural safety is a rational choice.

For the safety evaluation of category I concrete structures under various static and dynamic loads, a probability-based reliability analysis method has been developed.[7,12] An important feature of this method is that finite element analysis and random vibration theory have been incorporated into the reliability analysis. In the method, an appropriate probabilistic model is established for each load. For example, accidental pressure is idealized as a rectangular pulse with random intensity and duration and is assumed to occur according to the Poisson arrival law. Earthquake ground acceleration is represented by a segment of a stationary Gaussian process with a zero mean and Kanai-Tajimi spectrum. Furthermore, all possible seismic hazards at a site, which is represented by a hazard curve, are also included in the analysis. The limit state of the structure is then analytically defined and the corresponding limit state surface is established. Finally, limit state probabilities for various load combinations are evaluated.

Currently, the reliability analysis method for concrete containments subjected to dead load, live load, accidental pressure, tornado, SRV load and ground earthquake acceleration has been established. This reliability analysis method has also been applied to selected existing containment structures in order to assess their safety margins under various load combinations. The details of these reliability assessments are described in Refs. 7 and 9.

3. LOAD COMBINATION CRITERIA FOR DESIGN OF CONCRETE CONTAINMENT STRUCTURES

In principle, the reliability analysis method described above could be utilized directly in structural design. However, the probabilistic method requires expert judgement on the probabilistic models of loads and resistance, and on the target limit state probability etc., thus, it is not suitable for the routine design of nuclear structures.[6] Load combination criteria, which are in a deterministic format and yet reflect the probabilistic nature of the design parameters, are more appropriate for routine design purposes. The procedure for developing probability-based load combination criteria for the design of containments and other category I structures is as follows:

1. Select an appropriate load combination format. (e.g., LRFD format)
2. Establish representative structures.
3. Select a target limit state probability.
4. Assign initial values for all parameters (load factors etc.) associated with the selected load combination format.
5. Design each representative structure.
6. Determine the limit state probability of each representative structure.
7. Compute the objective function measuring the difference between the target limit state probability and the computed limit state probability.
8. Determine a new set of parameters (load factors) along the direction of maximum descent with respect to the objective function.
9. Repeat steps 5 to 8 until a set of parameters that minimize the objective function is found.

The procedure has been utilized in determining load factors for concrete containments as described in Ref. 8.

4. LOAD FACTORS FOR ACCIDENTAL PRESSURE AND SAFE SHUTDOWN EARTHQUAKE

The derivations of the load factors for the accidental pressure due to a design basis accident (DBA) and safe shutdown earthquake (SSE) for three target limit state probabilities are described in this section.

4.1 Load Combination Format

The development of probability-based load combinations for designing nuclear structures requires the selection of an appropriate load combination format. Several different formats have been proposed.[6] The format that has been selected for this study is the "load and resistance factor design (LRFD)" format. The LRFD format is simple enough to be used in routine design while offering sufficient flexibility to achieve consistent reliabilities in various design situations.

If three loads, i.e., dead load, earthquake and accidental pressure are considered, the load combinations in the LRFD format are expressed as follows:

$$0.9D + \gamma_p P_a \leq \phi_i R_i \tag{1}$$

$$1.2D + \gamma_{ES} E_{ss} \leq \phi_i R_i \tag{2a}$$

$$0.9D - \gamma_{ES} E_{ss} \leq \phi_i R_i \tag{2b}$$

where

D = load effect due to design dead load

P_a = load effect due to design pressure

E_{ss} = load effect due to safe shutdown earthquake (SSE)

γ_p = load factor for accidental pressure

γ_{ES} = load factor for safe shutdown earthquake

ϕ_i = resistance factor for the i-th limit state under consideration

R_i = nominal structural resistance for the i-th limit state under consideration

94

Dead load factor and resistance factor are preset to simplify the optimization. The mean value of the dead load is approximately equal to its nominal value and its variability is quite small. A dead load factor of 1.2 (or 0.9 when the dead load has a stablizing effect) has been found to be more than adequate to account for uncertainty in dead load.[1,6] Thus, in Eqs. 1 and 2, the dead load factor is preset to be 1.2 or 0.9. The same factors also appear in the probability-based load criteria in the A58 Standard.[1] A proposed set of resistance factors for concrete design that are consistent with the A58 load requirements has been derived.[10] For axial tension or flexure with axial tension, $\phi = 0.85$. For axial compression or flexure with axial compression, $\phi = 0.65$. The ϕ value is increased linearly from 0.65 to 0.85 as axial compression decreases from 0.10 $f'_{cn} A_g$ to zero, where f'_{cn} is the specified concrete compressive strength and A_g is the area of cross section. These ϕ values will be used for this study.

4.2 Selection of Representative Containment Structures

An important requirement for codified structural design is that all the structures designed according to a code should meet the code performance objectives which are expressed in probabilistic terms. In order to test if this requirement is satisfied, a set of representative (sample) structures must be selected for evaluating the code. In this study, representative containments are determined from examining the inventory of PWR reinforced concrete containments in the United States. The ranges of the design parameters such as geometries, material strengths, and design loads are determined as shown in Table 1. For each design parameter, one, two or four representative values are selected to represent its range. These representative values are also listed in Table 1. The general PWR containment characteristics identified in Table 1 can be used, along with a Latin hypercube sampling technique, to construct the sample (representative) containments. A sample containment is identified by a sample vector, which consists of one of the representative values of each design parameter. Four sample containments thus selected are shown in Table 2. With the design variables in Table 2, specified only one design variable still needs to be determined, that is, the required reinforcement.

95

4.3 Limit State

A limit state represents a state of undesirable structural behavior. In general, a limit state is defined from the actual structural behavior under loads. For a particular structural system, it is probable that more than one limit state may be considered. In this study, the limit state for containments is defined according to the ultimate strength theory of reinforced concrete. It is assumed that the containment can be detailed to prevent failures at local stress concentrations such as penetrations, equipment hatches, etc., and can be stiffened to prevent local buckling. Thus, the limit state can be defined by membrane stresses and bending moments in the containment wall. It is described as follows: at any time during the service life of the structure, the state of structural response is considered to have reached the limit state if a maximum concrete compressive strain at the extreme fiber of the cross-section is equal to 0.003, while the yielding of rebars is permitted. Based on the above definition of the limit state and the theory of reinforced concrete, for each cross-section of a finite element, a limit state surface can be constructed in terms of the membrane stress and bending moment, which is taken about the center of the cross-section.[3] A typical limit state surface is shown in Fig. 1. In this figure, point "a" is determined from a stress state of uniform compression and point "e" from uniform tension. Points "c" and "c'" are the so-called "balanced points", at which a concrete compressive strain of 0.003 and a steel tensile strain of f_y/E_s (E_s = elasticity modulus of steel) are reached simultaneously. Furthermore, lines abc and ab'c' in Fig. 1 represent compression failure and lines cde and c'd'e represent tension failure. The tangential shear limit state is currently being investigated for this study.

4.4 Design of Containment Structures

Each sample containment as shown in Table 2, is assumed to be fixed at the base and has to be designed according to the proposed load combination with trial load and resistance factors, design loads and nominal resistance. For design loads and nominal resistance, the current values specified in codes

are generally used. However, certain modifications may be necessary in order to put the design values on a probabilistic basis.

For the structural analysis of containments, three-dimensional finite element models are used. The finite element utilized in the analysis is the shell element as described in the SAP V computer code. A detailed cross-section of the containment model is shown in Fig. 2. As can be seen from this figure, the containment is divided into 20 layers. Except at the top of the dome, each layer has 24 elements such that the nodal points are taken every 15° in the circumferential direction. This discretization requires a total of 481 nodes and 468 elements.

The element stress resultants for dead load and accidental pressure are obtained from static analysis. For seismic analysis, the response spectrum analysis method is employed. The horizontal and vertical response spectra used in this study are those specified in the Regulatory Guide 1.60. The damping ratio is taken to be 7 percent of criterial for SSE as specified in the Regulatory Guide 1.61. The square root of the sum of squares (SRSS) method is used to combine the responses in three directions. On the basis of the ultimate strength design of reinforced concrete, the minimum required re-bar area is determined as shown in Table 3. Designers usually provide rebar area larger than the minimum requirement. In this study, however, the minimum required rebar area will be used in design and reliability analysis.

4.5 Probabilistic Representations for Loads and Material Strength

Various static and dynamic loads act on a containment structure during its lifetime. These loads may be caused by normal operating, environmental and accidental conditions. Since the loads intrinsically involve random and other uncertainties, an appropriate probabilistic model for each load must be established in order to perform reliability analysis. The probabilistic load models for dead load, accidental pressure and earthquake ground acceleration are described as follows:

97

Dead Load

The dead load primarily arises from the weight of the containment wall. There is some uncertainty as to the actual magnitude of the dead load.[6] However, the large variabilities in earthquake and accidental pressure tend to overshadow the variability in dead load. As a result its effect on the limit state probabilities is minor. Thus, for the purpose of this analysis, dead load is assumed to be deterministic and is equal to the design value, which is computed on the basis of the unit weight of reinforced concrete as 150 lb/ft^3.

Accidental Pressure

The accidental pressure is considered as a quasi-static load that is uniformly distributed on the containment wall. The accidental pressure is idealized as a rectangular pulse that occurs in accordance with the Poisson law during the containment life. Under these assumptions, three parameters are required to model the accidental pressure: the mean occurrence rate, the mean duration, and the intensity P, intensity P is considered as a random variable. In this study, the mean occurrence rate and the mean duration are taken to be 1.68×10^{-3} per year and 1200 sec, respectively. The intensity is assumed to be normally distributed with a mean over design value of 0.9 and coefficient of variation of 0.12.

Earthquake Ground Acceleration

The basis for the statistical description of earthquake ground motion is given in Refs. 4 and 8. The seismic hazard at a site of a nuclear power plant is described by a seismic hazard curve. In this study, the probability distribution $F_A(a)$ of the annual peak ground acceleration A is assumed to be the Type II extreme value distribution,[4]

$$F_A(a) = \exp \left[- (a/u)^{-\alpha} \right] \qquad (3)$$

where α and μ are two parameters to be determined. The value of α for the U.S. is estimated to be 2.7.[8] The parameter μ is computed based on this α value and the assumption that the annual probability of exceeding the safe shutdown earthquake at a site is 4×10^{-4} per year.[11] Figure 3 shows the comparison of the hazard curve used in this study and the hazard curves with 50 percent confidence for eight specific plant sites in the Eastern United States.[2] From this figure, it can be seen that the hazard curve used in this study compares well with six out of the eight curves.

The lower and upper bounds of peak ground acceleration are required in the analysis. The lower bound, a_0, indicates the minimum peak ground acceleration for any ground shaking to be considered as an earthquake. a_0 is assumed to be 0.05 g. The upper bound, a_{max}, represents the largest earthquake possible at a site. In this paper, a_{max} is chosen to be $2a_{SSE}$.

Even though the structures are designed for three components of an earthquake, for reliability analysis the earthquake ground acceleration is assumed to act only along the global x direction. This simplification is made since the reliability analysis results from both assumptions are almost the same because of the symmetry of the containment structures. The earthqquake ground acceleration on the condition that an earthquake occurs, is idealized as a segment of a zero-mean stationary Gaussian process, described in the frequency domain by a Kanai-Tajimi power spectral density.

$$S_{ggxx}(\omega) = S_o \frac{1 + 4\zeta_g^2(\omega/\omega_g)^2}{\left[1 - (\omega/\omega_g)^2\right]^2 + 4\zeta_g^2(\omega/\omega_g)^2} \tag{4}$$

where the parameter S_o is a random varible and represents the intensity of an earthquake. The distribution of S_o can be determined as shown in Ref. 8. Parameters ω_g and ω_g are the dominant ground frequency and the critical damping, respectively, which depend on the site soil conditions. For rack and deep cohensionless soil conditions, ω_g, is taken to be 8π rad/sec and 5π rad/sec respectively. ω_g is taken to be 0.6 for both soil conditions.[4] The mean duration of the stationary phase of the earthquake acceleration is assumed to be 10 or 20 seconds in this study.

99

Material Strength

In the reliability analysis methodology, the geometry of the containments is assumed to be deterministic while the distributions of material strengths are included. Ellingwood[5] recommended that concrete compressive strength, f'_c, is normally distributed with coefficient of variation (CoV) of 0.14 and a mean value at 1 year, $\overline{f'_c}$,

$$\overline{f'_c} = 1219 + 1.02 \, f'_{cn} \text{ (psi)} \tag{5}$$

in which f'_{cn} = specified compressive strength of concrete. Using this relation, the mean value of concrete compressive strength for f'_{cn} = 4000 and 5000 psi at 28 days are 5299 psi and 6316 psi, respectively. For yield strength f_y of ASTM A 615 Grade 60 deformed bar reinforcement, the lognormal distribution is recommended with a mean value of 71.0 ksi and CoV of 0.11.[5]

4.6 Reliability Assessment

For reliability assessments of these containments, the reliability analysis method developed by BNL is used. By utilizing this method, it is able to determine limit state probabilities for structures under various static and dynamic loads. The methodology can also evaluate the coincidence probabilities of various load combinations. This is important since it is on the basis of the coincidence probabilities that a decision may be made on whether or not a particular load combination (among all the possible mutually exclusive load combinations) is to be considered for design. For example, because the coincidence probability of earthquake and accidental pressure is very small, it does not need to design nuclear structures under simultaneous action of SSE and P_a.

The limit state defined in Section 4.3 and the probabilistic models for loads and material strengths described in Section 4.5 are used in the reliability assessments of sample containments. The limit state probabilities for a reference period of 40 years are shown in Table 4.

100

4.7 Determination of Load Factors

The limit state probability is a quantitative measure of structural performance. The selection of a target limit state probability should consider many factors, e.g., the characteristics of the limit states, the consequence of failure, and the risk evaluation and damage cost. Hence, the target reliability may not necessarily be the same for different limit states.

If a target limit state probability $P_{f,T}$ is specified, the load and resistance factors can be determined such that the limit state probabilities of the sample containments are sufficiently close to the target limit state probability. The closeness is measured by an objective function defined as follows:

$$\Omega(\gamma_p, \gamma_{ES}) = \sum_{i=1}^{4} (\log P_{f,i} - \log P_{f,T})^2 \tag{6}$$

where N is the total number of representative containments and $P_{f,i}$ is the limit state probability computed for the i-th sample containment. w_i represents a weight factor for i-th sample containment. On the basis of the Latin hypercube sampling techique, it is assumed that each sample containment in Table 2 is equally representative, and thus, $w_i = 1.0$. The optimum load factors γ_{ES} and γ_p may be obtained using a minimization technique. However, the load factors are limited to first digit after the decimal point for practical purposes, then the optimum load factors can be determined by computing the objective function at a few combinations of preassigned γ_p and γ_{ES} as illustrated in Table 5.

The optimum load factors for different target limit state probabilities are determined as shown below.[8]

Target limit state probability	Optimum load factors	
$P_{f,T}$	γ_{ES}	γ_p
1.0×10^{-5}	1.6	1.1
1.0×10^{-6}	1.7	1.2
1.0×10^{-7}	2.0	1.2

101

5. OTHER LOAD FACTORS

Tentative load factors for other loads appearing in the load combinations for designing containments are presented in Ref. 8. These factors were not determined through the optimization process described previously for P_a and SSE, but rather on the basis of prior experience with probability-based design for ordinary building construction.[6] However, the load factors are consistent with the levels of uncertainty in the loads.

6. TENTATIVE LOAD COMBINATION CRITERIA

For a target limit state probability of 1.0×10^{-6} and $a_{max} = 2a_{SSE}$, tentative load combinations for designing concrete containments are:

$$\left.\begin{array}{l} 1.2\ D + 1.6\ L + T_0 + R_0 \\ 0.9\ D + 1.2\ P_a + T_a + R_a \\ 1.2\ D + L + 1.7\ E_{ss} + T_0 + R_0 \\ 0.9\ D - 1.7\ E_{ss} \end{array}\right\} \quad \leqslant \phi_i\ R_i \qquad (7)$$

It is clear that the use of such criteria would entail no major change in the way that routine structural design calculations are performed. However, in contrast to existing design procedures, the proposed criteria are risk-consistent and have a well-established rationale.

The major features of the proposed load combination criteria are summarized as follows:

1. The load combinations are in a Load and Resistance Factor Design (LRFD) format using the principal load-companion loads concept.
2. Load factors and resistance factors are, in general, selected on the basis of limit states and a target limit state probability.
3. The load factor for accidental pressure, γ_p, is equal to 1.2 for $P_{f,T} = 1.0 \times 10^{-6}$. This new γ_p is smaller than 1.5 used in current design criteria.

102

4. One design earthquake, i.e., SSE, is selected to represent seismic
    hazards. In current practice, however, two kinds of design earth-
    quake, i.e., SSE and OBE are employed. Furthermore, the annual
    probability of exceeding the SSE is assumed to be 4×10^{-4} per
    year. For $P_{f,T} = 1.0 \times 10^{-6}$ and $a_{max} = 2a_{SSE}$, the load
    factor for SSE is equal to 1.7.

5. The load combination involving both accidental pressure and SSE,
    i.e., abnormal/extreme environmental conditions in the current
    ASME code, is not recommended for inclusion in the proposed de-
    sign criteria.

6. The dead load factor is set to be 1.2 or 0.9 depending on whether
    or not dead load has a stabilizing effect. Furthermore, for per-
    manent equipment loads, which currently are considered as dead
    loads, the load factor is set to be 1.0.

7. The live load factor is set to be 1.6 or 1.0 depending on if it
    is a principal load or a companion load.

8. The load factor γ_{ps} on the prestress effect is set equal to 1.0
    if the limit state is ductile. However, if the prestress stabi-
    lizes the structure or has a beneficial effect (e.g., shear), γ_{ps}
    is set to be 0.9.

9. The load factors for temperature loads either due to operating or
    accidental conditions are set equal to 1.0.

10. The load factors for those loads which produce only local effects
    on structures, are tentatively set equal to 1.0.

11. The nontornadic wind load is not recommended for inclusion in the
    load combinations. The load factor for tornado loads is set equal
    to 1.0.

7. CONCLUDING REMARKS

This paper presents the latest results of the on-going program entitled, "Probability Based Load Combinations For Design of Category I Structures". The objective of this program is to develop a probabilistic approach for the safety evaluations of reactor containments and other seismic category I structures subjected to multiple static and dynamic loadings. Furthermore, based on the above developed probabilistic approach, a load combination criteria for design of seismic category I structures will also be established.

For the safety evaluation of category I concrete structures under various static and dynamic loads, a probability-based reliability analysis method has been developed. An important feature of this method is that finite element analysis and random vibration theory have been incorporated into the reliability analysis. In the method, an appropriate probabilistic model is established for each load. The limit state of the structure is analytically defined and the corresponding limit state surface is established. Finally, limit state probabilities for various load combinations are evaluated. Currently, the reliability analysis method for containment subjected to dead load, live load, accidental pressure, tornado, SRV loads and ground earthquake accelerations has been established. This reliability analysis method has also been applied to selected existing containment structures in order to assess their safety margins under various load combinations.

With respect to developing probability-based load combination criteria for design of category I structures, a general procedure has been established. In this procedure, the proposed load combinations is in the form of load and resistance factor design (LRFD) format which uses the principal load-companion load concept. The load and resistance factors are, in general, determined on the basis of limit states and target limit state probabilities. The procedure has been utilized in determining load factors for concrete containments. In this paper, the derivations of the load factors for accidental pressure due to a design basis accident and safe shutdown earthquake (SSE) for three target limit state probabilities are described and the tentative design load combinations are presented.

REFERENCES

1. American National Standard A58, "Minimum Design Loads for Buildings and
    Other Structures, American (ANSI A58.1-1982)", American National Standards
    Institute, New York, 1982.

2. Bernreuter, D.L., et al., "Seismic Hazard Characterization of the Eastern
    United States: Methodology and Interim Results for Ten Sites", NUREG/CR-
    3756, April, 1984.

3. Chang, M., et al., "Structural Modeling and Limit State Identification for
    Reliability Analysis of RC Containment Structures", SMiRT-7 Conference
    Paper M3/2, Aug. 22-26, 1983.

4. Ellingwood, B. and Batts, M., "Characterization of Earthquake Forces
    for Probability Based Design of Nuclear Structures", NUREG/CR-2945,
    U.S. Nuclear Regulatory Commission, Washington, D.C., September 1982.

5. Ellingwood, B., "Probabilistic Descriptions of Resistance of Safety-
    Related Nuclear Structures", NUREG/CR-3341, U.S. Nuclear Regulatory
    Commission, Washington, D.C., May 1983.

6. Ellingwood, B., "Probability Based Safety Checking of Nuclear Plant
    Structures", NUREG/CR-3628, BNL-NUREG-51737, Dec. 1983.

7. Hwang, H., et al., "Reliability Assessment of Reinforced Concrete
    Containment Structures", BNL-NUREG-51661, February 1983.

8. Hwang, H., et al., "Probability Based Load Combination Criteria for
    Design of Concrete Containment Structures" (Draft), BNL-NUREG-51795,
    NUREG/CR-3876, June 1984.

9. Kawakami, J., et al., "Reliability Assessment of Indian Point Unit 3
    Containment Structure", NUREG/CR-3641, BNL-NUREG/51740, January 1984.

REFERENCES (Cont'd)

10. MacGregor, J. "Load and Resistance Factors for Concrete Design",
    ACI Journal July-August, 1983, pp. 279-287.

11. Reiter, L. "Uses of Probabilistic Estimates of Seismic Hazard and
    Nuclear Power Plants in the U.S.", Second CSNI Specialist Meeting on
    Probabilistic Methods in Seismic Risk Assessment for Nuclear Power
    Plants, Livermore, CA, May 16-19, 1983.

12. Shinozuka, M., et al., "Development of a Reliability Analysis Method
    for Category I Structures", SMiRT-7 Conference Paper M 5/3, Chicago,
    IL, August 22-26, 1983.

Table 1. Design Parameters of PWR Reinforced
Concrete Containment.

Design Parameters	Design Range	Recommended Value
inside radius	60'-0" to 75'-0"	60'-0", 70'-0"
dome rise ratio	1.0	1.0
cylindrical height	145'-0" to 160'-0"	150'
cylindrical wall thickness	3'-6" to 5'-0"	3'-6", 4'-6"
dome wall thickness	2'-6" to 3'-6"	2'-6", 3'-6"
concrete compressive strength	3000 psi to 5000 psi	4000 psi, 5000 psi
yield strength of steel rebars	60 ksi	60 ksi
accidental pressure	40 psi to 60 psi	42, 47, 52, 57 psi
safe shutdown earthquake	0.10g to 0.75g	0.17g, 0.25g, 0.32g, 0.50g

Table 2. PWR Reinforced Concrete Containment Samples.

Design parameters	Sample 1	Sample 2	Sample 3	Sample 4
inside radius	70'-0"	60'-0"	60'-0"	70'-0"
dome rise ratio	1.0	1.0	1.0	1.0
cylindrical height	150'-0"	150'-0"	150'-0"	150'-0"
cylindrical wall thickness	4'-6"	3'-6"	4'-6"	3'-6"
dome wall thickness	3'-6"	2'-6"	3'-6"	2'-6"
concrete compressive strength (psi)	4000	4000	5000	5000
steel yield strength (psi)	60,000	60,000	60,000	60,000
dead load (lb/ft^3)	150	150	150	150
accidental pressure (psi)	47	42	52	57
safe shutdown earthquake (g)	0.17	0.32	0.50	0.25
Soil	Rock	Deep Cohesionless	Rock	Deep Cohesionless
earthquake duration (sec)	10	20	20	10

Table 3. Required Rebar Area (D+E$_{SS}$, D+P$_a$).

Sample	Y$_{ES}$	As (in^2/in)							
		γ_p = 1.0		γ_p = 1.1		γ_p = 1.2		γ_p = 1.3	
		X	Y	X	Y	X	Y	X	Y
1	1.5	0.411	0.265	0.452	0.303	0.493	0.341	0.534	0.380
	2.0	0.411	0.272	0.452	0.303	0.493	0.341	0.534	0.380
	2.5	0.411	0.362	0.452	0.362	0.493	0.362	0.534	0.380
	3.0	0.411	0.453	0.452	0.453	0.493	0.453	0.534	0.453
2	1.5	0.314	0.372	0.345	0.372	0.376	0.372	0.408	0.372
	2.0	0.314	0.518	0.345	0.518	0.376	0.518	0.408	0.518
	2.5	0.314	0.665	0.345	0.665	0.376	0.665	0.408	0.665
	3.0	0.314	0.811	0.345	0.811	0.376	0.811	0.408	0.817
3	1.5	0.394	0.932	0.433	0.932	0.472	0.932	0.511	0.932
	2.0	0.394	1.271	0.433	1.271	0.472	1.271	0.511	1.271
	2.5	0.394	1.611	0.433	1.611	0.472	1.611	0.511	1.611
	3.0	0.403	1.951	0.433	1.951	0.472	1.951	0.511	1.951
4	1.5	0.495	0.353	0.544	0.400	0.594	0.448	0.643	0.495
	2.0	0.495	0.363	0.544	0.400	0.594	0.448	0.643	0.495
	2.5	0.495	0.470	0.544	0.470	0.594	0.470	0.643	0.495
	3.0	0.495	0.578	0.544	0.578	0.594	0.578	0.643	0.578

Table 4. Limit State Probability ($D+P_a$, $D+E_{SS}$).

Sample	γ_{ES}	P_f			
		$\gamma_p = 1.0$	$\gamma_p = 1.1$	$\gamma_p = 1.2$	$\gamma_p = 1.3$
	1.2	3.502 -5	2.220 -7	3.830 -9	1.911 -10
	1.6	3.502 -5	2.220 -7	3.820 -9	1.911 -10
1	1.8	3.502 -5	2.220 -7	3.830 -9	
	2.0	1.518 -5	2.220 -7	3.830 -9	1.911 -10
	1.2	1.307 -4	1.306 -4	1.306 -4	1.306 -4
	1.6	1.036 -6	8.790 -7	8.788 -7	8.788 -7
2	1.8	2.020 -7	4.463 -8	4.447 -8	
	2.0	1.593 -7	1.932 -9	1.777 -9	1.777 -9
	1.2	9.781 -5	9.766 -5	9.766 -5	9.766 -5
	1.6	8.811 -7	7.262 -7	7.260 -7	7.260 -7
3	1.8	1.971 -7	4.262 -8	4.193 -8	
	2.0	1.569 -7	1.955 -9	1.797 -9	1.797 -9
	1.2	1.922 -5	6.935 -8	4.439 -11	6.959 -14
	1.6	1.922 -5	6.935 -8	4.439 -11	6.959 -14
4	1.8	1.922 -5	6.935 -8	4.439 -11	
	2.0	6.681 -6	6.935 -8	4.439 -11	6.959 -14

Table 5. Values of the Objective Function ($D+P_a$, $D+E_{SS}$).

		γ_p		
		1.1	1.2	1.3
γ_{ES}	1.6	5.53	1.09	11.00
	1.7	4.73	(0.23)	10.14
	1.8	4.42	0.30	10.24
	1.9		1.25	
	2.0	4.29	2.80	13.67

NOTE: 1. Value in circle is the optimum.

111
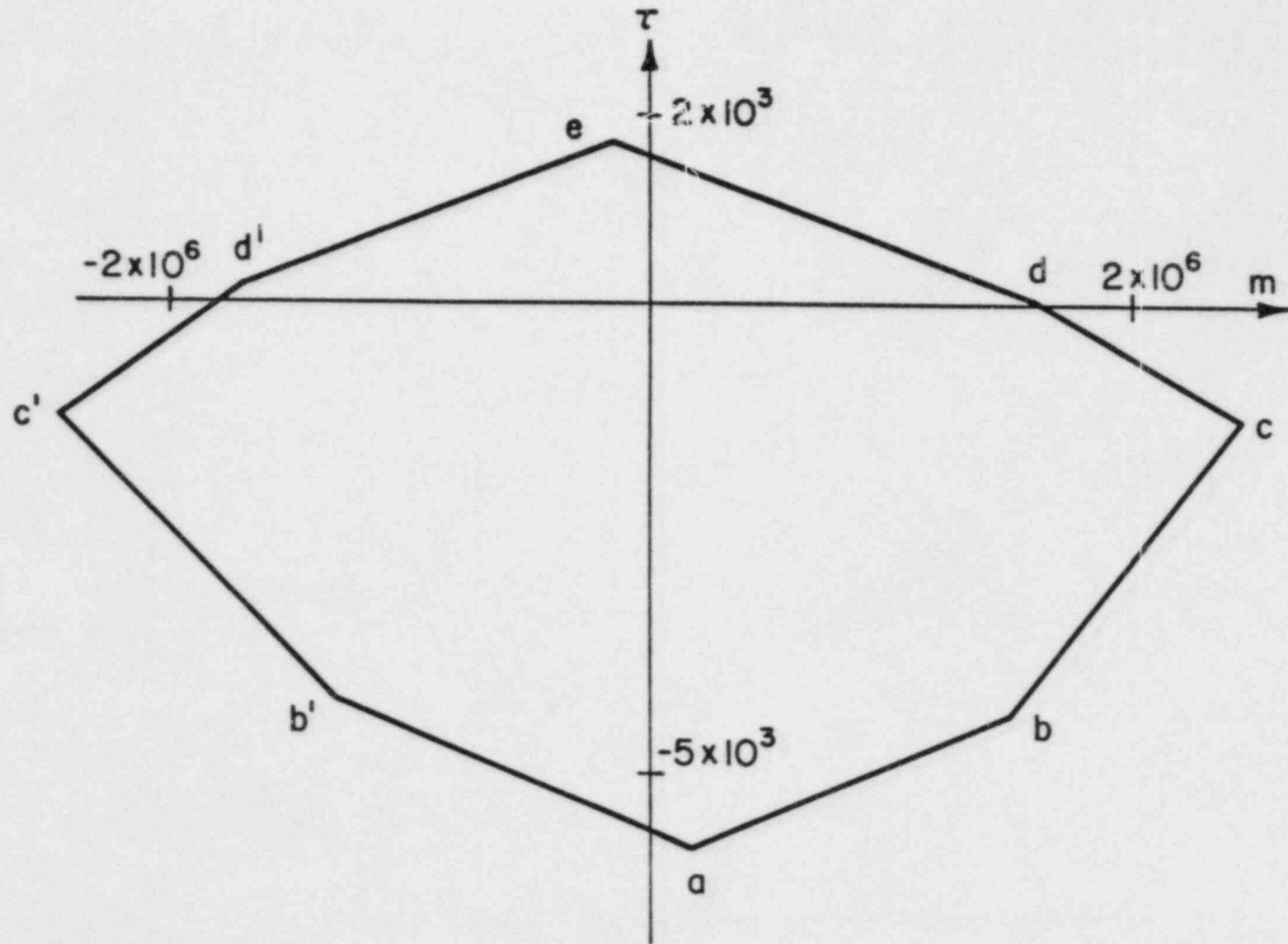
Fig. 1. Limit State Surface.

112
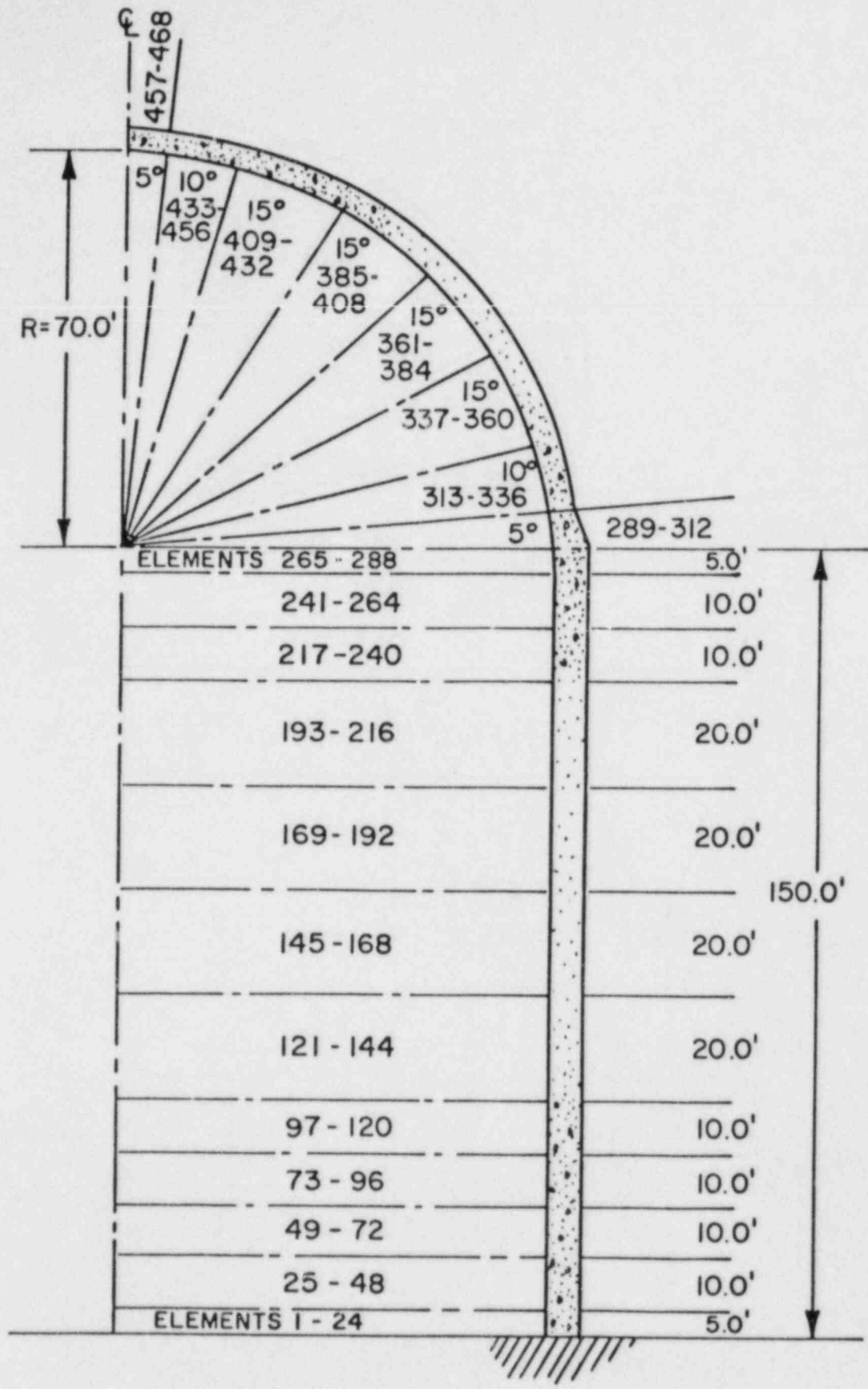
Fig. 2. Cross Section of Containment Model.

113
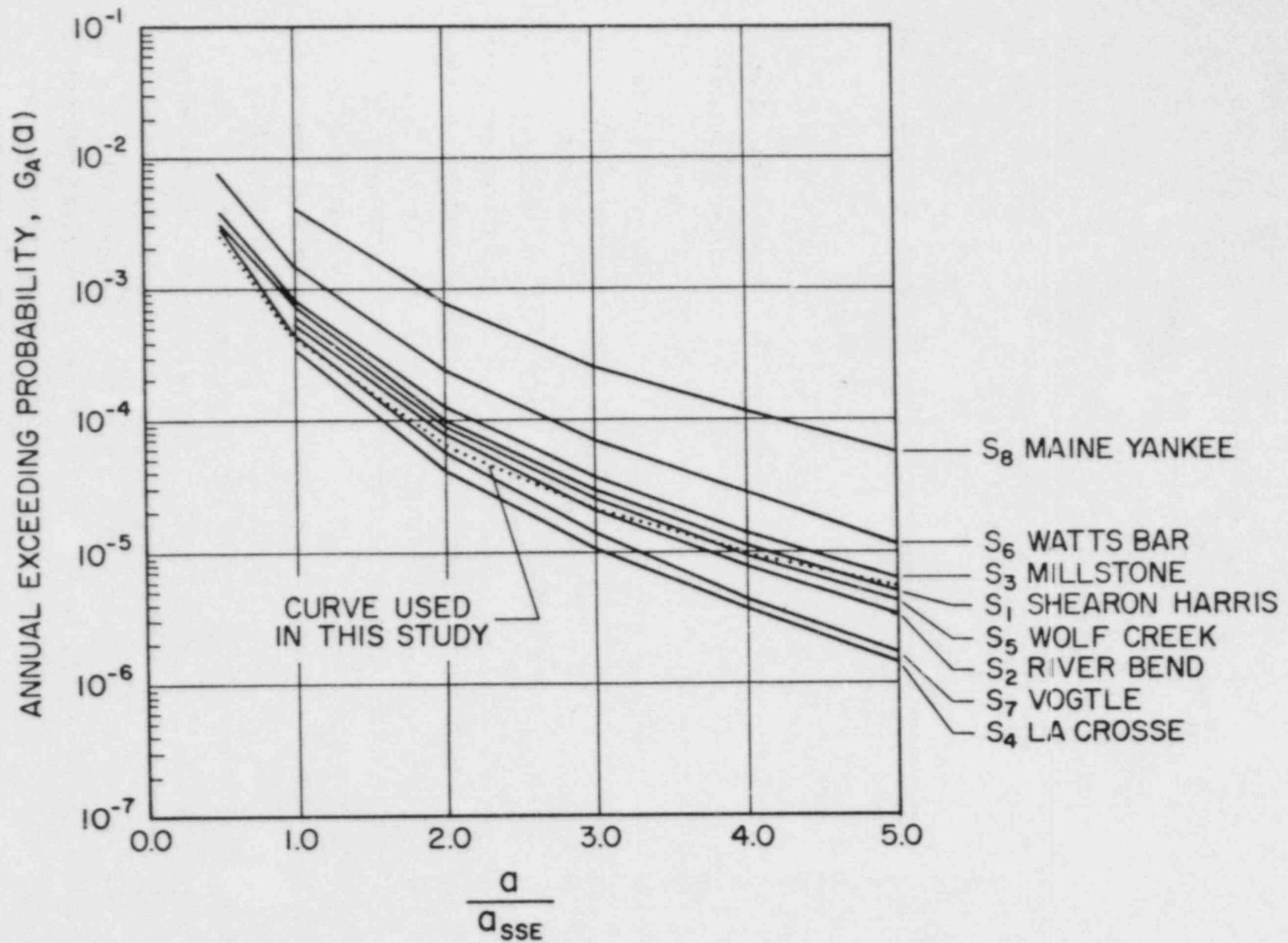
Fig. 3. Comparison of Seismic Hazard Curves.

SEISMIC CATEGORY I STRUCTURES PROGRAM

Elton G. Endebrock

Richard C. Dove

Charles A. Anderson

Los Alamos National Laboratory
Los Alamos, New Mexico

INTRODUCTION

The Seismic Category I Structures Program currently being carried out at the Los Alamos National Laboratory is sponsored by the Mechanical/Structural Engineering Branch, Division of Engineering Technology of the Nuclear Regulatory Commission (NRC). This project is part of a program designed to increase confidence in the assessment of Category I nuclear power plant structural behavior beyond the design limit. The project is focused on answering questions regarding safety issues that may arise when existing nuclear facilities are subjected to higher seismic loads than those considered in their original design. The program involves the design, construction, and testing of heavily reinforced concrete models of auxiliary buildings, fuel-handling buildings, etc., but does not include the reactor containment building. The overall goal of the program is to supply to the Nuclear Regulatory Commission experimental information and a validated procedure to establish the sensitivity of the dynamic response of these structures to earthquakes of magnitude beyond the design basis earthquake. The main purposes of the experimental program are (1) to obtain general information on how these structures behave in the inelastic range as compared with their elastic behavior, (2) to provide stiffness and damping values for more demanding loadings on the structures, (3) identify changes in floor response spectra that are used in design of systems and components as the structures are loaded into the inelastic range, and (4) to provide experimental data for benchmarking inelastic structural analysis codes.

More information on the background of this program is found in Ref. 1. During FY 82 preliminary experiments were conducted on small, reinforced-concrete isolated shear walls that had been identified as the most imporant element in the Category I structures of interest in this program. The results of these preliminary tests were reported at the 10th Water Reactor Safety Research Information Meeting and are reported on in more detail in Refs. (2) and (3).

The transition of the testing of isolated shear walls to small scale structures began in FY 83. The first complete structures tested were models of a prototypical Category I, isolated, two story, diesel generator building. The shape and dimensions of the assumed prototype structure are shown in Fig. 1, together with the dimensions of three scaled versions of this structure.* The 1/30 and 1/10-scale models were tested during FY 83 and 84 and the results of these tests are presented in this report. Although preliminary static tests were conducted on the 1/30-scale models, the emphasis was on the simulated seismic tests during which the models were driven by an appropriately scaled version of the 1940 El Centro earthquake N-S accelerogram.

The second structure of interest is a three-story, Category I auxiliary building. The shape and dimensions of this assumed prototype structure are shown in Fig. 2, together with the dimensions of two scaled versions of this structure. This second configuration will provide information on these structures that have a different set of fundamental characteristics than those of the diesel generator building. The 1/42-scale model has been tested to failure under simulated seismic conditions in FY 84. The 1/14-scale model has been constructed and is scheduled for test during FY 85.

MODEL CONSTRUCTION AND PROPERTIES

The smaller models (1/30-scale model of the diesel generator building and 1/42-scale model of the auxiliary building) were constructed with a wall thickness of 1 inch. Reinforcement consisted of 1/2-inch square mesh hardware cloth at each wall surface. This resulted in 0.28% reinforcement in each direction and on both wall surfaces. The larger models (1/10-scale model of the diesel generator building and the 1/14-scale model of the auxiliary building) were constructed with a wall thickness of 3 inches. These structures

---

* Figure 1 shows a two-story structure; however, several single story versions of the 1/30-scale structure were also constructed and tested.
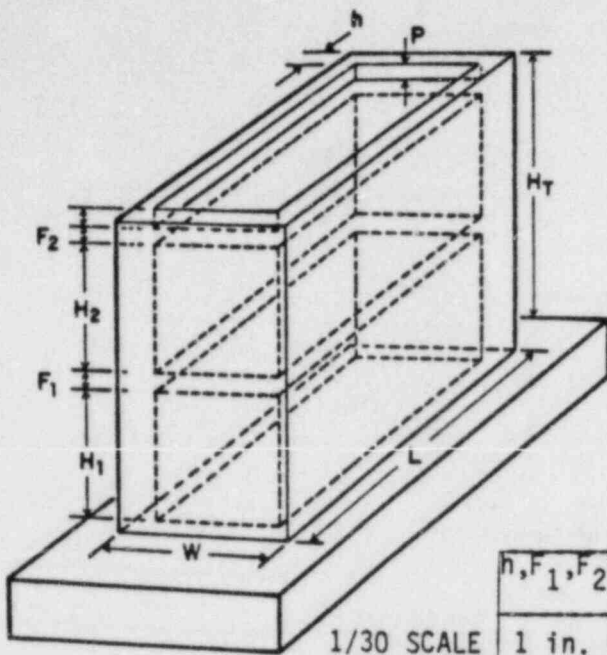
Fig. 1. Two-story deisel generator building

	h, F_1, F_2	W	L	H_1, H_2	P	Wt/STORY* (lb)
1/30 SCALE	1 in.	10 in.	18 in.	7.25 in.	1 in.	42
1/10 SCALE	3 in.	30 in.	54 in.	21.75 in.	3 in.	1134
1/5 SCALE	6 in.	60 in.	108 in.	43.5 in.	6 in.	9072
PROTOTYPE	30 in.	25 ft.	45 ft.	18ft.5in.	30 in.	1,134,000

* BASE NOT INCLUDED
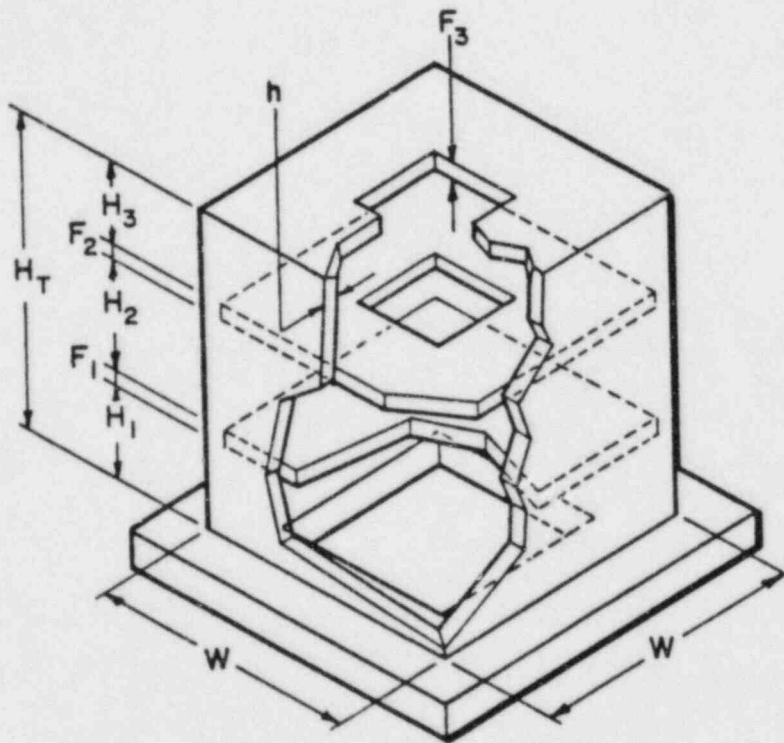
Fig. 2. Three-story auxiliary building

	h, F_1, F_2, F_3	W	H_1, H_2, H_3	Wt/STORY* (lb)
1/42 SCALE	1 in.	26 in.	10 in.	140
1/14 SCALE	3 in.	78 in.	30 in.	3780
PROTOTYPE	42 in.	1092 in.	42 in.	10,372,000

* BASE NOT INCLUDED

117

were fabricated using a larger aggregate microconcrete and a deformed model reinforcing steel (PCA designation D-1), which was tied in a 1.0-inch square mesh to give the same percentage reinforcement as was used in the smaller models. Tables I and II below give the concrete and reinforcing properties for the 1-in. and 3-in. thick wall models.

TABLE I

CONCRETE PROPERTIES FOR SCALE MODELS

Property	1-in. thick wall models	3-in. thick wall models
Ultimate compressive strength, f_c'	2500 - 3300 psi	2850 - 3500 psi
Tensile strength, f_t	300 - 420 psi	430 psi
Modulus of elasticity, E	2.3 - 2.6 x 10^6 psi	2.6 - 2.9 x 10^6 psi

TABLE II

REINFORCING PROPERTIES FOR SCALE MODELS

Property	1-in. thick wall models	3-in. thick wall models
Wire diameter	0.042 in.	0.113 in.
Yield stress	42,700 psi	42,400 psi
Ultimate tensile strength	53,100 psi	50,000 psi
Modulus of elasticity	25.6 x 10^6 psi	28.5 x 10^6 psi
Elongation	4 percent	13.1 percent

118

Figure 3 shows a 1/10-scale structure during construction. The base and first story have been cast and forms stripped and the second-story reinforcement and inside forms are in place.
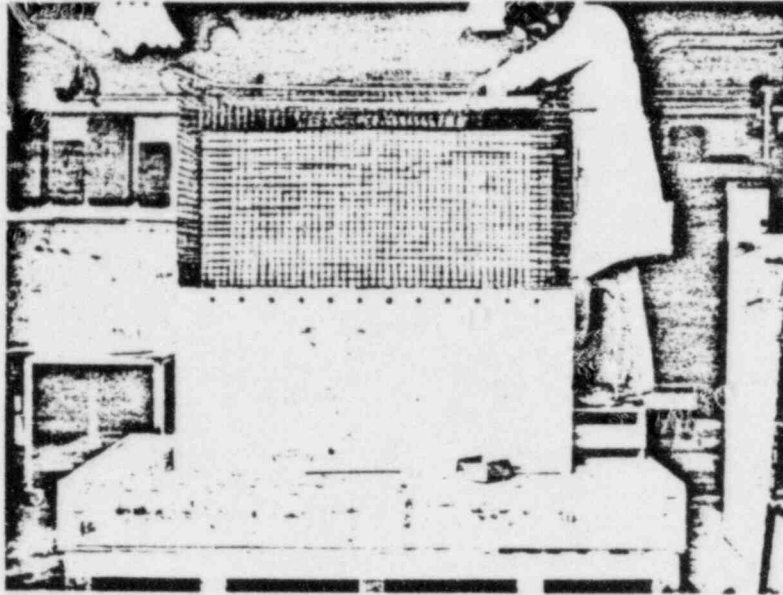
Fig. 3. View of a two-story, 1/10-scale model
structure under construction.

PRELIMINARY TESTS

Four, single-story, 1/30-scale models of the diesel generator building were statically tested to failure under both monotonic and cyclic load conditions. These tests were conducted using a horizontal, hydraulic testing machine. Models were tested with the load applied either parallel to the longer dimension or parallel to the shorter dimension. The load was applied through a 1-inch-thick steel plate, which was rigidly clamped around the entire perimeter at the top of the wall. Figure 4 shows a structure failed by monotonic loading applied parallel to the end walls.

The purpose of these tests was to compare measured values of stiffness, cracking load, and ultimate load with the values obtained by calculation using material properties and geometry. Figure 5 shows the force vs deformation diagram for structure 3D-2 (shown in Fig. 4), which was tested monotonically. Table III compares measured and calculated results. These results are typical for all of the tests (both directions, and with monotonic and cyclic loading),

and we conclude that the usual computational methods give good predictions for the cracking and ultimate strengths, but they predict structural stiffnesses that are much larger than the measured values.* Stiffness is very important in the dynamic analysis and, hence, this discrepancy is being investigated in additional static and dynamic tests.
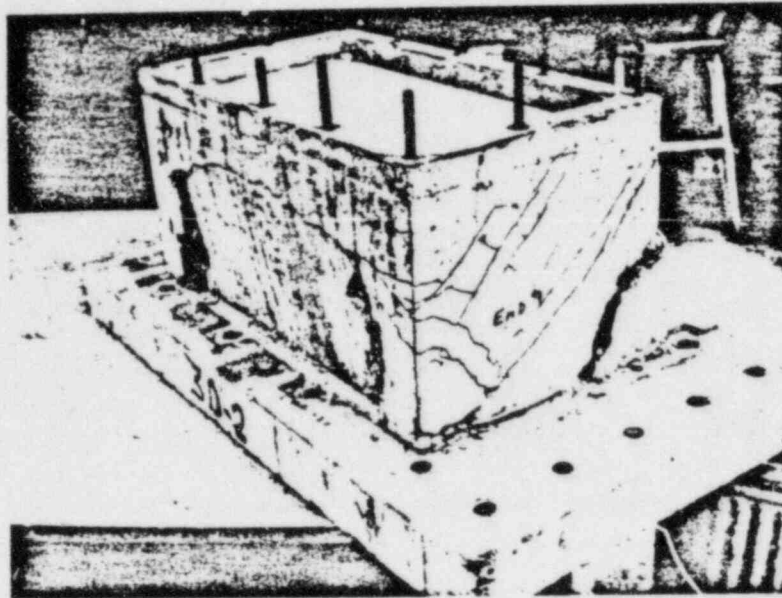
Fig. 4. Structure failed by monotonic load applied
parallel to the end walls.

---

* The stiffnesses (K) were computed assuming that the entire concrete cross section was uncracked. Both flexural and shear effects were considered in computing the initial stiffnesses. The "effective" shear area was based on the shape and size of the concrete cross section. The initial stiffness K is computed using the relationship:

$$K = \frac{GA_e}{h}\left(\frac{\alpha}{4 + \alpha}\right)$$

where

G = the concrete shear modulus;
h = the story height;
A_e = the effective shear area;
α = $12\ EI/GA_e h^2$;
E = the concrete elastic modulus; and
I = the section moment of inertia.

120

$K = 0.54 \times 10^6$ lb/in

$P_{ULT} = 8940$ lb

$U_{ULT} = 0.114$ in.

$P_{CR} = 5210$ lb

SPECIMEN No. 3D-2
TRANSVERSE LOAD

$U_{CR} = 0.0096$
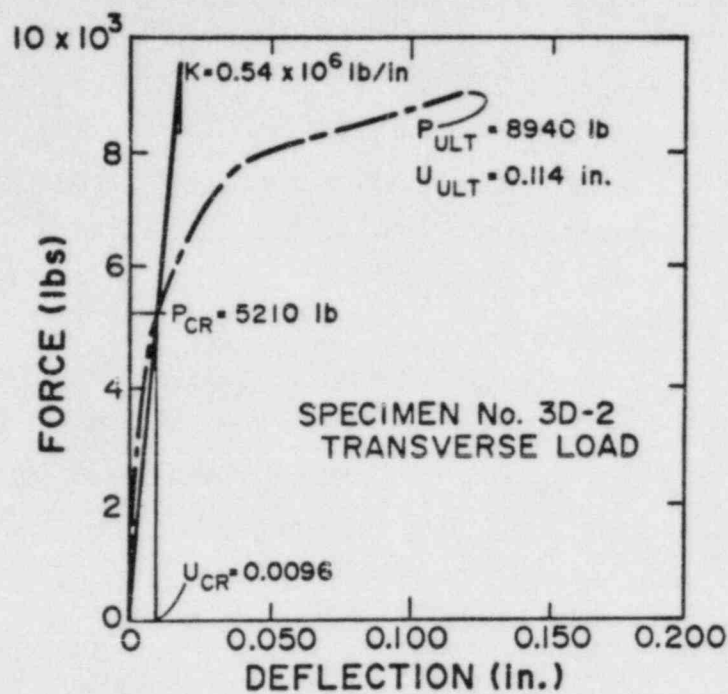
STATIC LOAD-DEFLECTION CURVE

Fig. 5. Force-deformation diagram for structure 3D-2.

TABLE III

COMPARISON OF CALCULATED AND MEASURED PROPERTIES
1/30-SCALE MODEL (3D-2)

Structural Property	Computed value	Measured Value
P_c - cracking load; lbs	6900	5210
P_{ult} - ultimate load; lbs	9040	8940
K - stiffness; lb/in. x 10^6	2.1	0.54

An investigation of the effects of aging and drying times on these models has also been carried out. Seven additional single-story, 1/30-scale models were statically tested after drying times from less than 1 hour (tested immediately after removal from the 100% humidity chamber) to 48 weeks. The data from these tests were plotted so that both tangent and secant modulus could be evaluated at various load levels. There was no apparent correlation between

121

measured stiffness and drying time[*]; however, a plot of stiffness, as measured by secant modulus, vs load level as shown in Fig. 6 is informative. The measured stiffness (K), taken as the zero load secant modulus (1.6×10^6 lbs/in.) is in better agreement with the computed value of 3.07×10^6 lbs/in.[**] Clearly under increasing load level the stiffness degradation indicates a measure of damage.

The difference between observed initial stiffnesses in these experiments and the computed uncracked stiffness is disturbing and an effort is currently underway to resolve the reasons for these differences. This effort includes reexamination of our scale modeling theory and the use of microconcrete, the

Secant Modulus vs Load
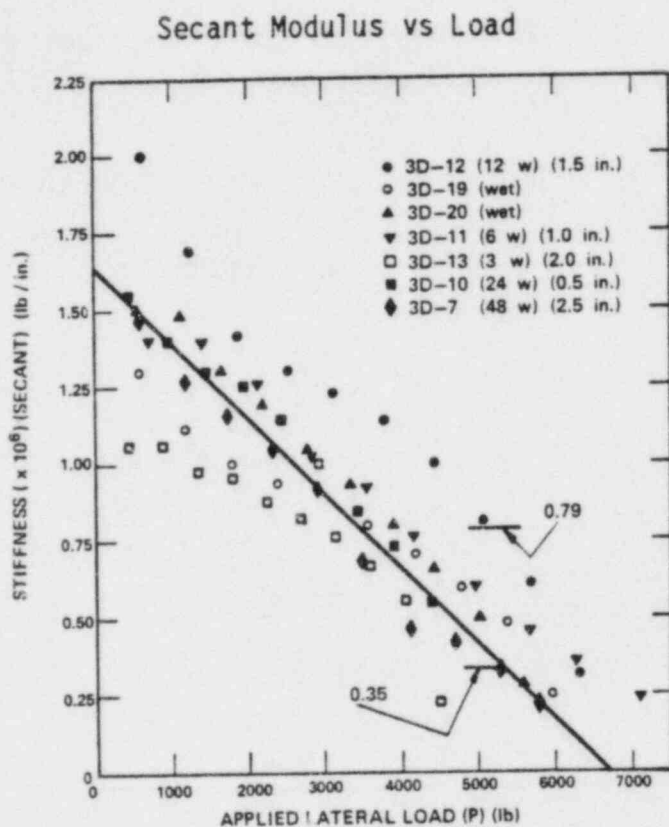
Fig. 6. Variation in secant modulus (Measured K)

---

[*] The measured stiffnesses of both structures tested with less than 1 hr. drying time (0.59×10^6 and 0.50×10^6 lbs/in. at 5000 lb load) fall between the values measured for structures tested with drying times of 48 weeks (0.35×10^6 lbs/in. at 5000 lbs load) and 12 weeks (0.79×10^6 lbs/in. at 5000 lb load).

[**] Computed using the average property value (E) of the models. E taken as $57000\sqrt{f_c'}$ average = 2.9×10^6 psi.

testing procedure, the test data itself, and the analyses and formulas used. Also a part of the difference between zero load stiffness and the computed value of stiffness may be accounted for by the difference between the actual boundary conditions during tests and the assumption of perfect rigidity; this possibility is currently being investigated. It is important to know the appropriate stiffness (K) to be used in dynamic response calculations.

Another obvious approach to the determination of effective stiffness involves dynamic testing of the structure of interest and the calculation of effective stiffness (K) from measured modal frequency. Two single-story, 1/30-scale models were used for this purpose.

Figure 7 shows a model mounted on the shake table ready for test in the transverse direction. Numerous accelerometer and displacement transducers were monitored during these tests, but the essential data were:

$\ddot{Y}(t)$ - the acceleration-time history of the input (base) motion, and

$\ddot{X}(t)$ - the acceleration-time history of the response motion at the roof level.

The modal frequency is measured as follows: The structure is subject to a base acceleration $(\ddot{Y})$ signal which is a properly scaled version of the 1940 El Centro N-S acceleration record. Both the input signal $\ddot{Y}(t)$, and the response signal $\ddot{X}(t)$ are recorded and the transfer function, $\ddot{X}(t)/\ddot{Y}(t)$, is computed.
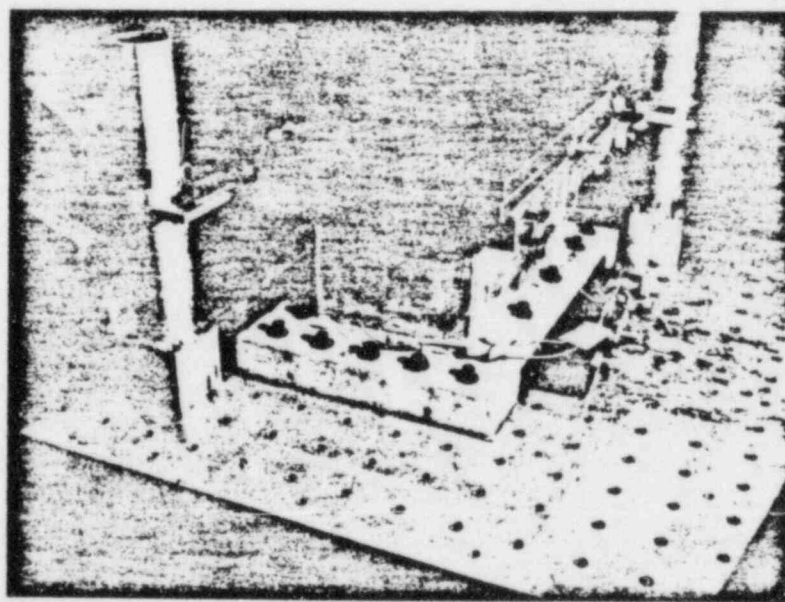
Fig. 7. A single-story, 1/30-scale structure mounted on shake table at Los Alamos.

123

The modal frequency is obtained from the transfer function presented in the phase and amplitude plots as shown in Fig. 8.

To compute the effective stiffness (K) from this dynamic test data, it is necessary to measure the modal frequency (as explained in the previous paragraph) using the same structure, but with different amounts of mass added to the structure. This model was tested at low acceleration levels under three conditions: (1) no mass added to the structure, (2) approximately 130 lbs added, and (3) approximately 230 lbs added. Mass was added by clamping steel plates to the top of the structure. Figure 7 shows the structure with 231 lbs of weight added.
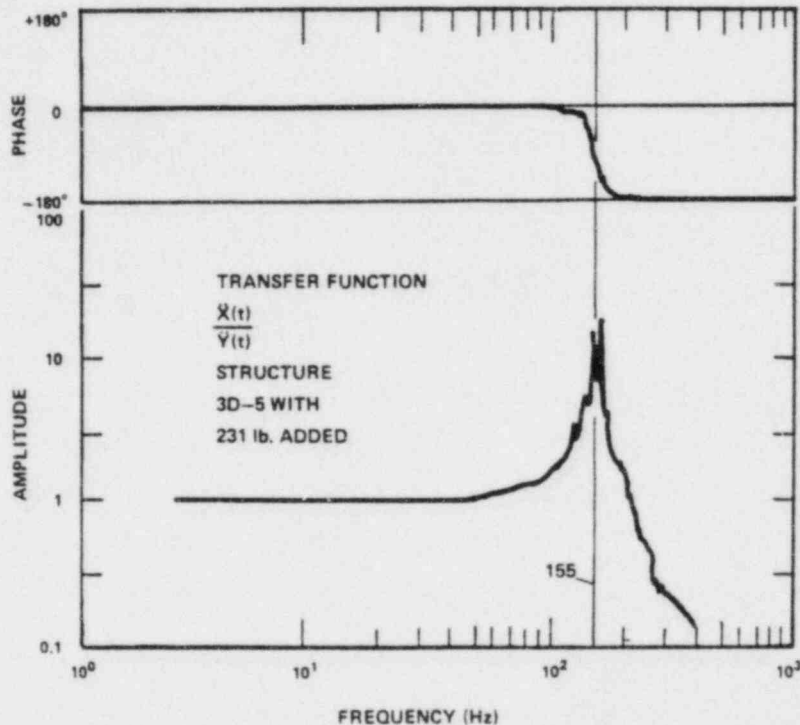
Fig. 8. Transfer functions.

Using the measured modal frequencies from two tests in which different amounts of mass $\left(M_A\right)$ were added to the structure, it is possible to eliminate the effective distributed mass of the structure $\left(M_0\right)$ from the relationship between modal frequency (ω), total mass $\left(M_T\right)$ and effective stiffness (K), thus:

$$K = \omega_0^2 \, M_0 = \omega_T^2 \left(M_0 + M_{ADDED}\right)$$

or

$$M_0 = M_{ADDED} / \left[\left(\omega_0/\omega_T\right)^2 - 1\right]$$

124

in which

ω_0 = the measured modal frequency with no added mass;
ω_T = the measured modal frequency with a given amount of mass added;
M_{ADDED} = the amount of mass added.

By substituting the second equation back into the first we can compute the structure's stiffness (K) from the data without the necessity of deciding upon the lumped mass equivalent of the structure's distributed mass. The stiffnesses obtained using the above method on the two single-story, 1/30-scale models are:

$K = 0.62 \times 10^6$ lbs/in (Model 3D-5, 231 lbs added);
$K = 0.69 \times 10^6$ lbs/in (Model 3D-5, 130 lbs added); and
$K = 0.71 \times 10^6$ lbs/in (Model 3D-6, 231 lbs added).

These values suggest that even during low level dynamic tests the effective stiffness is closer to the value determined from static tests after severe damage, than it is to the value of stiffness calculated using the uncracked cross section formula.

SIMULATED SEISMIC TESTS OF TWO-STORY MODELS OF A DIESEL GENERATOR BUILDING

Three, two-story, 1/30-scale models were fabricated and tested on the Los Alamos National Laboratory (LANL) electrodynamic shake table (Fig. 9). Two, 1/10-scale, two-story structures were built at the LANL and transported to Construction Engineering Research Laboratory (CERL) located at Champaign, Illinois. Figure 10 shows a 1/10-scale model mounted on the servohydraulically driven table at CERL.

Except during some preliminary tests at low acceleration levels, lumped masses (steel plates) were added to these structures so that the 1/30-scale structure was a true 1/3-scale model of the 1/10-scale structure. Also, except during these low acceleration level preliminary tests, the excitation signal was a properly scaled version of the 1940 El Centro, N-S accelerogram.

A test sequence on one of these structures consisted of subjecting the structure to a series of frequency scaled earthquake signals of increasing peak amplitudes $\left(\ddot{Y}_{pk}\right)$. During each of these earthquake events, the structure's response was monitored by means of numerous accelerometers and displacement transducers. From these data it is possible to determine how the structural

125
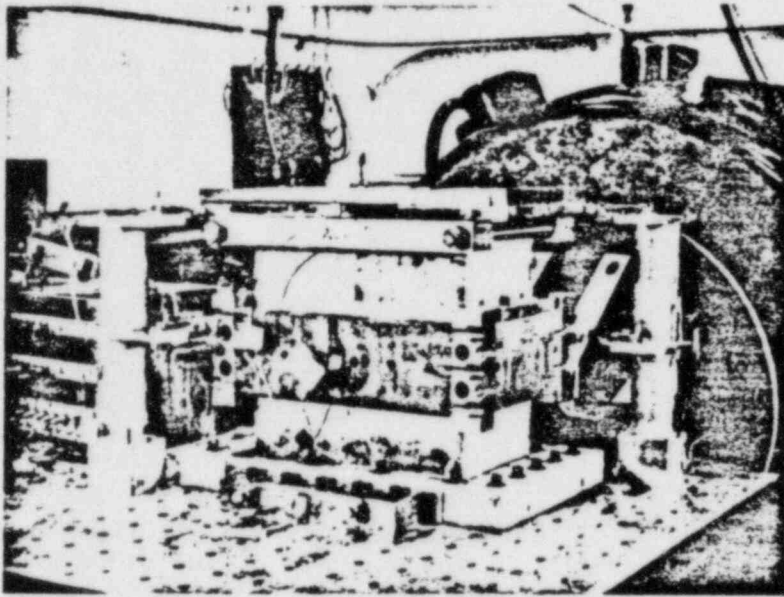
Fig. 9. A two-story, 1/30-scale structure mounted on shake table.
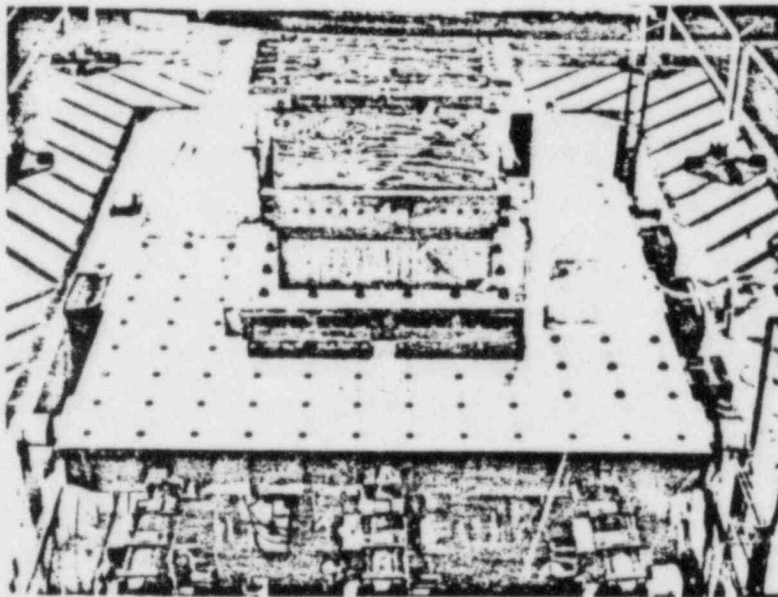
Fig. 10. A 1/10-scale structure mounted on the shake table at CERL.

properties (stiffness, K; damping, ζ) vary with earthquake magnitudes (as measured by peak acceleration, $\ddot{Y}_{pk}$). It is also possible to determine the acceleration amplitude $\left(\ddot{Y}_{pk}\right)$ necessary to produce nonlinear response and failure of the structure. Results obtained from the two sizes of structures (1/30-scale and 1/10-scale) can be compared thus providing a partial check of the scaling. Finally, the results obtained can be projected to predict proto-type behavior by utilizing the appropriate scaling laws.

The effect of earthquake intensity $\left(\ddot{Y}_{pk}\right)$ on structural stiffness (which is, in turn, related to modal frequency) is presented in Figs. 11 and 12. In these plots the first mode frequency, f_1, measured during a particular simulated seismic test, is plotted vs the peak acceleration level $\left(\ddot{Y}_{pk}\right)$ obtained during that test.*

Figure 11 shows the data taken during FY 83 from tests on two 1/30-scale models (3D-10-2 and 3D-11-2) and one 1/10-scale model (CERL≠1). All of these data can be plotted on the same sheet since under these test conditions (appropriate masses added to each model and the base motion properly frequency and acceleration scaled) the 1/30-scale structure is a 1/3-scale model of the 1/10-scale structure and both structures are models of the assumed prototype. In addition, when plotted in this manner, prototype behavior, predicted by each model, is shown directly.

Figure 12 shows the data taken during FY 84 from tests on an additional 1/30-scale model (3D-12-2) and on a second 1/10-scale model (CERL≠2). These tests differed from the FY 83 tests (Fig. 10) in two respects: First, the attached masses were adjusted slightly (mass added to the second-story was decreased) to better represent the equivalent distributed mass. Second, the drive signal ($\ddot{Y}$ vs t) used in the 1/30-scale test was refined to better match the drive signal used in the 1/10-scale test. As can be seen (by comparing Figs. 11 and 12) these two modifications had only minor effect and all of the data could have been plotted on a single sheet.

---

* The modal frequencies were determined from transfer function plots. In these tests using a properly time (or frequency) scaled El Centro accelerogram, the structure is so stiff relative to the frequency content of the input that the second mode response is very small and as a result the second mode frequency cannot be determined with any precision. For the same reason, the second mode response is of little practical importance; therefore, only first mode frequencies are considered.

Fig. 11

Variation in first mode frequency
for the FY 83 model tests.

Fig. 12

Variation in first mode frequency
for the FY 83 model tests

NOTES:

For 1/30 Scale, N_f = 1/11.8, $N_{\ddot{y}}$ = 1/4.6
For 1/10 Scale, N_f = 1/6.8, $N_{\ddot{y}}$ = 1/4.6

EXAMPLE:

At Point 'A' CERL Test No. 1

f_1 = 2.6 x 6.8 = 17.7 Hz
$\ddot{Y}_{pk}$= 3.5 x 4.6 = 16 g

NOTES:

For 1/30 Scale, N_f = 1/11.8, $N_{\ddot{y}}$ = 1/4.6
For 1/10 Scale, N_f = 1/6.8, $N_{\ddot{y}}$ = 1/4.6

EXAMPLE:

At Point 'B' CERL Test No. 2

f_1 = 3.7 x 6.8 = 25.2 Hz
$\ddot{Y}_{pk}$= 2.5 x 4.6 = 11.5g

The solid lines shown in Figs. 11 and 12 are not "best fit" curves for the
data points shown. Rather, they were added to suggest the following design
application of these data:

(1) All models suggest that the assumed prototype diesel generator
    building will have a virgin first mode frequency of between 7.8 and
    8.0 Hz:

128

(2) When subjected to the El Centro N-S earthquake of peak magnitude up to 0.2 g the prototype will respond with this virgin first mode frequency;

(3) If subjected to a peak intensity of greater than 0.2 g's, the prototypes will respond with a reduced effective first mode frequency. The greater the amplitude the lower the effective modal frequency. This implies that the floor response spectra for a given acceleration-vs-time excitation (in this case the El Centro, N-S) will vary with peak amplitude of input which is contrary to the usual linear design assumption;

(4) Inspection of the various models indicate that these reductions in modal frequency occur <u>without</u> visible signs of cracking;

(5) Low level, wide frequency band diagnostic tests, which were performed between the seismic tests, indicate that any reduction in the effective modal frequency is permanent; and

(6) The assumed prototype diesel generator building would not fail (cracking and breaking loose from the foundation at the lower walls) until the amplitude exceeded 2.5 g's.

Figure 13 illustrates the crack pattern on one of the lower-story end walls of a model after the test. The orientation of the cracks is consistent with the predominant development of shear stress in the end wall. Cracks did not appear until the seismic event which caused failure (wall-base slab separation) was applied. This diagonal crack pattern was not visible in the 1/30-scale models, probably because of the lower ultimate elongation of the reinforcement used in the 1/30-scale models, (4% for 1/30-scale, 13.1% for 1/10-scale).

The quantification of damping associated with the response of structures subject to transient loads which produce nonlinear and/or inelastic responses has proved to be a very difficult problem. This is especially true for reinforced concrete structures for which the exact damping mechanism is unknown (i.e., is damping viscous, structural, Coulomb, or perhaps a combination of all three?).
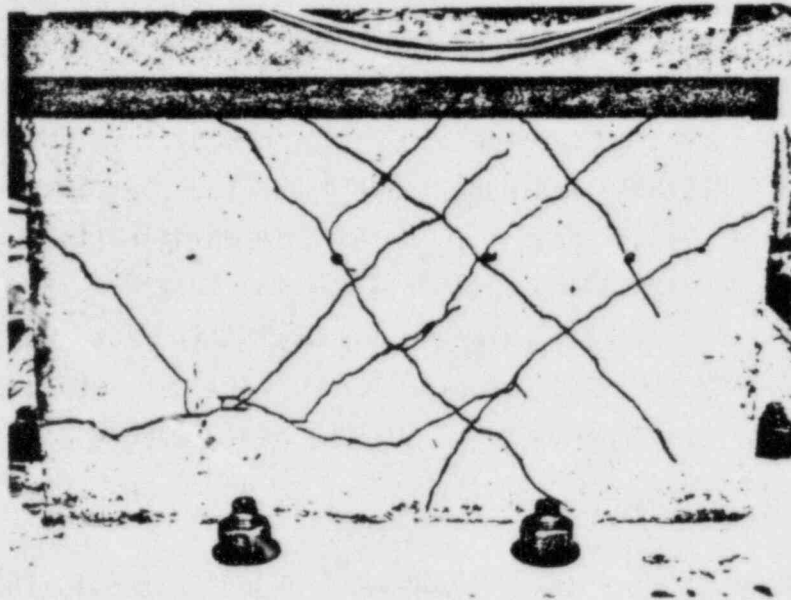
Fig. 13. Crack pattern in lower-story end wall of the
1/10-scale structure (CERL #1).

Since one of the objectives of this program is to improve our ability to
analyze structures loaded into their inelastic region, we have attempted to
characterize and quantify damping in a way which will be most useful in the
analysis process. Therefore, since most analysis methods utilize response
spectra and computations which involve equivalent viscous damping ratios, (ζ),
these tools and concepts are used in our evaluation and quantification of
damping.

Two methods of quantifying damping have been used. The first method will
be referred to as the "Floor Response Spectra (FRS) Matching Technique" and
the second method as the "Transfer Function Analysis Technique (TFAT)."

The "FRS Matching Technique" involves the use of a computer model and
iterating with different values of damping ratio (ζ) until the computer
generated FRS 'match' the FRS generated from response data measured during a
test at a given input acceleration level $\left(Y_{pk}\right)$.

---

* The use of and assigning values for 'equivalent viscous damping ratios (ζ)',
should not be taken to imply that the damping mechanism is viscous. Rather it
is only an attempt to assign an appropriate value to a term that is needed in
response spectra and other methods of analysis.

The "Transfer Function Analysis Technique" involves plotting the Fourier transform (FT) of the response acceleration, $\ddot{X}_1$ or $\ddot{X}_2$, at a given input acceleration level $\left(\ddot{Y}_{pk}\right)$. The real part of this FT is then examined to determine the damping ratio, ζ.

Both of these methods are discussed in detail in the project report to be issued in FY 85; only the results of these computations will be presented here. In Fig. 14 the computed values of damping ratio, ζ, from tests of these models are plotted vs the peak acceleration level $\left(\ddot{Y}_{pk}\right)$ of the test for which that value of damping ratio applies. All of the values, except the two points indicated as 'FRS Matching Tech', were determined using the 'Transfer Function Analysis Technique'. There is considerable scatter in the data, but the authors believe that the following observations are justified:

(1) These three models respond to inputs with magnitude of less than 4.6 g as if they have equivalent viscous damping ratios of between 5.5 and 8 ; and

(2) For input magnitudes between 4.6 and 9 g's the effective viscous damping tends to increase.

(3) At input magnitudes greater than 9'gs (where all of the models are known to be close to failure) the damping is uncertain.

The next important issue concerning damping is whether or not the damping effects are distorted in the models as compared to the prototype, and, if so, how are the effective damping ratios measured in these models related to the effective damping in the prototype As demonstrated in Ref. 4, we would expect that damping forces are distorted, between the 1/30 and the 1/10-scale models, only if the damping mechanism is viscous. Analysis of the data plotted in Fig. 14, confirms that the damping mechanism is not viscous and, hence, the values of equivalent damping ratios determined from these model tests are expected to apply to the prototype structure.*

----

* The details of this analysis are included in the project report to be issued during FY 85.

131

In connection with these observations, it is important to note that, since in both models (1/30 and 1/10-scale) acceleration is scaled by a factor of 4 6, the region of noticeably increasing damping (region A - B in Fig. 14) corresponds to input amplitude to the prototype in excess of 1 g peak acceleration.
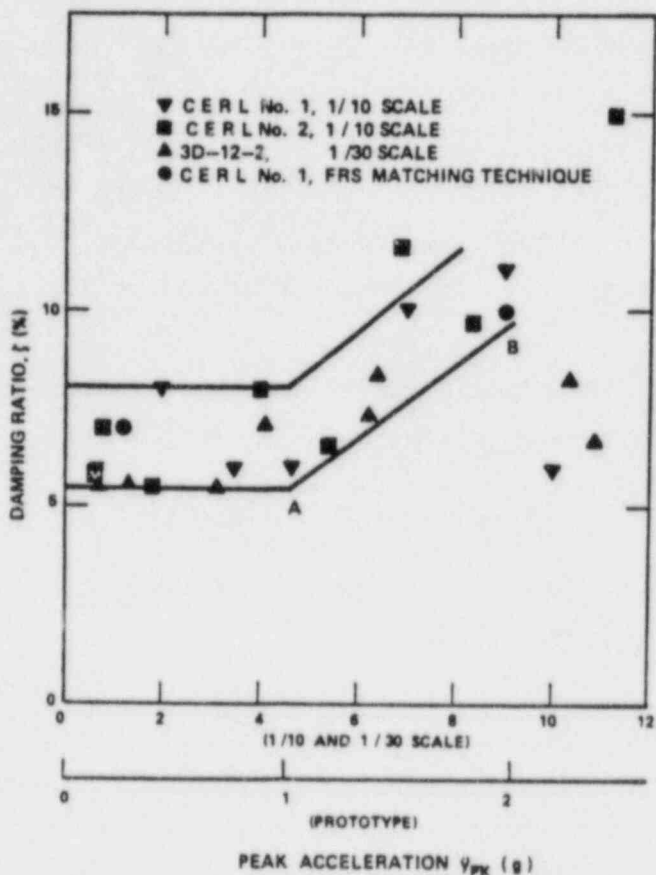
Fig. 14. Measured damping ratios.

A 1/5-scale model of the diesel generator building has been designed and will be constructed and tested during FY 85. The larger size structure (6" thick walls, see Fig. 2 for other dimensions) will give additional data for the evaluation of scaling effects on both stiffness and damping.

CONCLUSIONS

The results from this program to-date have indicated a number of potentially significant implications regarding Seismic Category-I shear wall structures. First, these structures have very large ultimate seismic capacities. Second, for input amplitudes as large as 0.2 g peak (El Centro, N-S) the prototype diesel generator building appears to respond linearly. However, in making the

usual linear analyses it is important to use the correct structural stiffness if the modal frequencies are to be accurately predicted. Third, in the range of practical interest (up to 1 g peak on the prototype) the effective equivalent viscous dumping ratio appears to be between 5.5 and 8%.

REFERENCES

1. Endebrock, E. G., Dove, R. C., and Anderson, C. A., "Margins to Failure-- Category-I Structures Program: Background and Experimental Program Plan," Los Alamos National Laboratory report LA-9030-MS, NUREG 2347, September, 1981.

2. Endebrock, E.G. and Dove, R. C., "Static and Dynamic Tests on Reinforced Concrete Shear Walls at High Loads," Proceedings, International Meeting on Thermal Nuclear Reactor Safety, NUREG/CP-0027, August, 1982, Vol. 3, pp. 2083-2091.

3. Endebrock, E. G. and Dove, R. C., "Nonlinear Seismic Response of Small-Scale Reinforced Concrete Shear Wall Structures," Transactions, 7th International Conference on Structural Mechanics in Reactor Technology, August, 1983, Vol. K(a), paper no. K4/1, pp. 259-266.

4. Anderson, C. A., Bennett, J. G. and Dove, R.C., "Seismic Category-I Structures Program: Current Status and Program Plan for FY 84 - FY 88," Appendix A, Los Alamos National Laboratory report to be published.

Joel G. Bennett,

Gerald W. Fly,

William E. Baker

Los Alamos National Laboratory
Los Alamos, New Mexico

INTRODUCTION

The Steel Containment Buckling program is in its fourth phase of work directed at the evaluation of the effects of the structural failure mode of steel containments when the membrane stresses are compressive. The structural failure mode for this state of stress is instability or buckling. Structural failure from buckling can result in large shell displacements that can potentially cause a loss-of-containment failure by the mechanisms of material splitting or tearing, seal warpage, leakage or seal failure around penetrations, or shell puncture from nearby hard points. The program to date has investigated (1) the effect on overall buckling capacity of the ASME area replacement method for reinforcing around circular penetrations, (2) a set of benchmark experiments on ring-stiffened shells having reinforced and framed penetrations, (3) large and small scale experiments on knuckle region buckling from internal pressure and post-buckling behavior to failure for vessel heads having torispherical geometries, and (4) buckling under time-dependent loadings (dynamic buckling). The first two investigations are complete, the knuckle buckling experimental efforts are complete with data analysis and reporting in progress, and the dynamic buckling experimental and analytical work is in progress. The results of the first two investigations have been reported in Refs. 1-4 as well as at previous LWR meetings and will not be summarized here.

KNUCKLE REGION BUCKLING CONCERN

After the overpressure condition occurred at Three Mile Island, some concern was raised as to the margin-to-failure above design for reactors with nonspherical head geometries. Some of these torispherical or ellipsoidal heads can undergo circumferential buckling in the torus region of the head when

subjected to internal pressure. This buckling causes large local strains and could therefore cause premature rupture of the head. Los Alamos National Laboratory has undertaken a combined analytical and experimental program to determine the margin-to-failure for such vessels. This program investigates both the bifurcation pressure and the post-buckling behavior of geometrically similar scale models of reactor heads. Both small-scale (1/64) and large-scale (1/8) models were tested and computer models of each were used to predict the buckling pressures and to examine the sensitivity of the shells to geometric, material, and fabrication variances. This information can then be used to confidently predict the margin-to-failure of existing structures.

KNUCKLE BUCKLING EXPERIMENTAL PROGRAM

The experimental program was two-fold. At Los Alamos, small-scale (2-ft. diam) heads were fabricated and tested, while a joint project between Los Alamos and several industry sponsors was put together to test two large-scale vessels at Chicago Bridge and Iron's Plainfield Research Center. The series of small-scale heads tested at Los Alamos formed a baseline for both the large scale tests and for the analytical modeling. These heads were 2 feet in diameter with a D/t ratio of about 750 and an as_ect ratio (D/H) of 4:1. The heads were hydraulically pressurized to determine both the buckling pressure and the rupture pressure. The displacement of the head was measured with a set of precision linear potentiometers mounted on an arm at various meridional positions. The arm was swept around the shell by a computer-controlled stepping-motor system and data at each meridional position was taken at three degree increments around the circumference by the computer. Thus both meridional and circumferential profiles of the head could be generated as a function of pressure. Strain gages both inside and outside the head measured local strains. This information provided not only corroboration of the displacement data but also gave a more precise indication of buckling.

SMALL SCALE TESTS OF SPUN HEADS AND SENSITIVITY ANALYSES

The small-scale tests were performed using spun steel heads. Figure 1 illustrates the head geometry and data acquisition. The spinning process caused several problems in modeling the tests. First there were large (50%)

135
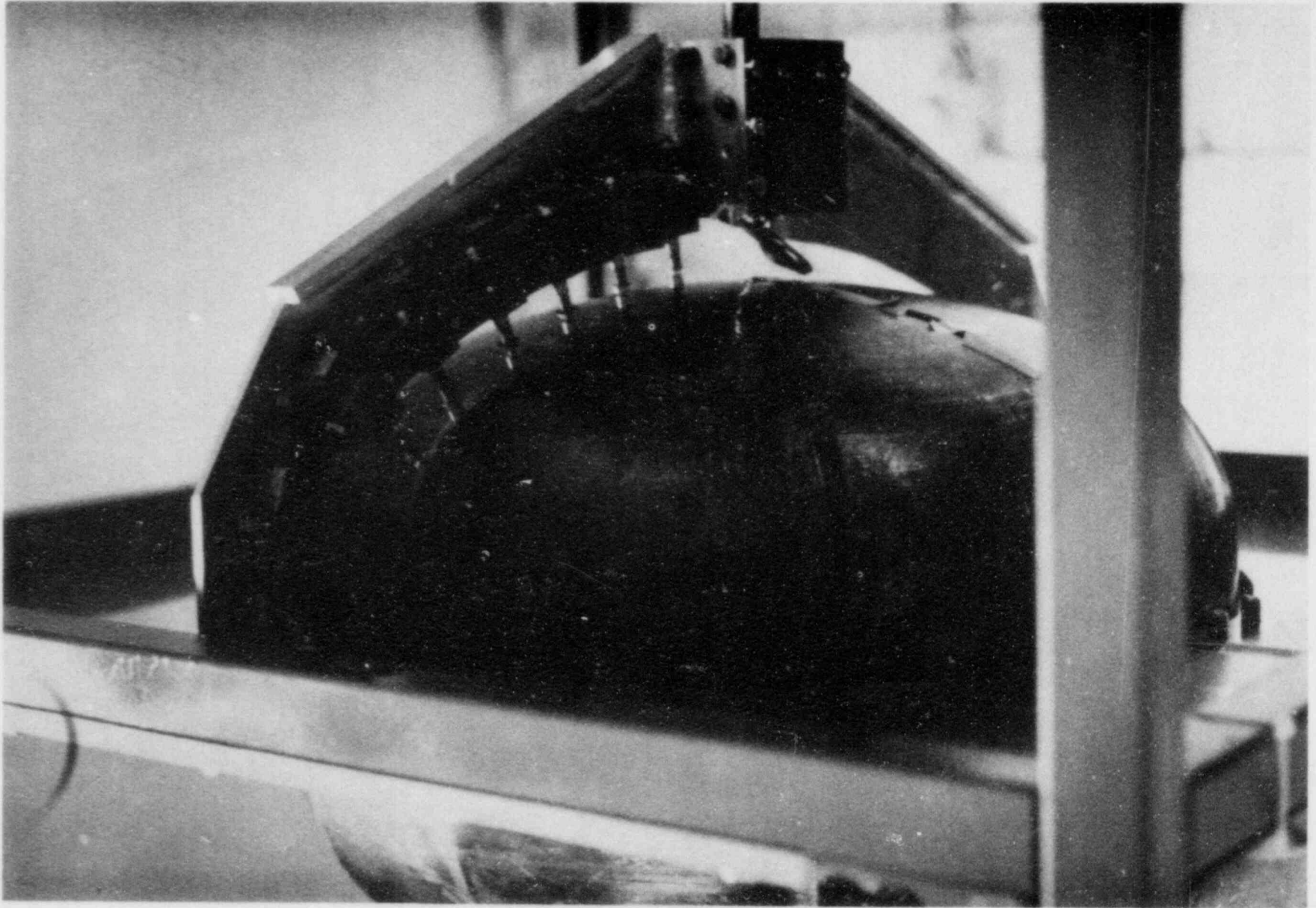
Fig. 1. Small scale knuckle buckling test and instrumentation.

thickness variations in the meridional direction and significant (20%) thickness variations in the circumferential direction. While the meridional variations could be directly modeled, the circumferential variations could not since the model is assumed to be axisymmetric. Although the heads were annealed to minimize the material property variations, there were still large differences both in the yield point and the tangent modulus from point to point. This was true both in the meridional direction as well as in the circumferential direction. Finally there were both large and small wavelength imperfections in the shells. Very detailed models were required to analyze these imperfections in the meridional direction but due to the axisymmetric model requirement, circumferentially oriented imperfections could not be adequately modeled. The relative importance of these problems caused by spinning can be determined by looking at the sensitivity analyses that were run.

These sensitivity analyses looked at the effects of thickness, yield point, tangent modulus, overall geometry, and imperfection wavelength and amplitude on bifurcation pressure. Because buckling occurs after most of the knuckle region has become plastic in compression, the buckling strength is essentially a linear function of shell thickness. As far as material properties are concerned, buckling strength tends to be most closely related to the stress at about 1% strain at the center of the knuckle region. Due to the geometry of the shells, most of the knuckle region has yielded at this point and the onset of buckling is imminent. Small variations in tangent modulus seem unimportant as long as a modulus representative of steel is chosen. This is true up to moduli as high as E/6. Buckling strength is then essentially linearly related to the 1% yield point. On the other hand, the shells are very sensitive to overall geometry variations because they directly affect the percentage of the knuckle region that undergoes plastic deformation. Since the elastic buckling pressure is almost three times the plastic buckling pressure, the extent of the plastic deformation zone is crucial to the buckling process. Small amplitude imperfections have little effect on buckling but clearly as the amplitude increases to the point where there is some reverse curvature, the structure is significantly weakened. For a wavelength of 10 degrees this amplitude is several material thicknesses. The critical imperfections are those which are not axisymmetric and these cannot currently be modeled, though some insight as to their behavior can be gained by looking at axisymmetric imperfections of similar amplitudes and wavelengths.

The predicted buckling pressures for the small models varied from 52 psi to 55 psi, while the experiments gave results from 42 psi to 46 psi for annealed shells. This variation is most likely attributable to circumferential variations in geometry and material properties. The predicted buckling pressures are somewhat low for a shell of the described geometry but this is because of the severe thinning of the snell in the knuckle region as a result of the spinning process. The buckles that formed all protruded outward and came in slowly. Buckles continued to form up to a pressure of about 110 psi and their wavelength was approximately the same as that predicted by the BOSOR5 model, though the full 39 waves predicted did not materialize. As the heads were pressurized beyond 110 psi the buckles began to disappear. The heads were pressurized to rupture which occurred at 140 psi to 160 psi. In all cases rupture occurred at the thinnest section that was at the base of the knuckle region. Rupture occurred at about 80% of the ultimate pressure of a hemisphereical shell with a thickness equal to the minimum thickness of each shell.

LARGE SCALE TESTS

The large-scale (16-ft diam) tests, jointly sponsored by Los Alamos and an industry consortium headed by the Pressure Vessel Research Council, looked at both scaling factors and the effect of field construction techniques on the buckling strength of the shells of a given geometry. Here both the material properties and the thickness were quite consistent throughout the shell, though there were clearly variations in yield point and ductility near the welds. However, the major variation was the imperfections caused by shrinkage of the welds in the knuckle region. The as-fabricated shells dipped inward at the welds by as much as several material thicknesses. These shells were 3/16 in. and 1/4 in. thick nominally with D/T ratios of 1024 and 768 respectively. The 1/4 in. shell had significantly less variation in geometry than did the 3/16 in. shell. The improved uniformity in material properties and thickness makes these larger heads somewhat easier to model. However the imperfections are the key to properly modeling these heads and since they are nonaxisymmetric in nature, they cannot currently be properly represented by the axisymmetric model.

The character of the buckling in the first large shell was much different than that of the small shells. The predicted buckling pressure for the 3/16 in. shell was 75 psi, but at 58 psi, a buckle snapped inward with a loud

138

bang. The buckle occurred at a weld that was severely pulled in due to shrinkage. Several other buckles occurred in the same manner but as the pressure increased beyond about 75 psi the buckling character changed. The later buckles grew slowly outward similar to those in the small-scale tests. Buckles continued to form up to a pressure of 138 psi. Above 150 psi the buckles began to pull out slightly. Pressurization continued up to rupture at 229 psi. Failure occurred in one of the knuckle plates at a point where an alignment bracket had been welded on for fit up.

The imperfection amplitude of the second head was significantly less and its buckling response was correspondingly different. The predicted buckling pressure for the second head was 102 psi. While many waves were apparent and had grown out as much as 1/2 in. at pressures as low as 75 psi, no reversal in strain nor drop in pressure occurred until approximately 105 psi. At this point, the circumferential strains in the knuckle region indicated the first bifurcation pressure. Though waves were visibly apparent at lower pressures, they were not true buckles. The buckles all grew slowly outward similar to the small scale tests. Buckles continued to form up to 234 psi. Above 260 psi the buckles began to pull out slightly. Rupture occurred in the spherical cap at 332 psi next to the weld seam.

The difference in behavior of the two shells is due to the difference in amplitude of the imperfections at the weld seams. The behavior of the second head demonstrates the validity of the scaling while the behavior of the first large scale head indicates the sensitivity to large amplitude imperfections.

KNUCKLE BUCKLING STUDY SUMMARY

The complete results for the knuckle buckling experiments will be reported in detail in both NUREG reports and in the open literature. Although complete results are not yet available, two firm conclusions from this study can be stated.

(1) Buckling pressures can be predicted accurately if both the geometry and material properties are well characterized and they can be properly modeled.

(2) A large margin-to-failure by rupture ($\sim$ 2-4) exists above the buckling pressure for ductile materials.

We believe many useful results have been obtained and will be documented from these experiments including the only data for buckling of large fabricated

139

heads that can be used for verifying design recommendations and including data for benchmarking computer codes that purport to be able to model the post-buckling response.

DYNAMIC BUCKLING STUDY USING SEISMIC EXCITATION

One of the ultimate goals for this program is an assessment of the currently used design and safety analysis techniques for buckling under time-dependent loadings, commonly referred to as dynamic buckling. In reality and in particular under accident conditions such as an earthquake, the loading is time-dependent. The traditional method of evaluating buckling potential from such a loading is to use a freezing-in-time method of evaluation. The structure is analyzed using some method of dynamic analysis and the worst state of membrane compressive stress is identified during the response. Time is "frozen" at this point and this worst state of stress is evaluated for its buckling potential against a static buckling criterion.

Implicit in this procedure is that a separation of time scale (buckling period, response period, and loading period) exists. Analysis of the various time scales has shown that this assumption is not always true over all response frequency regimes for steel containment structures. Yet no experimental data is available for containment-like structures to allow a ready assessment of the method.

The approach to verifying the freezing-in-time analysis method requires both experimental and analytical efforts composed of three basic steps. First, static buckling criteria in the form of interaction curves for stresses similar to the expected dynamic stress field should be available for the structure of interest. In this program, we developed these curves by the experimental means shown in Fig. 2. Note that because the static buckling criteria are developed experimentally, effects of imperfections and material anomalies are accounted for automatically.

Second, these same shells are now excited on a shaker using a properly time-scaled seismic record as base motion input. The amplitude of the excitation is increased and the test is repeated until buckling occurs. This information is now compared directly with the predicted buckling amplitude value that is determined from the third step, a freezing-in-time analysis of the model that uses the experimentally recorded base motion for input. This direct
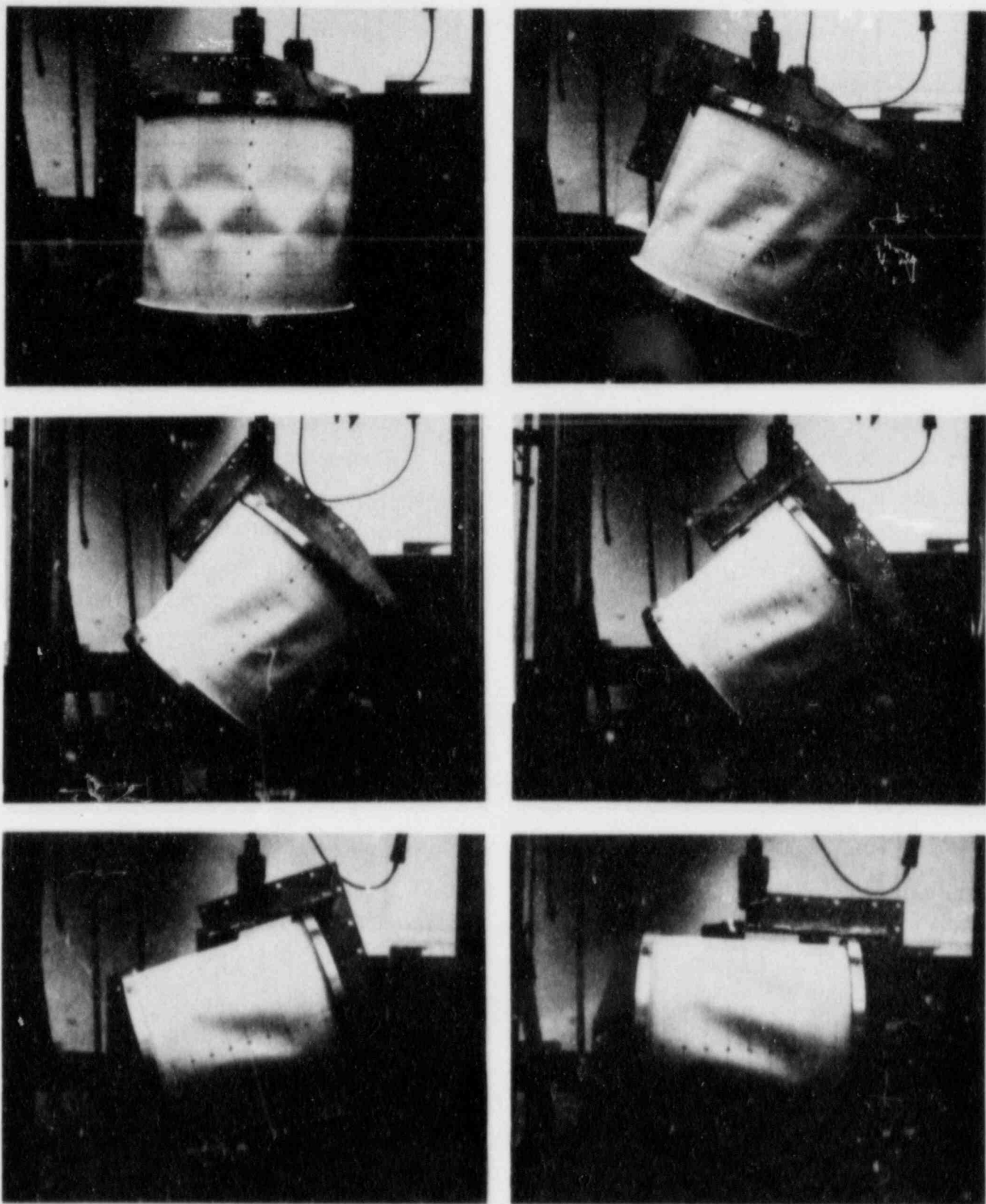
Fig. 2. Tests to determine static buckling interaction curves.

comparison along with the static buckling criteria allow the accuracy and adequacy of the method to be evaluated.

EXPERIMENTAL AND ANALYTICAL PROGRAM

Figure 3 illustrates the first and third steps described above. This figure shows that the results from both ring-stiffened and unstiffened shells generally fit a NASA recommended relationship when the membrane and maximum shear stress resultants are normalized by their critical values as determined from the tests shown in Fig. 2.

For step 3, a method for efficiently performing the freezing-in-time analysis had to be developed. We began with BOSOR-4, a well-known computer code for stress analysis of shells of revolution, which can carry out static stress analysis, bifurcation buckling analysis and vibration analysis. Using the information from the vibration analysis (i.e., mode shapes and frequencies), we developed a post processor to do a modal response analysis of the shell for a base input excitation. Then, using the El-Centro earthquake record, the response of the shell was computed for combined vertical and horizontal base motions (these can be shown to be composed of input harmonics of $n=0$ vertically and $n=1$ horizontally). By evaluating the maximum response (stress state) at a given meridional position and angle around the shell and plotting these maximum stress states on the static buckling interaction curves, the magnitude of an earthquake that would have a "frozen" stress state that will initiate buckling can be predicted. For example, Fig. 3 shows the normalized static buckling interaction curves determined experimentally and the predicted stress states around the shell from the analysis which used a 7.44 g horizontal and 2/3 7.44 g vertical properly time-scaled earthquake as input. (By the scaling laws, this input motion would correspond to 1 g for the actual structures.) As shown, the earthquake will have to be increased in magnitude by approximately 30% to initiate buckling by the freezing-in-time prediction method. Direct comparison with dynamic experiment is now possible.

As a side issue, it is imperative that if we are to pass judgement on the freezing-in-time analysis method by this means, we must have a verified analytical model. One method of verifying the model is to compare measured natural frequencies with the predictions. Figure 4 shows some of the comparisons we have made in verifying our analytical model. The results of such comparisons have been excellent to date.

142
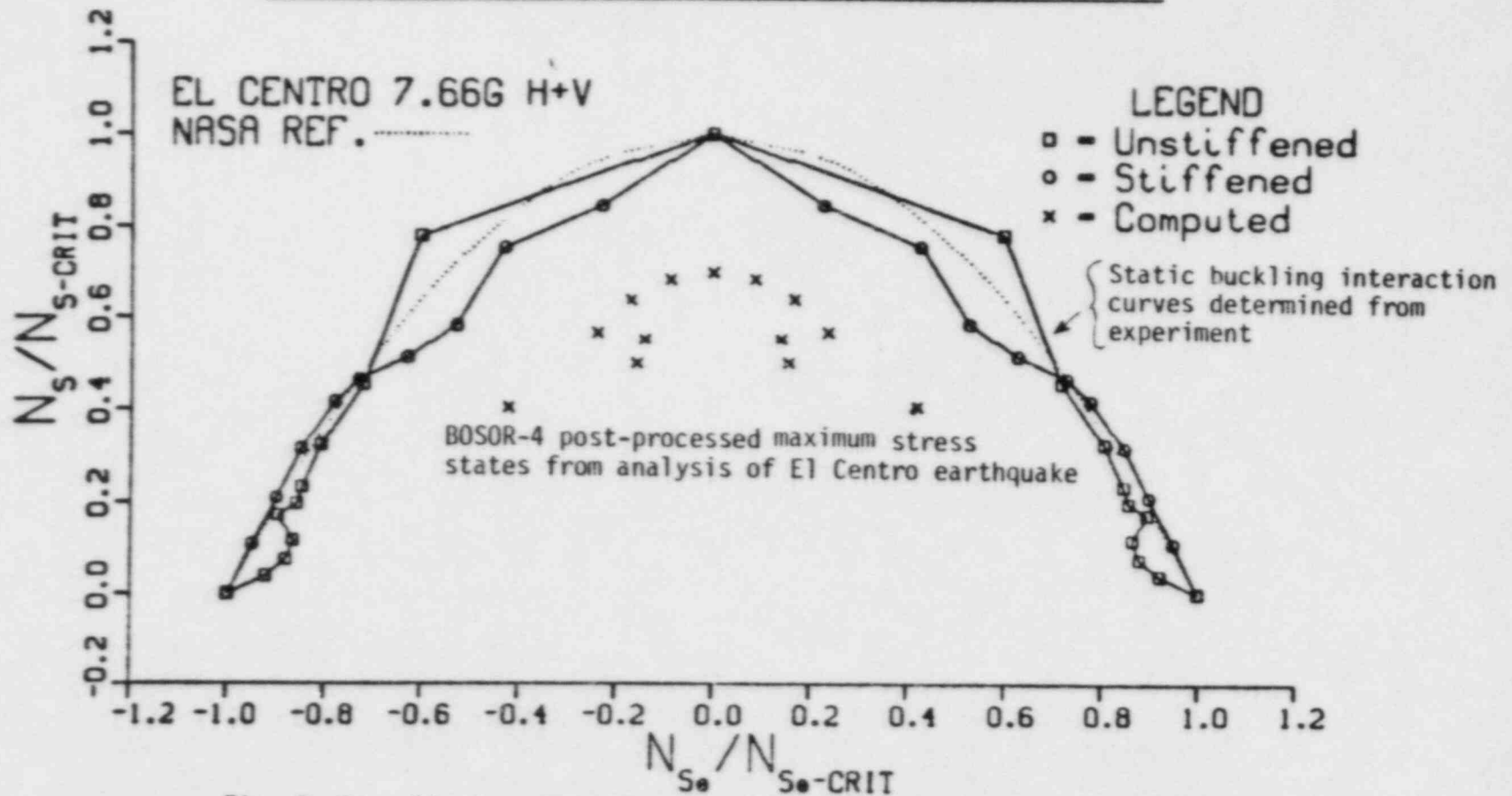
Fig. 3 Normalized meridional vs normalized shear stress to cause buckling and analysis prediction of maximum stress states from scaled El Centro earthquake.
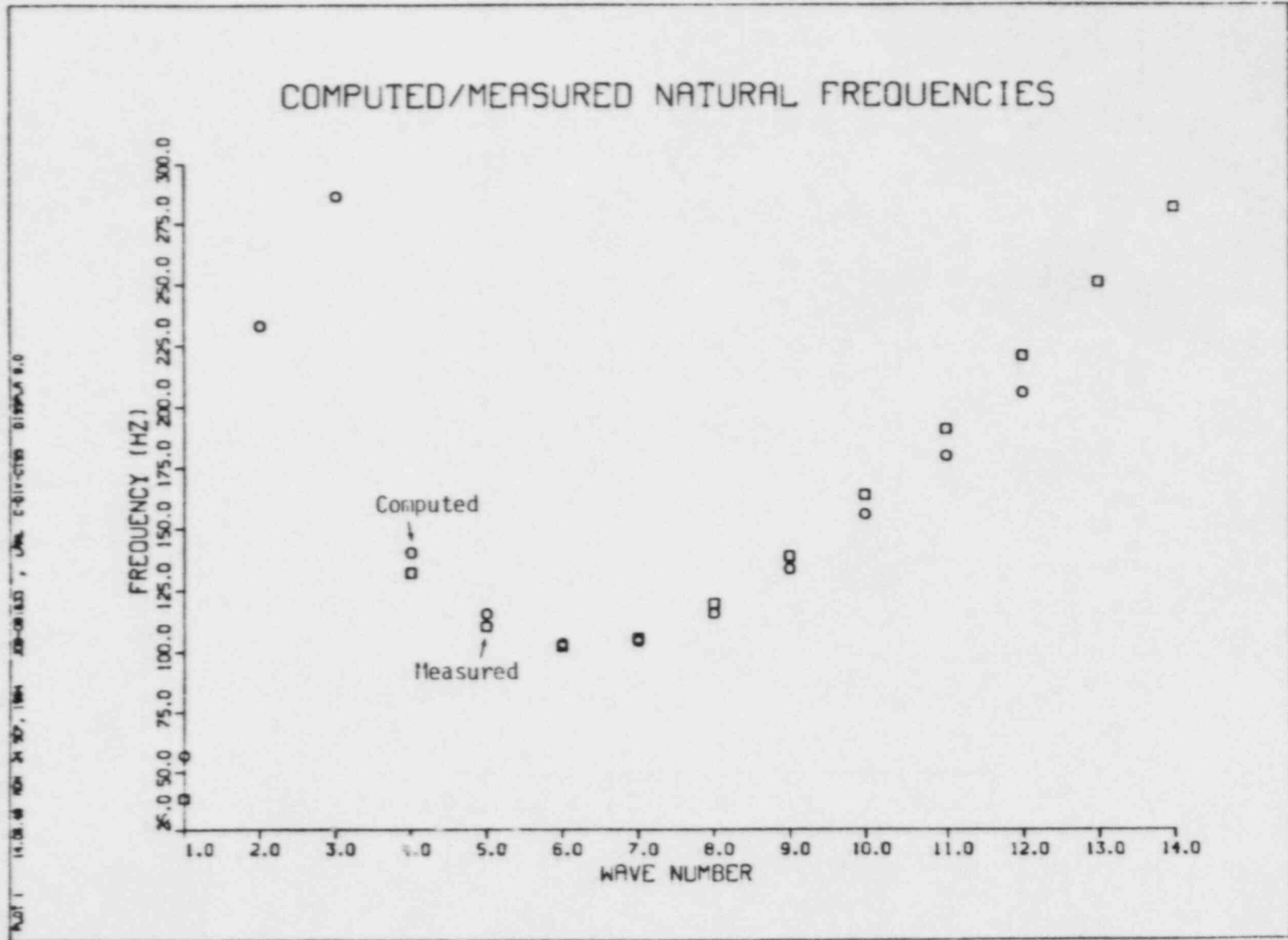
Fig. 4. Computed and measured natural frequencies for the 27.5 in. diameter ring-stiffened cylinder models of Fig. 1.

As explained, the dynamic buckling problem is further complicated by the possibility of response, excitation and buckling time scale overlap. Because the El Centro record is known to have a fairly narrow band of frequencies for which there is any significant power, another record that is power rich in all frequencies is also being used in this study. In addition, short time harmonic excitations that build up in acceleration magnitude are being used to develop curves of critical acceleration amplitude vs frequency, so that the magnitude of the effects of the time scale overlaps can be assessed. This experimental work is also in progress.

In summary we believe this study will answer significant questions concerning the dynamic loading effects on buckling of steel containments and can be used to establish regulatory positions and research directions for these problems.

REFERENCES

1. J. G. Bennett, R. C. Dove, and T. A. Butler, "An Investigation of Buckling of Steel Cylinders with Circular Reinforced Cutouts," Nuclear Engineering and Design 69 (1982), pp. 229-239.

2. J. G. Bennett, R. C. Dove, and T. A. Butler, "An Investigation of Buckling of Steel Cylinders with Circular Cutouts Reinforced in Accordance with ASME Rules," Los Alamos Scientific Laboratory report, NUREG/CR-2165 (June 1981).

3. W. E. Baker and J. G. Bennett, "Buckling Investigation of Ring-Stiffened Cylindrical Shells with Reinforced Openings Under Unsymmetrical Axial Loads," Los Alamos National Laboratory report, NUREG/CR-3135 (February 1983).

4. W. E. Baker, J. G. Bennett, and C. D. Babcock, "Experimental Buckling Investigation of Ring-Stiffened Cylindrical Shells Under Unsymmetrical Axial Loads," Journal of Pressure Vessel Technology, Vol. 105, pp. 342-346, November 1983.

5. C. D. Babcock, W. E. Baker, G. Fly, and J. G. Bennett, "Buckling of Steel Containment Shells Under Time-Dependent Loading," Los Alamos National Laboratory report, NUREG/CR-3742 (May 1984).

CONTAINMENT SAFETY MARGINS PROGRAM*

Thomas E. Blejwas

Containment Integrity Division
Sandia National Laboratories

Introduction

The Containment Safety Margins Program is one of three NRC-sponsored programs at Sandia in the area of containment integrity during severe accidents. In the subject program, models of containment structures with a variety of penetrations and other details are being analyzed and tested by quasi-static pressurization with nitrogen gas. The objective is to qualify methods for predicting the structural behavior and leakage of containments during severe accidents (beyond design basis). The larger models include operable equipment hatches, and the leakage through the hatches is being measured. The distortions of the hatches and of other penetrations are being measured with strain gages and displacement transducers. The strains and displacements near and on the penetrations that are simple representations of actual penetrations, e.g. nonoperable personnel airlock representations, will be used for planning leakage experiments with actual or large-scale penetrations in a companion program entitled Integrity of Containment Penetrations under Severe Accident Loads. In the third program, entitled Electrical Penetration Assemblies Program, actual electrical penetration assemblies will be pressurized with high temperature steam.

The testing to date and planned through the end of FY86 is the pneumatic pressurization of models of steel and concrete containments. Although the high temperatures of severe accidents are not modeled in these experiments, they will be included in the penetration tests and seal and gasket tests in the companion programs. Four 1/32 scale models of hybrid steel containments (often used with the PWR ice-condenser and BWR Mark III suppression systems) were tested between December 1982 and December 1983. Testing of a 1/8-scale steel model was initiated in September 1984. The conceptual design of a 1/6-scale model of a reinforced concrete containment has been completed; placement of a contract for final design and construction of the model is being negotiated.

Small Steel Models

Four steel containment models about 1/32 the size of U. S. hybrid steel containments were tested between December 1982 and December 1983. The three configurations of the models are shown in Figure 1. Two clean shell models were tested to provide baseline data. A ring reinforced shell was tested to determine the effect of
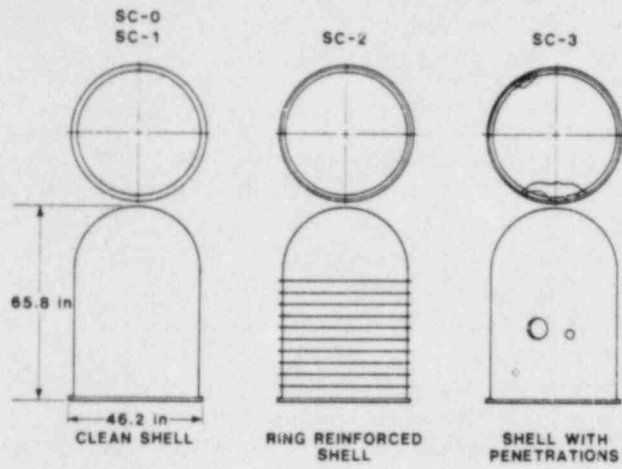
1/32 SCALE STEEL MODELS

Figure 1.   1/32-Scale Steel Models
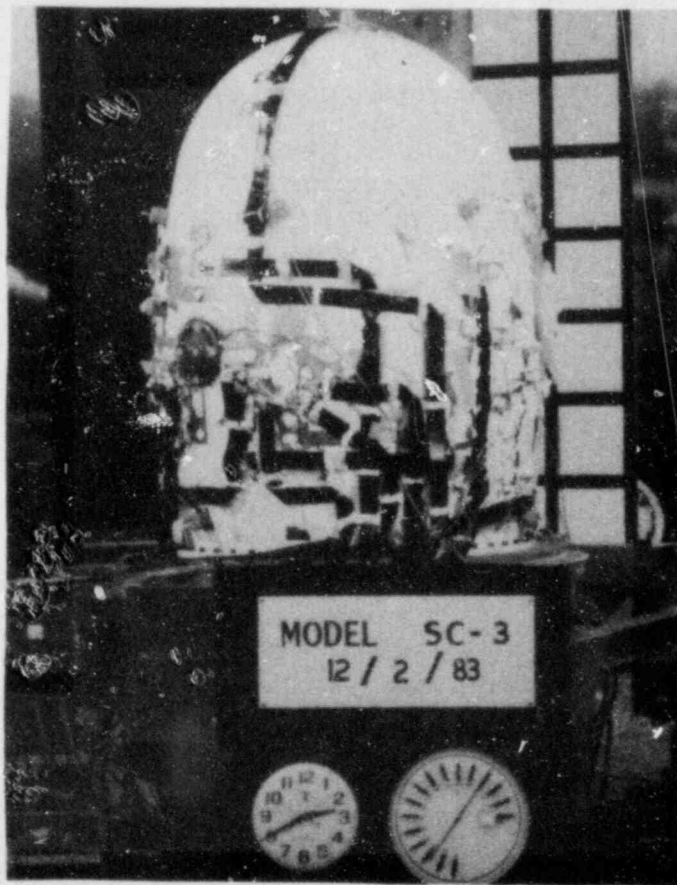
Figure 2.   Penetration Model at 120 psig (0.83 MPa)

stiffeners on post-yield containment behavior. The behavior of penetrations and their effect upon shell response were investigated during the pressurization of a model with simple representations of major penetrations. This last model is pictured (Figure 2) shortly before the model failed completely. Details of the testing of these small models are reported in [1]. Summaries of the testing are also available [2,3,4].

Experimental data and pretest analytical results have been compared for each configuration of the small steel models [1]. The comparisons are generally good for the first two configurations [4], but they are of varying quality for the penetration model. Examples of the comparisons for the penetration model are presented in Figures 3 and 4. In the first comparison, the strains for a location about three inches from the equipment hatch sleeve (three o'clock position) are presented. The major and minor principal strains from the two closest integration points in an analysis are plotted with sets of principal strains from two strain gage rosettes. (The principal strains are nearly the same for the two analytical points, and the two plots overlap.) The second comparison is for a location just below the six o'clock position of the equipment hatch sleeve. Strains from a single rosette and the two closest integration points in the finite element model are shown. The two sets of comparisons are representative of the range of differences between the experiment and the analysis near penetrations. The onset of yielding was generally overpredicted, but pressures corresponding to higher strains were both under and overestimated depending upon location. In areas of very high strain gradients, the finite size of the strain gages may contribute to less favorable comparisons.

Based on the testing and analysis of the small steel models, the following tentative conclusions have been drawn:

1. Steel containment structures can be analyzed with fair accuracy using existing methods. However, some areas of interest, such as the analytical overestimation of yield pressures and behavior in areas of very high strain gradients, require additional investigation.

2. Ring stiffeners increase the yield and ultimate strength of steel containments, such that the analytical "smearing" of the effect of stiffeners is reasonable for predicting global response. Bending distortions around stiffeners do not grow significantly during post-yield response.

3. Penetrations do not necessarily cause early failures of containment shells. However, the penetrations themselves require investigation for possible structural failure or leakage.

Each of these conclusions will be re-examined after testing of the 1/8th-scale steel model.

Large Steel Model

Low pressure testing of the large steel model began in late September 1984. Modifications of the instrumentation circuits and a complete system checkout are presently underway. Pressurization to levels well above design pressure is now expected to occur in November 1984. All testing is pneumatic pressurization with nitrogen gas.

Figure 3.   Strains About Three Inches From the Equipment Hatch

(Three O'clock Position)

Figure 4.   Strains Just Below the Equipment Hatch (Six O'clock Position)
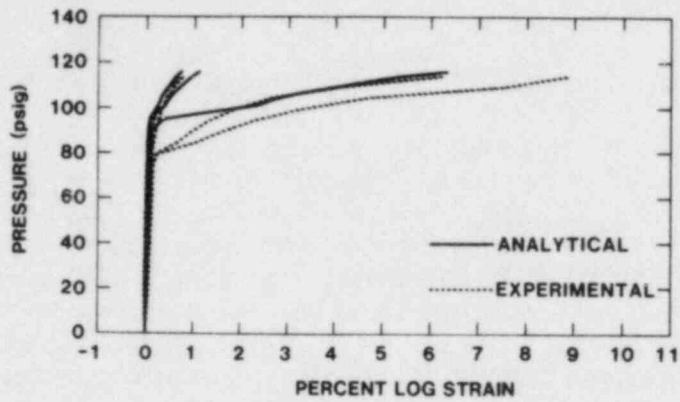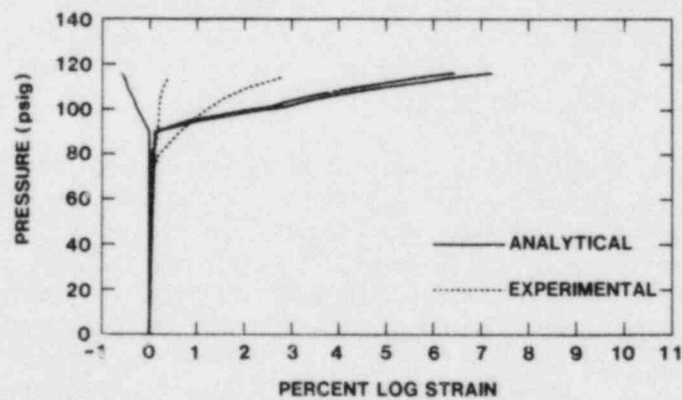
149

The model, about 1/8th the size of typical U. S. hybrid steel containments, was designed and fabricated for Sandia by Chicago Bridge and Iron Co. Dimensions and features of the model are shown in Figure 5. The upper part of the structure that is shown in white in Figure 6 has a design pressure of 40 psig (0.28 MPa) and was fabricated from A516 steel, a material that is used in many steel containments and for liners in concrete containments. The bottom torospherical head serves as a test fixture and is not representative of actual containments. A detailed description of the model, including measurements of the as-built geometry and actual material properties, will be published shortly [5].

The large steel model was instrumented with over 700 strain gages, about 50 displacement transducers, and nearly 40 thermocouples. A high accuracy pressure transducer and ten resistance temperature detectors provide data on the gas state for integrated leakage measurements. An acoustic emission system will be used to locate the source of any leakage. Photogrammetrics data and a theodolite-based coordinate determination system provide additional displacement information. Figures 7, 8 and 9 show the instrumentation near some of the model penetrations. The bars and grating in these figures are part of the interior structure that is attached to the base fixture but is not connected to the upper part of the model. Connections for the over one thousand channels of data are shown in Figure 10.

Initial testing of the model at 30 psig (0.21 MPa) has revealed an integrated leak rate of about 2.3 percent per day. After attempts to locate and eliminate existing leaks, the model will be pressurized to 46 psig (115% of design pressure), followed by an integrated leak rate test at design pressure (40 psig). High pressure testing will then be conducted in slowly applied steps using a computer-operated pressure controller. The valve gallery for the controller is shown in Figure 11. Structural data will be recorded at each pressure step using a computerized data acquisition system. At some pressure levels, the model will be isolated from the pressure controller, and the integrated leak rate will be determined from temperature and pressure readings. If large leaks develop (~100% per day), the pressure controller will be used to feed the leak while the flow into the model is measured. If the capabilities of the pressure controller or the nitrogen supply are exceeded, the test will be stopped and modifications to the model will be considered. Final testing will be halted when the maximum membrane strains in the cylinder walls away from penetrations reach a level of 8 to 10 percent.

Based on extensive analyses of the model and of the individual major penetrations using the MARC finite element code [6], the equipment hatch representations will be the first leakage/failure areas. At pressure levels near those for which the containment cylinder yields globally (about 180 psig or 1.24 MPa), the equipment hatch sleeve (that is attached to the shell) will begin to become noticeably oval in shape. In Figure 12 the predicted change in diameter of the sleeve at the sealing surface is plotted for both the meridional (3 to 9 o'clock) and vertical (6 to 12 o'clock) positions. These results were obtained using the MARC finite element code and estimated material properties. Updated results with actual measured material properties will be completed prior to high-pressure testing. As discussed previously, if leakage from the hatches exceeds the capabilities of the pressure equipment, the model may be modified and retested.
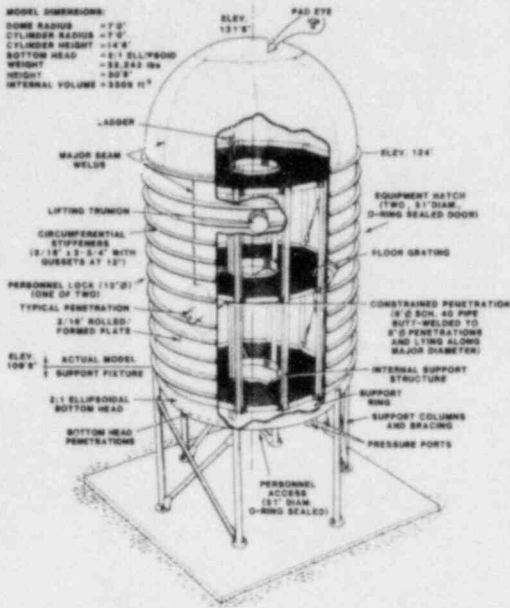
Figure 5.   Large Steel Model
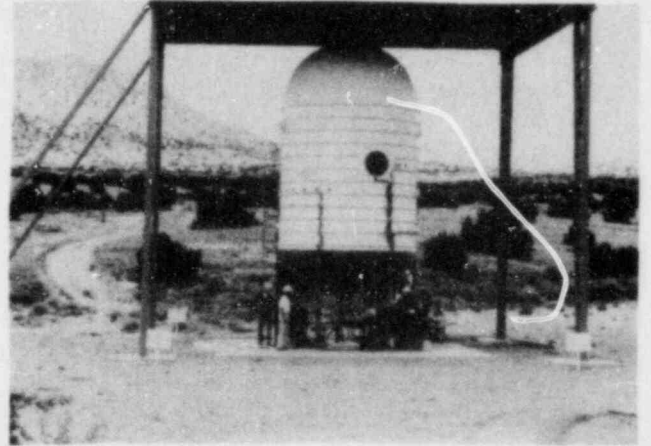
Figure 6.   Model with Open Equipment Hatch
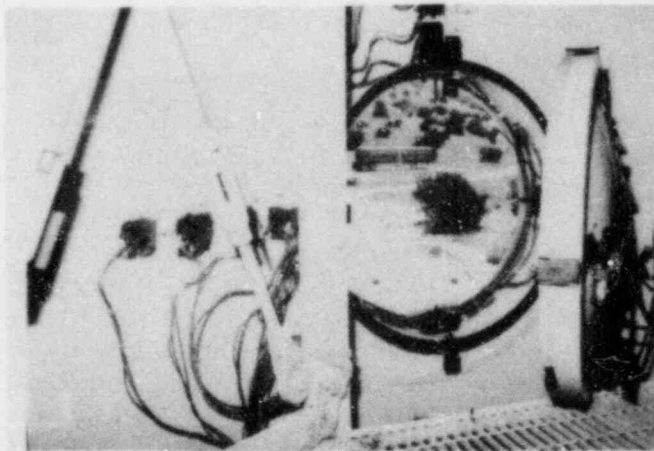
Figure 7.   Equipment Hatch with Installed

Strain Gages
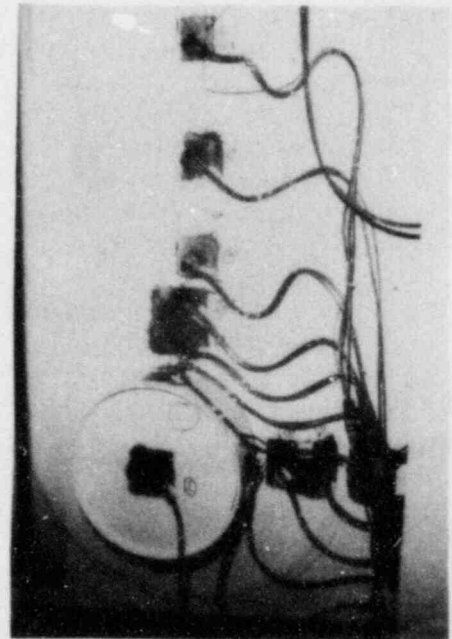
Figure 8.   Strain Gages Around Personnel

Airlock Representation

151
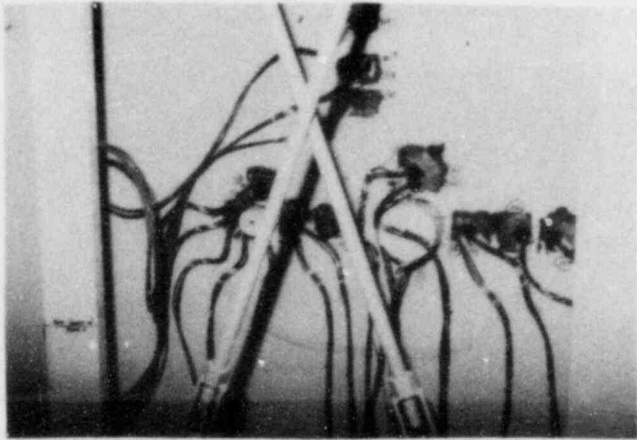
Figure 9.   Instrumentation of Pipe Penetrations
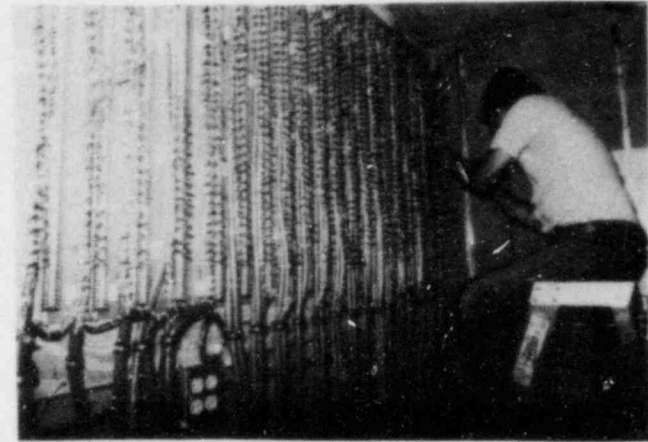
Figure 10.   Wire Connections for Instrumentation Channels
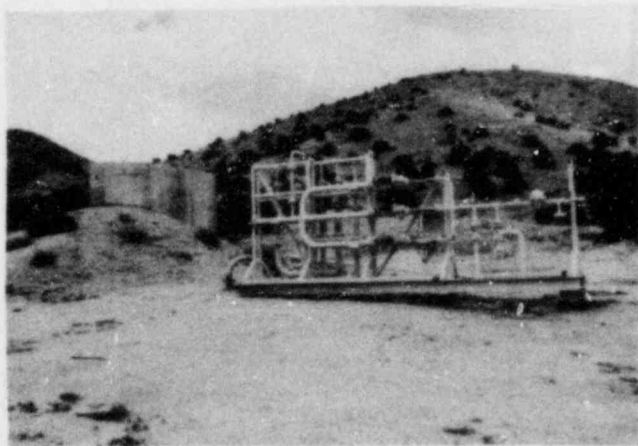
Figure 11.   Valve Gallery for Pressure Controller
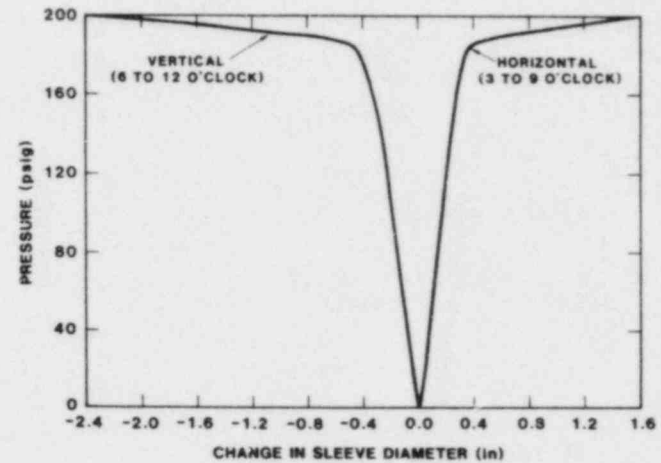
Figure 12.   Deformation of Equipment Hatch Sleeve at Sealing Surfaces

Reinforced Concrete Model

The conceptual design of a model of a typical U. S. reinforced concrete containment has been completed, proposals from prospective contractors have been received, and review of the proposals is underway. The concrete model will have the following features:

1. 1/6 scale
2. #3 rebar (10 mm) as major reinforcement
3. 1/16-inch (1.6 mm) thick steel liner with stud attachments
4. Two operating equipment hatches with seals
5. Two personnel lock representations
6. Restrained pipe penetrations
7. Other pipe penetrations
8. Thickened liner sections around penetrations
9. A "flat" basemat
10. A hemispherical dome
11. Diagonal seismic rebar that is scaled from actual containments
12. A design pressure of 46 psig (0.32 MPa)

A conceptual drawing of the model is shown in Figure 13. An example of a possible reinforcing plan is shown in Figure 14.

Expected Results

When testing and analysis of the models of containments is completed, the following results are expected. Some methods for the structural analysis of containments will be qualified or deficiencies will be noted. Benchmark data will be available for others to qualify their methods. The large model tests will yield data on the distortion and resulting leakage through equipment hatches and data on the tearing and leakage of steel shells and steel liners. Distortion data around penetrations will be used on companion programs to plan additional penetration experiments. When data from all of the containment integrity programs is available, a methodology for predicting containment leakage during postulated severe accidents will be possible.

Acknowledgements

The components of work described herein are being directed by Sandia staff members D. S. Horschel, L. N. Koenig, L. D. Lambert, P. E. Matson and D. B. Clauss. W. A. von Riesemann is the responsible Sandia supervisor. J. F. Costello and H. Ashar are the NRC program managers.

References

1. Horschel, D. S., "The Design, Fabrication, Testing, and Analysis of Four 1:32 Scale Steel Containment Models," NUREG/CR-3902, Sandia National Laboratories, Albuquerque, NM, to be published.

2. Blejwas, T. E., "Testing and Analysis of Containment Models," Proceedings of the International Meeting on Thermal Nuclear Reactor Safety, September 10-13, 1984, Karlsruhe, Federal Republic of Germany.

3. Horschel, D. S., "Experimental and Analytical Results of Steel Containment Tests," Proceedings of the 2nd Workshop on Containment Integrity, NUREG/CP-0056, Sandia National Laboratories, Albuquerque, NM, October 1984.

4. Blejwas, T. E. and von Riesemann, W. A., "Pneumatic Pressure Tests of Steel Containment Recent Developments," Nuclear Engineering and Design, Vol. 79, No. 2, May 1984.

5. Reese, R. T. and Horschel, D. S., Design and Fabrication of a 1/8-Scale Steel Containment Model, NUREG/CR-3647, Sandia National Laboratories, Albuquerque, NM, October 1984.

6. Clauss, D. B., "Analysis of a 1:8 Scale Steel Containment Model Subject to Internal Static Pressurization," Proceedings of the 2nd Workshop on Containment Integrity, NUREG/CP-0056, Sandia National Laboratories, Albuquerque, NM, October 1984.
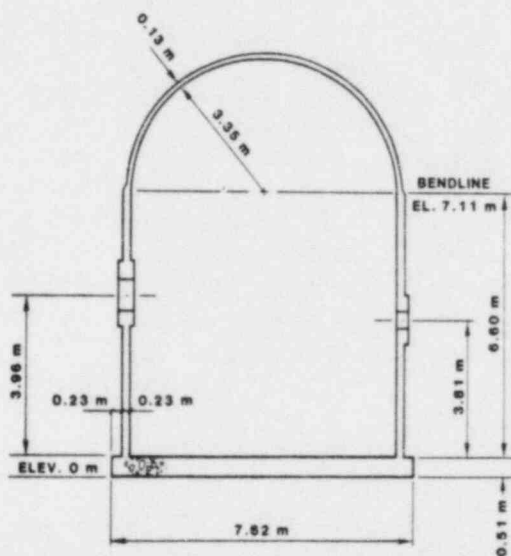
Figure 13.   Conceptual Drawing of
              Reinfored Concrete Model
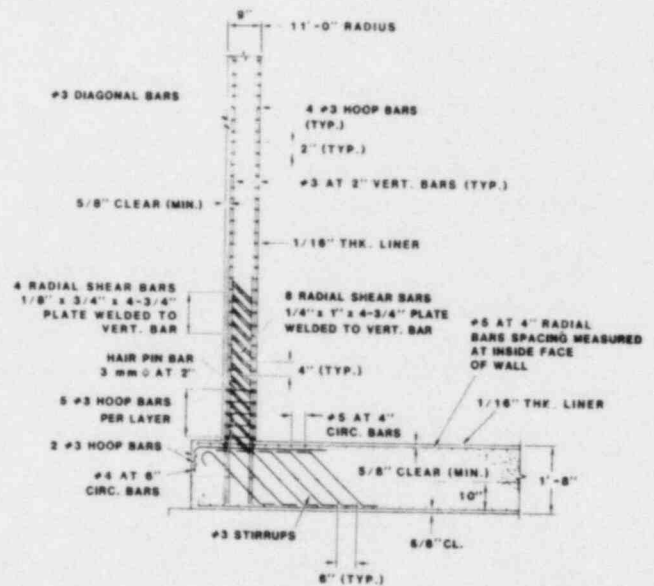
Figure 14.   Reinforcement Plan at Cylinder-Wall
              and Basemat Junction

154

INTERPRETATION OF SEISMIC SOURCE ZONES FOR SEISMIC HAZARD CALCULATIONS

by

Jerry L. King and J. Carl Stepp
Electric Power Research Institute

ABSTRACT

A current EPRI research program is to develop a state-of-the-art method of seismic hazard analysis applicable in intraplate regions. The program emphasis is on the interpretation of seismic source zones that are capable of producing moderate-to-large (magnitude 5.0 or greater) earthquakes. The methodology is first being applied to the Eastern United States, with preliminary hazard calculations for ten nuclear power plant sites scheduled for completion by April, 1985.

The source zone interpretations are based on assessments of the current tectonic stress regime and the potential response of tectonic structures to the applied stresses. A structured approach for evaluating the probability that individual tectonic features are capable of producing moderate-to-large earthquakes has been developed that explicitly quantifies both scientific uncertainty about earthquake processes and informational uncertainty due to inadequate data. The structured approach provides fully trackable documentation of the reasoning behind each source zone interpretation.

The interpretations are being made in parallel by six expert teams, each spanning the disciplines of geology, seismology and geophysics. To provide a common and as-complete-as-possible data base for the interpretations, an earthquake catalog and a number of relevant geophysical data sets were compiled and map products produced on a common scale. Extensive analyses of catalog completeness, dependent events (foreshocks and aftershocks) and non-stationarity were performed to aid the expert teams in determining seismicity parameters for the source zones.

1. INTRODUCTION

The definition of seismic source zones is the first and most fundamental element in a seismic hazard analysis. In intraplate regions of low seismicity, such as the Eastern United States, our knowledge of earthquake processes is poor, and the definition of source zones is difficult and uncertain. Recent hazard studies for the Eastern United States have attempted to capture and accommodate this uncertainty by soliciting multiple zoning alternatives from multiple experts [1]. In this approach, each expert is asked to subjectively weight the zones according to his or her degree of belief that each zone reflects the true state of nature and to estimate uncertainties in the seismicity parameters for each zone. The alternative hypotheses are incorporated in the hazard analysis, resulting in, for a given site, a probability distribution of calculated hazard levels. The spread of this distribution is taken as the uncertainty measure for the seismic hazard estimate.

The zonation approach cited above is a legitimate one. It has, however, several limitations that are being addressed by the current EPRI research program. The most important limitation is the lack of documentation of the reasoning behind the experts' zonation choices, which makes it impossible to review the criteria that were applied in identifying source zones or the consistency with which the criteria were applied. In the EPRI program, a structured approach to determining source zones has been developed that results in fully trackable documentation of the logic leading to the identification of source zones. The structured approach also explicitly decomposes zonation uncertainty into scientific uncertainty about earthquake processes and informational uncertainty due to inadequate data, as will be illustrated later.

The polling of individual experts in previous studies has several limitations. First, the interpretation of seismic source zones requires knowledge of geology, seismology, geophysics and tectonophysics -- an interdisciplinary breadth not commanded by many individuals. Second, a consistent and minimally uncertain interpretation of source zones for the entire Eastern United States requires good knowledge of data for the entire region, but most individuals have geographically limited experience. These concerns are being addressed in the EPRI study by employing expert teams whose members collectively span the disciplines of geology, seismology and geophysics and who have broad geographical experience. In addition, a comprehensive data base of seismicity and geophysical data for the Eastern United States has been compiled and made available to the expert teams [2]. Needed tectonophysics insights were obtained through a series of seminars by eminent academic researchers [3,4].

The use of interdisciplinary teams, the common data base, and the structured approach to interpreting source zones were designed to: (1) achieve an interpretation of seismic source zones that is based on a consistent, scientific procedure, to the extent possible given current knowledge; (2) minimize and quantify the uncertainty in interpreting source zones; and (3) produce fully trackable documentation of the logic and information leading to any source zone interpretation.

The purpose of this paper is to describe the structured approach to interpreting seismic source zones that has been developed by the EPRI program.

2. INTERPRETATION OF SEISMIC SOURCE ZONES

2.1 Models for Earthquake Generation

In the first workshop of the EPRI Seismic Hazards Program, the expert teams were asked to list all models or hypotheses for the generation of moderate-to-large earthquakes in the Eastern United States that they thought had any credibility. A list of all proposed models is shown in Table 1. It can be seen that the list is a mixed bag of classes of tectonic features thought to be localizing earthquakes, physical processes that create stresses in the Earth's crust, stress concentrators, and failure mechanisms. "None of the above" and "random" are expressions of uncertainty, of doubt that any of the models are correct or that we know how to apply them. After much discussion [4,5] about what constitutes a model of earthquake generation, about the state of stress in eastern North America, and about failure mechanisms, the following model evolved:

156

1. To first order, the North American lithospheric plate is acting as a stress guide.

2. Stresses within the plate primarily reflect plate-tectonic driving forces.

3. Earthquakes occur on pre-existing zones of weakness when some local stress-concentrating mechanism creates stresses that exceed the local material breaking strength, or when some weakening mechanism causes the breaking strength to drop below the ambient stress level.

The above model leads to the important conclusion that candidate sources of earthquakes in the Eastern United States are existing tectonic structures that are favorably oriented for shear failure in the present plate-tectonic stress field.

2.2 Tectonic Stress Regime in the Eastern United States

Available stress information for the Eastern United States has been compiled by Zoback and Zoback [6] from stress measurements (overcoring, hydrofracturing), earthquake fault plane solutions, and geologic data (fault and dike orientations), and augmented in this study by the expert teams. Figure 1 is the generalized azimuthal distribution of the maximum principal stress direction based on the Zoback and Zoback compilation [7]. Relatively uniform northeast-southwest compression persists throughout the central mid-continent region. This observation is consistent with "ridge-push" forces acting on the North American lithospheric plate. (The change in thickness and elevation of the oceanic crust between the continental margin and the Mid-Atlantic Ridge results in a net gravitational force that "pushes" the lithospheric plate away from the ridge [4].) Data not yet completely evaluated suggests that maximum principal stress is also in the northeast-southwest quadrant along the Atlantic Coast [5]. Locally induced stresses due to lateral density contrasts at the oceanic-continental crust boundary may be present in this region [3,4]. However, the magnitude of this force is small relative to the driving force at the plate boundary. Similarly, local stress concentration due to sediment loading and plate flexure may be important along the Gulf Coast [4,5].

Most of the Eastern United States exhibits a remarkably uniform orientation of maximum principal stress that is consistent with boundary forces acting on the North American plate. If we accept that boundary forces are the first order cause of stress in the plate interior, then the stress field can be predicted, approximately. The limited observational data base can be supplemented where observations are sparse by predicted values to obtain an interpretation of the tectonic stress regime at any location. This forms a basis for assessing the seismogenic potential of tectonic structures.

2.3 Tectonic Framework

Earthquakes in the Eastern United States are expected to occur on existing tectonic structures that are favorably oriented in the present tectonic stress regime. Classes of potentially seismogenic structures, identified by the expert teams, are shown in Table 2. The locations and configurations of these structures are mapped using geological, seismological, and geophysical data.

157

The mapped distribution of these structures, together with an interpreted tectonic stress regime, forms a tectonic framework for the interpretation of seismic source zones.

2.4 Evaluating the Seismogenic Potential of Tectonic Structures

A structured approach for assessing the seismogenic potential of each structural element in a tectonic framework has been developed as part of the EPRI study [8]. The basis of the approach is a set of observational criteria that can be evaluated for a given structure using geological, geophysical, and seismological data. A list of possible criteria is shown in Table 3. The resolving power of each criterion differs significantly due both to the state of scientific understanding of the phenomenon and to limitations on our ability to observe and evaluate it. For example, the most powerful criterion for assessing the potential for future activity on a structure is a spatial association of the structure with historical earthquakes. In contrast, evidence for local stress amplification or low material strength currently has low resolving power because our ability to measure and apply such evidence is poor.

The assessment of the subjective probability that a particular tectonic structure is seismogenic can be decomposed into an assessment of (1) the generic probability that a given criterion (e.g., association with seismicity) implies a seismogenic state and (2) the probability that the criterion actually applies to the particular structures. The first assessment may be viewed as an expression of scientific uncertainty about the implications of the criterion, while the second is an expression of informational uncertainty due to incomplete data.

Each of the six expert teams independently identified criteria that, in their opinion, have significant resolving power and that can be applied to most tectonic structures in the Eastern United States. These were then put into a matrix format, as illustrated in Figure 2. The values for each matrix element are subjectively assessed probabilities that a hypothetical tectonic structure would be seismogenic, given that the criteria associated with each element apply. The values reflect scientific uncertainty about the geologic causes of earthquakes and are, therefore, expected to be constant for a particular tectonic region (a region with similar tectonic deformation rates). The values and the criteria would be expected to vary significantly from region to region.

The subjective probabilities that criteria, in fact, apply to particular tectonic structures are assessed in a second matrix, an example of which is shown in Figure 3. The values in this matrix reflect the expert team's informational uncertainty about the structure. Unlike the generic, first matrix, which only has to be filled out once, the second matrix has to be filled out for each tectonic structure or class of structures being evaluated. The subjective probability that a structure is seismogenic is the product of the first, generic matrix and the structure-specific matrix.

The matrices are calibrated by comparing the calculated probabilities with the teams' "gut" or direct assessments of the probabilities that specific structures are seismogenic. When the matrices are properly defined and calibrated, good agreement is obtained. An exception may occur when significant information is available that is not represented in the matrices, such as unusual

158

knowledge of ongoing deformation or evidence of reactivation. In this case, the calculated probabilities must be modified to be in accord with the teams' gut feelings.

The matrix formulation described here has several advantages. First, it succinctly describes the scientific reasoning behind each assessment. Together with written justification of the values assigned to each matrix element, the matrix formulation provides completely trackable documentation for future peer review. Second, the matrices ensure a consistent evaluation of all structures considered. Third, the matrices explicitly and separately quantify scientific and informational uncertainty. The advantage of this is that the impact of future gains in knowledge and understanding on the hazard estimates can be easily calculated by appropriately modifying the matrices.

The seismic hazard analysis methodology requires that seismic source zones be defined that have a uniform probability of being seismogenic. (In this study, "seismogenic" means a potential for producing a magnitude $m_b > 5.0$ earthquake in the present tectonic stress regime.) A single tectonic structure may be defined as a source zone, or an aggregation of structures having similar properties can be defined to be a source zone. In these cases, the probability of the source zone being seismogenic is the probability that the structure is seismogenic, as calculated using the matrices. An area of seismicity not associated with any known structure can also be defined to be a source zone. In this case, the matrix formulation is not applicable, and the subjective probability of the area being seismogenic has to be assessed directly.

2.6 Determining Seismicity Parameters

The expert teams are currently considering earthquake recurrence models, model parameters, and maximum earthquake magnitudes for their seismic source zones. Extensive analyses of earthquake catalog completeness as a function of time and space, number of dependent events (foreshocks and aftershocks), and non-stationarity of historical seismicity have been performed to aid the teams in determining seismicity parameters [9]. State-of-the-art reviews of candidate earthquake recurrence models (Poisson-exponential, characteristic, etc.) and of methods of estimating maximum magnitudes have also been provided to the expert teams [9].

3. CONCLUSIONS

A structured approach to interpreting seismic source zones has been developed that has several advantages. First, it produces completely trackable documentation of the reasoning behind each source zone interpretation. Second, it explicitly identifies and quantifies uncertainties so that the impact of future gains in knowledge and understanding on calculated hazard levels can be easily assessed. Third, the approach ensures a consistent treatment of all tectonic structures thought to have any credibility of producing a moderate-to-large earthquake.

The seventh and final workshop of the program, to discuss the teams' assessments of seismicity parameters, is scheduled for late January, 1985, in Denver, Colorado. Hazard calculations for ten test sites will be available in April, 1985.

ACKNOWLEDGMENTS

REFERENCES

1. Bernreuter, D.L., J.B. Savy, R.W. Mensing and D.H. Chung (1984). Seismic hazard characterization of the Eastern United States: methodology and interim results for ten sites, NUREG/CR-3756, U.S. Nuclear Regulatory Commission.

2. King, J.L. and J.C. Stepp (1984). National geophysical data sets for assessing earthquake potential in the central and eastern United States, Proceedings of NOAA Conference on Pathways and Future Directions for Environmental Data and Information Users, Denver, Colorado.

3. EPRI (1984). Defining tectonic mechanisms causing earthquakes in the Eastern United States, Proceedings of a Seminar held March 22-23, 1984 in Salt Lake City, Utah, EPRI Seismic Hazards Research Program.

4. EPRI (1984). Tectonic processes of intraplate stress generation and concentration, Proceedings of Workshop No. 2, EPRI Seismic Hazards Research Program, Washington, DC.

5. EPRI Tectonic Evaluation Contractors (1984). Working papers prepared for Workshop No. 3, Tectonic Stress Regime and Potential Stress Concentrators, EPRI Seismic Hazards Research Program, Washington, DC.

6. Zoback, M.L. and M.D. Zoback (1980). State of stress in the conterminous United States, Journ. Geophys. Res., Vol. 85, pp. 6113-6156.

7. Zoback, M.D. (1983). Intraplate earthquakes, crustal deformation, and in-situ stress, Proceedings of Conference XX: A workshop on "The 1886 Charleston, South Carolina, Earthquake and its Implications for Today," USGS Open File Report 83-843.

8. Woodward-Clyde Consultants (1984). Approaches to developing tectonic frameworks and seismic sources, Proceedings of Workshop No. 4, EPRI Seismic Hazards Research Program, Washington, DC.

9. Dames and Moore (1984). Methods of estimating seismicity parameters, Proceedings of Workshop No. 6, EPRI Seismic Hazards Research Program, St. Louis, Missouri.

Table 1

INITIAL LIST OF "TECTONIC MODELS"

1. Reactivation of Failed Rifts/Aulacogens

2. Isostasy

3. Reactivation of Decollement Structures

4. Reactivation of Mesozoic Rift Structures

5. Epeirogenic Structures

6. Deep-Seated Structural Boundaries

7. Onshore Extensions of Oceanic Fracture Zones

8. Block Tectonics

9. Intrusive Bodies

10. Thermal Expansion/Contraction

11. Structural Intersections

12. Induced Seismicity

13. Growth Faults

14. Eastern Piedmont Ductile Shear Zones

15. Cenozoic Reverse Faults

16. Areas of Intensive Jointing/Fracturing

17. None of the Above

18. Random

19. Initiation of New Faults

20. Meteorite Impacts

Table 2

CLASSES OF POTENTIALLY SEISMOGENIC TECTONIC STRUCTURES

Failed Rifts/Aulocogens

Decollement Structures

Mesozoic Rift Structures

Epeirogenic Structures

Deep-Seated Structural Boundaries

Onshore Extensions of Oceanic Fracture Zones

Block Tectonic Structures

Intrusive Bodies

Growth Faults

Ductile Shear Zones

Cenozoic Reverse Faults

Areas of Intensive Jointing/Fracturing

Table 3

CRITERIA FOR EVALUATING SEISMOGENIC POTENTIAL
OF TECTONIC STRUCTURES

ASSOCIATION WITH SEISMICITY

Moderate-to-large earthquakes
Small earthquakes only
No association

ONGOING STRAIN DEFORMATION

FAULT ORIENTATION RELATIVE TO TECTONIC STRESS REGIME

Favorable
Unfavorable

CRUSTAL EXPRESSION

Deep, near intersections or barriers
Deep, not near intersections or barriers
Shallow only

GEOLOGIC EVIDENCE OF REACTIVATION

Brittle slip superimposed on ductile deformation
Paleoseismicity

EVIDENCE FOR LOCAL STRESS AMPLIFICATION

Localized stress anomalies
Rigidity contrasts

EVIDENCE FOR LOW STRENGTH MATERIALS
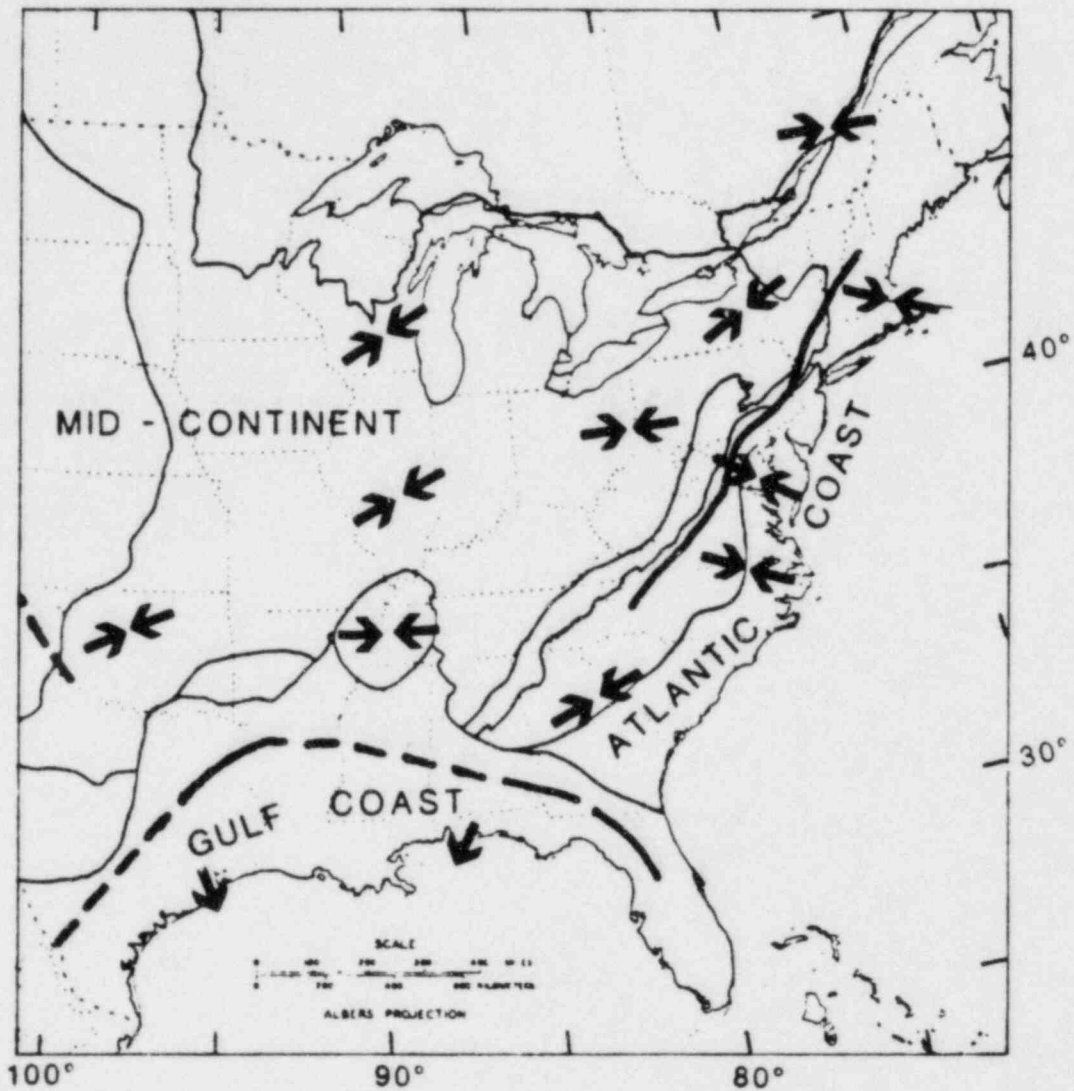
Figure 1. Generalized stress map of Central and Eastern United States (modified after Zoback and Zoback, 1980). Relatively uniform northeast-southwest compression seems to persist through the mid-continent and Southeastern U.S.

MATRIX OF PHYSICAL CHARACTERISTICS

		MODERATE TO LARGE EARTHQUAKES $\geq 5.0\,m_b$		SMALL EARTHQUAKES ONLY $< 5.0\,m_b$		NO SEISMICITY	
SPATIAL ASSOCIATION WITH SEISMICITY / GEOMETRY RELATIVE TO REGIONAL FABRIC, STRESS ORIENTATION and/or SENSE OF SLIP / DIMENSION AND NATURE OF TECTONIC FEATURE		FAVORABLE	NOT FAVORABLE	FAVORABLE	NOT FAVORABLE	FAVORABLE	NOT FAVORABLE
DEEP CRUSTAL EXPRESSION WITH A BARRIER		.95	.85	.80	.65	.15	.05
DEEP CRUSTAL EXPRESSION WITHOUT A BARRIER		.90	.60	.65	.40	.05	.01
JUST SHALLOW CRUSTAL EXPRESSION		.60	.50	.30	.20	.01	.005

Figure 2.

PROBABILISTIC ASSESSMENT OF FEATURE CHARACTERISTICS

FEATURE NAME: Clarendon-Linden Structure	**Probability that physical characteristic is associated with tectonic feature**	
PHYSICAL CHARACTERISTIC:	**Probability**	**Basis for Probability**

1. ASSOCIATION WITH SEISMICITY

A.	Moderate-to-large earthquakes [≥ 5.0 m$_b$]	.8	Attica - 1929
B.	Small earthquakes only [<5.0 m$_b$]	.1	
C.	No seismicity	.1	
		1.0	

2. GEOMETRY OF FEATURE RELATIVE TO REGIONAL FABRIC, STRESS ORIENTATION, and/or SENSE OF SLIP

A.	Favorable geometry	1.0	N-S Orientation
B.	Unfavorable geometry	0	
		1.0	

3. CRUSTAL EXPRESSION & NATURE

A.	Deep crustal expression with barrier	.6	Possible west-striking structural intersection; expressed in geophysical anomalies, seismicity trend, and nodal plane of focal mechanism solution.
B.	Deep crustal expression without a barrier	.4	
C.	Just shallow crustal expression [with or without barrier]	0	
		1.0	

REFERENCES:

Fletcher & Sykes (1977)
Hutchinson, et al. (1979)
Herrmann (1978)
Revetta (1971)

ADDITIONAL CHARACTERISTICS:

Calculated probability of activity = 0.83

Figure 3
166

THE SEISMIC SAFETY MARGINS RESEARCH PROGRAM - A CONCLUDING LOOK

By

G. E. Cummings
Lawrence Livermore National Laboratory

The Seismic Safety Margins Research Program (SSMRP) was started at LLNL in 1978 with the goal of developing tools and data bases to compute the probability of earthquake - caused radioactive release from commercial nuclear power plants. These tools and data bases were to help the sponsoring agency, NRC, assess seismic safety at nuclear plants. The methodology to be used was finalized in 1982 and applied to the Zion Nuclear Power Station. Results of this application were reported at the last Water Reactor Safety Research Information Meeting. The SSMRP will be completed this year with the development of a more simplified method of analysis and a demonstration of its use on Zion. This simplified method is also being applied to a boiling-water-reactor, the LaSalle Nuclear Power Plant, as part of another NRC sponsored program.

DESCRIPTION OF SSMRP METHOD

There are five steps in the SSMRP method for calculating the seismic risk at a nuclear power plant:

1. Determine the local earthquake hazard.

2. Identify potential accident scenarios for the plant which lead to radioactive release.

3. Determine failure modes for the plant emergency safety systems.

4. Compute failure probabilities of the critical components in the emergency safety systems.

5. Compute probability of radioactive release using information from Steps 1 through 4.

A brief discussion of each of these steps is given below and illustrated in Figure 1.

Step 1 - Determine the Earthquake Hazard

The earthquake hazard at a given power plant site is characterized by a frequency plot which gives the probability of occurrence (per year) of earthquakes causing different peak ground accelerations. This curve is derived from a combination of recorded earthquake data, estimated earthquake magnitudes of known events for which no data are available, review of local geological investigations, and use of expert opinion based on a survey of seismologists and geologists familiar with the region in question.

In addition to computing the seismic hazard curve, a number (usually 30) of random synthetic earthquakes are generated by using the data just discussed and a Monte Carlo procedure incorporated in our HAZARD code. These earthquake time histories provide the random ground motion uncertainty inherent in real earthquakes, and are used as input to the building response calculations described below. Each synthetic earthquake is described by three time histories in three orthogonal directions.

Step 2 - Identify Accident Sequences

In the event of an earthquake or other abnormal condition in a power plant, the plant safety systems act to bring the plant to a safe shutdown condition. In this step of the risk analysis process, we identify the possible paths that a reactor system could follow during a shutdown, given that an earthquake-related event has occurred which causes shutdown. These paths are referred to as accident sequences. For the SSMRP analysis of Zion, 315 accident sequences were identified and analyzed.

All the accident sequences result from one or more seismically-induced initiating events (events resulting in immediate shutdown of the plant). For the Zion plant, we considered seven classes of initiating events. Four LOCA's of different severity were considered, and two types of transients. In addition, an initiating event "Reactor Vessel Rupture" was identified which is a LOCA for which the ECCS cannot effectively flood the core.

168

For each of these initiating events, an event tree is constructed. Each branch of an event tree is an accident sequence. In computing the probability of core melt, we compute the probability of each accident sequence occurring. The sum of the probabilities of all accident sequence leading to core melt is the core melt probability.

Step 3 - Determine Failure Modes of Safety Systems

To determine failure modes for the plant safety systems, we use fault tree methodology. Construction of a fault tree begins by identifying the immediate causes of system failure. Then each of these causes is examined for more fundamental causes, until one has constructed a downward branching tree, at the bottom of which are failures not further reducible, i.e., failures of mechanical or electrical components due to all causes such as structural failure, human error, etc. These lowest order failures on the fault tree are called basic events.

Fault trees are required for each safety system identified on the event trees. For Zion, seven safety systems were modeled. The emergency core cooling system was modeled with fault trees for the Safety Injection System, Charging System, Residual Heat Removal System and the Accumulator System. The emergency core cooling function is provided by different combinations of these systems in the injection and recirculation phases of a LOCA, dependent on break size. The auxiliary feedwater system (AFWS) is of primary importance, and a complete fault tree was developed for this system. All the above systems (except the accumulators) require both electric power and service water, so detailed fault trees were also developed for both these systems.

The basic failure events which resulted after all fault trees were constructed fell into three categories: (1) human and maintenance errors, 533; (2) other random failures, 20; and (3) seismically-induced component failures, 1923. In all, a total of 2476 basic failure events were considered.

169

Step 4 - Compute Failure Probabilities of Critical Components in the Safety Systems

To compute the failure of critical components and safety systems, it is necessary to have both a measure of the maximum load or acceleration that the component experiences during an earthquake as well as a measure of the load or acceleration level at which it fails. Both the maximum load and the strength at failure are random variables. The strength at failure of the buildings and the mechanical and electrical equipment is never known exactly, for there is usually wide variation in the results of tests to determine their failure characteristics. Uncertainties in material properties, soil layering, wall dimensions and joint connectivity influence the response of the building to an earthquake. All of these uncertainties give rise to uncertainties in calculating the response and onset of failure of each building and component in the power plant. The most important feature of the SSMRP is that these uncertainties are explicitly recognized and propagated through the calculational scheme, so that the result is not a single number, but rather, the statistical probability of the occurrence of core melt and radioactive release.

(a)   Response Calculations

The buildings, foundations, major components, and piping systems are all modeled by the finite element method. SSI and structure response were calculated by the substructure approach. Piping analysis was performed by multi-support time history analysis. Models were developed for four buildings and five different piping systems in the Zion power plant analysis. For Zion, responses at over 400 points in the buildings and over 1000 points in the piping systems were computed for each input time history. The computer code, SMACS, was developed to do response calculations for SSMRP.

To incorporate the uncertainties, multiple analyses of the entire power plant are made. In each of these repeated calculations, the magnitudes of the input parameters are varied in a random fashion, and each calculation is performed using a different set of three input time histories. Typically, 30 calculations are made (at each

170

earthquake level) with the result that 30 values of response are computed for <u>each</u> building wall, slab, pipe segment, valve and component. From these 30 values, a statistical distribution of the response of each wall, component, etc., can be constructed. Such distribution functions were determined for the responses of every wall, slab, pipe segment, and electro-mechanical component identified on the fault trees.

(b)   <u>Determination of Fragility Functions</u>

Component failure is defined as either loss of operability or pressure boundary integrity. Failure (fragility) is characterized by a cumulative distribution function which describes the probability that failure has occurred given a value of load. Loading may be local spectral acceleration or moment, depending on the component and failure mode under consideration. Contrary to previous work, fragility is related to the appropriate local response, rather than being related directly to the free-field peak ground acceleration.

A data base of the necessary fragility functions was developed. As a first step, all components identified on the fault trees were grouped into 37 generic categories. Fragility functions for each generic category were developed based on a combination of design analysis reports, experimental data and an extensive expert opinion survey. Statistical methods were used to combine data from several sources.

<u>Step 5 - Compute Probability of Core Melt and Radioactive Release</u>

Accident sequence probabilities are calculated to determine radioactive release probabilities. Core melt probability is the sum of the probability of all accident sequences leading to core melt.

171

(a)   Calculation of Cut Set Probabilities

Each accident sequence consists of the statistical union of sets of
events (successes or failures of components) which must occur
together (in systems analysis terminology, called min cut sets).
The Zion accident sequences each contained up to 5000 of these
component failure groups and each component failure group (min cut
set) was allowed to have up to ten basic events (component failures).

The computer code SEISIM was written expressly to calculate the
probability of such component failure groups including all common-
cause failures. Given the individual component responses and
fragilities (in terms of the means and variances of their
distributions) and given the computed correlations between the
responses (obtained from the 30 time history response calculations
at each earthquake level), SEISIM constructs a multi-variate
lognormal distribution for each component failure group, and then
uses n-dimensional numerical integration to compute the probability
of the component failure group occurring.

(b)   Calculations of Probability of Radioactive Release

Once the component failure group probabilities have been computed,
the probability of each accident sequence can be found using the
expression for the statistical union of independent cut sets, which
is an upper bound to the accident sequence probability. Then each
accident sequence probability is multiplied by the probability of
the earthquake's occurrence and the probability of failure of the
containment to obtain the probability of radioactive release.
Several different containment failure modes of different severity
were identified, ranging from rupture of the containment shell down
to leakage of the containment isolation valves. Different
containment failure modes are assigned to different accident
sequences depending on our understanding of the physical processes
involved. One accident sequence can result in one or more
containment failure modes.

172

Finally, accident sequence probabilities are assigned to different release categories to reflect their severity with respect to radioactive release to the surrounding population. These release categories relate to the type and energy content of the radioactive fission product release, as well as the mode and timing of the release. They range from rupture of the top of the containment with a rapid, high energetic release (due to a fuel/water explosion or due to steam overpressure) down to slow melt-through of the containment concrete foundation, which is expected to have the least effect on the surrounding population. The containment failure modes and the release categories are those derived and used in the Reactor Safety Study.

IMPORTANCE AND SENSITIVITY

Results from SSMRP analyses of the Zion Nuclear Power Plant have been reported previously[1,2]. More recently, importance and sensitivity studies have been completed to help in prioritizing and testing the results.

A recent study[3] identified key accident sequences found from the Zion risk study. These are shown in Table 1. Systems found important to seismic risk at Zion where the containment spray and fan cooler systems, the auxiliary feedwater and secondary steam relief systems and the RHR system in LOCA mode.

Another study[4] was done using marginal, importance and sensitivity studies to identify changes in structures, systems, equipment, components and parameters that affect seismic risk, to estimate the effect and rank the changes. This study would be useful if an allocation of available resources to reduce seismic risk or uncertainty were felt to be desirable. Although the results are specific to Zion, they have some generic implications for similar plants of that generation.

Areas found most important to seismic risk by this study are listed below. Some of these areas are now receiving further study.

o   Local Site Effects

o   Piping Between Buildings

o   Piping Fragility

o   Crib House Pump Enclosure Roof Fragility

o   Base Slab Uplift Fragility

More detailed categories are in our report.

Local site effects refers to a phenomenon that occurs at 20 to 30 sites in the eastern United States including Zion. These sites have relatively shallow soil deposits on crystalline bedrock. The available information from past earthquakes and SSMRP calculations reveals that these sites may simultaneously have accelerations and spectral values at certain frequencies that are amplified by factors of as much as 2 to 10 times that obtained if the special physical features typical of these sites are not considered. It is thus not surprising that this area ranks high.

Previous SSMRP results have identified piping between buildings as important. This piping is important when it is restrained in close proximity at two buildings that have independent soil foundations. The relative motion of these buildings at accelerations greater than the safe shutdown earthquake (SSE) causes high stresses and strains in such piping. The relative motion of buildings is a known problem area from past earthquake data. This area would probably not be as important if the piping supports fail before the piping does or in the case of a rock site.

It is surprising that piping fragility ranks so high. Previous seismic risk analyses, including the SSMRP, have found that only a few piping systems were important in safety systems and then under special circumstances such as piping between buildings. Our result in this study arises because pipe breaks are initiating events for the more severe initiators such as LOCAS as well as the assumption that the possible error or bias in the estimated fragility of all piping in the plant is simultaneously biased high or low. This piping fragility is an important input but piping failures are not necessarily key contributors to risk except between buildings.

Crib house pump enclosure roof fragility ranks high because of (1) the relatively low capacity of this roof at accelerations beyond the SSE due to the detail of the connection between the roof and the supporting walls and (2) the assumption that the collapse of this roof causes the loss of function of all six service water pumps. While this category is specific to Zion, it points out: (1) the importance of connection detail (which is a known problem area from past earthquakes) and (2) the capability of structures to act as common-cause failure contributors, as two generic interpretations of our results.

Base slab uplift fragility refers to the failure of the soil foundation of the reactor building at accelerations beyond the SSE. This category is important because it is assumed to lead to failure of the piping between the reactor building and the auxiliary-fuel-turbine complex at Zion. This category points out the importance of soil and foundation failure which is also a known problem area from past earthquakes.

Finally, there is an important category that is not on the above list: relay chatter and breaker trip of electrical equipment.[5] In the SSMRP seismic risk analyses and thus also in our study, relay chatter and breaker trip were assumed not to lead to loss of function or accident initiation at the levels indicated by fragility test data. If this assumption is not made then relay chatter and breaker trip would have a "significant" effect on the SSMRP risk results and hence on our study. These analyses have not been performed and so we can give no accurate indication of how much "significant" is. However, we estimate the inclusion of these failures would lead to an order of magnitude or more increase in the median annual probability of core melt of 3×10^{-5} that was found. This would be a significant increase. Recent SSMRP results lead us to believe that relay chatter and breaker trip could be a much more important factor than we previously assumed in the SSMRP analyses; thus our inclusion of this category here.

Sensitivity studies relating to soil-structure-interaction effects were conducted in three areas: flexible foundation modeling, structure-to-structure interaction and basemat uplift.[6] The auxiliary-fuel handling-turbine building (AFT) complex was modeled to behave ridgidly and also modeled

as a series of rigid segments interconnected by structural elements. It turned out that modeling as rigid provided adequate response predictions at locations of interest.

During an earthquake, the vibration of one structure can affect the motion of an adjacent structure due to through-soil coupling. This phenomena is called structure-to-structure interaction and is of significance when small distances separate adjacent structures or massive structure-foundation systems are involved as at Zion. Sensitivity studies were conducted to determine the effect of including or excluding modeling of this phenomena. It was found that the responses of piping systems running between the containment and AFT complex were significantly affected by structure-to-structure interaction effects. Response increases of up to a factor of 2 were noted. The effect on risk was found less significant, a 20% increase in core-melt frequency.

Another soil-structure-interaction phenomena investigated was the separation of the foundation from the soil during an earthquake. This phenomena is called basemat uplift. The separation of the foundation from the soil may not in itself be a problem but upon resettlement, the potential exists for large soil pressures due to stress redistribution. Soil failure may result leading to increased relative displacement between adjacent structures. Basemat uplift was found to be important and as noted previously, basemat fragility is an important effect when considering earthquakes at nuclear power plants.

SIMPLIFIED METHOD

The basic objectives of the SSMRP simplified seismic PRA methodology are to save time and money but to adequately estimate seismic risk. Several assumptions serve as a point of departure for our development efforts:

o   Systems information about the plant is available and an
     identification of unique features relating to seismic risk has been
     made. Simultaneous development of plant logic models for all
     initiators is the best way to achieve consistency in the calculated
     risk estimates from the various initiators.

o   The seismic hazard models (site specific hazard functions and
        response spectra) for any eastern United States (EUS) site will be
        available from the NRC EUS Seismicity Projects.[7] Western U.S.
        sites will probably have to be treated separately.

o   Seismic design data is available for all structures, systems,
        components and equipment.

In the most simple general perspective of a seismic PRA, three different
kinds of data are sought:

o   Seismic hazard
o   Response and fragility and
o   Plant logic

In the seismic hazard models we generally eliminated the need for the
development of time histories and rely instead primarily on response spectra.
In some cases, it may be prudent to develop time histories for limited site-
and plant-specific calibration purposes.

The major change in methodology is in response and fragility models. We
generally eliminated the need for detailed time history seismic response
analysis and rely instead primarily on calibration factors to provide this
information. These calibration factors are based on generic studies such as
those performed as part of our development efforts or on a limited re-analysis
of the nuclear power plant for which the seismic PRA is being performed. The
studies that led to the generic calibration factors we recommend formed the
bulk of our efforts.

We have developed selected simplifications in plant logic models.
However, we believe full-scope PRA needs will dictate requirements here.

The primary focus of our simplification efforts is in the seismic response
of structures, piping systems, components and equipment. The SSMRP detailed

177

seismic PRA method involves detailed response calculations as a means to relate free-field acceleration to fragility based on local response quantities. It is thus logical to focus on response as an area to simplify.

The most important aspect of the response simplification effort is to "calibrate" seismic design data. By calibration we mean: To develop a calibration factor F_c that provides a relationship:

$$R_{BE} = R_D/F_c \qquad (1)$$

between seismic responses used in the plant design, R_D, and a best estimate response, R_{BE}. This calibration factor is a key element in the development of fragility functions. R_D is developed for the design earthquake and thus keys the responses to free-field acceleration at that level.

F_c is in general larger than 1.0 and in many cases it is much larger than 1.0. This is a reflection of conservatisms or margin in the calculational methods of analysis used in nuclear design practice. Calibration factors for shear wall structures are shown in Table 2.

A number of sensitivity studies were performed to obtain the calibration factors F_c in equation (1). They assessed the potential influence of many factors that might vary in the design of the various plants to which the SSMRP simplified seismic PRA methodology might be applied. The factors studied included parameters such as damping as well as alternative methods of analysis that are used in nuclear practice. For example, one study showed the relative unimportance of structural damping - particularly at soil sites. Another study revealed that there was surprisingly little difference in results between over ten different methods of analysis of piping systems.

We compared estimates of core melt probability obtained using the SSMRP detailed and simplified seismic PRA methodology. The results are given in Table 3. As shown in this table, the core melt probability for the simplified method is about four times the base case results from the detailed methodology and the dose is twice as much. The major contributors remain to be basemat uplift and inter-building pipes. The absolute results, although different,

178

are well within the uncertainty bounds and the key contributors remain much the same. Further investigation will be necessary to investigate the difference.

CONCLUSION

SSMRP has been a multi-year program to develop probabilistic analysis techniques to determine the seismic behavior of nuclear power plants. These techniques have been applied to Zion in both a detailed and simplified manner. The simplified method is now being applied to LaSalle. Seismic risk assessments are now commonly being conducted by utilities at plants both in the U.S. and offshore. The SSMRP stands as the most detailed of these type seismic risk assessments and provides a benchmark and resource for further work concerning seismic safety.

FIGURE 1: DESCRIPTION OF SSMRP SEISMIC RISK CALCULATION METHOD - HAZARD, SMACS AND SEISIM ARE THE THREE COMPUTER CODES USED TO DO THE CALCULATION
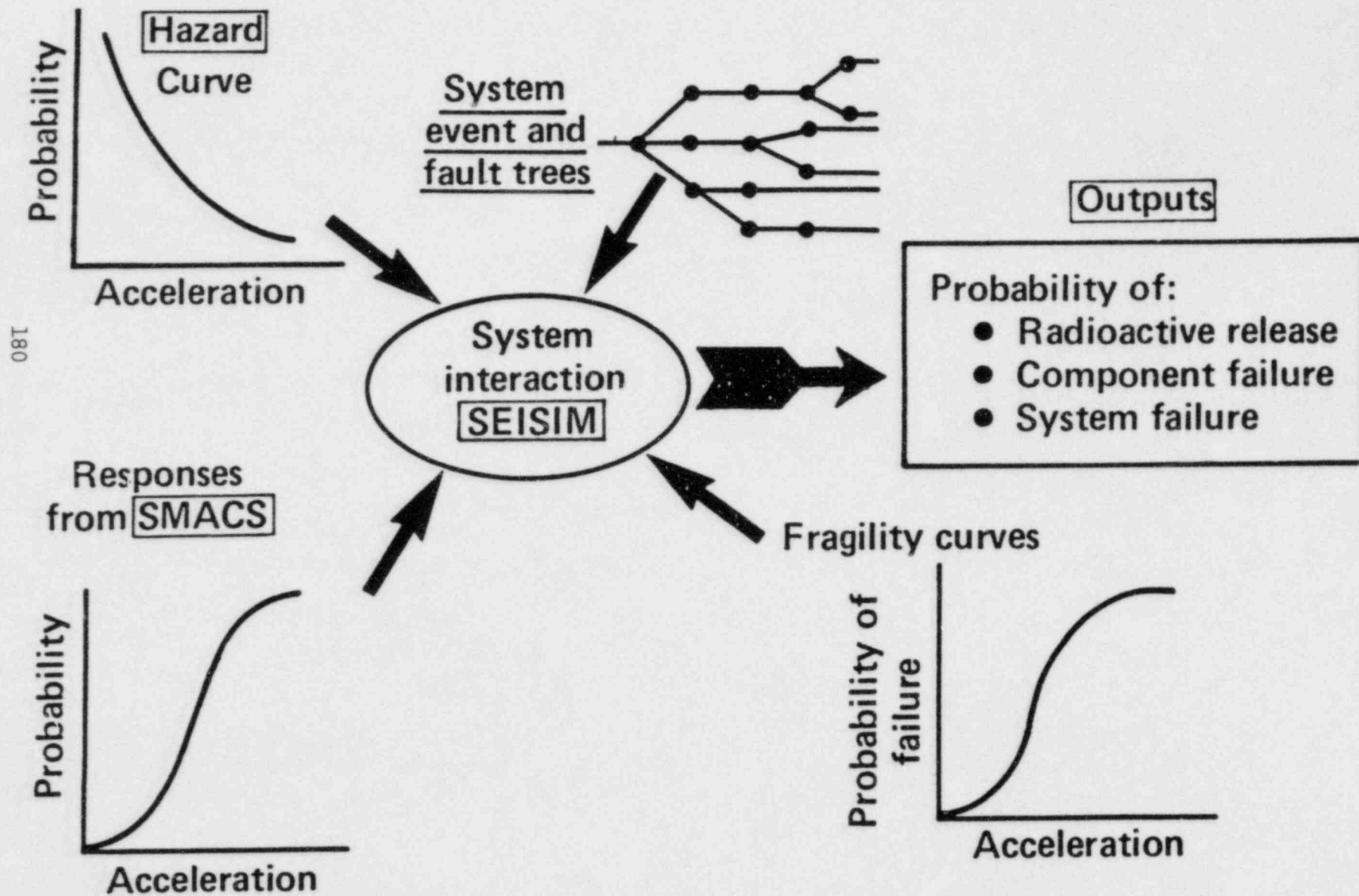
TABLE 1:   ZION TOP SEVEN ACCIDENT SEQUENCES
(82% of Core-Melt Probability)

Rank	Initiating Event	Accident Sequence	Core-Melt Probability (Per Year)
1	Transient with no PCS (T2)	* $\overline{K}$ L $\overline{B}$ $\overline{P}$ $\overline{Q}$ $\overline{C}$	** 1.3e-6
2	Small-Small LOCA (S2)	$\overline{K}$ L C F	4.1e-7
3	Small LOCA (S1)	$\overline{K}$ C $\overline{D}$ $\overline{J}$ F $\overline{H}$	3.4e-7
4	Small LOCA (S1)	$\overline{K}$ C D F	3.2e-7
5	Large LOCA (A)	$\overline{C}$ D $\overline{E}$	2.3e-7
6	Reactor Pressure Vessel Rupture (R)	C F	1.6e-7
7	Large LOCA (A)	C D F	1.3e-7

Systems

K - RPS
L - AFW
B - Bleed & Feed
P - PORV (open)

Q - PORV (close)
C - CSIS & CPCS (inject)
D - ECI
J - core geometry

F - RHR
H - ECR
E - CFCS (recirculation)
PCS - Pwr. Conversion Sys.

---

* Bar over letter means system success. No bar means system failure.
** Base Case point estimate for comparison.

Table 2: Calibration Factors for Shear Wall Structures

Soil Stiffness Characteristic V_S (fps)	Peak Accelerations		Peak Forces	
	Mean	Cov	Mean	Cov
3500	1.07	.261	1.23	.178
2000	1.25	.389	1.42	.289
1000	1.47	.500	1.64	.360
500	2.02	.601	2.14	.403

Assumes half-space modeling of the soil with soil density of 130 pcf, Poisson's ratio of 0.4, and soil material damping of 5%.

182

Table 3: Comparison Between Detailed & Simplified Analysis of Zion

	Release Probability/Year		Man-Rem/Year	
Release Category	Detailed	Simplified	Detailed	Simplified
1	2.9E-8	1.6E-7	0.2	0.9
2	1.4E-6	3.7E-6	6.5	17.8
3	5.4E-7	1.1E-7	2.9	0.6
4	0	0	0	0
5	8.3E-10	0	0	0
6	1.7E-7	6.3E-8	0	0
7	1.5E-6	9.5E-6	0	0.2
TOTALS:	3.6E-6*	1.3E-5*	9.6	19.5

* Base case point estimate for comparison purposes.

REFERENCES

1. P.D. Smith, et al., Seismic Safety Mardgins Research Program Phase I Final Report, Lawrence Livermore National Laboratory, Livermore, CA, UCRL-53021, Vols. 1-10, NUREG/CR-2015, Vols. 1-10 (1982).

2. M.P. Bohn, et al., Application of the SSMRP Methodology to the Seismic Risk at the Zion Nuclear Power Plant, Lawrence Livermore National Laboratory, Livermore, CA, UCRL-53483, NUREG/CR-3428 (1983).

3. C.Y. Kimura, J.E. Wells, Categorization of PWR Accident Sequences and Guidelines for Fault Trees: Seismic Initiators, Lawrence Livermore National Laboratory, Livermore, CA, UCID-20211 (1984).

4. L.L. George, W.J. O'Connell, Importance and Sensitivity of Parameters Affecting the Zion Seismic Risk, Lawrence Livermore National Laboratory, Livermore, CA, (To Be Published).

5. H.E. Lambert, Circuit Breaker Operation and Potential Failure Modes During an Earthquake: A Preliminary Investigation, Lawrence Livermore National Laboratory, Livermore, CA, UCID-20086 (1984).

6. J.J. Johnson, et al., SSI Sensitivity Studies and Model Improvements for the U.S. NRC Seismic Safety Margins Research Program, Lawrence Livermore National Laboratory, Livermore, CA, UCID-20212, NUREG/CR-4018 (1984).

7. D. Bernreuter, et al., Seismic Hazard Characterization of the Eastern United States: Methodology and Interim Results for Ten Sites, Lawrence Livermore National Laboratory, Livermore, CA, UCRL-53527, NUREG/CR-3756 (1984).

VALIDATION OF SEISMIC PROBABILISTIC RISK
ANALYSIS (PRA) METHODS

C. A. Kot and M. G. Srinivasan
Argonne National Laboratory
Argonne, Illinois

1. INTRODUCTION

Seismic PRA methods have been applied in recent years to clarify safety issues for nuclear power plants. The reason for this is the realization that seismic events can affect many plant systems simultaneously, and therefore, can be a significant or even dominant contributor to overall risk. The randomness of the seismic hazard, the uncertainties and variabilities of the needed data, and the approximate nature of the methodology raise questions of credibility with respect to the results of seismic PRAs. This, in turn, leads to questions as to the conclusions that can be drawn from the results concerning safety implications and regulatory actions. While the ultimate answer to these questions depends on the intended end-use of seismic PRAs, it is nevertheless useful to attempt to validate the methodologies. The objective of validation research is to obtain information that can be used by NRC to develop acceptance criteria for seismic PRAs and thus improve the regulatory process. Work on seismic PRA validation was initiated during FY 1984 as part of the research effort of the Mechanical-Structural Branch, DET-NRC/RES.

2. BACKGROUND

Seismic PRAs are performed at different levels of sophistication and detail, but in general, in all analyses three aspects are considered and technical information is sought in three areas as inputs to a seismic PRA, these are:

- A description of the seismic hazard at the site.
- A description of the level and parameters of the hazard that will cause vital plant components and systems to fail including descriptions of failure modes.

- A description of failure scenarios (event trees and fault trees) for the plant.

A calculation procedure assembles this information to produce the results of the PRA. Thus the seismic hazard, given usually in terms of a functional relationship between probability and site acceleration, is used to determine spacial distributions and accelerations at the plant foundation. The susceptibility of the nuclear power plant to the seismic excitation is then determined. This part is most often called an estimate plant fragility. In its most general form this estimate requires a response analysis of the soil-structure systems, to establish among other things the base motion at component supports. Also needed are predictions of component response, and a determination of component fragilities and structural capacities. The final aspect of the seismic PRA is the systems analysis which defines accident scenarios and consequences, and provides estimates of risk. All of the parts of seismic PRAs contain stochastic elements, and all of them are in need of validation. The effort under discussion here focuses its attention, (at least initially), on the center part of a seismic PRA, that is, it is primarily concerned with the validation of methods and data which are used to determine plant response and fragility. However, it should be remembered that research results in the plant response and fragility area must be characterized in terms of parameters specified in the seismic hazard and must be useful in performing the plant systems (risk) analysis. This requires that there be close coordination between research in all these areas to ensure compatibility of results. While a specific effort may be limited to one area, cognizance must be taken of the interrelationships to other seismic PRA elements.

The current effort is concerned with the validation of the seismic PRA method through the use of data from testing. The term "testing" is used here in a broad sense. It includes test data from specific laboratory and field experiments as well as measurements obtained from earthquakes or other natural environments. The immediate objective of this work then is to assess the potential of using test data, in the areas of plant response and fragility, to improve the predictive capability and enhance the understanding of the results of seismic PRAs. Ultimately research related to seismic PRAs must address the question: What information can PRAs provide and with what level of

confidence? Another goal is to improve the modeling of the phenomena and to develop better data bases including fragility information in order to enhance confidence in seismic PRA outcomes.

3. VALIDATION NEEDS

The first step in this effort is the assessment of validation needs for seismic PRA methods. This includes both the determination of verification requirements for the calculational procedures and the identification of deficiences in data bases. Of particular concern is the adequacy of linear analysis, which is generally used, to predict the expected nonlinear response of structures and components under seismic loading. Further of interest is the validation of response variability caused by uncertainties in input parameters and by variabilities in analysis methods. Identification of the needed fragility data for structures and components is also a major concern. Again the probabilistic nature of the information must be kept in mind, both mean values and distributions about the mean are of interest.

A first attempt to assess the requirements for seismic PRA validation has been completed. This was accomplished through the collective efforts of a working group from the National Laboratories, Consultants, and NRC which was coordinated by ANL. Further refinements in the assessment of validation needs, developed through the interaction with an advisory panel of internationally recognized experts in structural analysis and PRA methodology.

The initial identification of PRA validation needs gave little consideration to the relative importance of the selected items and was primarily based on perceived need or lack of information, i.e., identification of "soft spots" in the methodology. However, it did become apparent that ranking of potential validation tasks according to a measure of how much their successful execution would contribute to increasing the usefulness of seismic PRAs would significantly enhance the value of this study. Criteria used for ranking have to be compatible with the objectives of the effort as stated earlier. For this study validation is also considered to include the broader objective of confidence building or improvement of seismic PRA methodology that can be achieved by comparison with or through the use of physical data and

187

experience. Three steps were used to determine priorities and focus on the most effective research. First, elements of seismic PRAs that are amenable to validation by experiments or existing data were identified. Second, criteria were selected for assessing the potential benefits of experiments for improving the utility of seismic PRAs. Finally, an evaluation of the utility of testing based on these criteria was performed.

The following set of criteria was used to help prioritize the choices of seismic PRA validation needs:

- Significance as indicated by past earthquake experience
- Significance as indicated by past seismic PRAs
- Contribution to common mode failures
- Contribution to uncertainty in risk
- Potential for reducing modeling uncertainties
- Contribution to uncertainty in loads
- Potential for simplification in methods and models
- Applicability to a large number of plants

No claim is made that the above criteria are all inclusive. However, they cover most of the problem areas concerning current PRA methodology. The first six criteria deal with improving the results of seismic PRAs and with confidence building. The last two criteria are concerned with streamlining the analysis procedures, a worthwhile goal in itself considering the large effort required in performing seismic PRAs. While many specific items in need of validation were identified, they all fall into four categories

- Soil-structure interaction (SSI)
- Structural response
- Structural capacity
- Component and equipment fragilities

Seismic response of the soil-structure-component system is important in two aspects. First, the soil-structure system or component is intended to perform its design (safety) function during and after an earthquake. For buildings this includes providing support for systems contained therein; for vessels

this includes providing a leak tight pressure boundary; etc. Second, the soil, structure, and subsystem also act as transmitters and filters of vibratory motion to the safety systems whose fragility is of interest. Thus, their response is important because it modifies the loads to vital components and equipment. The key question is: Given an ear uake described by its seismic hazard curve parameters, what are the median (m an) level of seismic response, variability of responses, and correlation of seismic responses? The variability of seismic response addresses the major stochastic aspect of seismic PRAs, and response correlation deals with the system characteristics which lead to responses of like intensity throughout the plant. The validation effort must address all the aspects of seismic response.

Among the inputs required for seismic PRA evaluations are estimates of failure data and descriptions of damage mechanisms for structures, equipment and components. These may be described as stress levels, deflections, accelerations that cause failures, etc., together with information on the failure mechanisms, i.e., rupture, relay chatter, binding of valve stem. Again these component fragilities and structural capacities are subject to variabilities due both to randomness and uncertainty and validation of all aspects is of interest.

3.1 Soil-Structure Interaction Analysis

The overall soil-structure interaction (SSI) analysis which uses linear methods and a substructuring approach is in need of validation. The deconvolution methods for determining the loads at the foundation must be verified and the spacial variation of the seismic loading in an earthquake need to be better defined. While some aspects of these methods may be validated in experiments with sufficiently strong SSI such that nonlinear behavior is induced, the latter two items can only be addressed through measurements during actual earthquakes.

With respect to spacial variations of the seismic free-field motion, there are a number of aspects that need to be assessed. First, the exact nature of the waves that transmit the earthquake disturbance is not well defined. Second, a simplified procedure, i.e., deconvolution, is typically used in nuclear power

189

plant soil-structure interaction analysis. Third, the presence of inclined bedrock and/or lateral boundaries and water tables may influence the spacial variation of free-field motions. The latter are not accounted for in typical analyses. No experimental validation of any of these items currently exist.

Another generic problem associated with the strong earthquakes is soil failure. Specifically soil liquefaction or collapse may occur. These are highly nonlinear phenomena and depend on many factors including water content and compaction. Due to their complexities these phenomena are typically not modeled in a seismic PRA and their significance needs to be evaluated. A problem of similar nature is the so-called basemat uplift where the basemat separates from the soil. The level of excitation, site properties and foundation geometry influence the magnitude of uplift which in turn significantly modifies the floor response spectra. Typical SSI analysis, being based on linear methods, including that used for seismic PRAs cannot directly model uplift. When uplift is found to be important it is treated outside the direct methodology by a fragility approach. These methods are in need of validation.

3.2 Structural Response

Structural analysis in seismic PRAs deals with the response and behavior of large structures (buildings) and major components, e.g., steam generators. In most cases the best estimate of response is obtained on the basis of design safety margins. In general, the calculations must also yield accelerations at support locations of smaller components and piping in order to estimate their response. Even though excitation magnitudes exceeding design levels are of interest in seismic PRAs, the entire procedure is based on linear-elastic analysis and uses a substructuring approach. The accuracy to which these procedures represent high-level nonlinear response has not been verified. It is thought that experiments with sufficiently strong excitations to induce nonlinear effects are needed to provide validation of the methods. The question that must be addressed in this validation is this: Given an earthquake, how well does the best estimate analysis procedure predict behavior of structures and components, or alternatively, how conservative is a design procedure.

190

3.3 Variability of Response

Most seismic PRA methodologies require both the median values and the variability of the seismic response. This variability depends on: variations (randomness) in earthquake excitation, variations in physical properties (random and uncertain) of the soil/structure/piping/component system, and variations (uncertainties) in modeling ability. These variations contain a deterministic component which depends on the level of excitation, as well as a random (statistical) component. Since both response variations with excitation level and random variability can have significant impact on the final risk estimate and since many uncertainties exist in this area, it is considered to be an important candidate for validation.

In seismic PRAs large numbers of like equipment are often grouped into generic categories with estimates of dispersion or item to item variability at a given level of base excitation. This applies both for response and fragility. Validation of these variabilities may also be addressed by the use of test data from complex plant systems.

3.4 Correlation of Response

The correlation of responses, i.e., the tendency for responses to be simultaneously high or low, may significantly affect the overall risk depending on the correlations between fragilities and the fundamental characteristics of the system. Response correlations may be due to the level of earthquake or the dynamic characteristics of the system. Little hard information exists concerning correlations to be expected under typical seismic loading. Thus this is an area in need of validation.

3.5 Structural Capacity and Failure

In the seismic PRAs, nonlinear response of structures beyond yield as well as failures have to be considered. Two aspects of this nonlinear behavior are important: the state of stress in the structure and the effect on subsystem input motion. The first is important to local and global failure of the structure, the second can significantly influence the response of

191

subsystems. There is no simple well established procedure of analysis for concrete structures under such a condition. For steel structures consisting of beams, columns, and/or rigid frames the analysis may be accomplished through the assumption of plastic hinges, collapse mechanisms, and the use of pseudo-static loads representing the seismic loads. For concrete structures, other techniques are necessary for modeling the nonlinear behavior, (e.g., cracking) and the discrete reinforcement. Validation of models in this area is necessary.

In seismic PRAs where higher than design loads are considered, the concrete structures are often analyzed as linear elastic structures without taking into consideration the geometrical nonlinearity nor the material nonlinearities of concrete cracking or rebar yielding. However, some PRA methodologies use ductility factors in developing fragility estimates for concrete structures. These techniques were initially introduced by Newmark and were based on single-degree-of-freedom models. The validity of using such factors coupled to the linear-elastic analysis in modeling actual power plant structures needs to be established. In order to validate this methodology there is also need to establish the modes of failure of such unconventional rigid structures.

Interactions between adjacent buildings may be another element to consider in seismic PRAs. For closely spaced buildings the possibility of impact between buildings under earthquake loading cannot be excluded, and, in fact, has been identified in some cases as a problem of concern. Verification that such impacts may or may not occur is of importance.

3.6 Component and Equipment Fragilities

For components and equipment, fragility is normally represented as probability of failure vs "load" level. This information includes median values and uncertanties characterizing the capacity data. In addition, it is necessary to assume and describe the failure mechanism leading to failure.

The existing data base is sparse and the applicability of some of the data (derived from experience not related to nuclear power plants) to nuclear components is questionable. Since the quality of the end product of a seismic

192

PRA (probability of failure and frequency of radioactive release) is directly related to the quality of the fragility data, an effort should be undertaken to expand and improve the existing data base.

Fragility of piping systems is an important element in the seismic PRA methodology. Often a single master piping fragility curve is used and representative scale factors are applied to estimate the fragilities of specific piping systems. The master piping fragility curve is based on analytic predictions of ductile collapse mechanisms (the possibility of cracks is considered to a limited extent). The "elastically" calculated moment at the highest stress point in a piping system is used as the key input parameter for piping fragility.

In reality, the seismically induced failure of piping systems is likely to be much more complex than that assumed. Progressive support failure, multiple plastic hinge formation in the piping, ratcheting, etc., are mechanisms that may have to be specifically addressed in predicting failure. Current pipe test data indicates that piping has large seismic margins, but information regarding actual failure levels is either limited, or nonexistent. Again extension of the data base, i.e., validation is needed.

In most analysis practices, the PRA methodology tends to separate response and fragility estimates between structures and attached components. The effect of possible interaction at the boundaries between structures and components is not addressed. For example, the prediction of anchorage failures for components and piping fragilities does not specifically consider the combined effects of concrete wall cracking and seismic loads at the anchorage. It should be determined whether there have been significant oversights regarding boundary interaction effects between components and structures.

3.7 Ranking of Validation Needs

Each of the seismic PRA elements identified above as a candidate for validation was assessed in light of the criteria stated earlier. A judgment was made if additional information or data, i.e., validation by testing, in this area would contribute significantly to improving seismic PRAs as

expressed in each of the specific criteria. A simple three level ranking was used in the process by assigning numerical values as follows:

2 - Yes, important contribution
1 - Yes, moderate contribution
0 - No, little or no contribution

The results of this evaluation are presented in matrix form in the following table. This is a very coarse and preliminary evaluation and is in some respects not very satisfactory and in need of refinement. For example, equal weights are given to all criteria used in the evaluation. This obviously can and should be modified. Nevertheless the ranking provides some indication of the importance of the seismic PRA elements identified for validation. The areas of highest priority for validation are:

Soil-Structure Interactions
Capacity/Failure of Structures
Equipment Fragility
Structural Response
Variability of Response
Spacial Variation of Free-Field Motion

4. VALIDATION THROUGH TESTING

Testing that could serve to validate each of the critical elements, i.e., "soft spots," of seismic PRAs is discussed here. At this preliminary stage, the testing is only described in general terms. The possible role of certain ongoing or planned large scale testing efforts in seismic PRA validation is also described briefly.

Since testing in general requires large resources, it is imperative that prior to making specific test recommendations all available existing data be reviewed as to their appropriateness for validation. Where possible, participation in ongoing or planned experimental efforts that could provide some of the needed data should be explored.

VALIDATION MATRIX

Criteria / Validation Items	Contribution to Uncertainty in Risk	Contribution to Uncertainty in Loads	Reduction of Modeling Uncertainty	Contribution to Common Mode Effects	Past Physical Experience	PRA Experience	Applicability to Large No. of Plants	Potential for Method Simplification	Total Points
Free Field Spatial Variations	2	2	1	1	2	0	2	1	11
Soil-Structure Interaction	2	2	2	2	2	1	2	1	14
Soil Failure/Liquefaction	1	1	1	2	1	1	1	1	9
Basemat Uplift	1	1	1	1	1	1	1	0	7
Structural Response	2	2	2	1	1	1	2	1	12
Component & Piping Response	1	1	1	1	1	0	1	1	7
Variability of Response	2	2	2	1	1	1	2	1	12
Correlation of Response	1	1	1	2	1	1	1	1	9
Structural Capacity/Failure	2	0	2	2	1	2	2	1	12
Piping Fragility	1	0	1	1	0	1	1	2	7
Equipment Fragility	2	0	2	1	1	2	2	2	12
Component/Structure Interfaces	1	1	1	1	1	1	2	1	9

4.1 Testing to Validate Soil-Structure Interaction (SSI)

Testing suitable to establish the validity of seismic PRA soil-structure interaction (SSI) analyses must be conducted with systems that are of sufficient size to somewhat simulate prototypic behavior, i.e., frequency response, magnitude of motions and gravitational effects similar to those of the actual nuclear power plant structures. Small scale testing for the verification of SSI analyses is not very satisfactory, since scale effects may mask some salient behavior while exaggerating other phenomena. While excitation through the ground similar to an earthquake is preferable, some features of the SSI analysis may be evaluated for other loading, e.g., by shaker, as long as the SSI response is significant. The latter is necessary regardless of what testing approach is used and it is preferable that the motion be sufficiently strong to induce nonlinear effects so as to challenge the analyses which use linear equivalent methods. The test data used in SSI analysis validation should also provide information on the adequacy of the substructuring approach used in most calculations.

At this juncture two testing programs have been identified as possible sources of data for SSI analysis validation. These are: The HDR Program conducted by KfK in the Federal Republic of Germany and the planned 1/4 scale containment earthquake testing by EPRI in Taiwan. While the HDR tests will use excitations by a large shaker on the operating floor, significant rocking of the entire structure is expected so that at least some aspects of SSI analyses may be verified. The 1/4 scale containment experiment in Taiwan is specifically being designed to provide data for SSI analysis verification and should indeed be useful for validating all aspects of analyses used in seismic PRAs. The major drawback of this test program is that one has to await the earthquakes. Since downhole instrumentation will be provided, the earthquake experiments in Taiwan should also yield information on the spacial variation of free field motions and can thus serve the validation of deconvolution techniques used in estimating that variation. The only other possibility of validating this aspect is through the use of weapons test data such as that obtained at the Nevada test site. In addition, all data from previous earthquakes recorded at different depths and/or locations in the free field

should be reviewed for possible use in the validation of analytical procedures.

Soil failure and liquefaction have been simulated under many testing conditions, e.g., high explosive testing and centrifuge experiments. Data from such testing may provide insight into error bounds of analyses which neglect these phenomena. The data may also permit improvement in the determination of impedance functions and damping values for soils prone to failure. However, data from such testing should be used with great caution because of the difficulties of scaling such effects. Existing data in this area should be systematically reviewed and evaluated as to their usefulness.

Test data on the phenomenon of basemat uplift are of interest for assessing the errors introduced in analyses that neglect this process and also for the purpose of developing other approaches to treat the phenomenon. Strong uplift has been observed in some high explosive model testing. This, however, is not prototypical data and may be too severe a challenge of the analyses used for seismic PRAs. However, the data may yield some insight into the relative importance of various phenomena. The only other data source may be from instrumented structures at the Nevada Site which have been subjected to strong ground motion during weapons testing.

4.2 Testing for Structural Analysis Validation

Testing to validate the response analyses for large structures, components and piping used in seismic PRAs should include benchmark type tests for each of the subsystems separately and also for integral structure/component/piping configurations. Response levels in the testing should extend well into the nonlinear and plastic regime to bound the errors expected from the linear equivalent analyses.

Tests for piping should include base motion excitation and appropriate test data may become available from the tests conducted by ANCO for EPRI/NRC. For simple structures some data may be available from recent EERC testing. However, to really challenge the analyses procedures structural configurations of significant complexity are needed. Here again the Phase II HDR shaker

197

tests with high accelerations and large displacement may play a significant role. Also the 1/4 scale containment earthquake experiments to be conducted in Taiwan under EPRI sponsorship should be of value. While the structure is simpler than a real power plant, it will contain a large componment (steam generator) and piping to provide sufficient complexity to challenge the structural analysis methods.

4.3 Testing to Validate the Variability of Response

Variations in earthquake excitation cannot easily be addressed by testing and one must rely on collecting more complete earthquake information and on validating the computational procedures against this data. Variations in physical parameters may include the shear moduli and material damping for the soil, and frequencies and modal damping for the structures and subsystems. To estimate variability of response due to variations in physical properties and soil/structure parameters, multiple testing of reasonably complex systems under various loads is required. An alternative is to subject multiple "identical" test items to a smaller number of excitations. Both of these approaches require large efforts. It is more cost effective to validate variability of response by analyzing data from structures which for other reasons are subjected to multiple testing. Thus, any well-instrumented large structural system which has been subjected to multiple earthquakes or other excitation, may provide data for establishing variability limits of physical properties and structural parameters. Similarly, if a number of analyses with models of varying complexity were used to predict the response of such systems and/or if different analysts performed such calculations, each with his own model, a measure of the expected modeling variability could be obtained. Should such a structure also contain a number of equipment items in a generic category, e.g., many valves, it should be possible to obtain some measure of response variability for given equipment categories.

The HDR plant system (which is well instrumented) was subjected to a variety of loadings during Phase I of its test program and will experience multiple loadings at higher excitation levels during Phase II testing. Thus, the analysis of past and future HDR tests in the light of seismic PRA requirements, should provide good insight into the variability of response and

198

physical properties of complex reactor systems. While the loading in HDR is not seismic, such an exercise should give an indication of how structural and component frequencies and damping vary with load magnitude, type, and duration. Similarly the HDR tests can be used to evaluate modeling variability by performing a number of predictive analyses, each by different analysts, for a given test. Some insight into both parameter variability and modeling uncertainties can be readily gained from the Phase I testing experience and can be enhanced during Phase II testing. Since HDR contains many equipment items belonging to single generic categories, the possibility of obtaining variability estimates for the response in a generic group of equipment exists.

The planned surveillance by EPRI of the 1/4 scale containment model in Taiwan, which will be subjected to multiple earthquakes, may also yield data which can contribute to the validation of response variability. Again if multiple predictive analyses are undertaken in conjunction with the earthquake experiments, information on modeling variability can be generated.

4.4 Testing to Validate Correlation of Response

Again validation data in this area can only be obtained from multiple testing of large complex structures preferably containing a significant number of equipment items. Response correlation produced by earthquake level excitation can only be simulated through significant ground shaking. However, it may be possible to ascertain response correlation related to structural configurations in other vibrational testing, since it is essentially related to structural load transmission.

The HDR offers an integral structure-equipment system of significant complexity. It is thus likely that response correlations during high level loadings will occur. This holds particularly for correlations arising from the structural configurations. The use of HDR data for establishing the expected correlations should therefore be explored.

4.5 Testing to Validate Structural Capacity and Failure

As indicated earlier there is a need for seismic PRA to assess the effect of neglecting the geometrical and material nonlinearities and to establish the modes and levels of failure for concrete and steel structures. In view of the coupled uncertainties in damping, modeling, material properties, ductility, etc., it is difficult to devise tests for validation.

Since ductility factors are used in determining the capacity of concrete structures it is essential that validation testing be done at least at the level of incipient failure and with subassemblies which include the proper boundary conditions, e.g., box structures. Testing to failure of as-built structures is, in general, not feasible, unless a well instrumented structure experiences failures during an earthquake event. The 1/4 scale containment structure that will be subjected to earthquakes in Taiwan may provide such data. While the response and failure of models subjected to severe loading may not be prototypic, such testing may provide information on possible failure modes and may be helpful in validating computational approaches.

The HDR reinforced concrete shield building will be subjected to high excitation levels and is well instrumented. However, safety requirement precludes gross structural failures. The most that can be expected is some cracking of concrete and separation in interior shear walls. Thus no real failure data will be forthcoming, but the data may be useful for determining the effect of such structural softening on global response. Further, it appears possible that during the large shaker tests an experiment simulating impact between building (containment and equipment tower) may be designed.

4.6 Testing to Validate Component and Equipment Fragility

To define the fragilities, i.e., probability of failure vs. load level, and the descriptions of failure mechanisms for nuclear power plant equipment, it is best to rely on separate effects tests such as shake table experiments. To obtain such data for the multitude of plant equipment is an extremely costly undertaking. Therefore to reduce this effort, existing data, even if not

fully applicable, should first be evaluated. Next the components most important to plant safety and whose failure has a large contribution to risk must be identified and testing must concentrate on these items.

Where available, use should also be made of equipment qualification data. While the applicability of these data is limited, it may nevertheless define the tail end (at low level of excitation) of the fragility curve. Also used should be experience data from actual earthquakes. However, this data base is limited and documentation often is poor. On the other hand, some of this information could be especially useful since the equipment may have been in use for some time, thus the data could contain the effect of aging and possible construction errors.

For piping it is essential to obtain failure data for total piping systems (including pipe runs, supports, nozzles, components, anchors, branch connections, etc.) and for a variety of piping configurations. Once knowledge is gained concerning overall failure mechanisms, it may be most cost effective to proceed with separate effects testing in those areas indicated to be most critical to failure, e.g., pipe elbow collapse, crack propagation, etc. Empirical data on subelement behavior would then be combined by analysis to better predict piping behavior.

It is desirable that pipe system tests simulate earthquake conditions, i.e., loading through support anchors and earthquake-like load histories. The NRC/EPRI funded pipe tests performed by ANCO use this type of loading but load levels may not be high enough to induce many failures.

High level testing of integral facilities are needed to discover oversights in seismic PRAs regarding interactions of interfaces and boundaries between structures and components, between walls and penetrations, between piping and components, etc. If particular boundary effects are found, then it may be best to quantify these through supplemental testing that includes boundary modeling.

The large shaker tests of HDR are not sufficient in number and their excitation levels are not sufficiently high to cause significant failures in

components and piping. With proper instrumentation it is possible to obtain some limited information such as correlation between support excitation and nonlinear component response. Also the HDR large shaker testing appears to present favorable conditions under which boundary and interface effects may be discovered. This may only be qualitative information, but it will serve to identify areas requiring attention.

Higher excitation levels will be achieved in the HDR tests when direct loading will be applied to piping systems by hydraulic actuators. Testing to failure and/or pipe plastification will take place. To make these experiments meaningful for the validation of piping fragility, careful experimental design is necessary so that failure is not dictated by the points of load application. To obtain appropriate excitation, multiple shakers may be required. Since HDR equipment and piping has undergone much testing and loading it may be necessary, prior to using any of the new test data, to estimate the useful life degradation which may have occurred in the equipment.

5. CONCLUSIONS

The needs for validation and experimental data in seismic PRA methodologies are assessed to be in the following areas:

- definition of seismic hazards (seismic input)
- capacity and failure data for equipment, piping and structures
- response analyses of nuclear power plant systems (structure-site-components)

Improvements in the definition of seismic hazards are outside the scope of the current study. It is thought that failure data for equipment and the associated statistical variations are best addressed in separate effects laboratory testing. Piping fragility information requires both system and component testing. Failure information for structures is difficult to obtain because it is not practical to excite as-built structures to damage levels and the scaling of model tests is of doubtful value. Validation of response analyses requires extensive comparisons with experimental data from reasonably complex and complete site-structure-component systems.

Two major testing programs promise to provide significant information for the validation of seismic PRA methods. They are (1) the HDR Program conducted by KfK in the Federal Republic of Germany and (2) the 1/4 scale containment earthquake experiments to be conducted by EPRI in Taiwan. NRC participation in these efforts is therefore recommended.

In the HDR Phase II tests, the structure-equipment system will be subjected to high excitation by a large shaker. However, due to safety considerations, which preclude breaching of containment, the tests are expected to yield little in terms of hard failure data for structures and components. Some damage (plastification) of piping is anticipated and strong nonlinear interactions between structures, equipment, and piping is expected. Similarly significant soil-structure interaction (particularly in the rocking mode) is expected.

Therefore, the HDR experiments primarily provide a good means for validating the response analyses of seismic PRA procedures for piping, structures and soil-structure interactions. In particular it will be possible to evaluate the adequacy of the linear analyses in representing the nonlinear response and interactions of complex plant systems. Further, the existing and newly generated (Phase II) HDR data can be used in evaluating the expected variability of response due to variations in physical parameters and differences in modeling.

The earthquake testing of the 1/4 scale containment in Taiwan is primarily intended to provide data on soil-structure interaction (SSI) of nuclear power plant buildings. The data should permit the validation of all important aspects of SSI analysis methods, including such items as deconvolution techniques, substructuring approaches with their impedance functions, and the adequacy of linear analysis. Information should be forthcoming on the spacial variation of free field excitation. Since some large equipment and piping will be located in the building, the experiments may also serve to validate other aspects of seismic PRA response analysis.

203

HEISSDAMPFREAKTOR (HDR)
PHASE II
VIBRATION TESTS

Lothar Malcher
Kernforschungszentrum Karlsruhe
Federal Republic of Germany

Helmut Steinhilber
Labor für Betriebsfestigkeit Darmstadt
Federal Republic of Germany

The "Heißdampfreaktor (HDR) Phase II Vibration Tests" are part of the HDR Safety Program, which is being carried out by the Kernforschungszentrum Karlsruhe (KfK) on behalf of the German Federal Ministry for Research and Technology (BMFT). KfK is responsible for the technical, organizational and budgetary control of this project. Phase I of the project lasted from 1974 to 1983; Phase II started at the beginning of this year and is planned to be terminated in 1987.

The HDR safety program was subdivided into several Specific Projects corresponding with main items of interest within the overall Reactor Safety Research Program of the BMFT. Subject of this presentation are the structural dynamics investigations with the topics earthquake and aircraft impact (Fig. 1). The investigations chain comprehends the determination of the structural responses and stresses (partially of failure mechanisms) due to earthquake- and aircraft impact-like excitations.

The field of verification in the HDR studies (Fig. 2) serves to show the balance of the two essential parts of it,

- on one side the evaluation of the physical reality by means of experiments,
- on the other side the mathematical simulation of the reality by means of calculations.

The comparison of the results of these both parts - experiments and calculations - should result in the verification phase with:

- Improvement of our understanding of the properties and structural behavior of systems and components
- Quantification of the available safety margins
- Demonstration of the reliability of present design methods
- Optimization and improvement of analytical techniques.

The HDR (on Fig. 3 left) lies on the River Main approximately 50 km east of Frankfurt. In the immediate neighbourhood of HDR there are the first German nuclear power station (VAK) and a conventional coal and oil fired station not to be seen here.

The 100 MWth experimental reactor HDR was decommissioned in 1971 because of extensive fuel element damage after less then 2000 hours of operation. In type, the HDR largely corresponds to a German light water reactor of 1967/68 design status.

Thus, the specific HDR-conditions can be summarized as follows:

- The HDR components and safety relevant systems can be examined on full scale.
- The HDR components and systems are comparable with those in present Light-Water Reactors with respect to material and design.
- The HDR tests can be performed under pressure and temperature (operating conditions).
- Because of the unrestricted clearance granted to HDR for this program, experiments can be carried out to the actual limits of the load carrying capacity of individual reactor components.

Within the structural dynamics investigations testing and accompanying calculations are performed for the

- reactor building
- reactor pressure vessel with corebarrel
- different piping systems
- vessels and tanks

under shaker, snapback and impulse excitation at progressive levels of intensity.

Fig. 4 shows the reactor pressure vessel, the HDU-vessel and the primary steam piping system connecting them. In Fig. 5 the HDU-vessel and the VKL piping system is to be seen.

An overview of PHDR Phase II test groups within SP 4000 (= Structural dynamics investigations) and the corresponding main objectives is given as follows:

TEST GROUPS	MAIN OBJECTIVES
"SHAG" Shakertests of the Reactor Building	Behavior of Building and Mechanical Equipment at High Excitation Levels
"SHAM" Servo-Hydraulic Excitation of the Mechanical Equipment	Behavior of the Mechanical Equipment under Extreme Dynamic Loads
"STO" Impulse Excitation of Outer Containment Shell	Global Effects on Building and Mechanical Equipment due to Local Loading
"RAU" Seismometer Measurements under Environmental Noise Excitation	Validate Ambient Testing as a Simple Means to Quantify Changes in Structural Behavior after Strong Excitations and Provide a Basis for Matching Analytic Models to Real Situation

206

A few remarks on the individual test groups are given below:

"SHAG"

The reactor building was previously excited by means of rotating eccentric mass-shakers and explosive charges buried in the sur- rounding soil to investigate its vibrational response to earth- quake excitation. The results obtained to date for the reactor building (e.g., damping values) suffer from the fact that suffi- ciently high excitation could not be produced. In order to remedy this disadvantage, and in consideration of load and response regi- mes of interest in the licensing process, the test group "SHAG" was conceived. Because no high-explosive tests with larger charges are possible (because of safety considerations for the VAK reactor neighboring the HDR), the only remaining way for "high-level" ex- citation of the reactor building without affecting the surroun- dings is from inside (intended accelerations at the 30 m elevation at the first natural frequency were 0.5 - 1 g).

"SHAM"

The mechanical components, in particular pipes, were in fact exci- ted to relatively high levels during shaker and snapback tests, comparable to levels assumed for real earthquakes. But in order to achieve plastification, the excitation force must be increased by at least a factor of ten. Shaker of appropriate force capacity cannot be mounted on pipes because they would falsify the pipe mass and therefore pipe eigenfrequencies. Snapback excitation has the disadvantage that the maximum load is typically brought about by the static displacement of the pipe. In contrast, the servo- hydraulic shakers should be able to subject the investigated com- ponents to typical earthquake loads, up to the point of failure, without any of the previously mentioned disadvantages.

The excitation and evaluation of prior tests on mechanical components focussed on earthquakes and the relevant frequency range up to 20 Hz. The behavior of systems under high-frequency external loading up to 80 or 100 Hz (aircraft impact) is to be investigated by special tests. Here the load level must be sufficiently large to assure that the "clamp and rattle" regime of the components, particularly constant-force hangers and sway braces, can be overcome. For the same reasons discussed before servohydraulic shakers are suited for this excitation case.

"STO"

This test group will also relate to aircraft impact. Pre-tests with a maximum of four solid fuel rockets on the outer dome of the reactor building were successfully conducted (400 kN force), but the burn time of 500 ms was too long and the resultant load function of too low a frequency. While the so called "Drittler" aircraft impact (this is the design basis force-time history prescribed in the German Reactor Safety Commission guidelines) is characterized by an impulse period of 70 ms, these tests can be better realized by a 20 tonne weight falling from 5 m (200 kN sec impulse) and a corresponding crush zone. Pretests have already been successfully perfomed in autumn 84.

"RAU"

In the forefront of this test group is the systematizing of the vibrational characteristics of structures and components by means of seismometer measurements during excitation by ambient noise, so that the analytically evaluated response characteristics of a structure (which provide the input for analysis of mechanical equipment) can be controlled through routine measurements. Test measurements at HDR have shown that excitation through microseismic soil disturbances and ambient shaking is sufficient to define the desired measurement quantities. One of the most significant

advantages is that the measurements can be performed without any danger whatsoever of damaging the systems in the investigated structure.

Another main objective of this test group is to identify possible changes in the fundamental eigenfrequencies of the reactor building due to strong excitations.

In the following we concentrate on the test group SHAG with shakerexcitation of the reactor building. Because of the high response levels of the building and mechanical equipment expected during these test, a cooperation between the U.S. NRC and KfK-PHDR has been established. The mutual basis of interest of both partners is, that these tests allow to achieve in a large scale integrated system vibration levels in the internal structures and components at sufficient levels to:

1. evaluate structural and mechanical response prediction computer codes at design levels and damage levels for selected subsystems
2. evaluate range of frequency shifts due to nonlinear behavior in the concrete to verify techniques used to develop floor response spectra
3. evaluate pipe damping due to the effects of various supports up to and including limit state conditions
4. evaluate the behavior of various items of energized mechanical and electrical equipment under limit state
5. evaluate the correlation of structural response from low level (including ambient) to high level excitations

As already mentioned, the shaker technique will be used to excite the building up to its own limits, because desired response levels cannot be achieved via blast excitation with respect to the safety of adjacent plants.

209

A standard eccentric mass shaker of an appropriate size, capable to perform steady state vibration tests needs:

- a fine frequency control (1:1000)
- and very high drive power (about 5000 kW)

Additionally, at the desired high levels of force, the structure should not be exposed to steady state vibrations with a large number of load cycles.

It was therefore decided to use a "coast down" shaker technique, that means to bring the vibrator up to speed in a balanced condition and then to unbalance and decouple it from the drive system. The shaker will then run down through the building resonances.

A coast down shaker needs

- no fine frequency control
- smaller drive power (about 750 kW)
- and should achieve the desired high levels of excitation for only a few transient cycles.

Fig. 6 gives an impression of the size of the vibrator, designed by ANCO Engineers, Los Angeles. The eccentric mass of 50 - 80 tons is composed of two equal sectors on a common shaft. These two sectors are shown in this figure in the unbalanced position.

The shaker will be mounted on the 30-m-floor of the reactor building (Fig. 7) and remotely controlled.

In Fig. 8 the shaker force and frequency range are compared with the excitation systems previously installed at the HDR. The force output will be about 20 times higher then during the last shaker test series in 1979.

To get an impression of the building accelerations, displacements, dynamic loads on the mechanical equipment and the number of vibration cycles in resonance, design calculations were performed using a nonlinear, coupled model of the shaker and the building.

Fig. 9 shows typical results of the simulations, in this special case for a test run with approximately 50 % of the projected maximum shaker eccentricity.

For the 100 % load case the calculations indicated building accelerations of 4 - 5 m/sec^2 at the operating floor. Because these values refer to the fundamental rocking mode at 1 - 1.4 Hz, the corresponding displacements are $\pm$ 7 cm. The mechanical equipment will be strongly eccited.

This can be seen in Fig. 10. It shows, that the envelope of the calculated response spectra at the HDR operating floor from several shaker tests with different eccentricities and frequency ranges is comparable to the SSE-design spectrum at the operating floor of modern PWR-buildings in Germany.

This leeds to the question of the safety for the HDR building and its neighbourhood. So, in parallel to the design-calculations a number of safety studies were carried out to determine the limit load carrying capacity of the HDR building and other critical points.

Basically we want to state, that a global structural failure of the building must be avoided, while local damage would be accepted.

The safety aspects, which were considered up to now, are summarized in Fig. 11.

211

There are:

1   the solidity of the shaker itself
2   its connection to the 30-m-floor
3   the connection of the internal and external structure, which we call the "egg-cup" effect
4   the overall stability of the building against tilting and thus the allowable edge-pressure of the basemat
5   the problem of soil liquefaction and
6   the excitation of the adjacent buildings.

Expected test loads due to different shaker runs and estimated load carrying capacity of the HDR are given in Fig. 12. The "egg-cup" effect turned out being most critical. But this limitation can be overcome by constructive measures to prevent the steel containment with the inner concrete structure from slipping in the egg-cup.

So, the unavoidable limitation will result from the maximum allo-wable soil pressure at the edge of the basemat, while exciting the building in its fundamental rocking mode and from possible over-stressing of the basemat, while exciting the building in its out-of-phase bending mode of external and internal structure. We be-lieve the estimated limit values established up to now are conser-vative. Therefore the vibrator will be constructed such, that it will be capable to double its maximum eccentricity.

More detailed calculations will be carried out to establish non-conservative limits for the critical points.

Further steps in preparing these tests are:

-    to start construction of the shaker still this year
-    to perform pretests at the end of 1985

212

- to establish detailed instrumentation plans for about 400 transducers at the building, vessels and pipes
- to establish the final test plan after the more detailed safety calculations are finished.

The main test runs are scheduled for may/june 1986. Thus it should be possible to report at the 1986 meeting on experiences and first results of these vibration tests.

213

INVESTIGATION \ LOAD T-GR.	EARTH-QUAKE SHA, RAU	AIRCRAFT IMPACT STO	BLOWDOWN CON	RBE	RORB	OVERCOOLING TRANSIENTS TEHR	RORV	EMERGENCY COOLING (SMALL LEAK) TEMB	NOT	THERMAL-SHOCK THE
a. FLUID+THERMOD LOAD										
b. STRUCTURAL RESPONSE										
c. STRESS										
d. FAILURE MECHANISM	(SHAM)									
e. DAMAGE ANALYSIS										
f. FUNCTION-ABILITY										

INVESTIGATIONS CHAIN (INVESTIGATIONS FIELD) Fig.1

A   Evaluation of Physical Reality

A1   Physical Phenomena

A2   Dominant Parameters

A3   Boundary Conditions

B   Mathematical Simulation of Reality

B1   Mathematical Model, Method of Solution

B2   Mathem. Simulation of Dominant Parameters

B3   Simulation of Boundary Conditions

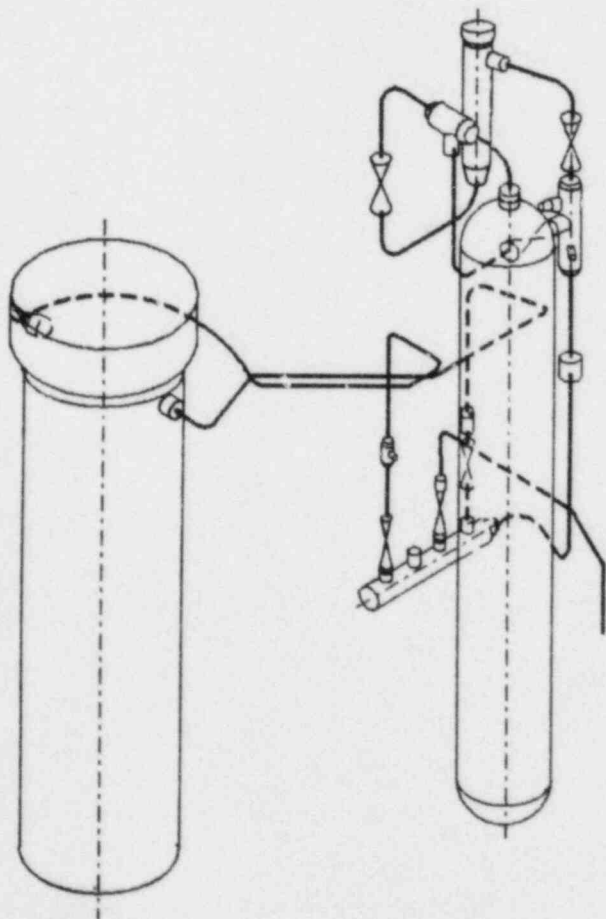System Bound
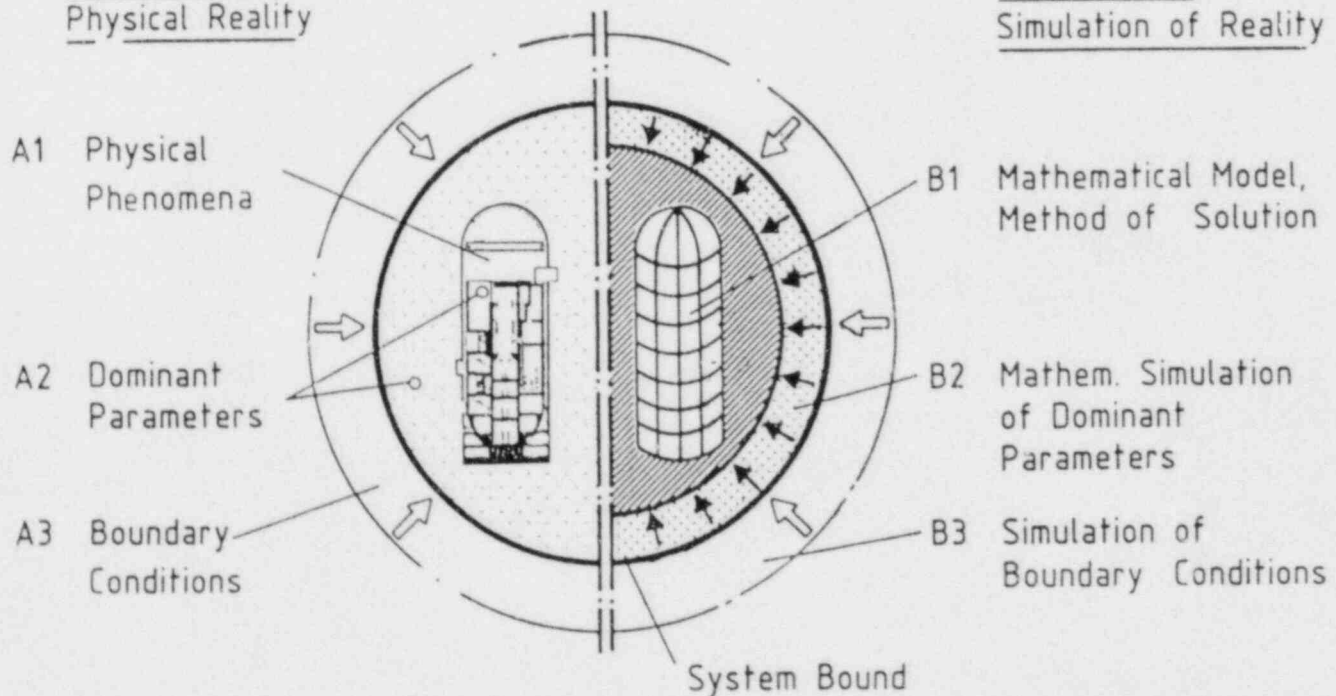
FIELD OF VERIFICATION IN HDR STUDIES Fig.2   214
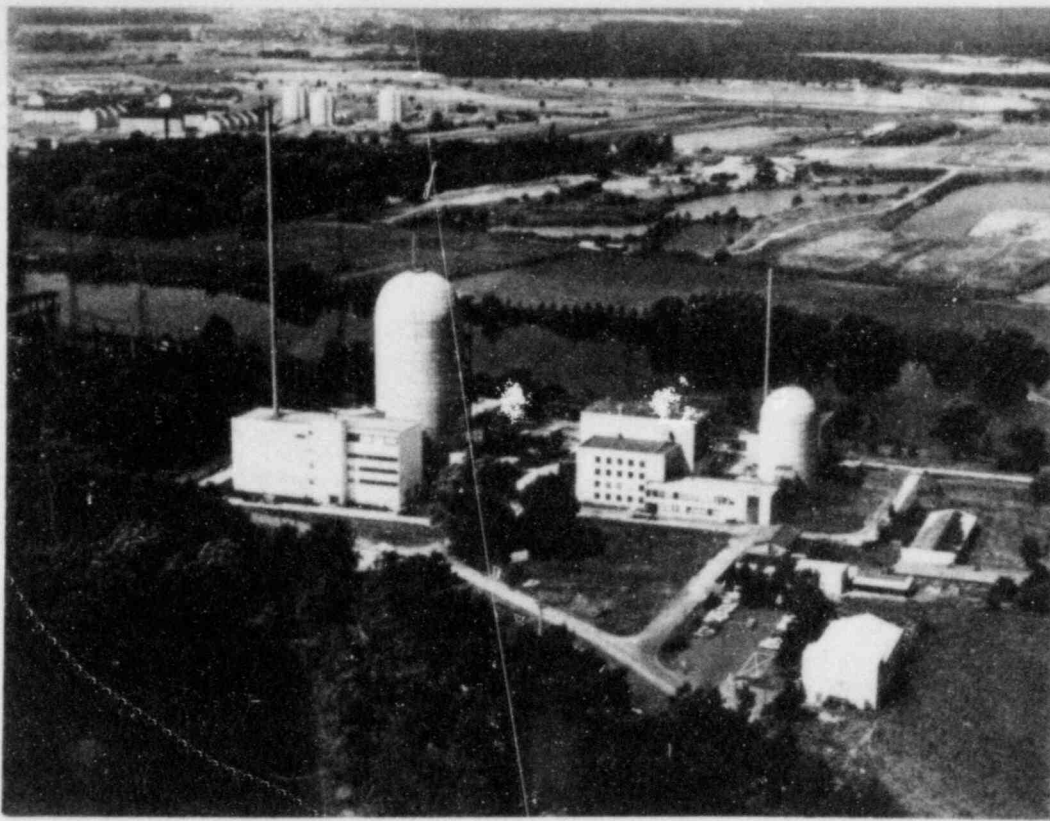
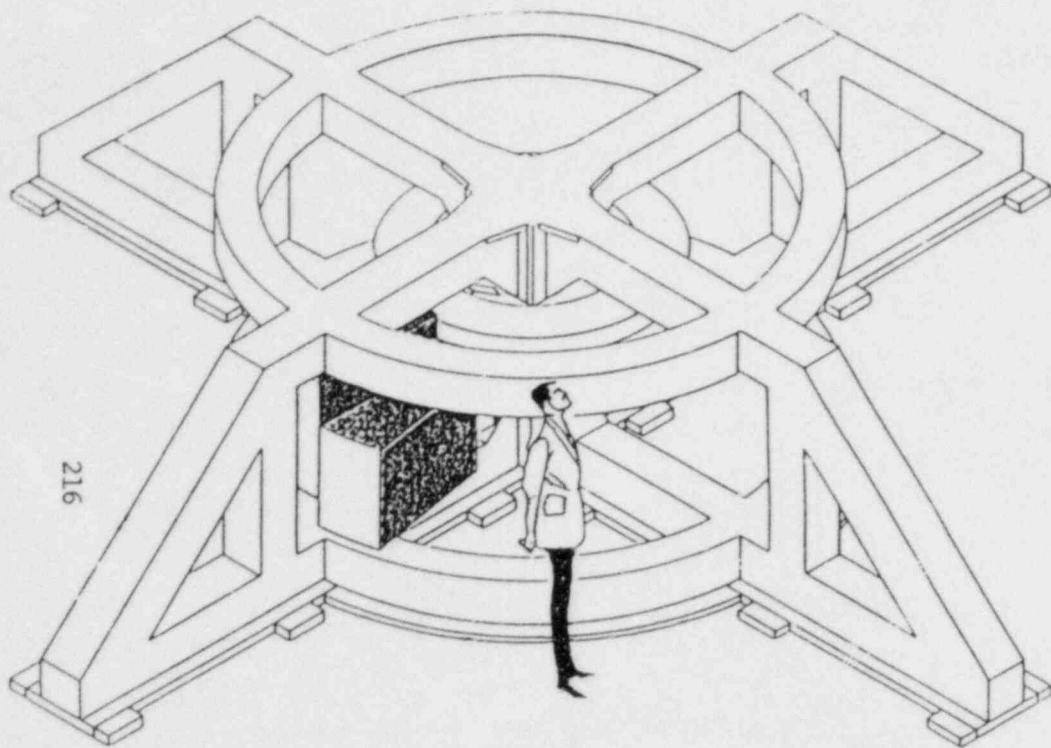HDR TEST FACILITY (LEFT) AND NEIGHBOURGING VAK   Fig.3
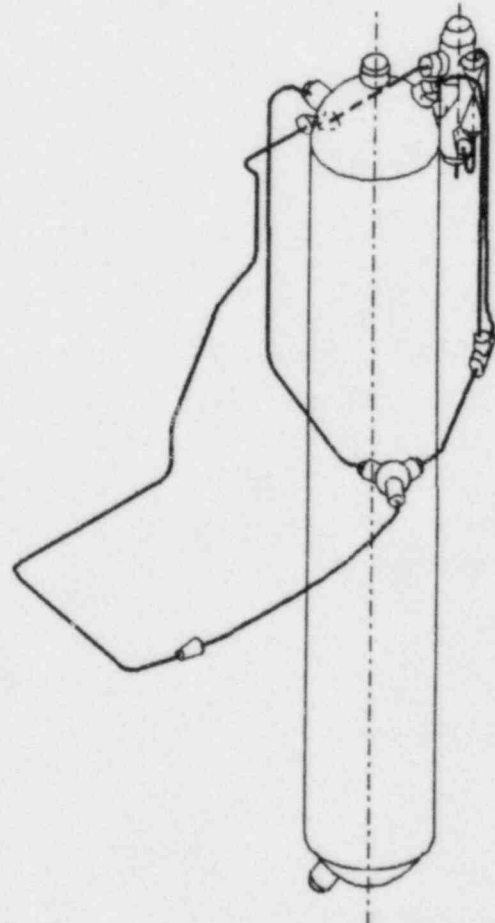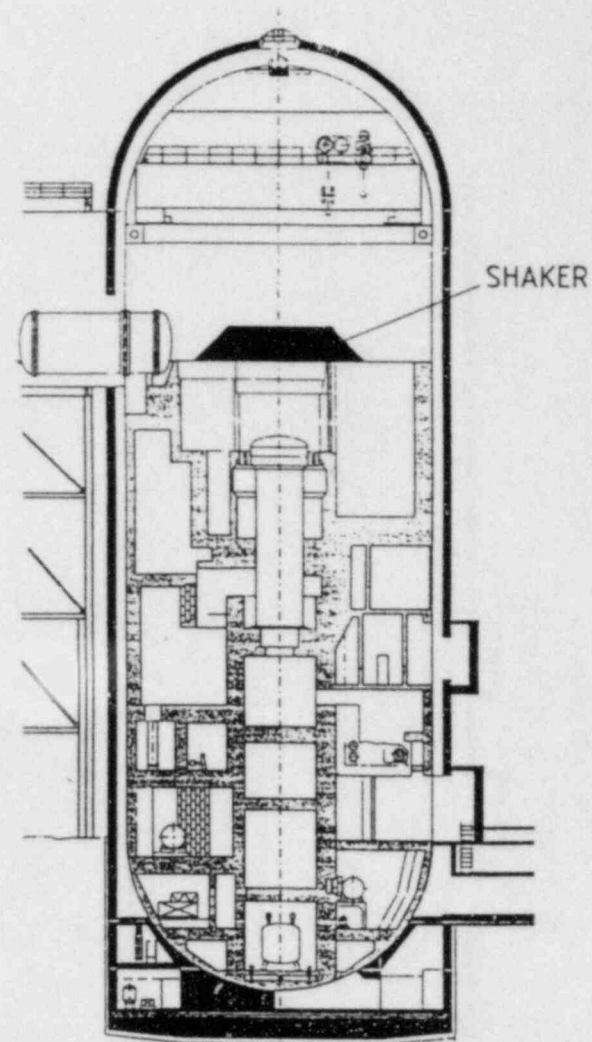
RPV AND PRIMARY STEAM PIPING SYSTEM   Fig.4   HDU-VESSEL AND VKL-PIPING SYSTEM   Fig.5
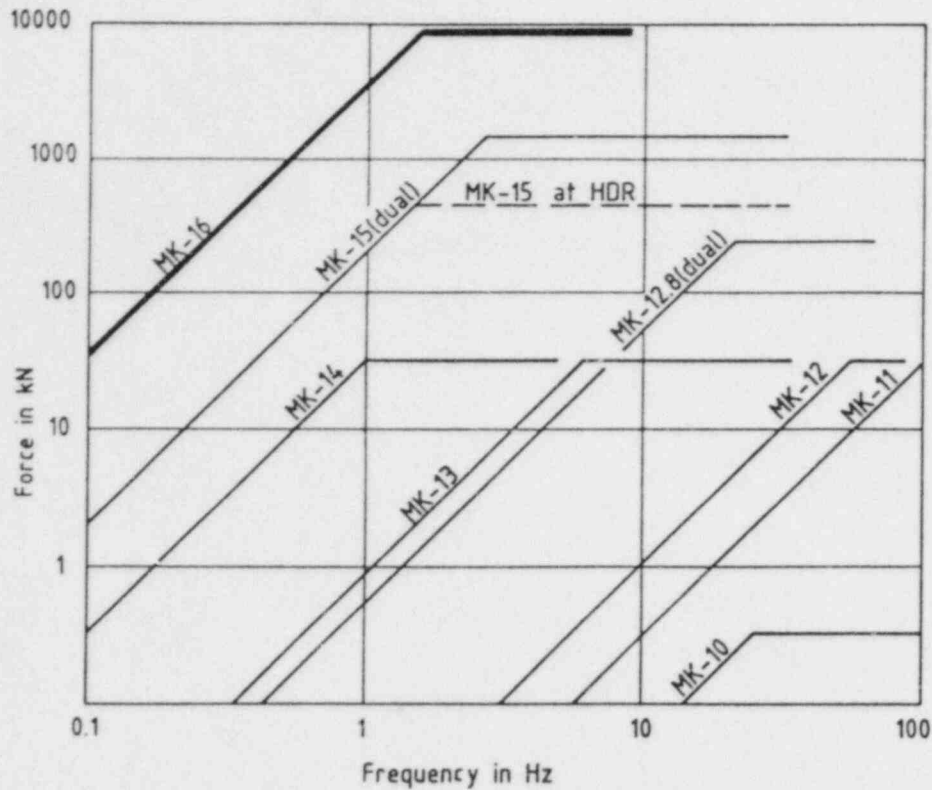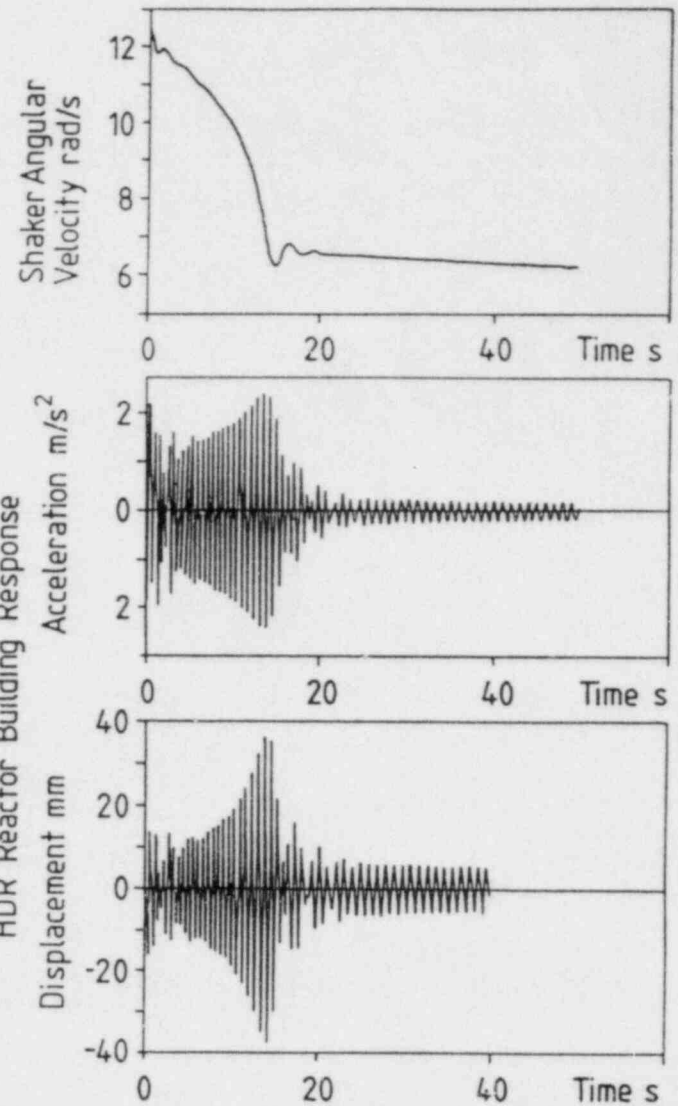
216

ANCO MK16 ECCENTRIC MASS VIBRATOR   FIG.6
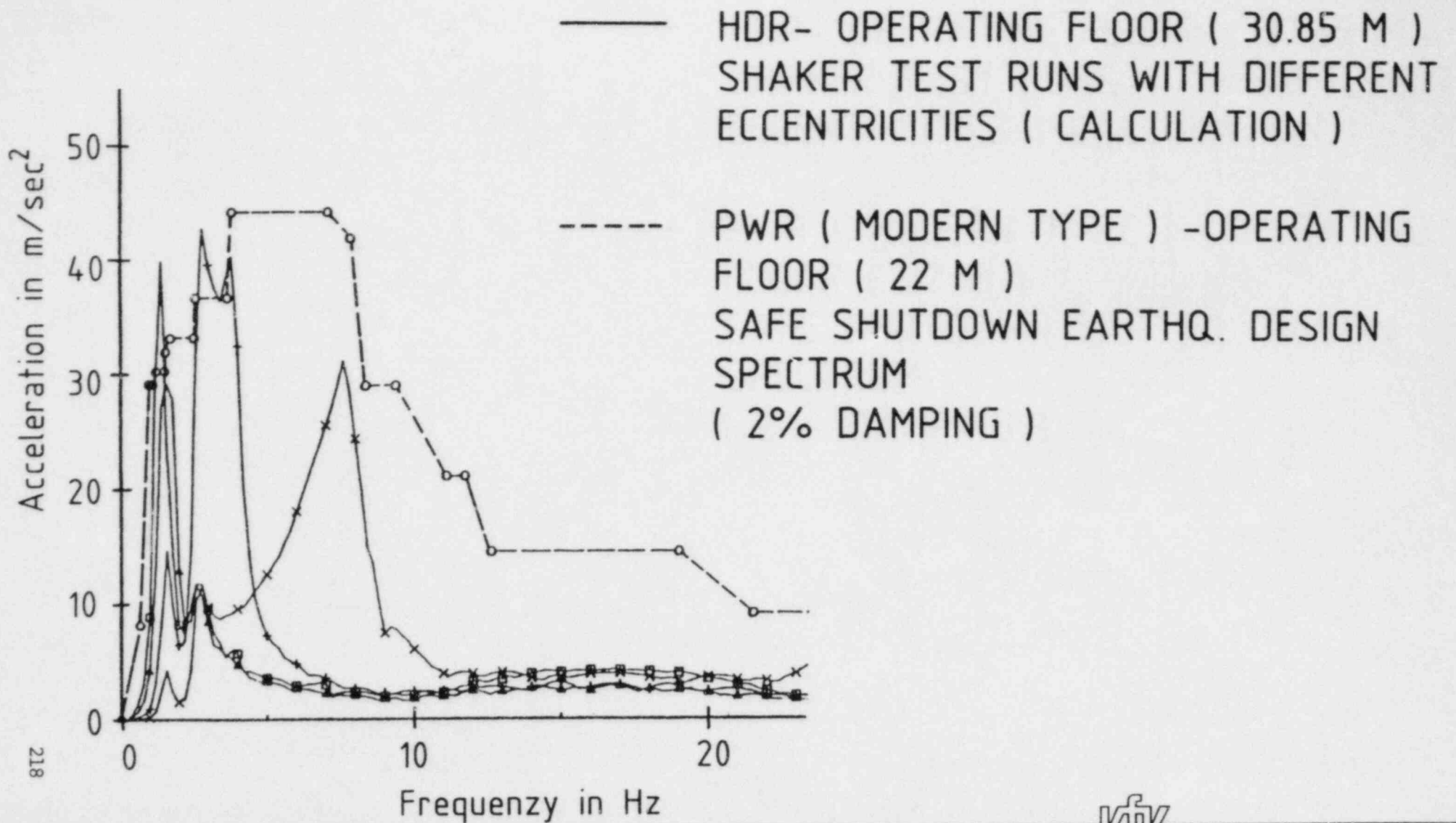

SHAKER

REACTOR BUILDING WITH SHAKER   FIG.7

STRUCTURAL VIBRATORS FORCE
AND FREQUENCY RANGE (ANCO)

Fig. 8
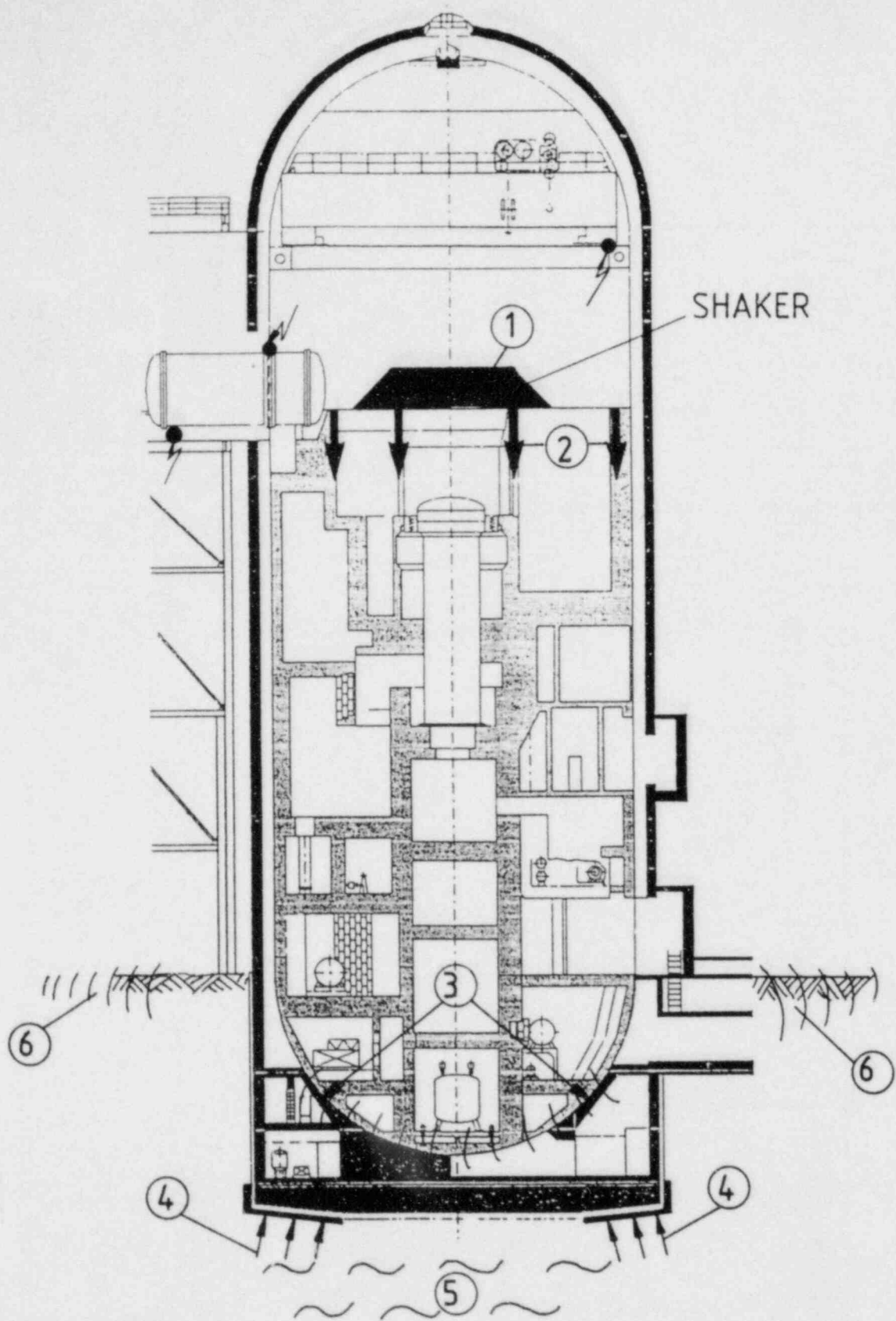

SIMULATION OF COAST-DOWN
SHAKER TEST SH.ECC.64000 Kg m

Fig.9

RESPONSESPECTRA HDR- SHAKER TESTS VS. GERMAN DESIGN SPECTRUM

Fig.10

SHAKER

SAFETY ASPECTS FOR SHAKER TESTS   FIG.11

	EXPECTED TEST LOADS			ESTIMATED LOAD CARRYING CAPACITY OF HDR
SHAKER ECCENTRICITY kg m	100 000	32 000	4 000	
STARTING FREQUENCY Hz	1.6	2.8	8	
MAX. DYNAMIC SHAKER FORCE kN	10 000	12 000	9 750	15 000
MAX. MOMENT "EGG-CUP" MNm	980	890	240	500 *
MAX. MOMENT BASEMAT MNm	1840	880	135	1000 -1400

* This value can be raised by constructive measures

220

RESULTS OF HDR-BUILDING SAFETY INVESTIGATION

Fig.12

EVALUATION OF NUCLEAR FACILITY DECOMMISSIONING PROJECTS PROGRAM - Status
B. L. Baumann - UNC Nuclear Industries, Decommissioning Programs
Department

In recent years major studies have been undertaken by the U.S. Nuclear
Regulatory Commission (NRC) and others concerning the technology,
safety, and costs associated with decommissioning nuclear facilities.
The Evaluation of Nuclear Facility Decommissioning Projects (ENFDP)
program described in this presentation is being undertaken by the NRC to
compile and evaluate the activities of ongoing decommissioning projects.
Assessment and evaluation of the methods, impacts, radiation exposure,
and costs will provide a basis for evaluating licensee's decommissioning
proposals and for future decommissioning direction and regulation.

Program participants include the U.S. Nuclear Regulatory Commission
(NRC) through the Office of Regulatory Research, UNC Nuclear Industries
(UNC) through the Decommissioning Programs Department, and nuclear
facility licensees.

A computerized data collection system has been developed to store and
manipulate relevant data from the nuclear facility decommissioning
projects in this study. The decommissioning information included in
this data base includes but is not limited to:

- Costs for labor, waste disposal and shipping.
- Radiation exposure and facility dose rates.
- Volume and curie content of generated waste.
- And lessons learned.

Decommissioning projects for which data have been collected include the
following:

Research Reactors
   - Ames Laboratory Research Reactor
   - North Carolina State University Reactor
   - PNL Estimates for Decommissioning a Reference Research Reactor
Test and Demonstration Reactors
   - Elk River Demonstration Reactor
   - Fermi 1 Demonstration Reactor
   - Plum Brook Test Reactor
   - PNL estimates for Decommissioning a Reference Test Reactor
Pressurized Water Reactors
   *Shippingport Atomic Power Station
   -PNL estimates for Decommissioning a Pressurized Water Reactor
   *Data from the Recovery Efforts at Three Mile Island 2
Boiling Water Reactors
   * Humboldt Bay 3
   - PNL Estimates for the Decommissioning of a Reference Boiling
     Water Reactor

   *Facilities where data collection is ongoing

221

This presentation will primarily status the progress of the program with emphasis on projects not yet completed. These are Humboldt Bay Unit 3, the Shippingport Atomic Power Station Decommissioning and the Three Mile Island Unit 2 recovery efforts.

HUMBOLDT BAY UNIT 3

The Humboldt Bay Power Plant (HBPP) Unit No. 3 is a nuclear unit owned and operated by Pacific Gas and Electric Company (PG&E) and located approximately 4 miles southwest of Eureka, California. Unit No. 3 is a single cycle, natural circulation, 65 MWe boiling water reactor (BWR) operated for the production of electricity. Also on the plant site are two oil and/or natural gas fueled units and two gas turbine mobile emergency power plants.

The reactor achieved criticality on February 16, 1963 and operated commercially from August 1963 until July 1976. On July 2, 1976, Unit No. 3 was shutdown for annual refueling and for the performance of seismic modifications. Seismic and geologic studies were already in progress. In December 1980, it became apparent that the cost of completing the backfits required may make it uneconomical to restart the unit. Work was suspended at that time awaiting further guidance regarding backfitting requirements. In 1983 updated economic analyses indicated that restarting Unit No. 3 probably would not be economical, and in June 1983 PG&E announced the decision to decommission the unit. The Humboldt Bay Unit 3 Decommissioning Plan describes the activities required to implement that decision.

During the 13 years of commercial operation, 11 core operating cycles were completed. In general, the operating history of HBPP Unit No. 3 is similar to that of other boiling water reactor designs. However, early fuel failures (stainless-steel-clad fuel elements), and minor leakage from the fuel storage pool, had occurred during reactor operation. Spills and leaks have caused some soil contamination within the Unit No. 3 restricted area. Off-site concentrations of nuclides are within the range of background.

The alternatives that the NRC has defined for decommissioning (SAFSTOR, DECON, ENTOMB) all include shipment of spent fuel off-site prior to amending an operating license to a possession-only license. The NRC definition of custodial SAFSTOR is placement and maintenance of the facility in a state of protected surveilled storage. The facility may be left intact except that all fuel, radioactive fluids and wastes would be removed from the site. There are currently no facilities in the U.S. to receive spent fuel since none of the following is either currently operating or accepting uncontracted spent fuel:
- Spent Fuel Reprocessing Facility
- Away-From-Reactor Storage Facility
- Geologic Repository

Consequently, PG& E has concluded that spent fuel storage at HBPP falls within the definition of custodial SAFSTOR.

PG&E plans to place UNIT No. 3 into custodial SAFSTOR for a dormancy

period of up to 30 years. The spent fuel assemblies will be stored on site until a federal repository is operating and able to receive the spent fuel. Custodial SAFSTOR assumes that operations and security personnel will remain on-site to maintain and provide continual surveillance. PG&E has executed and submitted a contract for the disposal of spent nuclear fuel to the Department of Energy in accordance with the terms of the Nuclear Waste Policy Act of 1982.

Several activities will be performed prior to beginning SAFSTOR decommissioning. These are:

- Removal of fuel assemblies from reactor core (completed February 1984).
- Storage of spent fuel assemblies in the spent fuel storage pool (completed February 1984).
- Decontamination of 44 new fuel assemblies and return to the vendor.
- Drain and flush plant systems not required by the Unit No. 3 operating license.
- Processing and disposal of radwaste stored on-site.
- On-going facility decontamination activities.

Following approval of the possession-only license amendment application by NRC, the following decommissioning activities will be completed to establish custodial SAFSTOR.

- Selective system/component layup.
- Selective system/component modification for operations during SAFSTOR.
- Selective system/component facility decontamination.
- Waste consolidation, treatment, solidification, and shipment.
- Baseline radiation and contamination survey and baseline environmental characterization to establish initial SAFSTOR conditions.

Completion of preparations for safe storage is expected by January of 1986.

During the custodial SAFSTOR period, significant activities will include operation of the Spent Fuel Storage Pool and related waste management facilities and maintenance of those components required for fuel removal and facility dismantlement. In addition, security, facility and environmental monitoring, periodic reporting to the NRC, and periodic revision of the Dismantlement Plan will continue throughout the SAFSTOR period.

THE SHIPPINGPORT STATION DECOMMISSIONING PROJECT

The Shippingport Atomic Power Station is a prototype reactor built to generate electrical power. This pressurized water reactor operated from December 1957 to September 1982 with three different cores. It's thermal power has ranged from 230 to 505 megawatts over its lifetime

223

because of changes in reactor core configuration.

The plant site is located 25 miles west of Pittsburg, Pennsylvania. The reactor, although not as large as current power reactors serves as a good model for future commercial reactor decommissionings. This reactor will be decommissioned by the immediate dismantlement or "DECON" option. This entails removal & disposal of all radioactive material from the site and final release of the site for unrestricted use.

The current schedule calls for actual decommissioning work to begin September 1985 with project completion scheduled for September 1988. About $72 million will be spent on actual decommissioning activities with an additional $8 million to be spent through 1984 for planning, engineering and environmental studies. Most of the planning and engineering have already been completed. As a result of the engineering study, the decision was made to remove the reactor vessel in one piece rather than segmenting it as originally planned. The one-piece removal technique is expected to save millions of dollars in costs, a year's time, a significant amount of worker exposure, and about 80 overland truck shipments of radioactive material.

The 25-foot-high, 10-1/2 foot diameter vessel will be encased in a poured shielding material such as concrete, sealed, and transferred to a barge docked in the Ohio River within the Shippingport site boundary. From there, the vessel will be barged to the Hanford site for burial.

THREE MILE ISLAND UNIT 2 - POLAR CRANE RECOVERY

On March 28, 1979 the Three Mile Island Nuclear Station, Unit-2 (TMI-2) experienced a partial loss of coolant water which exposed the upper portion of the reactor core. Resulting temperatures in the core region were in excess of 2500 F causing considerable damage to the core and possibly to other reactor components.

Contaminated reactor coolant water was released to the reactor building basement and to the auxiliary and fuel handling buildings. Release of the contaminated water resulted in gross contamination of the interior of the reactor building and the auxiliary and fuel handling buildings requiring extensive decontamination and waste handling operations to restore these buildings. Decontamination and equipment repair activities have required many manhours of labor and many manrem of exposure to the workers.

Because of the vast quantity of information generated during decontamination, equipment recovery and waste handling activities at TMI-2, the Nuclear Regulatory Commission (NRC) requested that this information be assembled, analyzed and entered into a computer data base for historical purposes. The information also serves as a comprehensive base line for future planning, estimates and actions required should an incident of this type occur again.

The TMI-2 polar crane suffered severe damage as a result of the

accident. Beside being grossly contaminated, the crane electrical components were damaged by hydrogen ignition and exposure to the excessive moisture in the containment building atmosphere. Restoration of the crane is required to accomplish defueling and other cleanup activities.

The TMI-2 polar crane recovery required approximately 2184 manhours of radiation area work, and 155 1/2 manrem of exposure. Table 1 summarizes the exposure by major element. Approximately 60% of the labor and exposure were incurred by the contractor hired for the job. Contractor personnel included all crafts (electricians, ironworkers, carpenters, pipefitters, welders, radiation monitors, laborers, etc.) Plant maintenance, health physics, and quality assurance support account for approximately 21%, 14%, and 1.2% of the labor and exposure for the polar crane recovery respectively. The actual report contains more detail but this summary is presented as an example of how the data base can be used. These figures for recovery of the polar crane do not include general support outside the radiation area, decontamination and characterization of the containment prior to July 1982 or preventative maintenance since December 1983.

Table 1 - Summary of Labor and Exposure for Recovery of the Three
Mile Island Unit 2 Polar Crane

	Labor (Manhours)	Exposure(Manrem)
Contractor (Catalytic)	1324.	91.7
Maintenance	477.	31.2
Health Physics (Rad Engineering)	287.	24.5
Quality Assurance	27.	1.8
Other	69.	6.3
Total	2184.	155.5

ENFDP REPORTS

The following is a listing of reports generated to date by the ENFDP program. As additional projects are completed or in the case of Three Mile Island Unit 2 as additional portions of the project are completed additional reports will be released.

Program Plan	NUREG/CR-2522 REV 1
Elk River Reactor	NUREG/CR-2985
Enrico Fermi-1 Reactor	NUREG/CR-3116
Ames Laboratory Research Reactor	NUREG/CR-3336
North Carolina State University Reactor	NUREG/CR-3370
Plum Brook Reactor Facility	NUREG/CR-3605
Annual Summary Report	NUREG/CR-3550
Reference Boiling Water Reactor	UNI-2461
Reference Pressurized Water Reactor	UNI-2462
Reference Test Reactor	UNI-2463
Reference Research Reactor	UNI-2596
Three Mile Island Unit 2 Polar Crane Recovery	NUREG/CR-3884

Copies of these reports can be obtained by contacting:

U.S. Nuclear Regulatory Commission
5650 Nicholson Lane
Rockville, Maryland 20852
ATTN: D.W.Reisenweaver, Program Manager

CONCLUSION

The ENFDP program is following the decommissioning of reactors to provide the NRC with data to evaluate the methods, impacts, radiation exposures and costs of reactor decommissioning. Collecting the experience from these ongoing decommissioning projects and from future projects to be added to the program will aid the NRC in evaluating licensee decommissioning proposals and developing decommissioning direction and regulation.

THE PERFORMANCE OF DEFECTED SPENT LWR FUEL
RODS IN INERT AND DRY AIR STORAGE ATMOSPHERES[a]

C. S. Olsen
EG&G Idaho, Inc.

ABSTRACT

A testing program using eight commercial PWR and BWR spent fuel rods was conducted to investigate their long-term stability under a variety of possible dry storage conditions. The objective of this project is to provide the Nuclear Regulatory Commission (NRC) with the information to confirm or establish spent-fuel, dry storage licensing positions regarding long-term, low-temperature (<523 K) spent fuel rod behavior during dry storage, and for radioactive contamination arising from spallation of cladding crud. Until now, the testing program has included three interim nondestructive examinations and one destructive examination. This paper presents the results of the third examination conducted to determine any degradation in eight fuel rods after being subjected to 13 168 h at temperature. During this examination, visual observations, diametrical measurements, and isotopic analysis of smears were used to assess the fuel rod behavior and particulate release.

The PWR fuel showed no measurable change from the pretest condition. The artificial defects had not changed and no diametrical growth in the cladding occurred. A BWR fuel rod replaced one that breached after the second interim examination, and a 1.9 cm crack developed in this rod at the bottom defect. About 17% cladding deformation was observed at the defect. Minute amounts of crud consisting of the cobalt-60 isotope fell into the

fuel rod capsules. A slight amount of fuel (0.1 g) from the breached BWR fuel rod was found in the capsule. The BWR fuel rod removed after the second interim examination was destructively examined. The fuel was oxidized to U_3O_8 in the area of the cladding defect. The extent of oxidation decreased further away from the breach, also corresponding to smaller cladding deformation. The extensive fuel oxidation may result from intergranular diffusion of oxygen through the open porosity. Release of fission gases in a sealed fuel rod capsule may also be attributed to fuel oxidation along grain boundaries which are open.

The results of the testing with the BWR fuel indicate that dry storage above 490 to 502 K is not acceptable for this particular fuel used. This fuel may be atypical of current fuel design and fabrication techniques. The BWR results may not be applicable to PWR fuel because of the wide differences observed between PWR and BWR fuel rod behavior. The PWR fuel rods are being destructively examined to determine the extent of oxidation, but additional effort is required to determine oxidation mechanisms and identify the causes of the differences in behavior between PWR and BWR fuel.

INTRODUCTION

The contamination potential of spent fuel during long-term, low-temperature (<523 K) dry storage depends on the fuel rod performance in the atmosphere selected for storage. Because breached rods which occur in-reactor are not routinely isolated, some rods with cladding perforations may be stored in dry environments. Contamination may result from spallation of the crud coating or fuel particulate and fission-gas releases from a perforated rod which fails during storage.

A long-term, eight-rod, fuel rod test using commercial fuel was initiated at 502 K covering a wide range of storage atmospheres, rod types, and cladding conditions. These tests were part of a long-range project to evaluate the behavior of spent fuel during dry fuel storage conditions. Results from this project will provide the NRC with the information to confirm or establish spent-fuel, dry storage licensing positions regarding

long-term, low-temperature (<523 K) spent fuel rod behavior during dry storage, and for radioactive contamination arising from spallation of cladding crud.

In an unlimited air atmosphere, oxidation of UO_2 may occur with a concurrent volume expansion and rupture of the cladding. The contamination potential may be enhanced by (a) oxidation of the fuel along the grain boundaries which would release fission gasses trapped in the grain boundaries, (b) fallout of fuel particulate from the rupture, and (c) spallation of the crud from stresses imposed on the cladding by fuel expansion. Similar behavior, although at different rates, may occur with other atmospheres containing impurities such as an inert atmosphere with moisture or some other oxidant. Estimates have been made of maximum storage temperatures expected,[1] but information is needed to assess a satisfactory storage temperature with regards to defected rods in an oxidizing environment.

Four intact and four defected rods were tested. The four defected rods were examined during the first and second nondestructive interim examinations.[2,3] The first interim examination was conducted after 2235 h exposure at temperature, and a second interim examination was conducted after a total of 5962 h at temperature. The third and final nondestructive examination was conducted after 13 168 h; and, a breached rod from the second interim examination, which was replaced with another fuel rod was destructively examined. This paper presents the results of the third interim nondestructive examination and a summary of the destructive examination of the breached fuel rod.

EXPERIMENTAL PROCEDURE

Four PWR fuel rods from the H. B. Robinson reactor and four BWR rods from the Peach Bottom reactor were heated in a furnace to simulate temperatures occurring during dry storage conditions. These fuel rods were described previously.[4,5] Four rods (two PWR and two BWR) each contained artificial defects in the form of 0.76 mm dia holes placed at different orientations and axial positions (Table 1). Stainless steel capsules with

Table 1. Defect Locations

Fuel Rod	Defect Locations[a] (cm)					
	Defect Number 1		Defect Number 2		Defect Number 3	
	Location	Orientation	Location	Orientation	Location	Orientation
B05-E7	36.8	90	179.1	240		
B05-G7	27.9	200	205.7	0		
PH462-D6	52.1	90	224.8	270		
PH462-C5	401.3	0	236.2	0	66.0	0

a. Measured from the top of the fuel rod.

S4 1804

a 1.75 cm inside diameter were used to contain the fuel rods with each one in its own atmosphere (Table 2). One defective rod of each type was placed in a sealed capsule containing 0.1 MPa of an argon-1% helium mixture. The other two defected rods were placed in capsules which terminated at each end with a series of 2 μm and 15 μm in-line filters open to the cell atmosphere. These filter sizes were based on fuel particle sizes expected from ruptured fuel rods.[6] The intact rods were handled in a similar fashion. One intact rod of each type was placed in a sealed capsule containing 0.1 MPa of an argon-1% helium mixture. Also, one intact rod of each type was placed in a capsule containing air-1% helium mixture. The leak rate on the sealed capsules was a minimum of 2.5×10^{-7} cm^3/s.

The fuel rods were heated in a shielded 14-zone, 12.8-m long clamshell furnace capable of holding the eight encapsulated, unmodified LWR fuel rods (Figure 1). The fuel rod capsules were placed around an instrument train which contained 10 axially located thermocouples (Figure 2), and furnace-control thermocouples indicated a 3 K radial temperature gradient, with the center of the furnace being the hottest. The axial variation of the hot zone temperature was 2 K with a time variation of 2 K.

The furnace temperatures were read and printed on paper tape once an hour with a Fluke data logger. During the last 10 weeks prior to shutting the furnace down for the final nondestructive examination, the Fluke data logger was connected to an Apple II+[a] personal computer for storing the temperature data on floppy diskettes for subsequent data reduction.

For each furnace campaign, the furnace was brought to temperature over a 12-h period and, other than for power outages, ran continuously until the interim examinations (Figure 3). The furnace was allowed to cool by natural means at a rate less than 5 K/h. The furnace was operated at 502 K for 5932 h, and then gradually decreased to 490 K during the next 7206 h (Table 3).

Peach Bottom rod PH462-E3 was removed from the furnace after 5962 h at 502 K. This rod was replaced with PH462-C5 which was heated for 7206 h at temperatures decreasing from 502 to 490 K. The remaining seven rods were heated for 13 168 h, 5962 at 502 K and 7206 h from 502 to 490 K.

231

Table 2. Fuel Rod Storage Conditions

Reactor Type	Assembly and Rod Number	Capsule Atmosphere	Capsule Pressure (MPa)	Fuel Rod Condition
PWR	BO-5-G7	Ar/1%-He	0.1	defected (2 holes)
PWR	BO-5-E7	Air	0.1	defected (2 holes)
PWR	BO-5-08	Ar/1%-He	0.1	intact
PWR	BO-5-B8	Air/1%-He	0.1	Intact
BWR	PH462-D6	Ar/1%-He	0.1	defected (2 holes)
BWR	PH462-E4	Air/1%-He	0.1	Intact
BWR	PH462-E5	Ar/1%-He	0.1	Intact
BWR	PH462-C5	Air	0.1	defected (3 holes)

S4 1805
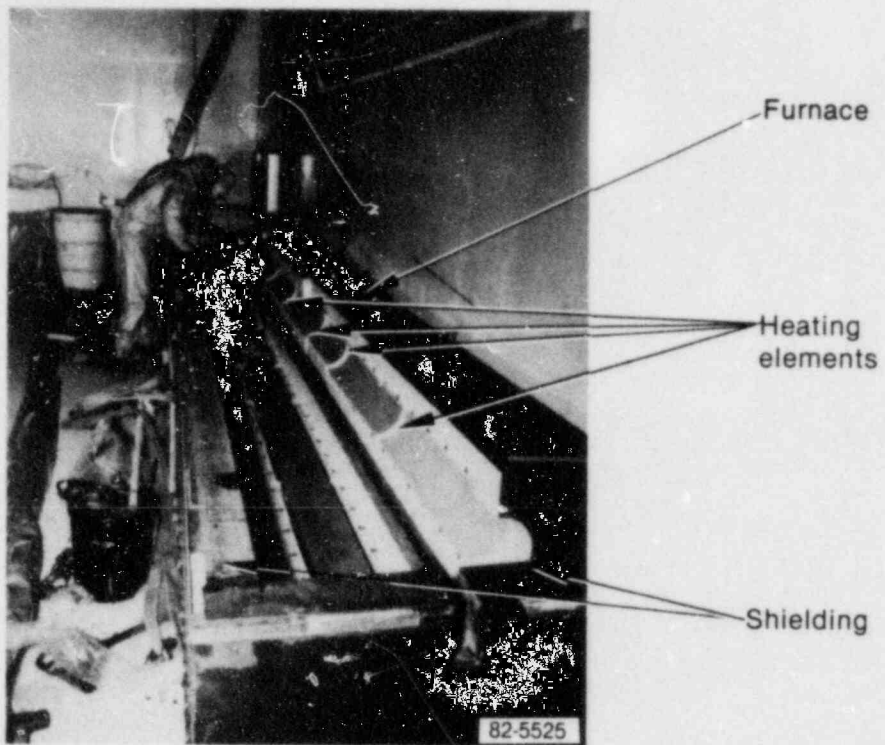
Figure 1. Dry fuel storage furnace.
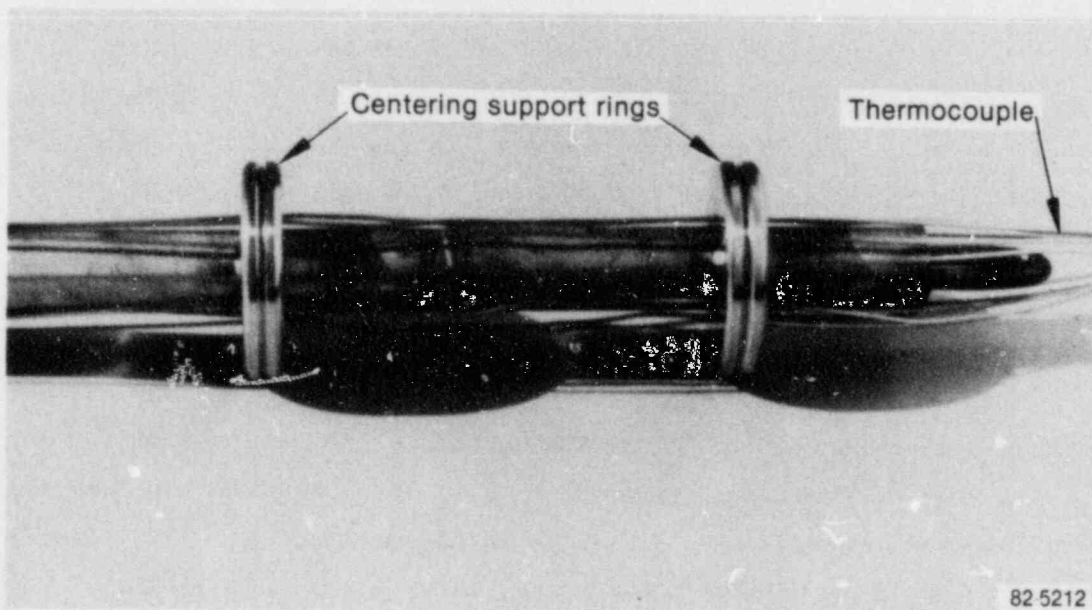
Figure 2. Thermocouple train.

233
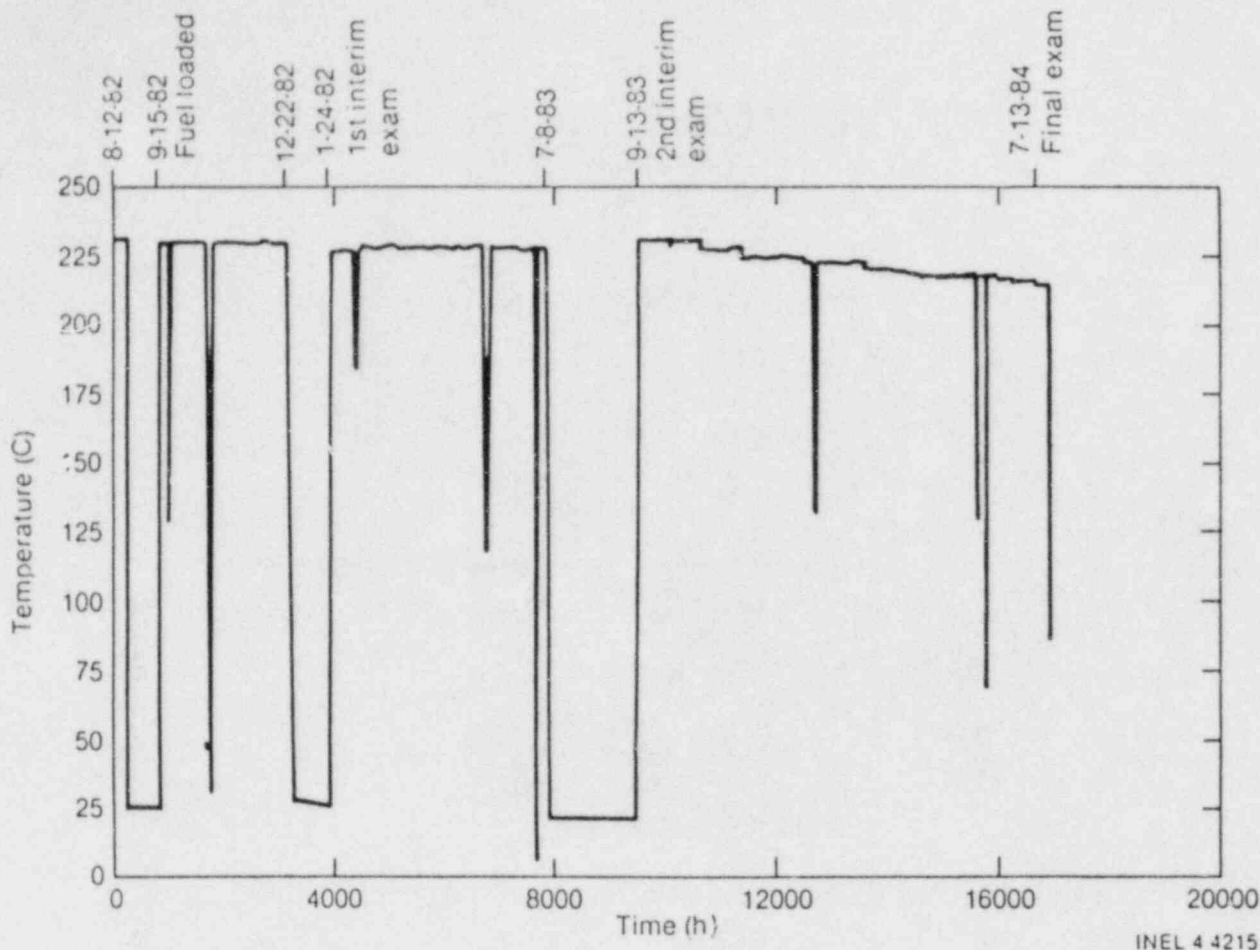
Figure 3. Dry fuel storage temperature history.

The fuel rod capsules were removed from the furnace on July 13, 1984. Gas samples were taken from the sealed capsules, and then the fuel rods were removed from the capsules. The capsules were swabbed to check for any loose crud or fuel particulate. The filters and swabs were weighed to determine the amount of material picked up from the capsules. The swabs were gamma-scanned to determine isotopes and will undergo neutron activation analysis to determine the fissile content.

EXPERIMENTAL RESULTS

The results presented below from the fuel rod nondestructive examination are for the visual examinations and fuel rod strain. Results from the crud measurements which include weight measurements and isotopic analysis of capsule swabs and capsule gas analysis are also presented. The results from the destructive examination of PH462-E3 are summarized since these results were published previously (Reference 3).

234

Table 3. Furnace Temperature Schedule During FY-1984

Date	Actual Temperature (K)
9-14-83	504.3
9-30-83	504.3
10-31-83	501.0
11-30-83	498.5
1-16-84	496.5
2-29-84	493.9
4-16-84	493.5
4-30-84	492.2
5-30-84	491.2
6-29-84	490.2
7-13-84	0.0

S4 1806

Visual Examination

All eight rods were visually examined. The general surface condition of the H. B. Robinson fuel rods appeared to be unchanged. The fuel rods heated in air (both intact and defected) were similar in appearance to those heated in Argon (Figures 4 and 5).

The general surface appearance of the four BWR fuel rods also appeared not to have changed. The artificial defect at the top of rod PH462-C5 did not appear to be fully open. When this hole was drilled into the cladding, indications were that the drill bit had penetrated through the wall. Debris may have been pulled into the hole upon removal of the drill bit. The defect located at the bottom showed significant enlargement and developed an axial crack emanating from both sides of the original hole (Figure 6). Also the top defect in rod PH462-D6 did not appear to be fully open to the atmosphere.

Fuel Rod Strain

Significant fuel rod strain was measured in the BWR PH462-C5 fuel rod. The crack size in PH462-C5 was asymmetrical extending 8.6 mm up the rod and 10.2 mm down the rod. Its width at the widest point was 1.3 mm. The original defect, which was 0.76 mm, increased by 0.25 mm neglecting the crack opening. The fuel rod expanded 17% at 90 degrees from the crack and 7% at 30 degrees (almost parallel) to the crack. The deformation of the failed BWR fuel rods was apparently constrained by the fuel rod capsule. The maximum deformation of the fuel rod was 1.73 cm compared with 1.75 cm inside diameter of the capsule. The fuel rod was stuck inside the capsule when the capsule was being unloaded. No apparent fuel rod strain occurred in the other three BWR fuel rods, based upon the fuel rod diameter measurements. However, although the fuel rod diameter indicated no strain, the middle defect in PH462-D6 slightly increased in diameter by 0.11 mm. The top defect was apparently closed, and measurements indicated nominal defect size.
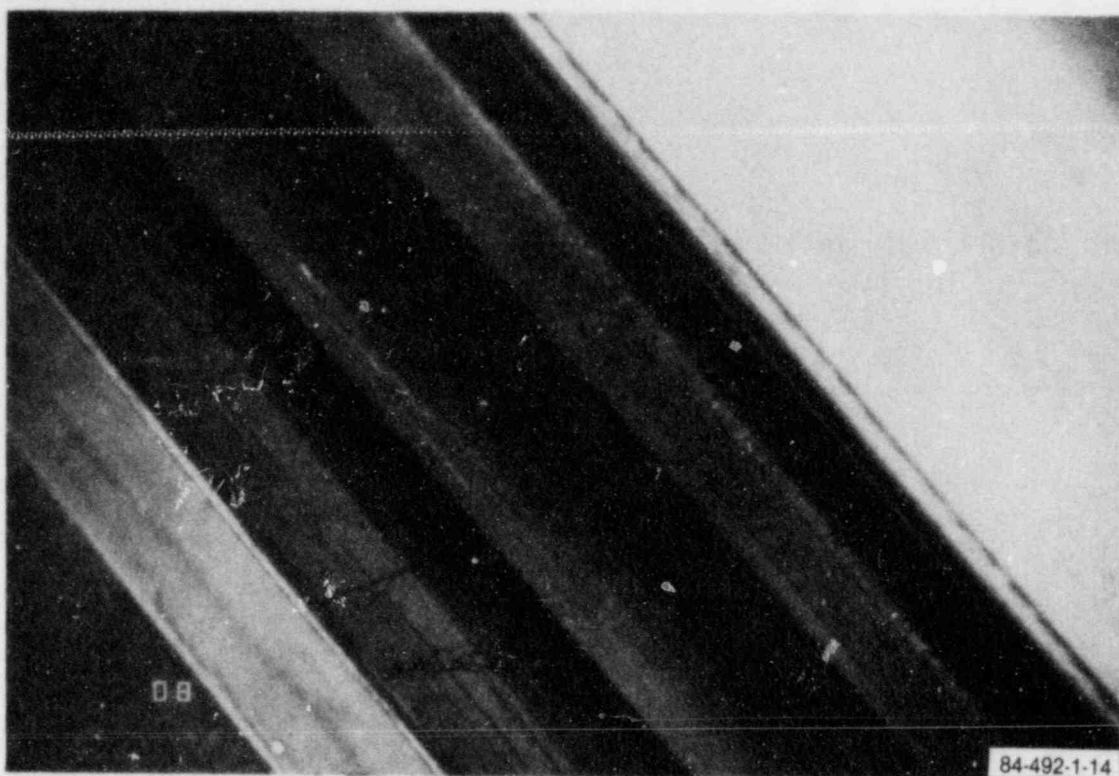
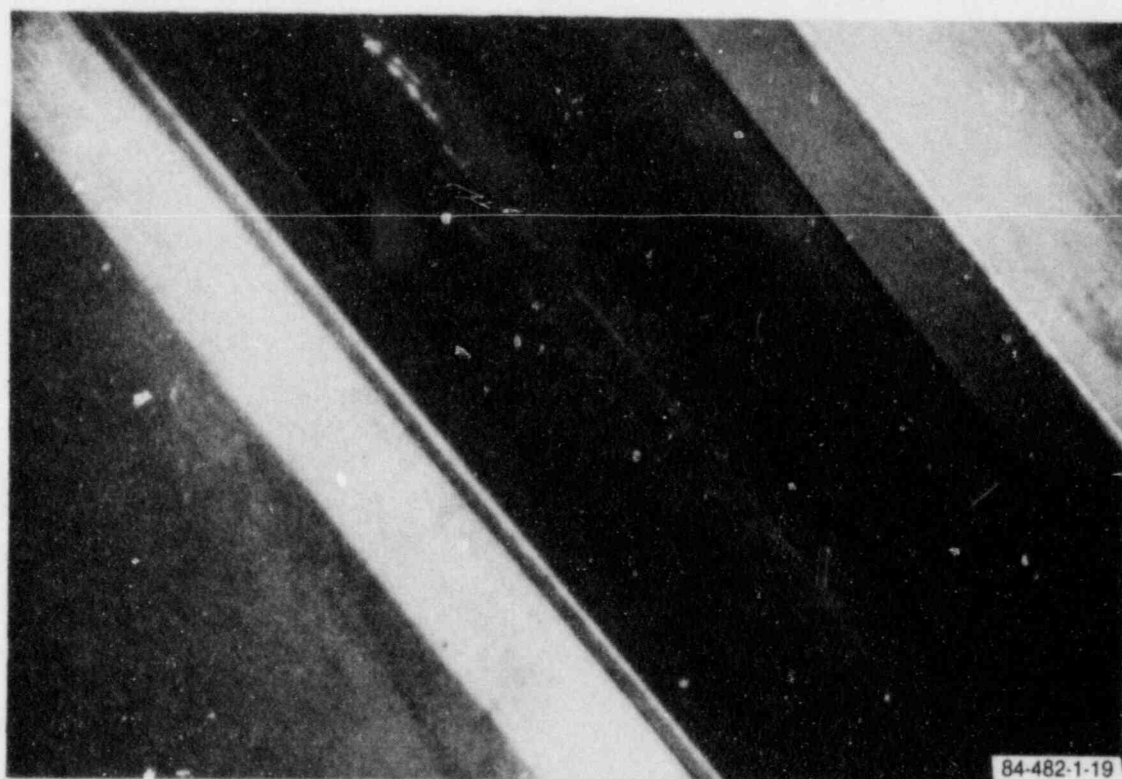Figure 4. Top defect in fuel rod HBR-G7 heated in argon.

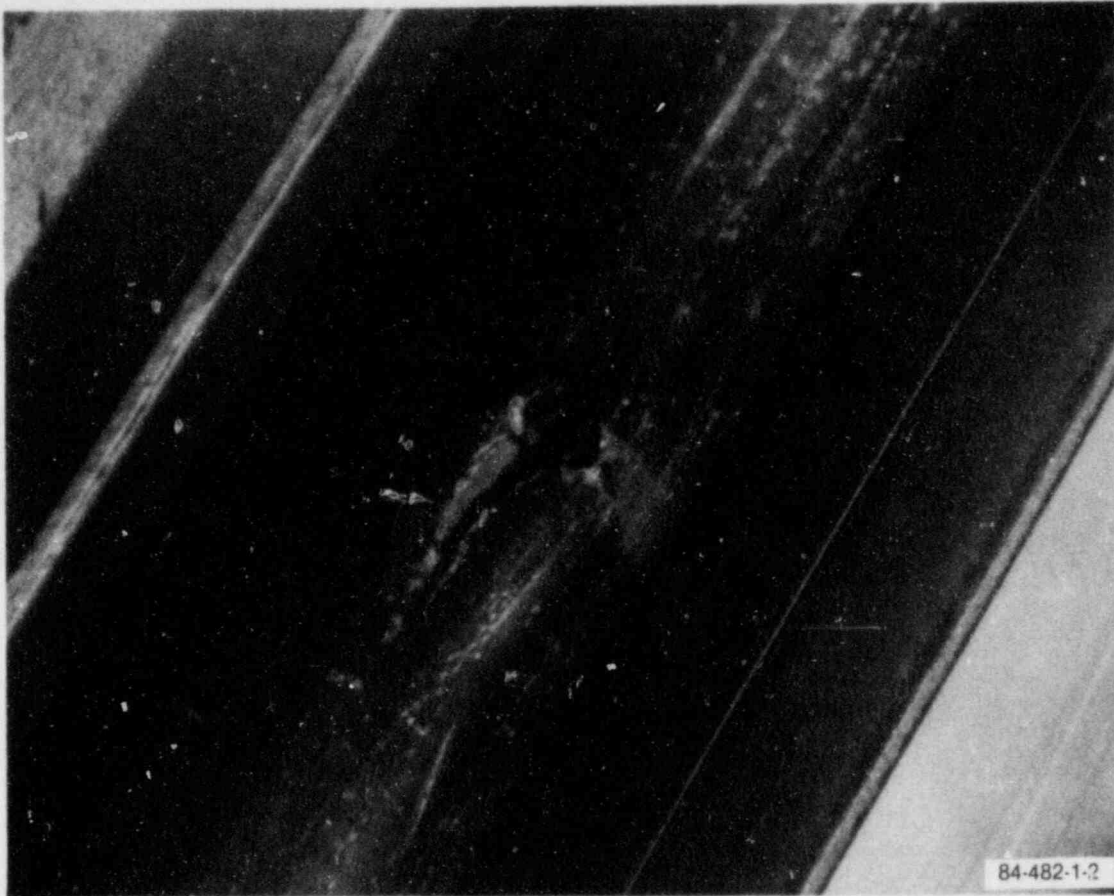Figure 5. Top defect in fuel rod HBR-E7 heated in air.

237

Figure 6. Crack in fuel rod PH462-C5,158 in. from the top.

The fuel rod diameters for the PWR fuel rods did not change much from the nominal dimensions. The fuel rod diameters varied from 10.46 to 10.67 mm, slightly less than the nominal 10.72 mm. The smaller diameter may be attributed to cladding creep during steady-state irradiation in the reactor. These values are comparable to the values measured previously (Reference 2 and 3). Similarly the defect sizes did not increase.

Gas Release

Gas samples were taken from the six sealed fuel rod capsules (Table 4). The gas sample from PH462-E4 proved to be invalid because the valve on the capsule was found to be opened when the gas sample was taken. Air had apparently leaked into the argon-filled capsules, but this is consistent with a 2.5×10^{-7} cm^3/s leak rate for 7206 h. A higher than normal amount of CO_2 was found in HBR-G7 (0.39%) and in HBR-B8 (0.59%). The reason for this high CO_2 content is not known.

Table 4. Fuel Rod Capsule Gas Concentrations

Rod	PH462-E5	B05-67	B05-08	PH462-D6	B05-B8	PH462-D4
Capsule No.	1	2	3	4	5	6
Rod Condition	Intact	Defected	Intact	Defected	Intact	Intact
Initial Atmosphere	Ar/1% He	Ar/1% He	Ar/1% He	Ar/1% He	Air	Air
H_2	0.05	0.05	0.01	0.09	0.01	0.01
He	1.10	0.78	0.01	0.91	0.88	0.01
N_2	0.82	5.80	70.80	5.20	79.90	78.00
O_2	0.13	0.98	18.80	1.20	18.40	21.00
Ar	97.30	92.30	10.40	92.50	0.18	0.93
CO_2	0.39	0.09	0.09	0.03	0.59	0.06
Organic	0.10	0.01	0.01	0.10	0.03	0.01
Kr				0.003		
Xe				0.027		

S4 1807

With PH462-D6, there was a significant amount of fission products released in the capsule. These gases may have been released from the grain boundaries as the fuel was oxidized. These products were the long-lived isotopes of krypton and xenon. Fission gas may have been released from PH462-C5, but this fuel rod was open to the atmosphere and the fission gases would be too low to detect with the stack monitor. These products were not detected in the sealed capsules of the PWR fuel rods.

Crud and Fuel Particulate Release

Each of the stainless steel capsules containing a fuel rod was swabbed with a cotton swab in order to capture any crud which may have fallen from the rod or any fuel which may have been released from a breached fuel rod. In addition, each of the individual filters was weighed to determine the amount of any fuel or crud captured in the filters. Table 5 lists the pre- and posttest weight measurements. The negative values for the filters reflect the balance drift for the size of loads being measured. The weight changes are insignificant. All of the swabs indicate a weight gain, even the control swabs which were just placed in the cell during the time the capsules were being swabbed. The largest weight gain occurred with PH462-C5, because this rod was breached and a minute amount of fuel escaped. The weight gains of the other swabs do not appear to be significant compared to the control samples.

Each of the filters and swabs were measured for isotopes by gamma-scanning. Table 6 shows these results. Only the 15 μm filter for the PWR fuel rod B05-E7 exhibited cesium-137, but the other fission products attributed to fuel are not present. This measurement may be anomalous. The swab measurements indicate that some crud was found in all the capsules, and some fuel in capsules which contain defected fuel rods except B05-G7. This rod was defected, but the isotopes indicate only crud. PH462-E5 is an intact rod, but the isotopes indicate the presence of fuel.

240

Table 5. Weight Gain Measurements

Component	Pretest	Posttest	Change
Filter 7I	121.0036	120.9848	-0.0188
Filter 7J	121.3335	121.3588	0.0253
Filter 7K	121.2179	121.2007	-0.0172
Filter 7L	121.8049	121.7869	-0.0180
Filter 8I	121.0928	121.0652	-0.0276
Filter 8J	121.1773	121.1583	-0.0190
Filter 8K	121.5669	121.5481	-0.0188
Filter 8L	122.2114	122.1994	-0.0170
PB-C5 Capsule	10.4177	10.5200	0.1023
PB-C5 Control	10.3306	10.3593	0.0287
HBR-E7 Capsule	11.4783	11.5100	0.0317
PB-E4 Capsule	11.7060	11.7366	0.0306
HBR-B8 Capsule	11.4358	11.4758	0.0400
PB-D6 CAPSULE	11.8274	11.8573	0.0299
HBR-08 Capsule	12.0726	12.1073	0.0347
HBR-67 Capsule	11.7096	11.7424	0.0328
HBR-E5 Capsule	11.8481	11.8805	0.0324
HBR-E7 Control	11.5159	11.5396	0.0237
-D6, -B8, -E4 Controls	11.0964	11.1314	0.0350
E5, -67, -03 Controls	11.5291	11.5965	0.0674

S4 1808

Table 6. Isotopic Gamma Analysis of Swabs and Filters

Component	Co-60	Cs-134	Cs-137	Eu-154	Cs-144	Am-241	Sb-125	Eu-155	Rh-106	Zn-65
Filter 7K			0.001 (0.0002)							
PB-C5 Capsule	28.7 (0.09)	1.25 (0.04)	55.6 (1.7)	0.36 (0.02)	0.59 (0.08)	0.38 (0.04)	0.78 (0.08)	0.47 (0.03)	0.73 (0.08)	
PB-C5 Control	0.004 (0.001)									
HBR-E7 Capsule	8.42 (0.25)	0.033 (0.003)	0.78 (0.03)	0.015 (0.002)	0.012 (0.004)	0.01 (0.003)	0.025 0.006			
PB-E4 Capsule	25.9 (0.6)		0.71 (0.03)				0.26 (0.03)			0.14 (0.04)
HBR-B8 Capsule	125 (4)		0.08 (0.04)							0.46 (0.016)
PB-D6 Capsule	13.5 (0.4)	0.84 (0.03)	16.4 (0.4)	0.13 (0.01)	0.13 (0.03)	0.11 (0.01)	0.23 (0.03)	0.085 (0.009)		
HBR-08 Capsule	32 (1)		0.08 (0.02)							
HBR-67 Capsule	61.7 0.2		0.34 (0.03)				0.26 (0.03)			
HBR-E5 Capsule	18.3 (0.6)	0.33 (0.01)	6.8 (0.2)	0.12 (0.08)	0.063 (0.012)	0.092 (0.01)	0.23 (0.03)	0.07 (0.008)	0.14 (0.04)	
HBR-E7 Control	0.014 (0.002)		0.001 (0.0008)							
-D6, -B8, -E4 Controls	0.008 (0.002)		0.001 (0.0009)							
-E5, -67, -08 Controls	0.009 (0.002)		0.002 (0.0004)							

S4 1809

Summary of Results of Destructive Examination of PH462-E3

The crack in PH462-E3 grew from 1.3 cm to 6.35 cm during the last
3727 h at 502 K (Figure 7), and the cladding swelled to 16% from fuel
oxidation. The largest strain occurred where the fuel oxidized to
U_3O_8. Further away from the crack less oxidation occurred. In Sample
TF at 7.0 cm from the artificial defect, the fuel was primarily oxidized to
U_4O_9, but some U_3O_8 was present. The fuel was oxidized about 11 cm
from the breach, and extended to the center of the fuel pellets. The
oxidation occurred intergranularly. With even an unetched sample, the
grain structure was revealed by oxidation in the grain boundaries
(Figure 8).

A particle which was released from the crack area was determined by
X-ray diffraction to be U_3O_8. This particle was very easily pulverized
into face powder, and contamination problems resulted just in handling this
powder for X-ray diffraction measurements. Similar behavior was observed
in metallographic preparation of the other samples containing oxidized
fuel. Individual grains of fuel were pulled from the pellet during
polishing and smeared across the cladding leaving a stain.

The fuel at the center defect was oxidized primarily to U_4O_9 with
some U_3O_8. Correspondingly, the cladding deformation was small, on the
order of 0.3%. The oxidized fuel in this area also pulled from the fuel
and stained the cladding.

DISCUSSION

In unlimited air, cracks were initiated from the artificial defects
located at the ends of the BWR fuel rods PH462-E3 and -C5. The defect at
the top of PH462-C5 did not enlarge because the defect may be blocked. A
fuel rod destructive examination will show the condition of this defect, as
well as that of the defects in other fuel rods. Crack initiation and
propagation in the cladding appears to require extensive fuel oxidation
from UO_2 to where most of fuel would be U_3O_8. The extent of
oxidation in BWR fuel may be indicative of extensive open porosity for the
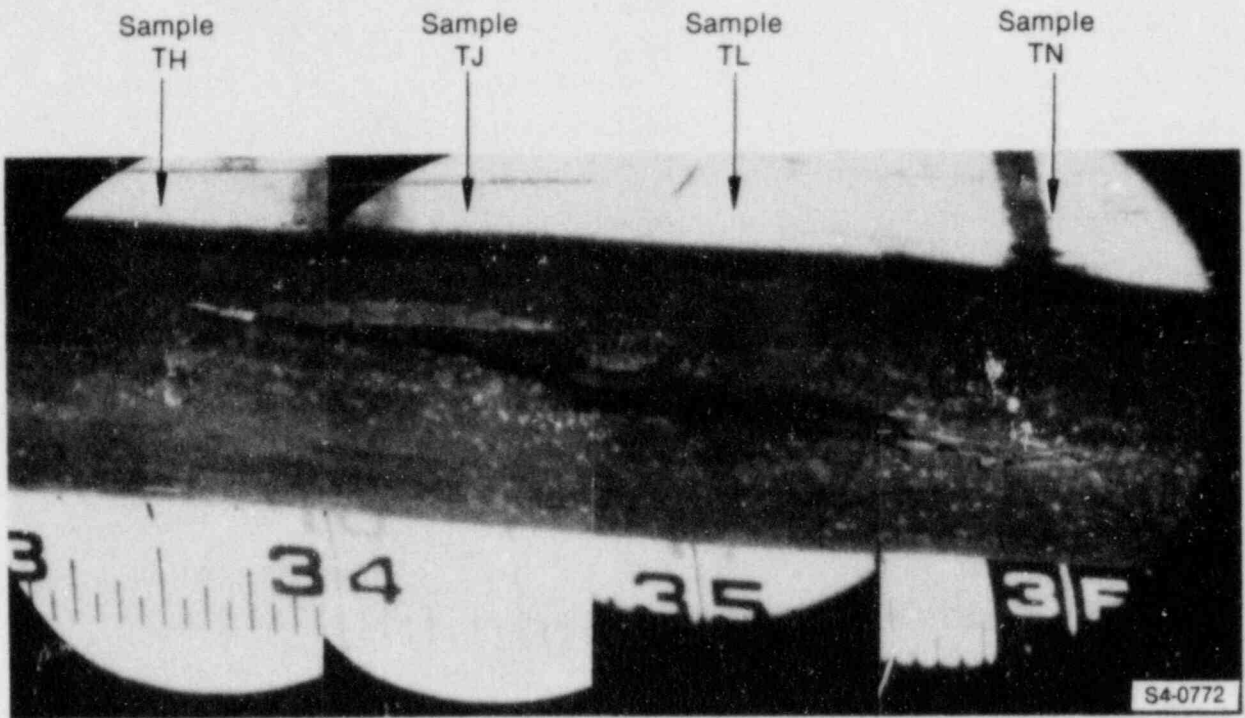
243

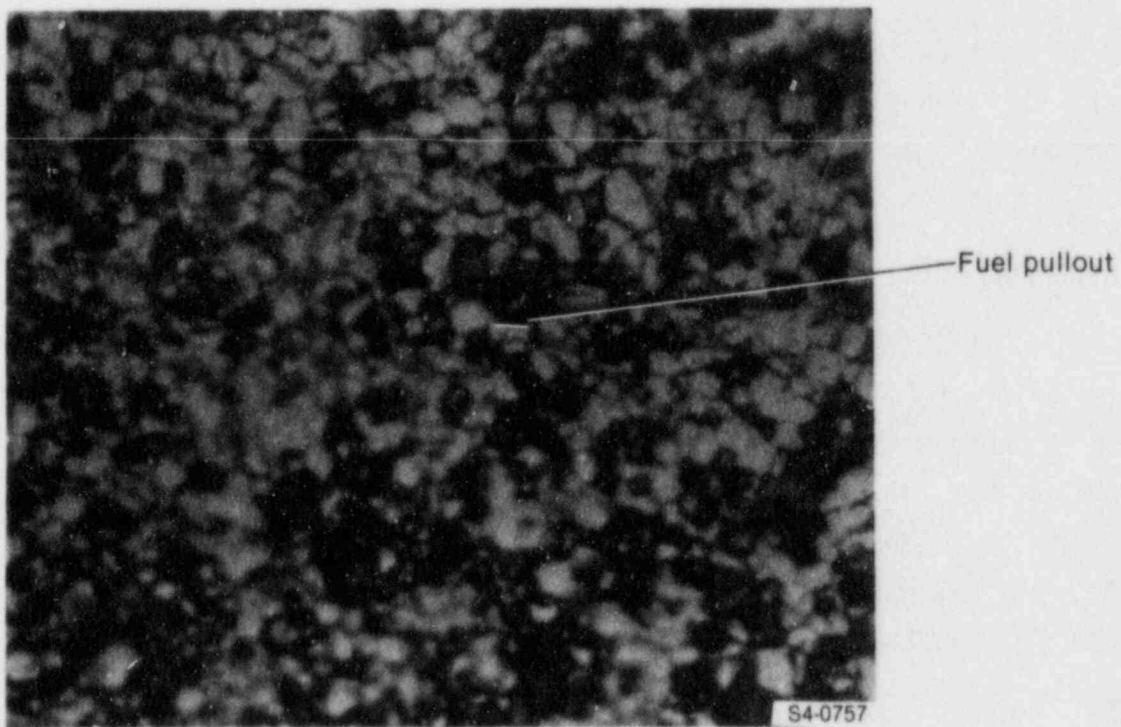Figure 7. Cladding defect in PH 462-E3 after two furnace campaigns.

Figure 8. Oxidized fuel as-polished condition.

244

amount of oxidation in the relative short time at temperature. The oxidation process consists of transport of oxygen through the open channels between grains and the subsequent oxidation of the UO_2. This mechanism may explain the apparent induction period observed by Simpson and Wood[7] where the induction period may be due to the time for oxygen to migrate through the channels and react with the UO_2 to produce measurable weight gains.

The extent of the oxidation, which occurred in the BWR fuel rods, did not occur in the PWR fuel rods based on dimensional changes. Densification in the BWR fuel and the rod gap volume may be contributing factors to the extensive BWR fuel oxidation. Oxidation of PWR fuel will be determined during the destructive examination of these rods.

Although the BWR fuel rod PH462-D6 may not have oxidized as evidenced by the lack of fuel rod deformation, this defected fuel rod continued to release fission gases. Fission gas release from this rod also occurred during the second nondestructive examination, and may indicate open porosity in the fuel in PH462-D6, and some oxidation similar to that in PH462-C5.

The crud release inside the capsules was very minimal; but, the crud layer on both the PWR and BWR fuel rods is also very small, as evidenced by the visual examination of the fuel rods.

CONCLUSIONS

These tests have shown that, at least with BWR fuel, storage of defected fuel rods in an unlimited air atmosphere at temperatures between 490 and 502 K may result in cladding failure and loss of the fuel out the breached cladding. The oxidation also appeared to cause further fission gas release. Because of its age, the BWR fuel may be atypical of current fuel design and fabrication techniques. The oxidized fuel results in contamination of the surrounding area which will be difficult to decontaminate.

The storage of PWR fuel rods in unlimited air at 502 K is uncertain. A destructive examination is planned for the PWR rods, as well as the BWR rods, so that more information will be gained on the extent of the oxidation and the cause of fission gas release from PH462-D6.

The crud release in the capsules was primarily in the form of cobalt-60 and was minimal.

REFERENCES

1. L. D. Blackburn et al, Maximum Allowable Temperature for Storage of Spent Nuclear Fuel, HEDL-TME 7837, May 1978.

2. R. E. Einziger and J. A. Cook, "First Interim Examination of Defected BWR and PWR Rods Tested in Unlimited Air at 229°C," presented at Workshop on Spent Fuel/Cladding Reaction During Dry Storage in Gaithersburg, Maryland, August 17-18, 1983.

3. R. E. Einziger and J. A. Cook, LWR Spent Fuel Dry Storage Behavior at 229°C, NUREG/CR-3708 HEDL-TME 84-17, July 1984.

4. R. E. Einziger and R. L. Fish, Characterization of LWR Spent Fuel Rods Used in the NRC Low-Temperature Whole Rod and Crud Performance Test, NUREG/CR-2871 HEDL-TME 82-27, September 1982.

5. R. E. Einziger and J. A. Cook, Pre-Test Visual Examination and Crud Characterization of LWR Rods Used in the Long-Term, Low-Temperature Whole Rod Test, NUREG/CR-3285 HEDL-TME 83-9, March 1984.

6. R. A. Lorenz et al, Fission Product Release from Highly Irradiated LWR Fuel, ORNL/NUREG/TM-287, February 1980.

7. K. A. Simpson and P. Wood, "Uranium Dioxide Fuel Oxidation in Air Below 350°C," presented at the Workshop on Spent Fuel/Cladding Reaction During Dry Storage in Gaithersburg, Maryland, August 17-18, 1983.

Performance Assessment of Class 1E Pressure Transmitters
Subjected to Environmental Stresses*

David T. Furgal
Charles M. Craft
Sandia National Laboratories
Albuquerque, New Mexico

1.0   INTRODUCTION

Research has been conducted at Sandia National Laboratories (SNL) within the Component Assessment Program to evaluate the failure and degradation modes of unaged instruments exposed to environments within and beyond the design basis. Current qualification test requirements as they relate to electronic components in containment were also evaluated. This paper summarizes the salient findings of an experimental evaluation of pressure transmitter performance in harsh environments. A more complete account of this work is reported in NUREG/CR-3863 [1].

Transmitters were chosen for testing because they are a basic component in Class 1E instrumentation circuits, provide critical reactor and plant state information, and may provide vital information for accident management. To implement the program, one typically used model of nuclear power plant pressure transmitter was chosen for testing. The specific choice of model was based on the results of a survey of transmitter usage [2], and the availability of instruments for testing. Emphasis was placed on determining the instrument's fragility (i.e., failure and degradation modes) in separate and simultaneous environmental exposures. Specific objectives were (1) to determine and isolate the effects of individual and simultaneous environmental stresses, (2) to address severe accident questions by testing beyond the normal design basis environmental envelope, (3) to investigate the current qualification test methodology as it pertains to electronic components, and (4) to identify and analyze any weak-link circuit components for the mechanisms contributing to their degradation. In addition, this test effort was able to independently evaluate the merits of a modification recommended by the vendor to improve the temperature stability of the transmitter model tested.

Our test matrix exposed five ITT Barton Model 763, 0-1000 psig, 4-20mA pressure transmitters to five separate environments. One transmitter was exposed to each environment. The five environments were (1) simulated Loss of Coolant Accident (LOCA) steam conditions alone (transmitter T1), (2) temperature alone (transmitter T2), (3) radiation alone (transmitter T3), (4) simultaneous radiation and LOCA temperature (no steam) conditions (transmitter T4), and (5) simultaneous radiation and simulated LOCA steam conditions (transmitter T5). Unaged equipment was tested to establish a baseline performance and to avoid introducing failures which might result from an accelerated aging process.

Subsequent to the main test, a special test was conducted to evaluate a modification recommended by Barton to improve the transmitters' temperature stability. This temperature sensitivity has been reported by Barton in a series of 10CFR21 disclosures [3,4,5]. In this special test, four of the already-tested transmitters were modified as recommended by Barton and then exposed to the first high temperature peak of the IEEE 323-1974, Appendix A [6] simulated LOCA profile. Subsequent to the testing, the span and zero calibration potentiometers were disassembled and evaluated to determine the root cause of the temperature instability.

2.0 EXPERIMENTAL PROCEDURE

The tests were performed at the SNL High Intensity Adjustable Cobalt Array facility [7]. Transmitter T1, exposed to the LOCA steam environment for 24 days without radiation, was installed in a steam chamber located outside the radiation cell. This chamber was connected to the steam supply system in parallel with a second, similar chamber located inside the radiation cell and hence both chambers experienced identical LOCA profiles. Figures 3 and 4 show the achieved LOCA temperature profile. This profile closely approximates the recommended IEEE 323-1974, Appendix A temperature profile [6]. However since saturated steam conditions were maintained throughout the steam exposure, the achieved pressure profile was more severe than the recommended pressure profile. Chemical solution, made in accordance with the IEEE 323-1974, Appendix A [6] recommendation, was sprayed into both steam chambers during the first 24 hours of the LOCA profile.

To verify that the observed errors were related only to the temperature and not to the combination of environments present in the steam chambers, transmitter T2 was subjected to a temperature only environment. This transmitter was located inside an air circulating oven and experienced temperatures from 105°C to 180°C (221°F to 356°F). However, the sequence of temperatures did not follow the LOCA profile sequence. Rather, the sequence was controlled somewhat arbitrarily to enhance the investigation of the temperature instability experienced by the transmitters. The ramp time between temperature plateaus was significantly longer in the oven than it was for steam chambers.

Figure 1 shows transmitters T3, T4, and T5 being readied for the test. Transmitter T3 was located in the radiation cell in an ambient temperature environment. Transmitters T4 and T5 were installed in the steam chamber inside the radiation cell. To achieve the radiation and temperature (no steam) environment, transmitter T4 was sealed inside a stainless steel enclosure that was in turn placed inside the steam chamber. Figure 2 shows this enclosure and Figure 1 shows how it was installed in the steam chamber. Transmitter T5 was exposed simultaneously to the radiation and full LOCA steam environments.

Transmitter T3, exposed to radiation alone, received a total integrated dose (TID) of 527 Mrd (air) at a dose rate of 413 krd per hour. The ambient temperature of the radiation cell varied between 18°C (64°F) and 35°C (95°F) over the approximately 58 days of irradiation. Transmitters T4 and T5 inside the steam chamber received a TID of 482 Mrd at a dose rate of 603 krd per hour. Their total exposure time was approximately 33 days.

The test configuration for each transmitter is shown schematically in Figure 5. As shown, the transmitters were connected in series with two 500-ohm resistors and a dc power supply which was set to 40 V. The current in the transmitter instrumentation loop was monitored via the voltage drop across one of the resistors. The reference pressure gauges located in an ambient temperature, nonradiation environment were used to monitor the applied pressure. During most of the test sequence, 600 psig nitrogen was applied to the transmitters as the pressure stimulus. To obtain data on transmitter response over the entire calibrated range of the electronics, ten functional tests were conducted during the first 172 hours of the exposure. These functional tests exercised the transmitters over their 0 to 1000 psig range in 200 psi increments. Both upscale (0-1000 psig) and downscale (1000-0 psig) measurements were made to investigate instrument hysteresis.

3.0 RESULTS

3.1 Radiation Effects. Radiation exposure produced a small gradual degradation in transmitter output. This degradation was observed for the transmitter exposed to radiation alone and for the transmitter exposed to the radiation and LOCA steam environment. The radiation effects were manifested as a negative shift in transmitter calibration. The shift averaged -0.7% of full scale per 100 Mrd of exposure for transmitter T3. For this transmitter, Figure 6 shows the shift in calibration as a function of time. Measurements made after 200 Mrd exposure compared favorably with the published specification of $\pm$ 10% of full scale [8].

For the three transmitters exposed to radiation, Table 1 tabulates the error values experienced initially and at 100 Mrd TID increments. For transmitters T4 and T5, exposed to combined environments, some of the error is due to temperature effects. By comparing errors in the output of transmitters T1 and T5 (see Table 2) and observing that the relative change in these errors followed the same negative trend as the errors observed in transmitter T3, we conclude that no significant synergistic effects existed. For transmitter T3, temporary suspensions in the radiation exposure caused changes in transmitter error ranging from -0.2% to -1.2%; the error returned to prior values when irradiation was resumed. Transmitters T4 and T5 showed the same general response.

Table 1

Percent Errors for Radiation-Exposed Transmitters
at 100 Mrd Intervals
(Percent of Full Scale)

| Exposure | Transmitter | | |
(Mrd)	T3	T4	T5
Initial	+0.01	-0.06	-0.002
100	-0.4	-2.0	-2.7
200	-1.2	-2.9	-3.4
300	-1.9	-3.4	-5.1
400	-2.8	-5.0	N/A

Table 2

Temperature-Exposed Transmitter Error
Observations at Selected Intervals
(Percent of Full Scale Reading)

	Temperature °C (°F)	T1	T4	T5	Error* Specification T1/T4 & T5
Maximum Error 1st LOCA Peak	173 (343)	+21.1%	-9.0%	+26.8%	±4.0%/±4.0%
End 1st LOCA Peak	173 (343)	+10.7%	+5.7%	+12.4%	±4.0%/±4.1%
Maximum Error 2nd LOCA Peak	173 (343)	+10.3%	+5.5%	+12.0%	±4.0%/±4.2%
End 2nd LOCA Peak	173 (343)	+8.3%	+4.4%	+8.8%	±4.0%/4.3%
Beginning 1st Plateau	160 (320)	+3.6%	+2.3%	+4.3%	±3.7%/±4.1%
End 1st Plateau	160 (320)	+3.0%	+1.2%	+3.2%	±3.7%/±4.2%
Beginning 2nd Plateau	140 (381)	-0.7%	-7.0%	-0.2%	±3.1%/±3.6%
End 2nd Plateau	140 (381)	-0.4%	-7.1%	+0.1%	±3.1%/±3.5%
Beginning 3rd Plateau	122 (252)	-1.8%	-1.3%	-1.0%	±2.6%/±3.3%
End 3rd Plateau	122 (252)	-0.9%	-1.7%	-1.4%	±2.6%/±5.4%
Beginning 4th Plateau	105 (221)	-1.4%	-1.8% ~66**	-1.8% ~66**	±2.2%/±5.0%
At 500 Hrs Elapsed Time	105 (221)	+1.0%	-3.4% ~300**	-4.9% ~300**	±2.2%/±12.2%

* Maximum allowable temperature error from ITT Barton published specification [8]. Specification values for transmitters T4 and T5 include allowance for radiation effects proportional to exposure dose based on a 10% maximum error at 200 Mrd.

** Total Integrated Dose in Mrd.

3.2 Temperature Effects. Temperature was the primary environmental stress affecting transmitter performance. The four transmitters exposed to a thermal environment all experienced temperature-related and time-at-temperature-related effects. The temperature effects appeared as distinct shifts in transmitter output at exposure temperature transitions above 122°C (252°F), and as decreases in these shifts as the time-at-temperature increased. The direction of these shifts generally followed the direction of the temperature change.

Transmitters T1, T5, and T4 exhibited similar responses during the initial 100 hours of the exposure. Figures 7, 8, and 9 show the responses for these transmitters, respectively. The temperature profile for this period is given in Figure 4. Using Figures 4, 7, and 8 together, large positive shifts in transmitter output can be observed during each of the increasing temperature transitions to the 173°C (343°F) and 160°C (320°F) plateaus. Large negative shifts in transmitter output can be observed during the decreasing temperature transitions at the end of each plateau. The transition ending the 160°C (320°C) plateau caused a negative shift large enough to make the transmitter error negative. The transition from 140°C (284°F) to 122°C (252°F) shifted the transmitter outputs even further negatively. A corresponding permanent shift in transmitter output was not observed during the 122°C (252°F) to 105°C (221°F) temperature transition. During each temperature plateau, the shift in transmitter output decreased exponentially as Figures 7 and 8 illustrate.

Figure 9 shows a somewhat different error profile for transmitter T4. The output of this transmitter shifted negatively with the initial increasing temperature transition to 173°C (343°F); but then, approximately two thirds of the way through this temperature plateau, it reversed its negative error trend with a positive shift of approximately 16% and began to follow the pattern of transmitters T1 and T5. We speculate that this difference in response is related to the fact that transmitter T4 was enclosed in a stainless steel canister inside the test chamber. One obvious difference is the rate and mode of heat transfer to the transmitter. The responses of transmitters T1, T4, and T5 are compared in Table 2.

As shown by Figures 7, 8, and 9 and Table 2, the maximum errors observed at approximately 30 minutes into the first 173°C (343°F) plateau were +21.1%, +26.8% and -9.0% of full scale reading. These values are up to a factor of 6 greater than the error specification for the instruments . When these errors are expressed as a percent of the base reading (600 psi), the error percentages become +32.5%, +44.7% and -15.0%, respectively. The Barton error specification allows a maximum of $\pm$ 4% of full scale ($\pm$ 6.6% of 600 psi base) at 173°C (343°F) [8].

The response of transmitter T2 exposed to the temperature only environment agreed with the responses observed for the transmitters in the steam chambers. However, the magnitudes of the errors observed from this transmitter were less than the errors produced by transmitters T1 and T5, exposed to the LOCA steam environments. We speculate that the more rapid temperature transient experienced in the steam chamber led to the increased shifts observed in the outputs of transmitters T1 and T5.

3.3 Functional Tests. The functional tests evaluated whether or not the behavior observed at a constant pressure of 600 psig was consistent over the entire operating range of the transmitter, and whether any nonlinearities in transmitter response existed. The asterisks in Figures 3 and 4 indicate when the functional tests were made.

For transmitter T3, the radiation exposure alone produced little change in its response over the calibrated range. The small changes observed were basically linear and followed the error profile shown in Figure 6. The shift in calibration at 1000 psig was up to -0.65% greater than the shift at 0 psig. Table 3 summarizes the shifts in output observed for transmitter T3 at 0 and 1000 psig for the initial and final functional tests.

Table 3

Percent Change in Output for Transmitter T3
for First and Last Functional Test
(Percent of Full Scale)

	0 psig	1000 psig
Pre-exposure	-0.1	-0.1
Last Functional Test (~70 Mrd)	-0.6	-1.1

The functional tests allowed us to characterize the observed temperature shifts in terms of zero and span errors. The calibration of this model of transmitter is set by two potentiometers. The zero potentiometer sets the transmitter's output to 4 mA when zero pressure is applied, while the span potentiometer sets the slope of the transmitter's correlation curve relating output to applied pressure. Zero error refers to the error observed at zero psig or the shift in the correlation curve, and span error refers to the deviation in slope of this curve from a preset value.

At elevated temperatures, both zero and span errors occurred. Figures 10 and 11 show the correlation curve for transmitter T5 before the test began and early in the first 173°C (343°F) temperature plateau. The positive shifts in zero and span are evident. Figure 12, which gives the Figure 11 data with the ordinate scale changed, shows that the error at 1000 psig for transmitter T5 was approximately 25% of full scale, while at 0 psig the error was only 6% of full scale. As shown in the correlation curve in Figure 13, this pressure sensitivity was not observed at 122°C (252°F). Similarly, no pressure sensitivity was observed below 122°C (252°F). Figure 12 also shows a hysteresis between upscale and downscale measurements. As time-at-temperature increased, the magnitude of the zero and span shifts decreased, though at different rates. Later in the first 173°C (343°F) plateau, Figure 14 shows a slight bend in the correlation curve at 200 psig, indicating that the span shift is decreasing in a nonlinear fashion. By changing the ordinate scale this bend is emphasized in Figure 15. A similar bend was observed in the correlation curves constructed at different temperature levels, indicating that this nonlinearity existed at each elevated temperature. A summary of the errors observed at 0, 200, and 1000 psig during the 10 functional tests is given in Table 4.

Figures 16, 17 and 18 show the stability of transmitter T1 at three functional test pressures (0, 200 and 1000 psig) for the ten functional tests conducted. These

252

Table 4

Errors Observed During Functional Test Measurements
For 0, 200, and 1000 psig Measurements
(Percent of Full Scale)

	T4 & T5 Exposure Dose (Mrd)	Temp °C (°F)	Error* Specification T1/T4 & T5	T1	T4	T5
Cal 0 0 psi		21 (70)	±0.3/±0.3	-0.1	-0.0	-0.2
200 psi	0			-0.0	-0.1	-0.2
1000 psi				-0.0	-0.1	-0.2
Cal 1 0 psi		173 (343)	±4.0/±4.1	+6.6	+1.2	+6.9
200 psi	0.9			+9.4	-15.0	+10.9
1000 psi				+19.0	+5.7	+23.6
Cal 2 0 psi		173 (343)	±4.0/±4.2	+5.0	+4.4	+4.4
200 psi	3.0			+6.6	+2.1	+6.0
1000 psi				+13.1	+9.0	+15.5
Cal 3 0 psi		160 (320)	±3.7/±4.0	+2.8	+3.2	+2.3
200 psi	6.6			+2.7	+0.2	+1.8
1000 psi				+4.1	+4.2	+6.8
Cal 4 0 psi		122 (242)	±2.6/±3.2	+0.9	+1.3	+0.2
200 psi	12.3			-1.3	-1.3	-1.4
1000 psi				-2.2	-0.9	-1.0
Cal 5 0 psi		122 (242)	±2.6/±3.2	+1.0	+1.1	+0.2
200 psi	16.2			-1.1	-1.1	-1.0
1000 psi				-1.6	-0.4	-0.3
Cal 6 0 psi		105 (221)	±2.2/±3.5	+0.9	+0.7	-0.2
200 psi	56.3			-0.6	-1.5	-1.7
1000 psi				-1.4	-1.5	-1.5
Cal 7 0 psi		105 (221)	±2.2/±3.5	+0.8	+0.7	-0.1
200 psi	71.5			-0.7	-1.5	-2.2
1000 psi				-1.3	-1.5	-1.7
Cal 8 0 psi		105 (221)	±2.2/±7.2	+0.7	+0.7	-0.2
200 psi	99.3			-0.6	-1.7	-3.0
1000 psi				-1.2	-2.0	-2.5
Cal 9 0 psi		105 (221)	±2.2/±7.4	+0.9	+0.7	-0.1
200 psi	103			-0.4	-1.6	-3.0
1000 psi				-1.0	-2.0	-2.5

*Error specification for T4 and T5 includes allowances for radiation effects proportional to exposure dose based on 10% maximum error at 200 Mrd exposure.

plots reemphasize the pressure relationship of the temperature instability and confirm that the behavior observed through time at 600 psig was representative of the behavior across the full range of instrument calibration.

3.4 Failure Mode Analysis. One and possibly two common mode failures were identified during the test. Both appeared to be thermally activated and both were related to the zero and span potentiometers. The first was the thermal instability problem already reported by Barton [3,4,5]. The instabilities observed in our tests were, however, greater than those reported by Barton. The second potential common mode failure was the opening of the span potentiometer which caused the transmitter to exhibit short circuit conditions. Each of these failure modes is discussed below.

3.4.1 Evaluation of the Thermal Instability Problem. Our analyses confirmed that the primary cause of the thermal instability problem was leakage current from the zero and span calibration adjustment potentiometers to the transmitter housing. This cause has been previously reported by Barton [4].

We hypothesize that the basic cause of the leakage currents is a materials related problem. Internally, the potentiometer's shaft is molded into a nylon rotor assembly. This rotor assembly provides both the mechanical support for the wiper and the electrical isolation between the shaft and the wiper. The shaft itself is in intimate mechanical and electrical contact with the potentiometer case. Thus, the only electrical isolation between the circuit elements and the potentiometer case (and hence the transmitter housing) is the nylon rotor assembly.

Nylon has a hydrogen bonded molecular structure and hence has a strong affinity to absorb moisture. Over time, moisture trapped in the transmitter housing or diffusing into the transmitter housing [9] is absorbed by the nylon. This absorbed moisture reduces the dielectric qualities of the nylon. Presumably, when the instruments are calibrated, equilibrium values of these qualities are present, and some small amount of leakage current occurs. These small leakage currents are accounted for in the calibration, and as long as they remain constant, cause no problem. However, as temperature is increased, the moisture causes the dielectric qualities of the nylon to degrade, which in turn enhances the conducting path between the electronics and the potentiometer case. As time-at-temperature increases, some of the absorbed moisture is driven off partially restoring the dielectric qualities of the nylon. Also, as the temperature is lowered, the dielectric qualities of the nylon tend to restore and, because moisture has been driven off, may even be better than the original equilibrium values. Thus, after a thermal transient, the amount of leakage current that occurs at reduced or ambient temperatures may be less than prior to the transient. This results in a possible negative shift in output. At the lower temperatures, the moisture is reabsorbed by the nylon. Therefore, over time the dielectric qualities of the nylon tend to return to their original equilibrium values and the original calibration of the transmitter may be restored. We did not characterize the rate of reabsorption and hence we cannot say how long the reabsorption process might take. However, we believe that the reabsorption process is slow compared to the initial desorption at elevated temperatures. This reabsorption process may account for the slow drift back toward calibration observed in the long, low temperature portions of our test.

This hypothesis is consistent with the shifts in transmitter output observed at environmental profile temperature transition points, and with the observed

time-at-temperature behavior. Thus, we infer that the root cause of the leakage currents is a deterioration of the dielectric qualities of the nylon rotor material caused by elevated temperature and absorbed moisture. To be more definitive would require more testing of the potentiometers. However, an initial step toward eliminating this failure mechanism would be to use a nonhydrogen bonded dielectric material in the potentiometer rotor assembly.

3.4.2 Evaluation of Barton's Thermal Instability Modification. To enhance the temperature stability of the transmitter design, Barton has recommended the installation new potentiometer mounting brackets and fiberglass washers to electrically isolate the potentiometers from the transmitter housing [5]. As such, this corrective action does not address what we believe is the basic mechanism causing the leakage current, but does isolate the leakage path by the addition of dielectric material.

To evaluate Barton's recommended modification a special test was conducted after the main test was completed. Transmitters T1, T2, T3, and T5 were modified using modification kits supplied by Barton. New O-rings were used in the housing covers to reseal the units after modification. Figure 19 shows the temperature profile achieved for this special test. As in the main test, saturated steam was used, and 600 psig nitrogen was used as the process stimulus pressure.

The special test sequence exposed the four modified transmitters to 175°C (347°F) saturated steam for approximately 1.3 hours. The maximum stable errors observed for three of the transmitters before and after the modification are compared in Table 5. Transmitter T3 failed completely 1 minute 40 seconds after introduction of the steam. Insufficient stable test data was obtained to make any comparisons for this transmitter. We attribute this failure to the high level of radiation received by the unit which caused embrittlement of the insulation on wires external to the instrument. As shown in Table 5, the maximum stable errors range from +0.9% to +7.8% of full scale reading. Significant improvements were observed for transmitters T1 and T5 which had been exposed to the LOCA steam environment. However, transmitters T2, T3, and T5 produced large error spikes of less than 15 second duration within the first 40 seconds after introduction of the steam. These spikes ranged from +14.9% to +19.4% of full scale reading. We cannot satisfactorily explain these transient error spikes. Figure 20 shows the response during the special test of the transmitter T2. In general, our data shows that the modification produced significant improvement in transmitter thermal stability. Without further testing and investigation we cannot comment on the source or significance of the error spikes observed.

3.4.3 Evaluation of Potentiometer Open Failure. The second potential common mode failure mechanism is corrosion of the potentiometer's resistive element. Approximately 550 hours into the initial test, output from the transmitter exposed to the LOCA steam only environment exhibited short circuit conditions. Upon examination, we found that the resistive element in the span potentiometer had opened, thus breaking the circuit. Figure 21 is a scanning electron micrograph (SEM) of the failure point. The ends of the wire show distinct characteristics of corrosion. The timing of the failure is also consistent with the operation of a corrosion mechanism activated by high temperatures. Analysis of the corrosion point and the underlying mandrel wire showed the presence of chlorine, sulphur and potassium all of which tend to initiate and enhance corrosion processes.

Table 5

Pre- and Post-Modification Performance of
Transmitters T1, T2, and T5 at 173°C-175°C
(Percent of Full Scale)

	T1	T2	T5
Pre-	+21.1	+6.4	+26.8
Post-	+ 0.9	-2.0	+ 7.8

Error Specification: ±4.1% at 175°C [8]

We traced the origin of these elements to a lubricant applied during the manufacture of the potentiometers. Though the potentiometer manufacturer reported that this lubricant has not been used since late 1982 to mid-1983, transmitters manufactured before this time may contain potentiometers with this lubricant, and may, therefore, be susceptible to this failure mode. Further evaluation of this problem is necessary to confirm its generic implications. It is our understanding that one of the original transmitters returned to Barton for evaluation of the thermal instability problem had exhibited similar behavior [10]. An evaluation of its potentiometers would show whether or not this corrosion mechanism had caused that transmitter to fail. We were unable to obtain this transmitter or its potentiometers for evaluation.

4.0   CONCLUSIONS

This research has provided both specific equipment performance and general qualification methodology insights. By testing in individual and combined environments we were able to isolate environmental effects on equipment performance. The primary environmental stress affecting the model of transmitter tested is temperature. We confirmed the Barton finding that leakage current originating in the zero and span potentiometers was the major contributor to the transmitters' thermal instability and that the modification kit, though only palliative in nature, does significantly improve transmitter performance. We also observed that the time-at-temperature significantly reduced the magnitude of the output shifts. Analyses of the potentiometer piece parts indicated that the root cause of the temperature instability was a thermally activated decrease in the dielectric qualities of the nylon insulating material used in the construction of the potentiometer. We also experienced a possible second, thermally activated, common mode failure mechanism which causes the potentiometer(s) to open, resulting in the transmitter circuit exhibiting short circuit conditions.

The effects of radiation on this transmitter design are secondary to thermal effects. In fact, the transmitter electronics proved to be exceptionally hard to the effects of the gamma radiation. Simultaneous exposure to radiation and thermal environments did not produce noticeable synergistic effects relative to the operation of the transmitter electronics. There was, however, a noticeable

256

embrittlement of some of the polymer materials used in the transmitter construction such as the wire insulation and circuit board conformal coating.

The observed thermal behavior coupled with the hypothesized mechanism causing this behavior, raises a question about whether accelerated aging to an intended end-of-life condition produces the most vulnerable operational state for this transmitter. Since the magnitude of the error decreased with the time at temperature, the thermal aging exposure of a qualification sequence may mask or diminish the errors observed during a subsequent LOCA exposure. Thus, thermal aging may not place this transmitter in its most vulnerable state prior to the LOCA exposure. This possibility is recognized by IEEE Standard 381-1977 [11] which states in section 5.8.1 that "in some instances, aging may actually improve equipment capability to perform." Even though we did not investigate the response of aged equipment, our testing appears to have discovered an example where such an effect may occur. We therefore agree with the recommendation of IEEE 381-1977 that an understanding of equipment failure modes is essential to the qualification process. Obtaining this understanding may dictate that "more than one piece of equipment or component thereof may have to be tested such that samples are aged to different degrees of advanced life and then analyzed/tested to establish limiting cases [11]." It is also important that the instruments' performance be recorded at each temperature level and across its entire range of operation.

5.0 REFERENCES

1.   D. T. Furgal, E. A. Salazar, and C. M. Craft, "Assessment of Class 1E Pressure Transmitters When Subjected to Harsh Environment Screening Tests," NUREG/CR-3863, SAND84-1264, Sandia National Laboratories. To be published.

2.   E. A. Salazar, "Preliminary Review of Pressure Transmitters Used in the Nuclear Power Industry," RS/6445/83-01, Sandia National Laboratories, June 1983.

3.   10 CFR 21 Notification: Telex to R. C. DeYoung, Office of Inspection and Enforcement, USNRC, from T. J. Shideler, Barton Instrument Co., October 29, 1982.

4.   10 CFR 21 Notification: Telex to R. C. DeYoung, Office of Inspection and Enforcement, USNRC, from T. J. Shideler, Barton Instrument Co., November 19, 1982.

5.   10 CFR 21 Notification: Telex to R. C. DeYoung, Office of Inspection and Enforcement, USNRC, from T. J. Shideler, Barton Instrument Co., May 18, 1983.

6.   IEEE Standard 323-1974, "IEEE Standard for Qualifying Class 1E Equipment for Nuclear Power Generating Stations," Institute of Electrical and Electronic Engineers, New York, 1974.

7.   W. H. Buckalew and F. V. Thome, "Radiation Capabilities of the Sandia High Intensity Adjustable Cobalt Array," NUREG/CR-1682, SAND81-2655, Sandia National Laboratories, March 1982.

8. Technical Manual Model 763 Gauge Pressure Electronic Transmitter, Report R3-763-6, ITT Barton Instrument Co., City of Industry, CA.

9. M. R. Keenan, "Moisture Permeation into Nuclear Reactor Pressure Transmitters," SAND83-2165, Sandia National Laboratories, March 1984.

10. Presentation to USNRC by ITT Barton, Subject: Review of actions taken by ITT Barton Instruments Company and Westinghouse Electric Corporation in resolving potential defects reported to the NRC on the Barton Electronic Transmitter Models 763 and 764, February 23, 1984.

11. IEEE Standard 381-1977, "IEEE Standard Criteria for Type Tests of Class 1E Modules Used in Nuclear Power Generating Stations," Institute of Electrical and Electronic Engineers, New York, 1977.

Figure 1. Steam Exposure Test Chamber Showing Transmitters T3, T4 & T5
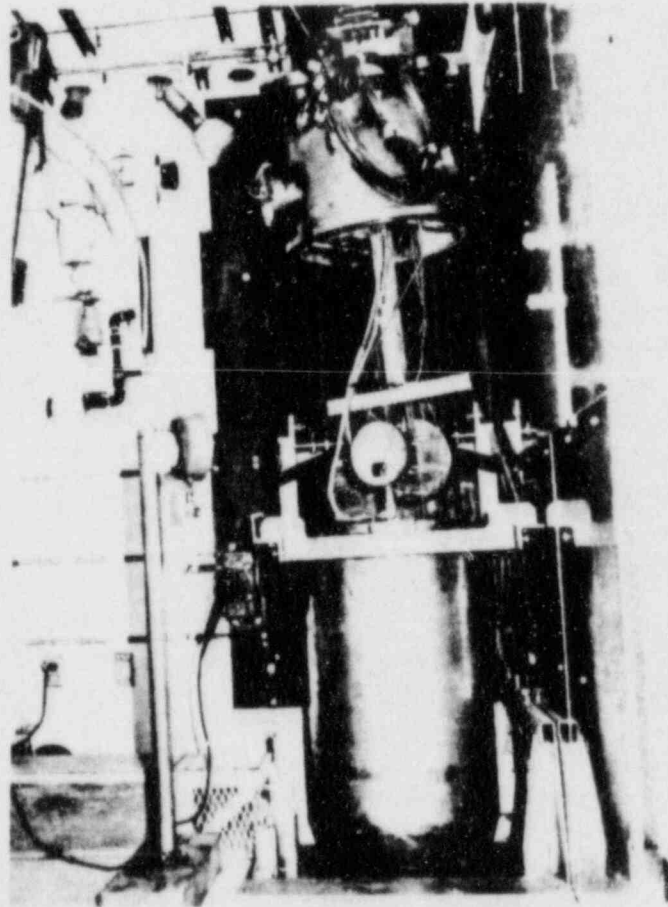
Figure 2. Transmitter T4 In Stainless Steel Enclosure
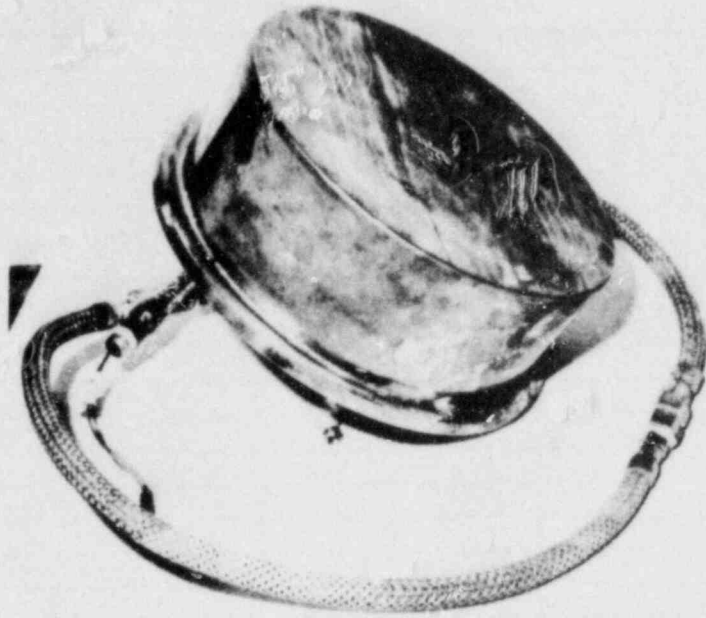
Figure 3. LOCA Exposure Temperature Profile
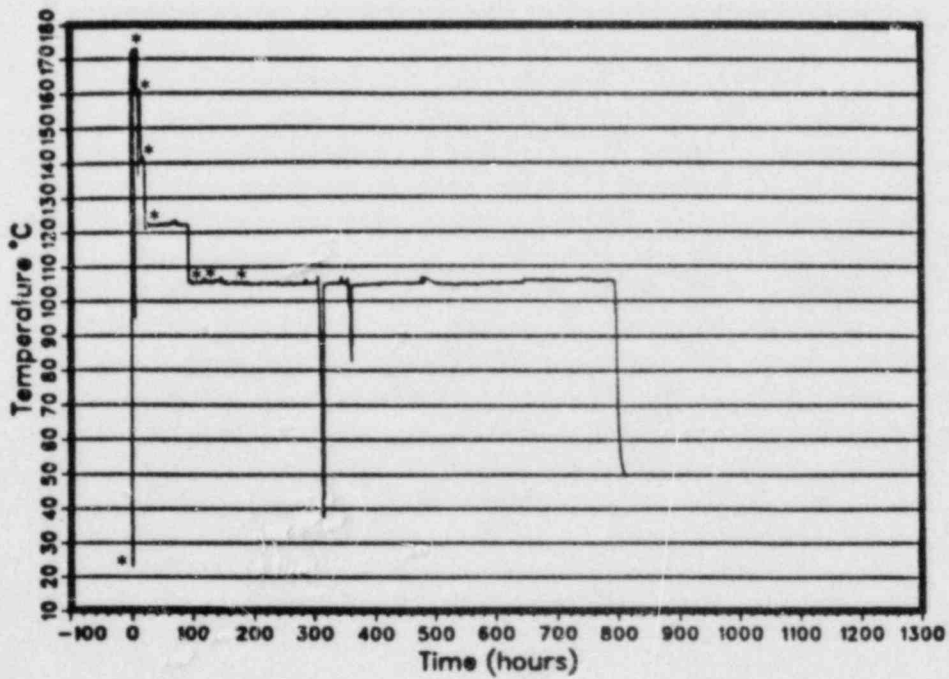
Figure 4. LOCA Exposure Temperature Profile for First 100 Hours
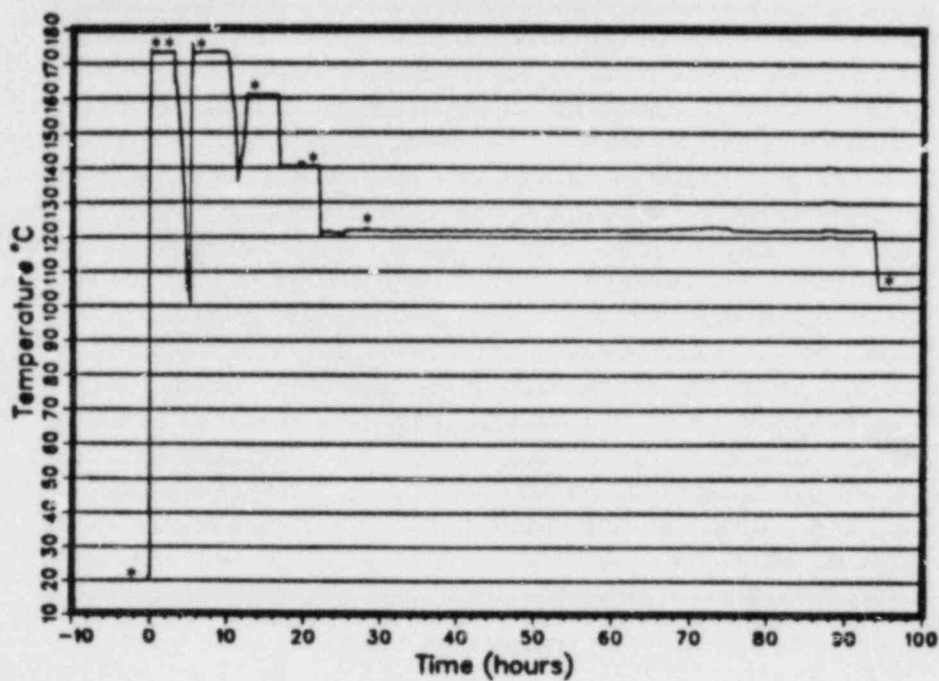
Figure 5. Test Setup Schematic

260
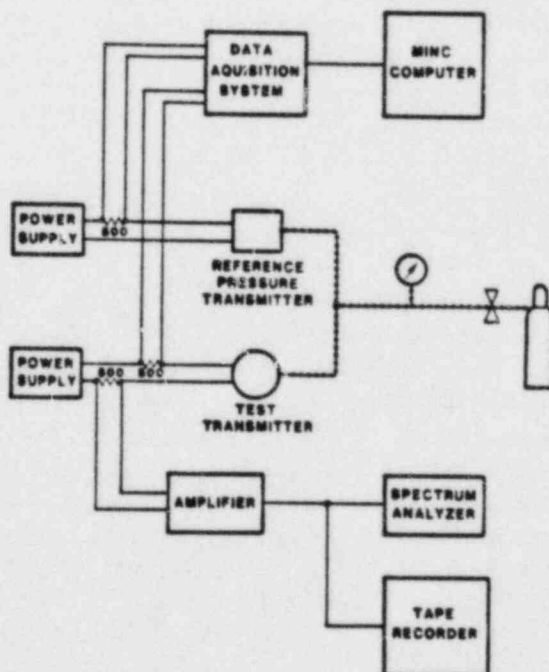
Figure 6. Error Profile for Transmitter T3
Exposed to Radiation Environment
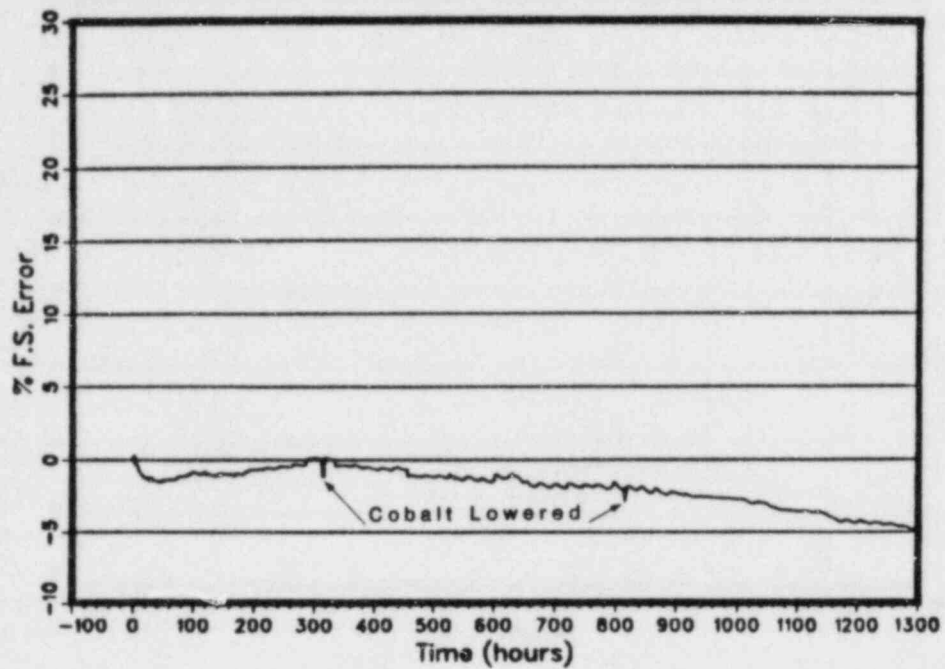
Figure 7. Error Profile for Transmitter T1
Exposed to LOCA Steam Environment
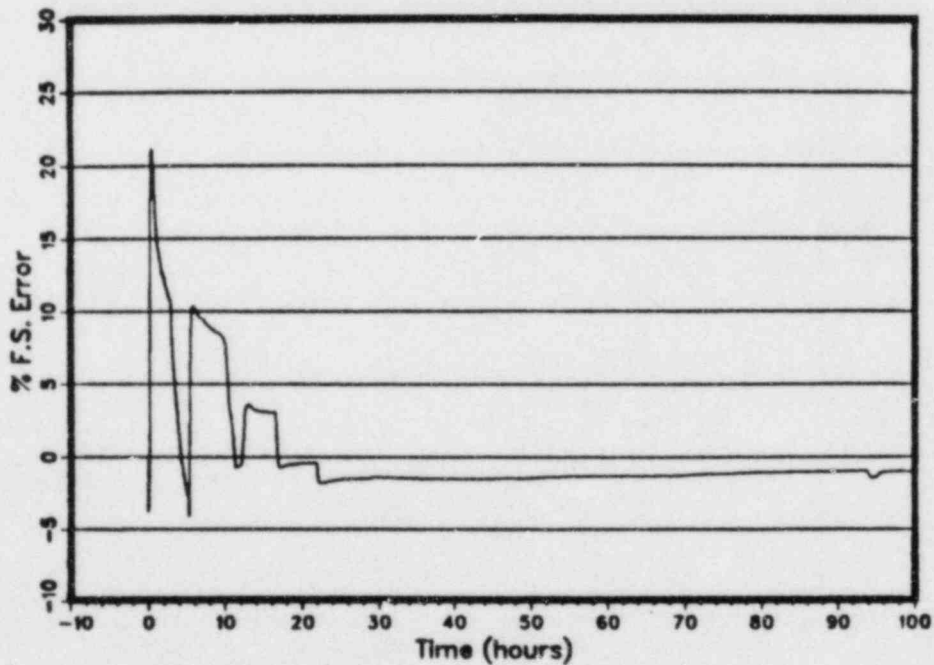
Figure 8. Error Profile for Transmitter T5 Exposed to Radiation & LOCA Steam Environment
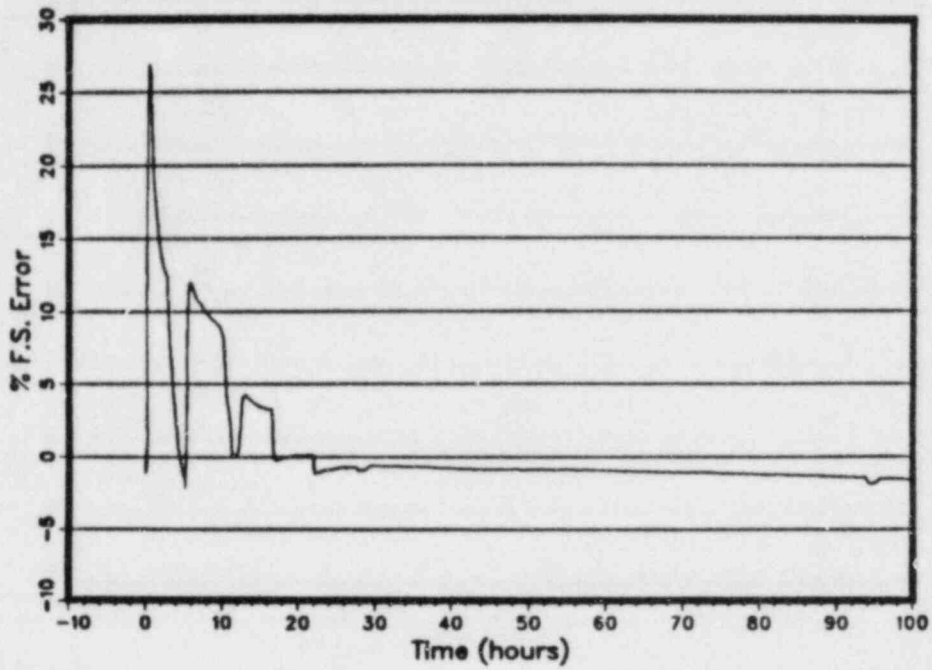
Figure 9. Error Profile for Transmitter T4 Exposed to Radiation & LOCA Temperature Environment
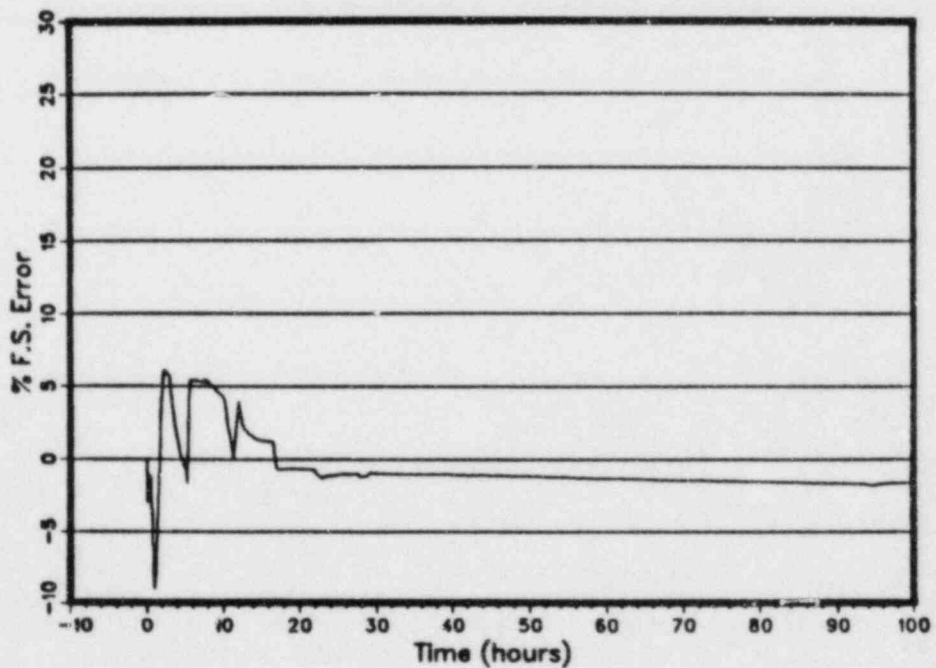
Figure 10. Transmitter T5 Correlation Curve
at Ambient Temperature
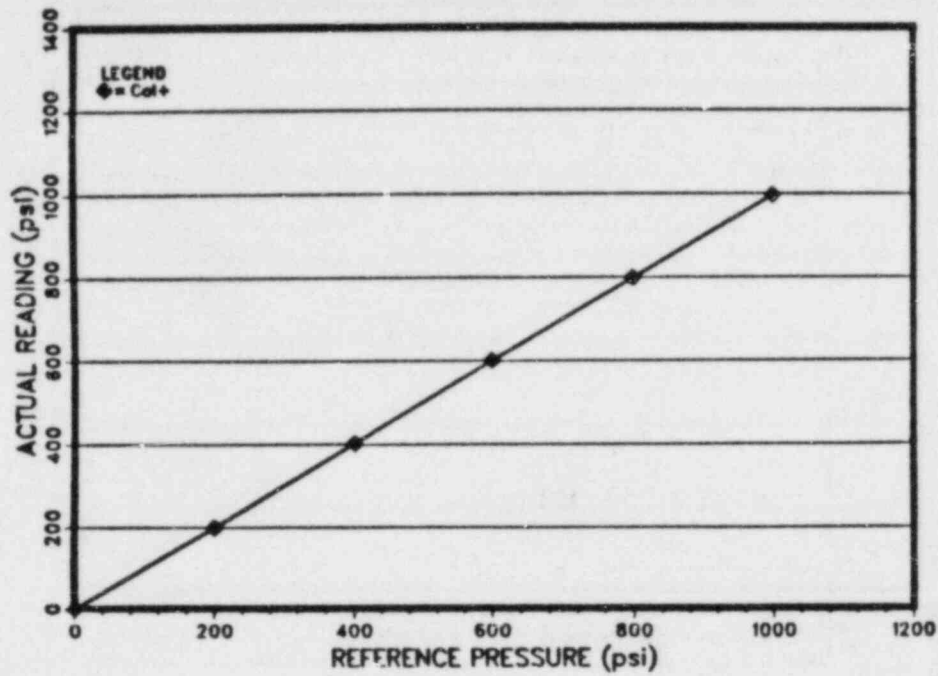
Figure 11. Transmitter T5 Correlation Curve Early
in First 173°C Plateau

263
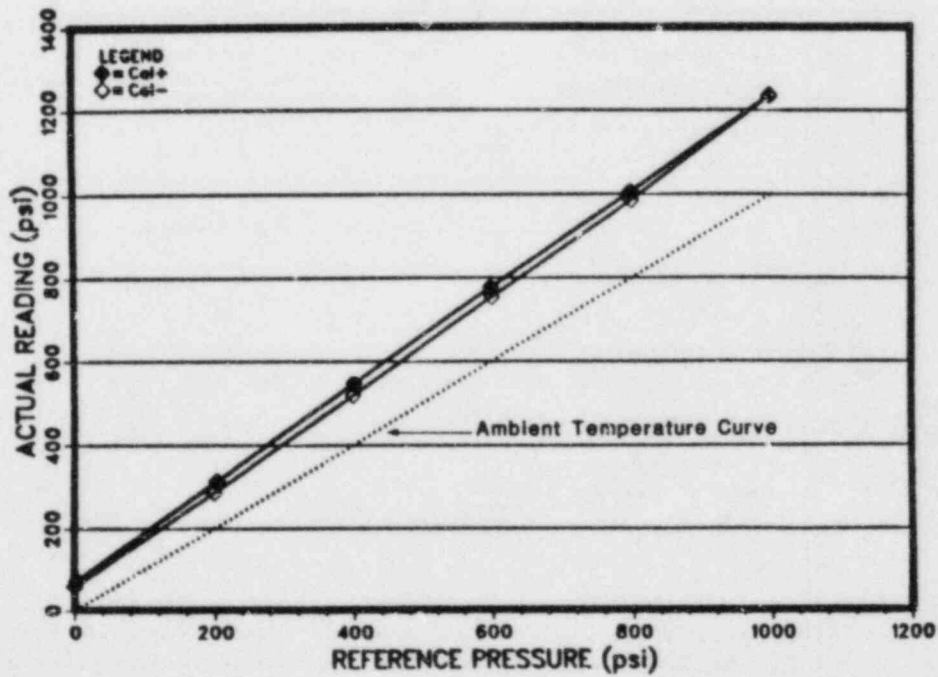
Figure 12. Transmitter T5 Response Showing Pressure Sensitivity at 173°C
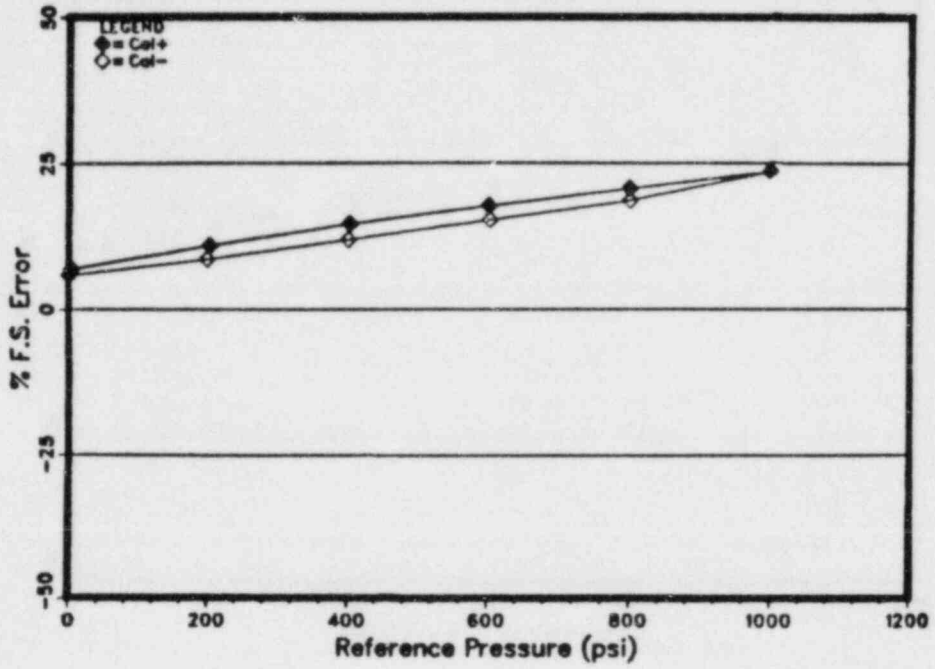
Figure 13. Transmitter T5 Response Showing Pressure Sensitivity at 122°C
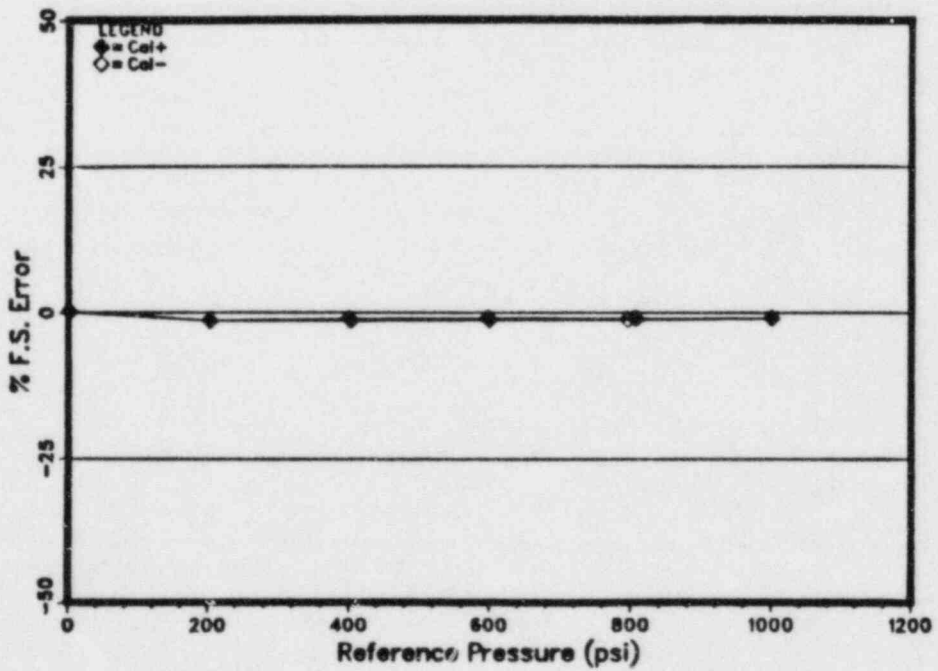
Figure 14. Transmitter T5 Correlation Curve Showing Nonlinearity at 173°C
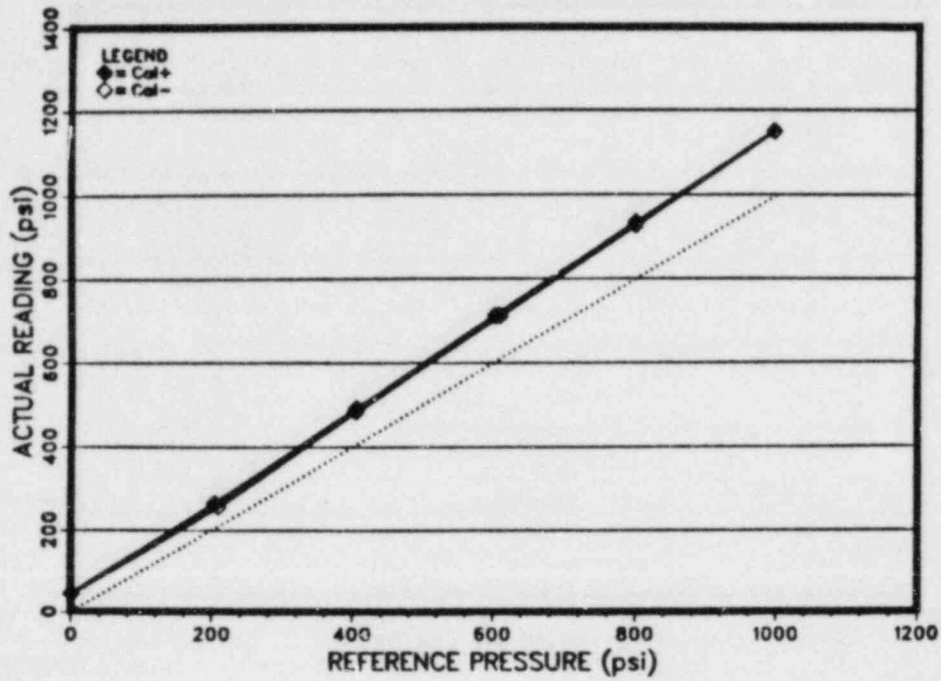
Figure 15. Transmitter T5 Correlation Curve Emphasizing Nonlinearity at 173°C
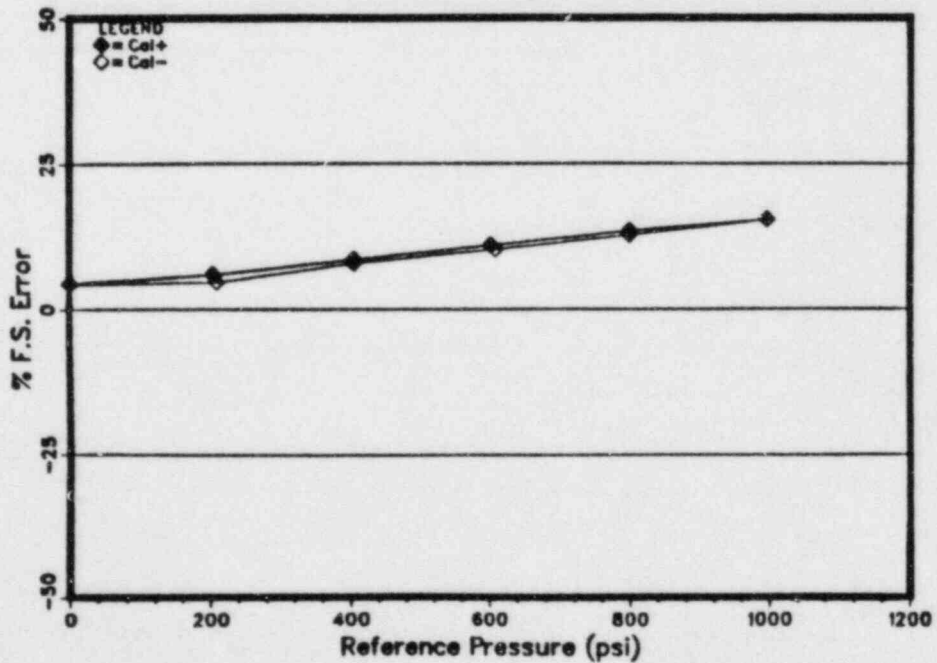
Figure 16. Transmitter T1 Functional Test Sequence Error Profile at 0 psi
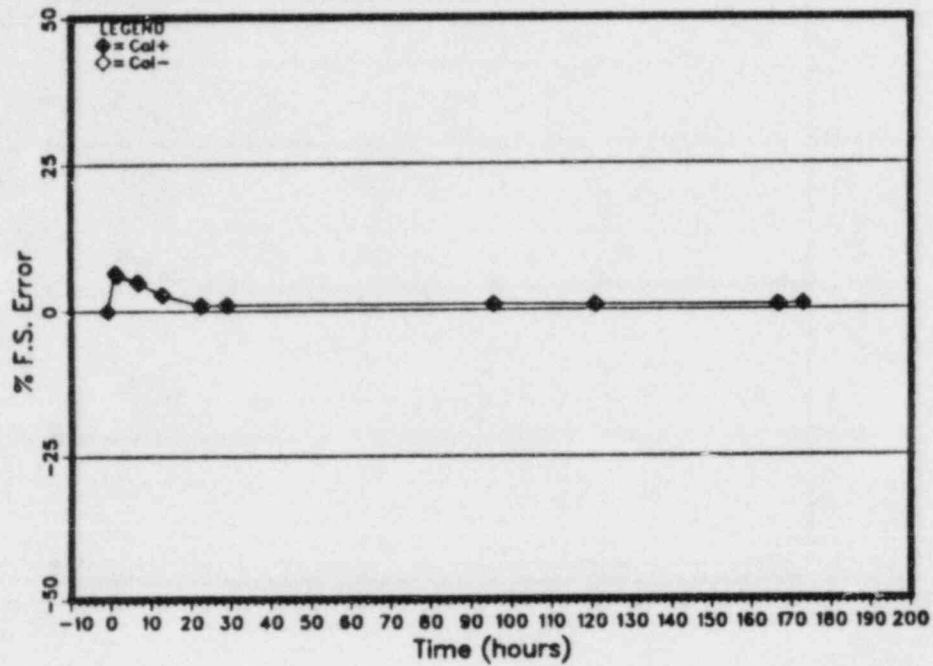
Figure 17. Transmitter T1 Functional Test Sequence Error Profile at 200 psi
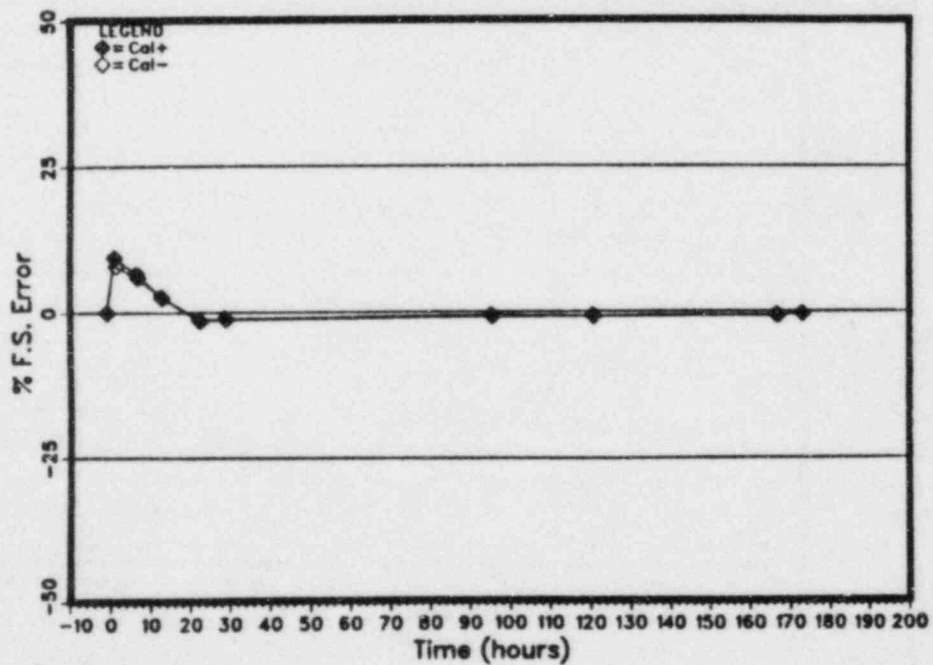
Figure 18. Transmitter T1 Functional Test Sequence Error Profile at 1000 psi
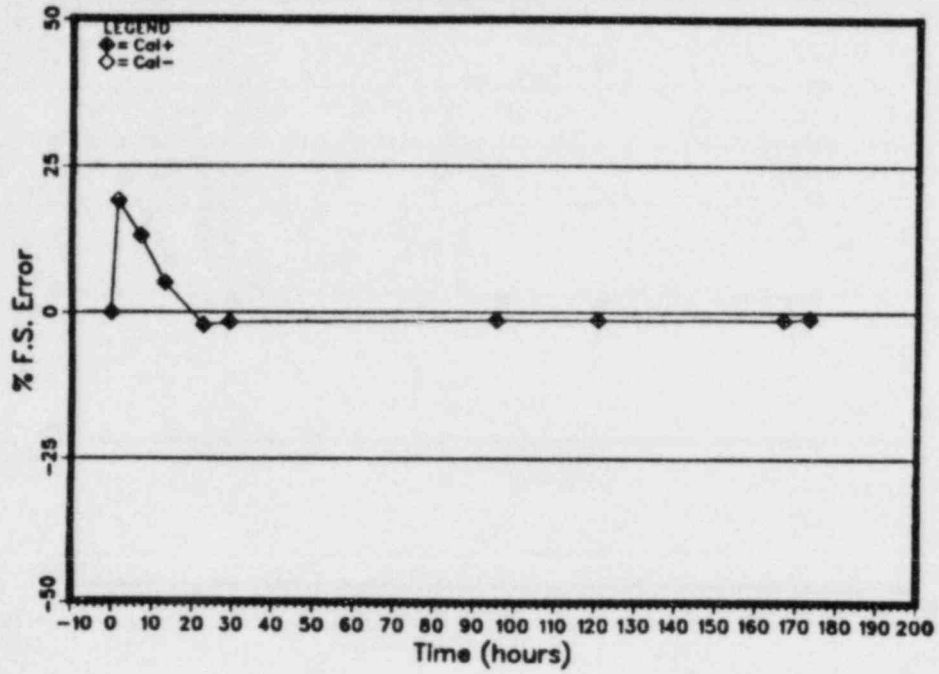
Figure 19. Special Test Sequence Temperature Profile

267
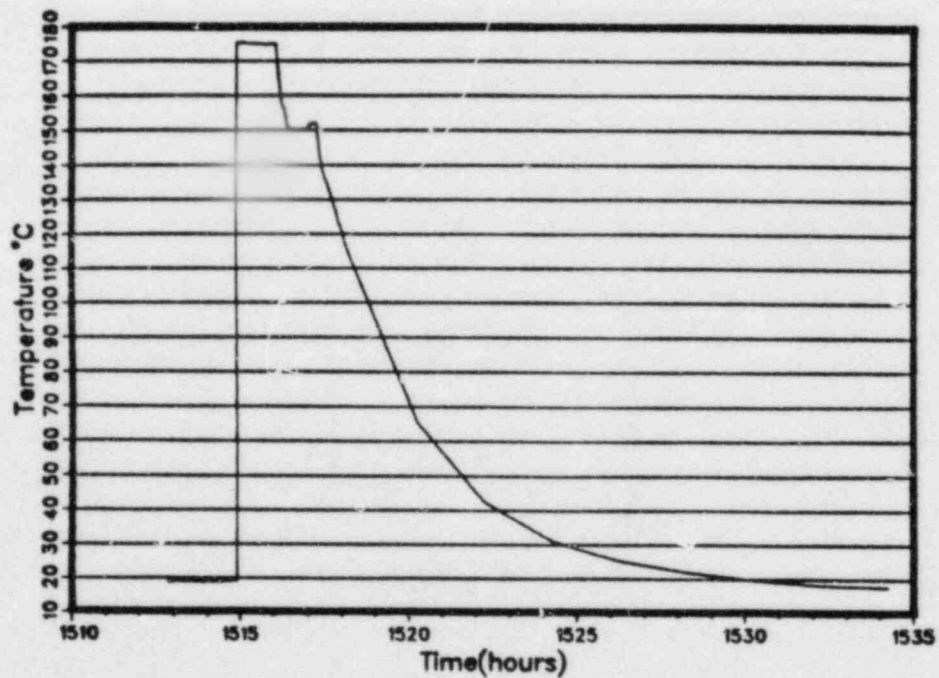
Figure 20. Special Test Sequence Error Profile for Transmitter T2
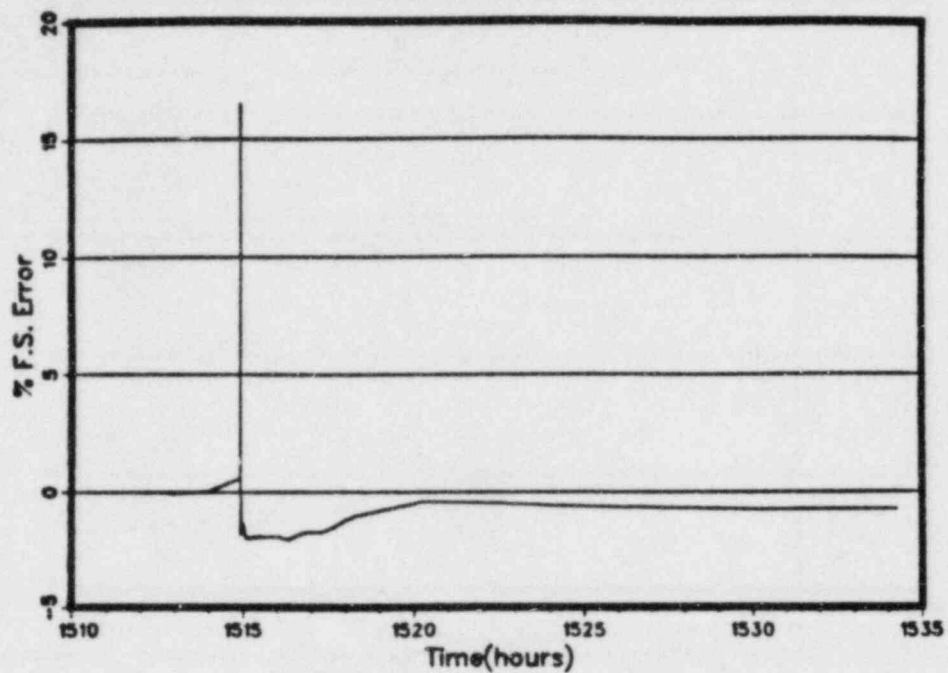
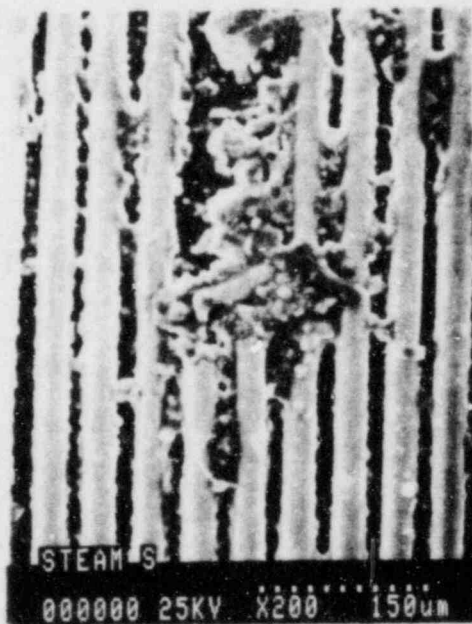Figure 21. SEM Photograph of Potentiometer Resistive Element Showing Corrosion

268

DIAGNOSTIC INSTRUMENTATION FOR DETECTION OF THE ONSET
OF STEAM TUBE LEAKS IN PWRs

W. H. Roach
EG&G Idaho, Inc.
Idaho National Engineering Laboratory

SUMMARY

This report discusses the third, and final, year's work on an NRC-funded project examining diagnostic instrumentation in water reactors. The first two years were broad in coverage, concentrating on anticipatory measurements for detection of potential problems in both pressurized- and boiling-water reactors, with recommendations for areas of further study. One of these areas - the early detection of small steam tube leaks in pressurized water reactors - formed the basis of study for the last year of the project.

Four tasks are addressed in this study of the detection of steam tube leaks.

1. Determination of which physical parameters indicate the onset of steam generator tube leaks.

2. Establishing performance goals for diagnostic instruments which could be used for early detection of steam generator tube leaks.

3. Defining the diagnostic instrumentation and their location which satisfy Items 1 and 2 above.

4. Assessing the need for diagnostic data processing and display.

Parameters are identified, performance goals established and sensor types and locations are specified in the report, with emphasis on the use of existing instrumentation with a minimum of retrofitting. A simple algorithm is developed which yields the leak rate as a function of known or measurable quantities. The conclusion is that leak rates of less than one-tenth gram per second should be detectable with existing instrumentation.

1.0 PREVIOUS WORK

Year 1: (See Reference 1)

During the first year of the project, event tree analysis was used
to assess anticipatory measurement requirements for nuclear power plants.
Events studied were those that could lead to breach of cladding, breach
of pressure boundary and breach of containment. Several hundred events
were identified; from the analysis a list of fifty-one useful anticipatory
measurements was developed, covering potential problems in: reactor
power, core heat removal, secondary side heat removal, primary pressure
boundary integrity and containment integrity. Diagnostic instrument
performance characteristics for these measurements were then developed
and listed. The report concluded with recommendations for future work
in three areas:

o   Valve status monitoring by acoustic analysis

o   Leak detection and location by acoustic analysis

o   Instrument integrity methodology development
     (Self test capability)

Year 2: (See Reference 2)

The potentially useful anticipatory measurements identified during
the first years work were ranked in importance according to the expected
frequency of occurrence of the accidents that the measurement might
prevent or mitigate. Development and implementation costs were also
estimated. Cost and benefit were then combined to arrive at a qualitative
estimate of the cost/benefit ratio for each measurement. Several types
of measurements were recommended for implementation and/or further investigation.
Three major areas were suggested: acoustic techniques, instrument performance
diagnostics and general signature analysis. Several specific tasks
were also suggested:

270

o   Flow rate pressure drop for pumps

o   Lateral shaft motion detection

o   Secondary coolant monitoring to detect steam generator tube
     leaks.

   2.0   DIAGNOSTIC INSTRUMENTATION EVALUATION TASK FOR FY-84

The broad, non-specific nature of this project during the first
two years, FY-82 and FY-83, changed considerably for FY-84. One of
the recommended areas of work in the final report for FY-83 was to examine
methods for the early detection of steam generator tube leaks in pressurized
water reactors. This task was drafted into a statement of work which
is included as Appendix A.

A literature survey showed that some work has been done on steam
tube leak location after reactor shut down[3] and a mathematically oriented
study[4] has been done in which loop equations were developed for radiation
levels in the PWR secondary. No reference was found which specifically
addressed the tasks given in the statement of work. Monitoring of the
secondary to detect steam tube leaks is done at many, if not all, operating
PWRs and is described in varying detail in plant Final Safety Analysis
Reports (FSARs).

   2.1   Task 2.1.1: Physical Parameter Identification

Task 2.1.1 of the Statement of Work, became a search to determine
what physical parameters would indicate onset of steam generator tube
leaks since there appeared to be no way to determine an impending leak
condition. Further, very small leaks are probably difficult, if not
impossible, to detect through any of the coolant parameters such as
pressure, fluid flow or coolant level. For such leaks, the parameter
to choose is one which is unique to the primary system, in a no-leak
condition, and which is detectable, with great sensitivity, in the secondary
when a leak occurs.

Radioactive isotopes formed in the primary as a result of fission or neutron capture fulfill the above requirement and are monitored in some PWRs to indicate primary-secondary leakage. Task 2.1.1 thus became a search for suitable radioactive isotopes which are born in the primary and can migrate to the secondary via small steam tube leaks.

In-plant measurements[5], conducted during the past years, did examine secondary coolant and steam in those plants where steam tube leaks were known to exist. Isotopes which transport readily from primary to secondary are listed in Table 1. Some fission products plate out, to varying degrees, hence are not useful as quantitative indicators of leakage and are not listed. Not all of the isostopes in Table 1 are suitable as leak detectors. For example, ^3H (Tritium) decays by a weak beta, hence it is difficult to detect in a plant situation. In addition, tritium cannot be scrubbed from coolant, and make-up water may contain tritium which has entered the water through some other process than leakage.

TABLE 1. PARAMETERS FOR STEAM TUBE LEAK DETECTION

Isotope(s)	Formation	Predominant Decay Mode	$T_{\frac{1}{2}}$	Remarks
^3H	Neutron Capture Tertiary Fission	β	12.7 yr	Low Energy β
^{16}N	Neutron Capture	γ	7 s	High Energy γ Short Half-Life
^{24}Na	Neutron Capture	γ	15 hr	Energetic γ Good Half-Life
Noble Gases	Fission	γ and β	Several*	Follow Steam Cycle
Iodines	Fission	γ and β	Several*	Follow Water Cycle

*See Table 2.

Of the isotopes in Table 1, those selected for further scrutiny were the iodines, the noble gases, and sodium-24. Analysis shows that the iodines, to a large extent, remain in the steam generator rather than following the steam path. Detection of the iodines would be the most productive, then, in the steam generator water; for example, in the downcomer. Physical access to the downcomer, which is in reactor containment, plus the high radiation background expected in such a location,

272

largely precludes a monitoring site on the steam generator itself.
In addition, retrofitting costs for existing plants would be high even
if the location were feasible.

Sodium-24, with an energetic gamma ray decay and a useful half-life,
is one of the isotopes which existing plants monitor at the steam generator
blowdown line, either on-line or on a grab sample-laboratory basis. Two
items suggest that the blowdown line location is not ideal: one, the
possibly high background level and two, the relatively long time between
leak onset and detection at the blowdown line location.

Noble gases are non-condensible and follow the steam path from the
secondary. A separation of the non-condensible gases and water occurs
at the condensor, the gases then proceeding to the steam generator air
ejector. The air ejector location for a radiation monitor is acceptable
since expected radiation background is low. Finally, some existing
plants have air ejector monitors already in place.

The detection of noble gases at the air ejector appears to be the
best method to use to detect early onset of steam generator tube leaks.
This selection is based on the following facts:

o   Noble gases leaving the steam generator are totally discharged
     via the air ejector. None are returned to the steam generator.

o   The transit time from steam tube leak to air ejector is less
     than two minutes.

o   The air ejector is located in an acceptable environment from
     a sensor point of view.

2.2 Task 2.1.2: Establish Performance Goals

This task, the establishment of performance goals for diagnostic
instruments being evaluated, was closely tied to the actual selection
of the instrumentation, Task 2.1.3. In order to define performance
goals in a quantitative sense it was felt that some small, but realistic,

273

radiation level in the secondary must be assumed. An American National Standard[6] has addressed the problem of source term specifications for both PWRs and Boiling Water Reactors (BWRs). In particular, numerical examples are given in the report for both primary and secondary radiation levels in a PWR, assuming nominal radiation build-up mechanisms in the primary and a small (0.4 g/second) leak in the steam generator tubes. Since this document, now in a draft stage, should soon be available as a national standard, the calculated radiation levels in Reference 6, assuming a 0.4 g/second leak rate, were used here to establish performance goals for diagnostic instrumentation.

In the following development, expressions are derived for the build-up of noble gases in the steam generator secondary after leak onset; for the noble gas arrival rate, in μCi/second, at the steam generator air ejector; and for the primary-to-secondary leak rate. These expressions are then used in a sample calculation which shows what activity might be expected at the air ejector in a typical PWR with a small steam tube leak. Performance goals are then given for the required monitoring systems. Several assumptions are made:

o   The noble gas activity in the primary coolant is in equilibrium or a slowly varying function of time;

o   The half-lives of the most abundant noble gas isotopes are long compared to both the transit time of steam from the steam generator to the air ejector and the cycle time from steam generator through the turbines and condensor and return to the steam generator, the latter time being of the order of two minutes or less for a typical PWR;

o   Complete mixing of the noble gases with the secondary coolant occurs in times much less than the steam generator cycle time.

The time rate of increase of total noble gas activity in the steam generator secondary coolant after leak onset is

$$\frac{dA_s(t)}{dt} = \ell\, C_p - \frac{m}{M}\, A_s(t),\qquad\qquad\qquad(1)$$

where

$A_s(t)$ = the total noble gas, in µCi, in the steam generator secondary at time t

C_p = the primary coolant noble gas activity, in µCi/g

ℓ = leak rate, primary to secondary, g/s

m = mass of water per second converted to steam

M = mass of water in steam generator

Equation (1) assumes steady-state conditions in the primary coolant and for the leak rate. The transient case, where either or both ℓ and C_p are time dependent is not treated here.

Solving Equation (1) for $A_s(t)$,

$$A_s(t) = \ell\, C_p\, \frac{M}{m}\left(1 - e^{-\frac{m}{M}t}\right).\qquad\qquad\qquad(2)$$

For times long after leak onset, the total noble gas activity in the steam generator secondary is

$$A_s(t \to \infty) = \ell\, C_p\, \frac{M}{m}.$$

The noble gas activity per second arriving at the air ejector, A_E, is the same as that leaving the steam generator per second, neglecting noble gas decay in the short transit time between steam generator and air ejector. From Equation (2), this quantity is

$$A_E = \frac{m}{M}\, A_s(t) = \ell\, C_p\left(1 - e^{-\frac{m}{M}t}\right)\qquad\qquad\qquad(3)$$

in µCi/second.

275

A_E approaches the product ℓC_p after a few steam generator cycle times, $\frac{M}{m}$, which is typically about 100 seconds. Figure 1 plots the dimensionless quantity $A_E/\ell C_p$ as a function of steam generator cycles after onset, $\frac{m}{M} t$.
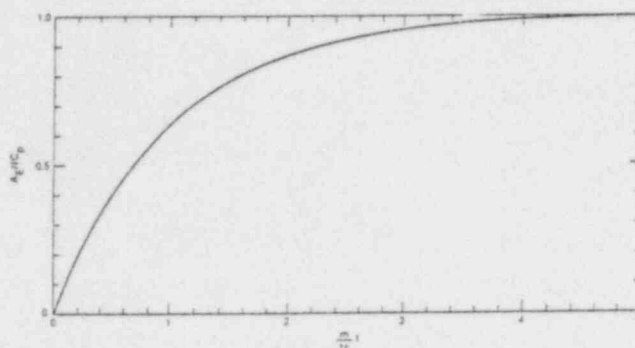

Figure 1. Normalized air ejector activity vs. number of steam generator cycles.

The separation of the noble gases from the secondary loop return coolant appears to be complete. The source term survey (See Reference 5) did not detect any noble gas activity in the return water in those plants where steam tube leakage was observed.

Solving Equation (3) for the leak rate yields

$$\ell = \frac{A_E(t)}{C_p(1 - e^{-\frac{m}{M} t})} \qquad (4)$$

Equation (4) assumes that the noble gas activity at both the air ejector and in the primary coolant are known. An existing air ejector monitoring system, shown schematically in Figure 2, (See Reference 7 and Appendix B) counts activity from noble gases only, hence are only required to be gross activity detectors. To obtain the noble gas activity in the primary coolant, however, requires an isotopic analysis, since the primary contains all the fission products in addition to radio-nuclides produced by other (e.g., neutron capture) processes. Such analyses are routinely done using, for example, a Ge(Li) detector in a gamma ray spectrometer system. Since the above development for leak rate has assumed that the primary activity is approximately constant with time, on-line real-time spectral analysis in the primary would not be required. Grab samples at regular (each shift) intervals should be sufficient, with the precaution that such samples must be kept sealed.
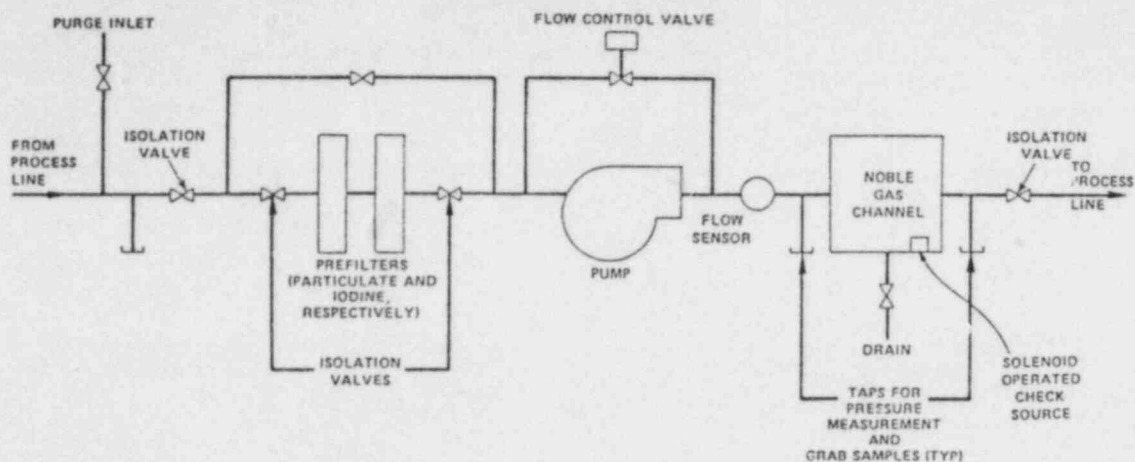
Figure 2. Single stage gaseous monitor.

A sample calculation of what the air ejector activity would be, using assumptions from the references, is included here in order to estimate what performance goals should be set for the two monitors, air ejector and primary coolant.

The activity per second at the air ejector, from Equation (3), must be converted to activity per unit volume, since it is the latter quantity which is obtainable from a count rate. Such a conversion requires that the gas flow rate, in cm^3/second, is known in the air ejector sampling system. Reference (7), included in part in Appendix B, gives the specifications for an air ejector monitoring system and assumes a flow rate at the air ejector sample system of one standard cubic foot per minute (scfm). That assumption will be used in this sample calculation.

From Table 2 (See Reference 6) the sum of the isotopic noble gas activities in the primary coolant yields

TABLE 2. REPRESENTATIVE SOURCE TERMS[1]
(μCi/g)

| Nuclide | $T_\frac{1}{2}$ | Reactor[a] Coolant | Secondary Coolant[b] | |
			Water[c]	Steam[d]
Kr-85m	4.5 hr	1.6(-1)	0	3.4(-8)
Kr-85	10.7 yr	4.3(-1)	0	8.9(-8)
Kr-87	76 min	1.5(-1)	0	3.0(-8)
Kr-88	2.8 hr	2.8(-1)	0	5.9(-8)
Xe-131m	12 day	7.3(-1)	0	1.5(-7)
Xe-133m	2.2 day	7.0(-2)	0	1.5(-8)
Xe-133	5.2 day	2.6(0)	0	5.4(-7)
Xe-135m	15.3 min	1.3(-1)	0	2.7(-8)
Xe-135	9.1 hr	8.5(-1)	0	1.8(-7)
Xe-137	3.8 min	3.4(-2)	0	7.1(-9)
Xe-138	14.1 min	1.2(-1)	0	2.5(-8)
I-131	8 day	4.5(-2)	1.8(-6)	1.8(-8)
I-132	2 hr	2.0(-1)	2.9(-6)	2.9(-8)
I-133	20 hr	1.4(-1)	4.8(-6)	4.8(-8)
I-134	53 min	3.4(-1)	2.5(-6)	2.5(-8)
I-135	6.7 hr	2.6(-1)	6.6(-6)	6.6(-8)
H-3	12.7 yr	1.0(0)	1.0(-3)	1.0(-3)
N-16	7 sec	4.0(+1)	1.0(-6)	1.0(-7)
Na-24	15 hr	4.7(-2)	1.5(-6)	7.6(-9)

a. Coolant entering letdown line (Notation: 1.6(-1) = 1.6 x 10⁻¹).
b. Primary-to-secondary leakage rate of 0.4 g/s (/5 lb./day)
c. Water in steam generator.
d. Steam leaving steam generator.

277

$C_p = 5.6 \ \mu Ci/g.$

The air ejector activity per cm^3 is given by

$$A'_E = \frac{A_E}{\text{(Sample Flow Rate)}} = \frac{\ell \, C_p}{\dot{V}_E} \,, \qquad (5)$$

where it is assumed that A_E has attained a steady-state value and where

$\dot{V}_E$ = volumetric flow rate in the air ejector sample line, cm^3/s.

Assume a leak rate (See Reference 6)

$\ell = 0.4 \ g/s.$

Equation (5) then gives

$A'_E = 4.7 \times 10^{-3} \ \mu Ci/cm^3.$

This activity is some three orders of magnitude greater than the detection limit given for existing single stage gaseous monitoring systems (See Appendix B) and perhaps five orders of magnitude greater than the $10^{-8} \ \mu Ci/cm^3$ or better attainable with available gamma ray spectrometers using Ge(Li) detectors. (See Reference 5).

Performance goals for the air ejector and primary coolant monitoring systems are taken from Reference (7) and are given as system specifications which are probably representative of commercially available systems. Appendix B, from the same reference, discusses these systems in greater detail.

2.2.1 Specfication for Air Ejector Monitor

The air ejector monitor will be a single-stage gaseous monitor consisting of a beta sensitive plastic scintillation radiation detector, coupled to a photomultiplier tube which is protected by an electromagnetic shield. Figure 2 is a block diagram showing the components of the monitor.

278

The minimum detectable limit of the monitor for Xe-133 in a 1 mr/hr background at a 95% confidence level is 1×10^{-6} $\mu Ci/cm^3$, based on a sample flow rate of 1 standard cu. ft. per minute (scfm) and a one-half minute counting time. The response of the detector is at least three times the square root of the background above background.

2.2.2 Specification for Primary Coolant Monitor

The primary coolant monitor will be a single-stage liquid monitor consisting of a gamma sensitive scintillation detector, coupled to a photomultiplier tube which is protected by an electro-magnetic shield. The minimum detection limit of the monitor for Cs-137 in a 1 mr/hr background of Co-60 gamma radiation at a 95% confidence level is 1×10^{-6} $\mu Ci/cm^3$ for one minute counting time. The resolution of the detector is less than 10% Full Width at Half Maximum (FWHM) at 0.662 MeV (Cs-137).

It is noted that existing Ge(Li) gamma ray pulse height analyzers have sensitivities which exceed those in the above specification by several orders of magnitude and typically can resolve 1 to 2 keV peaks at several MeV energy. Such a primary coolant monitor should be able to resolve the noble gas photo peaks at a 95% or greater confidence level.

Self-test capability for the systems described in Appendix B is provided by means of a built-in, pop-up source, remotely or manually operated. A self-test capability, which tests everything except the detector itself, is incorporated in many of the gamma ray spectrometer systems in use at the Idaho National Engineering Laboratory. This consists of an electronic pulser which injects double pulses of known energy equivalent and repetition rate into the counting data. Since the energies are precisely known, the pulser acts also as a system calibration and, by knowing the pulse rate, indicates whether or not counts are being lost due to excessive count rate. Such a modification to existing gamma ray systems is recommended.

The drift rate during the data taking interval of the referenced gross beta detector is not known. However, the short counting interval (30 seconds) coupled with good design, should assure that the drift rate

279

is within the 0.5% requirement of the Work Statement. Gamma ray
spectrometers, with the detector kept at constant temperature, are well
within the above stability criteria over long periods of time.

The analysis suggested here-isotopic noble gas activity in the primary
coolant using a Ge(Li) based gamma ray spectrometer and a beta detector
at the air ejector-attempts to utilize existing, or commercially available,
monitoring systems.

2.3 Task 2.1.3: Define Diagnostic Instrumentation

This task, the defining of the diagnostic instrumentation, is covered
in the preceding section. Only a summary is given here.

2.3.1 Secondary Monitor

Location: Air Ejector
Suggested System: Gross Beta Detector
Detected Species: Noble Gases
Duty Cycle: Continuous

2.3.2 Primary Monitor

Location: Existing or Grab Sample Line
Suggested System: Ge(Li) Gamma Ray Spectrometer Pulse Height
              Analyzer
Detected Species: Isotopic Abundance of Noble Gases
Duty Cycle: Grab sample during operating shift; more often if
         primary conditions are altered.

2.4 Task 2.1.4: Assess Need for Data Processing and Display

This task is defined to assess the need for diagnostic data processing
and display in order to provide plant operators with primary-secondary
leak information.

For control room display purposes, both primary and air ejector noble gas activities must be available. These are used, together with the ratio m/M, to determine leak rate, in g/s, from Equation (4), where t is measured from the first indication of leak onset. Since the water/steam cycle time, M/m, is of the order of a few minutes, the leak rate quite rapidly approaches its limiting value. If the leak rate, ℓ, is a slowly varying function of time, i.e., leak rate slowly increasing, then the time dependent leak rate can be approximated as

$$\frac{\Delta \ell}{\Delta t} \simeq \frac{1}{C_p} \frac{\Delta A_E(t)}{t},$$

for C_p = a constant. Thus the rate of change of leak rate can be determined, at least in principle, by successive measurements of A_E, for time long compared to M/m.

To convert count rate at the air ejector to leak rate requires data reduction as outlined below. The count rate at the air ejector should be the sum of count rate due to noble gases and any background count rate, presuming that the monitoring system filters particulates and iodines upstream of the noble gas counting geometry. After background subtraction, the count rate must be reduced to units of μCi/s. To accomplish this, from gross count rate, one must know the relative abundances of the noble gases, their decay constants, and counting efficiencies for each of the isotopic energies. To obtain A_E, in μCi/s requires that flow rate, $\dot{V}_E$, in cm^3/s, be known. Decay constants for the noble gases are known; counting efficiencies must be determined at the time the counting system is calibrated. (Gross beta counting system such as described here are routinely used for monitoring air ejectors in BWRs; calibration requirements and frequencies are part of BWR technical specifications). Relative isotopic abundances are determined from analysis of the primary coolant, yielding C_p. The ratio, $\frac{m}{M}$, is known from reactor design specifications. The air ejector count rate can then be converted to the total activity, A_E, in μCi/s. The leak rate is then obtained from Equation (4).

3.0 CONCLUDING REMARKS

This study has examined the early detection of onset of steam tube leaks in pressurized water reactors. It has identified which physical parameters in an operating reactor may be used in identifying a steam tube leak condition; has established performance goals required for detection of small leaks; has defined monitoring instruments and their locations for detection of early onset of a leak condition; and has discussed requirements for data processing and display. Steam tube leaks of less than 0.1 g/s should be detectable with existing instrumentation at existing sensor locations, i.e., the combination of a gross beta detection system for noble gases at the steam generator air ejector, installed at some operating plants, and a high resolution gamma ray spectrometer for a detection of noble gas activity in the primary coolant, also a part of some plants' instrumentation inventory.

Close monitoring of a steam generator tube leak could allow a scheduled shut down of the reactor for steam tube repair, with attendant savings. Complete tube rupture could possibly be averted by instrumenting the derivative of the leak rate and providing the necessary alarms.

4.0 REFERENCES

1. J. R. Fincke, G. D. Lassahn, Report on Diagnostic Instrumentation Evaluation, EGG-ID-6037, September 1982.

2. G. D. Lassahn, Diagnostic Instrument Evaluation, 1983 Annual Report, EGG-PBS-6408, September 1983.

3. Proceedings on Workshop on U-Bend Tube Cracking in Steam Generators, C. E. Shoemaker, Editor, Palo Alto, California, 1981, EPRI-WS-80-136, p. 343.

4. M. Chiruvolu, G. A. Pettinger, "Calculating Radioactivity in Nuclear Steam Generator Fluids", Power Engineering, January 1980.

5. J. W. Mandler et al, In-Plant Source Term Measurements at Four PWRs, NUREG/CR-1992, August 1981.

6. American National Standard Source Term Specification, N237-1976 (ANS-18.1), Revision 1 (Draft), March 1983.

7. Final Safety Analysis Report, Vol. 12, St. Lucie Unit No. 2, Florida Power and Light.

APPENDIX A

STATEMENT OF WORK
DIAGNOSTIC INSTRUMENT EVALUATION

B&R: 60190102

FIN: A6380

CONTRACTOR: IDAHO NATIONAL ENGINEERING LABORATORY

PRINCIPAL INVESTIGATOR: W. H. Roach

SITE: Idaho Falls

STATE: Idaho

FY 1984 PROGRAM BUDGET: $100,000

1.0 Background

Diagnostic instrumentation is desirable to (a) detect plant and equipment anomalies, (b) detect precursors to accidents, and (c) supply the plant operator with information on the status of systems important to the safety of a nuclear power plant (NPP).

The objective of this project is to evaluate key instrumentation that would diagnose plant status during normal, abnormal and shutdown conditions.

An evaluation of the state of the art (theory and hardware) and current practice in the use of diagnostic instrumentation and corresponding measurement methods important to safety was begun in FY 1982 and is scheduled for completion in FY 1984. Performance goals will be established and used as a guide in evaluating current diagnostic instrumentation system capabilities and needed improvements. Special emphasis will be given diagnostic instrumentation needs associated with the detection of PWR steam generator leaks in the FY 1984 efforts. Diagnostic measurements may include selected instrument readings, their trends, signatures and other significant information.

2.0 Work Required

The following tasks shall be performed by the contractor in FY 1984:

2.1 PWR Steam Generator Tube Leak Diagnostics

Complete detailed evaluation of diagnostic instrumentation needs for the timely detection of PWR Steam Generator tube leaks, which would include the identification of optimal sensor location.

2.1.1   Determine what physical parameters indicate degrading perfor-
         mance or onset of PWR steam generator tube leaks. List
         these parameters.

2.1.2   Establish performance goals for the diagnostic instruments
         being evaluated. These goals should be a trade-off between
         their reliability and cost. A suggested goal for the reliability
         should be 95% for the measuring system self-test and 90%
         for diagnostic abi ity, with appropriate confidence levels.
         Also, the system must be stable with time and for most measurements,
         the instrument channel drift should be smaller than 0.5%
         during the surveillance interval.

2.1.3   Define diagnostic instrumentation to monitor the parameters
         identified in Subtask 2.1.1, that will fulfill the performance
         goals established in Subtask 2.1.2. Evaluate the need to
         implement (periodic or on-line) self-testing, in these instruments
         to ensure fulfillment of these performance goals.

2.1.4   Assess needs for diagnostic data processing and display.
         Needs should be identified in sufficient detail to enable
         comparison with existing plant data processing and display
         capabilities.

APPENDIX B

Radiation Detectors

The detector assembly is a completely weatherproof assembly, housing a detector, photomultipliers, and radiation check source. The assembly is capable of withstanding the design pressure and temperature of the piping system of which it is a part.

The detector assembly is incorporated in the sampler assembly. All detector assemblies are designed to detect over their specified ranges in a 2.5 mr/hr (1 MeV gamma) external field.

A shielded photomultiplier is provided integral with the detector to ensure reliable transmission of a high signal-to-noise ratio.

Scintillation detectors are beta- or gamma-sensitive detectors suitable for analysis of photopeaks up to 2.5 MeV and beta energy up to 5.0 MeV.

The detector is one of the following types.

Single-Stage Liquid Monitor

A single-stage liquid monitor consists of a gamma sensitive scintillation detector, coupled to a photomultiplier tube which is protected by an electromagnetic shield. The minimum detection limit of the monitor for Cs-137 in a 1 mr/hr background of Co-60 gamma radiation at a 95 percent confidence level is 1×10^{-6} $\mu Ci/cm^3$ for one minute counting time. The resolution of the detector is less than 10 percent Full Width at Half Maximum (FWHM) at 0.662 MeV (Cs-137).

Single-Stage Gaseous Monitor

A single-stage gaseous monitor consists of a beta sensitive plastic scintillation radiation detector, coupled to a photomultiplier tube which is protected by an electromagnetic shield. Figure 2 is a block diagram showing the components of the monitor.

The minimum detectable limit of the monitor for Xe-133 in a 1 mr/hr background at a 95% confidence level is 1×10^{-6} $\mu Ci/cm^3$, based on a sample flow rate of 1 scfm and a one-half minute counting time. The response of the detector is a least three times the square root of background above background.

Condenser Air Ejector Monitor

The condenser air ejector monitor is a single-stage gaseous monitor. The monitor measures noncondensable fission product gases in the condenser air ejector discharge to detect any primary-to-secondary leakage. The presence of radioactivity in this line indicates a primary-to-secondary leak in the steam generators. The predominant isotopes would be Kr-85 and Xe-133, with presence of iodine. The function of this monitor is to alarm in the event of a primary-to-secondary steam generator tube leak.

The monitor is located on the common header downstream of the air ejector after condensers discharge. The alarm setpoint would be set slightly higher than expected plant background.

Calibration and Inspection

A remotely-or manually-operated check source is provided with each detector assembly. The check source isotope has a half-life greater than seven years, with emissions in the energy range and of the same type as being monitored, and is usable as a convenient operational and gross cali-bration check of the associated detection and readout equipment. The

check source strength provides a count rate of approximately 1.5 decades above background. The check source controls are mounted on the channel indicator module in the control cabinets. These check sources can be activated automatically through the CRT keyboards in the control room, the health physics office or radiochemistry laboratory.

Isotopic calibration of the complete radiation monitoring system are performed at the factory. Field calibration sources, with their decay curves, are provided with the system hardware. For the high range in containment monitor, a current source will be used for calibration of the radiation ranges above 10R/hr.

Further isotopic calibrations are not required, since the geometry cannot be altered significantly within the sampler. Calibration of samplers is then performed, based on a known correlation between the detector responses and field calibration standards.

This single-point calibration confirms the detector sensitivity. The field calibration is performed by removing the detector and placing the calibration source on the sensitive area of the detector.

The radiation monitoring channels are checked and inspected in accordance with the Technical Specifications. Grab samples are collected for isotopic analysis weeekly as described in the subsequent sections. Set point adjustment and functional testing are done on a monthly basis, and calibration is performed at each refueling shutdown or indication of equipment malfunction.

Controls and Alarms

All monitors are provided with either a local control and display unit located near the monitor or a portable indicator control box capable of accessing the monitor control features and data base. Either of the two units provide information relating to operational mode, alarm status and data output. Purging, check source actuation, valve and pump control, and various test mode actuations may be done locally and with the exception of valve control, within the cabinets at the various operator's terminals.

The digital information from all channels is stored by the redundant computers and displayed at the three operator consoles on cathode-ray tube (CRT) displays. If an alarm condition is detected, a status change occurs at each of the three CRTs and logging of the alarm occurs automatically. Monitor status, radiation level, and alarm status are displayed. Alarms include two up-scale trips to indicate high radiation levels and one downscale trip to indicate instrument trouble. For those channels designated as safety related, data displays and strip-chart recorders are also present in a safety related panel in the control room.

For those channels which perform control action, any one of the following automatically sends an isolation signal to the valve located on the monitored line to prevent further flow; radionuclide concentrations abvove the preset "high" radiation trip point, failure of the detector or sample pump, or loss of flow to the sampling chamber.

Alarm set points are variable over the entire dynamic range and are set from the control room. Alarm setpoints may be introduced or changed from the following locations, a) for safety related monitors; from the individual channel control and display units located in the control room safety cabinets, and b) for non-safety related monitors; from any of the three CRTs, locally by means of the local control and display unit, or by the portable indicator control unit. All alarm set points are protected and changed only by means of proper access identification. Exact setpoint depends on background and plant conditions. For effluent monitors, high-high alarms indicate before 10CFR20 limits are reached.

MEASUREMENT OF RESPONSE TIME AND DETECTION OF DEGRADATION IN PRESSURE SENSOR/SENSING-LINE SYSTEMS

M. E. Buchanan,* L. F. Miller,** J. A. Thie,***
T. W. Kerlin,** G. Ragan,** J. March-Leuba**

*Oak Ridge National Laboratory, Oak Ridge, Tennessee 37831[1]
**The University of Tennessee, Knoxville, Tennessee 37916
***Analysis & Measurement Services, Inc., Knoxville, Tennessee 37919

INTRODUCTION

Remote in situ methods to detect degradation in the response time of nuclear plant pressure sensor/sensing-line systems were evaluated. This research was performed at the request of the Electrical Engineering Instrumentation and Control Branch of the U.S. Nuclear Regulatory Commission Office of Nuclear Regulatory Research.

Pressure-sensing systems are used in nuclear plant protection systems to trip the reactor and initiate engineered safety features within a specified, finite time period. Pressure sensor/sensing-line systems include the pressure sensor and sensing line and any associated snubbers, valves, and signal-conditioning equipment. At present the in situ response-time testing of pressure sensors recommended in Regulatory Guide 1.118 necessitates entering containment; testing is therefore limited to periods of plant shutdown. Furthermore, the industry currently has no method to remotely verify the response time of pressure- sensing lines. The availability of a remote, in situ method for response-time testing would enable confirmation of the satisfactory operability of pressure sensors and associated sensing lines whenever desired rather than only during plant shutdown.

The current response-time measurement technique requires that the transmitter be isolated from the sensing line and that a pressure ramp be injected into the transmitter to test its operability. However, this method does not address sensing-line problems and cannot verify response time while the plant is operating. The methods evaluated in this work have the potential for overcoming these limitations.

Three methods were evaluated for remote in situ testing: (1) interruption of ac power to the power supply of force-balance type pressure transmitters (referred to as the off-on method) to verify sensor response time; (2) a pressure perturbation method (referred to as the BURP method) that involves introducing a small pressure impulse into the sensing line by means of a remotely operated solenoid valve to verify line response time; and (3) analysis of the frequency spectrum of naturally occurring pressure fluctuations (referred to as noise analysis) to continuously monitor the complete pressure-sensing system (line, sensor, electronics, etc.) for degradation that may affect system response time.

These three methods were evaluated in the laboratory at pressures up to 1000 psi and in the Forced Convection Test Facility (FCTF) at ORNL, which simulates the flow, temperature, and pressure conditions of a commercial pressurized water reactor (PWR). The ability of the various methods to detect degradation in pressure-sensing systems was evaluated by introducing blockages and air into sensing lines and by degrading the response of the pressure sensor. A nuclear-qualified force-balance pressure sensor, together with a prototypical pressure-sensing system (sensing line, valves, etc.), was used to evaluate the methods. Laboratory- grade fast-response pressure sensors were used as references to verify the response time of the prototypical system. A theoretical model describing the dynamic response of the sensing system was developed and used to aid in evaluating the test results.

This paper describes some of the methodology employed in this research and presents the results of our evaluation of the above methods.

290

Recommendations and procedures to verify response time and to monitor for degradation in pressure sensor/sensing-line systems are suggested.

METHODOLOGY AND DISCUSSION OF RESULTS

Remote Testing of Foxboro Pressure Transmitters

Force-balance pressure transmitters can be tested remotely because system pressure can be utilized to introduce a perturbation by deactivating the electromechanical force acting on the diaphragm that balances the force associated with system pressure. The simplified illustration of the Foxboro pressure transmitter shown in Fig. 1 exemplifies this observation. Note that when the current to the force motor coil is turned off, system pressure displaces the diaphragm in the same manner as would occur with a positive pressure transient, and the lever system is displaced to the high-pressure stop. When power is restored, current returns to the force motor coil and the system responds with essentially the same characteristics as it responds to a positive pressure perturbation. In Fig. 2 a comparison of the off-on response is shown by the dotted curve and a large-step pressure perturbation is shown by the solid curve. The initial portion of the two responses differ since the electronics must be first initialized in the case of the off-on test. The straight-line portion of the response corresponds to the integral action of the controller while sufficient current builds up for the force motor to overcome system pressure. The terminal end of the response, which corresponds to the final exponential form of the responses, contains the dynamic data of interest.

The analysis of the remote test data, which begins at the point where the response makes a transition from straight-line to exponential, is accomplished by parameter identification of a physically based model for the case of non-zero initial conditions. In particular, the first derivative is not zero at the start of the transient. After model parameters are identified from the remote test data, the asymptotic ramp delay time is determined by integrating the step response of the model for the

291
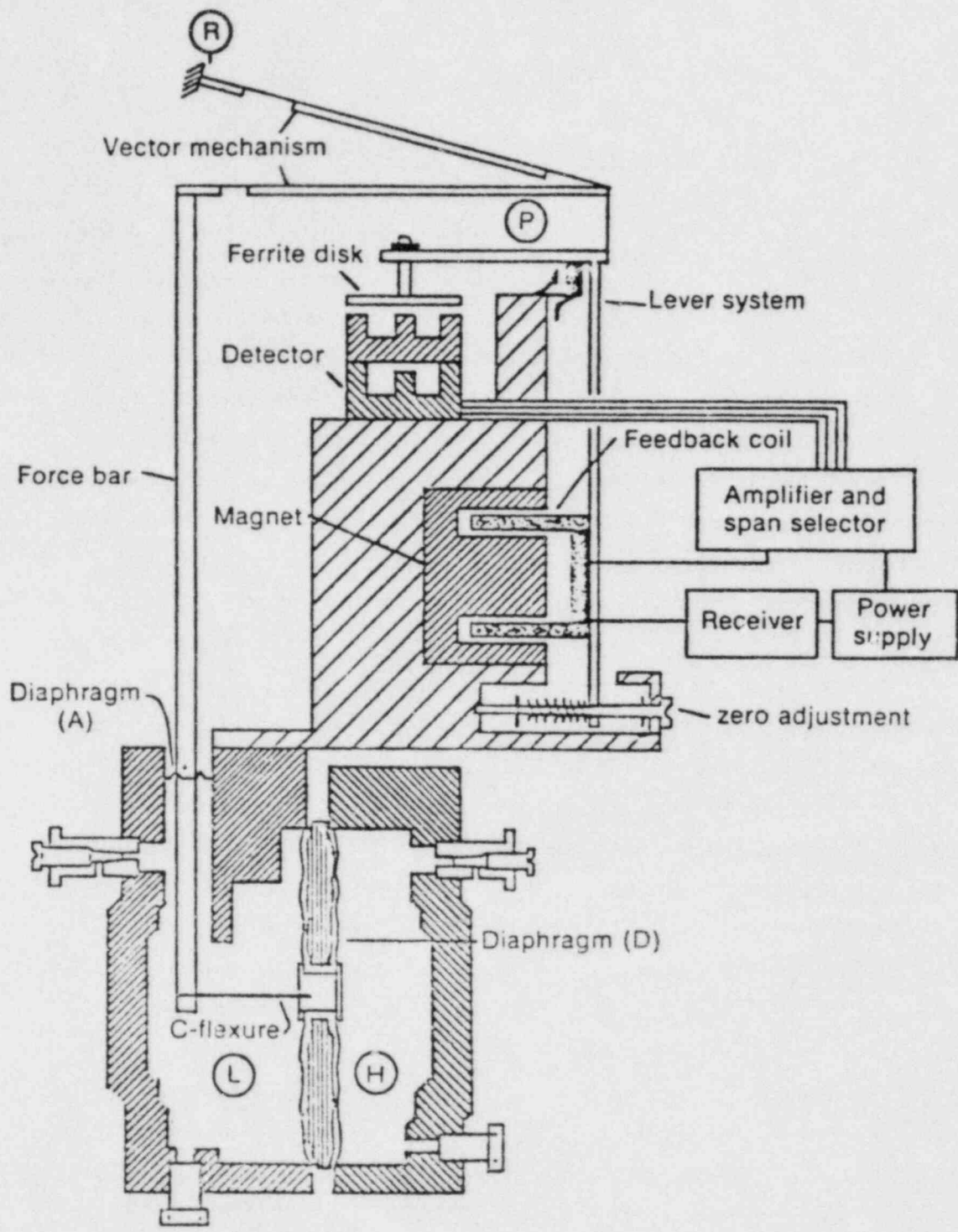
Fig. 1. Simplified illustration of a Model E13DM Foxboro pressure transducer.
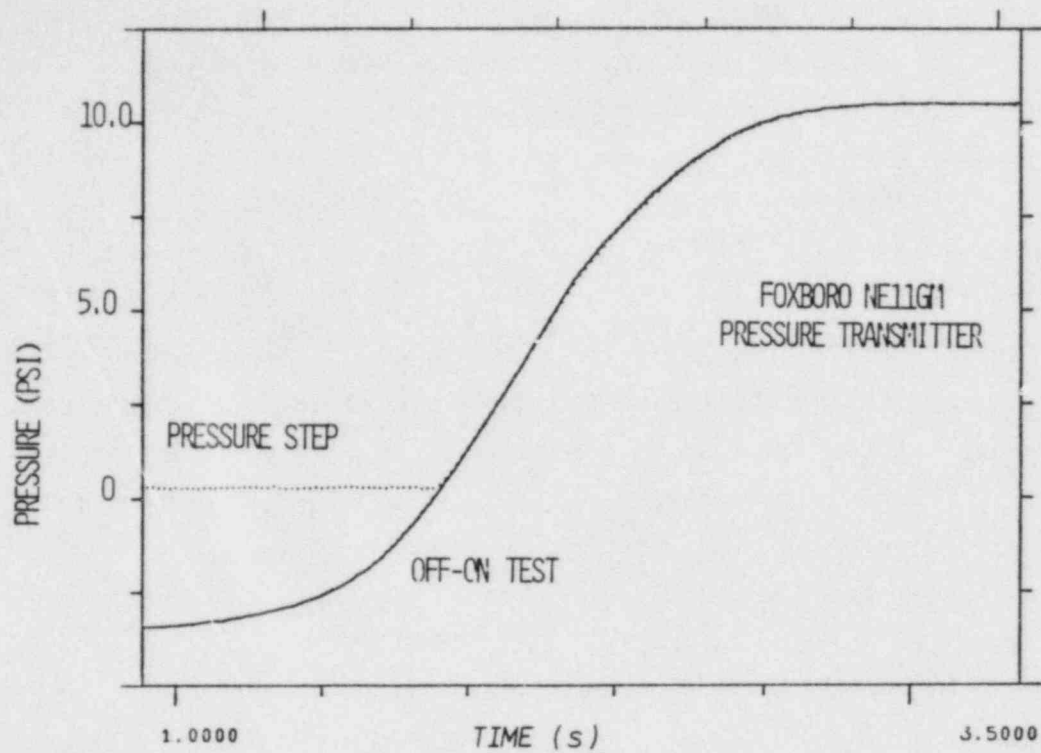
Fig. 2. Nuclear grade transmitter response to OFF-ON test. The solid line corresponds to a remote test and the dotted line is obtained from a large-step pressure perturbation.

case of zero initial conditions. A comparison between measured ramp delay times and those determined from remote test data are shown in Table 1. Observations of experimental data and analyses of remote test data suggest that differences as large as 100 ms should be expected.

Pressure Perturbation Tests

Dynamic models of sensing lines developed in conjunction with this research, and experimental data from previous research projects, indicate that several types of resonant frequencies can be excited in sensing lines. Thus, distributed-parameter models and lumped-parameter models were studied in order to understand the pressure sensor/sensing-line system and to implement a pressure perturbation experiment for measuring the response time of the sensing line.

The solution of the one-dimensional wave equation with the terminal end reflected, a ramp pressure input at the other end, and no resistance illustrates that the asymptotic time delay for this case is positive or negative and may have a magnitude as large as the sensing-line length divided by the speed of sound in water. If resistance is introduced, one obtains the damped wave equation. Based on an analysis of this equation, it is apparent that resistance is the parameter of primary concern in determining delay times associated with sensing lines. Other parameters such as inertia and elasticity also play important roles in determining the response characteristics of the sensing line. Although complicated nonlinear distributed-parameter models of the pressure sensor/sensing-line system are available and may be utilized, a second-order linear lumped-parameter model accurately predicts the response due to a pressure perturbation. In addition, it provides a good estimate of the asymptotic time delay of the sensing line.

The method used to excite oscillations in the sensing line employs a fast-acting solenoid valve and a small chamber downstream of the solenoid valve. Conditions prior to introduction of the perturbation into the sensing line consist of a pressure differential across the solenoid valve with the perturbation chamber empty and isolated. When the solenoid

294

Table 1. Foxboro transmitter remote test results

Transmitter Type	Response Time (ms)	
	Direct	Remote
E11DM	140	160
E11DM	107	160
E11DM	139	143
E11DM	121	156
E11DM	155	182
E11DM	154	189
E11DM	205	135
E11DM	177	172
NE11GM	360	411
E13DM Differential	321	287
E13DM Differential	492	382
E13DM Differential	438	346
E13DM Differential	412	331
E13DM Differential	392	450
E11GM Absolute	179	146
E11GM Absolute	155	203
E13DM Differential	180	156

valve is opened, fluid from the sensing line (and system) flows rapidly into the pressure perturbation chamber and initiates oscillations. Experiments of this type were performed at low pressure (~10 psi), medium pressure (~1000 psi), and high pressure (~2000 psi). However, only results obtained from the high-pressure test facility and pressure perturbation test fixture are discussed here.

The high-pressure test fixture was installed in the Forced Convection Test Facility (FCTF) shown in Fig. 3; the fixture itself is illustrated by Fig. 4. Note that approximately 120 ft of sensing line is installed between the process pressure transmitter (The Foxboro) and the root penetration into the system. Specific hardware components are shown in Figs. 4 and 5. Tubing sizes and configurations were selected to be consistent with those typical of commercial nuclear power plants. Figure 6 is a schematic diagram that illustrates the valve and transmitter locations. Procedures for initializing and initiating pressure perturbation tests should be apparent after some study of Fig. 6.

An example of a typical pressure perturbation transient obtained at the FCTF is shown in Fig. 7. Only two parameters associated with the response are required in order to obtain the asymptotic ramp time delay. They are (1) the frequency, and (2) the decay rate of the oscillations. In particular, these two parameters may be substituted into the second-order lumped-parameter model to obtain the delay time of interest. Applicable equations are included in Fig. 7. Table 2 lists delay times based on this method for several values of line resistance simulated with a needle valve. Note that these delay times are approximately a factor of 10 less than the length of the sensing line divided by the speed of sound in water (~25 ms). This result is consistent with solutions of the one-dimensional wave equation. If the needle valve is closed to one turn open, the induced oscillations are small and it is then difficult to obtain a good estimate of the asymptotic delay time by t' s method. Another pressure perturbation experiment was performed to investigate large simulated values of line resistance. In particular, a small pressure differential was introduced across V_{17} (cf., see Fig. 6), and V_{17} was then opened rapidly. Results of these experiments are shown in
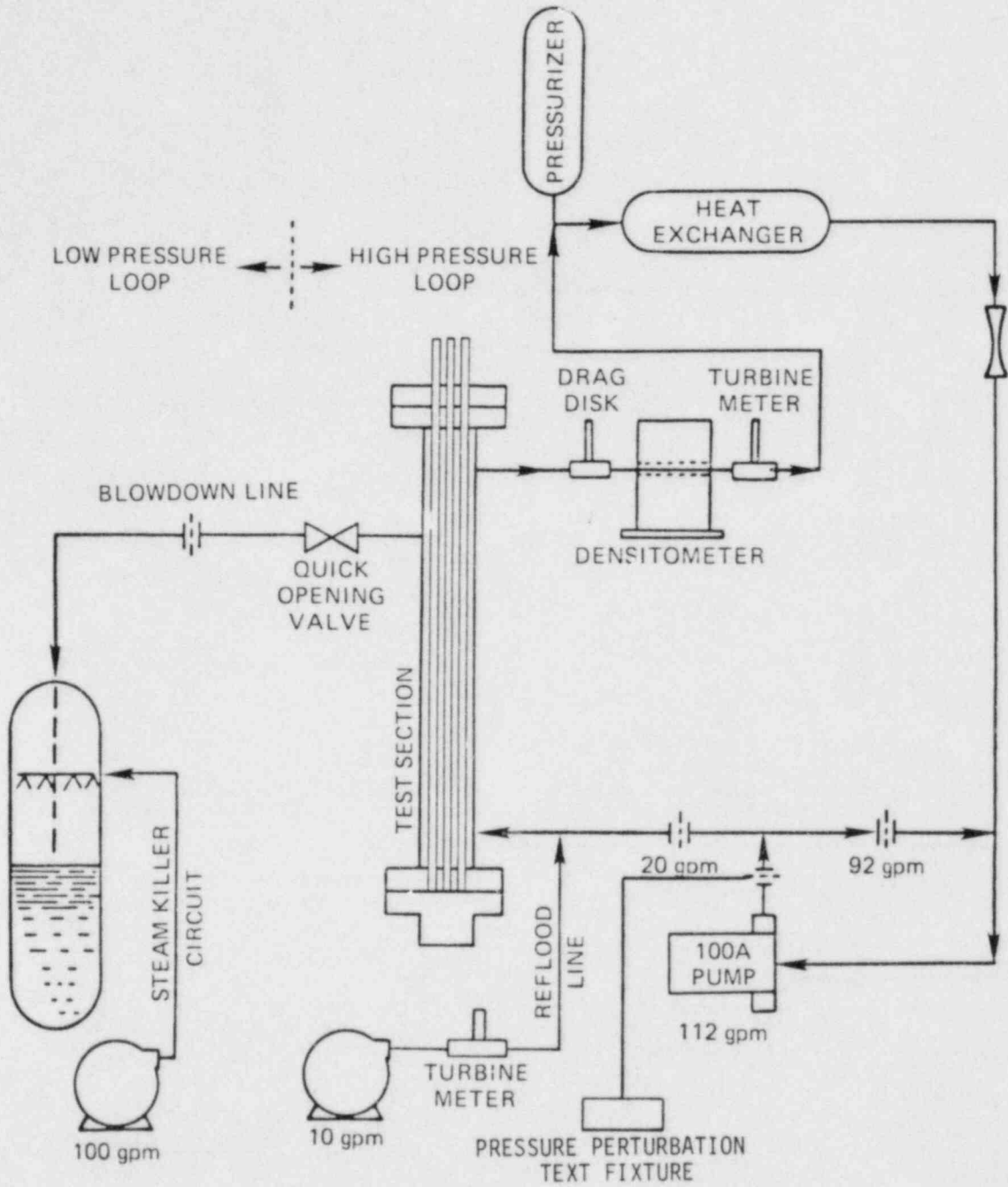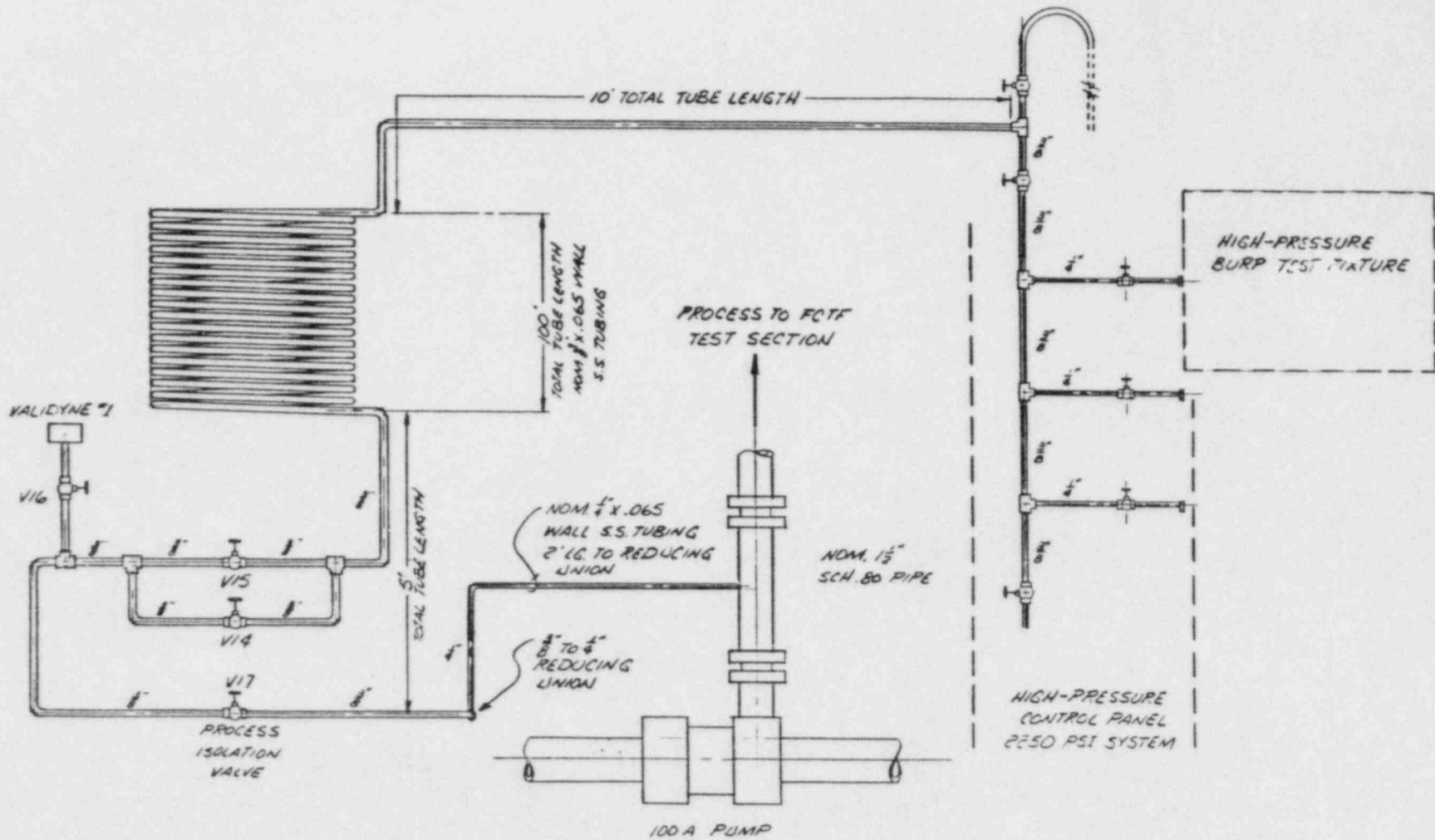
Fig. 3. Forced convection test facility.

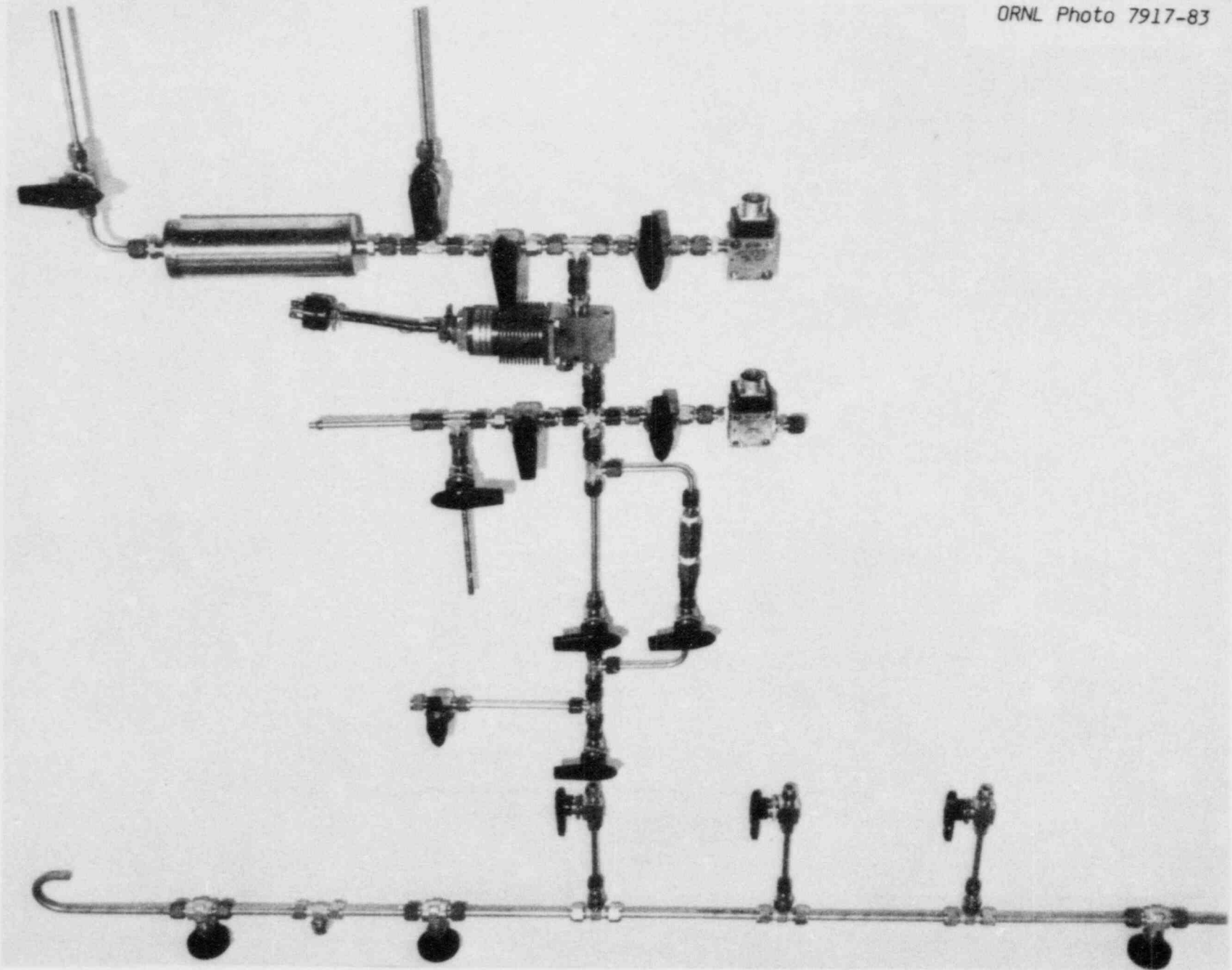Fig. 4. ORNL high-pressure perturbation test configuration.

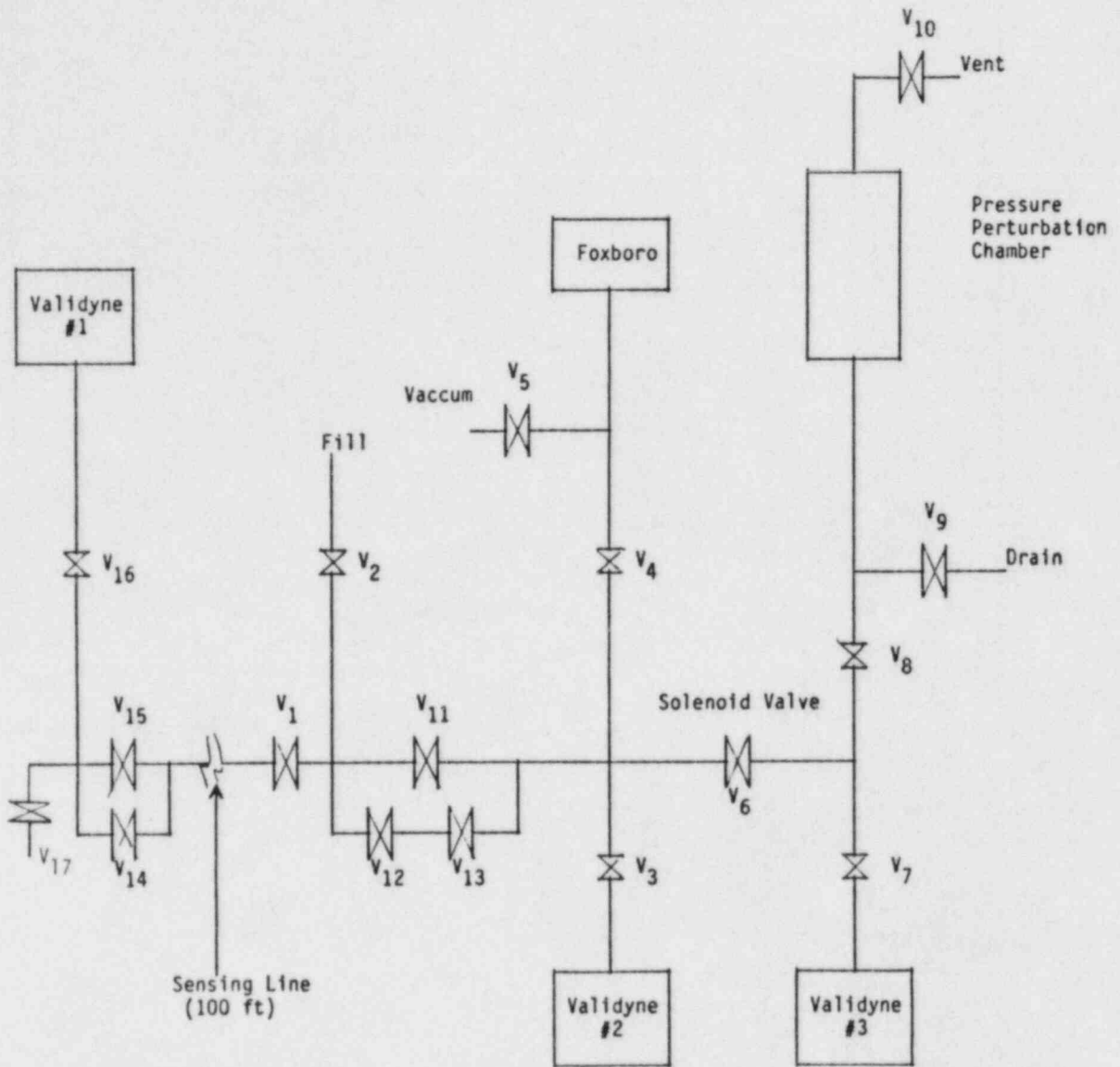Fig. 5. Photograph of the high-pressure perturbation test fixture for the ORNL FCTF experiments.

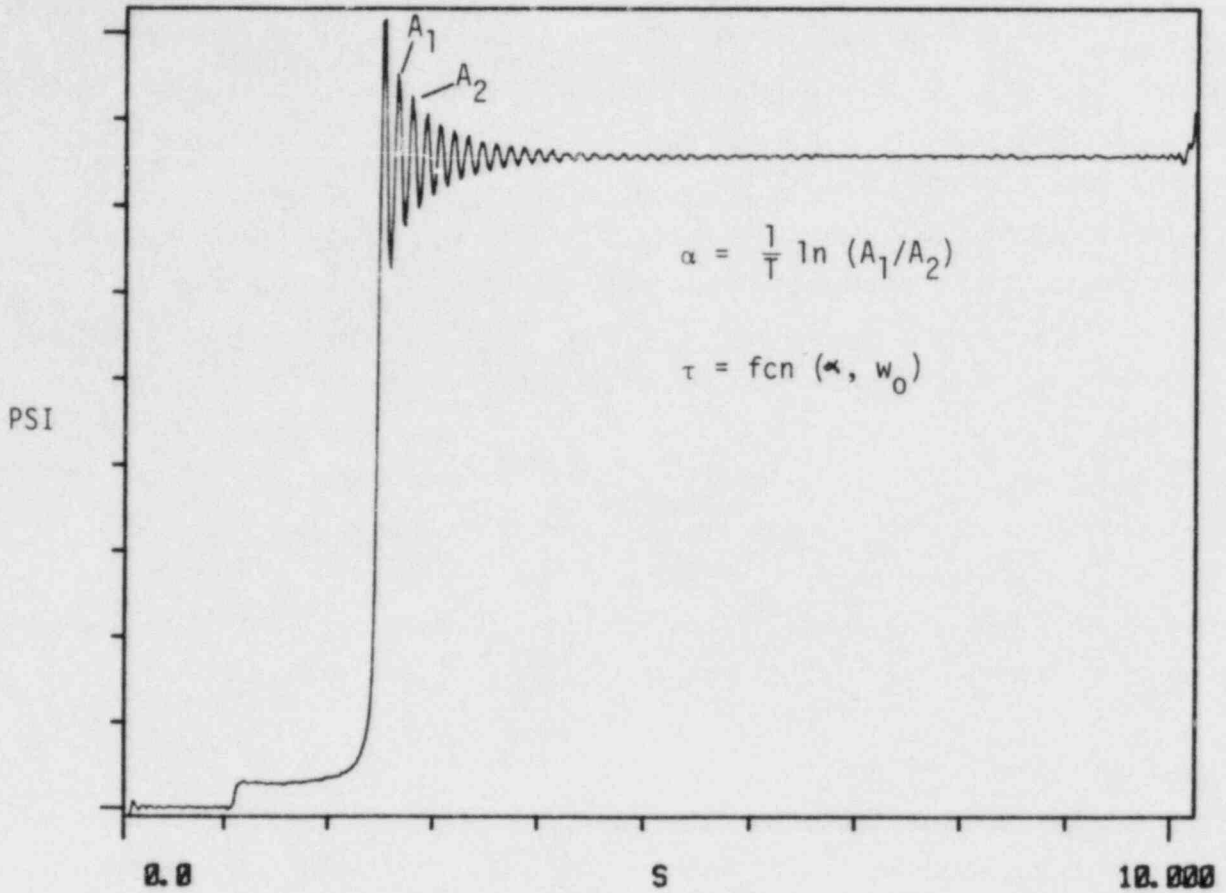Fig. 6. Schematic diagram of ORNL high-pressure perturbation test equipment.

300

PSI

$$\alpha = \frac{1}{T} \ln (A_1/A_2)$$

$$\tau = fcn \ (\alpha, \ w_0)$$

0.0   S   10.000

Fig. 7. Response from a high-pressure perturbation experiment at the ORNL FCTF. Equations for identifying the asymptotic ramp delay time are included on the plot.

Table 2. Pressure perturbation tests for several values of line resistance

VALVE CONDITION (TURNS OPEN)	ASYMPTOTIC RAMP DELAY TIME
2	4.6 MS
3	2.6
5	2.7
7	3.7
FULL OPEN	2.7

301

Table 3. In this case transport delay times (defined as the time for the output to reach 63% of its final value) are obtained. Thus, the smallest value is near the time for a signal to travel from V_{17} to Validyne #3. Significant time delays (~1 s) are not obtained until the line is more than 99% blocked (a nine-turn needle valve is open only 1/16 of a turn). Thus it is apparent that the response time obtained from the pressure oscillations is very sensitive to sensing-line resistance and that it can detect line restrictions of considerably less resistance than required to introduce long time delays into the sensing line. It is also apparent from experiments with pressure perturbation experiments that the sensing line must change from an underdamped system to a highly overdamped system before it introduces significant time delay into the pressure sensor/sensing-line systems. Thus, spectral measurements should provide essential dynamic information for appropriate circumstances.

Noise Analysis Experiments

Spectral measurements of the pressure sensor/sensing-line system are obtained for conditions characteristic of ideal experimental circumstances as well as those expected in field conditions. Transfer function measurements of the sensing line (based on Validynes #1 and 3, shown in Fig. 6) are illustrated in Fig. 8 for essentially no line resistance as well as for cases with the sensing line nearly blocked. Note from the gain versus phase plot that the system becomes overdamped when the nine-turn needle valve is 1/4 turn open. At 1/8 turn open, the asymptotic time delay is approximately 0.2 s, and thus the line must be at least 99% blocked in order to introduce a time delay near the response time of a typical process pressure transmitter. Table 4 lists results from transfer function measurements as well as those from the power spectral density (PSD) measurements with Validyne #3 and with the Foxboro transmitter (Fig. 9). It is apparent from Fig. 9 that even the Foxboro alone could be utilized to detect blockages in a sensing line. This observation is quantified by the results listed in Table 4. Differences between asymptotic ramp response times obtained from transfer function measurements (Validynes #1 and #3) and from PSDs of Validyne #3 (or the Foxboro) are
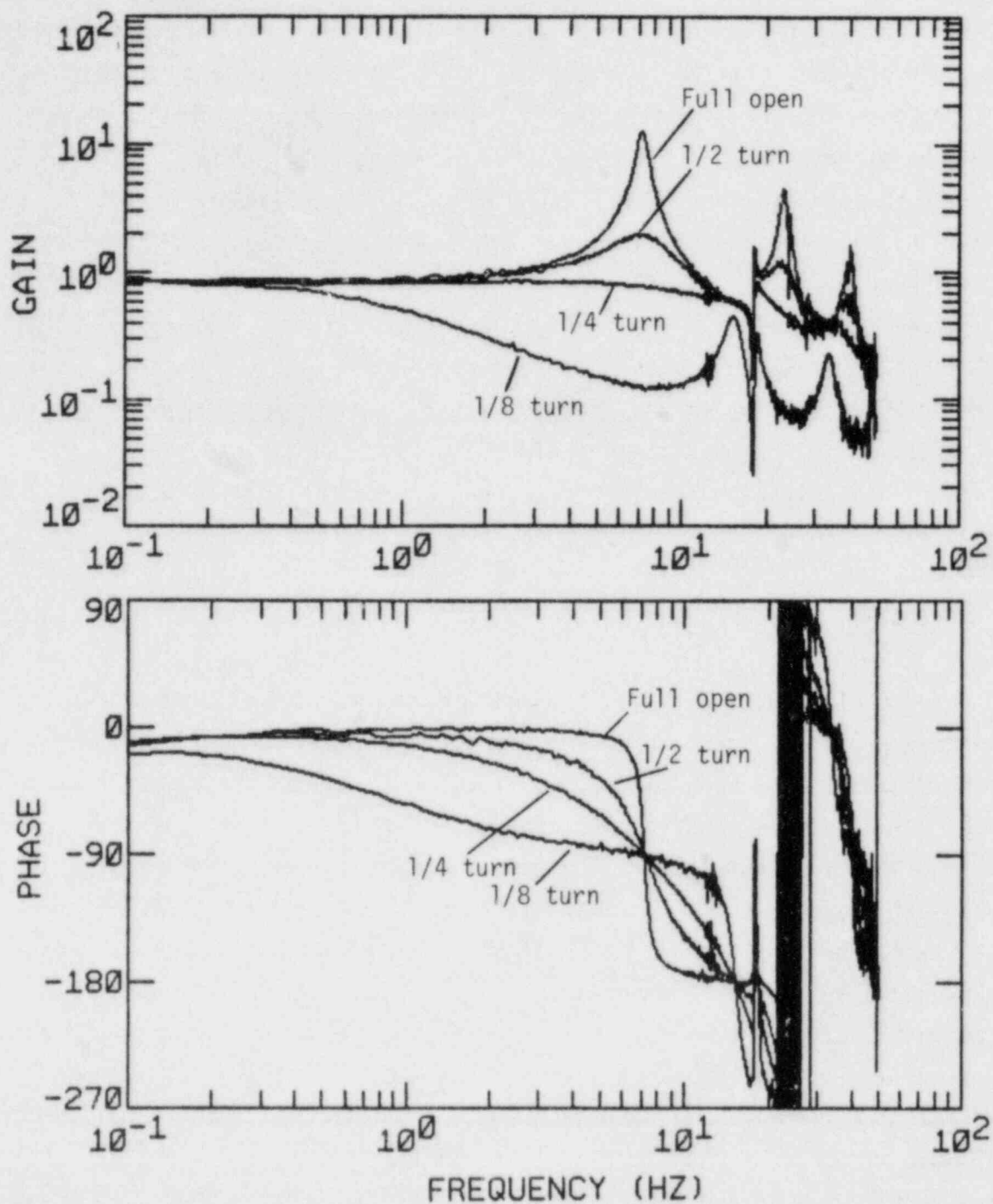
302

Fig. 8. Transfer function measurements of the sensing line based on
Validynes #1 and #3 (cf. Figs. 4 and 6). Transfer functions (gain and
phase) are shown for an open line and for cases with large line resis-
tances. Restrictions are obtained by positioning a nine-turn needle
valve open 1/8, 1/4, and 1/2 of one turn. (At 1/4 turn open, the line is
approximately 99% blocked).

303

Table 3. Sensing-line response times for several simulated
line restrictions at the ORNL High-Pressure Test Facility

Value configuration*	Transport delay time (ms)
V14 1/16 T Open	1300
V14 1/4 T Open	230
V14 1/2 T Open	100
V14 1 T Open	45
V15 Full Open	30

*Nine turn needle valve

Table 4. Asymptotic time delays (ms) estimated from noise analysis

Method	Valve position[A]			
	Open	1/2 turn	1/4 turn	1/8 turn
Transfer function nonlinear fit[B]	1.8	10.5	13.0	215.1
Transfer function[B] −45 degrees frequency	23.2	28.9	45.5	227.4
Valydine PSD:[C] nonlinear fit	2.6	14.7	28.8	212.5
Valydine PSD:[C] RMS value	--	42.0	96.0	425.0
Foxboro PSD:[C] nonlinear fit	3.1	12.7	24.3	240.8
Foxboro PSD:[C] RMS value	--	6.0	225.0	>500

[A]Nine-turn needle valve
[B]Open loop
[C]Closed loop
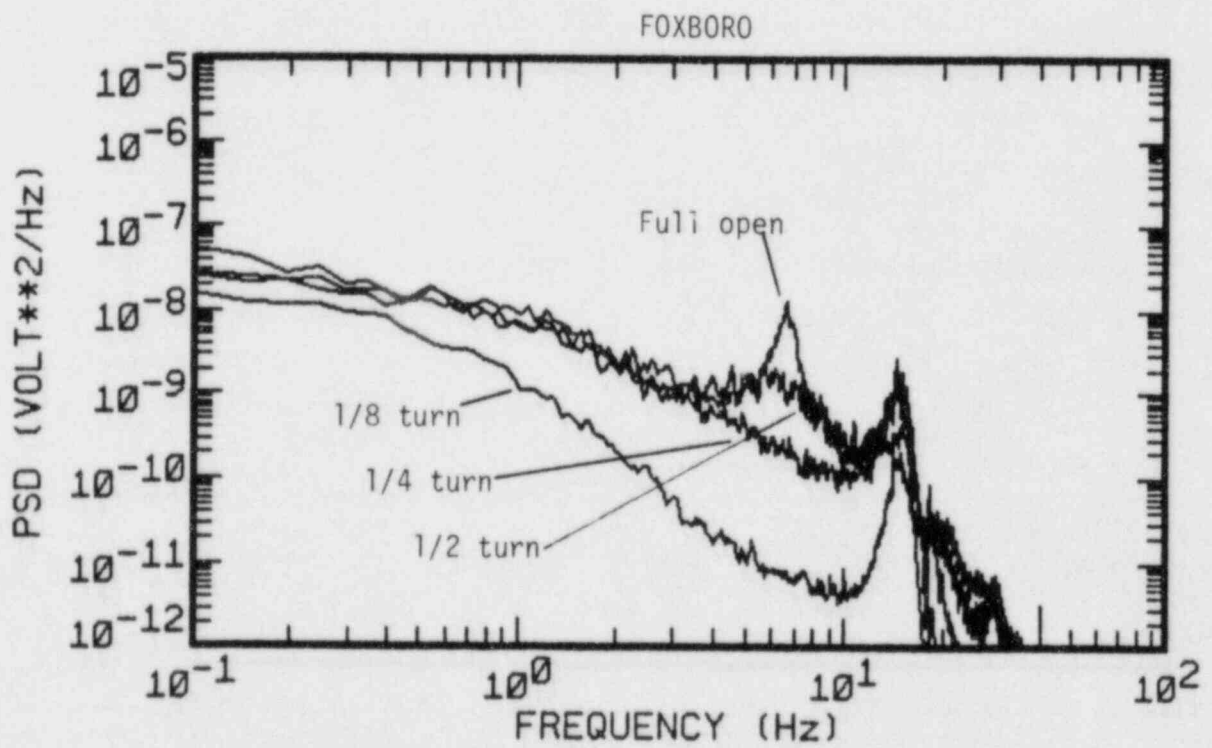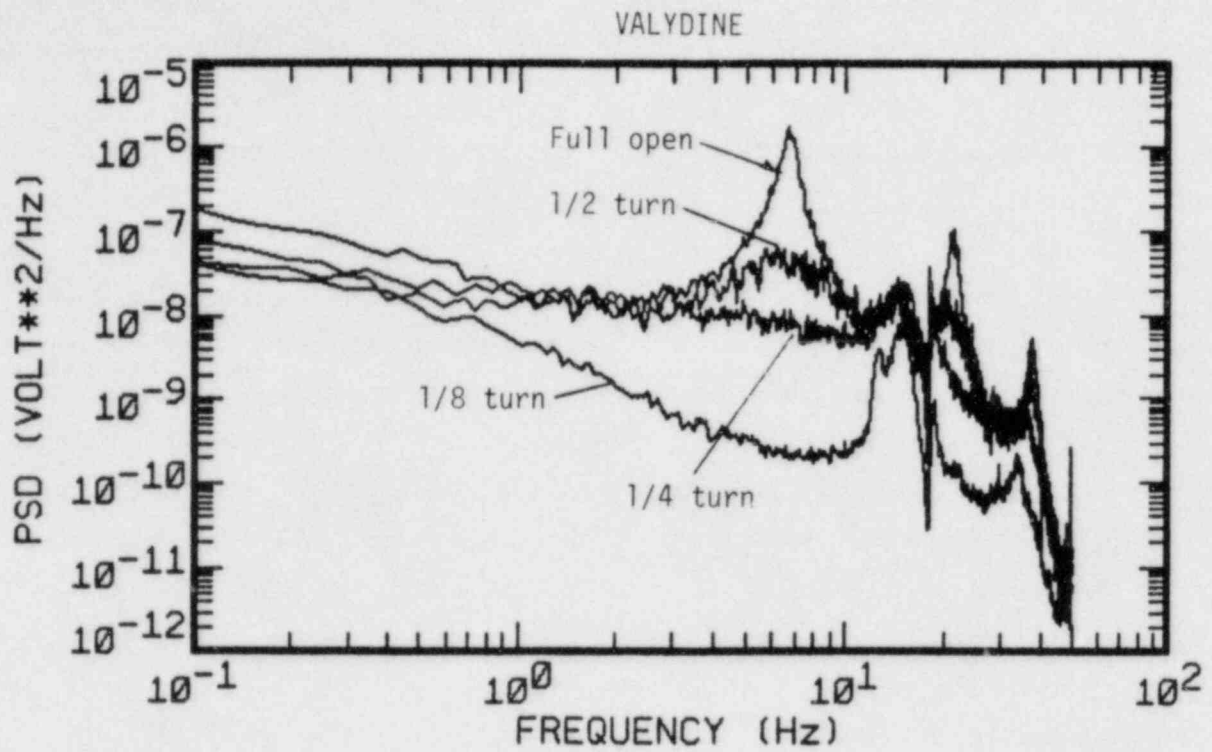
Fig. 9. Power spectral density parametric in sensing-line resistance.

not very significant. This is especially true for conditions of practical interest. In practice, the frequency response characteristics of the process transmitter may not always be sufficient to permit an accurate determination of the response time by this method. This shortcoming could be eliminated, however, by attaching a Validyne to the sensing line of interest.

A very straightforward method for determining sensing-line blockage was also evaluated. In particular, the root mean square (RMS) of the integral of the PSD was correlated with the asymptotic time delay through a single-pole exponential model. This method requires a baseline measurement that could be obtained when the sensing line is verified to perform suitably based on a PSD measurement with a broadband frequency response. Once the baseline measurement is obtained, however, the time delay prediction by this method is computationally easy and is robust.

Conclusions

The results of this research have led to a better understanding of the dynamics of pressure sensors and sensing lines through the use of complex analytical models and through computational results from lumped-parameter models. In particular, experimental results agree well with model predictions.

The current method of testing pressure sensors is to remove them from service and impose a pressure ramp to obtain an estimate of the response time. This method requires personnel to enter containment and can yield misleading results. It also does not address the response associated with the sensing line.

The Remote (OFF-ON) test applies only to force-balance type sensors (in particular the Foxboro Model E11 series of tranducers) but has the advantages that the sensor is only momentarily removed from service and that personnel are not required to enter containment. In addition, results from this method agree well with equivalent direct measurements.

306

Model predictions and laboratory tests with prototypical sensing lines indicate that an open sensing line makes a negligible contribution to the overall pressure measurement response time (i.e., typically less than 10 ms for a 120-ft-long sensing line); however, a severely blocked line can affect the overall response time, and a large void in the sensing line at high pressure may also degrade the response time up to 100 ms.

The pressure perturbation (BURP) test was found not to yield quantitative sensing-line response time measurements when response time of the sensing line was greater than 10 ms. However, the results indicated that this test method is suitable for obtaining quantitative measurements for normally operating sensing lines which have an asymptotic delay time of less than 10 ms. This test method will also give a clear indication of a severely blocked sensing line. It is not a continuous method, however, and would require comparison with a baseline test to give an indication of the blockage. The presence of voids in the system may also be detected by comparing baseline tests with subsequent measurements. Also, this test would be difficult to perform under remote or field conditions and should consequently be viewed as a useful laboratory methodology.

It is apparent from data reported herein and other data obtained during this research that spectral measurements at the FCTF provided good estimates of the sensing-line response time for the case when the line is not blocked. In the case of the highly blocked case (>99%), the process transmitter provided sufficient sensitivity to identify this problem by the RMS of the PSD and by a nonlinear fit to the PSD. Adequate estimates of sensing-line delay times can be obtained by correlating the RMS with delay times through a single-pole exponential model. Measuring the PSD with a broadband transmitter and fitting it to a physically based model would permit an accurate determination of the asymptotic delay time of the sensing line as well as identify blockage.

307

IN-CORE COOLANT FLOW MONITORING OF PRESSURIZED WATER REACTORS USING TEMPERATURE AND NEUTRON NOISE[1]

F. J. Sweeney,* B. R. Upadhyaya,** and D. J. Shieh**

*Oak Ridge National Laboratory, Oak Ridge, Tennessee 37831
**The University of Tennessee, Knoxville, Tennessee 37916

ABSTRACT

Noise measurements were performed at the Loss-of-Fluid-Test (LOFT) and Sequoyah-1 pressurized water reactors (PWRs) in order to investigate the possibility of inferring in-core coolant velocities from cross-power spectral density (CPSD) phases of core-exit thermocouple and in-core neutron detector signals. These noise measurements were used to investigate the effects of inlet coolant temperature, core flow, reactor power, and random heat transfer fluctuations on the noise-inferred coolant velocities. The effect on the inferred velocities of varying in-core neutron detector and core-exit thermocouple locations was also investigated. Theoretical models of temperature noise were developed, and the results were used to interpret the experimental measurements.

Results of these studies indicate that the neutron detector/thermocouple phase is useful for monitoring core flow in PWRs. Our results show that the interpretation of the phase between these signals depends on the source of temperature noise, the response times and locations of the sensors, and the neutron dynamics of the reactor. At Sequoyah-1 we found that the in-core neutron detector/core-exit thermocouple phase can be used to infer in-core coolant velocities, provided that the measurements are corrected for the thermocouple response time.

KEYWORDS

Reactor noise; PWRs; noise analysis; Sequoyah-1 reactor; temperature noise; neutron noise; coolant velocity; flow measurements.

INTRODUCTION

Previous experimental noise measurements (Sweeney and Upadhyaya, 1982, 1983) in pressurized water reactors (PWRs) have indicated that the linear phase versus frequency behavior of the cross-power spectral density (CPSD) phase between a neutron detector and core-exit thermocouple might be utilized to infer in-core coolant velocities. Pór (1981) and Katona and colleagues (1982), however, observed that coolant velocities inferred from the CPSD phase between neutron detectors and a core-exit thermocouple at the Borssele reactor [a 470 MW(e) KWU PWR] were approximately 50% lower than design values.

To investigate the feasibility of using in-core neutron detector and core-exit thermocouple noise signals to monitor in-core coolant flow, experimental measurements were performed at the Loss-of-Fluid-Test (LOFT) reactor [a highly instrumented 55 MW(th) scale model of a PWR] and the Sequoyah-1 PWR [a Westinghouse 1100 MW(e) reactor]. Theoretical models of temperature and neutron noise were also developed to interpret the experimental results.

IN-CORE COOLANT VELOCITY MEASUREMENTS

LOFT Measurements

In-Core, Cobalt-60 self-powered neutron detector (SPND) and 0.16-cm diam K-type, core-exit thermocouple noise signals at the LOFT reactor were cross correlated. The neutron detectors were located at axial levels of 28, 68, 112, and 155 cm above the core bottom and core-exit thermocouples at 2.5, 33, and 124 cm above the top of the core (the LOFT core is 168 cm high). We observed that the

maximum coherence was approximately 0.4 and the CPSD phase was linear over the 0.1 to 2-Hz frequency range for the thermocouple located at 2.5 cm and all neutron detector locations. The coherence and slope of the CPSD phase versus frequency were independent of the axial or radial location of the neutron detectors. A measurement using an in-core flow venturi yielded a coolant velocity of 3.8 m/s for 100% of design coolant flow rate. Using this value and the time delay of 0.25 s inferred from the slope of the neutron detector/thermocouple CPSD phase, an "equivalent transport distance" of 94.3 cm between the sensors was obtained. When the coolant flow was reduced to 65%, the coolant velocity inferred from the CPSD phase (Fig. 1) and the equivalent transport distance of 94.3 cm was 2.7 m/s, which agreed well with the 2.6 m/s value obtained with the flow venturi. This result indicates that even if the neutron noise generated by coolant temperature perturbations is space independent (point kinetic behavior), it may be possible to infer coolant velocities and to monitor core flow using neutron noise/core-exit thermocouple noise signals.

A neutron detector located 66 cm from the core bottom was cross correlated with thermocouples located at 2.5, 33, and 124 cm above the core at 100% flow. We observed that as the thermocouple distance from the top of the core increased, the coherence decreased (Fig. 2) and the slope of the phase versus frequency line (Fig. 3) increased (indicating increasing time delay between the two signals). The inferred coolant velocities were 3.8, 2.5, and 1.9 m/s, respectively, for thermocouples located 2.5, 33, and 124 cm above the core. The assumed transport distance for these inferred velocities was the previously mentioned 94.3-cm equivalent transport distance added to the distance of the thermocouple above the core top. These results indicate that, as expected, thermocouples located far from the top of the core are unlikely to yield good estimates of the coolant velocity inside the core. It is likely that the 50-cm distance between the top of the core and the core-exit thermocouple at the Borssele reactor is the cause of the discrepancy observed by Katona and colleagues (1982) between inferred and expected in-core coolant velocities.

Sequoyah-1 Measurements

Noise measurements were performed at Sequoyah-1 utilizing a movable in-core, flux-mapping fission chamber and a 0.32-cm diam, K-type, core-exit thermocouple located approximately 10 cm from the top of the core. The neutron detector was positioned radially near the core center and at various axial positions.

It was observed that the CPSD phases between the two signals were nearly linear over the 0.1 to 1.5-Hz range, and the slopes of the phase versus frequency plots decreased as the neutron detector was moved from near the bottom of the core (measurement 1) to near the top of the core (measurement 6) as shown in Fig. 4. Coolant velocities were inferred from these slopes using the actual
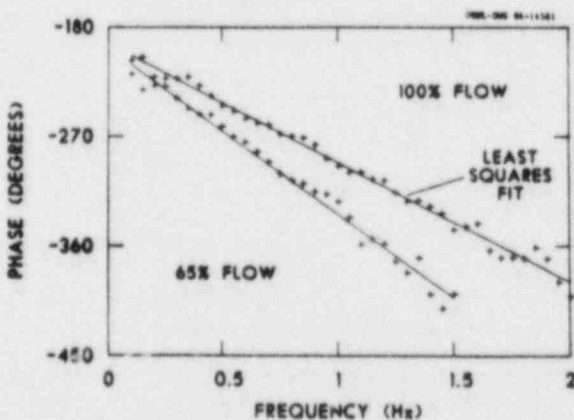

Fig. 1. CPSD phase between an in-core neutron detector and a core exit thermocouple 2.5 cm above the core for 65 and 100% flow at LOFT.
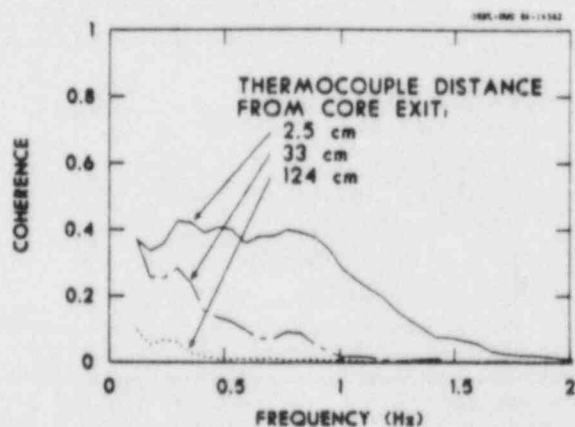
Fig. 2. CPSD coherences between an in-core neutron detector at 66 cm from the core bottom and core-exit thermocouples located at 2.5, 33, and 124 cm above the top of the LOFT core.

distance separating the detectors, and the results are summarized in Table 1. The discrepancies between the noise-inferred and expected (4.82 m/s indicated in the Sequoyah-1 Final Safety Analysis Report) coolant velocities increased as the distance between the sensors decreased. It was postulated that this trend is a consequence of the increasing contribution of the thermocouple time response to the total time delay (coolant transport time + thermocouple response) between signals as the detectors are moved closer together.
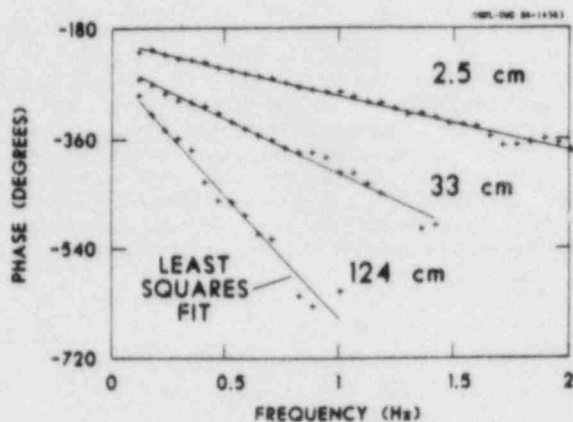
309

Fig. 3. CPSD phases between an in-core neutron detector at 66 cm from the core bottom and core-exit thermocouples located at 2.5, 33, and 124 cm above the top of the LOFT core.
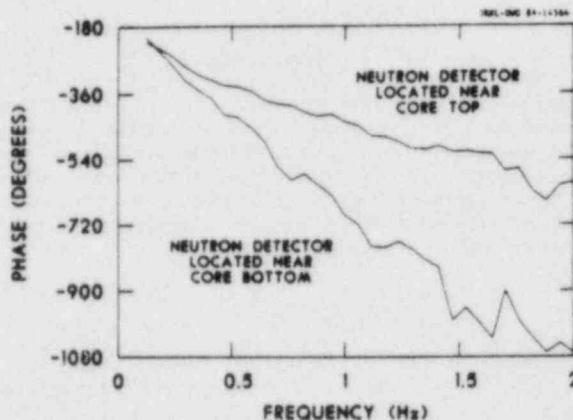
Fig. 4. CPSD phases between a movable in-core neutron detector at near the core bottom (measurement 1) and core top (measurement 6) in the Sequoyah-1 reactor.

TABLE 1 Coolant Flow Velocities Inferred from In-core Neutron/Core-exit Temperature Noise CPSD Phase with No Correction for Thermocouple Response Time at Sequoyah-1 PWR

Measurement	Distance between neutron detector and thermocouple (cm)	Maximum coherence*	Inferred coolant velocity (m/s)†
1	403.6	0.11	3.1
2	317.7	0.35	2.9
3	287.3	0.40	3.1
4	135.1	0.43	1.9
5	102.1	0.45	1.6
6	63.5	0.50	1.1

*Frequency range 0.1 to 1.5 Hz.
†For comparison, the Sequoyah-1 Final Safety Analysis Report lists the design average coolant velocity as 4.82 m/s.

It was also observed that the maximum coherence over the 0.1 to 1.5-Hz range increased from less than 0.1 when the neutron detector was near the core bottom to more than 0.4 when the detector was near the top of the core as shown in Table 1. These results suggest that the sources of temperature noise at Sequoyah-1 are spatially distributed and statistically uncorrelated (i.e., spatially independent) and therefore are probably the result of turbulence or random heat transfer processes rather than perturbations in the core-inlet temperature or flow. The observed spatial dependence of the neutron detector/thermocouple phase and coherence shows that neutronically, Sequoyah-1 does not respond as a "point reactor" to coolant temperature fluctuations above 0.1 Hz.

Previous studies by Sweeney and Upadhyaya (1982, 1983) have shown that the relatively long thermocouple response time (estimated to be 0.7 to 1.0 s) at Sequoyah-1 compared to the coolant transport time adversely affects coolant velocities inferred from ex-core neutron/thermocouple noise measurements.

To remove the effect of the thermocouple time response from the in-core measurements at Sequoyah-1, it was assumed that the in-core neutron detector spatial sensitivity was small in the axial direction. The neutron detector/thermocouple CPSD can then be described by (Sweeney and Upadhyaya, 1983, 1984)

310

$$CPSD(\omega) = \left| \delta S(\omega) \right|^2 \left| G(\omega) \right| e^{j[\theta(\omega) - \omega\tau]} , \tag{1}$$

where $\left| \delta S(\omega) \right|^2$ is the temperature noise power spectral density (PSD), $\left| G(\omega) \right|$ is the coolant temperature-to-thermocouple output transfer function magnitude, $\theta(\omega)$ is the transfer function phase (due to its response time characteristics), and τ is the true coolant transport time between the neutron detector and thermocouple locations. By dividing two CPSDs (subscript 1 and 2) obtained with the same core-exit thermocouple/in-core neutron detector pair but with the neutron detector located at different axial positions for each measurement, the thermocouple phase is removed and the resulting phase behavior is due solely to the coolant transport time between the neutron detector locations:

$$\frac{CPSD_1(\omega)}{CPSD_2(\omega)} = \frac{\left| \delta S_1(\omega) \right|^2}{\left| \delta S_2(\omega) \right|^2} e^{-j\omega(\tau_1 - \tau_2)} , \tag{2}$$

where $\tau_1 - \tau_2$ is the net coolant transport time between neutron detector locations 1 and 2.

A typical pair of combined (ratioed) measurements yield a linear phase versus frequency plot as shown in Fig. 5 with an intercept near 0°. The results of applying this correction are summarized in Table 2. In general, best agreement between the expected and noise-inferred coolant velocities is obtained when the neutron detector locations are separated by at least 90 cm. It was also found that small errors in transit time resolution (as a result of relatively slow sampling rates) or low signal coherence can lead to large errors in the inferred velocities when the detectors are closely spaced.

The above results indicate that by virtue of the space-dependent nature of temperature noise sources and its associated neutron noise, it may be possible both to monitor for and locate localized in-core flow blockages in a large commercial PWR.

CORE-EXIT TEMPERATURE NOISE ROOT MEAN SQUARE (RMS) VERSUS CORE ΔT

Tsunoda (1976) observed in an out-of-core test loop that the RMS temperature noise of a fuel assembly exit thermocouple increased linearly with increasing ΔT across the assembly under normal conditions. When localized blockages or power skews were introduced, the RMS noise deviated from the original behavior. To investigate the possibility of monitoring core-exit temperature noise alone for indications of localized coolant flow abnormalities, the RMS of core-exit temperature noise was measured over the 0.1 to 1-Hz range at LOFT and Sequoyah-1 at various power levels thereby measuring various temperatures (core ΔT). We observed that the RMS temperature noise varies linearly with core ΔT and as the core ΔT approaches 0°C, the temperature noise also approaches 0°C RMS for both LOFT and Sequoyah-1 as shown in Fig. 6. We concluded from these results that core-exit temperature noise may be useful in detecting localized power skews, flow blockages, or hot spots.
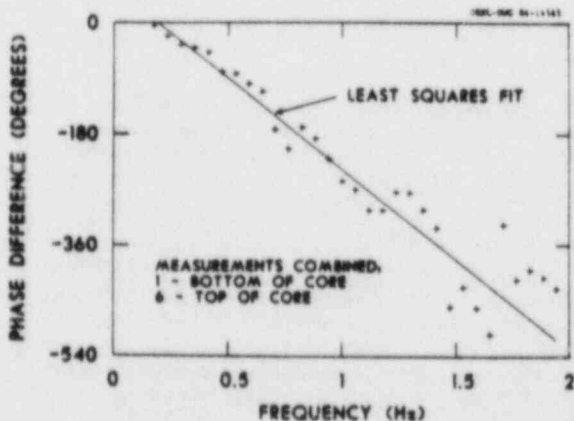

Fig. 5. CPSD phase difference between two sets of neutron detector/thermocouple measurements (measurements 1 and 6) at Sequoyah-1, which removes the effects of the thermocouple response time.
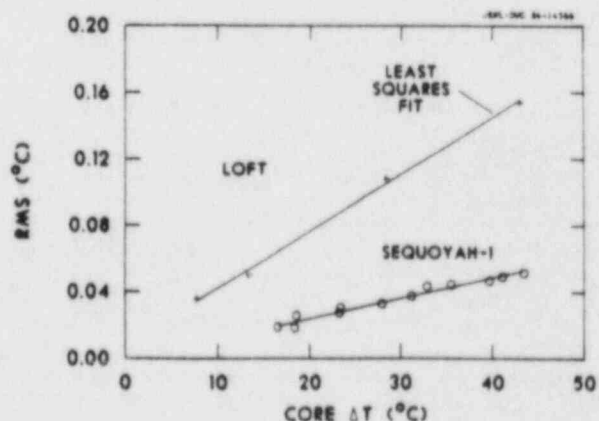
Fig. 6. Core-exit thermocouple root mean square (RMS) noise versus core temperature rise (ΔT) at LOFT and Sequoyah-1.

311

TABLE 2 Inferred Coolant Flow Velocities Corrected
for Thermocouple Response Time at
Sequoyah-1 PWR

Measurements combined	Distance between neutron detector locations (cm)	Inferred coolant velocity (m/s)
1,3	116.3	4.8
1,6	340.1	4.5
2,6	254.2	3.9
3,5	185.2	4.3
3,6	223.8	4.4
4,6	71.6	4.6

THEORETICAL MODELS OF TEMPERATURE AND NEUTRON NOISE

The work of Katona and colleagues (1981) indicated that the CPSD phase between a neutron detector and core-exit thermocouple depended on the source of the coolant temperature fluctuations. They concluded that only core-inlet coolant temperature fluctuations can lead to time delays that are directly related to the coolant transport time between the two sensors. We therefore developed nodal and distributed parameter models to interpret experimental observations.

Nodal Models

Single and multi-node models of thermal-hydraulics and heat transfer processes were developed to investigate the contribution of reactor power, coolant flow, and core-inlet temperature fluctuations to core-exit temperature noise (Sweeney and Upadhyaya, 1983; Upadhyaya and Sweeney, 1983). The results of these models indicate that core flow perturbations produce a core-exit temperature dependence on core ΔT of the form

$$\delta T_i = \frac{\delta \dot{m}}{\bar{\dot{m}}} \Delta T_i \qquad (3)$$

where

δT_i - temperature fluctuations at the outlet of the ith node

$\delta \dot{m}$ - coolant flow rate (velocity) fluctuations

$\bar{\dot{m}}$ - mean coolant flow rate

ΔT_i - coolant temperature rise between the outlet of the ith node

A similar relationship is obtained for random heat transfer processes, which would lead to the previously mentioned linear dependence of core-exit temperature noise on core ΔT at LOFT and Sequoyah-1. These results also indicated that the core-exit temperature noise would not be a linear function of core ΔT nor pass through 0°C RMS at 0°C core ΔT if core-inlet temperature fluctuations were significant.

These results were confirmed by noise measurements at LOFT in which the coherence of a core-inlet thermocouple was found to be low (<0.1) with both a core-exit thermocouple and a neutron detector, and a linear phase versus frequency behavior was not observed. Coherence of a core pressure drop (core ΔP) sensor with both the neutron detector and core-exit thermocouple was >0.4 over the 0.1 to 1-Hz range at LOFT. The contribution of flow-rate fluctuations to neutron noise was also observed by Cannon and Clemmo (1980). We concluded from these results that core flow fluctuations rather than core-inlet temperature fluctuations are the dominant temperature noise source at LOFT.

Distributed Parameter Model

A distributed parameter dynamic model of fuel heat conduction, heat transfer, and coolant transport was developed that included direct neutronic heating of the coolant (Shieh and Upadhyaya, 1984).

312

Coolant temperature fluctuations were assumed to arise from the fluctuations of four sources: heat generation (power), flow rate (velocity), coolant inlet temperature, and random heat transfer (turbulence).

LOFT results. The distributed parameter model was applied to the LOFT reactor by assuming coolant- and fuel-temperature reactivity feedback and a point kinetic model of the reactor dynamics. A summary of the results follows.

- The neutron detector/core-exit thermocouple phase is linear, with frequency for each of the perturbation sources.
- The frequency range over which a linear phase versus frequency is obtained is bounded by feedback effects which are important below 0.1 Hz, and a sink (minimum) or resonance at frequencies above 2 Hz that is dependent upon the perturbation source and the coolant transport time through the core (similar to the results of Mogilner, 1971).
- Because of the time required for fuel to coolant heat transfer (up to several seconds), heat source fluctuations are important only below 0.1 Hz, and the resulting neutron/thermocouple phase does not approach 180° at low frequencies. Random heat transfer sources yield very low (approximately 0) coherence between the detectors because of the spatial averaging effect of the point kinetics assumption. The predicted slope of the neutron detector/thermocouple phase is 79.5°/Hz for coolant velocity perturbations, which agrees well with the 89.3°/Hz obtained from experimental measurements.

On the basis of predicted and experimental evidence it was concluded that coolant velocity (flow) fluctuations are the dominant source of coolant temperature noise in the 0.1 to 2-Hz range at LOFT.

Sequoyah-1 results. Because of the similarities in the behavior of the RMS temperature noise versus core ΔT at LOFT and Sequoyah-1, it was postulated that coolant velocity fluctuations were also the dominant source of core-exit temperature noise at Sequoyah-1. The distributed parameter model was applied to the Sequoyah-1 reactor, and a highly localized (space-dependent) neutron detector sensitivity to coolant temperature fluctuations was assumed. In contrast to the LOFT results, coolant flow fluctuations lead to predicted velocities that are approximately twice the coolant flow velocity observed at Sequoyah-1. The previously mentioned increasing coherence with decreasing separation distance between the neutron detector and thermocouple observed at Sequoyah-1 would also require an axially-increasing, nonpropagating contamination of the neutron detector signal for any assumed noise source other than random heat transfer. Based on these results, we concluded that the most likely source of core-exit temperature noise at Sequoyah-1 is a random heat transfer process such as turbulence.

SUMMARY AND CONCLUSIONS

Experimental and theoretical results from LOFT and Sequoyah indicate that neutron detector/ thermocouple phase is useful for monitoring core flow in PWRs. Our results show that the interpretation of the coolant velocities inferred from these signals depends on the source of temperature noise, the response times and locations of the sensors, and the neutron dynamics of the reactor. At Sequoyah-1 we found that the neutron detector/core-exit thermocouple phase can be used to infer in-core coolant velocities provided that the measurements are corrected for the thermocouple response time. We also observed at LOFT that in-core coolant velocities can be inferred and core flow can be monitored with these signals even in a reactor with point kinetic neutron dynamics. These results combined with the observed RMS temperature noise behavior and the out-of-pile test results of Tsunoda (1976) show that temperature noise can provide useful diagnostic information in PWRs.

REFERENCES

Cannon, J. W. and T. M. Clemo (1980). Flow-induced power fluctuations at LOFT. Trans. Am. Nucl. Soc., 35, 591.

Katona, T. and colleagues (1982). Some aspects of the theory of neutron noise due to propagating disturbances. Prog. Nucl. Energy, 9, 209.

Pór, G. (1981). Investigations on the phase at low frequencies of CPSD between detectors in the Borssele PWR power plant. Netherlands Energy Research Foundation Report ECN-81-131.

Shieh, D.J. and B. R. Upadhyaya (1984). Inference of core coolant flow parameters from neutron-coolant temperature noise analysis in PWRs. Trans. Am. Nucl. Soc., 46, 847.

Sweeney, F. J. (1982). Behavior of core exit temperature noise RMS in PWRs. Trans. Am. Nucl. Soc. 43, 789.

Sweeney, F. J. and B. R. Upadhyaya (1982). Measurement of core coolant flow velocities in PWRs using temperature-neutron noise cross-correlation. Trans. Am. Nucl. Soc., 43, 795.

Sweeney, F. J. and B. R. Upadhyaya (1983). Relationship of core exit temperature noise to thermal-hydraulic conditions in PWRs. Proceedings of The Second International Topical Meeting on Nuclear Reactor Thermal-Hydraulics, Santa Barbara, California. Volume II, 1511.

Sweeney, F. J. and B. R. Upadhyaya (1984). In-core coolant velocity measurements in a pressurized water reactor using temperature-neutron noise cross-correlation. Trans. Am. Nucl. Soc. 46, 736.

Tsunoda, T. (1976). Application of temperature fluctuation to anomaly detection in fuel assemblies. J. Nucl. Sci. Technol., 13, 103.

Upadhyaya, B. R. and F. J. Sweeney (1983). Theoretical and experimental stochastic modeling analysis of PWR core heat transfer. Proceedings of the Fifth Power Plant Dynamics, Control and Testing Symposium, Knoxville, Tennessee. Volume 2, 46.01.

Safety Implications of Control Systems

R. S. Stone

Oak Ridge National Laboratory*

ABSTRACT

As part of an overall program to determine the extent to which failures of
control can impact plant safety control failures in the Oconee-1 nuclear plant
were examined. Plant systems capable of initiating plant overcooling and under-
cooling were identified, as well as those with potential for overfilling events
in the steam generators. Failure mode and effects analyses were conducted on
these candidate plant systems, with computer analysis applied where appropriate.
This latter process utilized a detailed hybrid computer model of Oconee-1,
developed as part of this program. Where failures with safety consequences were
found, probabilities of the pertinent scenarios were developed. Tentative
recommendations for corrective actions have been sought.

INTRODUCTION

Objectives

The overall program is intended to assess the safety implications of nuclear
power plant control systems by examining the consequences of control system
failures and action, both planned and unplanned. A properly performing control
system can correct for failure in other parts of the plant, thus aborting a
challenge to the safety system; contrarily a malfunctioning control system can
create such a challenge. A principle of nuclear plant design is that the safety
system must be capable of countering any conceivable action or inaction of the
control system without danger to the plant or to the public. These concepts are
being examined in practice by means of a thorough analysis of control/safety
dynamics and interactions from a plant system perspective. As described above,
the objectives of the overall task define three interrelated goals:

° To assess the safety implications of control systems by examining the
  effects of control system malfunctions on plant dynamic behavior and by
  investigating the interactions of such malfunctioning controls with other
  plant systems.
° To formulate a method for assessing the failure mode and effects of
  control systems on the basis of common cause, common mode, and other
  multiple failures such as cascade failures.
° To develop criteria for establishing the relative importance of control
  systems important to safety and to recommend importance to safety classi-
  fications and any changes to regulatory requirements as may be indicated
  by the results of this work.

In performing these tasks, a major objective is to assist in the resolution of Unresolved Safety Issue (USI) A-47 on Safety Implications of Control Systems. The Task Action Plan for that USI states that its objective "...is to perform an indepth evaluation of the control systems that are typically used during normal plant operation and to verify the adequacy of current licensing design requirements or propose additional guidelines and criteria to assure that nuclear power plants do not pose an unacceptable risk due to inadvertent non-safety grade control system failures."

In its approach, this task is specifically responsive to the four principal foci of NRC Task Action Plan A-47:

1. Evaluate control system failures that could lead to steam generator overfill transients.
2. Evaluate control system failures that could lead to reactor overcooling transients.
3. Evaluate other control system actions that have safety implications.
4. Evaluate the effect of loss of control system power sources (ac, dc, pneumatic, and hydraulic).

This study has future plans beyond the objectives of A-47, however, since this study will address operator errors, sabotage, and harsh environments to a degree not included in the guidelines for A-47.

This work is being done in a plant-specific fashion, and the first task provides a careful examination of reactor transients in one specific plant of Babcock and Wilcox (B&W) design, i.e., Oconee 1.

Approach

The standard FMEA provides an orderly method for studying the possible failure modes of a single component in an important system, treating all the causes and consequences of each such failure mode. In a plant with components numbered in tens or hundreds of thousands it is manifestly impossible to cover each of them in such a study. Accordingly, a number of steps are taken to pre-focus the effort. Some systems are excluded from consideration by the scope of the study, e.g., safety systems. Some classes of events are excluded because they are studied elsewhere, e.g., ATWS. The most important focusing is accomplished by categorizing the kinds of system failures that we search for: steam generator overfill, primary coolant overcool, overheat.

The first step in performing an FMEA is to define the system to be analyzed. In the present case, this has meant an exhaustive listing of every system in the nuclear plant under study. Until the systems under consideration are narrowed to the fine details of specific designs, all PWRs involve much the same functions. This has permitted us to create a so-called generic systems list. These descriptions and interface identifications are prepared for each system. On a plant-specific inquiry the listing continues to the finest system level. Such lists and interfaces are crucial to the FMEA process. It is unlikely that a serious failure mode will be uncovered if the system affected is omitted during system definition.

Having defined the plant systems and described their operation, it is necessary to limit the cases examined to a manageable set by identifying the failure categories which will be examined. In general these are the overfilling, over-cooling, and overheating areas outlined above. At this point the first judgmental decisions are made. Those systems without input to the failure classes of interest are eliminated, using as basis the previously developed functional descriptions, interfaces, and criteria.

The FMEA process continues by conceptually failing each of the systems potentially contributory to one of the three classes of safety consequences, with the results determined (so far as this is possible) on an a priori basis. This process is referred to as a "broad FMEA." At this stage both single and double failures are postulated. Probabilities of these events will be estimated at a later time, but only for those which prove to be of interest.

Many of the failures lead to events which are clearly benign. These will be dropped from further consideration. Other events will be found to be precursors for accident sequences already considered elsewhere (e.g., in the PTS program, or in Chapter 15 studies for licensing reports). Where such cases have safety-related consequences the precursor events will be documented, but no further computer analysis need be done.

There will remain some residuum of system failures with potential safety consequences. These will be addressed through computer simulations in an activity referred to as the "augmented FMEA." As outlined above, two criteria must be satisfied for a scenario from the FMEA process to be selected for the computer program:

  A. There must be potential for overfilling, overcooling, or over-
     heating, as determined by the broad FMEA, but without certainty
     as to the extent of the consequences
  B. There must be no satisfactory alternate source (e.g., the PTS
     program or Chapter 15 studies) for computations from which the
   consequences in question can be determined.

The above sequence is the primary approach to the FMEA process, i.e., an orderly assessment of the failure consequences of each identified system in the plant. Where failure of a control element produces actual or potential compromises to safety, interfacing systems are examined for contributions to the failure or to the consequences. Where a double failure is required to produce the hazard in question, common sources for the two failures will be sought, particularly in control logic sequence.

Figure 1 shows the process described in flow chart form.

The modality for computer analysis of the Oconee-1 plant is a hybrid computer model developed at ORNL. Before modeling or analysis could start, it was necessary to obtain detailed design information regarding the plant to be studied. The first task was to establish a collection of drawings and reports on each assigned plant. The information was obtained from the following sources:

317

Figure 1

PROGRAM FLOW FOR STUDY OF SAFETY EFFECTS OF

NUCLEAR POWER PLANT CONTROL SYSTEM FAILURES

318
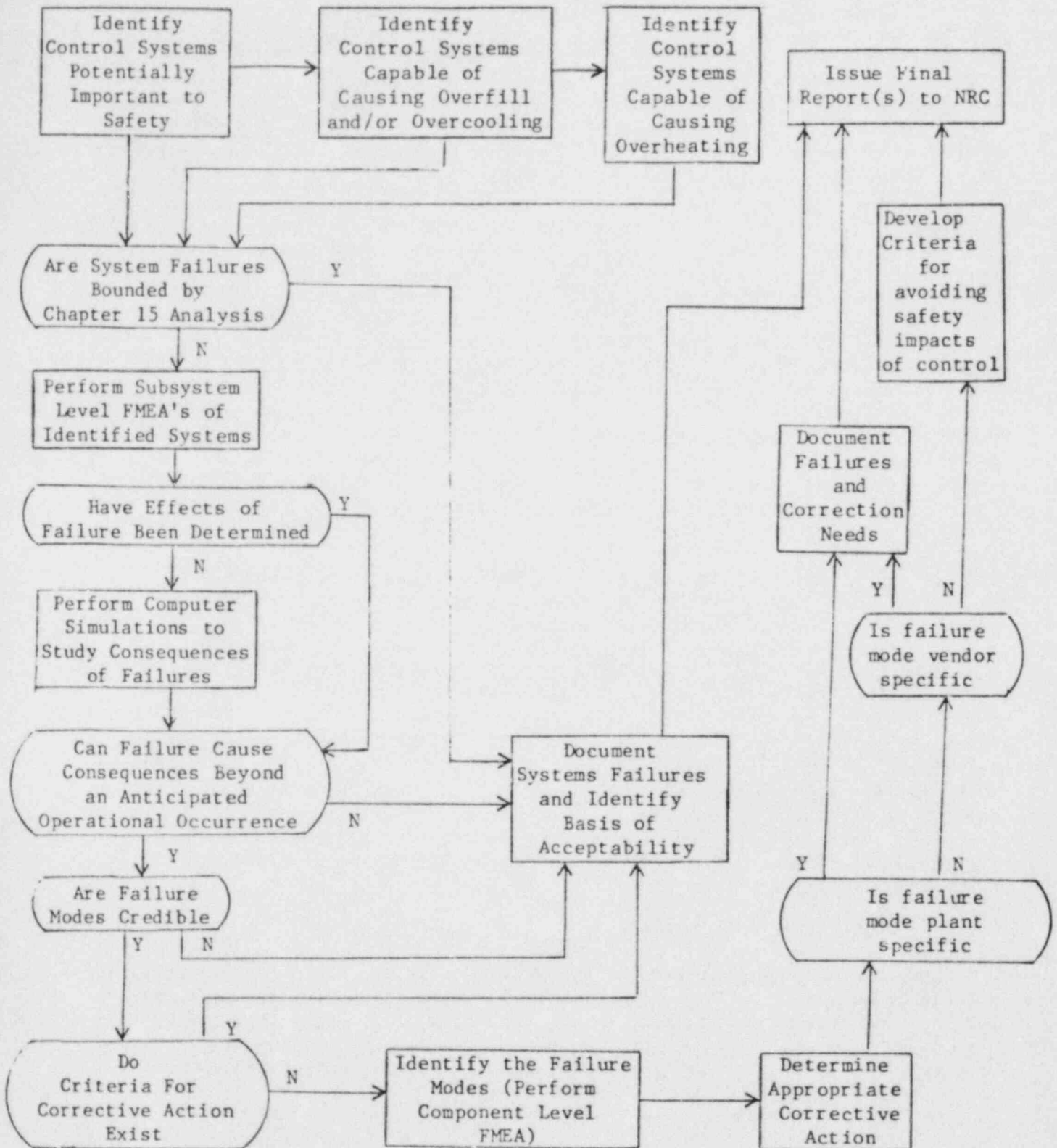
° the applicable utility, where possible
° various dockets and resources of the NRC
° other ORNL projects
° staff experience
° subcontractors and their sources

The computer analysis is discussed by O. L. Smith in the following paper.

Cases selected as requiring analysis were prioritized in order of estimated importance, grouping them in lots of similar runs to minimize programming changes. The results of these runs were then fed back to the (thus) augmented FMEA process for the final determination of the consequences of controls failures.

Limitations of the Studies

No external events have been considered in this controls study. The neglected categories include earthquakes, fires, and floods (external and internal to the containment), as well as sabotage. These initiating events are important, and they will be addressed in a later extension of the program but are outside the scope of the present report. Actions that the operator could take were identified. However, all possibilities were not studied nor, in general, were alternatives beyond the first identified.

In part because disclosures of controls dynamics and configurations have not been required for licensing or for other regulatory oversight, the controls data required for this study have not been routinely available. Collection of this information has been a time-consuming operation, and though the final computer model is impressively complete, some exacerbating or ameliorating features may be missing from some transients through lack of information or the time to acquire it.

This report does not reflect the results of sensitivity studies; these are planned but not yet undertaken. The objective is to determine the effects of variations in input data, plant conditions, or parameter values (trip points, for example) on our conclusions and results. These variations can reflect limitations in detailed knowledge of the Oconee-1 plant but, more importantly, should allow for differences between Oconee-1 and other plants in its class. This latter requirement may be important when our major conclusions are examined for generic implications.

<div align="center">SUMMARY OF RESULTS</div>

FMEA for Steam Generator Overfill

Steam generator overfill comes about when the feedwater flow rate overbalances the inflow heat rate to the steam generator. Heat input can be diminished by a drop in feedwater temperature or a drop in core power. Water flow can be increased by failures in the steam generator/feedwater control system. Our studies indicate that credible decreases in main feedwater temperatures are

initially well compensated by control system action and that substantial additional failures would be required to bring on a serious safety problem in the primary. However, decrease in core power can aggravate steam generator overfill, and such a decrease will occur in most important overfills because scram is expected to occur. We have found that excess water feed, as a result of improper actions of steam generator or main feedwater controls, may induce serious overfill with a credibly small number of control failures.

Steam generator overfill is a concern because it appears to have the potential to

a. produce secondary side damage which might compromise safety equipment or produce a cascade of events which might have primary side effects including radiological leakage,
b. cause densification of primary coolant, reducing pressure, possibly losing pressurizer control, possibly vapor-locking the primary flow path, possibly introducing excess reactivity from cold flow, and
c. provide excess cooling which might in some cases contribute to PTS.

We have found that a number of control system failure scenarios can lead to water entry into the steam line. In one case a single failure causes this; in several other cases, a preexisting undetected failure and one additional failure can bring on the event. Such events have occurred and have caused extensive damage to the affected steam system. Items which can be damaged include turbine drives on main feedwater and emergency feedwater pumps, turbine bypass valves, steam safety valves, steam line supports and the steam line itself. If we assume a steam line, which is not qualified for this environment, could rupture, then a cascade of dependent events might follow, including multiple steam generator tube rupture with small break LOCA vented direct to the atmosphere.

FMEA for Overcooling the Primary System

A number of failure modes have been identified which could cause the RCS temperature to decrease. The rate and amount of such decreases and their possible subsequent effects require simulation of the system's response to the control system failures.

Conditions that cause RCS temperature to drop 100°F or more in an hour are considered to be overcooling. Also, tentatively, RCS cooling to a degree that causes system variables to assume values that should cause ESPS actuation is considered overcooling.

To aid in subsequent analyses, the overcooling criteria were related to RCS transient classes. These classes were (1) a release of reactor coolant from the RCS, (2) opening the pressurizer spray valve, and (3) increased heat transfer through the steam generator tubes.

Failures judged to be significant include:

Class 1 - (a) PORV fails open or fails to close, producing a small break LOCA.
        (b) RC pump seals fail.
        (c) Steam generator tube ruptures.

320

Class 2 - Pressurizer spray valve fails open or fails to close.

Class 3 - (a) Steam generator overfills - see steam generator overfill section.
(b) Turbine bypass valve or main steam safety valve fails open or fails to close.

Three failure modes were identified which resulted in more than one effect on the RCS. Failure of the RCS narrow range pressure signal would result in both the PORV and spray valves opening and deenergizing the pressurizer heaters. The differences between this transient and the effects of the open PORV alone are not expected to be significant.

There are single electrical branch circuit failures which result in transferring many ICS controls stations to manual and freezing the controlled components in position, including the turbine bypass valves and main feedwater control valves. If the auto power failure occurred followed by a reactor trip, a steam generator overfeed transient would occur with the turbine bypass valves remaining closed. If the auto power fails following a turbine trip (possibly in response to the same initiating failure), both the turbine bypass and feedwater control valves may be held open resulting in a combined steam generator overfeed and steam generator depressurization transient. Although this sequence appears unlikely, similar sequenced power failures have occurred.

FMEA for Overheating the Primary System

Plant systems potentially affecting the ability to replace reactor coolant lost from the RCS or affecting the ability to remove heat through the steam generators were selected for detailed FMEA.

Several failures were found to result in a loss of reactor coolant or a loss of main feedwater flow to the steam generators. Most of these failures resulted in automatic initiation of HPI safety injection or emergency feedwater injection which would prevent the insufficient core cooling failure mode. Three failure modes, however, were found to create a situation where operator action would be required to prevent insufficient core cooling.

The first two failure modes comprise failure of two ICS power supply branch circuits either (1) auto power or (2) hand power, which result in loss of automatic control of main feedwater flow.

The transients resulting from these power supply failures are expected to proceed relatively slowly. The operator is expected to have approximately one-half hour to reestablish steam generator cooling or approximately one hour to initiate HPI safety injection to avert insufficient core cooling. However, the transients are important for two reasons. First, the transients include inoperability of the operating system (main feedwater) with the simultaneous loss of automatic actuation for the emergency back-up systems. Second, both power supply failures cases result in numerous spurious control room alarms and indications. While these failures would not prevent successful operator action, they would tend to distract the operators and make successful operator action less likely.

321

The third transient consists of a letdown cooler tube failure combined with operator failure to maintain adequate flow to the HPI pumps. Following a tube failure (an isolatable small LOCA or RCS leak), the operating HPI pumps will be transferring the inventory of the letdown storage tank (LST) to the RCS. To the extent the operator fails to recognize the failed tube or fails to isolate the leak once recognized, the reduction in LST inventory will continue. This transient may result in ESPS actuation which would automatically terminate the transient. However, if it does not and the operator allows the LST to drain, the operating HPI pumps will be damaged.

Because of the HPI pump redundancy (three pumps), recovery, even with a damaged HPI pump, is likely. However, the transient does represent a case of a small LOCA potentially including degraded HPI safety injection. Furthermore, the transient does present the operator with the situation of decreasing pressurizer level and degraded makeup flowrate and the potential for a serious error. If the operator mistakenly starts the second or third HPI pumps, these pumps also would be damaged and the transient risk significantly increased.

Recommendations

Several modifications have been identified which could make the plant less susceptible to unacceptable control system failures. Most important of these would make the high level main feedwater pump trip less apt to fail. Other suggestions included (1) greater use of the plant computer to identify inconsistent sensor readings, and (2) classification of emergency procedures to call upon the operator explicitly to consult backup instrumentation in certain situations.

A PWR HYBRID COMPUTER MODEL FOR ASSESSING
THE SAFETY IMPLICATIONS OF CONTROL SYSTEMS

O. L. Smith, R. S. Booth, N. E. Clapp,
F. C. DiFilippo, J.-P. Renier, and A. Sozer

Oak Ridge National Laboratory

The ORNL study of safety-related aspects of control systems consists of two interrelated tasks, (1) a failure mode and effects analysis that, in part, identifies single and multiple component failures that may lead to significant plant upsets, and (2) a hybrid computer model that uses these failures as initial conditions and traces the dynamic impact on the control system and remainder of the plant. The first of these tasks is dicussed in a companion paper by R. S. Stone. The second is reported here.

The initial step in model development was to define a suitable interface between the FMEA and computer simulation tasks. This involved identifying primary plant components that must be simulated in dynamic detail and secondary components that can be treated adequately by the FMEA alone. The resulting model is shown in Figs. 1 through 3. The FMEA in general explores broader spectra of initiating events that may collapse into a reduced number of computer runs. A portion of the FMEA includes consideration of power supply failures. Consequences of the transients may feedback on the initiating causes, and there may be an interactive relationship between the FMEA and the computer simulation.

Since the thrust of this program is to investigate control system behavior, the controls are modeled in detail to accurately reproduce characteristic response under normal and off-normal transients. The balance of the model, including neutronics, thermohydraulics and component submodels, is developed in sufficient detail to provide a suitable support for the control system. The overall approach predominantly uses existing advanced state-of-the-art procedures available in production codes or in the literature. At the expense of generality, attempts were made to simplify and streamline programming, tailor it to a specific plant, and improve computational speed and maneuverability as compared with large production codes.

MODEL VALIDATION

The use of previously confirmed modeling techniques wherever possible provided a leg up on verification of the hybrid model of Oconee-1. Testing is progressing along two fronts. The first is comparison with data from B&W plants including Oconee-1. Figure 4 shows steam generator water level measured in a B&W plant similar to Oconee-1; the level indication is obtained from the pressure difference between taps and is the sum of static and dynamic heads. Simulation of this measurement as a function of load is seen to be in agreement with data.

Figure 5 shows the primary and secondary temperature profiles in the Oconee-type once-through steam generator, and Fig. 6 indicates the heat transfer surface utilization, that is, the fraction of tube length in the boiling mode as a function of load. The measured values were taken from standard B&W design reports. The model tracks closely.

Figure 7 shows the measured and calculated feedwater temperature as a function of feed flow after turbine trip and reactor runback in a plant very similar in design and operation to Oconee-1. Feed flow was a boundary condition in this test of the balance-of-plant portion of the model. Because the measurements were made near the input to the steam generator while the calculations are upstream of this point by about 20 seconds, there is a small delay before the measured values begin to decline.

Figure 8 compares the core flood tank simulation with TMI data (Ref. 1). The right scale is coolant injection as a function of primary pressure. The left scale is the nitrogen over-volume during tank evacuation.

In March of 1980 a turbine trip at Oconee-3, sister plant to Oconee-1, was accompanied by an ICS malfunction that resulted in overfeed of the steam generators. Overfilling continued for approximately 120 seconds until the high level trip in generator A caused feedpump trip. Data from the first 180 seconds of the transient were available for model testing. No design data for Oconee-3 were available and the Oconee-1 design was assumed. Because the Oconee-3 transient data are proprietary, only a summary of the comparison is given here. Secondary side information included feedwater flow, and pressure and water levels for both generators. Primary side data included power level, pressurizer water level, pressure, and the hot and cold leg temperatures of both loops. In general, the model tracked these data closely with the exception of the B generator water level which, after the first minute, fell below the measured value.

As part of the Pressurized Thermal Shock Program, this overfill transient was also run on the RELAP5 code. Good agreement was found with the exception of the B generator water level which, after the first minute, fell below the measured value, as was found with the hybrid model. The PTS study speculated that the emergency feedwater system may have been running, though not detectably in the available information, possibly explaining the higher measured water level in generator B. The hybrid model shows the same degree of agreement with the Oconee-3 data as RELAP5, and consequently compares well not only with the data but also with this validated production code.

These tests largely exhaust the available plant transient data. In the second phase of validation the hybrid model will be further tested against RETRAN2, another extensively verified production code.

APPLICATION OF THE MODEL

The simulation is being used primarily to address mild to moderate transients that can occur at least partially under action of the non-safety control system. Attention initially focused on overfill events that assumed single or multiple failures of feed valves or the generator low and high level set points and the trips that regulate these valves. Cases were run at 20%, 50%, and 100% initial power levels, with failures occuring either in loop A or in loop A in combination with loop B. The following classes of events were considered. In the first six sets the initiating event was failure high of the low level set point.

1. Intermediate overfeed failure insufficient to activate steam generator level protective features other than ICS interaction.
2. Overfeed failure when the high level control transfer is approached but not reached.
3. Slow main feedwater control valve action in combination with overfeed failure when the high level control transfer is approached but not reached.
4. Overfeed in which high level control transfer fails and the high level pump trip is approached but not reached.
5. Overfeed with high level control transfer and high level pump trip failed.
6. Overfeed with high level control transfer and high level pump trip failed in combination with a steam leak in line A.
7. Main feedwater blocking valve position indicator falsely indicated closed; flow reading taken from the startup meter in loop A.

In general, these calculations showed that for single generator overfeed, water inventory in the affected generator increased to a sufficiently high level to saturate the generator fluid, quench superheat, and inject water into the steam line. In some cases of two generator overfill, the transient terminated on low suction trip of the main feed pumps. Overcooling of the primary side was usually modest.

Other events studied with the model include depressurization of the secondary side and overheating of the primary:

8. Secondary side depressurization induced by steam line rupture or by dump valves or turbine bypass valves failing open in loop A or in combination with loop B at low and high power levels.
9. Insufficient main feedwater cooling induced by steam generator high level setpoint failing low, potentially drying out the generator.

SIMULATION RESULTS

In this section selected cases from the above classes of events will be described in more detail. Transients were normally run for ten minutes of plant time; the model has restart capabilities for continuation. Although all available information on plant trips was included, it is possible that trips unknown to the authors would terminate some of the transients. In particular, recent information suggests that the turbine may have a steam quality trip. Possible action of this trip was not provided in the simulation, but was examined in the FMEA process. Also excluded was operator intervention.

Classes 1 through 5 represent increasing levels of overfill. Near the lower end of the range, in Class 2, the high level control transfer was approached but not reached; the low level setpoint in generator A was failed to 240 in., near but below the high level setpoint. The impact of this degree of overfill on the primary side was minor, but as the generator filled to the setpoint, the outlet quality* decreased below 1 and liquid was injected into the steam line. These effects at 100% power are shown in Figs. 9 through 11. Fig. 11 is the time integral of liquid exiting the generator, indicating the total water passing into but not necessarily accumulating in the line. Phase separation and any attendant accumulation were not considered. Runs at 20% and 50% power showed approximately half as much injection into line A in 10 minutes.

*Throughout this paper quality is defined as the thermodynamic quality.

325

The above runs were repeated with level failure occuring in generator B in combination with A. At power levels above approximately 50% the results for both steam lines were comparable to those for line A above. At lower initial powers the main feed pumps tripped on low suction pressure and terminated the overfill before water was injected into the steam lines.

At the upper end of the overfill spectrum, class 5 events assumed that the high level control transfer and the high level pump trip failed. The low level set point in generator A was assumed to fail arbitrarily high; a value of 700 in. was used in the simulation. All high level control points in generator A could thus be exceeded.

Depending upon initial power level, the ICS took different courses of action to reestablish balance between reactor power and feedwater flow. At 20% power the failed setpoint caused the generator A feed valve to run full open in a few seconds (Fig. 12). Generator level increased to 350 in. and stabilized below the failed setpoint because 1) the maximum pumping power in line A was reached, and 2) balance between power and flow was reestablished at 60% (Fig. 13), with most of the heat transferred in generator A. Superheat in generator A was lost in approximately 1 min. (Fig. 14). Total water injection was 38,000 lbs. after 10 min. (Fig. 15). On the primary side, pressurizer pressure decreased 200 psi in 2.5 min. and recovered (Fig. 16). Pressurizer level indication dropped 5 ft. and was beginning to rise when the simulation was terminated. The cold leg temperature of the affected loop decreased 35°F in 2.5 min.

At 100% initial power the ICS was limited in its capacity to adjust power to match overfeed. In this case the control system reduced flow to generator B to compensate for the increase in A (Figs. 17 and 18). The level indication in generator A stabilized near 260 in. Water injected into line A was 68,000 lbs in 10 min. Primary and secondary temperature variations are generally smaller than at 20% power since the overfeed at 100% is a smaller percentage change in flow.

In both of these transients, action of the ICS to match power and feed flow resulted in a stabilized system with the generator water level below the failed low level setpoint. If the turbine does not trip on low quality, this configuration may be sustainable.

In the Class 7 event, the main feedwater blocking valve position indicator falsely indicated closed; flow reading was taken from the startup meter in loop A. Initial power was 100%. The feedwater flow signal for generator A was 15%. The ICS reduced reactor power to 65% (Fig. 19). Total feed flow was reduced less rapidly (Fig. 20) and some overcooling of the primary occurred. Primary pressure decreased 230 psi, and pressurizer level fell from 18 ft to 9 ft in 2 min. (Fig. 21). Core average temperature as calculated from the hot and cold legs of the affected loop decreased 18°F in 1.5 min. and then began a slow recovery. Water injection into steam line A was 20,000 lbs in 10 min.

In Class 8 events, secondary side depressurization was induced by partial steam valve failure or steam line rupture in loop A or in combination with loop B, at low and high power levels. At 20% power a fault in steam line A was sized to accommodate the line's total available flow. An initial modest pressure reduction in the generator resulted in a temporary increase in feed flow. The ICS increased reactor output and reestablished equilibrium at 35% power. The ICS maintained header pressure by throttling turbine flow, forcing virtually all

line A flow through the fault. Impact on the primary and secondary pressures and temperatures was minor (Fig. 22). Plant conditions appeared to remain manageable by the ICS. Without operator intervention, the system would be expected to trip on depleted feedwater inventory.

At 100% power, over the time interval considered, the ICS appeared to be capable of managing single line faults that released up to 100% of one line's nominal flow. Perhaps the most noteworthy imbalance was the substantial downtrend in feedwater temperature that resulted from loss of half of the bleed steam to the heaters (Fig. 23). Leaks of this magnitude or larger in both lines resulted in depressurization of the secondary side and system trip within one minute on low steam flow to the turbine.

PRELIMINARY CONCLUSIONS

A number of general conclusions may be drawn from these simulations. The integrated control system shows considerable ability to deal appropriately with many of the off-normal conditions investigated. The feedforward and feedback control matrix which matches feedwater and reactor power has a versatility that tends to buffer the disturbances. This is seen particularly in the class 5 overfeed events in which all high level control is inoperative. The ICS manipulated either the power level at low powers or the distribution of feed flow between generators at high power to maintain Btu balance.

In a substantial number of the simulations, superheat was lost, steam generator quality fell below 1, and water was injected into the steam lines. While these cases presume no quality trip, conditions could exist in which the quality hovered just above any trip setpoint and injected water into the lines for a sustained period. For example, in the class 2 event in which the low level set point in generator A failed to 240 in., the quality was marginally below unity (Fig. 10), water was injected into the line (Fig. 11), and the condition appeared sustainable in the absence of operator intervention.

Overfeed of both generators tended to inject water into the lines at powers above approximately 50%, whereas the calculations indicated that at lower powers the system would trip on low feedwater suction pressure before water was injected.

In the majority of the cases studied, overfill of the generators appeared to have minor effects on the temperatures and pressures of the primary side. An exception appeared to be the class 7 event in which the main feedwater blocking valve position indicator falsely indicated closed and the flow reading was taken from the startup meter in loop A. The ICS ran the power back more rapidly than feed flow, and primary pressures and temperatures dropped significantly.

The ICS demonstrated ability to manage single line steam leaks up to the full normal flow in the line for the existing power level. In the simulations there was a tradeoff of flow between the leak and the turbine, with consequent reduction in turbine power. Turbine trip may occur even though the leaks appeared otherwise controllable by the ICS in the short term.

REFERENCE - 1. Analysis of Three Mile Island, Unit 2 Accident, NSAC-1, July 79.

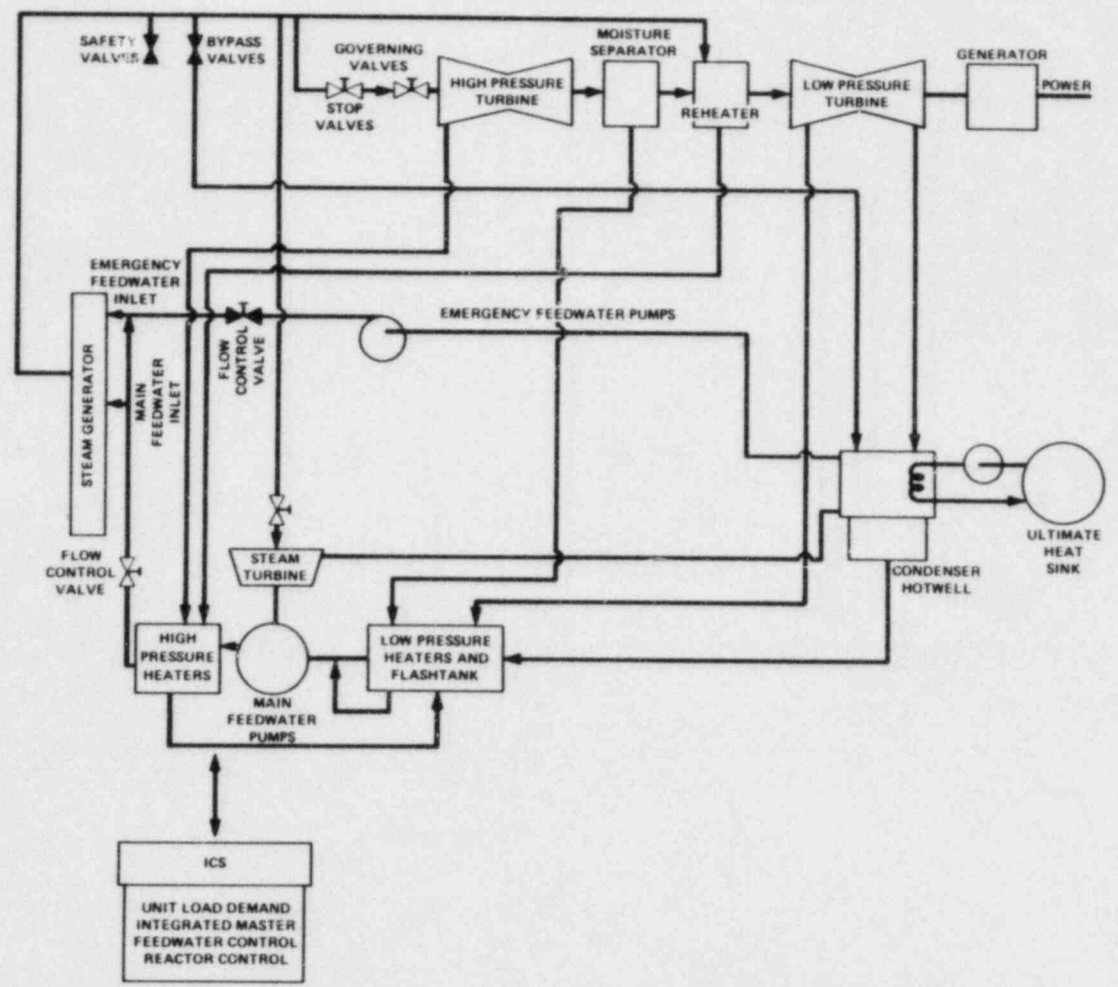# ORNL MODEL LAYOUT OF OCONEE 1
PRIMARY SYSTEM

Fig. 1

ORNL DWG 83-8948
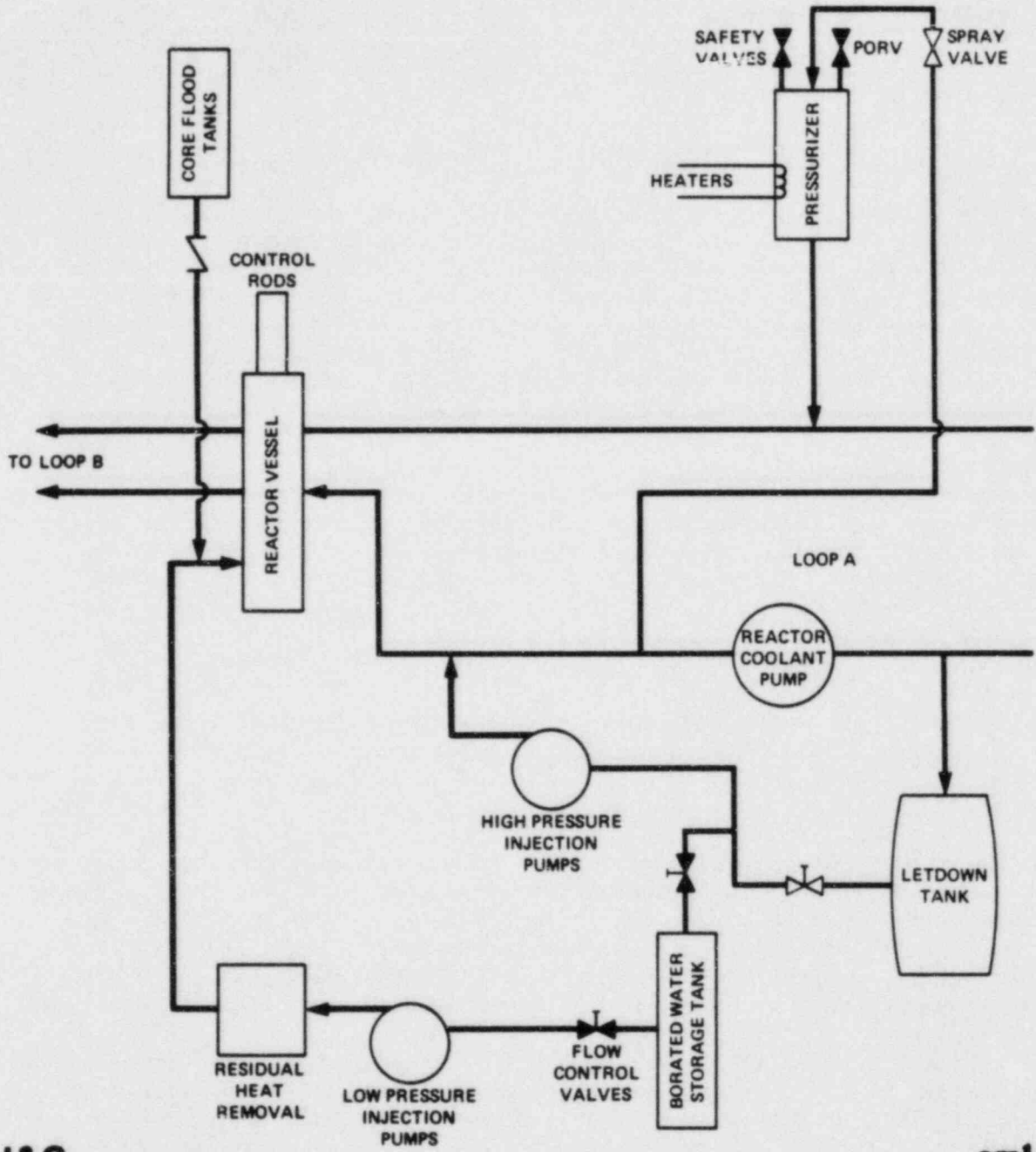
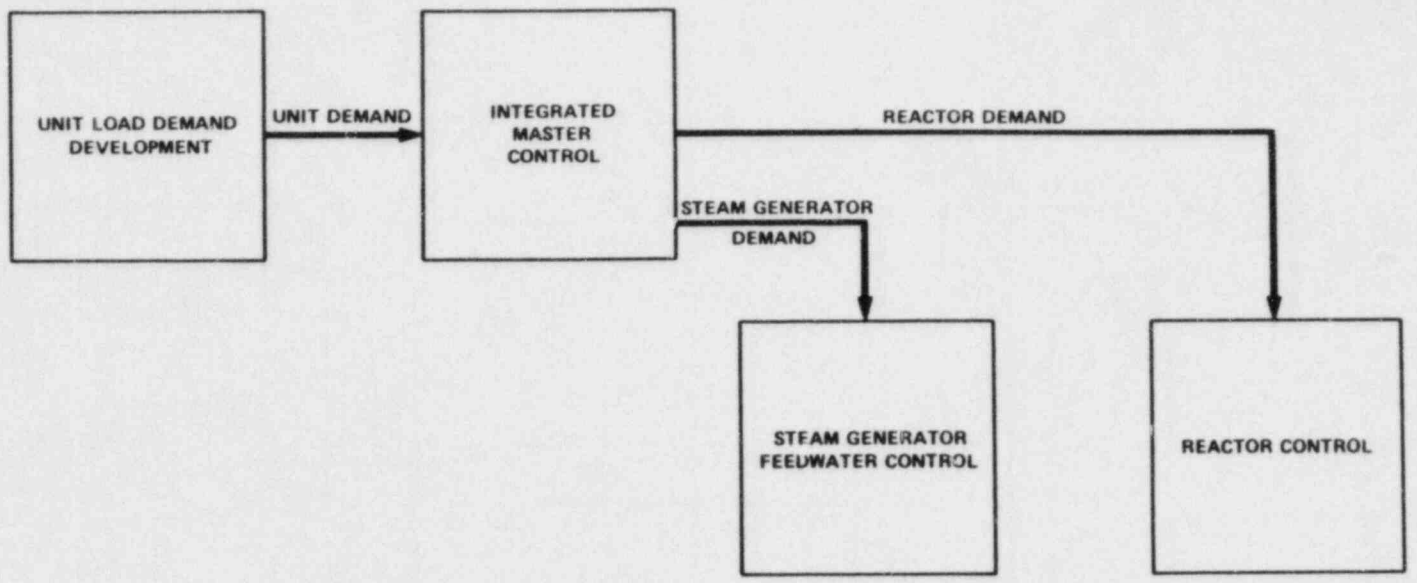**ORNL MODEL LAYOUT OF OCONEE 1**
SECONDARY SYSTEM

329

I&C

ornl

Fig. 2

INTEGRATED CONTROL SYSTEM

Fig. 3

STEAM GENERATOR ΔP SIGNAL vs LOAD
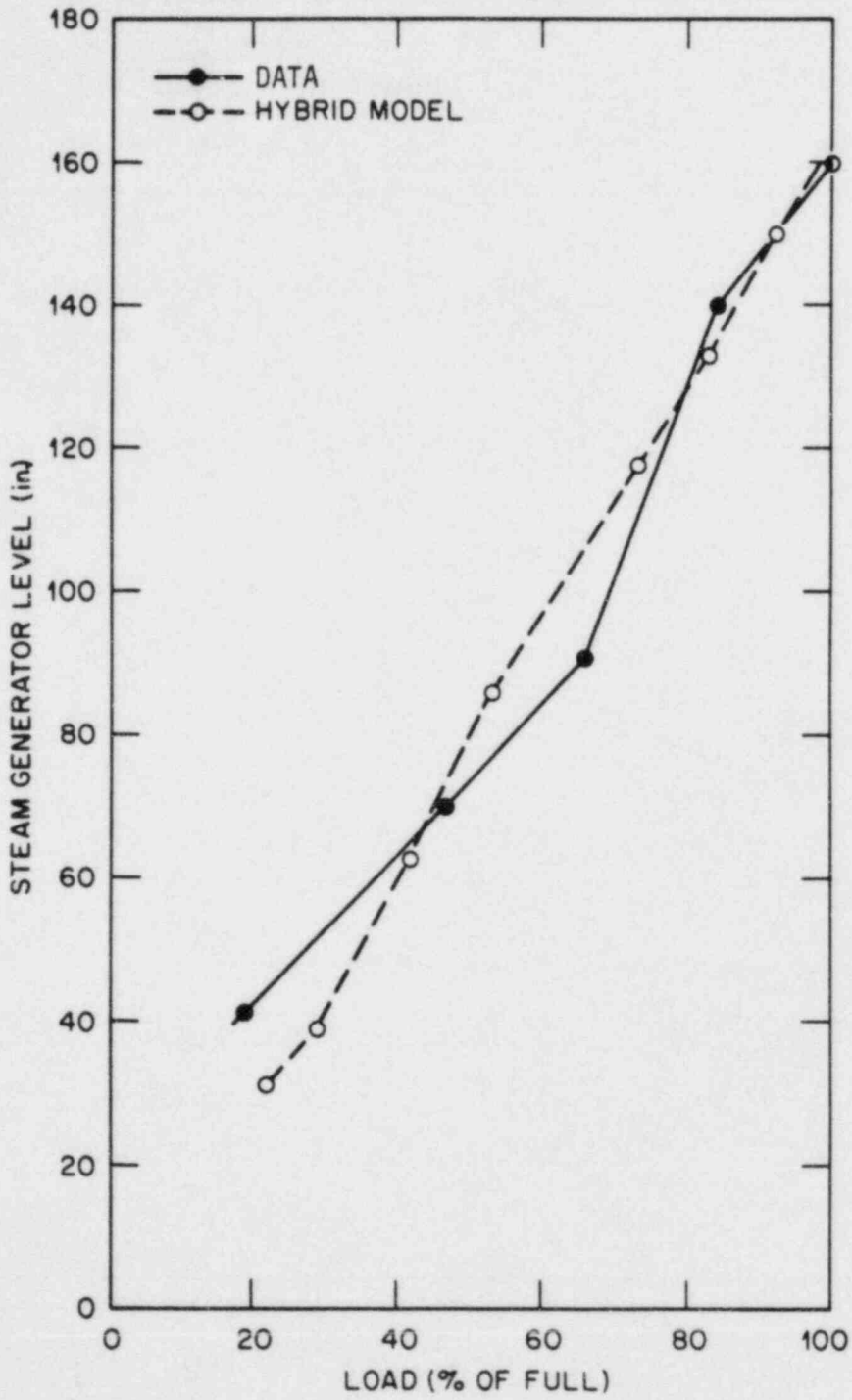

Fig. 4

STEAM GENERATOR
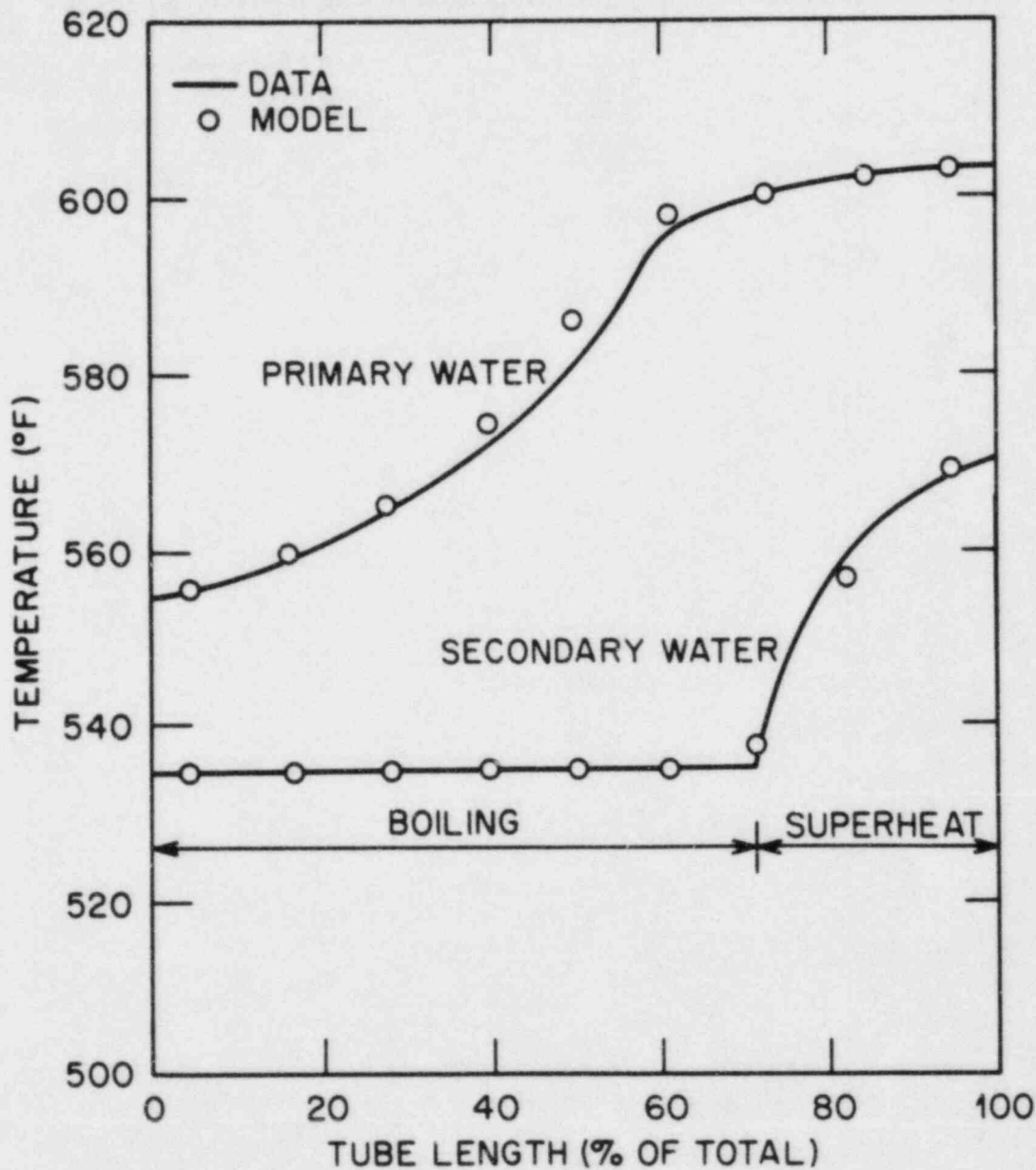# PRIMARY AND SECONDARY TEMPERATURE
PROFILES AT 100% LOAD

Fig. 5

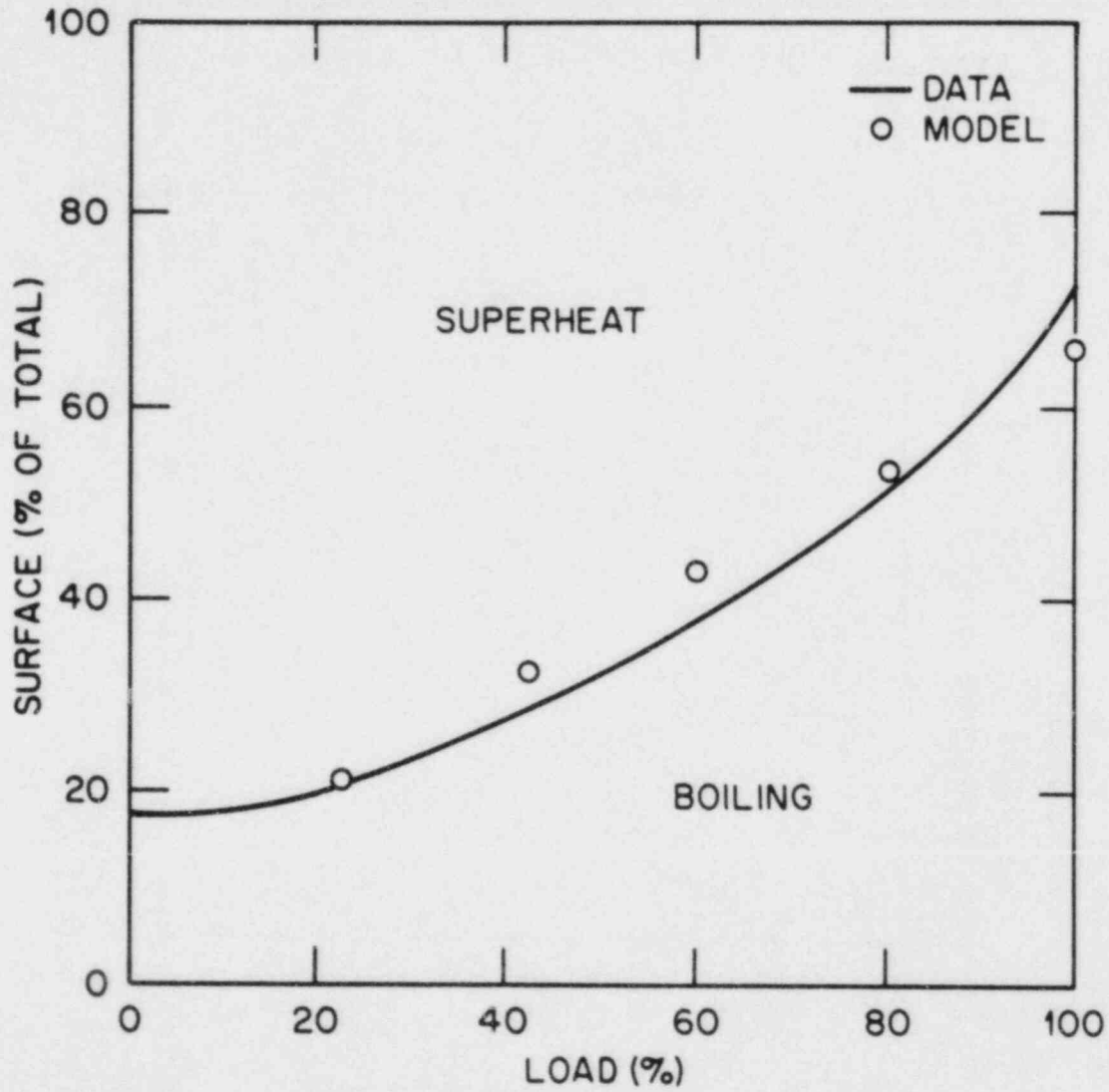## STEAM GENERATOR HEAT TRANSFER
SURFACE UTILIZATION vs FLOW

Fig. 6

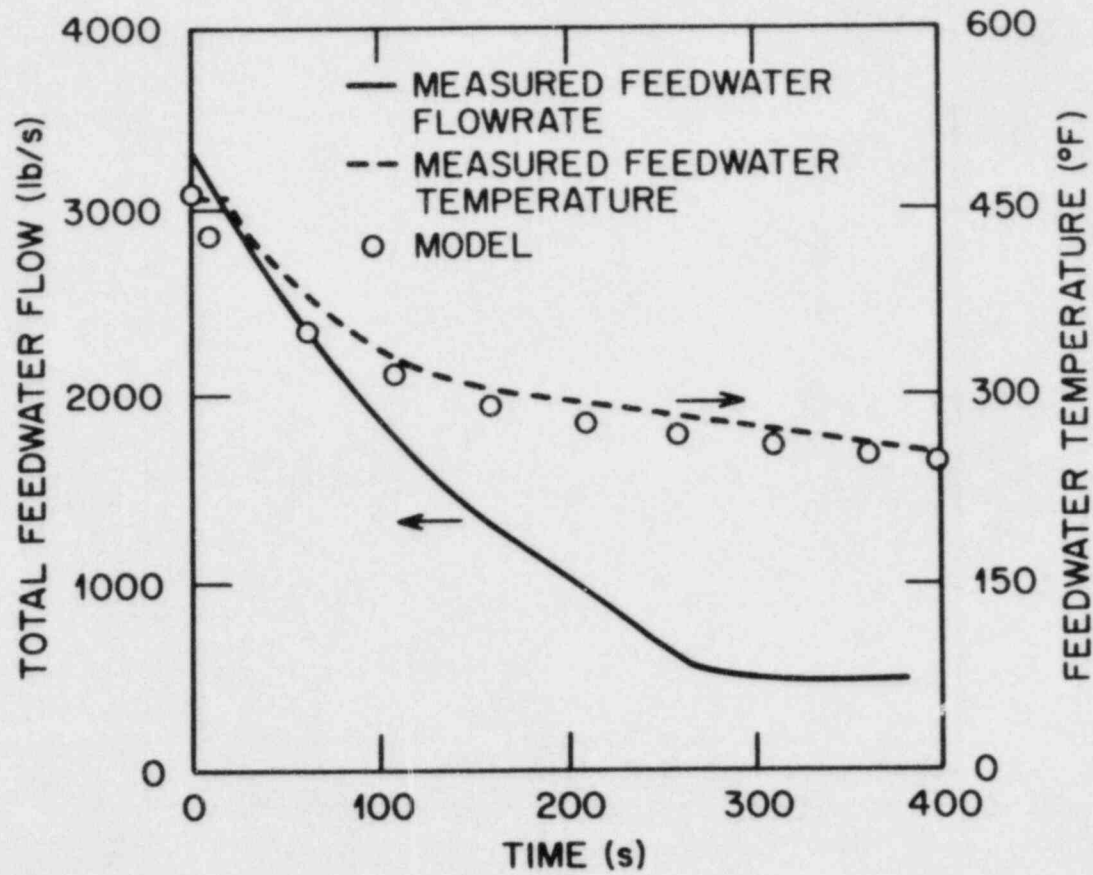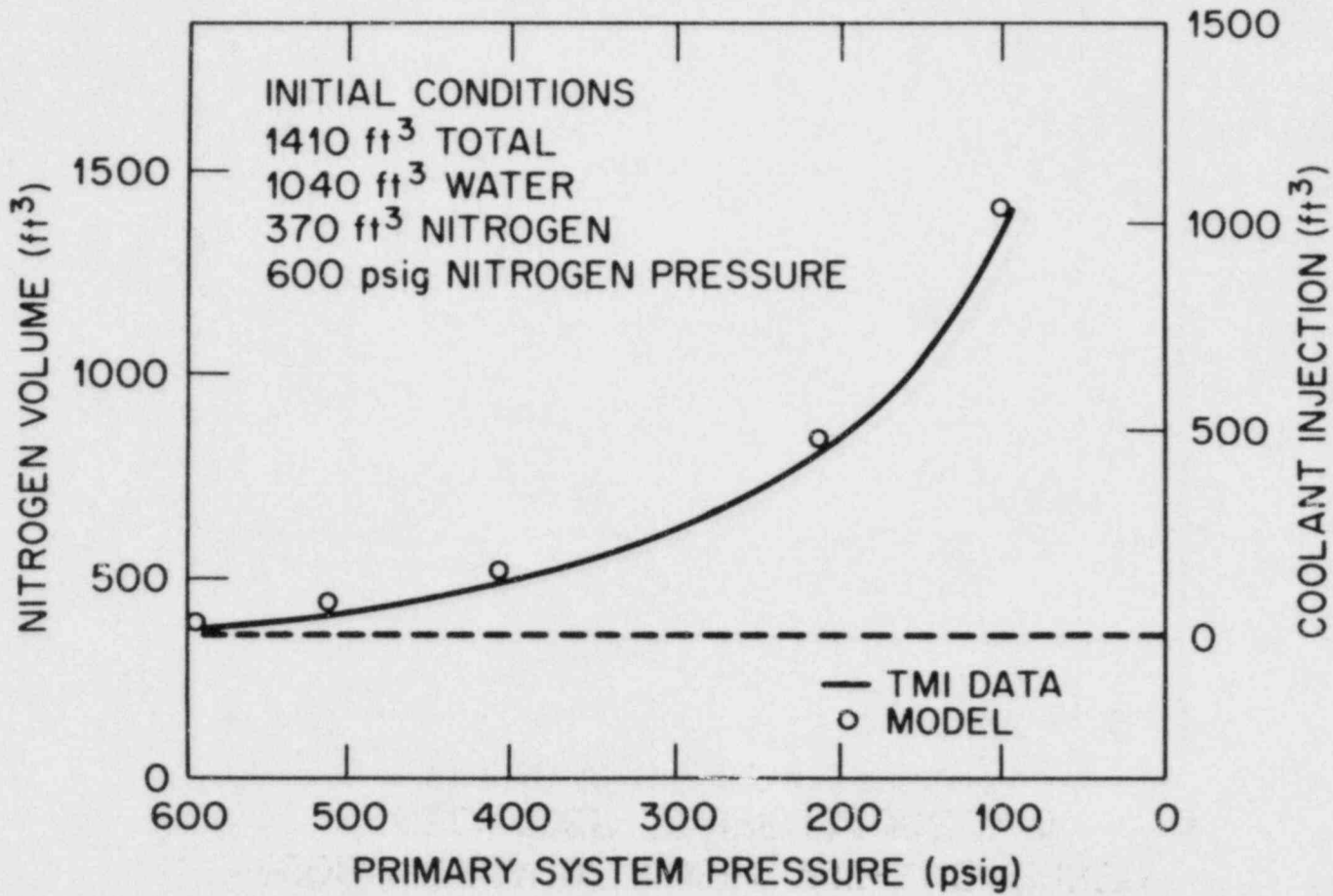## COMPARISON OF MODEL WITH MEASURED
FEEDWATER TEMPERATURE IN A
B AND W NUCLEAR PLANT

Fig. 7

Fig. 8

CLASS 1 CORE OUTLET TEMPERATURE

Fig. 9

ORNL-DWG 84-15617
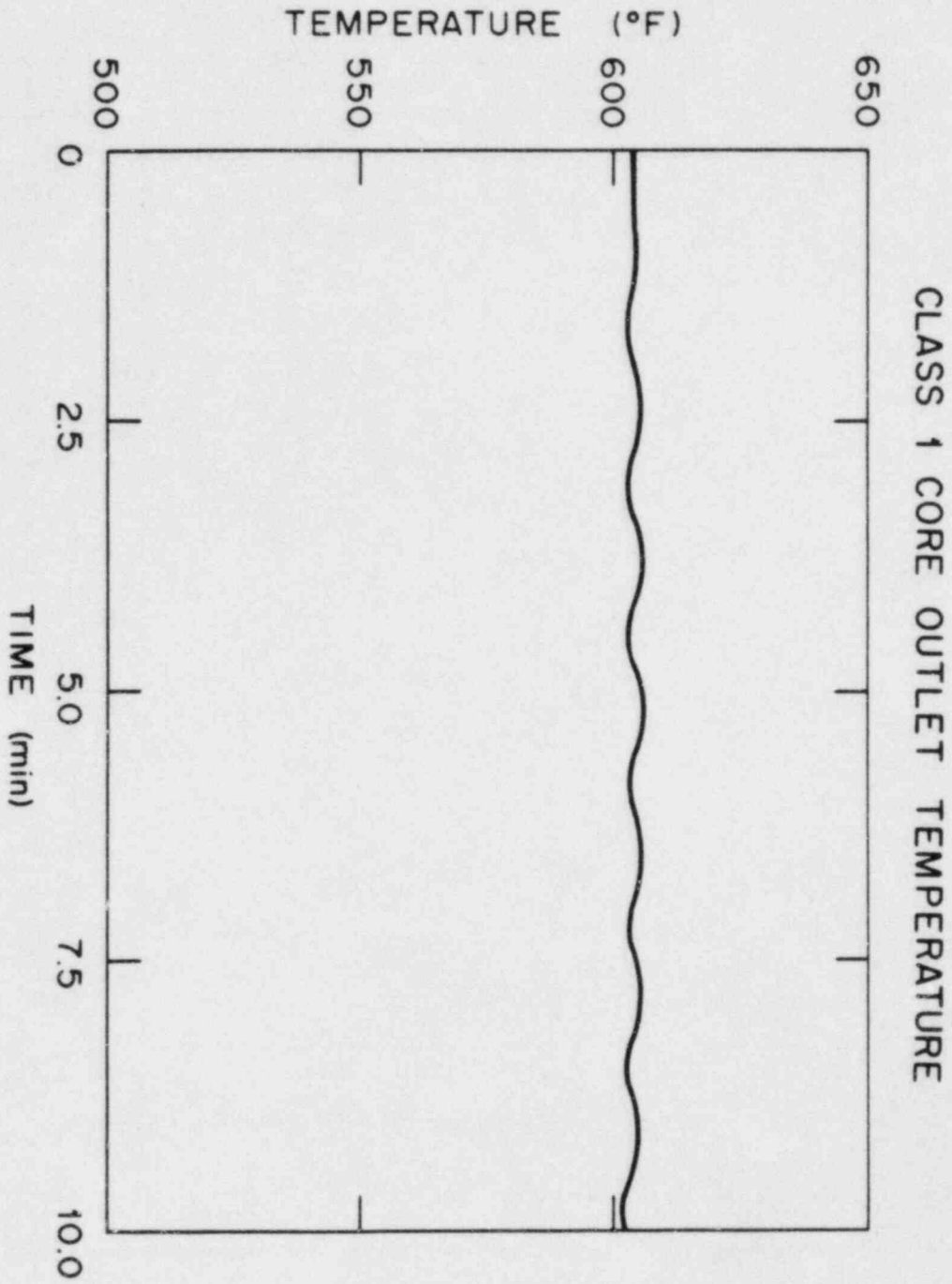
CLASS 2 STEAM GENERATOR A OUTLET QUALITY
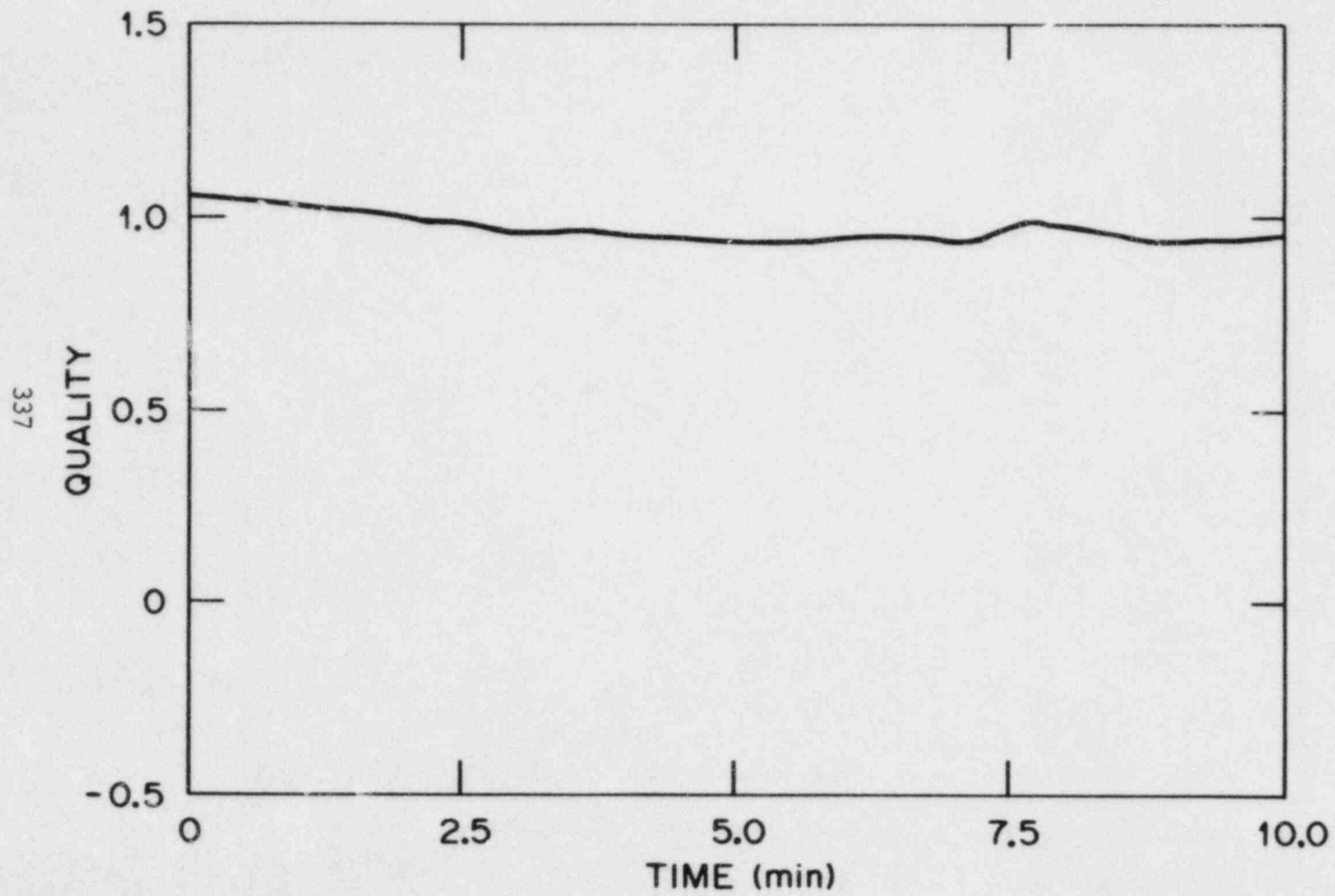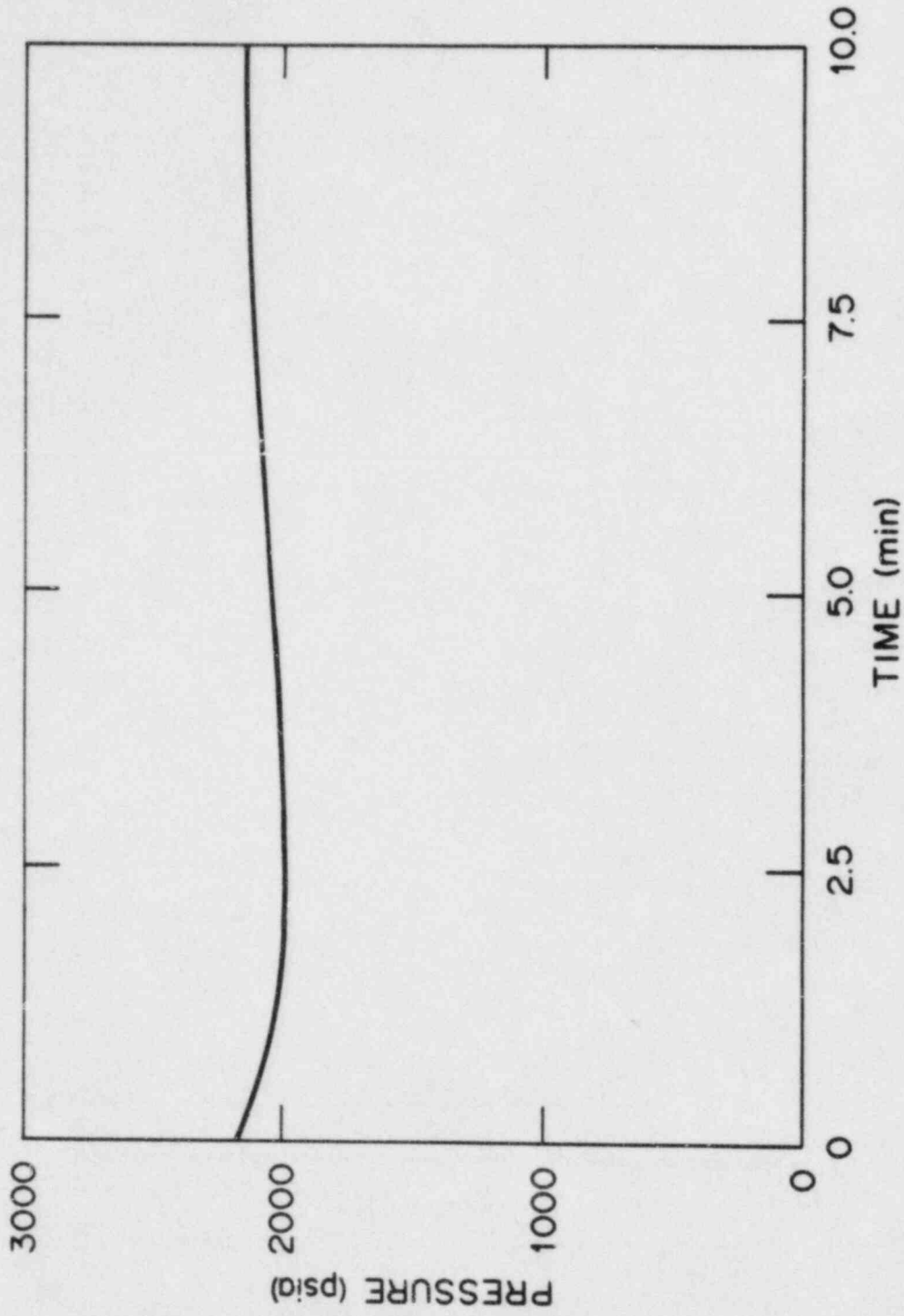

Fig. 10

CLASS 2 WATER INJECTION INTO STEAM LINE A
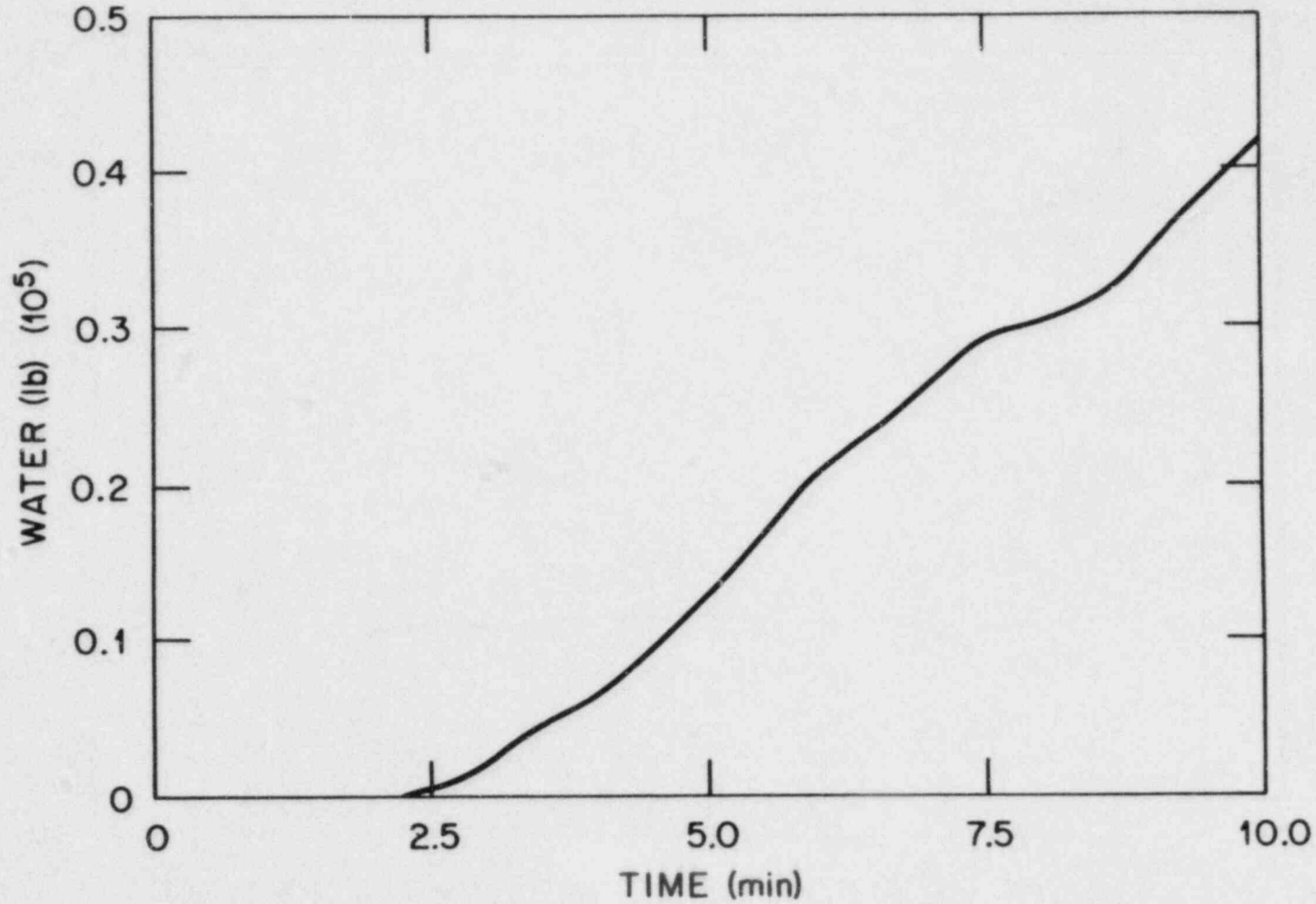
Fig. 11

CLASS 5 (20% POWER)
STEAM GENERATOR A FEEDWATER FLOW
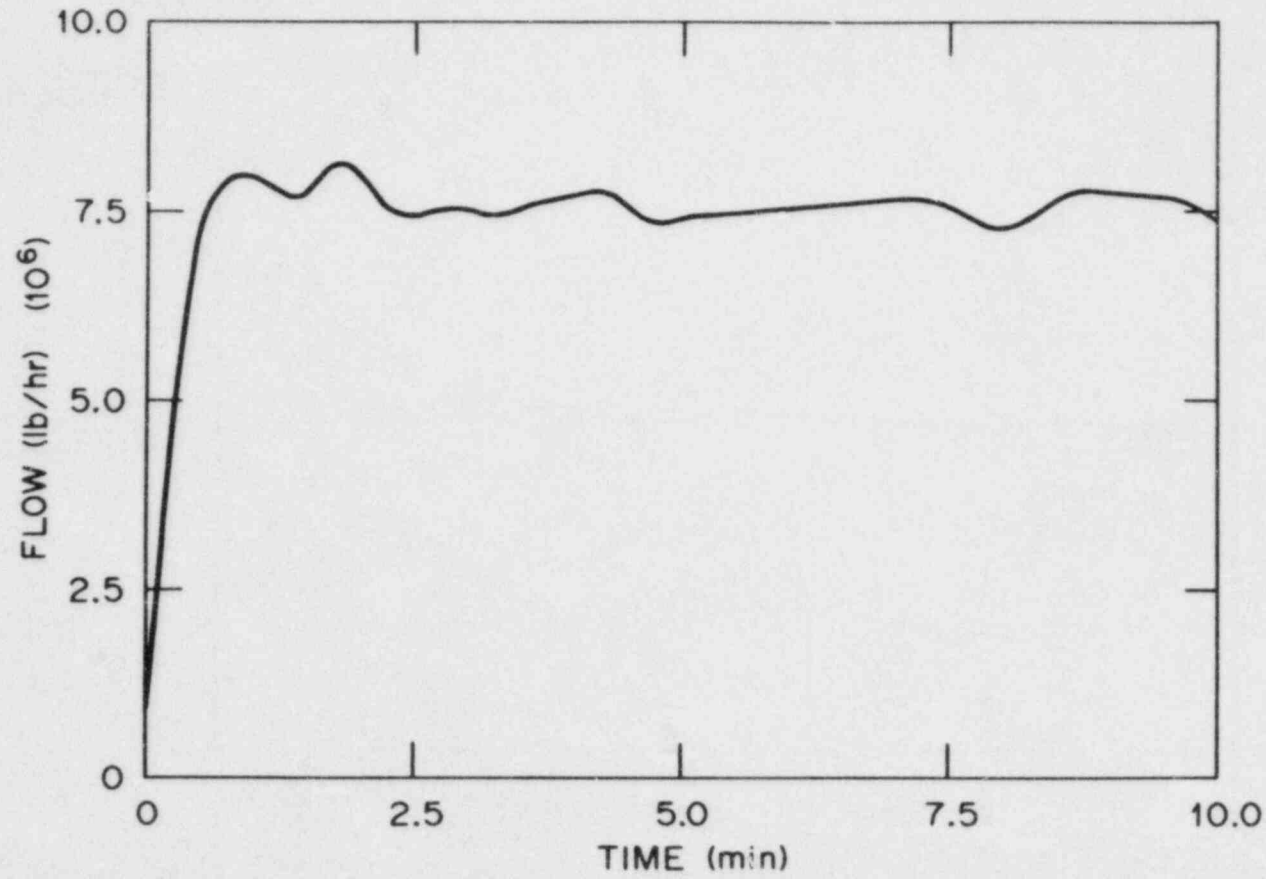
Fig. 12

CORE POWER FRACTION (%)
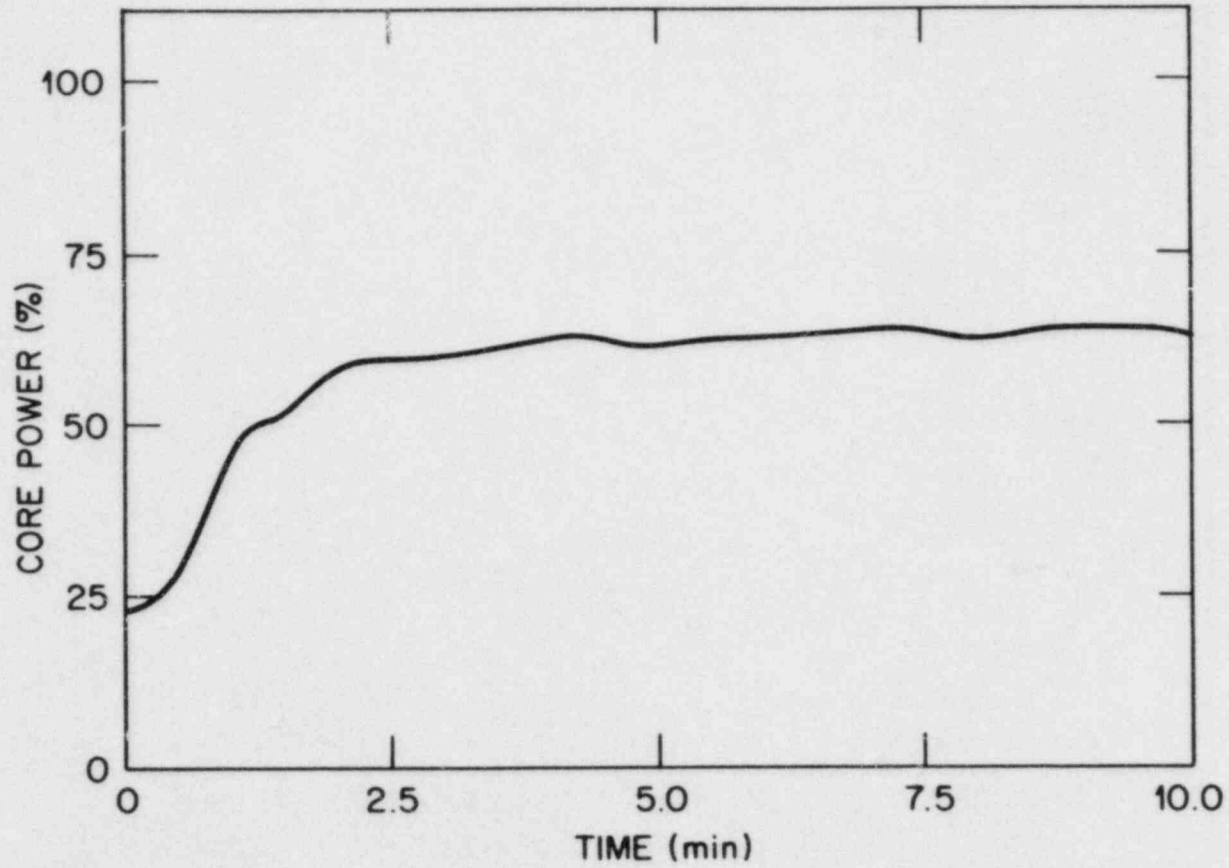
Fig. 13

CLASS 5 (20% POWER)
STEAM GENERATOR OUTLET QUALITY

ORNL __u 84-15623

Fig. 14

341
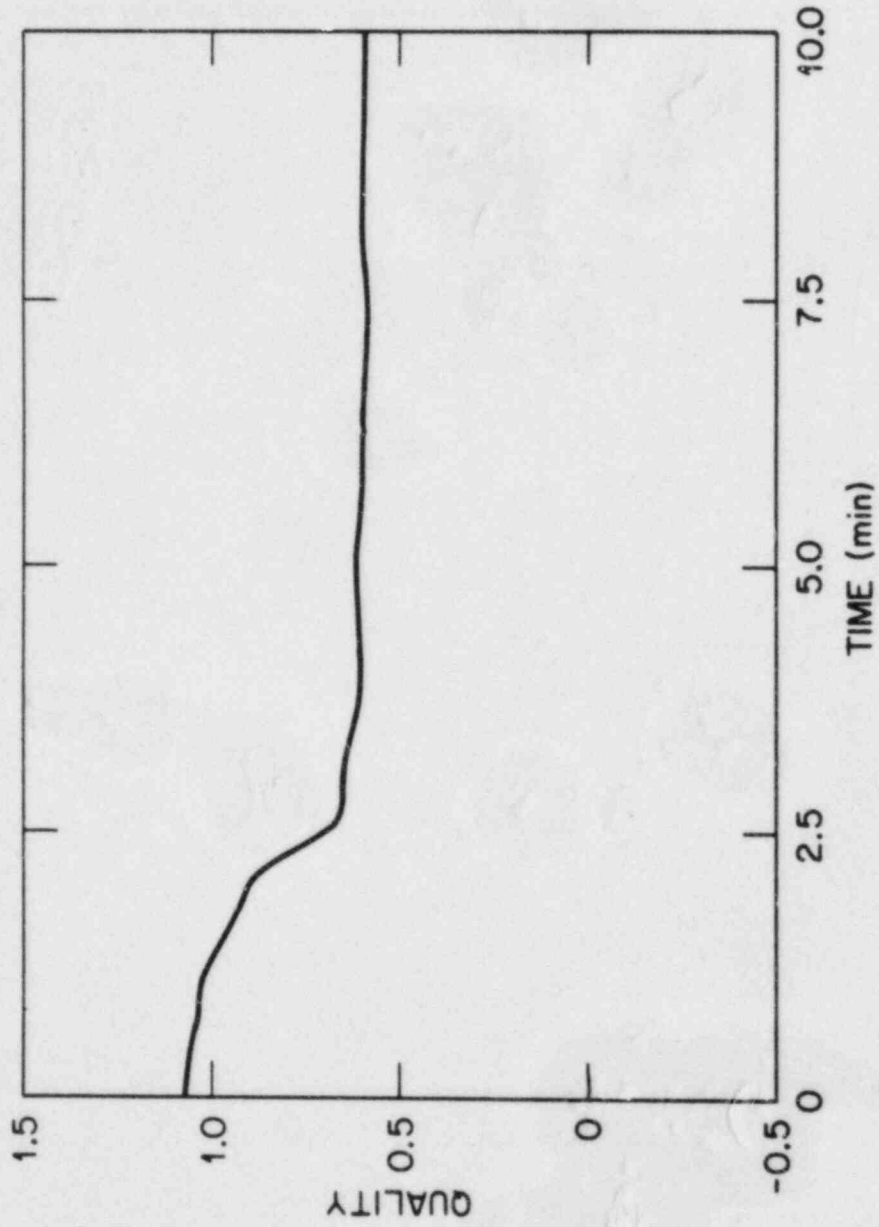
CLASS 5 (20% POWER)
WATER INJECTION INTO STEAM LINE A

ORNL-DWG 84-15625

Fig. 15

342
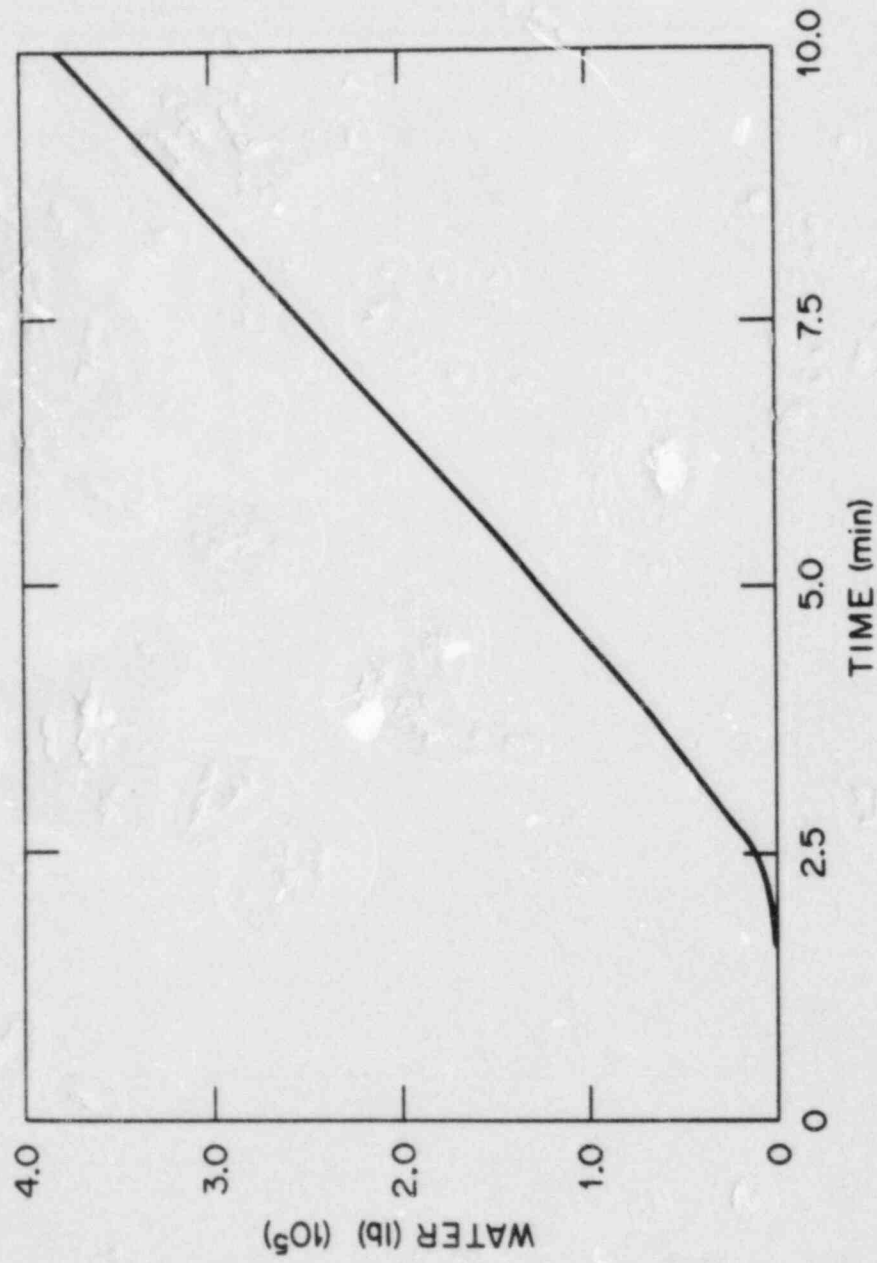
ORNL - DWG 84 - 15626
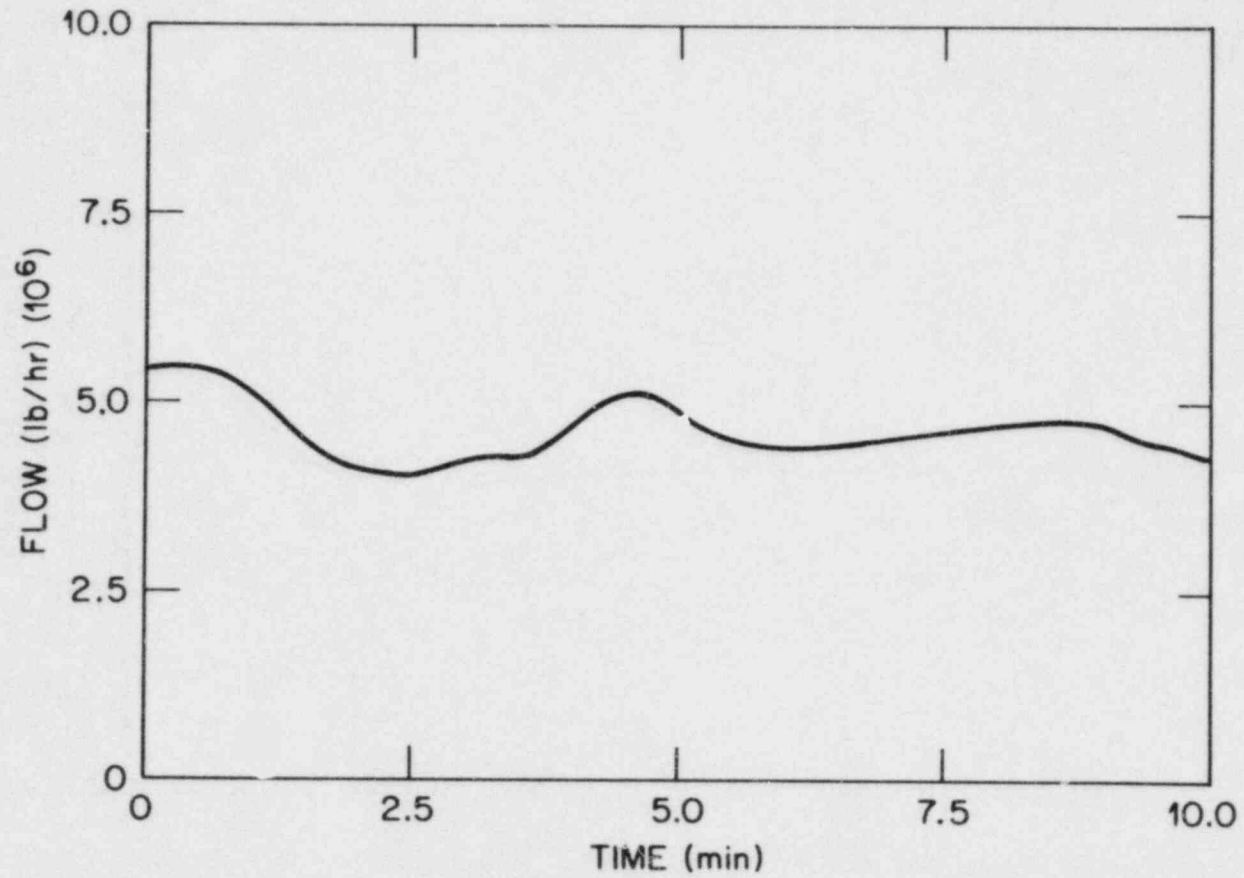
CLASS 5 (20% POWER) PRESSURIZER PRESSURE

Fig. 16

CLASS 5 (100% POWER)
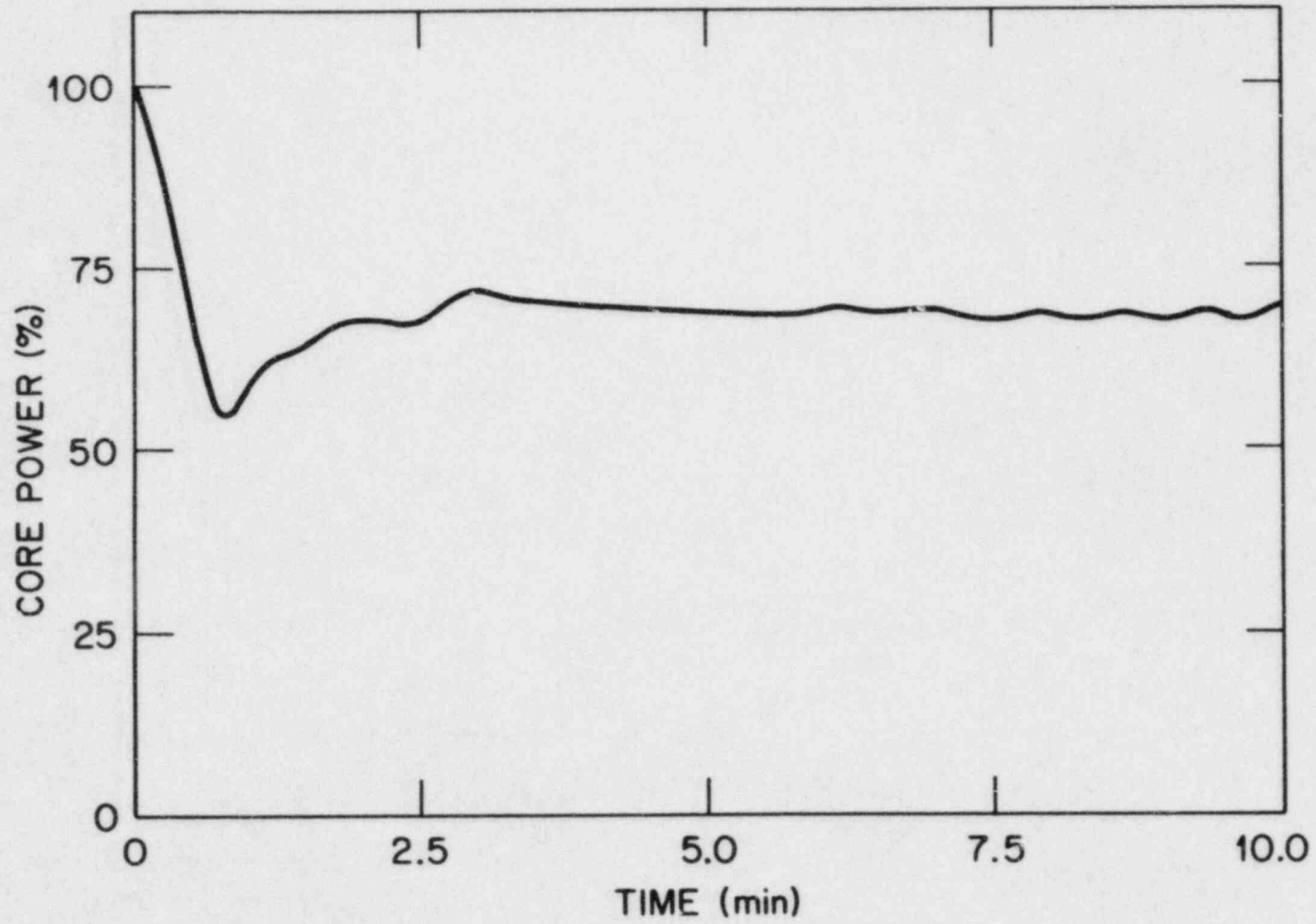## STEAM GENERATOR A FEEDWATER FLOW
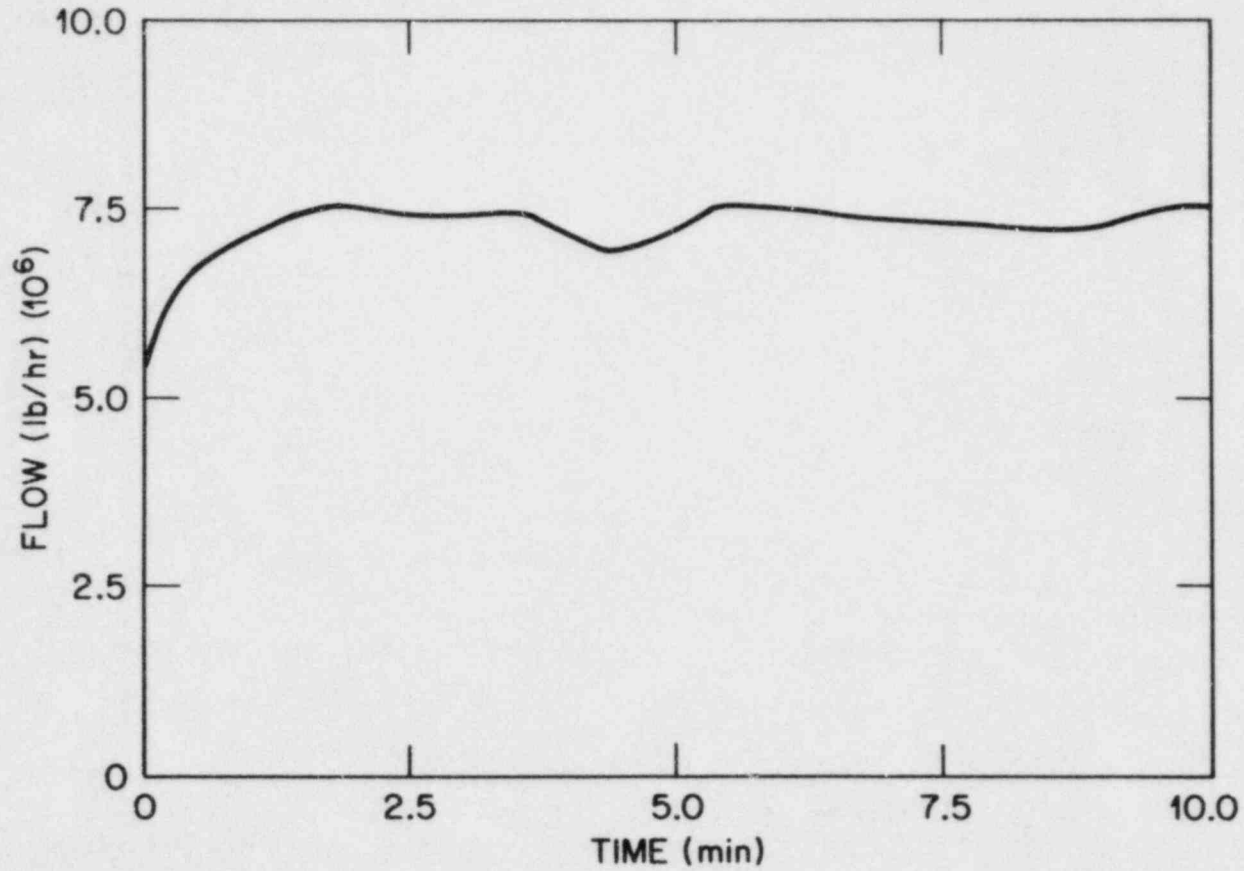
Fig. 17

CLASS 5 (100% POWER)
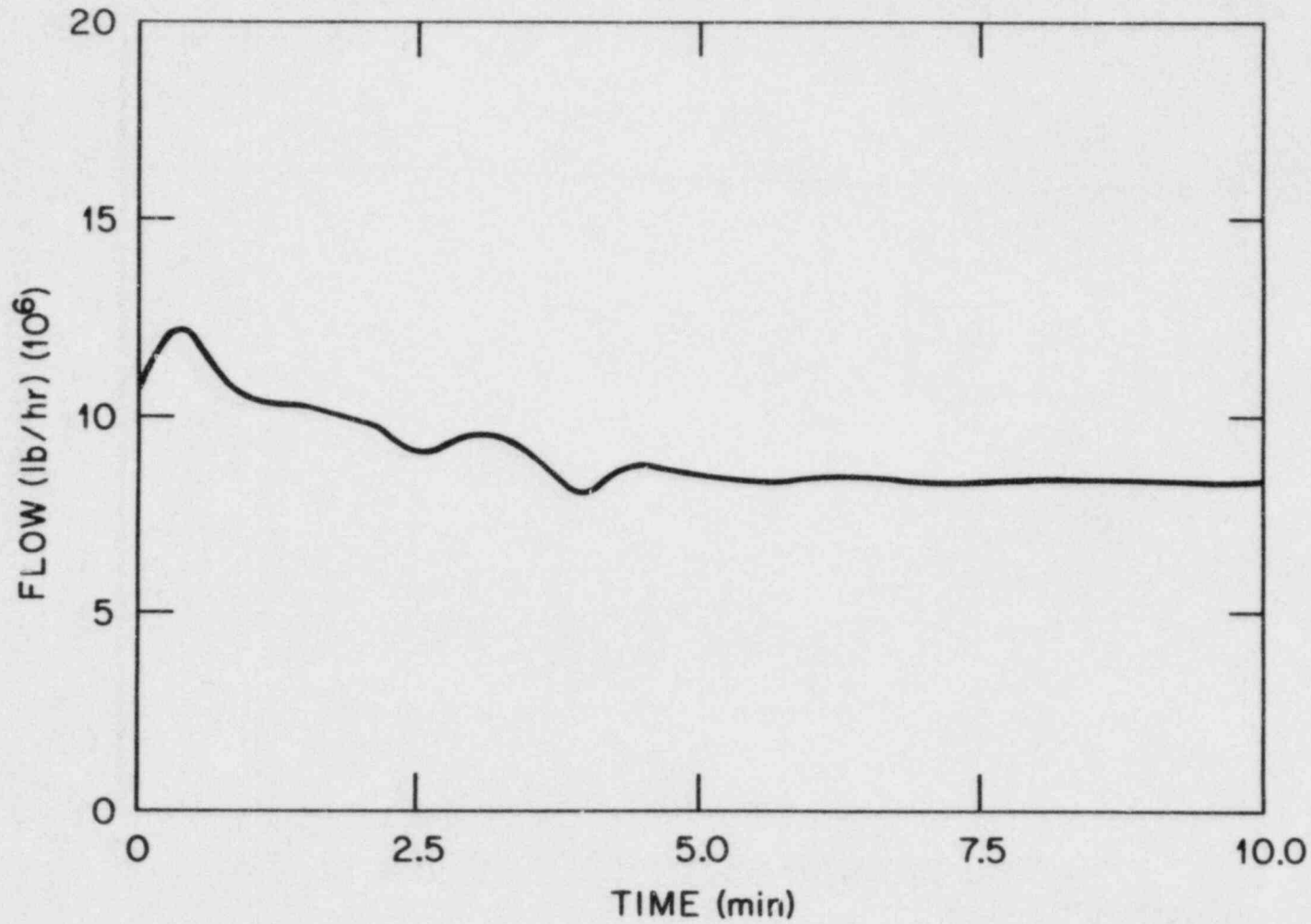## STEAM GENERATOR B FEEDWATER FLOW

Fig. 18

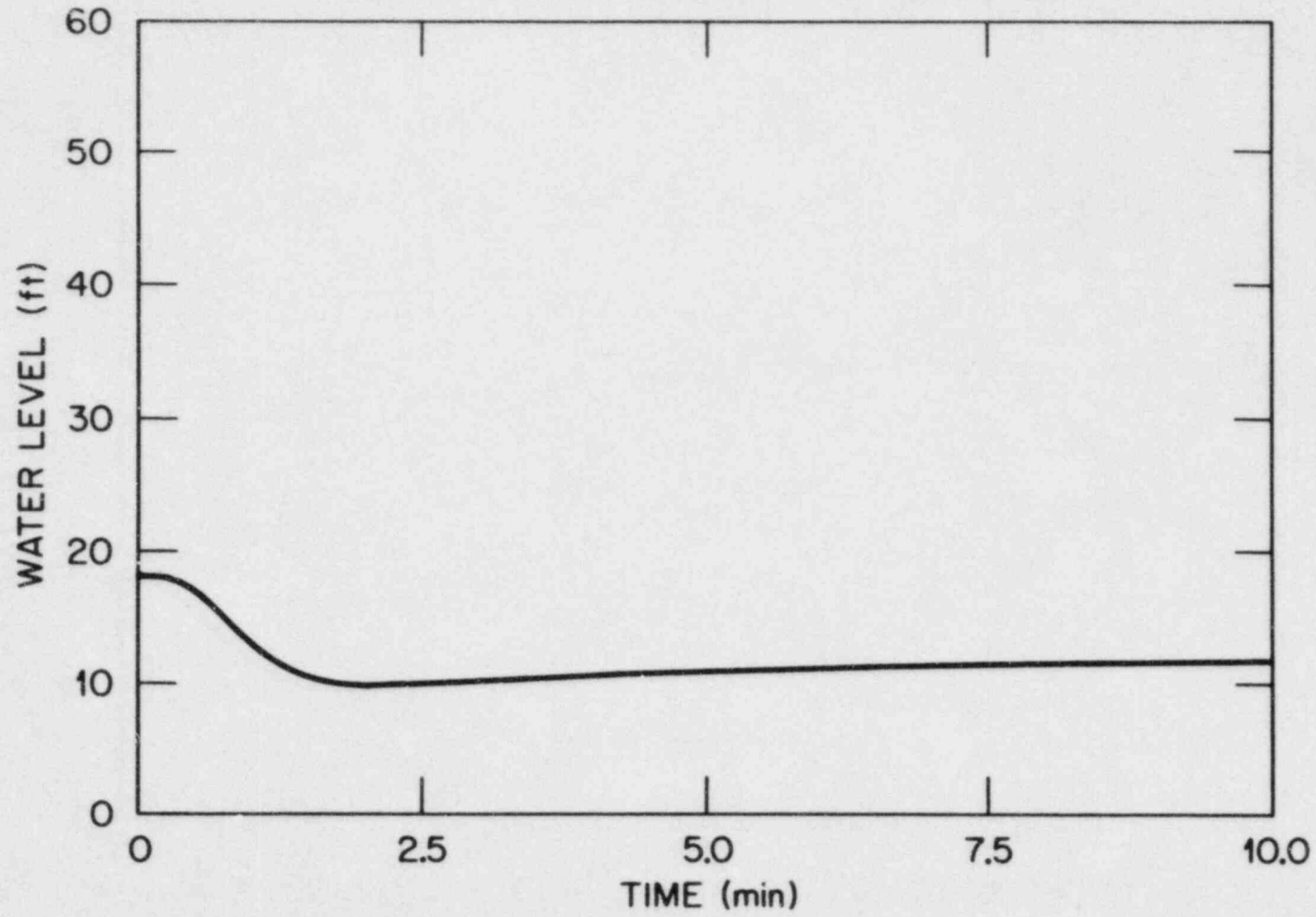## CLASS 7 CORE POWER (%)
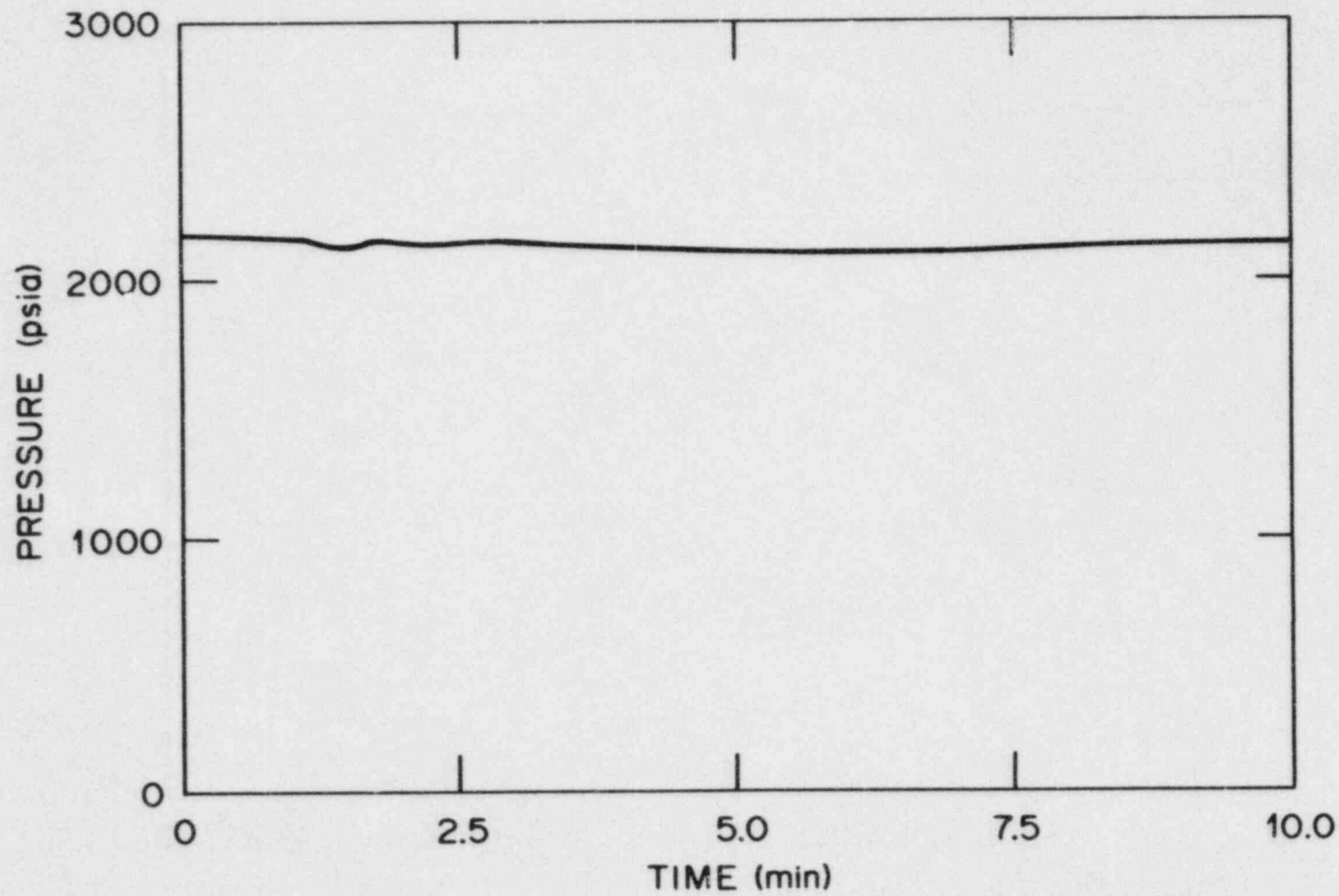

Fig. 19

CLASS 7 TOTAL MAIN FEEDWATER FLOW

Fig. 20

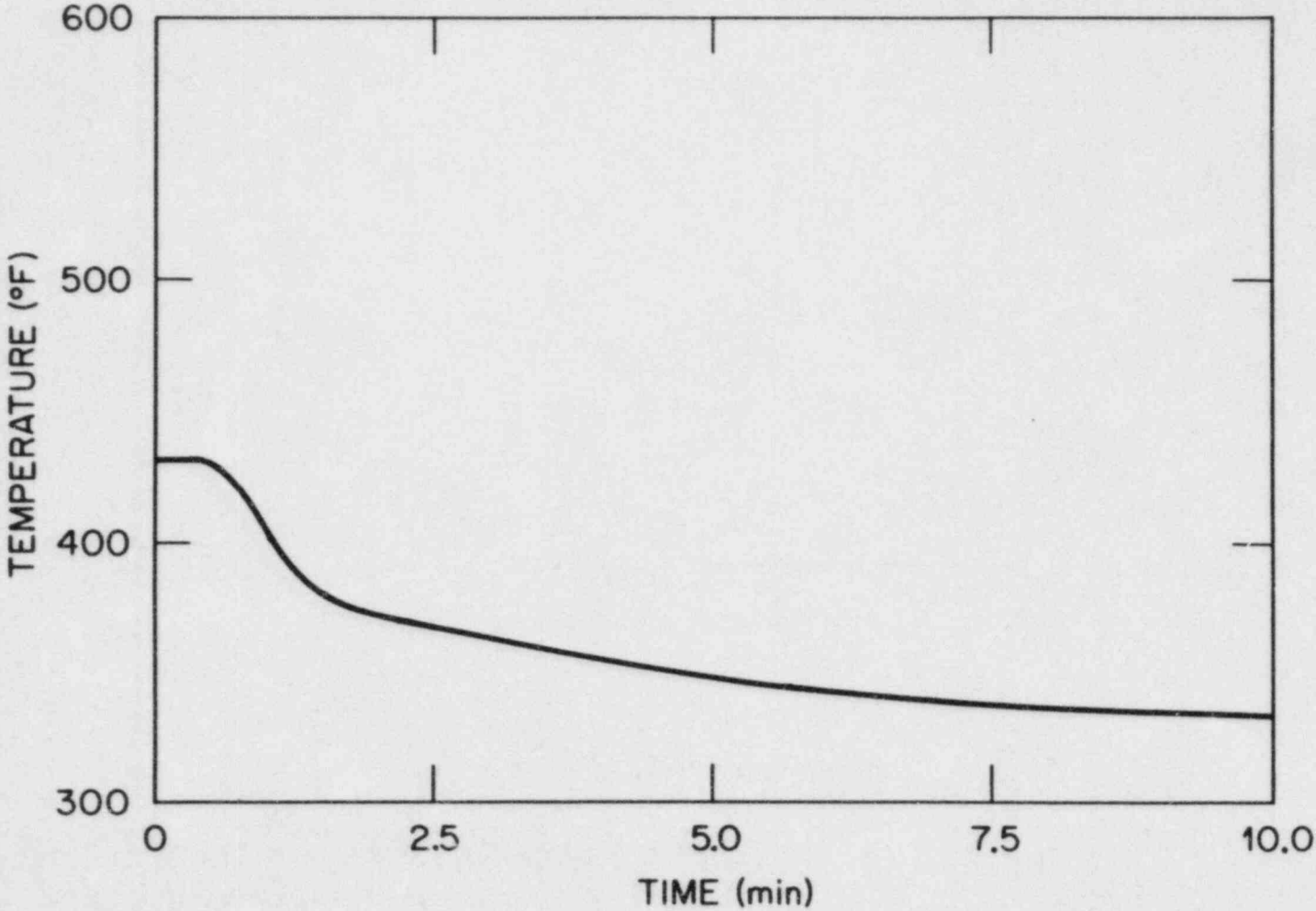## CLASS 7 PRESSURIZER WATER LEVEL

Fig. 21

348

CLASS 8 PRESSURIZER PRESSURE

Fig. 22

349

CLASS 8 STEAM GENERATOR A FEEDWATER TEMPERATURE

350

Fig. 23

Progress on Qualification Testing Methodology Study
of Electric Cables

M.Ito, Y.Kusama, T.Yagi, S.Okada, M.Yoshikawa, and K.Yoshida
Takasaki Radiation Chemistry Research Establishment, JAERI

Introduction

A LOCA, one of design basis events, is estimated to continue
more than one year including a post-LOCA period. It is difficult
to demonstrate the capabilities of cables through such a long
period by the test. The accelerated test is desired for practical
uses. For this purpose, the post-LOCA period which occupies the
most part of the accident is usually cut out because the degra-
dation in this period assumes to be small owing to its low dose
rate and low temperature. By recent aging studies, it was found
that the low dose rate irradiation gave rise to a significant
degradation even at room temperature.

We conducted the simultaneous LOCA tests exceeding three
months at relatively low dose rate and compared the results with
one week's LOCA tests at high dose rate in order to verify the
above assumption. Besides usual LOCA simulation by satulated
steam, simulation by air containing steam was tested.

Experimental

(1) Pre-conditioning

After the thermal aging(121°C, 7days), samples were
irradiated by Co-60 gamma rays at room temperature. Dose-
rate was 0.7-0.95 Mrad/h and total dose was 50 Mrad.

(2) LOCA Conditions

The test profile for steam/chemical spray exposure is
shown in Fig. 1. The aged samples were irradiated up to
about 150 Mrad under steam/chemical spray exposure(dose rate:
0.055 Mrad/h for the three months test and 0.925 Mrad/h for
the one week test).

Results

(1) Mechanical Properties

In case of the simulation by saturated steam, the differences of the degradation between the one week test and the three months test results were not observed for ethylene-propylene rubber(EPR), but clearly observed for chlorosulfonated polyethylene(CSPE).

In case of air containing steam, the differences between both tests were significant even for EPR.

(2) Volume Resistivity

The decrease in volume resistivity of EPR after test is less than two orders of magnitude when the samples are exposed to LOCA environments by saturated steam. The influence of the exposure length is obscure.

For LOCA tests simulated by air containing steam, the influence of the exposure length was remarkable. The value decreases about five orders of magnitude after the three months test, whereas the drop is only two orders for the one week test.

Conclusion

(1) Effect of oxgen is significant on the degradation of the sheet shape samples during the three months LOCA simulation.
(2) Cable structure gives higher reliability to the insulators in the air contaning LOCA simulation.

Fig.1 Simultaneous Test Profile (Air added: non or 0.05 MPa)
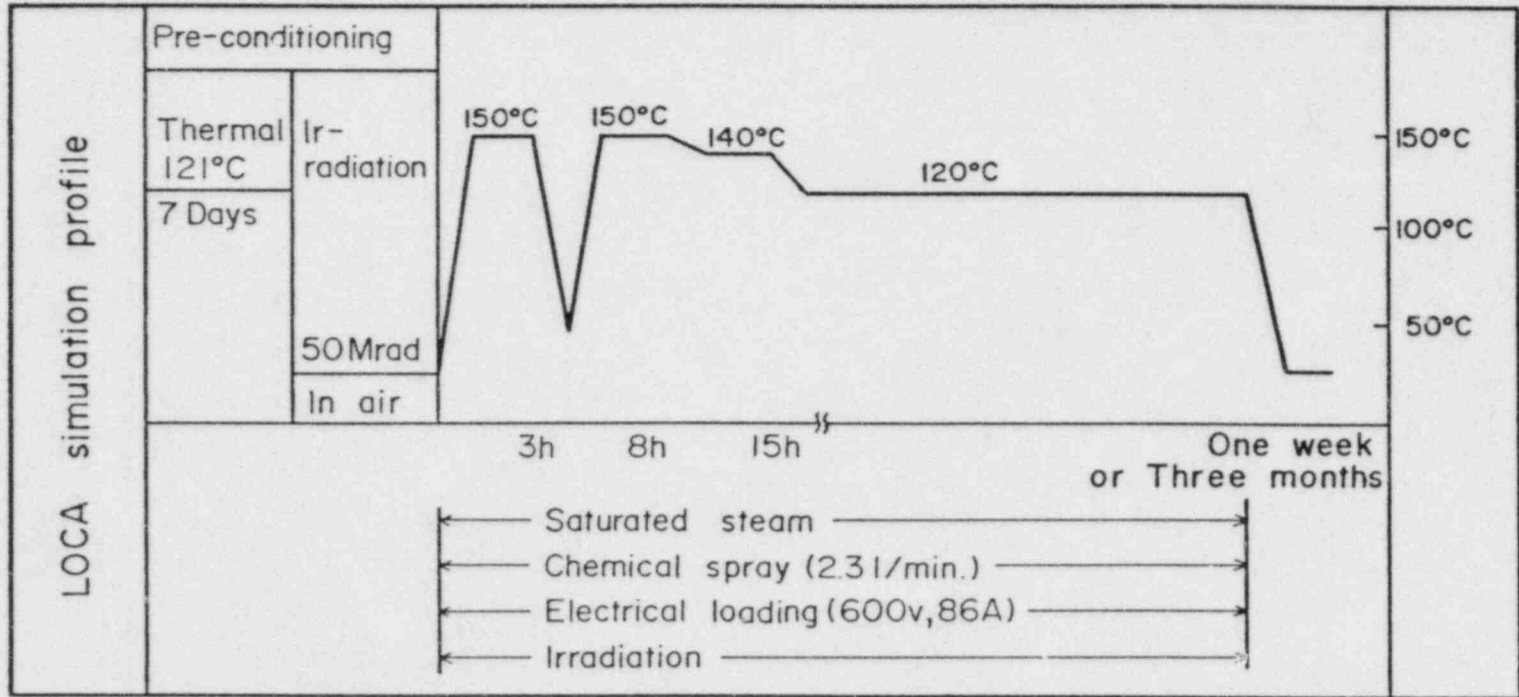
Fig.2 Ultimate tensile elongation of EPR-A as a
function of dose   under LOCA condition.

354

Fig.3 Relative tensile strength at break of EPR-A
as a function of dose under LOCA condition.
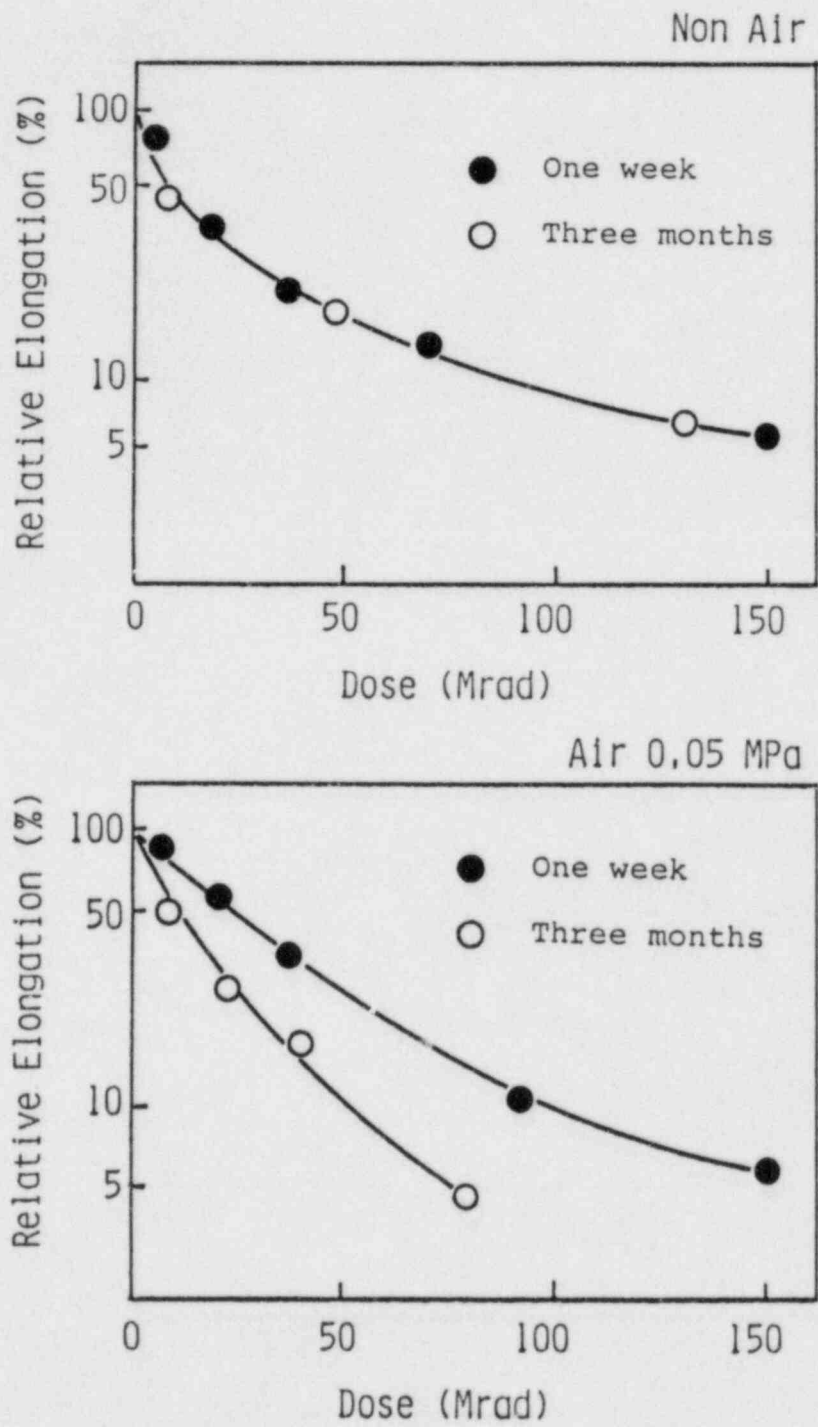
Fig.4 Ultimate tensile elongation of EPR-B as a
function of dose   under LOCA condition.
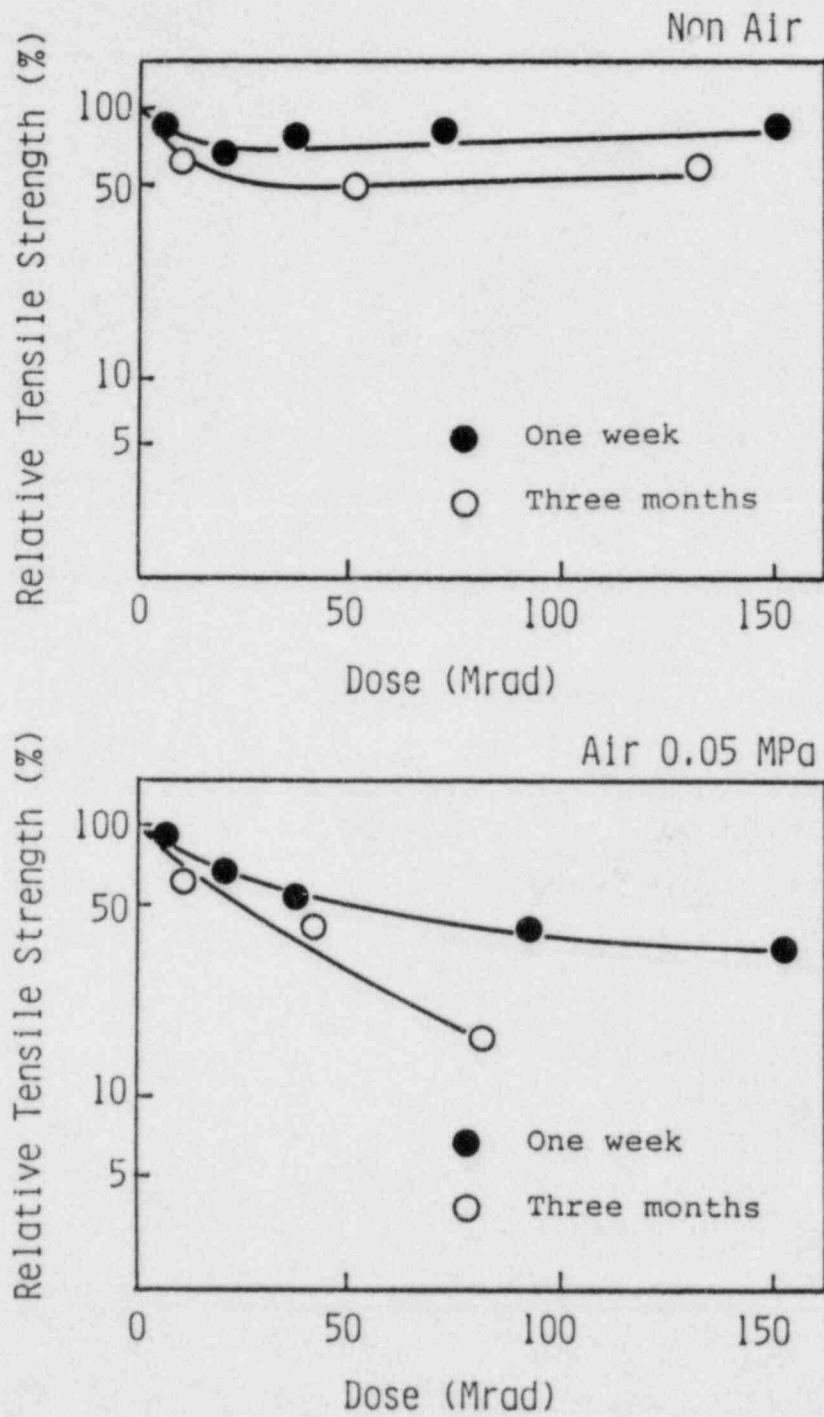
Fig.5 Relative tensile strength at break of EPR-B
as a function of dose under LOCA condition.
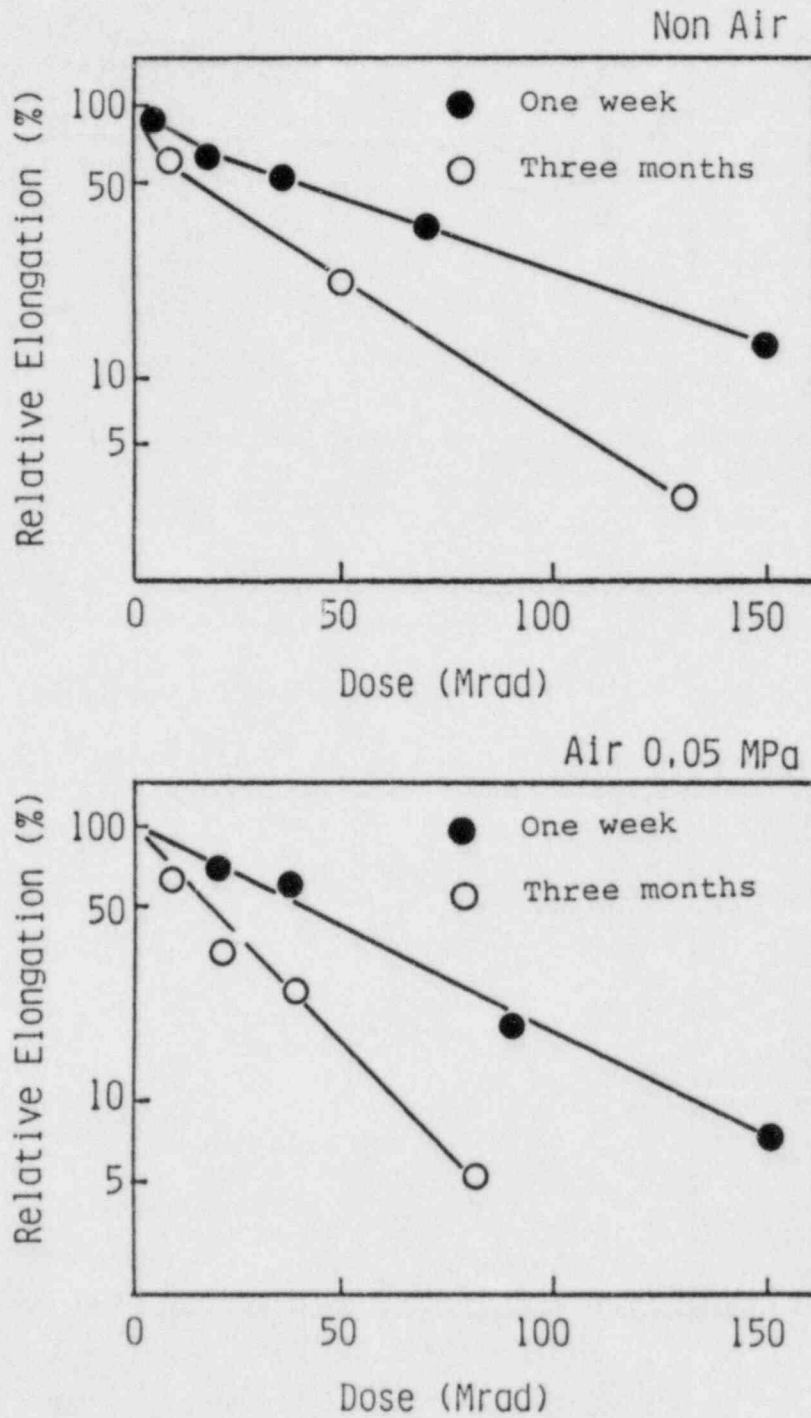
Fig.6 Ultimate tensile elongation of CSPE-A as a
function of dose under LOCA condition.

358
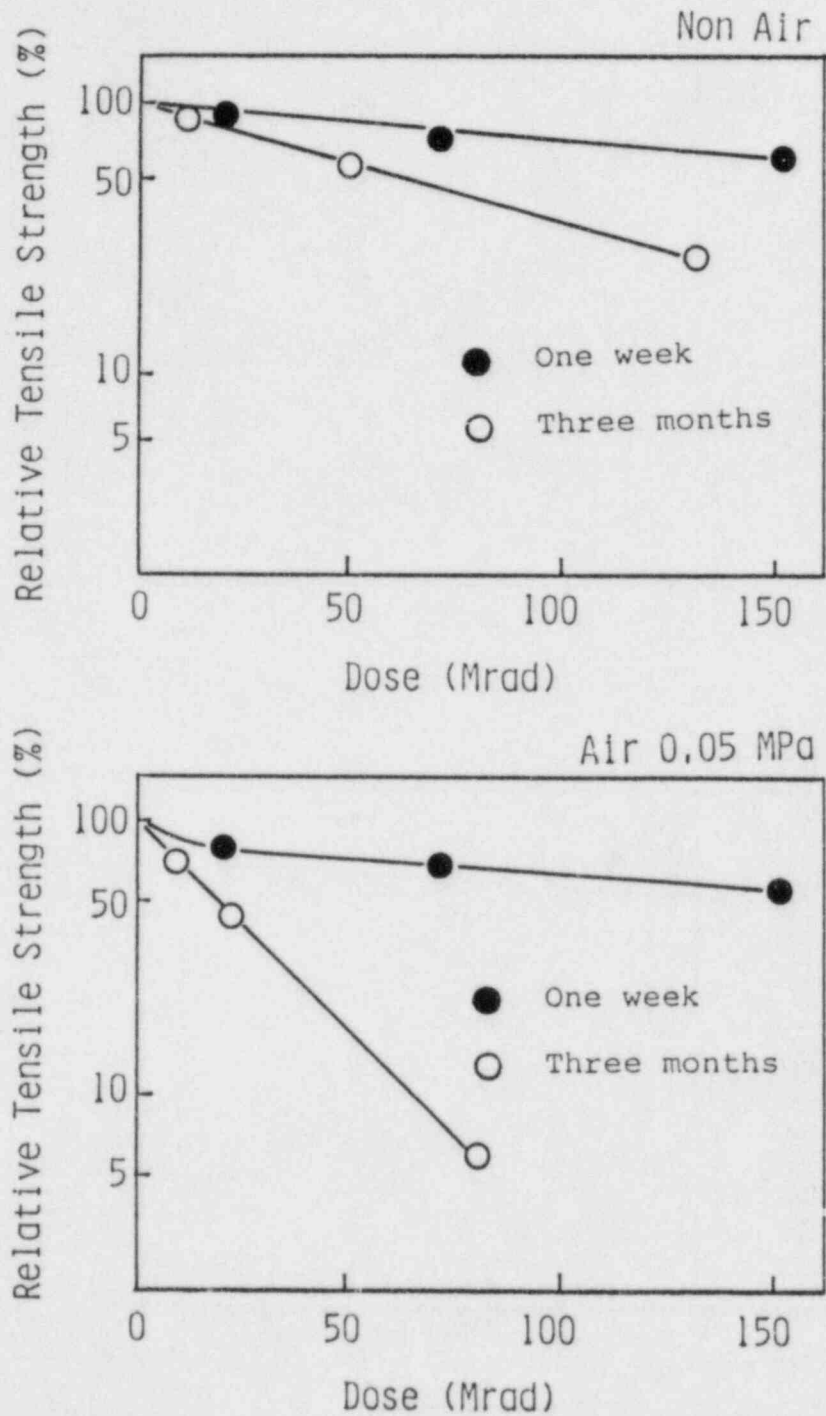
Fig.7 Relative tensile strength at break of CSPE-A
as a function of dose under LOCA condition.
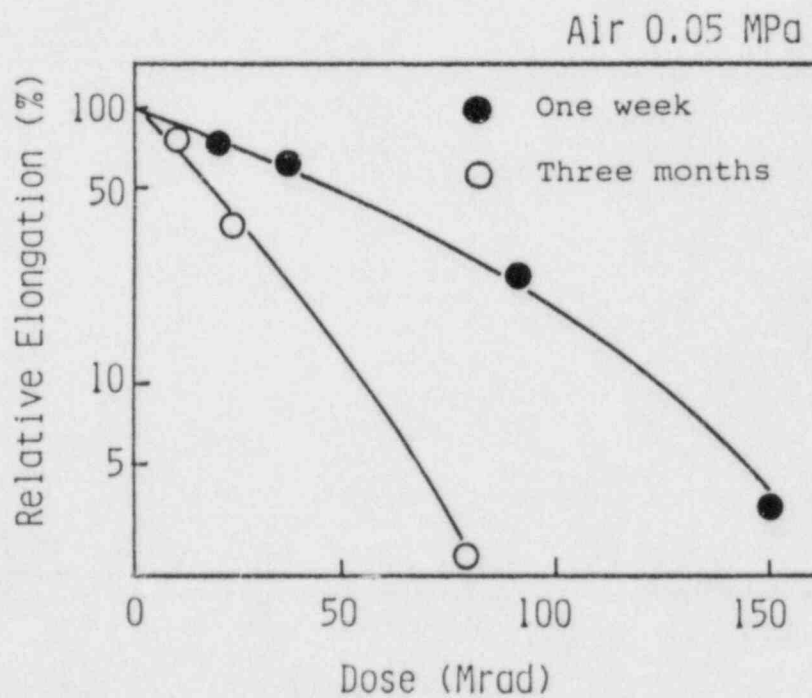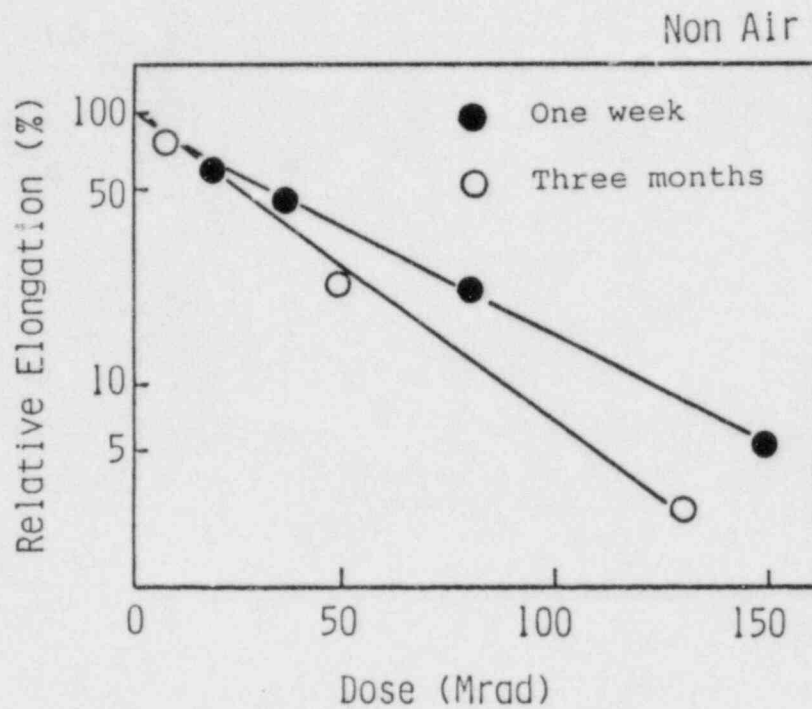
Fig.8 Ultimate tensile elongation of CSPE-B as a function of dose under LOCA condition.

360
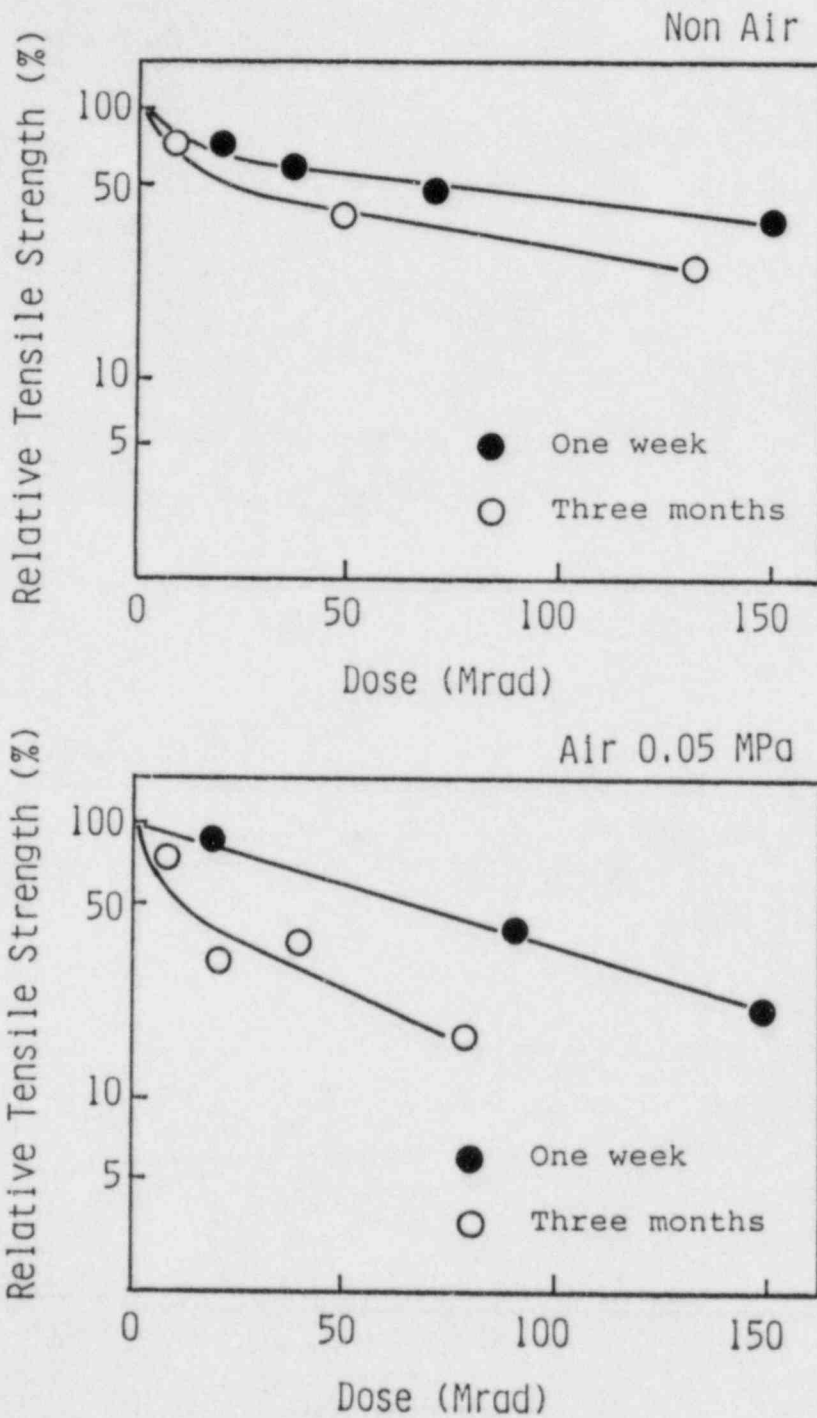
Fig. 9 Relative tensile strength at break of CSPE-B
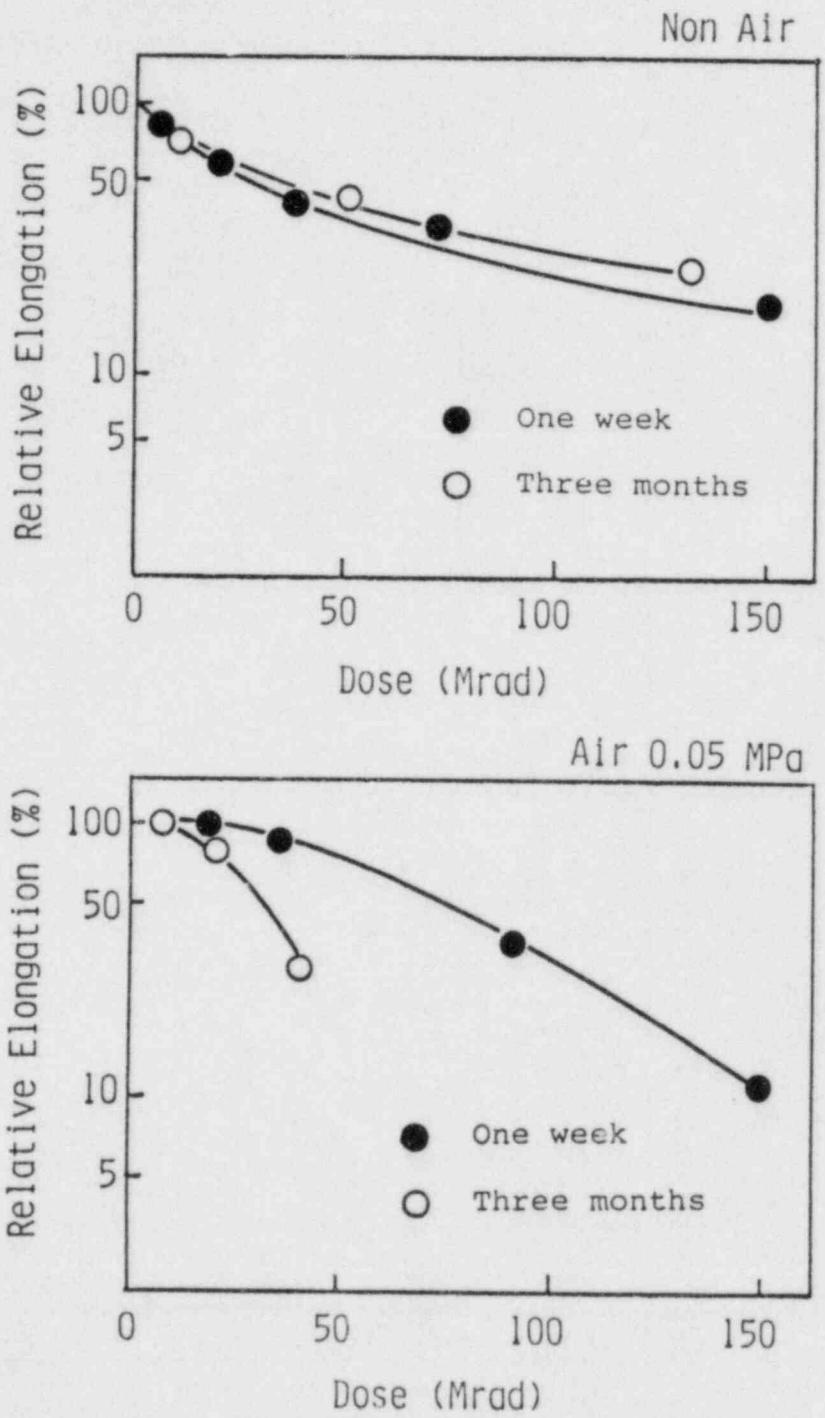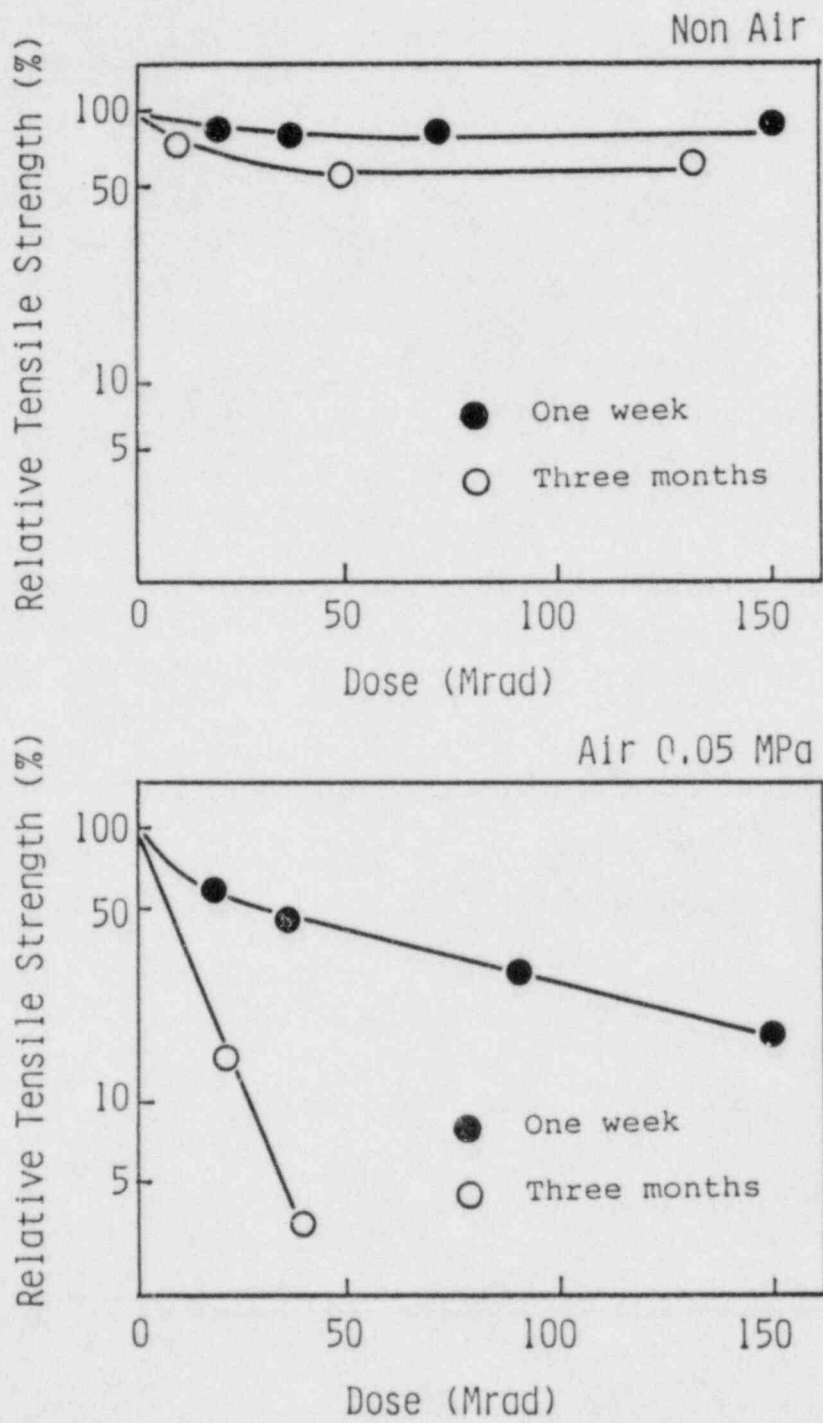as a function of dose under LOCA condition.
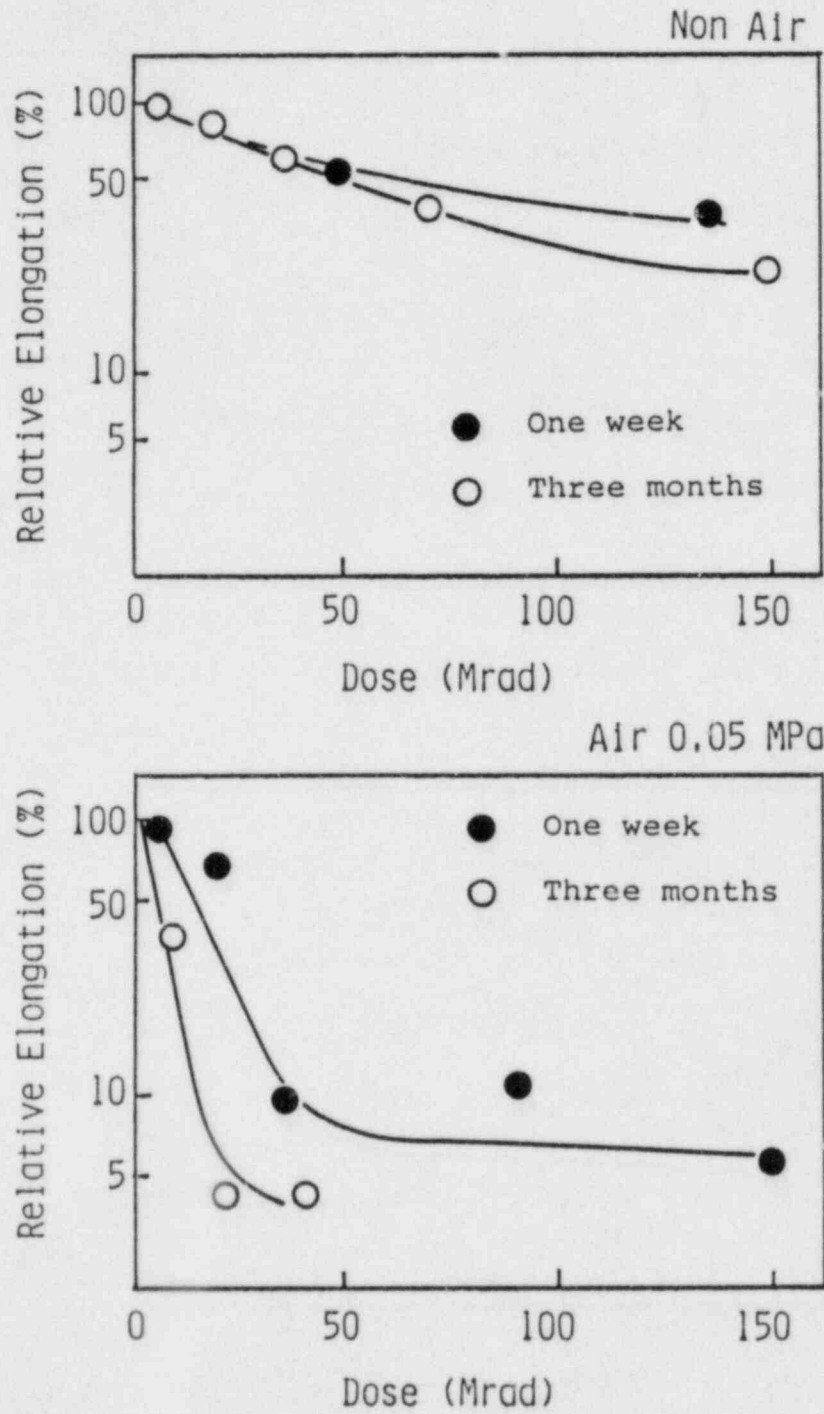
Fig.10 Ultimate tensile elongation of XLPE as a
function of dose   under LOCA condition.
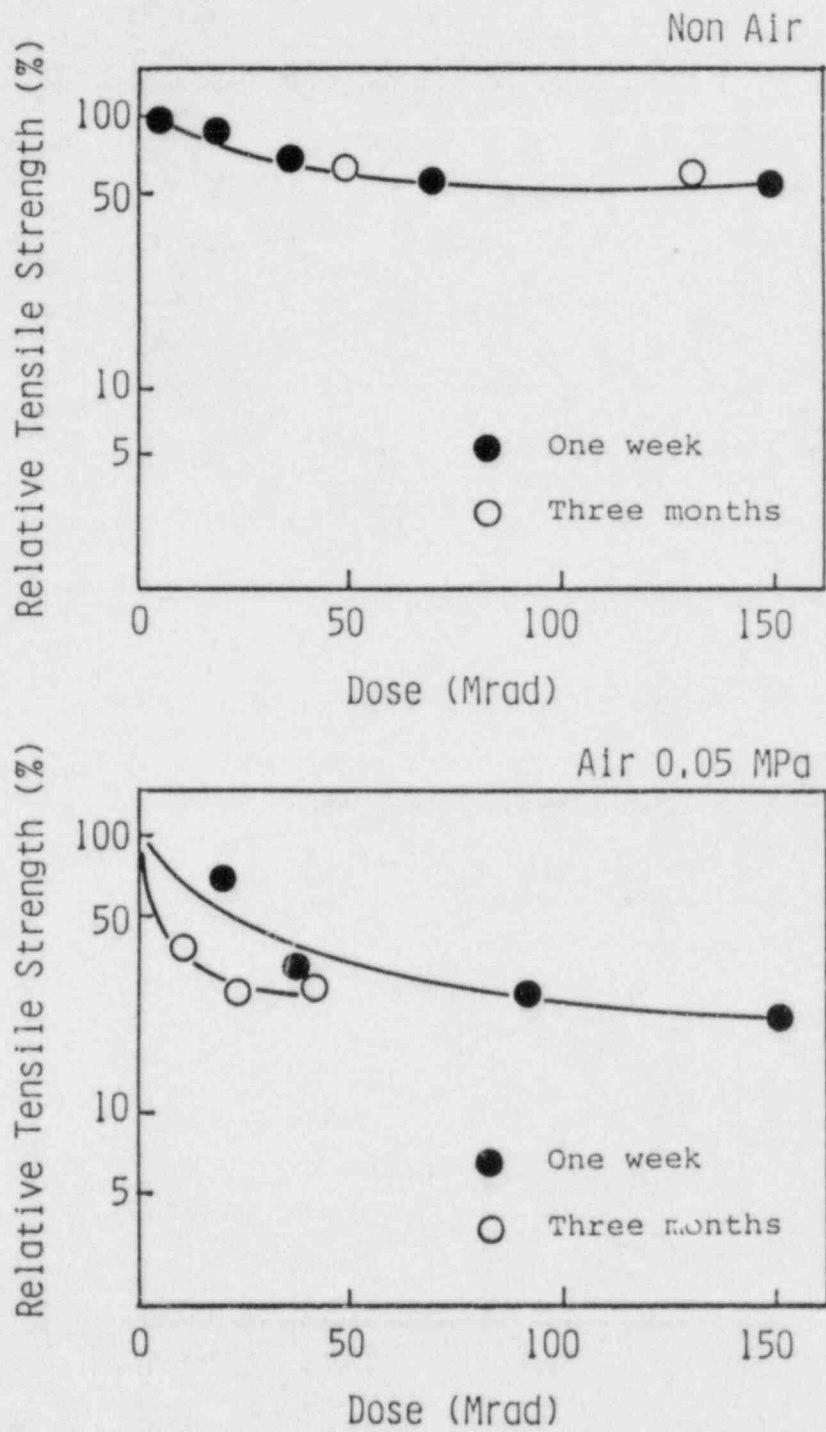
Fig.11 Relative tensile strength at break of XLPE
as a function of dose under LOCA condition.
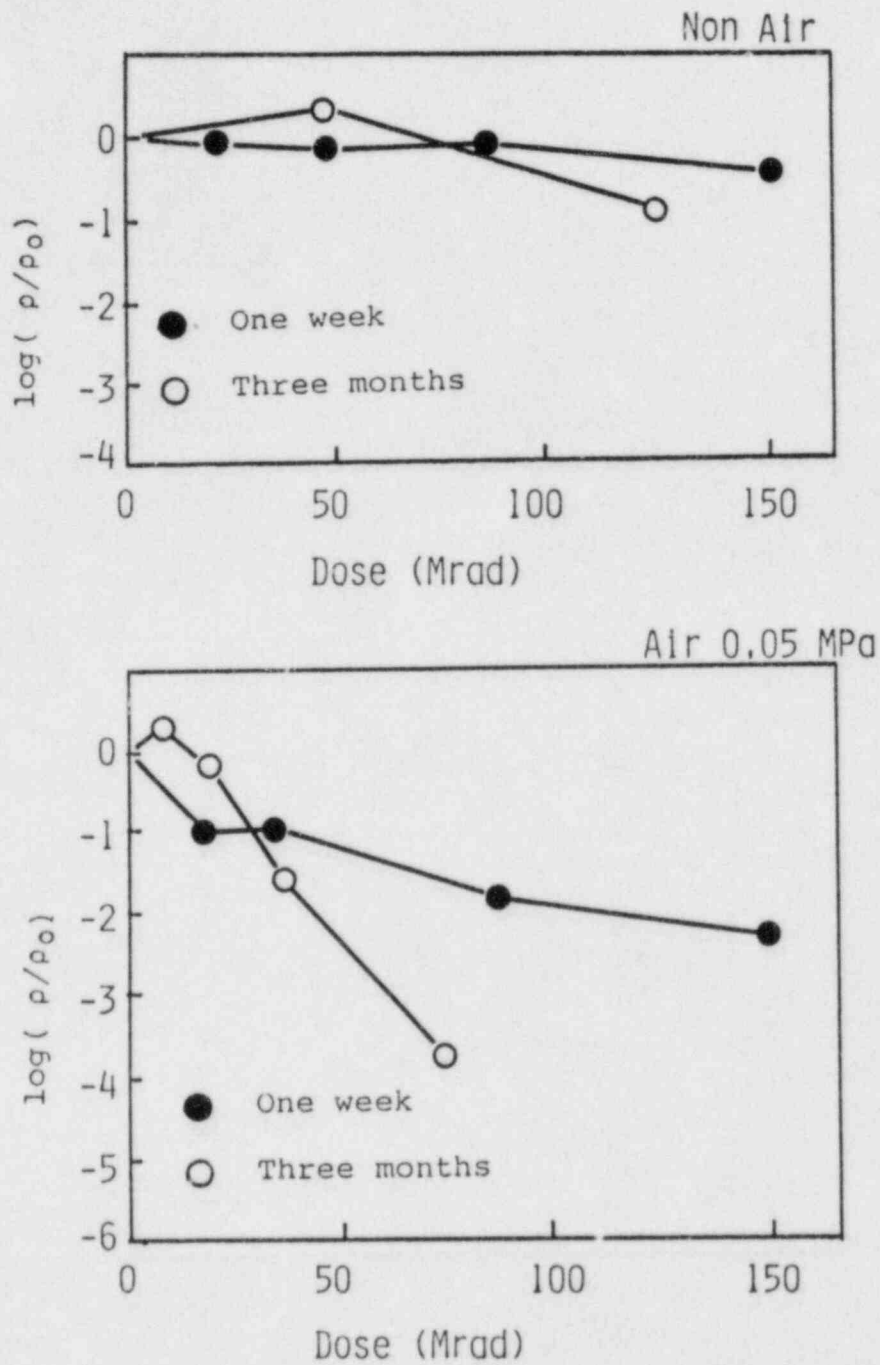
Fig. 12 Relative volume resistivity of EPR-A
   as a function of dose under LOCA
   condition.
   ρ: Volume resistivity.
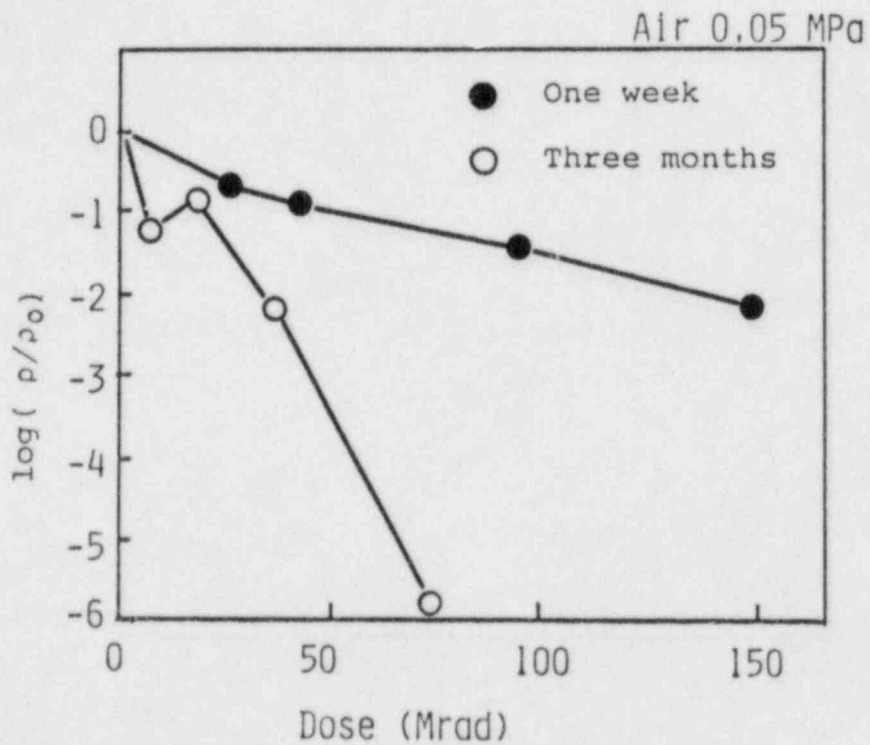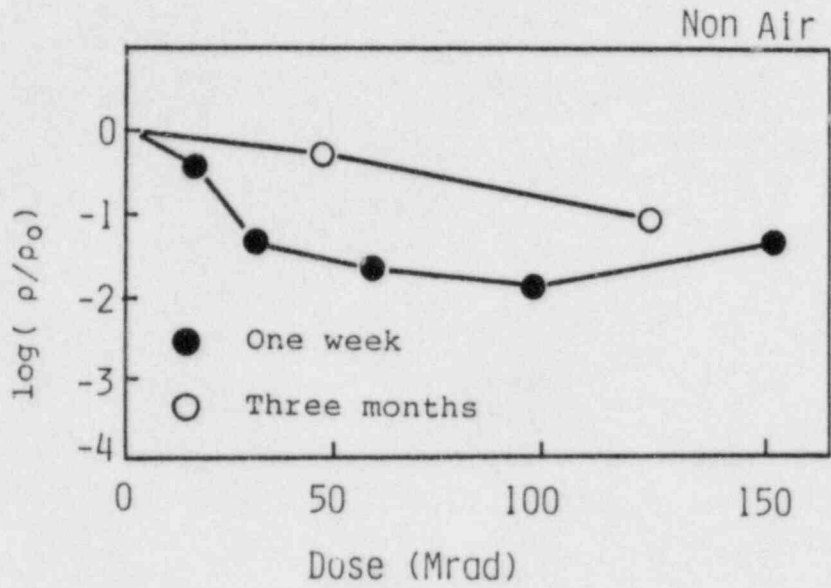
Fig. 13 Relative volume resistivity of EPR-B
as a function of dose under LOCA
condition.

ρ: Volume resistivity.
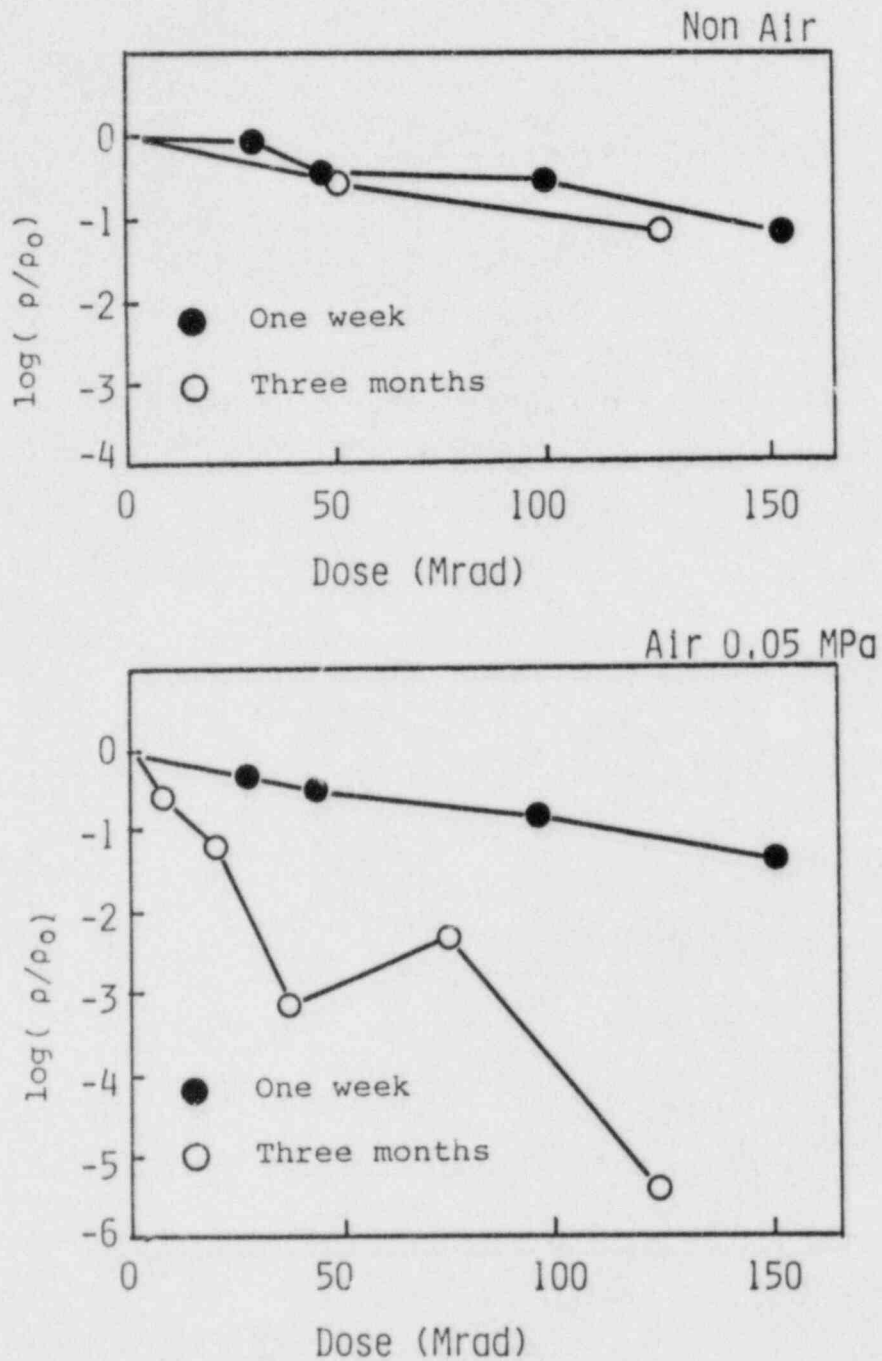
Fig.14 Relative volume resistivity of EPR-C
as a function of dose under LOCA
condition.
ρ: Volume resistivity.

Table 1 Rate of decrease in ultimate elongation
under LOCA condition. (1/100Mrad)

	Non Air		Air 0.05MPa	
Sample	One Week	Three Months	One Week	Three Months
EPR-A	0.40	0.40	0.83	1.57
EPR-B	0.46	0.46	0.74	1.46
CSPE-A	0.56	1.00	0.77	1.60
CSPE-B	0.80	1.11	1.09	2.14

Decay curves are taken as Maxwellian.

Table 2 Rate of decrease in volume resistivity
under LOCA condition. (1/100 Mrad)

	Non Air		Air 0.05MPa	
Sample	One Week	Three Months	One Week	Three Months
EPR-A	<1.0	<1.0	2.2	7.1
EPR-B	<1.0	<1.0	2.2	11.2
EPR-C	<1.0	<1.0	1.3	6.6

Decay curves are taken as Maxwellian.

Fig.15 Insulation Resistance Changes of Electric Cables under LOCA,
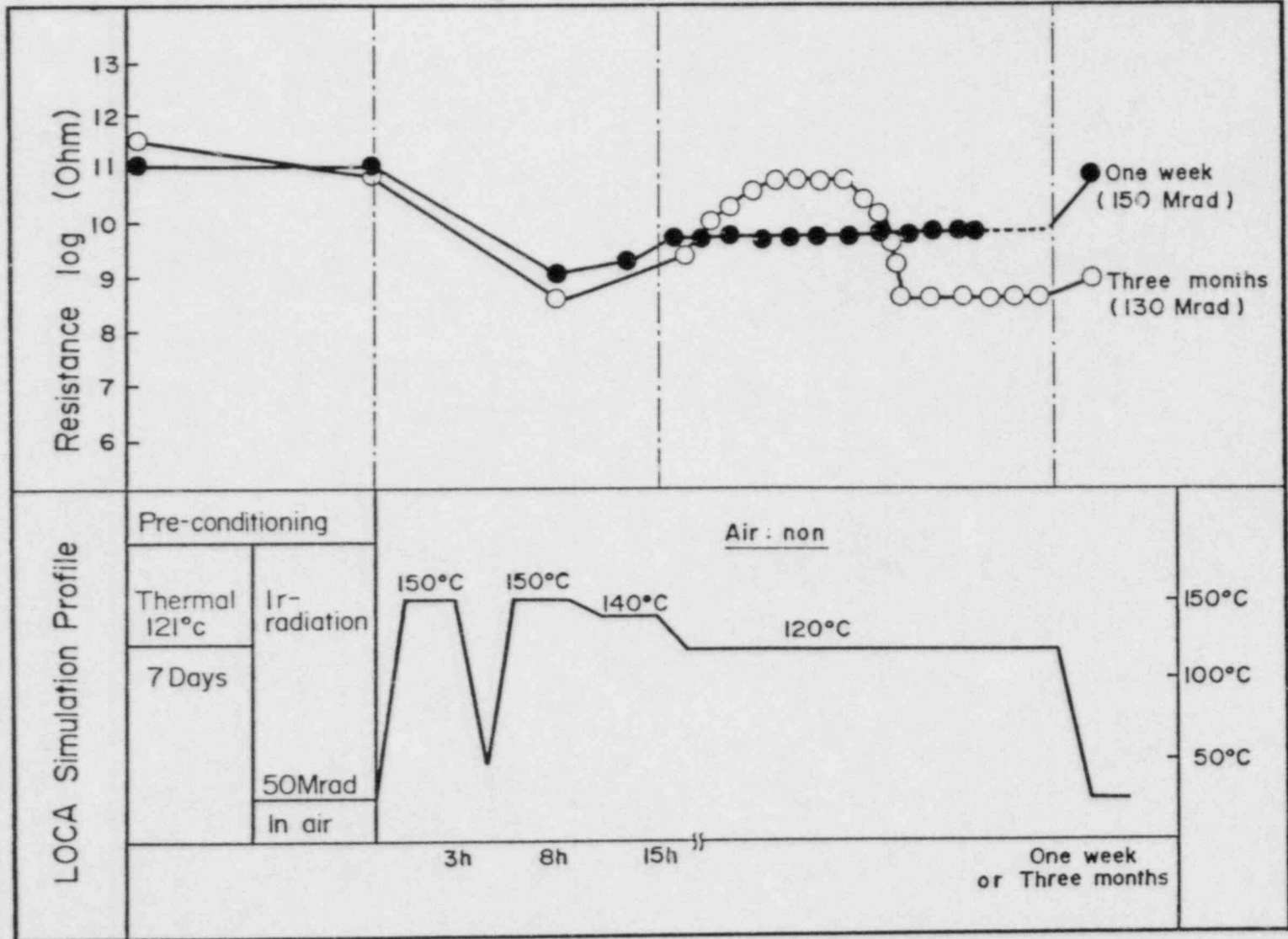
Fig.16 Insulation Resistance Changes of Electric Cables under LOCA,
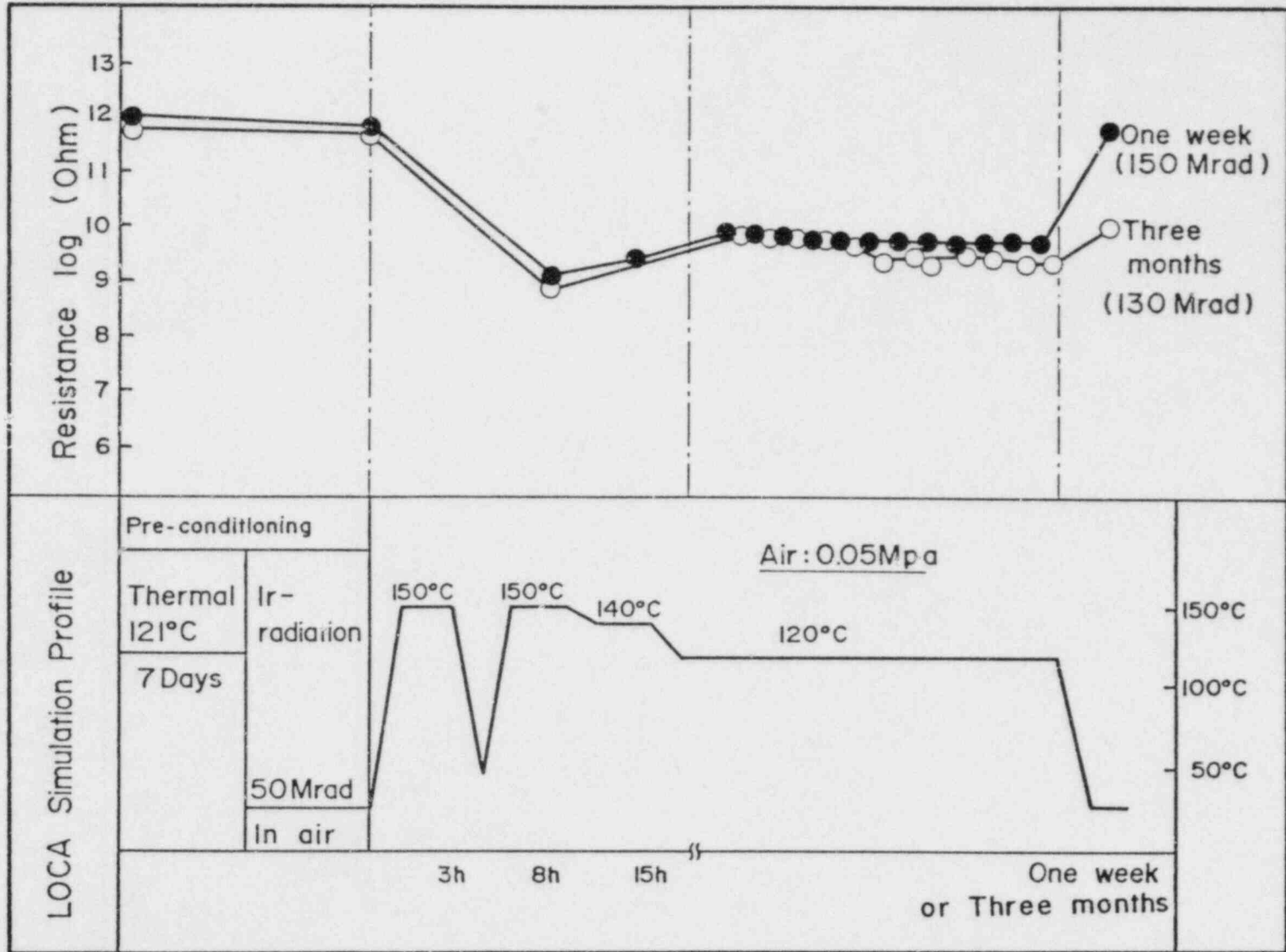
Fig. 17 Insulation Resistance Changes of Electric Cables under LOCA,
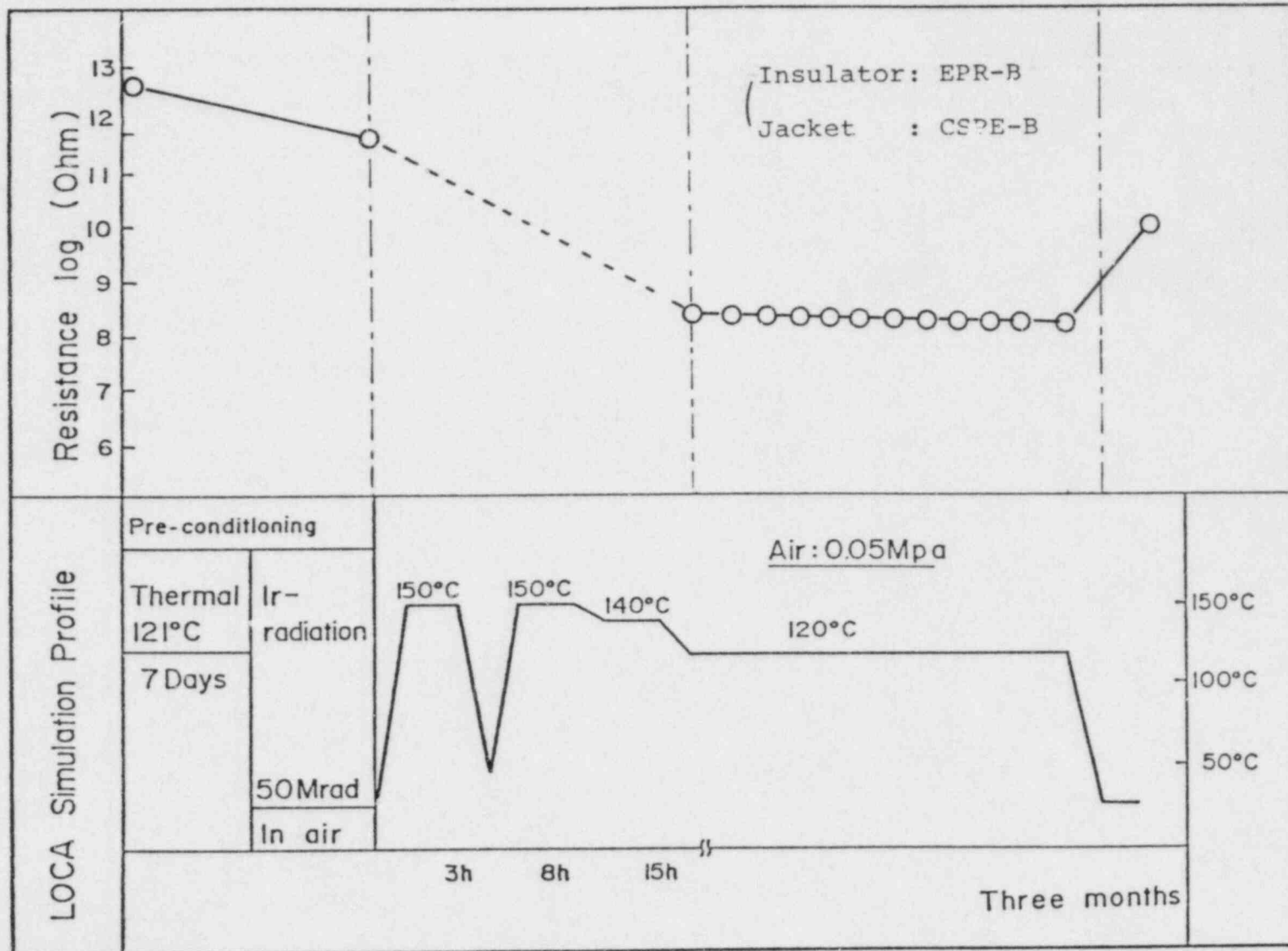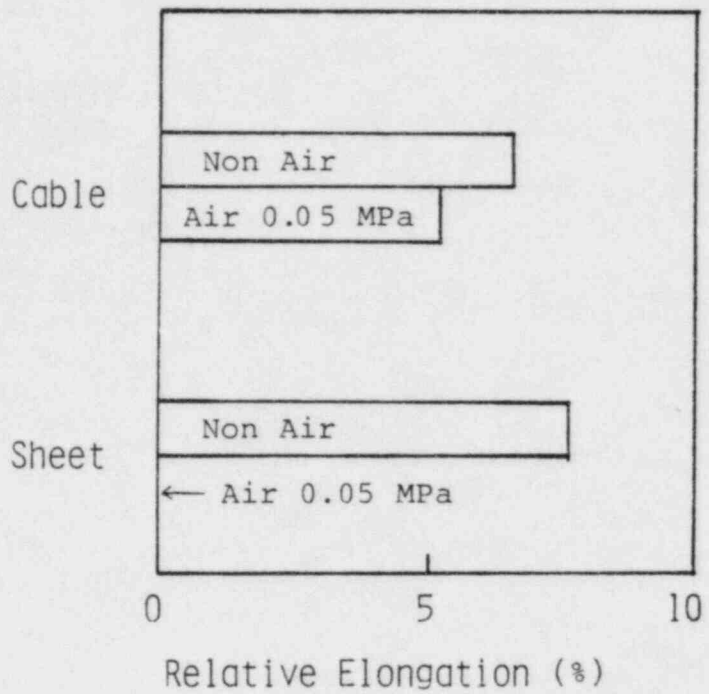
Fig.18 Comparison between degradation
of sheet shape samples and
degradation of cables under
three months LOCA test.

SEISMIC FRAGILITY TESTING OF
NATURALLY-AGED, SAFETY-RELATED, CLASS 1E BATTERY CELLS*

L. L. Bonzon
D. B. Hente

Sandia National Laboratories
Albuquerque, NM 87185

Bharat M. Kukreti   James D. Tulk
Jerry Schendel   W. John Janis
David A. Black   Brian D. Aucoin
Gordon D. Paulsen

Ontario Hydro
Toronto, Ontario, Canada

BACKGROUND

The concern over seismic susceptibility of naturally-aged lead-acid batteries used for safety-related emergency power in nuclear power stations was brought about by battery problems that periodically had been reported in Licensee Event Reports (LERs). The Turkey Point Station had reported cracked and buckled plates in several cells in October, 1974 (LER 75-5).[1] The Fitzpatrick Station had reported cracked battery cell cases in October, 1977 (LER 77-55)[2] and again in September, 1979 (LER 79-59).[3] The Browns Ferry Station had reported a cracked cell leaking a small quantity of electrolyte in July, 1981 (LER 81-42).[4] The Indian Point Station had reported cracked and leaking cells in both February (LER 82-7)[5] and April, 1982 (LER 82-16);[6] both of these LERs indicated the cracked cells were due to expansion (i.e., growth) of the positive plates.

Similar problems at the Connecticut Yankee Station in June and September, 1982 (LER 82-6)[7] prompted the NRC staff to conduct a general investigation which included a visit to Connecticut Yankee and discussions with manufacturers of Class 1E** batteries. The visit revealed a number of cells with case cracks which were attributed to swelling of the positive plates. This swelling or growth of positive plates has always been reported as typical of aged battery cells. (Also associated with aging has been the embrittlement and cracking of the lead plates and the sloughing of plate material.) A report of the investigation by NRC staff concluded that aged batteries may be vulnerable to common-mode failure because of a seismic event.[8] Such a seismic event, even a relatively mild one, could cause otherwise electrically acceptable batteries to suffer plate or cell cracking or shorting due to the sloughing of plate material.

The report[8] also concluded that the existing technical specifications for surveillance are designed to ensure the availability of sufficient battery capacity without regard to the effect of a seismic event on an aged battery. To make nuclear power plant personnel aware of the findings, the NRC Office of Inspection and Enforcement issued Information Notice 83-11, "Possible Seismic Vulnerability of Old Lead Storage Batteries" on March 14, 1983.[9] The notice provided the circumstances which led to the concern of the NRC regarding the potential vulnerability of aged batteries to a seismic event and gave possible reasons for a battery to undergo accelerated aging.

There is no information available on how the battery cells identified in the LERs would have responded to a seismic event (or performed their electrical function) just prior to their replacement. There is, however, a general belief that the electrical life of these type of battery cells is longer than their "seismic" life. That is because past experience with aged batteries has shown the cells will pass all their surveillance requirements, meet all technical specifications, and provide adequate capacity after it appears the plates are too embrittled to survive a mild seismic test.[10]

PROGRAMMATIC PERSPECTIVE

In response to the increasing NRC staff concern over aged-battery behavior in seismic events, the NRC-sponsored Qualification Testing Evaluation (QTE) research program [11] initiated

---

** Class 1E is the safety-class designation as defined in IEEE 323-1974.

an effort to evaluate the adequacy of batteries to survive a seismic event. It has a two-fold goal: to determine actual failure modes and thresholds, and to determine the validity of using the electrical capacity of individual cells as an indicator of the "end-of-life" of a battery, given a seismic event. The choice of nuclear station batteries as the equipment for evaluation was supported by two other specific developments.

First, Sandia National Laboratories (SNL) staff were made aware of a 1977 Ontario Hydro test report[12] in which results of seismic fragility tests on naturally-aged batteries showed that a 9-year battery cell and a 16-year old battery cell showed differences in failure threshold. While the data was sparse, age-related effects were indicated.

Second, naturally-aged battery cells became available to SNL from the decommissioned Shippingport Station. This, in turn, prompted a search for naturally-aged batteries more typical of those currently used in U. S. nuclear power stations.

The first test program of a more extensive testing effort involved the use of 12-year old lead-calcium Gould NCX-2250 battery cells from the James A. Fitzpatrick Nuclear Power Station.[13] The cells were seismically tested in three different cell configurations on a triaxial shaker table: (1) single-cell tests with rigidly mounted, electrically active cells; (2) multi-cell (three) tests mounted in a typical battery rack with one or more cells electrically active; and (3) single cell tests with both rigidly and "loosely mounted," non-active cells. The purpose of the first and second series of tests was to determine the electrical fragility level of the cells. This was done by monitoring the electrical properties and discharge capacity of the cells through a graduated series of g-level step increases until either the shake-table limits were reached or the cells failed. The third series of tests was used to examine the propagation of pre-existing case cracks, again by exposing the cells to increasing g-levels.

This paper describes the conditioning of the cells and their seismic-fragility testing, and discusses the test results and subsequent cell and materials analyses.

CELL RECEIPT AND CONDITIONING

The first lead-calcium cells obtained – 20 in number – came from the James A. Fitzpatrick Nuclear Station through the courtesy of the New York Power Authority; the cells were 12-year old Gould NCX-2250s. They were sent to Ontario Hydro in Toronto, Canada, for conditioning and seismic testing.

Of the 20 cells sent to Ontario Hydro, six were crazed and had cracks in them so they were shipped without electrolyte; these were used for subsequent crack propagation tests as were three other cells that developed leaks during transit (Figure 1). The results of an inspection of the cells and a measurement of their specific gravity upon arrival is shown in Table 1. Water and electrolyte were added to cells 12 and 13 and along with the other nine cells with electrolyte, placed on an equalizing and then a float charge at 2.25 and 2.15 volts per cells, respectively (Figure 2). Cells were also placed on float charge prior to, and between, capacity tests to minimize capacity loss through self-discharge.
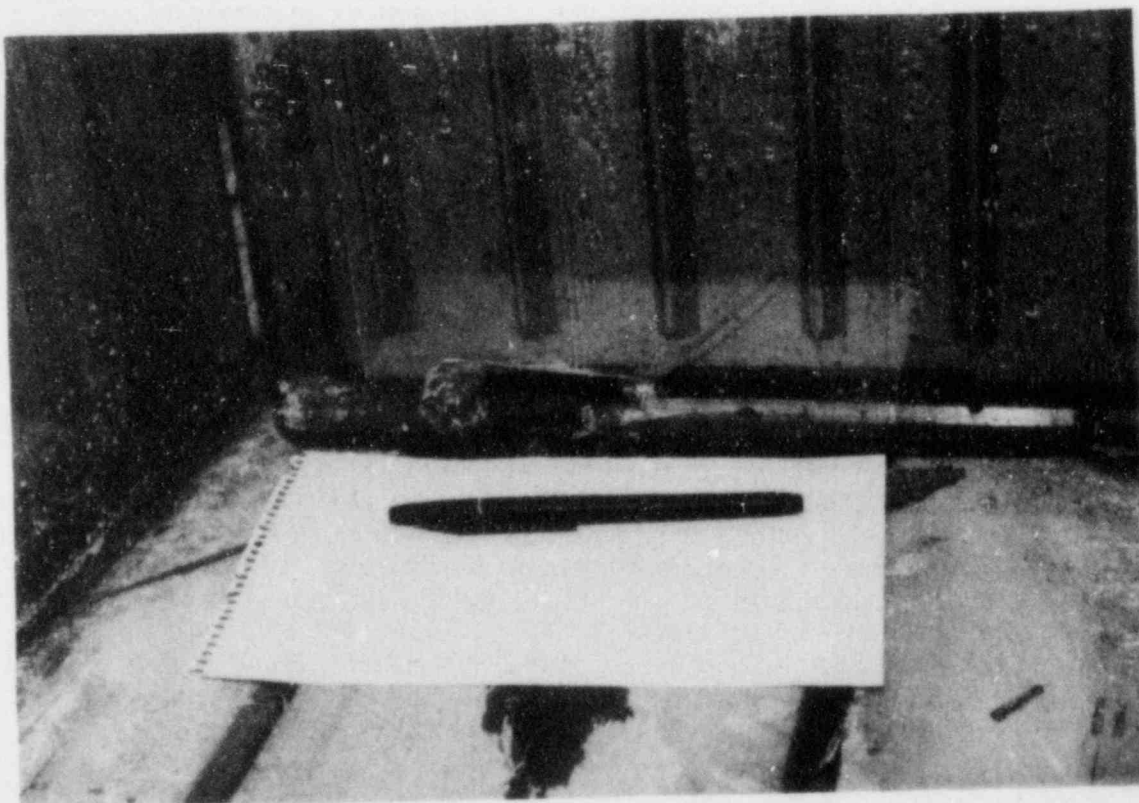
FIGURE 1
Punctured Battery Cell Case

TABLE 1

Cell Inspection Record

Fitzpatrick Cell ID Number	Gould Serial Number	Specific Gravity		Observations
		In Plant (1983)	As Received at OHRD	
3	00155	1.230	1.194	No visible damage
6	K1148	1.232	1.205	No visible damage
7	00154	1.228	1.195	No visible damage
8	K74	1.238	1.209	No visible damage
9*	00024	-	-	No electrolyte but no visible damage
12	00130	1.236	N/A**	Slightly low electrolyte level
13	00144	1.232	N/A**	Slightly low electrolyte level
14	00022	1.230	1.195	No visible damage
15*	00158	-	-	No electrolyte but no visible damage
16***	00177	-	-	No electrolyte - cracked seam
17***	00167	-	-	No electrolyte - large hole in base
22	K1149	1.230	1.210	No visible damage
23	C0152	1.238	1.200	No visible damage
24*	00156	-	-	No electrolyte - crack at bottom corner
25***	00143	-	-	Leaking - crack on bottom
30*	00014	-	-	No electrolyte but no visible damage
42*	00135	-	-	Little electrolyte -crack on bottom
43	00141	1.230	1.194	No visible damage
48	00032	1.236	1.200	No visible damage
49*	00181	-	-	No electrolyte but No visible damage

*   Cells shipped without electrolyte.

**   Electrolyte level too low for accurate determination.

*** Developed leaks during transit (no measurements of transportation shocks were made during transit).
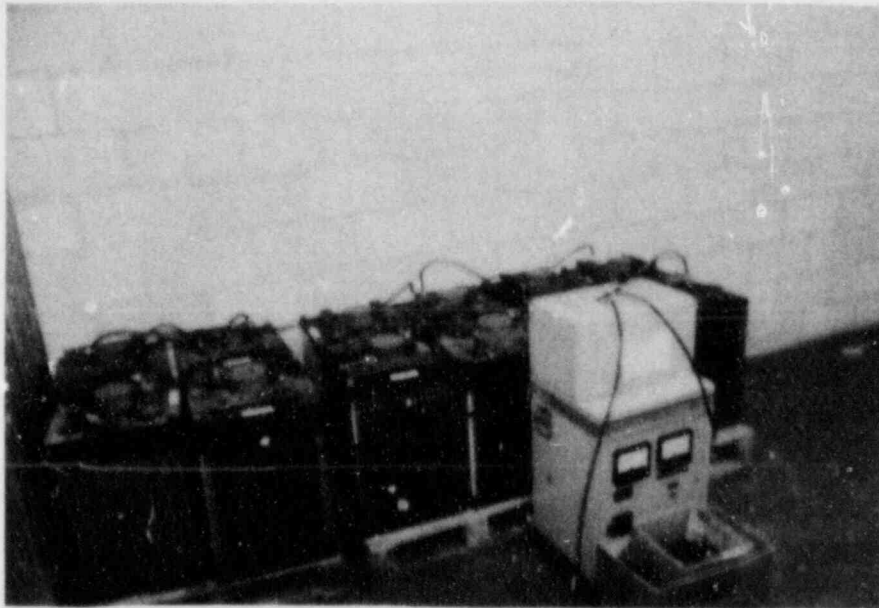
FIGURE 2
Naturally-Aged Cells on Float Charge

While on float, the specific gravity of the cells was maintained
between 1.200 and 1.220, corrected to 25°C per IEEE Standard
450-1980. In addition, the cell voltage, electrolyte level and
temperature were monitored and adjusted as necessary to maintain
the cells in a serviceable condition.

Following this cell conditioning and a minimum of 24 hours on a
float charge, the 11 active cells were discharged at the manu-
facturer's specified 3-hour rate to a final cell potential of
1.75 volts per cell. These discharge tests provided the bench-
mark capacity data for the cells which were used for comparison
in the subsequent seismic testing. The capacity data is shown
in Table 2. The discharged cells were then recharged at a
potential of 2.25 volts for 35 to 70 hours and then placed on a
sustained float charge at 2.15 volts until they were subjected
to seismic-fragility tests.

TABLE 2

Capacity Test Data

Cell Number	25°C Gravity Prior to Discharge	Open Circuit Potential (Volts)	Time to 1.75 VPC at 3-h rate of 585 A (minutes)	Percent Rated Capacity at 3-h Rate
3	1.208	2.19	194	108
6	1.213	2.19	173	96
7	1.208	2.20	124	69
8	1.209	2.10	175	97
12	1.190	2.20	176	98
13	1.195	2.20	208	116
14	1.200	2.23	186	103
22	1.213	2.13	175	97
23	1.200	2.10	191	106
43	1.200	2.21	183	102
48	1.200	2.12	183	102

SEISMIC TESTING

The seismic testing was conducted on Ontario Hydro's triaxial shaker table which has a maximum load capacity of 2000 kg and the following limitations in each axis:

Displacement:	152 mm (6 in.)
Velocity:	820 m/s (2690 ft/sec.)
Acceleration:	4g (no load)
	1.6g (fully loaded)

The shaker system consists of generators and hydraulic actuators which provide a random signal to drive the shaker in three directions simultaneously. The signal is filtered to match the frequency content of a typical earthquake. The vibration levels in the three directions are individually controlled by adjusting a "span" potentiometer to give nominally similar levels. The span setting has no significance in itself except the same "span" settings nominally provide equivalent vibration levels. Because of the random signal used though, the vibration or input acceleration is never exactly the same from one test to the next. There is, however, an approximate relationship between "span" settings and maximum acceleration response levels. That relationship is shown in Table 3.

378

TABLE 3

Span Setting	Maximum Acceleration
2	2
3	3
4	4
5	5
6	6
6.8	6.5

A series of three different kinds of seismic tests were
performed on these Gould cells: (1) single-cell tests with
rigidly mounted, electrically active cells (Figure 3); (2) multi-
cell (three) tests mounted in a typical battery rack with one
or two cells electrically active (Figure 4), and (3) single-cell
tests with both rigidly and loosely mounted, non-active cells
(Figure 5). The purpose of the first and second series of tests
was to determine the fragility level of the cells. This was
done by monitoring the electrical properties and discharge ca-
pacity of the cells through a graduated series of g-level step
increases until the shake-table limits were reached or the cells
failed. A discharge rate of 1.5 hours was used during the
seismic testing to simulate a high emergency load service con-
dition. Failure occurred when the cell potential dropped to
1.75 volts. The third series of tests was to examine the prop-
agation of pre-existing case cracks again by exposing the cells
to increasing g-levels.
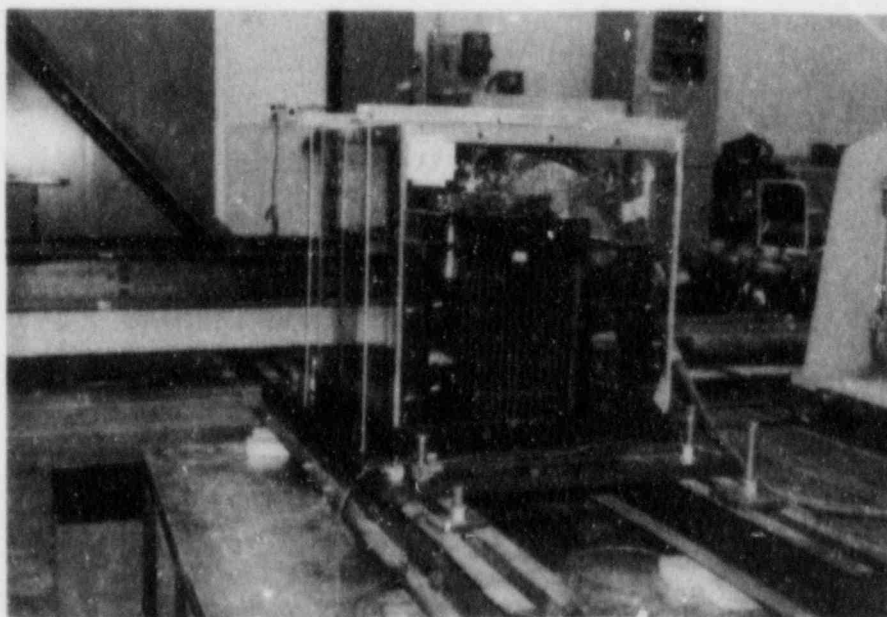
FIGURE 3
Rigidly Mounted Single-Cell Test Configuration
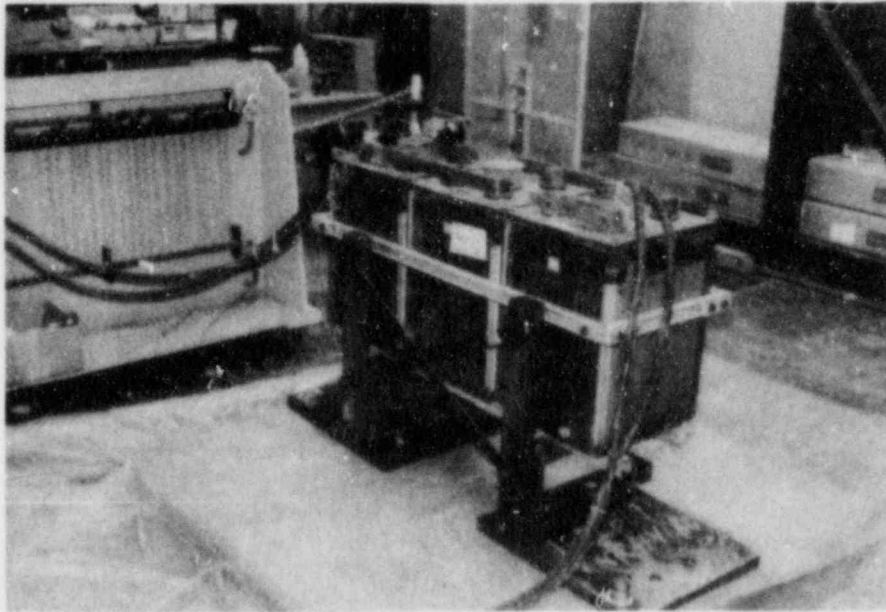
FIGURE 4.
Multi-Cell (Rack) Test Configuration
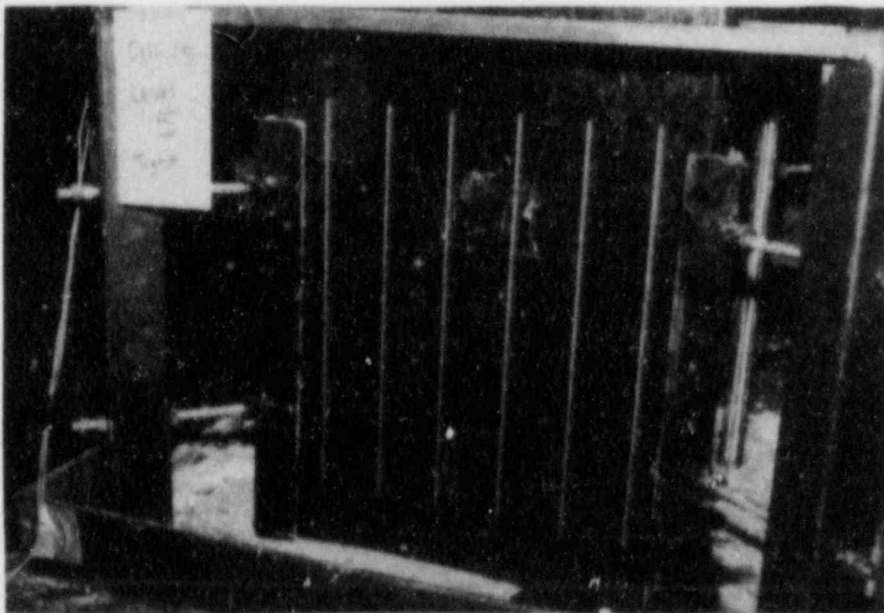
FIGURE 5
Single Cell Crack Propagation Test Configuration

Single-Cell Tests

The g-level responses were recorded by accelerometers mounted on a cell terminal post and on the shake table mounting jig. The results of the single-cell electrical tests are shown in Table 4. The "Best Fit" response levels will be discussed shortly. (It subsequently was learned that cell 48 lost voltage as a result of a loose electrical connection and so the results of testing cell 48 should be disregarded.)

The failure mode in each of the cells that failed electrically was a fracture of the connection between one or both of the positive posts and the bus bars connecting the posts to the positive plates. The details of this failure mode will be presented shortly.

Figures 6 and 7 show the actual response spectrum (in the X axis) of a cell (13) that failed and a cell (6) that survived. As can be seen, there is nothing obviously different that would indicate either failure or survival. What can be seen though is a convenient means to compare the acceleration levels encountered during the various tests - each test spectrum is compared to a normalized spectral shape which is defined in IEEE Standard 501-1978.

This spectral shape is intended to represent the frequency content of a "typical" seismic environment for electrical equipment. According to this representation, the intensity of the simulated seismic motion is expressed in terms of the ZPA (Zero Period Acceleration), i.e., the peak acceleration of a hypothetical oscillator with a natural frequency above 33 Hz. Because a high frequency oscillator is stiff, it will tend to follow the base motion quite closely so that the ZPA effectively represents the peak acceleration of the base.

According to the IEEE 501 Standard, the normalized spectrum curve is to be scaled to lie below the experimental spectrum at all frequencies between 1 and 33 Hz. The dashed lines in Figures 6 and 7 show the normalized IEEE 501 spectra that were scaled to meet this standard. Examination of these figures as well as the results from the other cells reveals that in many instances, the scaling level of the IEEE 501 curve is set by a relatively low level of response at the low end of the frequency scale. As a result, the normalized spectrum may lie substantially below the test spectrum over much of the frequency range. Because the battery cells and racks are relatively stiff structures, with no natural frequencies below 10 Hz, the low frequency component of the shaker motion has little influence on the response of the cells. This means that the normalized curves, for which the scaling level is dominated by low

381

TABLE 4

Single-Cell Electrical Tests

Cell No.	Test Sequence Span Setting	"Best-Fit" ZPA Response Levels-g (x/y/z)	Comments
13	2		
	3		
	4		
	5	1.6/1.9/1.9	-Loss of voltage, considerable loss of electrolyte around terminal posts
	6		
3	2		
	3		-Voltage increased
	4		-Voltage dropped, then recovered
	4		
	5		
	6	1.7/2.0/2.2	-Voltage dropped steadily, below 1.7 V
6	4		
	5		
	6		
	6.8	1.8/2.5/2.2	-No failure
7	4	1.4/1.8/1.8	-Rapid loss of voltage
43	5		
	6	1.6/1.9/2.0	-Loss of voltage to failure
12	5		-Loss of voltage but not to failure
	6	2.0/2.1/2.2	-Loss of voltage but not to failure
	5		-Voltage loss to failure
14	5		
	6		
	6.8	1.9/2.0/2.5	-No failure
48	5	1.3/1.6/1.7	-Cell lost voltage almost as soon as shaking started (loose electrical connection found later)

RESPONSE SPECTRUM
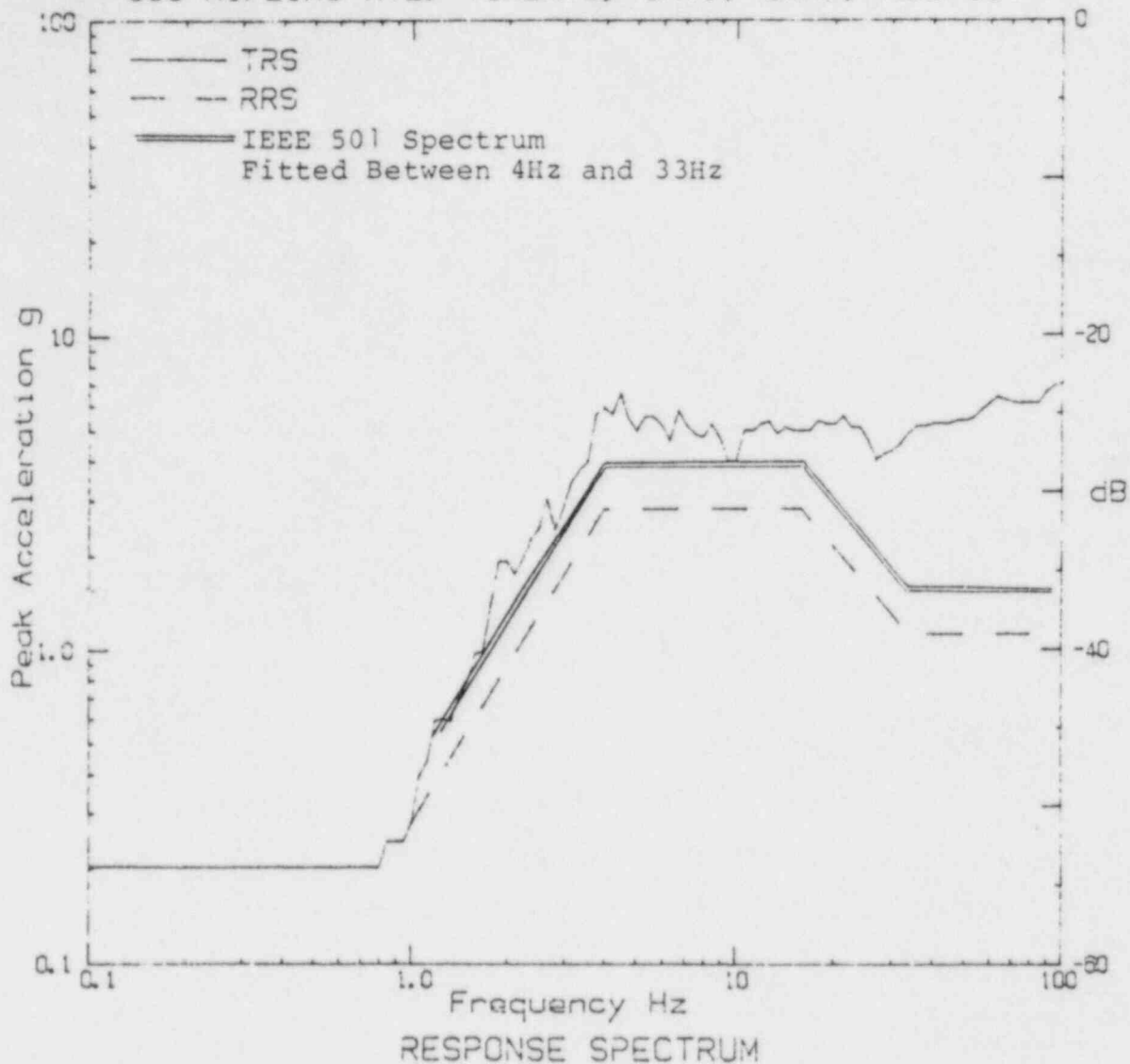
FIGURE 6

TEST ITEM
station calls, Gould, Model NCX 2250, #13

PARTICULARS
Jan 16/84, Time 1:35, Temp('C) 23, Humidity(%) 22, Press (kPa)100.3,
Graph 4963

SPECIFICATIONS
Specs IEEE 501, Conditions operating, 3-hour rate, fragility level

ANALYSIS
Type Maximax, Damping (%)5, B.W.= 1/12 Octaves, Axis X,
Shaker tri-axial, ZPA= 1.6 g

ACCELEROMETER
Wilcoxon, Serial S757, Range d858, Location base-mounting jig,
TT 558, Channel 1

RESPONSE SPECTRUM
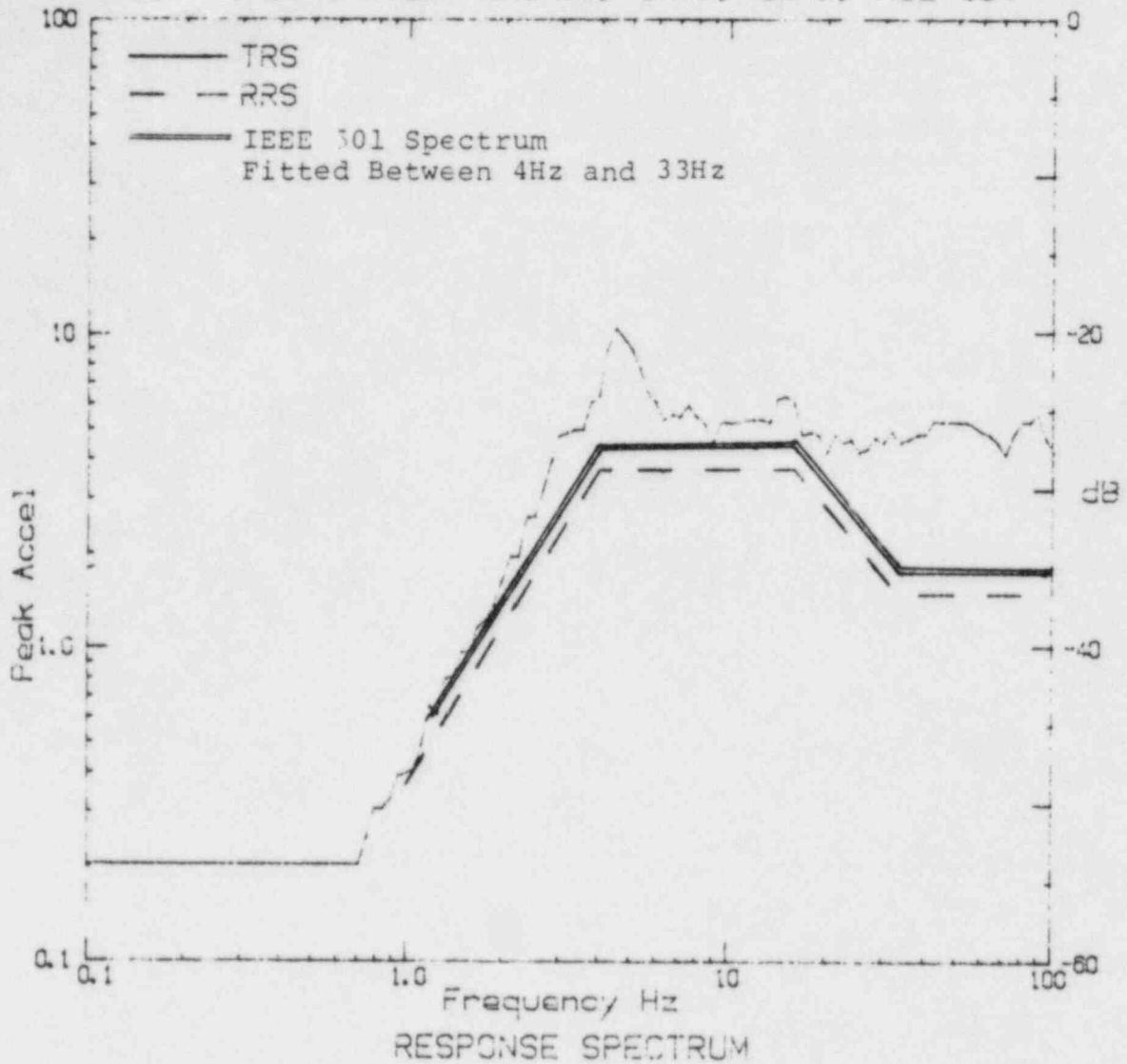
FIGURE 7

ST ITEM
station cells. Gould. Model NCX 2250. #6

PARTICULARS
Jan 16/84. Time 1:20. Temp('C) 23. Humidity(%) 22. Press (kPa)100.3.
Graph 4975

SPECIFICATIONS
Specs IEEE 501. Conditions operating. 8-hour rate. shaker limit

ANALYSIS
Type Maximax. Damping (%)5. B.W.= 1/12 Octaves. Axis X.
Shaker tri-axial. ZPA 1.8g

ACCELEROMETER
Wilcoxon. Serial S757. Range dB58. Location base-mounting jig.
TT 584. Channel 1

frequency response, will not reflect the true acceleration
levels. To provide more meaningful ZPA data, an alternative set
of normalized spectra has been fitted to the experimental data
over the 4 to 33 Hz range. These alternative spectra are shown
as double lines. The response levels shown in Table 4, are ZPA
levels determined for IEEE 501 normalized spectra fitted over
the 4 to 33 Hz range using this "best-fit" approach.

Multi-Cell Tests

The mounting arrangement for the single cell tests was designed
to minimize the possibility of jar failure. This meant that the
tests focused on failure modes of internal components. To
examine the failure modes of cell-to-cell interactions normally
encountered with standard in-plant mounting arrangements, shaker
tests were carried out using a three-cell battery rack based on
the designs for seismically qualified station battery racks as
shown in Figure 4.

The first set of cells tested was selected from the group with
significant pre-existing case cracks. The electrolyte was
replaced with water to reduce the safety hazard in the event of
a jar failure. The electrical connections, including the copper
tie bars, were in place, however. Two failure modes were
observed: cracking on the bottom of one of the end cells,
Figure 8 (subsequently the bottom of this cell broke off), and
lifting of the connecting posts of the middle cell.

FIGURE 8
Simulated Electrolyte Leaking
from a Cracked Battery Cell Case

For the second set of tests, two electrically active cells were used, combined with one water-filled "dummy." Again, the cells were mounted in the rack and electrically interconnected with copper tie bars. The cells were subjected to a series of tests at increasing amplitudes. In this instance, the middle cell failed electrically on the third test due to a fracture of the connection between the posts and the internal positive bus bar. The pre-cracked end cell showed some leakage after this test. The electrical active end cell showed some cracking, but had not failed at the point when the testing stopped.

Table 5 shows the results of the multi-cell testing. Figures 9 and 10 show the response spectra (in the X axis) for a setting of Span 5 for each of the two multi-cell tests.

Crack Propagation Tests

Crack and craze propagation was examined to investigate the integrity of the jar material for those cells with significant prior cracks. The cracks were located on the bottoms of the cells as well as on the sides where the side rails of the battery racks contacted the cells (Figure 11). The side cracks were in the order of 50mm in length and 5mm deep (wall thickness was about 8mm). For testing, the cells were filled with water and neutralized with sodium bicarbonate to reduce the safety hazard. The cells were then shaken to see if any of the cracks in the jars could be made to propagate. For several of the test runs, the clamping mechanism on the support frame was loosened so that the cell was free to move around inside the frame thus increasing the shock loading.

These tests showed that the cracks could be made to grow. However, this required repeated high amplitude shaking. Short and shallow cracks showed little tendency to grow compared to longer, through-wall cracks. Most crack growth occurred when the cells were loose, indicating that much of the damage was done when the cases impacted the restraining frame. The loss of compressive stresses on the jars in the region of the cracks may also have contributed to crack growth. Table 6 summarizes the results of the crack propagation testing.

POST-TEST EVALUATIONS

Subsequent to the seismic fragility testing the two cells that did not fail in the single-cell configuration were subjected to capacity tests and both indicated rated capacity above the accepted standard of 80%; these values were 84% for cell 6 and 87% for cell 14.

TABLE 5

Multi-Cell, Rack-Mounted Tests

Cell No.	Test Sequence Span Setting	"Best Fit" ZPA Response Levels-g (x/y/z)	Comments
49 42, 25			-Test on three water-filled cells. Cells interconnected but no electrical monitoring.
	3		-Some leakage from previously cracked sample
	4		-Some spill from vents
	5	1.4/1.5.0.9	-Some spill from vents -End bar on rack loosened and cells shifted longitudinally
	6	1.5/2.0/1.0	-End cell (49) fractures on lower corner -no apparent previous cracking posts lift on center cell (42)
	6.8		-Bottom of cell 49 breaks off -Posts and bus bar broken on cell 42 -Overall - loosening of bolts on interconnection and frame
30 23, 8			-Cells 23 and 8 filled with electrolyte and loaded electrically
	3		-No apparent damage
	4	1.1/1.3/0.74	-No apparent damage. Frame bolts require retightening.
	5	1.5/1.7/0.93	-Cell 23 fails electrically. -Some jar cracking in cell 30 (water filled)

TRS
RRS
IEEE 501 Spectrum
Fitted Between 4Hz and 33Hz
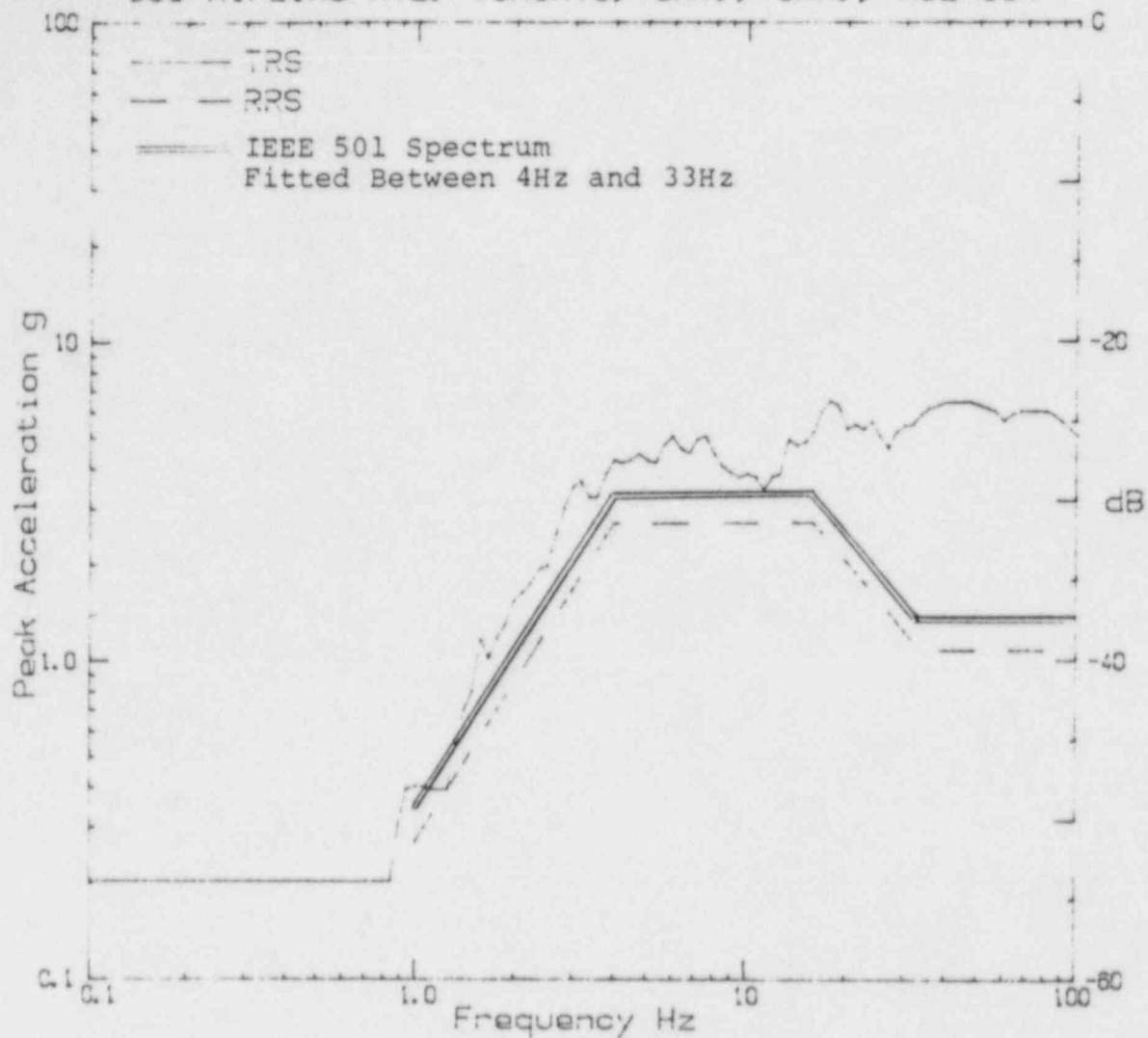
RESPONSE SPECTRUM

FIGURE 9

TEST ITEM
Station Cells & rack. Gould. Model NCX2250 & Gould type rack.
        Part 49; 42; 25

PARTICULARS
March 12/84. Time 10: 46. Temp('C) 24. Humidity(%) 39.
Press (kPa)100.9. Graph 5080

SPECIFICATIONS
Specs IEEE 501. Conditions 3 dummy cells : span 5. fragility level

ANALYSIS
Type Maximax. Damping (%)5. B.W.= 1/12 Octaves. Axis X.
Shaker tri-axial. ZPA =1.4g

ACCELEROMETER
Wilcoxon. Serial S757. Range dB58. Location base-mounting plate.
TT 868. Channel 1

388
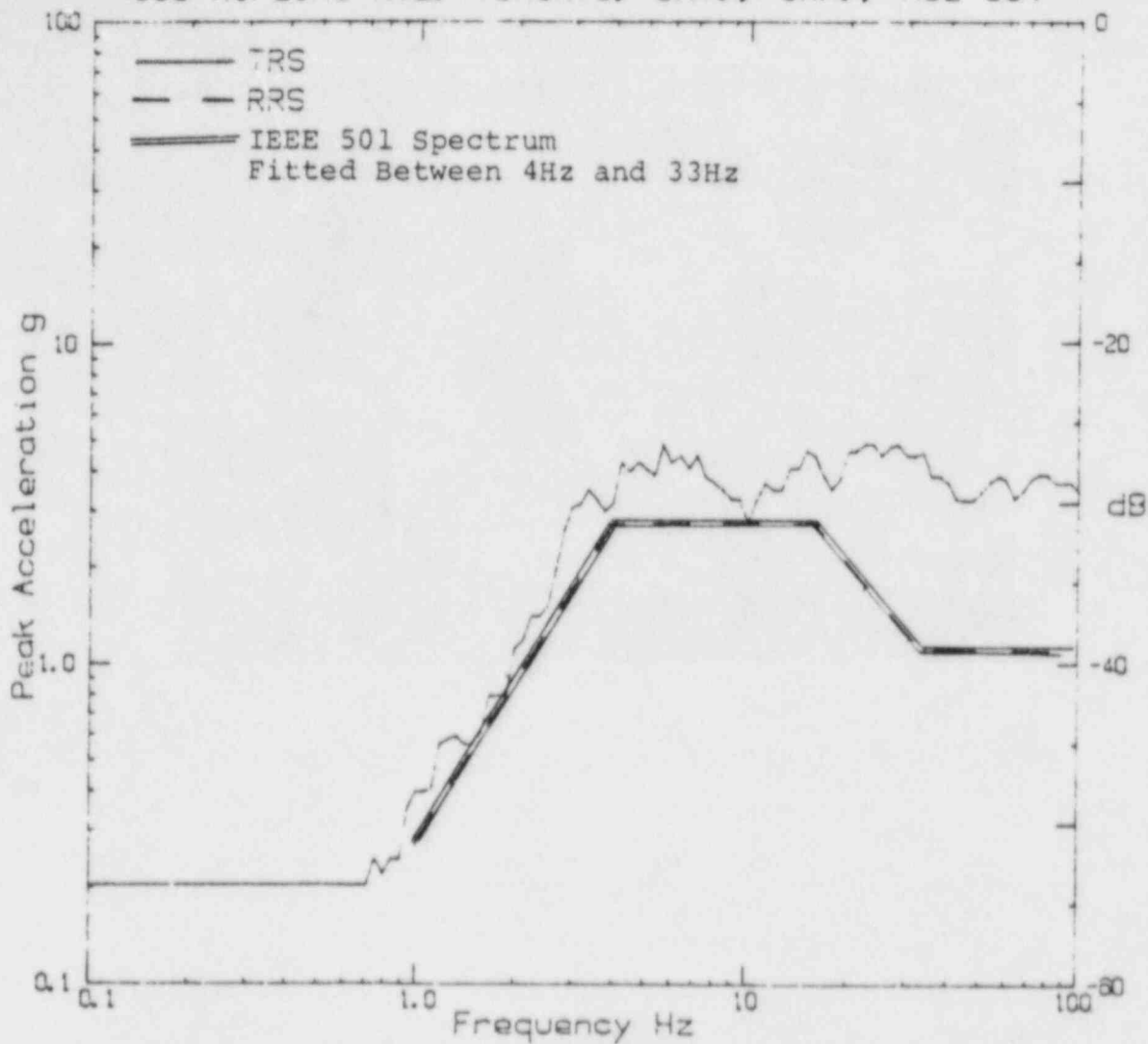
RESPONSE SPECTRUM

FIGURE 10

TEST ITEM
Station Cells & rack, Gould, Model NCX2250 & Gould type rack.
Part cells #30; 23; 8

PARTICULARS
March 12/84, Time 3:42, Temp('C) 24, Humidity(%) 39,
Press (kPa)100.9, Graph 5092, Record 0

SPECIFICATIONS
Specs IEEE 501, Conditions 2 live cells : 1 dummy, fragility level

ANALYSIS
Type Maximax, Damping (%)5, B.W.= 1/12 Octaves, Axis X,
Shaker tri-axial, ZPA=1.1g

ACCELEROMETER
Wilcoxon, Serial S757, Range d858, Location base-mounting plate,
TT 678, Channel 1

389
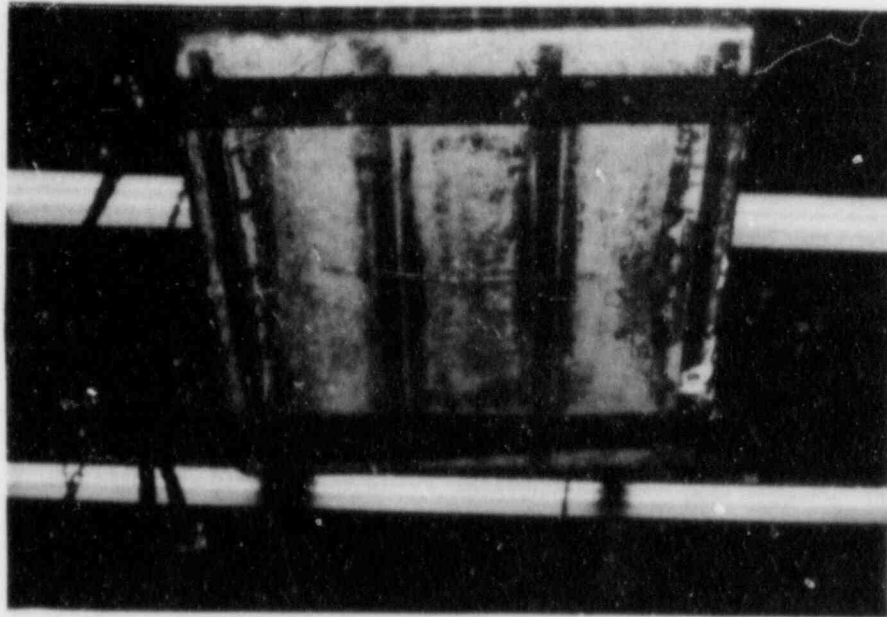
FIGURE 11
Crack on Bottom of Battery Cell Case

TABLE 6

Crack-Propagation Tests

Cell No.	Test Sequence Span Setting	"Best Fit" ZPA Response Levels-g (x/y/z)	Comments
15	3		-Jar clamped in jig -no crack propagation
	4		-Jar clamped -no crack propagation
	4		-Jar loose-sidecrack grew 3mm
	5		-Jar loose -no further cracking
	6		-Jar clamped; 103mm crack grew to 140mm
	6	1.5/2.5/2.3	-Jar clamped; 140mm crack grew to 310mm
25	4		-Jar loose
	5		-Run aborted when clamping bars fell off (repaired, tests continued)
	5		-No apparent crack propagation
	6,8	2.0/3.1/2.2	-No apparent crack propagation

390

Following the post-seismic capacity testing all seismically tested cells were disassembled and inspected for internal damage. Figure 12 shows the placement of cell posts, positive and negative bus bars, and plate connections. All cells that had failed electrically experienced fractures in the connection between the posts and the bus bars supporting the positive plates (Figures 13 and 14).
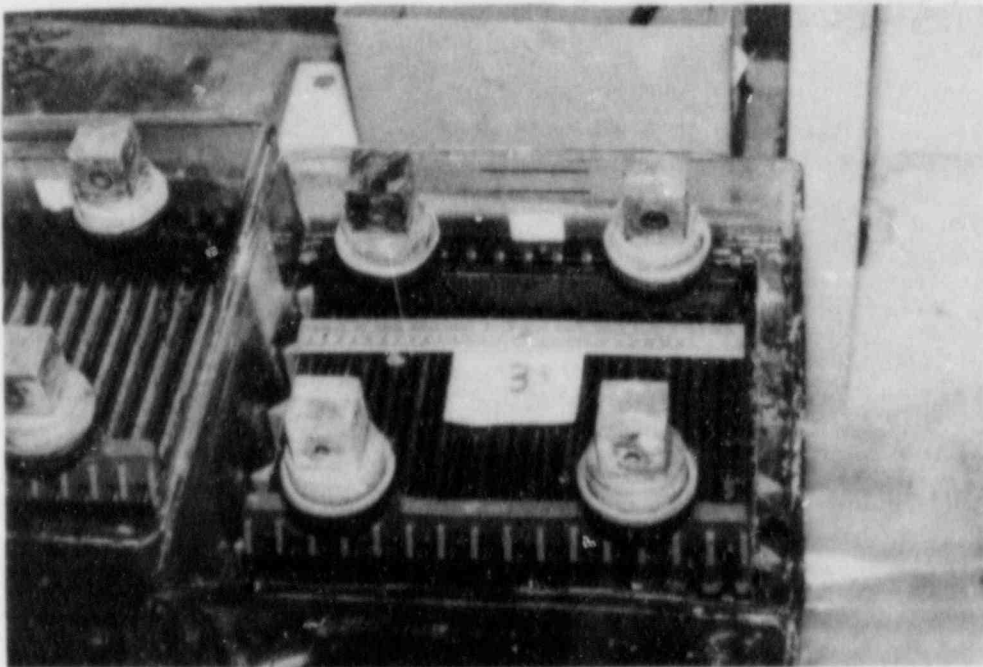
FIGURE 12
Battery Cell With Cover Removed

391
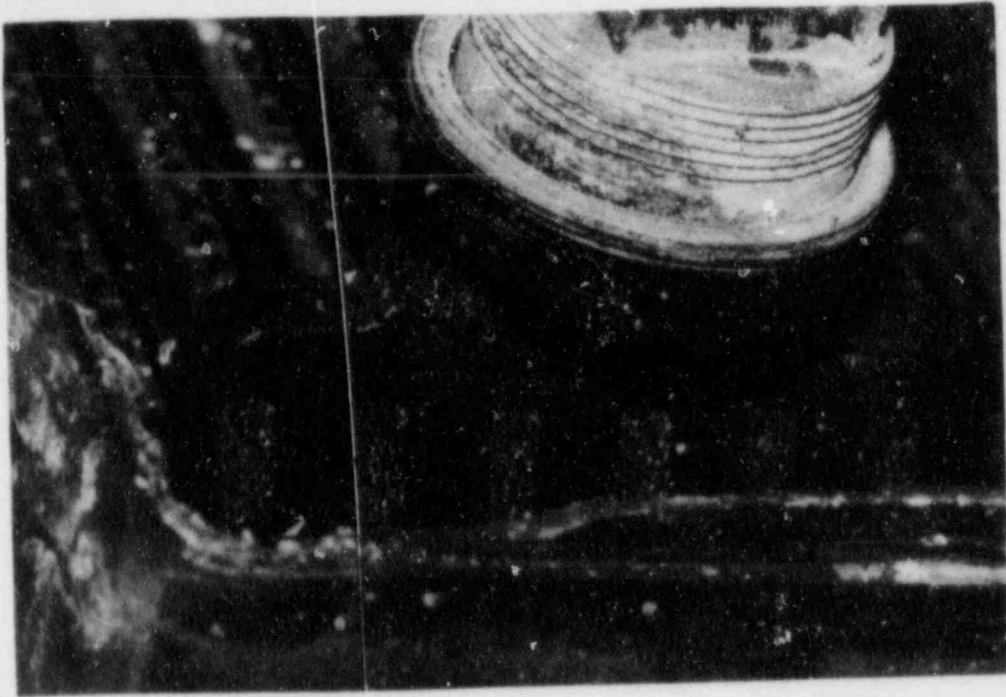
FIGURE 13
Crack at Postive Post-Plate Bus Bar Interface
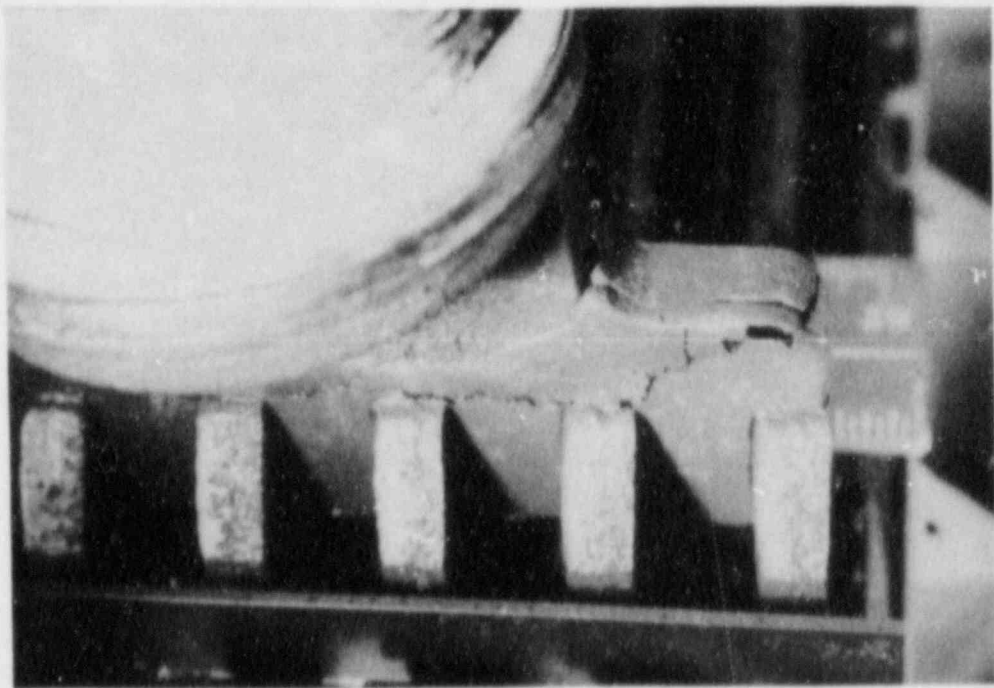
FIGURE 14
Positive Post-Bus Bar Interface Crack

The lead in the fractured area was heavily corroded and extremely weak. Figure 15 shows the results of gentle pressure applied to the positive posts of cell 3. The material was coarsely grained and porous and easily crumbled. The absence of silver-colored lead surfaces at the fracture indicated that significant chemical attack had occurred within the bus material. Microscopic examination of the material showed that corrosion had proceeded along the grain boundaries and that the grain size of the samples from cells which had failed in this region was relatively large. These observations were common to all cells which failed the seismic tests; all cracked areas were below the normal operating level of the electrolyte. Only one negative bar experienced cracking and that was only a very minor fracture. It appears the reason for the extensive bus bar failures may be, in part, because the chemistry involving the positive plates promotes heavier corrosion.
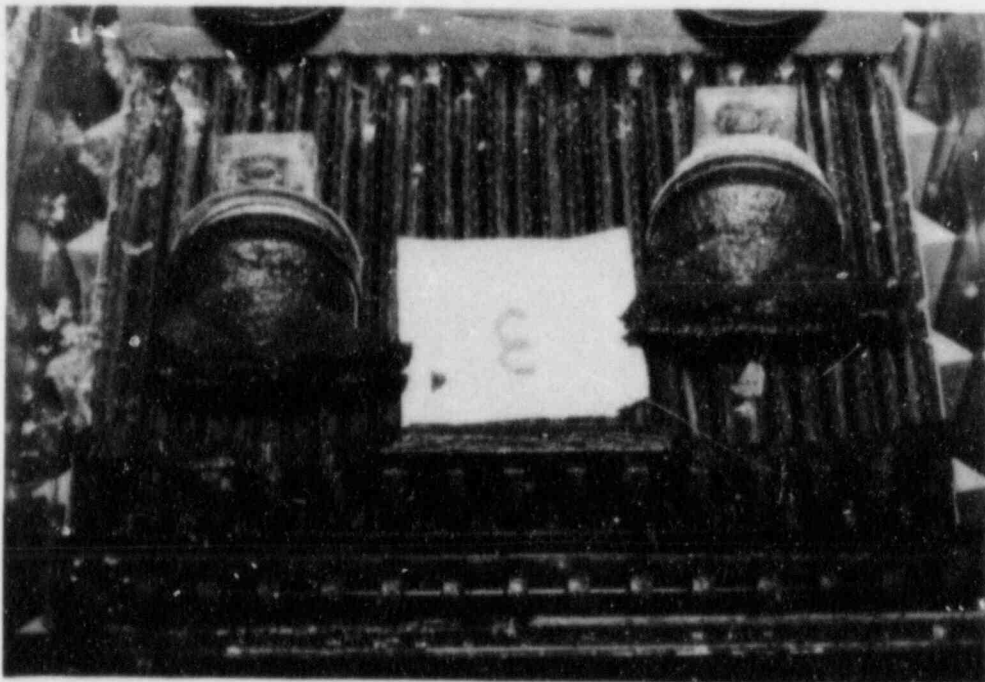
FIGURE 15
Failed Positive Posts

When samples from cells which had survived the shaker tests up to the machine limit were examined, it would found that the metal grain size was much smaller than for the failed cells and that the degree of corrosion was much more limited. This is seen in Figure 16 where some chemical attack has taken place at the fracture interface of a positive post that required several blows from a hammer before fracturing.

In an effort to determine the nature of brittle (failed cell) and ductile (passed cell) interface areas, metallurgical examinations of positive and negative post/bus bar interfaces were performed. These analyses identified the following:
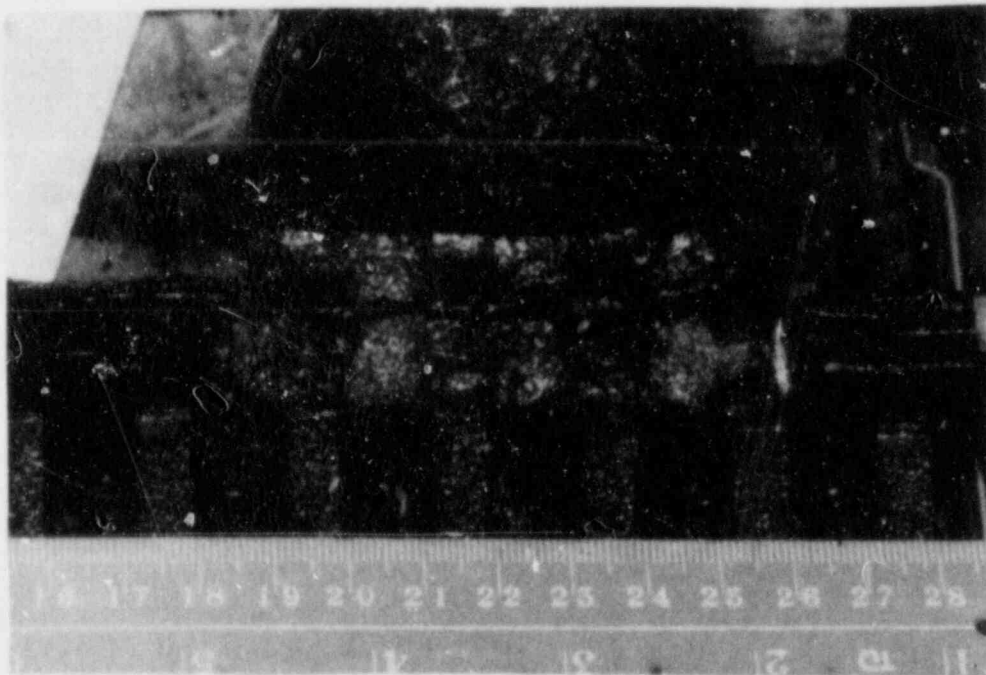
FIGURE 16
Corrosion Indications in a Seismically-Passed Battery Cell

394

1. Brittleness in seismically-failed cell positive or negative bus materials was characterized by an extremely coarse grain size material, which makes them prone to intergranular fracture.

2. Fracture paths deliberately induced in ductile material from seismically-passed cell positive or negative buses were primarily transgranular, and through sound, fine-grained material.

3. Brittle materials exhibited extensive intergranular decohesion behind the fracture face and interfacial decohesion between bus and post material.

4. Coarse grain size almost certainly originated with the cell manufacturer's casting process.*

5. Creep is a possible failure mechanism for brittle material but the precise failure mechanism remains obscure.

6. Intergranular corrosion may be a significant contributor to failure.

The results of these investigations suggest that the failure of the bus bars was due to a combination of unsuitable material properties and chemical attack. It was not immediately apparent why the grain size of the lead in the bus bars of the failed cells was larger than that in the surviving cells. To check whether this might be the result of manufacturing conditions, samples from the negative bus bars of both failed and surviving cells were compared. It was found that again, grain sizes were much larger in the cells where fracture had occurred. Oxidation was much less apparent on the negative side. This suggests that the large grain size was developed during the casting and burning process and was not due to in-service conditions. The hypothesis, that the problem arose during manufacturing, is supported by the observation that all of the cells which failed bore serial numbers between 130 and 155, while the serial numbers of the surviving cells were 022 and 1148.

Another failure that occurred during the multi-cell tests was the lifting and twisting of the connector posts. This was apparently due to the mechanical forces exerted by the rigid connecting bars jointing the cells. We believe that these forces

---

* Proof of a manufacturing process anomaly is not yet available.

could make the cells more vulnerable to failure in the bus bar region, but the test sample was too small to provide any estimate of the change in fragility level.

SUMMARY AND CONCLUSIONS

In summary, all plates and separators were in very good condition. The negative plates were easily scratched to reveal lead metal, and the positive grids showed minimal loss of active material. No evidence of significant plate or grid growth was detected and positive active material could be removed easily with a knife - it was not unduly compressed.

The lack of significant plate or grid growth is particularly significant in defining an acceptable accelerated-aging methodology. Contrary to IEEE 535-1979[14] expectations, the acceleration of plate or grid growth by aging at increased temperatures seems inappropriate when considering these 12-year old naturally aged cells.

The following conclusions were reached by Ontario Hydro personnel conducting the tests and evaluations:

1. Six of the nine 12-year old cells, selected at random from approximately 60 cells retired from service at the James A. Fitzpatrick Nuclear Power Station, failed under electrical load during shaking. One which did not fail electrically suffered significant internal damage.

2. Electrical failure of the test cells was caused by severe cracking of abnormally brittle positive bus material and/or disconnection of positive posts from the bus material.

3. Decohesion, leading to fracture, occurred mostly along the boundaries of extremely large lead grains and was assisted by chemical corrosion. Coarse grain structure can be attributed to abnormalities in the bus casting process.*

4. Internal components and connections in two cells without bus defects were extremely durable. These cells survived violent and repeated seismic testing and were capable of meeting the acceptance criterion of 80% of rated capacity after the test.

5. Plates and separators were generally in very good condition, with no significant plate growth.

---

* Proof of a manufacturing process anomaly is not yet available.

6. Failures in the cell jars also occurred, but only after repeated testing at high acceleration levels. These failures led to electrolyte leakage.

7. The fragility level of cells mounted together in batteries appears to be marginally lower than the fragility level of cells tested individually, due to amplification of seismic motion through the rack and because of relative movement between the cells and the rack.

8. The failure modes observed during these tests may be specific to this type of cell or even to this particular installation. Testing should continue to include samples from other manufacturers.

9. The tests described in this report do not imply that this type of cell is, or is not, seismically qualified for any particular installation. The objective of the tests was to identify failure modes in naturally-aged cells so that the cells were shaken repeatedly at high acceleration levels until damage occurred.

The manufacturing-process deficiency hypothesis suggested by Ontario Hydro staff may prove correct and is appealing. The data are not conclusive, and this issue will certainly be included in follow-on activities. For example, we are obtaining new cells of the same type and baseline evaluations of these cells as received and after accelerated aging will be conducted.

RECOMMENDATIONS

Recommendations made by Ontario Hydro staff as a result of this effort are:

1. The principal mode of deterioration of these cells was the corrosion at the grain boundaries of the positive bus bars. Where metal grain size was large, this corrosion seems to have reduced the electrical capacity of the cells and reduced their mechanical strength. We recommend that manufacturing processes and quality assurance procedures be reviewed to eliminate coarse grained structures in the internal components of lead-acid storage cells.

2. Because the failure mode may be specific to the cells that were tested, samples from other manufacturers should be tested before general conclusions are drawn about the fragility level of aged cells.

3. The battery rack used in these tests was designed to simulate the racks typically used in seismically qualified systems. On the basis of our observations of the behavior of a set of cells in this rack during a simulated earthquake, we offer the following suggestions:

   - Cells should be restrained vertically if the vertical component of the floor motions is expected to exceed 1-g.

   - Cells that are tied together with rigid connectors tend to move together. This means that a cell on the end of a long string could be subjected to large forces if it is crushed between its neighbors and the end of the rack. In severe seismic environments, it would be beneficial to separate the cells into groups of three or so, with rigid partitions on the rack and flexible electrical connections between groups.

FOLLOW-ON ACTIVITIES

Subsequent to this effort we tested naturally-aged 10-year old Exide FHC-19 cells used at Calvert Cliffs and naturally-aged 10-year old C&D LCU-13 cells used at North Anna. In none of the tests did we see any evidence of electrical failure. Examinations, analysis, and metallurgical evaluations of these cells are being accomplished at the present time; separate reports will be issued as SAND/NUREG reports in the near future.

Our follow-on efforts will include:

1. Conducting baseline tests of new cells from all three manufacturers, and subsequent accelerated aging and seismic testing of the new cells, and an attempt to address the question of manufacturing-process deficiences through other metallurgical evaluations.

2. Obtaining the required response spectrum (RRS) for battery locations at a number of nuclear power plants for comparison with the fragility levels obtained by this testing. (We anticipate the fragility levels of these Class 1E battery cells will exceed the RRS of most plants.)

3. Accelerating the age of naturally-aged battery cells and subsequent seismic testing of the aged cells.

4. Conducting additional lead-chemistry evaluations that may be necessary as a result of failure modes observed in subsequent testing.

REFERENCES

1. LER 75-4, Turkey Point-4, "Cracked and Buckled Plates," Event date: October 14, 1974, Report date: October 23, 1984.

2. LER 77-55, Fitzpatrick-1, "Cracked Battery Cell Case," Event date: October 20, 1977, Report date: November 14, 1977.

3. LER 79-59, Fitzpatrick-1, "Cracked Battery Cell Case," Event date: September 4, 1979, Report date: October 2, 1979.

4. LER 81-42, Browns Ferry-1, "Cracked Cell," Event date: July 22, 1981, Report date: August 14, 1981.

5. LER 82-7, Indian Point-2, "Battery Inoperable Due to Cracked Cell," Event date: February 2, 1982, Report date: March 19, 1982.

6. LER 82-16, Indian Point-2, "Battery Cell Cracks," Event date: April 23, 1982, Report date: May 24, 1982.

7. LER 82-6, Connecticut Yankee, "Cracked Emergency DC Battery Cells," Event date: September 19, 1982, Report date: October 5, 1982.

8. Eric W. Weiss, Possible Generic Battery Problem, Memo for R. William Mills, Chief, Events Analysis Branch, Office of Inspection and Enforcement, Nuclear Regulatory Commission, November 26, 1982.

9. IE Information Notice No. 83-11, Possible Seismic Vulnerability of Old Lead Storage Batteries, Office of Inspection and Enforcement, Nuclear Regulatory Commission, Washington, D. C., March 14, 1983.

10. Frank Ashe, Degradation of Safety-Related Batteries Due to Cracking of Battery Cell Cases and/or Other Possible Aging-Related Mechanisms, AEOD Engineering Evaluation Report, AEOD/E307, Nuclear Regulatory Commission, April 18, 1983.

11. L. L. Bonzon, et al., "An Overview of Equipment Survivability Studies at Sandia National Laboratories (SNL)," SAND83-0759C, Proceedings of the ANS/ENS International Meeting on Light Water Reactor Severe Accident Evaluation, Cambridge, Massachusetts, August 28 - September 1, 1983

12. T. Lowen, Ontario Hydro Report 77-221-H, <u>Seismic Qualification Tests for Nuclear Generating Station Batteries</u>, Toronto, Ontario, Canada, May 17, 1977.

13. L. L. Bonzon, et al., <u>Test Series 1: Seismic-Fragility Tests of Naturally-Aged Class 1E Gould NCX-2250 Battery Cells</u>, SAND84-1737, NUREG/CR-3923, Sandia National Laboratories, Albuquerque, New Mexico, September 1984.

14. "IEEE Standard for Qualification of Class 1E Lead Storage Batteries for Nuclear Power Generating Stations," IEEE Std. 535-1979.

THE EFFECT OF ALTERNATIVE AGING AND ACCIDENT
SIMULATIONS ON POLYMER PROPERTIES*

L. D. Bustard
Sandia National Laboratories
Albuquerque, New Mexico 87185

J. Chenion, F. Carlin, C. Alba, G. Gaussens
Commissariat a l'Energie Atomique
Gif-Sur-Yvette, France

M. LeMeur
CEA/CEN-FAR
Fontenay-aux-Roses, France

INTRODUCTION

Polymer materials are important components of safety-related equipment both in the United States and France. In both countries, safety-related equipment containing polymer constituents is qualified by tests that simulate aging and postulated accident environments. These simulations rarely reproduce the environmental parameters exactly. In fact, it would be impossible to exactly reproduce aging environments because of the long times (~40 years) that would be required. Other constraints also limit the experimental ability to reproduce accident exposures exactly. Hence a necessary aspect of each qualification program is the choice of appropriate environmental simulation techniques and parameters.

The response of eighteen US and French polymer materials to variations in aging and accident simulation techniques has been determined by our experimental program. This information will provide a partial data base by which to judge appropriate simulation practices. Our overall research goal was to determine whether some aging and accident simulation techniques are better suited for qualification activities than other alternative simulation techniques. The test program varied the following parameters:

1. Accident simulations of irradiation and thermodynamic (steam and chemical spray) conditions were performed both sequentially and simultaneously.

2. Accident steam exposures were performed both with and without air present during the exposures. (Air was replaced by nitrogen during some test exposures.)

3. Age preconditioning (thermal and irradiation exposures) was performed both sequentially and simultaneously.

---

4. Aging and accident irradiations during the sequential exposures were performed both at 28°C and 70°C.

5. Sequential aging exposures were performed using two sequences: (1) thermal followed by irradiation and (2) irradiation followed by thermal exposures.

The individual effect of several of these parameters has been previously reported by numerous authors [1-8]. These previous research activities rarely combined accident and aging research into one comprehensive test program. Establishing the most severe aging or accident simulation technique was also typically the goal of these previous research efforts. Our goal was to vary several aging and accident test parameters in one research program. Thus the relative importance of each of these parameters could be assessed. Moreover, we wanted to identify those sequential simulation techniques that produced degradation similar to that achieved during our simultaneous radiation, steam, and chemical spray accident exposures. We consider our simultaneous accident simulation to be the best representation among our alternative simulations of postulated design basis event accident conditions.

Our study, however, did require a choice of the postulated aging and accident environments. We chose 25 Mrd as an aging radiation exposure and 60 Mrd as an accident radiation exposure. Dose rates of ~0.06 Mrd/h were used for aging of U.S. samples; dose rates of ~0.1 Mrd/h were used for the French samples. The accident irradiations for both the French and U.S. samples were done at ~0.3 Mrd/h. These doses and dose rates are consistent with qualification requirements at the start of our test program. Our accident simulation of thermodynamic conditions (steam and chemical spray) was also based on French qualification requirements. (Figure 1 illustrates a typical French qualification profile for thermodynamic conditions).

Irradiations in the United States that simulate aging and accident conditions are typically performed at ambient conditions. In contrast, in France both the aging and accident irradiations are performed at 70°C. This latter choice reflects typical maximum operating temperatures inside containment plus margin. Our test program varied the irradiation temperature to assess the importance of this difference between U.S. and French qualification practices; samples were irradiated at both 27°C and 70°C.

An important parameter not varied during our experimental program was the aging irradiation dose rate. Experimental studies [2,9] have demonstrated the importance of both physical and chemical contributions to dose rate effects. Physical dose rate effects are caused by diffusion-limited oxidation. Our aging irradiation dose rate of ~0.1 Mrd/h (an order of magnitude less than sometimes used in U.S. qualification efforts) will reduce the impact of this dose rate mechanism. Chemical dose rate effects are most commonly caused by the slow breakdown of intermediate hydroperoxide species. Such a process may be occurring if material properties depend on the test sequence of irradiation and thermal exposures. Our experiments do vary the test sequence; thus our experimental strategy recognized the possible importance of physical and chemical dose rate effects.

SAMPLES

The U.S. samples consisted of six insulation materials and two jacket materials. The insulation and jacket materials were carefully obtained by disassembling cable received from five U.S. manufacturers of Class 1E cables. The insulation specimens were tubular in shape; the jacket specimens were cut with a die into rectangular pieces. The materials are:

EPR 1   A radiation cross-linked fire-retardant EPDM insulation obtained from a shielded instrumentation cable.

EPR 2   A chemically cross-linked fire-retardant EPDM insulation obtained from a 600V, 3-conductor control cable.

XLPO 1   A cross-linked polyolefin insulation obtained from a shielded instrumentation cable.

XLPO 2   A cross-linked polyolefin insulation obtained from a 600V, 3-conductor control cable.

TEFZEL 1   A TEFZEL insulation removed from a thermocouple extension cable.

TEFZEL 2   A TEFZEL insulation removed from a shielded instrumentation cable.

CSPE   A chlorosulfonated polyethylene jacket removed from a 600V, 3-conductor control cable.

CPE   A chlorinated polyethylene jacket removed from a 600V, 3-conductor control cable.

The French samples consisted of six elastomer materials used in the manufacture of electrical cables (insulation and jacket materials), two O-ring seal materials and two thermoplastic and thermosetting materials used in the manufacture of connectors. The electrical cable materials were in the form of either insulating material stripped from the copper conductor (identified by "I"), dumbbells cut from jacket material and identified by "G", or standard dumbbells cut from compression molded sheets (identified by "H"). The six cable materials are:

82 I1 PRC   Chemically cross-linked polyethylene in the form of conductor insulation for 3-conductor cables.

82 I2 EPDM   Ethylene propylene diene terpolymer conductor insulation. Samples taken from a 3-conductor cable.

82 I9 EPDM   Bromine-loaded, ethylene propylene diene terpolymer conductor insulation. This material was removed from a 3-conductor cable.

82 G10 HYPALON   Chlorosulfonated polyethylene used in the manufacture of cable jackets.

403

82 H3 VAMAC Acrylic polyethylene in the form of sheets from which dumbbells were cut. Material is used in electrical cable jackets, mechanical parts, and connectors.

82 H4 EPR Copolymer ethylene-propylene rubber in the form of 3 mm sheets from which dumbbells were cut. Material is used in the manufacture of insulation for electrical cables sheathed with fire-proof EPDM.

The two O-ring seal samples (identified by "J") have an inner diameter of 12 mm and an outer diameter of 17 mm. They were enclosed and held under compression in aluminum grooves. The O-ring seal materials are:

82 J3 VAMAC Same material as 82 H3, used in the manufacture of O-ring seals.

82 J4 EPR Same material as 82 H4, used in the manufacture of O-ring seals.

The two thermoplastic and thermosetting materials used in the manufacture of connectors were in the form of International Organization for Standardization (ISO) dumbbells. The two materials are:

82 H5 Polydiallylphtalate Thermosetting polyester used in connectors and mechanical parts.

82 H6 PPS Phenylene polysulfide used in the manufacture of switches and connectors.

Additional details concerning both the U.S. and French samples are provided in Reference 1.

EXPERIMENTAL TECHNIQUES

The aging of all U.S. and French samples was performed in the United States at Sandia National Laboratories. Sandia's Low Intensity Cobalt Array (LICA) facility was employed for the irradiation exposures. Thermal aging was performed using air circulating ovens each of which had been modified to accommodate a number of self-contained aging cells. Both facilities are described in more detail in Reference 1.

The U.S. insulation and jacket samples were exposed to five different aging procedures. In addition, unaged samples were exposed to the accident simulation. These procedures (and the shorthand codes used in the rest of the report to describe them) are:

A = R70 → 120°C: A 16-day irradiation at ~65 krd/h and 70°C followed by a 16-day thermal exposure at 120°C.

B = R27 → 120°C: A 16-day irradiation at ~65 krd/h and ambient temperatures (~27°C) followed by a 16-day thermal exposure at 120°C.

404

C = 120°C → R70:   A 16-day thermal exposure at 120°C followed by a 16-day irradiation at ~65 krd/h and 70°C.

D = 120°C → R27:   A 16-day thermal exposure at 120°C followed by a 16-day irradiation at ~65 krd/h and ambient temperatures (~27°C).

E = R120:   A 16-day simultaneous exposure to 120°C thermal and ~65 krd/h irradiation environments.

U = Unaged.

The 120°C, 16-day elevated temperature exposure was chosen based on Arrhenius calculations which assumed a 40-year service operation at 45°C and cable material activation energy of 1.0 eV. The total integrated dose for each aging exposure was ~25 Mrd. Additional details concerning the aging techniques are provided in Reference 1.

Each French material was exposed to four different aging procedures. In addition, unaged samples were exposed to the accident simulations. These aging procedures (and the shorthand codes used in the rest of the report to describe them) are:

A = T → R70:   A 10-day thermal exposure followed by a 9- or 10-day irradiation at ~115 krd/h and 70°C.

B = R70 → T: A 9- or 10-day irradiation at ~115 krd/h and 70°C followed by a 10-day thermal exposure.

C = T → R27:   A 10-day thermal exposure followed by a 9- or 10-day irradiation at ~115 krd/h and ambient temperatures (~27°C).

D = R27 → T: A 9- or 10-day irradiation at ~115 krd/h and ambient temperatures (~27°C) followed by a 10-day thermal exposure.

U = Unaged.

The 10-day thermal aging temperature depended on the French specimen material. The VAMAC dumbbell and O-ring samples (82H3 and 82J3) were thermally aged at 120°C. The PRC, EPDM, EPR, and HYPALON samples (82I1, 82I2, 82I9, 82H4, 82J4, and 82G10) samples were thermally aged at 140°C. A 160°C thermal aging exposure was employed for the PPS and Polydiallylphtalate samples (82H6 and 82H5). Various sample groups were irradiated over a several month period. Co-60 decay during this time period necessitated varying the irradiation exposure time from 9 days to 10 days so that each sample group was irradiated to a similar dose (~25 Mrd). Additional details concerning the aging techniques are provided in Reference 1.

All accident simulations were performed in France in the laboratories (ORIS-LABRA) of the Ionizing Radiation Office at Saclay (the Radiation Biological Application Laboratories). The accident simulations were comprised

405

of three elements: the accident irradiation, the thermodynamic (steam and chemical spray) exposures, and the post-accident 100°C, 95-100% relative humidity, exposures. The thermodynamic exposure was applied either simultaneously with the accident irradiation, or sequentially. The post accident exposure followed the irradiation and thermodynamic exposures. All accident irradiations were carried out in the hot cave of the POSEIDON irradiator. The CESAR (Reference Accident Simulation Test Cell) was employed for the LOCA simulations. The CESAR chamber was positioned inside the POSEIDON irradiator whenever simultaneous thermodynamic and irradiation exposures were desired. The French facilities are further described in Reference 12.

Four different accident simulations were performed on each of the five groups of preaged (A,B,C,D, and U) French samples:

L1 = Accident irradiation at 70°C followed by thermodynamic and post-accident exposures with air (R70 → LOCA(air)).

L2 = Thermodynamic and post-accident exposures with air followed by an accident irradiation at 70°C (LOCA(air) → R70)).

L3 = Simultaneous accident irradiation and thermodynamic exposures with air followed by a post-accident exposure with air (R + LOCA(air)).

L4 = Accident irradiation at 28°C followed by LOCA and post-accident exposures with air (R28 → LOCA(air)).

Six different accident simulations were performed on each of the six groups of preaged (A,B,C,D,E, and U) U.S. samples:

L5 = Accident irradiation at 70°C followed by thermodynamic and post-accident exposures with air (R70 → Steam(air)).

L6 = Accident irradiation at 70°C followed by thermodynamic and post-accident exposures with nitrogen (air was replaced by nitrogen) (R70 → Steam(N_2)).

L7 = Accident irradiation at 28°C followed by thermodynamic and post-accident exposures with air (R28 → Steam(air)).

L8 = Accident irradiation at 28°C followed by thermodynamic and post-accident exposures with nitrogen (air was replaced by nitrogen) (R28 → Steam(N_2)).

L9 = Simultaneous accident irradiation and thermodynamic exposures with air followed by a post-accident exposure with air (R + Steam(air)).

L10 = Simultaneous accident irradiation and thermodynamic exposures with nitrogen (air was replaced by nitrogen) followed by a post-accident exposure with nitrogen (R + Steam (N_2)).

The accident dose rate was ~0.3 Mrd/h; the accident total dose was ~60 Mrd. The thermodynamic (steam and chemical spray) profile for the L1

exposure is shown in Figure 1. Since the thermodynamic exposure requirements for L1 were the same as for L4, both L1 and L4 samples were exposed to the thermodynamic profile concurrently. Hence Figure 1 also provides the thermodynamic profile for the L4 exposure. Similar reductions in experimental effort were achieved by combining the L5 and L7 exposures, the L3 and L9 exposures and the L6 and L8 exposures. The achieved thermodynamic conditions were similar to the L1 and L4 conditions shown in Figure 1. The chemical spray exposure started 220 seconds after the initiation of the second thermodynamic transient. The samples were sprayed for 24 hours with a borated solution having the following composition: $H_3BO_3 = 15$ g. ℓ^{-1} and $NaOH = 6$ g. ℓ^{-1} (consistent with French qualification requirements).

The pH value of the solution was maintained at 9.25. The post-accident exposure consisted of a 10 day, 100°C exposure at 95-100 % relative humidity. Either air or nitrogen was used as the nonwater vapor gas during this exposure. Additional details are provided in Reference 12.

Periodically during the aging and accident exposures, test specimens were removed from the test program for mechanical measurements. French tensile measurements were carried out on a Zwick traction machine, Model 7025/3. The samples, in the form of dumbbells or wiring insulation were clamped into the jaws of the test machine. The space between the jaws was 4.0 cm for dumbbells 82G10, 82H3 and 82H4, approximately 15.0 cm for dumbbells 82H5 and 82H6, and approximately 11.0 cm for insulations 82I1, 82I2, and 82I9. An extensometer was placed in the center of each sample. Its initial separation was 1.0 cm. The traction speed was 5.0 cm per minute for the elastomers and thermoplastics. The traction speed was reduced to 0.8 mm per minute for the thermoset sample.

Measurements of permanent set after compression were carried out at ORIS-LABRA on French elastomer O-ring samples 82J3 and 82J4. Measurement of the initial and final diameters of the core were carried out using Roche slide calipers, with an accuracy of 0.02 mm (French Standard No. NFT 46011).

INSTRON 1130 and 1000 tensile testing machines were used for testing of the U.S. samples. In general, at the time of the post-LOCA tensile tests, the weights of the U.S. samples were not more than ~2% greater than the weights of the samples prior to the LOCA exposures. (We allowed moisture absorbed by our samples during the LOCA simulation to desorb prior to performing tensile measurements. Moisture absorption data is presented in Reference 12.) The samples were gripped using pneumatic jaws; initial jaw separation was 5.1 cm and the samples were strained at 12.7 cm/min. The strain was monitored with an INSTRON electrical tape extensometer clamped to the sample.

Bend tests were performed on the U.S. TEFZEL 1 and TEFZEL 2 samples rather than tensile tests since aged specimen tubes shattered when gripped by the pneumatic jaws of the Instron tensile testing machine. Bend radii between 75 and 6 times the radii of the TEFZEL specimens were employed. Each specimen was successively wrapped around tubes of smaller diameter until insulation cracking was visually observed.

RESULTS AND DISCUSSION

Our overall research goal was to determine whether some combinations of aging and accident simulations are better suited for qualification activities than other alternative simulation techniques. To answer this question we looked for combinations of aging and accident simulation techniques that produced degradation similar to the worst degradation obtained during our simultaneous R + LOCA(air) tests. (Degradation variability for a given material during the R + LOCA(air) simulation is caused by differences in the aging simulations that preceded the accident exposure.) We consider the simultaneous R + LOCA(air) accident simulation to most reasonably reflect a design basis event accident scenario (except for inerted Boiling Water Reactor containments).

We performed this evaluation for each of the eighteen U.S. and French polymer materials that were included in our study. To help establish trends, we present our results in terms of generic material categories (such as cross-linked polyolefins).

Cross-linked Polyolefins: Our experimental program included three cross-linked polyolefin materials, namely the U.S. XLPO 1 and XLPO 2 samples and the French PRC samples. The U.S. materials were irradiation cross-linked, while the French material was chemically cross-linked.

The effect of alternative aging and accident simulation techniques on the three materials is shown in Figure 2. The effect of alternative simulation techniques on the two U.S. materials is vastly different than for the French material. For both U.S. materials, the R + steam(air) accident simulation produces less degradation of the ultimate tensile elongation than the other accident simulations. Since this is the most realistic accident simulation, any of the sequential accident simulation techniques would be appropriate. For neither of the U.S. cross-linked polyolefin materials was degradation strongly dependent on the aging technique.

The French material (PRC (82I1)), in contrast, was most severely degraded by the R + LOCA(air) accident exposure. The sequential accident technique best suited to simulate the simultaneous exposure results is the R70 → LOCA(air) accident simulation. The choice of aging simulation technique is less important than the choice of accident simulation technique.

Hence we conclude that a qualification profile applicable for all three cross-linked polyolefin materials would be an aging simulation followed by a R70 → LOCA(air) accident simulation. The choice of aging simulation technique (based on those used in our test program) is not critical provided the appropriate accident simulation technique is employed.

Ethylene Propylene Rubbers: Our experimental program included five ethylene propylene rubber materials, namely the U.S. fire-proof EPRs: EPR 1 and EPR 2; and the French EPDM (82I2), fire-proof EPDM (82I9), and EPR (82H4). In addition, EPR (82J4) was tested but we discuss it with the other compression set material VAMAC (82J3). The effect of alternative aging and accident simulations on the EPR materials is presented in Figures 2 and 3.

The French EPR materials 82I2 (Figure 3) and 82I9 (Figure 3) were most degraded by the R + LOCA(air) accident simulation. For 82I2, similar degradation is possible (for any accident simulation technique), provided a radiation followed by thermal (R → T) aging technique is employed. For 82I9, performing the R → T aging technique will enhance the conservatism of the qualification process, but no sequential accident technique is as degrading as the R + LOCA(air) technique. The R70 → LOCA(air) simulation most approaches the R + LOCA(air) results.

For the French 82H4 (Figure 3) EPR material, the R + LOCA(air) accident technique is least degrading. Any combination of sequential aging and accident simulation techniques is more degrading than this simultaneous accident exposure.

For the U.S. EPR 2 (Figure 3), the simultaneous R + steam(air) accident exposure is most conservatively simulated by the R70 → steam(air) technique. The R28 → steam(air or N$_2$) and the R + steam(N$_2$) techniques are less conservative. The R120 and T → R27 aging techniques would be less conservative than the other three aging techniques. For the U.S. EPR 1 (Figure 2) material, an appropriate aging and accident sequential qualification technique would be R(27 or 70) → T followed by R70 → LOCA(air).

Hence a qualification procedure appropriate for all our EPRs would be a R(27 or 70) → T aging simulation followed by a R70 → Steam(air) accident simulation.

TEFZEL: Our experimental program included two TEFZEL materials, namely the U.S. TEFZEL 1 and TEFZEL 2 samples. Test results at completion of the accident exposures are presented in Tables 1 and 2. For each combination of aging and accident simulations, we tested four specimens. The tables provide the largest bend radii for which at least one of the four samples had cracked as well as the radii by which all four samples had cracked. Both materials were more degraded when oxygen was present during simultaneous LOCA simulations (R + steam). If sequential qualification procedures are employed, then performing the aging and accident irradiations at elevated temperatures (i.e., 70°C) is desirable. The aging sequence should be R70 → T.

Chlorosulfonated Polyethylene (HYPALON): Two chlorosulfonated polyethylene materials were included in the data base, namely the U.S. CSPE and the French HYPALON (82G10) (Figure 4). For the French material the R + LOCA(air) exposure was less degrading than all the sequential aging and accident techniques. Hence any sequential qualification procedure is appropriate. For the U.S. CSPE, all accident techniques produced similar degradation, the R70 → T and R120 aging techniques produced more degradation than other techniques. A sequential qualification procedure appropriate for both materials would start with a R70 → T aging simulation followed by any convenient accident simulation technique.

O-ring Materials: Two O-ring materials were included in the test program, namely VAMAC (82J3) and EPR (82J4) (Figure 4). By the end of all accident simulations both were at the limit of their use. Hence any of the qualification procedures would be appropriate for these two materials.

Connector Materials: Two connector materials were included in our test program, namely the thermosetting material polydiallylphtalate (82H5) and the thermoplastic material PPS (82H6) (Figure 5). For both materials we monitored ultimate tensile strength behavior. For neither material were differences between alternative aging techniques important. For PPS (82H6) there also was little difference caused by alternative accident techniques. For polydiallylphtalate (82H5), the R28 → LOCA(air) accident simulation most closely matches the degradation achieved by the R + LOCA(air) technique. The R70 → LOCA(air) simulation is more conservative and might also be employed for qualification purposes.

VAMAC: One VAMAC sheet material (Figure 5) was tested, namely the French VAMAC (82H3). The R + LOCA(air) accident simulation technique was least degrading and therefore any sequential accident simulation technique would be appropriate. Any aging technique would provide appropriate preconditioning for a sequential accident exposure.

CPE: One chlorinated polyethylene jacket material (Figure 5) was tested, namely the U.S. CPE. For this material, the choice of accident technique is relatively unimportant; the R70 → T aging exposure is most conservative.

Table 3 summarizes our qualitative conclusions for each generic class of material. Examination of Table 3 indicates that the R70 → T aging technique followed by the R70 → LOCA(air) accident technique could be employed for all of our materials.

QUANTITATIVE EVALUATION OF DATA BASE

In addition to the qualitative evaluation summarized in Table 3, we have performed a quantitative evaluation to identify those aging and accident simulation techniques that dominate polymer degradation.

Tables 4 through 7 illustrate our evaluation technique and its results. In Tables 4 and 5 we list for each aging and accident technique combination those U.S. and French materials whose normalized elongation (i.e., e/e_0) was reduced to .05 or less. (For PPS and polydiallylphtalate, tensile strength was employed as the property of interest, while for the TEFZEL materials we listed those aging and accident combinations that caused all four samples of a sample group to crack at bend radii greater than or equal to 40 times the sample radii. We did not include the O-ring materials in our evaluation since all aging and accident combinations essentially placed these materials at their end of use condition.) Each table listing is provided a weight according to the number of times that material appears in the table. A low weight is given to each table entry if the material's degradation is insensitive to the choice of aging and accident simulation techniques. A high weight is given if the material's degradation is very sensitive to the choice of aging and accident simulation technique. For example, a material listed five times in the table is assigned a value of 0.2 for each listing. In contrast, a single listing rates a value of 1.0. This weighting process also ensures that each material contributes equally to the conclusions. We sum across each row of the table to evaluate the relative importance of each aging technique. (The aging technique with the largest sum is most significant.)

410

Similarly, summing down the column of each table provides a means to evaluate the relative importance of each accident simulation technique. Tables 6 and 7 provide results of a similar analysis employing a degradation threshold of 10% of initial unaged values.

Examination of Tables 4 through 7 provide insights concerning those aging and accident simulation techniques that dominate degradation. Note that only six U.S. materials contributed to Tables 4 and 6 (two U.S. materials did not exhibit sufficient degradation to be included) and only four French materials contributed to Tables 5 and 7 (four French materials did not exhibit sufficient degradation to be included and the two O-ring materials were not evaluated because they were at their end of use condition.) Hence our data base is small. The insights are:

1. Both Tables 4 and 5 suggest the possible importance of R → T aging techniques. In both tables the R → T aging techniques (at a given irradiation temperature) contribute more to degradation than do the corresponding T → R aging techniques at the same temperature.

2. Table 4 suggests that oxygen presence during LOCA exposures enhances degradation. The R + Steam(air) exposure was more degrading than the R + Steam(N_2)) exposure. Likewise, the R70 → Steam(air) exposure was more degrading than the R70 → Steam(N_2).

3. Tables 6 and 7 suggest that as the degradation threshold is raised, differences between alternative aging and accident simulations decrease.

4. The tables present conflicting data concerning the importance of elevated temperature irradiations (R70 versus R28). Table 4 suggests that an elevated temperature aging irradiation is important for the U.S. materials. It also indicates than an elevated temperature accident irradiation is more important when followed by a steam exposure with air. This conclusion is not confirmed in Table 5 which presents results for the French materials.

CONCLUSION

We have experimentally evaluated a number of polymer materials to determine the effect of alternative sequential and simultaneous aging and accident simulation procedures on material properties. Our overall research goal was to determine which aging and accident simulation technique most closely match anticipated real simultaneous conditions and therefore are better suited for qualification activities.

Some general conclusions have been identified from our experimental base. Results in Tables 3-5 indicate that radiation followed by a thermal exposure is a more conservative choice for an aging sequence than would a thermal followed by radiation exposure aging sequence. We also note that the presence or absence of air during accident simulations can influence the degree of degradation in some materials. The U.S. EPR and TEFZEL materials are examples where degradation is enhanced when air (oxygen) is present during accident simulations; the U.S. XLPO materials are examples where degradation

is reduced by the presence of air. Hence, since most reactor containments are not inerted, a conservative accident simulation for qualifying materials would include air in the LOCA test chamber.

We noted substantial variabiaity in test results because of differences in either the chemical composition or processing of test samples. For example, the response of the French cross-linked polyolefin material to alternative simulation techniques is different than the response of the two U.S. cross-linked polyolefin materials. Similar variability was noted both within and between other classes of materials.

We are encouraged that our empirically-based conclusions agree well with the findings of numerous research programs. Research reports have stressed the need to consider R $\rightarrow$ T aging simulations [1,2,7,10] and have recognized the importance to polymer degradation of oxygen during LOCA exposures [5,6].

We encourage the development of a larger data base. This will enable our preliminary insights to either be solidified or appropriately modified. In closing we would like to stress some of the limitations of our work. We monitored only mechanical properties of our polymer materials. Mechanical failure is an important but not the sole method by which polymers can contribute to functional degradation of Class 1E equipment. We also have tested a limited number of materials. Many important classes of polymers were not included in our study. Our conclusions, representing simply the dominant trends, may not apply to all materials. For some materials alternative aging and accident simulation techniques may be equally appropriate. Finally, we chose experimental test conditions (radiation dose, steam temperature and pressure profiles, etc.) that may not be applicable to all nuclear utilities. These limitations should be considered prior to incorporating our "preliminary" insights into a qualification program for Class 1E equipment.

REFERENCES

1. L. D. Bustard, E. Minor, J. Chenion, F. Carlin, C. Alba, G. Gaussens, and M. LeMeur, "The Effect of Thermal and Irradiation Aging Simulation Procedures on Polymer Properties," NUREG/CR-3629, SAND83-2651, Sandia National Laboratories, April 1984.

2. R. L. Clough, K. T. Gillen, J. L. Campan, G. Gaussens, H. Schonbacher, T. Seguchi, H. Wilski, and S. Machi, "Accelerated-Aging Tests for Predicting Radiation Degradation of Organic Material," NUCLEAR SAFETY, 25, 238 (March-April 1984).

3. L. D. Bustard, "The Effect of LOCA Simulation Procedures on Ethylene Propylene Rubber's Mechanical and Electrical Properties," NUREG/ CR-3538, SAND83-1258, Sandia National Laboratories, October 1983.

4. L. D. Bustard, "The Effect OF LOCA Simulation Procedures on Cross-linked Polyolefin Cable's Performance," NUREG/CR-3588, SAND83-2406, Sandia National Laboratories, April 1984.

5. K. T. Gillen, R. L. Clough, G. Ganouna-Cohen, J. Chenion, and G. Delmas, "The Importance of Oxygen in LOCA Simulation Tests," NUCLEAR ENGINEERING AND DESIGN, 74, 271 (1982).

6. Y. Kusama, S. Okada, M. Yoshikawa, M. Ito, T. Yagi, Y. Nakase, T. Seguchi, and K. Yoshida, "Methodology Study for Qualification Testing of Wire and Cable at LOCA Conditions," NUREG/CP-0041, Proceedings of the U.S. Nuclear Regulatory Commission Tenth Water Reactor Safety Research Information Meeting, Vol 5, p 330.

7. K. Yoshida, T. Seguchi, S. Okada, M. Ito, Y Kusama, T. Yagi, and M. Yoshikawa, "Progress on Qualification Testing Methodology Study of Electric Cables," NUREG/CP-0048, Proceedings of the U.S. Nuclear Regulatory Commission Eleventh Reactor Safety Research Information Meeting, Vol 5, p 283.

8. C. Alba, F. Carlin, J. Chenion, G. Gaussens, M. Le Meur, and M. Petitjean, "Synergetic Effects in Accident Simulation," Proceedings of the Colloque International 'Vieillissement Dans Les Essais De Materiel De Surete Pour Centrales Nucleaires', Paris, France, May 15-16, 1984.

9. R. L. Clough, K. T. Gillen, and C. A. Quintana, "Heterogeneous Oxidative Degradation in Irradiated Polymers," Sandia National Laboratories, SAND83-2493, NUREG/CR-3643, April 1984.

10. R. L. Clough, K. T. Gillen, "Combined Environment Aging Effects: Radiation-Thermal Degradation of Polyvinyl Chloride and Polyethylene, J. Polym. Sci., Polym. Chem. Ed., 19(8): 2041-2051, August 1981.

11. L. Bonzon, R. L. Clough, K. T. Gillen, and E. A. Salazar, "Qualification Testing Evaluation Program Light-Water Reactor Safety Research Quarterly Report, April-June 1979, Sandia National Laboratories, SAND80-0276, NUREG/CR-1343, April 1980).

12. L. D. Bustard, J. Chenion, F. Carlin, C. Alba, G. Gaussens, and M. LeMeur, "The Effect of Alternative Aging and Accident Simulations on Polymer Properties," Sandia National Laboratories. To be published.

Table 1

a. TEFZEL 1: Largest Bend Radii At Which One Sample Cracked. Table entries are expressed as multiples of the TEFZEL 1 sample radius.

ACCIDENT SIMULATIONS

Aging Technique	R70→ST(AIR)	R70→ST(N_2)	R28→ST(AIR)	R28→ST(N_2)	R + ST(AIR)	R + ST(N_2)
UNAGED	75.00	75.00	44.00	11.00	75.00	
R120	75.00	75.00	75.00		75.00	75.00
R70→120	75.00	75.00	75.00	75.00	75.00	50.00
120→R70	75.00	75.00	56.00	50.00	75.00	75.00
R27→120	75.00	75.00	75.00	75.00	75.00	31.00
120→R27	75.00	75.00	75.00	75.00	75.00	75.00

b. TEFZEL 1: Bend Radii By Which All Samples Cracked. Table entries are expressed as multiples of the TEFZEL 1 sample radius (i.e., 75 X).

ACCIDENT SIMULATIONS

Aging Technique	R70→ST(AIR)	R70→ST(N_2)	R28→ST(AIR)	R28→ST(N_2)	R + ST(AIR)	R + ST(N_2)
UNAGED	69.00	75.00	11.00	6.00	69.00	
R120	75.00	75.00	75.00		75.00	75.00
R70→120	75.00	75.00	69.00	50.00	75.00	44.00
120→R70	75.00	75.00	44.00	31.00	75.00	69.00
R27→120	75.00	75.00	44.00	75.00	75.00	22.00
120→R27	75.00	75.00	75.00	75.00	75.00	56.00

Table 2

a. TEFZEL 2: Largest Bend Radii At Which One Sample Cracked. Table entries are expressed as multiples of the TEFZEL 2 radius.

ACCIDENT SIMULATIONS

Aging Technique	R70→ST(AIR)	R70→ST(N_2)	R28→ST(AIR)	R28→ST(N_2)	R + ST(AIR)	R + ST(N_2)
UNAGED	11.00	6.00			75.00	
R120	75.00	75.00	75.00	75.00	75.00	75.00
R70→120	75.00	75.00	75.00	75.00	75.00	75.00
120→R70	75.00	75.00	75.00	75.00	75.00	75.00
R27→120	22.00	44.00	22.00	22.00	75.00	44.00
120→R27	75.00	31.00	22.00	31.00	75.00	69.00

b. TEFZEL 2: Radii By Which All Samples Cracked. Table entries are expressed as multiples of the TEFZEL 2 radius.

ACCIDENT SIMULATIONS

Aging Technique	R70→ST(AIR)	R70→ST(N_2)	R28→ST(AIR)	R28→ST(N_2)	R + ST(AIR)	R + ST(N_2)
UNAGED	6.00	6.00			75.00	
R120	75.00	75.00	75.00	75.00	75.00	75.00
R70→120	75.00	75.00	44.00	75.00	75.00	56.00
120→R70	22.00	75.00	75.00	56.00	75.00	75.00
R27→120	11.00	11.00	11.00	11.00	75.00	22.00
120→R27	22.00	11.00	11.00	22.00	75.00	44.00

415

Table 3

Qualitative Conclusions for Each Class of Material

Material Class	Appropriate Qualification Procedures For Our Test Materials
1. Cross-linked Polyolefins	Any aging sequence followed by R70 → LOCA(air) accident simulation
2. Ethylene Propylene Rubbers	A R → T aging sequence followed by R70 → LOCA(air) accident simulation
3. TEFZEL	R70 → T aging sequence followed by a R70 → LOCA(air) accident simulation
4. Chlorosulfonated Polyethylene	A R70 → T aging simulation followed by an accident simulation.
5. O-ring Materials	Any sequential aging and accident technique is appropriate
6. Connector Materials	Any aging sequence followed by R28 → LOCA(air) or R70 → LOCA(air)
7. VAMAC	Any sequential aging and accident technique is appropriate
8. Chlorinated Polyethylene	R70 → T aging followed by an accident simulation

Table 4

Aging and Accident Combinations That Resulted in Degradation for U.S. Samples of Ultimate Tensile Elongation to Less Than 5% of Initial Values. (For TEFZEL, failure to pass a 44X bend test (all samples) was the selection criteria). The numbers in the table refer to weighting averages as discussed in the text.

Aging Environment \ Accident Environment	R70→ST(AIR)	R70→ST(N_2)	R28→ST(AIR)	R28→ST(N_2)	R + ST(AIR)	R + ST(N_2)	Totals
R120	EPR1=.14 TEFZEL1=.04 TEFZEL2=.05	EPR2=.20 TEFZEL1=.04 TEFZEL2=.05	CSPE=.13 TEFZEL1=.04 TEFZEL2=.05	CSPE=.13 TEFZEL2=.05	EPR1=.14 EPR2=.20 TEFZEL1=.04 TEFZEL2=.05	TEFZEL1=.04 TEFZEL2=.05	1.44
R70 → 120	EPR1=.14 EPR2=.20 CSPE=.13 CPE=.17 TEFZEL1=.04 TEFZEL2=.05	CPSE=.13 TEFZEL1=.04 TEFZEL2=.05	CSPE=.13 CPE=.17 TEFZEL1=.04 TEFZEL2=.05	CSPE=.13 CPE=.17 TEFZEL1=.04 TEFZEL2=.05	CSPE=.13 CPE=.17 TEFZEL1=.04 TEFZEL2=.05	CSPE=.13 TEFZEL1=.04 TEFZEL2=.05	2.34
120 → R70	EPR2=.20 TEFZEL1=.04	TEFZEL1=.04 TEFZEL2=.05	TEFZEL1=.04 TEFZEL2=.05	CPE=.17 TEFZEL2=.05	EPR1=.14 TEFZEL1=.04 TEFZEL2=.05	TEFZEL1=.04 TEFZEL2=.05	.96
R27 → 120	EPR1=.14 EPR2=.20 TEFZEL1=.04	TEFZEL1=.04	CPE=.17 TEFZEL1=.04	TEFZEL1=.04	TEFZEL1=.04 TEFZEL2=.05		.76
120 → R27	EPR1=.14 TEFZEL1=.04	TEFZEL1=.04	TEFZEL1=.04	TEFZEL1=.04	EPR1=.14 TEFZEL1=.04 TEFZEL2=.05	TEFZEL1=.04 TEFZEL2=.05	.62
Totals	1.76	.68	.95	.87	1.37	.49	6.12

6.12

Table 5

Aging and Accident Combinations That Resulted in Degradation for French Samples of Mechanical Properties to Less Than 5% of Initial Values. The numbers in the table refer to weighting averages as discussed in the text.

Aging Environment \ Accident Environment	R70→ST(AIR)	LOCA(AIR)→R70	R + LOCA(AIR)	R28→LOCA(AIR)	Totals
T → R70	EPDM = 0.071 PRC = 0.083	PRC = 0.083	FP-EPDM = 0.25 EPDM = 0.011 PRC = 0.083	EPDM = 0.071	0.712
R70 → T	EPDM = 0.071 PRC = 0.083	HYPALON = 0.333 EPDM = 0.071 PRC = 0.083	FP-EPDM = 0.25 EPDM = 0.011	EPDM = 0.071 PRC = 0.083	1.116
T → R27	EPDM = 0.071 PRC = 0.083	PRC = 0.083	FP-EPDM = 0.25 EPDM = 0.071 PRC = 0.083	EPDM = 0.071	0.712
R27 → T	EPDM = 0.071 PRC = 0.083	HYPALON = 0.3333 EPDM = 0.071 PRC = 0.083	FP-EPDM = 0.25 EPDM = 0.011 PRC = 0.083	HYPALON = 0.333 EPDM = 0.071	1.449
Totals	0.616	1.140	1.533	0.700	3.99	3.99

418

Table 6

Aging and Accident Combinations That Resulted in Degradation for U.S. Samples of Ultimate Tensile Elongation to Less Than 10% of Initial Values. (For TEFZEL, failure to pass a 22X bend test (all samples) .as the selection criteria). The numbers in the table refer to weighting averages as discussed in the text.

Aging Environment	R70→ST(AIR)	R70→ST(N_2)	R28→ST(AIR)	R28→ST(N_2)	R + ST(AIR)	R + ST(N_2)	Totals
R120	EPR1=.10 CSPE=.05 CPE=.04 TEFZEL1=.03 TEFZEL2=.04	EPR2=.13 CSPE=.05 CPE=.04 TEFZEL1=.03 TEFZEL2=.04	CSPE=.05 CPE=.04 TEFZEL1=.03 TEFZEL2=.04	CSPE=.05 CPE=.04 TEFZEL2=.04	EPR1=.10 EPR2=.13 CSFE=.05 TEFZEL1=.03 TEFZEL2=.04	CSPE=.05 TEFZEL1=.03 TEFZEL2=.04	1.31
R70 → 120	EPR1=.10 EPR2=.13 CSPE=.05 CPE=.04 TEFZEL1=.03 TEFZEL2=.04	CPSE=.05 CPE=.04 TEFZEL1=.03 TEFZEL2=.04	CSPE=.05 CPE=.04 TEFZEL1=.03 TEFZEL2=.04	CSPE=.05 CPE=.04 TEFZEL1=.03 TEFZEL2=.04	EPR2=.13 CSPE=.05 CPE=.04 TEFZEL1=.03 TEFZEL2=.04	CSPE=.05 TEFZEL1=.03 TEFZEL2=.04	1.28
120 → R70	EPR2=.13 CSPE=.05 CPE=.04 TEFZEL1=.03 TEFZEL2=.04	CPE=.04 TEFZEL1=.03 TEFZEL2=.04	CSPE=.05 CPE=.04 TEFZEL1=.03 TEFZEL2=.04	CPE=.04 TEFZEL1=.03 TEFZEL2=.04	EPR1=.10 CPE=.04 TEFZEL1=.03 TEFZEL2=.04	TEFZEL1=.03 TEFZEL2=.04	.95
R27 → 120	EPR1=.10 EPR2=.13 CSPE=.05 CPE=.04 TEFZEL1=.03	CSPE=.05 CPE=.04 TEFZEL1=.03	CSPE=.05 CPE=.04 TEFZEL1=.03	CSPE=.05 CPE=.04 TEFZEL1=.03	EPR2=.13 CSPE=.05 CPE=.04 TEFZEL1=.03 TEFZEL2=.04	CPE=.04 TEFZEL1=.03 TEFZEL2=.04	1.07
120 → R27	EPR1=.10 CPE=.04 TEFZEL1=.03 TEFZEL2=.04	EPR1=.10 EPR2=.13 CPE=.04 TEFZEL1=.03	EPR1=.10 CPE=.04 TEFZEL1=.03	EPR1=.10 CPE=.04 TEFZEL1=.03 TEFZEL2=.04	EPR1=.10 CPE=.04 TEFZEL1=.03 TEFZEL2=.04	TEFZEL1=.03 TEFZEL2=.04	1.17
Totals	1.46	.98	.77	.73	1.35	.49	5.78

5.78

419

Table 7

Aging and Accident Combinations That Resulted in Degradation for French Samples of Mechanical Properties to Less Than 5% of Initial Values. The numbers in the table refer to weighting averages as discussed in the text.

| Aging Environment \ Accident Environment	R70→ST(AIR)	LOCA(AIR)→R70	R + LOCA(AIR)	R28→LOCA(AIR)	Totals
T → R70	HYPALON = 0.083 FP-EPDM = 0.111 EPDM = 0.067 PRC = 0.067	HYPALON = 0.083 EPDM = 0.067 PRC = 0.067	FP-EPDM = 0.111 EPDM = 0.067 PRC = 0.067	HYPALON = 0.083 EPDM = 0.067 PRC = 0.067	1.007
R70 → T	HYPALON = 0.083 FP-EPDM = 0.111 EPDM = 0.067 PRC = 0.067	HYPALON = 0.083 FP-EPDM = 0.111 EPDM = 0.067 PRC = 0.067	FP-EPDM = 0.111 EPDM = 0.067	HYPALON = 0.083 EPDM = 0.067 PRC = 0.067	1.051
T → R27	HYPALON = 0.083 EPDM = 0.067 PRC = 0.067	HYPALON = 0.083 PRC = 0.067	FP-EPDM = 0.111 EPDM = 0.067 PRC = 0.067	HYPALON = 0.083 EPDM = 0.067 PRC = 0.067	0.829
R27 → T	HYPALON = 0.083 FP-EPDM = 0.111 EPDM = 0.067 PRC = 0.067	HYPALON = 0.083 FP-EPDM = 0.111 EPDM = 0.067 PRC = 0.067	FP-EPDM = 0.111 EPDM = 0.067 PRC = 0.067	HYPALON = 0.083 EPDM = 0.067 PRC = 0.061	1.118
Totals	1.201	1.023	0.913	0.868 4.005	4.005

420
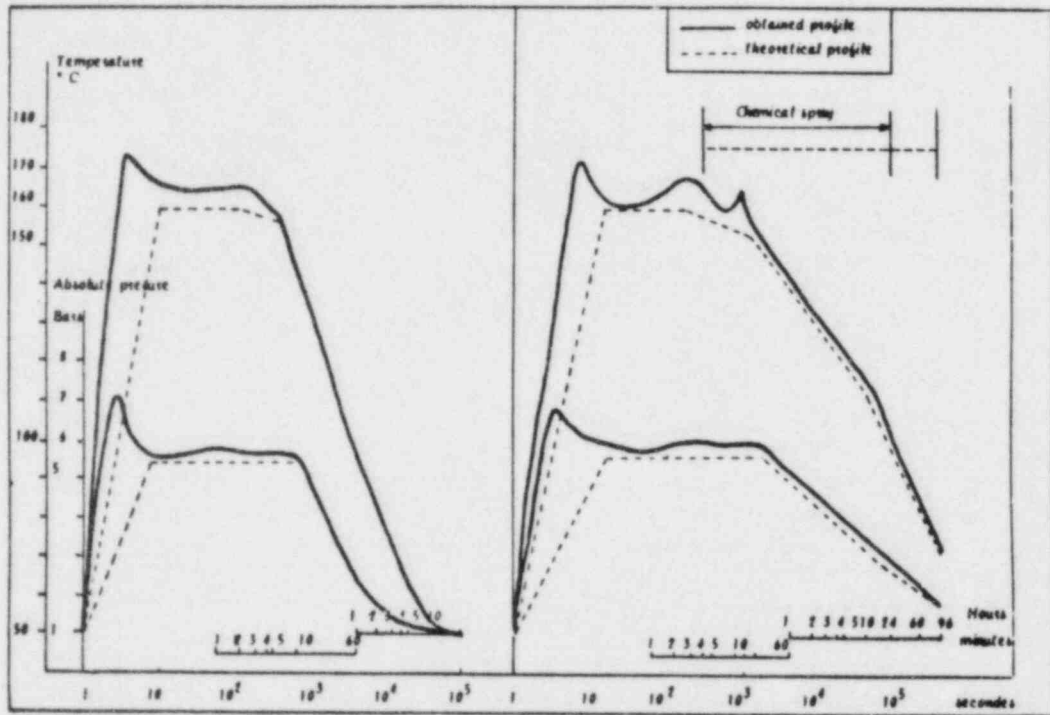
Figure 1: The Thermodynamic (Steam and Chemical Spray) Profile for Temperature (Upper Curve) and Pressure (Lower Curve) Employed During the L1 + L4 Test Exposure
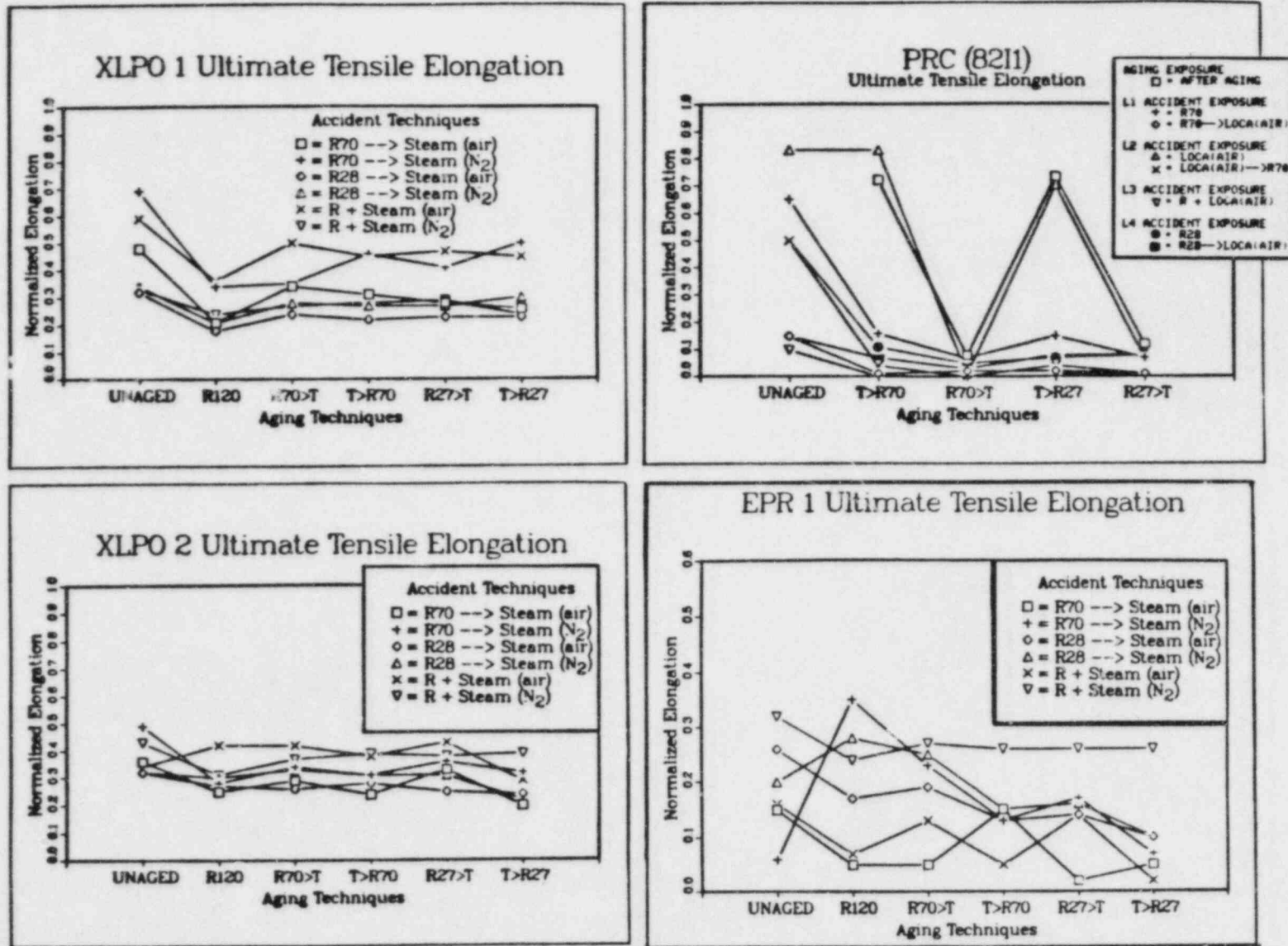
421

Figure 2: Ultimate Tensile Elongation of XLPO 1, XLPO 2, PRC (82I1), and EPR 1 at Completion of Various Phases of the Aging and Accident Exposures
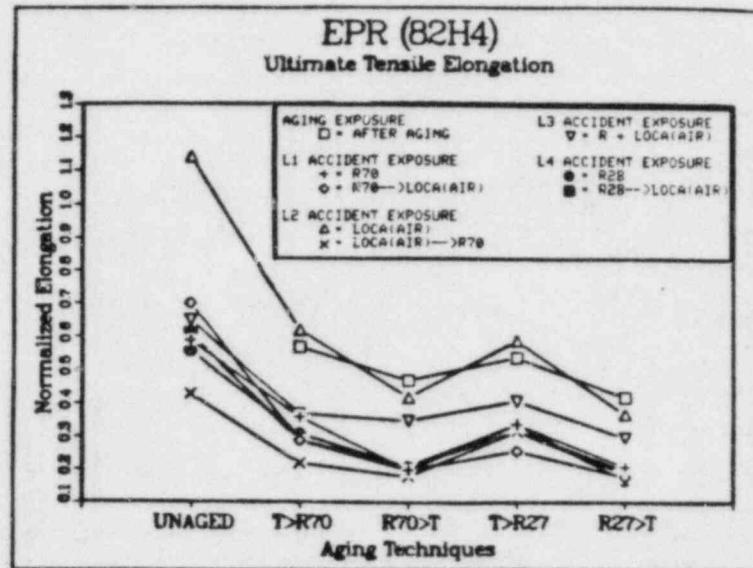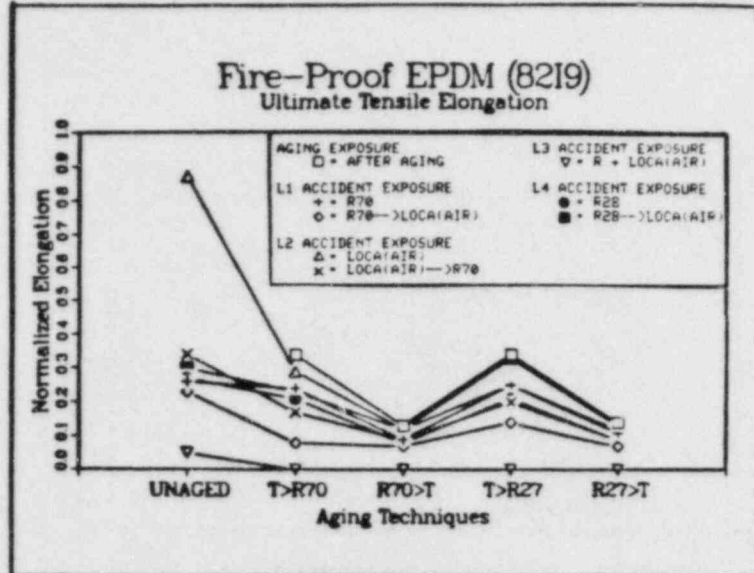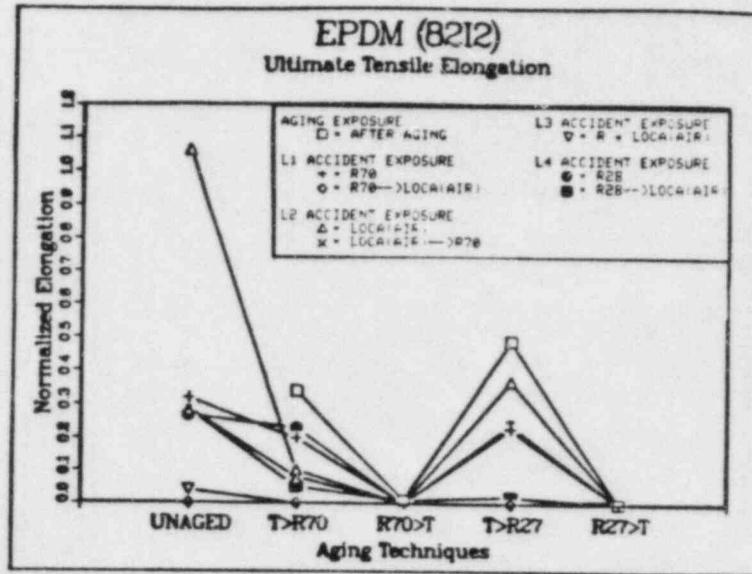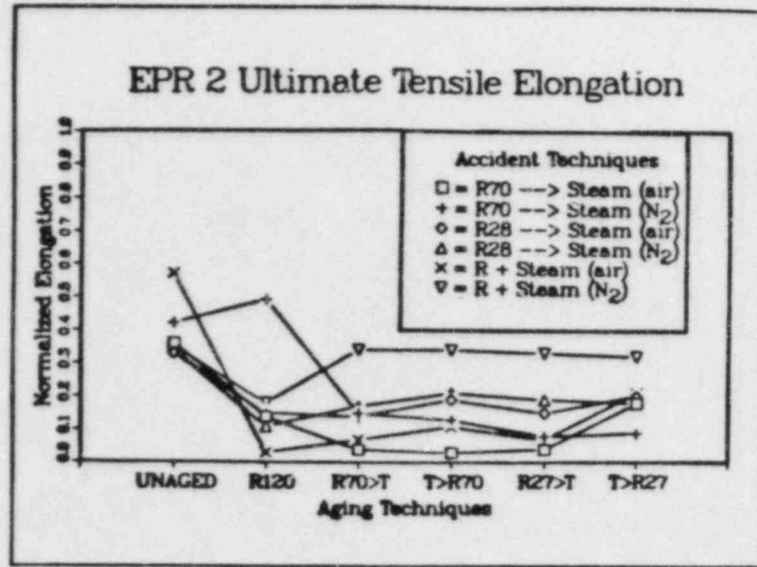
Figure 3: Ultimate Tensile Elongation of EPR 2, Fire-Proof EPDM (8219), EPDM (82I2), and EPR (82H4) at Completion of Various Phases of the Aging and Accident Exposures

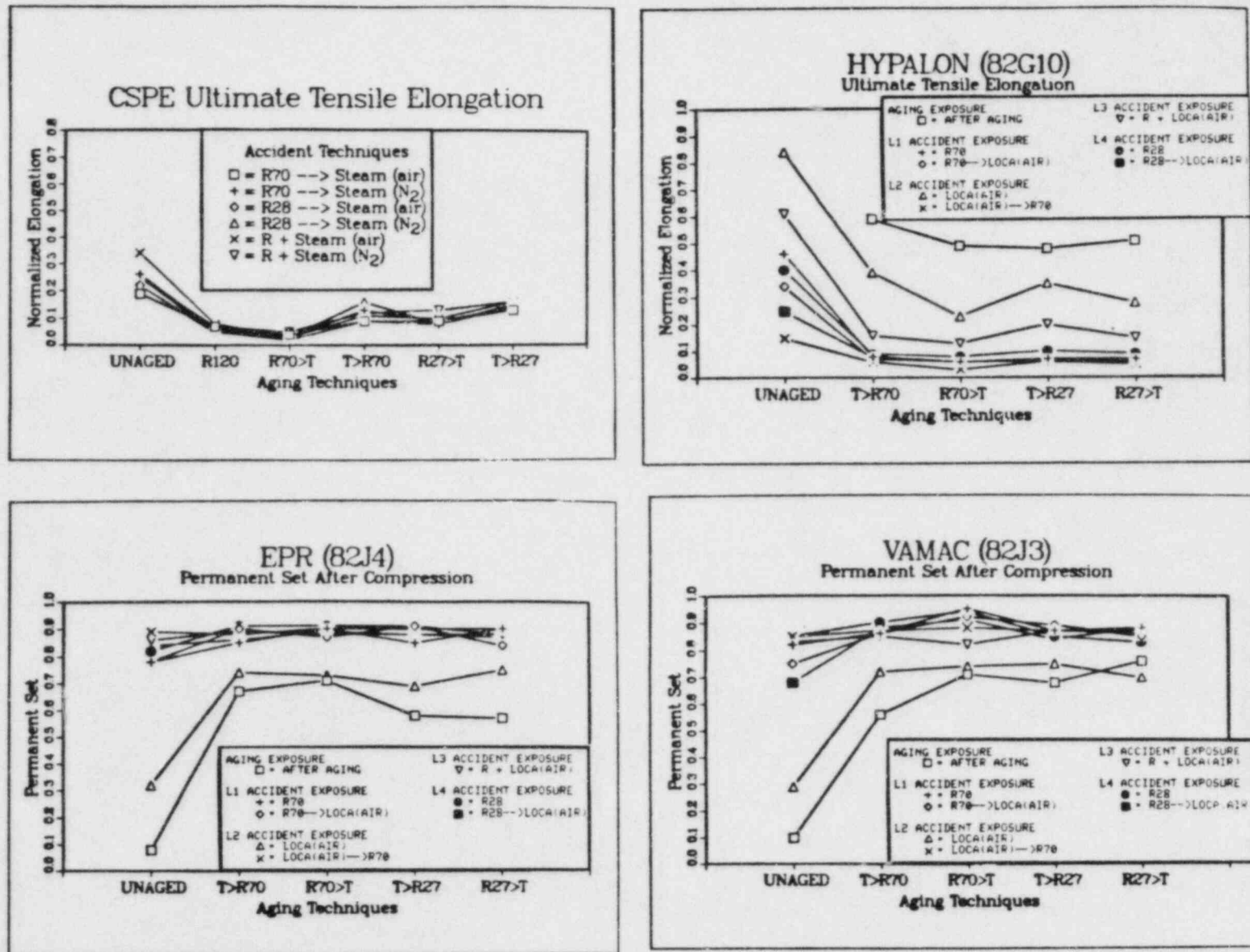Figure 4: Mechanical Properties for CSPE, HYPALON, and the O-ring Materials (EPR (82J4) and VAMAC (82J3)) at Completion of Various Phases of the Aging and Accident Exposures
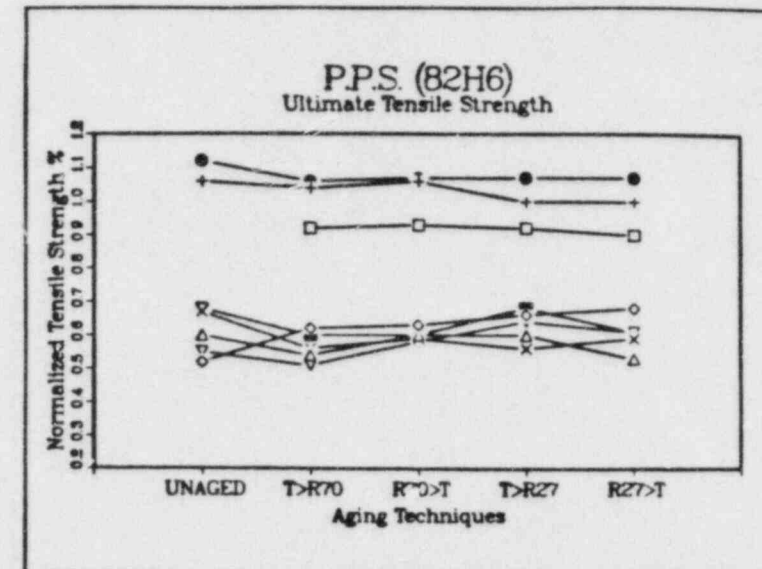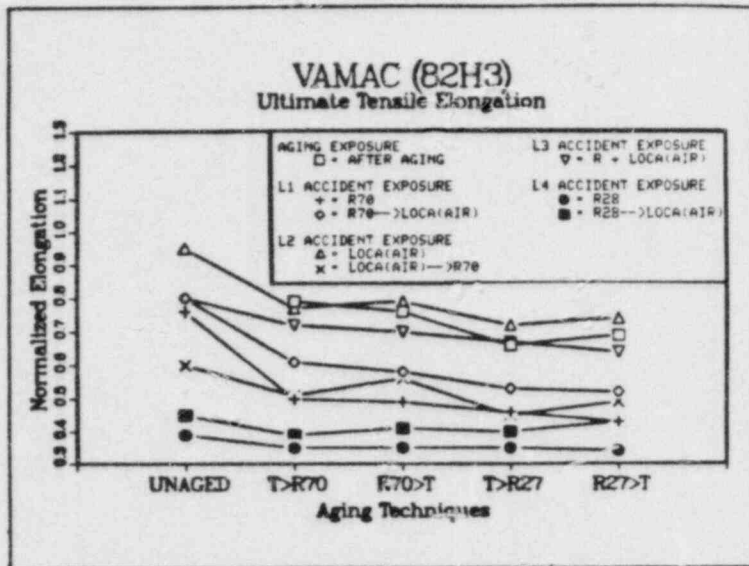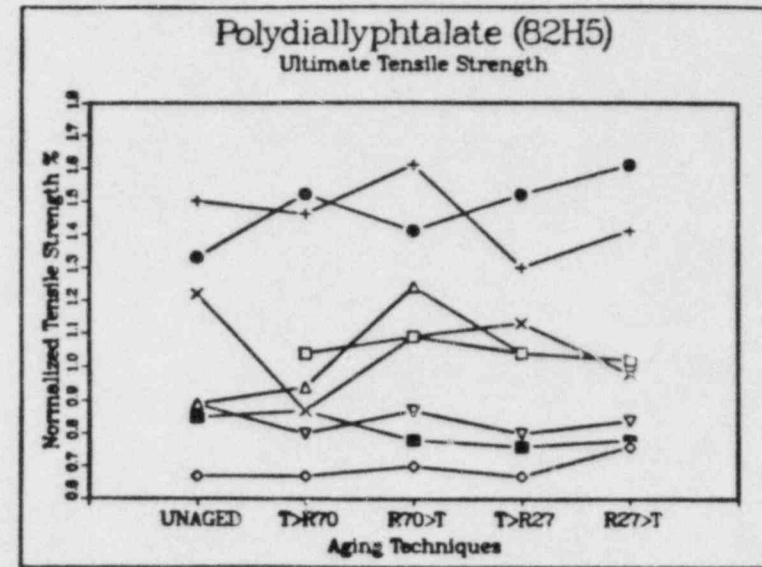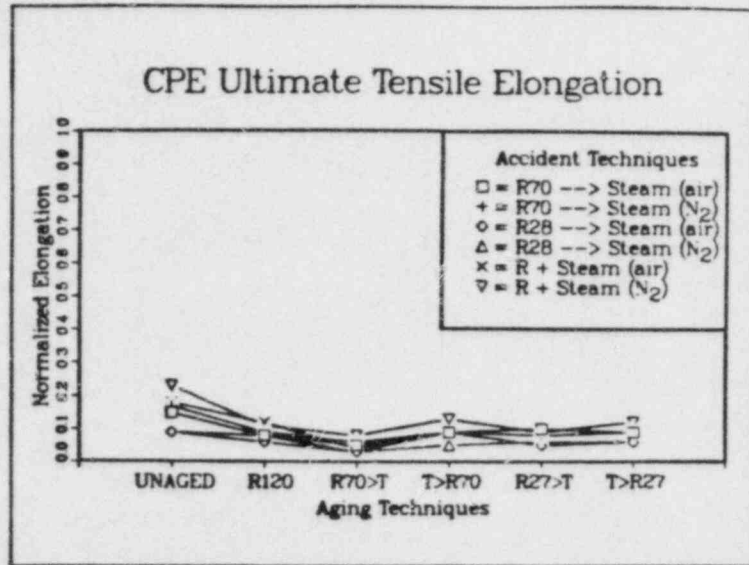
Figure 5: Ultimate Tensile Properties for CPE, Polydiallylphtalate (82H5),
VAMAC (82H3) and PPS (82H6) at Completion of Various Phases of the
Aging and Accident Exposures. The figure key for polydiallylphtalate
and PPS is the same as that for VAMAC.

NUCLEAR PLANT AGING RESEARCH - AN OVERVIEW
(ELECTRICAL AND MECHANICAL COMPONENTS)

J. P. VORA
OFFICE OF NUCLEAR REGULATORY RESEARCH
U. S. NUCLEAR REGULATORY COMMISSION

INTRODUCTION:

As the operating nuclear power plants advance in age there must be a conscious national and international effort to understand the influence and safety implications of aging and service wear of components and structures in nuclear power plants and develop measures which are practical and cost effective for timely mitigation of aging degradation that could significantly affect plant safety. In addition to following good maintenance practices, the safety of operating nuclear power plants may depend on making certain that component degradation with age is recognized and accommodated before it can cause significant reduction in safety, under normal operating conditions and during and after trigger events or accident conditions.

The Office of Nuclear Regulatory Research has, therefore, initiated a multi-year, multi-disciplinary program on Nuclear Plant Aging Research (NPAR). The overall goals identified for the program are as follows:

PROGRAM GOALS

o   To identify and characterize aging and service wear effects associated with electrical and mechanical components, interfaces, and systems whose failure could impair plant safety.

o   To identify and recommend methods of inspection, surveillance and condition monitoring of electrical and mechanical components and systems which will be effective in detecting significant aging effects prior to loss of safety function so that timely maintenance and repair or replacement can be implemented.

o   To identify and recommend acceptable maintenance practices which can be undertaken to mitigate the effects of aging and to diminish the rate and extent of degradation caused by aging and service wear.

The specific research activities to be implemented to achieve these goals include:

RESEARCH ACTIVITIES

I.   Risk and Systems Oriented Identification of Aging Effects
    A.   Correlation of Risk and Aging Trends
    B.   Integration and Analysis of the Impact of Component Aging
        on System Performance
    C.   LWR Operating Experience Survey to Identify Aging Trends
    D.   Selection of Components for Aging Assessments
    E.   Evaluation of Impact of Plant Cycling and Trips on Components
        and Structures

II. Component Aging Assessment

   A. Evaluation of Operating Experience
   B. Post-Service Examination and Testing
   C. Investigation of Aging/Seismic Stress Interaction (special topic)
   D. In-situ Monitoring and Testing of Operating Equipment

III. Evaluation of Inspection, Surveillance, and Condition Monitoring Methods

   A. Identification of Performance Indicators
   B. Review of Current Inspection, Surveillance, and Condition
       Monitoring Methods
   C. Verification of Monitoring Methods at Operating Facilities
   D. Evaluation of Occupational Exposure Associated with Monitoring
       Methods
   E. Evaluation of Service-Life Predicting Methods

IV. Evaluation of the Role of Maintenance in Counteracting Aging Effects

   A. Survey of Current Maintenance Practices to Counteract Aging
       and Service Wear of Components and Structures
   B. Evaluation of Relative Benefits of Preventive and Corrective
       Maintenance
   C. Identification of Potential Mechanisms Causing Equipment
       Degradation Through Improper Maintenance
   D. Development of Recommendations for Preferred Maintenance
       Practices

RESEARCH PROGRAM STRATEGY

The NPAR program has been planned so that the major program elements (the circled elements in Figure 1) can be applied uniformly to all components and systems under study. A number of supporting tasks, identified by blocks in Figure 1, have been selected and scheduled so that research on the major elements can proceed with the full benefit of necessary groundwork.

Emphasis has been placed on learning from operating experience, at the systems level and component level, avoiding duplication, attempting to coordinate research activities with willing organizations and institutions, and refraining from government sponsored research which the industry is best qualified and willing to pursue.

Where information is needed from manufacturers and utilities, consultation and communication by the NRC contractors will be pursued. Where related research is underway, liaison will be necessary. Insofar as practical, both government- and industry-supported programs and both domestic and foreign efforts will be included. The overall program plan will include establishment of a central data bank (component specific-systems specific), of information on research relevant to plant aging, standards and guides relevant to aging, and citations and sources of published information on plant aging. This central, integrated source of information will benefit not only the NRC in its plant aging research, but also all other organizations (laboratories, utilities,

427

professional societies, and manufacturers) concerned with plant aging. The program will identify gaps in existing aging related research that can be filled by government or industry sources depending on which is most appropriate.

Another element of the overall program strategy is to provide the maximum possible flow and exchange of information. In addition to the publication of reports on the research tasks, this will be accomplished through avenues such as preparation of technical papers, coordination of sessions at technical conferences, sponsorship of workshops and symposia, and exchange of visits with principal sources of related research.

A final product of the research program will be recommendations for the revision of existing standards and regulatory guides and the development of new standards and guides as necessary. A significant factor in this regard is that the program intends to provide the technical basis for all of its recommendations. Compliance is much more effective when the technical basis is clear and the guidelines are consistent with the state of technology. Revisions and additions to existing standards and guides will be recommended. When appropriate, recommendations for revisions to regulations, standard review plans, and technical specifications will be made.

The aging assessment of selected components has been contemplated in discrete phases for effective project management and for the optimum utilization of available resources. For a given component, Phase I would involve a collection of data from past experience, including a survey of current inspection and monitoring practices, and limited "screening type" post-service examinations. At the end of Phase I, an appropriate distribution of additional resources between assessment of advanced inspection and monitoring methods and equipment tests under accident conditions would be decided based on information obtained through that time. Phase II would include the recommended mixture of advanced inspection and monitoring assessment and testing and development of final recommendations. The steps for aging research with two phases of component assessment may involve:

I.   Risk/Aging/Systems Studies (Select Components)

II. Component Assessment

PHASE I

A.   Review of Past Operating Experience, Qualification Testing
     Performed, Design and Operating Environments as Basis for Preliminary
     Assessments of Failure Causes/Modes

B.   Survey of Current Inspection, Surveillance, Monitoring and Maintenance
     Methods

C.   Perform Screening-Type Post Service Examinations of Equipment
     from Decommissioned and Operating Reactors

D.   Perform In-situ Monitoring in Cooperation with Willing Utilities

E.   Perform Integrated Assessment of Aforementioned Activities and Make
     Interim Recommendations for an Appropriate Combination of Testing of
     Naturally Aged Equipment and Evaluation of Advanced Inspection,
     Surveillance, Monitoring Methods and Maintenance

PHASE II

F.   Review and Verify Advanced Inspection, Surveillance, Monitoring and Maintenance Techniques for Selected Components

G.   Perform Test on Selected Equipment (Naturally Aged, New with Artificially Implanted Defect)

H.   Value Impact Studies and Final Recommendation for Inspection, Surveillance, Monitoring and Maintenance

Within the resources allocated to the current NPAR program, it will not be possible to perform the comprehensive aging assessments, defect characterization, and provide recommendations for inspection, surveillance and maintenance of all vital components and systems in nuclear power plants. However, the benefits of the NPAR strategy will be demonstrated by applying it to selected components and systems. The intent is then to transfer the assessment strategy, backed up by illustrative examples, for the industry to use.

ACTIVITIES AND MILESTONE SCHEDULE

The currently estimated schedules and milestones for completing these activities are provided in Figure 2. These general schedules, and particularly schedules for evaluation of specific component types will depend on the assignment of components to priority groups (group 1, group 2, etc.), an activity to be completed early in the program, and the degree of participation by and coordination with other organizations. The NRC staff and its contractors will actively pursue such participation from domestic and foreign organizations. The degree and depth of component and systems aging assessments will depend upon the availability of funds and the cooperative and complimentary programs which can be initiated with other organizations and institutions.

DISSEMINATION OF RESEARCH RESULTS

The preferred format for implementing this goal will be the dissemination of information developed in the research program directly to national consensus standard writing groups (e.g., IEEE, ASME, ANS, and ASTM) and directly to utilities in cooperation with INPO and EPRI, equipment vendors, and architect engineering firms responsible for developing plant specific programs. In addition, it is anticipated that revisions to existing regulatory guides endorsing national consensus standards, development of new regulatory guides, and revision and addition to plant technical specifications will be initiated based on recommendations emanating from the research. It is the intent of the program that any recommendations for regulatory guidance will be justified through value impact analyses based on technical results and data generated through the research.

CONCLUDING REMARKS:

The NPAR goals enumerated in the beginning may appear ambitious but are achievable through cooperative programs, and with active participation and information exchanges among the utilities sharing their operating experiences and surveillance and maintenance practices, equipment manufacturers sharing their nonproprietary designs and construction know-hows, the architectural engineering firms sharing their knowledge pertaining to specifications, standards, systems interaction and installations and research organizations contributing their skills and expertise in understanding aging phenomena. We can then develop codes and standards and regulatory guidance based on strong technical understandings. It is envisioned that while achieving the identified NPAR goals, the industry will benefit further from the improved availability and reliability of plant components and systems and generate confidence in all of us for plant life extension considerations.

In the companion papers we have attempted to illustrate selected examples of the applicability of the overall NPAR strategy, as discussed in this overview, to the understanding of aging and defect characterization of motor operated valves, and a review of the concept of condition monitoring, and a review of surveillance and diagnostics technology as applicable to cables inside containment. At the technical level, these types of results are expected for various other components and systems which will be studied under the NPAR program.
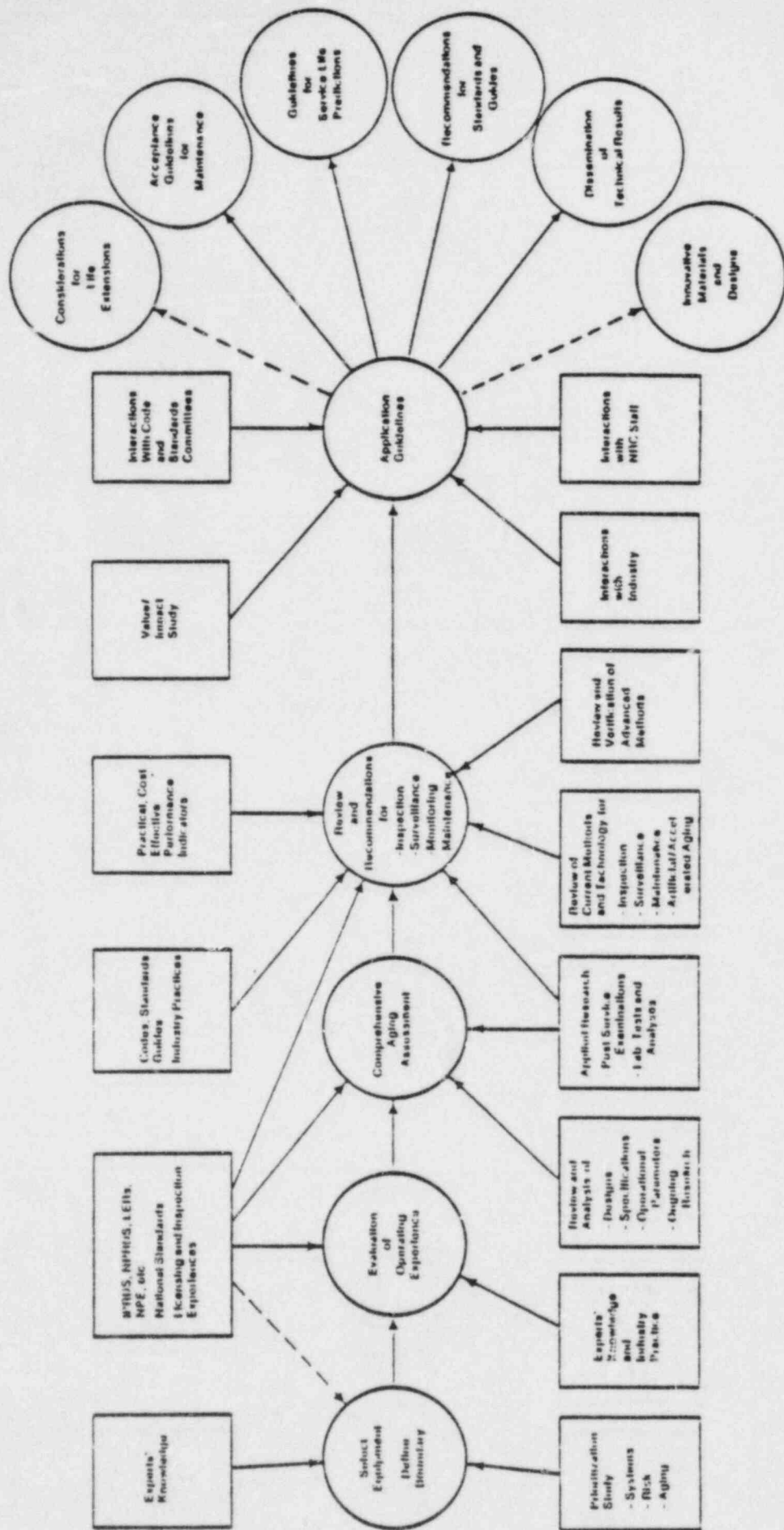
Figure 1 - NPAR Program Strategy

431

NPAR — MILESTONES AND SCHEDULE

END OF FISCAL YEAR

	R3	R4	R5	R6	R7	R8	R9

ACTIVITY DESCRIPTION

I. Risk Oriented Identification of Aging Effects
- A. Correlation of Risk and Aging Trends
- B. Analysis of Impact of Component Aging on System Performance
- C. LWR Operating Experience Survey to Identify Aging Trends
- D. Selection of Components for Aging Assessment (Groups 1, 2, 3, ...)
- E. Evaluation of Impact of Plant Cycling and Trips on Components and Structures

II. Component Aging Assessment
- A. Evaluation of Operating Experience
- B. Post-Service Examinations and Tests
- C. Investigation of Aging/Seismic Stress Interaction
- D. In-Situ Monitoring of Operating Equipment

III. Evaluation of Inspection, Surveillance, Monitoring Methods
- A. Identification of Performance Indicators
- B. Review of Current Surveillance/Inspection Technology
- C. Verification of Monitoring Methods at Operating Facilities
- D. Evaluation of Occupational Exposure Associated with Monitoring Methods
- E. Evaluation of Service-Life Prediction Methods

IV. Evaluation of Role of Maintenance In Counteracting Aging Effects
- A. Survey of Current Maintenance Practices to Counteract Aging and Service Wear of Components and Structures
- B. Evaluation of Relative Benefits of Preventive & Corrective Maintenance
- C. Identification of Potential Mechanisms Causing Equipment Degradation Through Improper Maintenance
- D. Development of Recommendations for Preferred Maintenance Practices

V. Recommendations for Standards and Guides
- A. Rev. of R.G. 1.89 and IEEE Std. 323
- B. Rev. of R.G. 1.100 and IEEE Std. 344
- C. Guidelines for Aging Assessment and Condition Monitoring

ELECTRICAL SYSTEM
FLUID SYSTEM

GR. 1
GR. 2, 3, ...
1
2, 3, ...
4
MOTOR
CHARGERS/INVERTERS
RELAYS
GR. 1; ELEC. EQUIP. IN HARSH ENVIRONMENT
GR. 2, 3
GR. 4
GR. 1
GR. 2, 3
GR. 4
GR. 2, 7

FIGURE 2

432

AGING AND DEFECT CHARACTERIZATION OF MOTOR-OPERATED VALVES:
PROGRESS BASED ON NPAR STRATEGY*

D. M. Eissenberg
Oak Ridge National Laboratory

Background

The Nuclear Plant Aging Research (NPAR) program strategy is directed at carrying out comprehensive aging assessments in order to define and resolve issues related to aging (including service wear) of electrical and mechanical components and structures at operating reactor facilities and their possible impact on plant safety. One currently used approach to dealing with aging degradation of electrical components consists of establishing a qualified life based on calculations or on tests (usually of equipment which has been aged by exposure to more severe stressors than anticipated in reactor service). A second approach, used both with electrical and mechanical equipment, is to carry out periodic surveillance tests. These tests are intended to establish that the component at the time of the test is in a state of operational readiness.

The NPAR approach to dealing with aging and service-wear effects is to develop the methodology of trending component parameters which are directly or indirectly related to aging degradation and, based on a-priori criteria, performing maintenance (repair, replacement, etc.) prior to failure. This methodology is frequently referred to as predictive maintenance.

Objective

This paper describes work recently completed at Oak Ridge National Laboratory which applied the NPAR strategy to motor-operated valves (MOVs). The objective of the work was primarily to develop an understanding of the operating history and conditions and the failure modes of MOVs in nuclear plant service as a preliminary to identifying and recommending methods for trending aging degradation. A second objective was to demonstrate, using MOVs as an example, that the NPAR strategy can be applied to many electrical and mechanical components of nuclear power plants.

The work reported here represents the completion of the first of three parts of the comprehensive aging assessment of MOVs. The contents of each of the three parts are shown in Table 1.

Table 1. Contents of comprehensive aging assessment

Part I

- Background information on motor-operated valves
- Regulatory requirements, guides, and standards
- Summary of operational and environmental stressors
- Summary of operating experience with motor-operated valves
- Manufacturers' input
- Tabulation of failure modes and causes
- Tabulation of measurable parameters suitable for trending defects

Part II

- Postservice examination and tests of aged equipment
- In-situ assessments of aged equipment
- Assessment of advanced monitoring techniques
- Controlled laboratory testing of monitoring techniques

Part III

- Cost/benefit impact analysis
- Guidelines for monitoring methods and maintenance philosophy
- Service-life prediction techniques

Valve Descriptions

Motor-operated valves of many sizes and types are used extensively in LWR power plants. A summary of the MOVs used in a typical BWR nuclear power plant is given in Table 2, which gives the valve numbers, size range, and types as utilized in the various safety systems. Similar usage occurs in PWR nuclear power plants.

Table 2. Typical motor-operated valve usage
in BWR nuclear power plants

System	Number of MOVS	Valve size (in.)*	Valve type
Low-pressure core spray	8-12	2-28	G, GL
High-pressure coolant injection	8-14	4-24	G, GL
Low-pressure coolant injection (includes RHR and containment spray)	28-50	4-24	G, GL
Reactor recirculation system	8-10	2-28	G
Reactor core isolation cooling	8-10	3-6	G, GL
Containment isolation	4-14	3-24	BF, G
Balance-of-plant systems	50-150	2-60	G, GL, BF

Legend: G - Gate Valve
         GL - Globe Valve
         BF - Butterfly Valve
         * Nominal Pipe Size

For this work, the MOV is defined as including the motor operator and the valve as separate assemblies. The functional subassemblies, individual parts, and materials of construction were identified for the valve (Fig. 1) and for the motor operator (Fig. 2) in enough detail to allow analysis of failure causes.

Operating stressors, acting on each subassembly and part, were identified and quantified, where possible, under both normal and emergency conditions. A tabulation of the stressors considered and the subcomponents which were determined to be affected by them is given in Table 3. The expected response of each subcomponent to the stressors was reviewed to provide a basis for relating the stressors to the observed degradation.
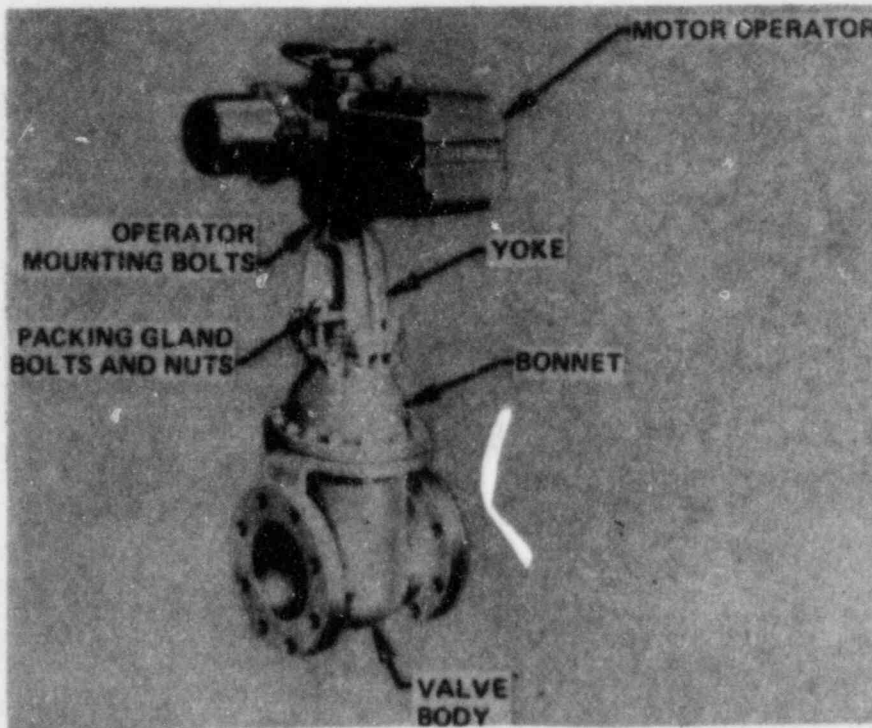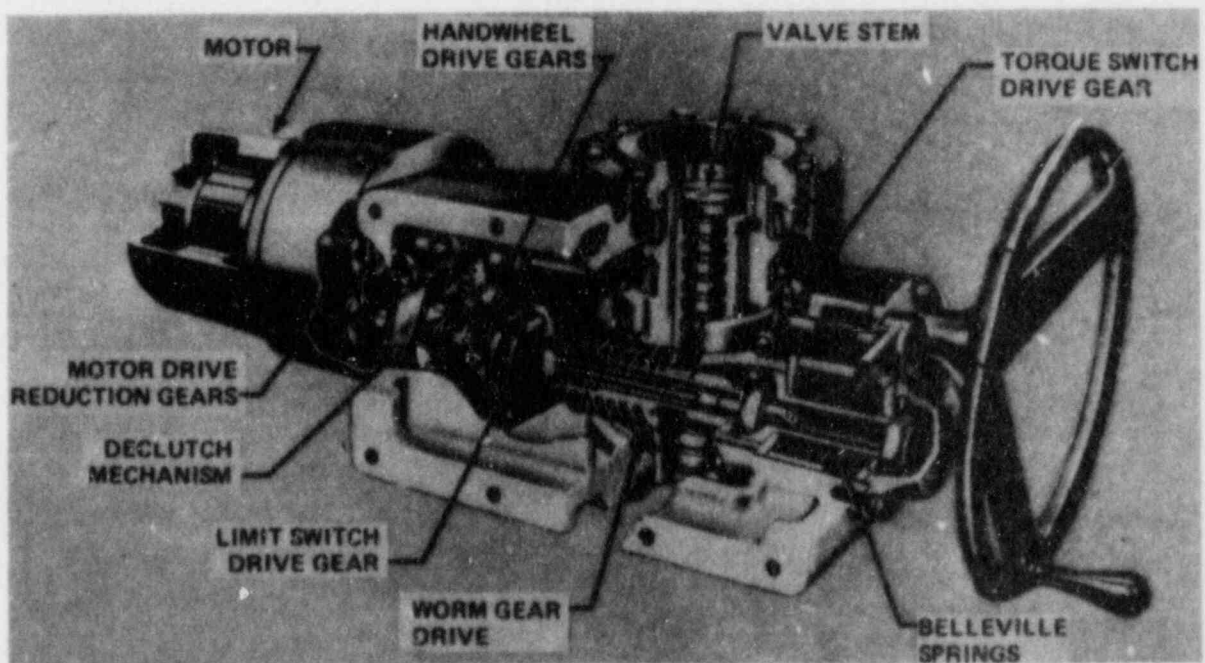
Fig. 1. Typical motor-operated valve assembly

Fig. 2. Typical motor-operator assembly

436

Table 3. Operational stressors acting on
motor-operated valve subassemblies

Stressors	Applicable subcomponents
Electrical	Motors, switches, cables
Mechanical	All subassemblies and parts
Thermal	Seals, lubricants, insulation
Chemical	Body assembly, seals
Radiation	Insulation, lubricants, seals, and gaskets
Environmental	External surfaces (especially valve stem)

A major part of the assessment consisted of identifying failure modes and causes. The first approach was to collect and review nuclear plant operating experience information in order to summarize and categorize MOV failures observed in operating plants. Four data bases were reviewed, as well as seven reports which dealt explicitly with observed valve failures in nuclear plants (Table 4). The failure information available from the various data bases was limited since it included only failures that had occurred in nuclear plants to date. Thus, the effects of long-term (>20 years) exposure to operating stressors could not be included. In addition, the information included in any data base was defined by the objective of the operator of the data base. The type of information available from each data base is summarized in Table 5.

Table 4. Data bases and reports providing
operating data on motor-operated valves

Data Bases

Licensee Event Report (LER) Data System
Nuclear Plant Reliability Data System (NPRDS)
In-Plant Reliability Data System (IPRDS)
Nuclear Power Experience (NPE)

Reports

NUREG/CR-0848, "Summary and Bibliography of Operating Experience
with Valves in Light-Water-Reactor Nuclear Power Plants for
the Period 1965-1978"

NUREG/CR-1363, "Data Summaries of Licensee Event Reports of
Valves at U.S. Commercial Nuclear Power Plants, January 1,
1976 - December 31, 1978"

ALO-73, "Investigation of Valve Failure Problems in LWR Power
Plants"

ALO-75, "Pilot Program to Identify Valve Failures Which Impact
the Safety and Operation of LWR Nuclear Power Plants"

EPRI NP-241, "Assessment of Industry Valve Problems"

AEOD/C203, "Survey of Valve Operator-Related Events Occurring
During 1978, 1979, and 1980"

INPO 83-037, "Assessment of Motor-Operated Valve Failures"

Table 5. Types of information available from data bases

Data/Source	Operating Experience Data Bases			
	LER	NPRDS	IPRDS	NPE
Valve type and description		0	X	0
Manufacturer and model number		X		0
Operating environment		X		
Failure mode	0	X		0
Failure cause	0	0		0
Discrete failed part	0	X		X
Maintenance action	0	0	X	X
Modification to prevent recurrence	0	0	X	0
Failure trend data				
Incipient failure detection			X	

X - Generally available
0 - Occasionally included in failure report

The optimum data source for operating experience information would be the plant-specific surveillance and maintenance records--including results of surveillance tests as required by Technical Specifications, as well as the result of inspections, surveillance testing, and condition monitoring as utilized in normal utility practice. These records are in general not readily accessible since many nuclear power plants do not currently utilize computer storage for maintenance and/or surveillance records.

Based on the information contained in the data bases, the most frequently reported failure mode of motor operators was "failure to change position." The most frequently cited causes were torque-switch or limit-switch misadjustments or failures, motor failures, and protective overload trips. These failure causes reflect premature aging, i.e., that due to inadequate maintenance or to nonoptimum sizing of the motor operator with reference to the valve requirements.

439

The most common failure mode for the valve subcomponent was internal leakage. The failure causes were the presence of foreign material and valve seat wear. Here, too, these causes may have resulted from premature aging as well as normal aging.

A more complete list of MOV failure modes and causes resulting from either normal or premature aging was compiled as part of this study, based on a review of designs and discussions with the manufacturers shown in Table 6. The resulting list of gate valve failure modes and causes associated with the body assembly is shown in Table 7. A similar list was derived for each of the other valve subcomponents and for each of the other valve types used in nuclear plant safety-related systems.

Table 6. Valve and motor-operator manufacturers
contacted for discussion of failure causes

Motor Operator	Valve
Limitorque Corporation	Atwood and Morrill Company, Inc.
Rotork Controls, Inc.	Masoneilan Division, McGraw Edison Co.
	Rockwell International, Flow Control Division
	Valtek
	Walworth Company

Table 7. Summary of gate valve body assembly
failure modes and causes

	Failure Modes				
Failure causes	Failure to open	Failure to close	Failure to operate as req'd	Internal leakage	External leakage
Body erosion, corrosion				X	X
Body rupture					X
Obturator guide wear, galling, erosion, corrosion	X	X	X		
Yoke bushing wear	X	X	X		
Fastener loosening, breakage	X	X	X		X

In a similar fashion, the failure causes associated with each subcomponent of the motor operator were identified. The gearbox assembly failure causes are tabulated in Table 8. It is noted that the list is not intended to prioritize failure causes either by their frequency of occurrence or by the severity of the consequences. Each failure cause would result ultimately in failure of the operator to change the position of the valve.

441

Table 8. Summary of motor-operator gearbox
assembly failure causes

Gear wear, breakage
Shaft wear, distortion, fracture
Shaft pin or key wear, breakage
Fastener loosening, breakage
Gearbox fracture
Stem wear, galling, distortion, breakage
Stem nut wear, galling, breakage
Stem locknut loosening, breakage
Spring pack response change, wear, fracture
Thrust compensator (or control attachment) response change,
   wear, fracture
Thrust assembly wear, fracture
Clutch mechanism, wear, breakage
Valve obturator/seat seizure due to inertia
Motor-to-operator mounting loosening, breakage
Seal wear, deterioration
Bearing wear, corrosion
Lubricant degradation, hardening

Identification of Measurable Parameters

A second major part of this study was to identify, for the various failure causes, measurable parameters which could be trended using suitable measuring techniques and which would give information regarding the approach to failure of the MOV. In order to provide guidance in selecting parameters, a generic "shopping" list was compiled (Table 9). This list is intended to apply to all components. Each parameter is thus defined as clearly as possible, given its general applicability. Thus, for example, chemical composition may apply to a lubricant or to insulation. Similarly, response time may apply to valve stroke, switch actuation, or time to reach full rotational speed.

442

Table 9. Generic list of measurable parameters applicable
to electrical and mechanical components

Visual appearance (color, roughness, cracks, etc.)
Dimensions
Relative position within component boundary
Chemical and metallurgical composition
Mechanical, chemical, physical, or electrical properties
Eddy-current response
Ultrasonic response
Vibration
Acoustic emissions
Electromagnetic emissions
Response time
Electrical power requirements
Thrust or torque generated (internal or external)
Temperature level or difference
Internal pressure level or difference
Internal or external flow rate

A list of specific measurable parameters which could potentially detect and trend valve defects prior to failure is shown in Table 10. A comparable list for motor operators is shown in Table 11.

Table 10. Measurable parameters useful
for trending valve defects

Stroke time
Dimensions (various parts)
Visual appearance (various parts)
Stem play
Stem torque
Leakage rate (external and internal)
Bonnet pressure
Obturator position during operation
Downstream internal pressure
Downstream piping temperature
Acoustic emission
Humidity

443

Table 11. Measurable parameters useful for trending
defects in motor operators

Stroke time	Alignments
Handwheel torque	Switch actuation times
Stem thrust	Worm shaft play
Acoustic emission	Current/voltage
Vibration	Resistance
Torque, limit-switch settings	Current decay time
Dimensions (gearbox assembly)	Elasticity
Lost motion	Bolt torque
Cracking	Grease lubricity
Lubricant leakage	Grease fluidity
	Grease chemical composition

These lists and the supporting discussions represent the current status of the assessment of MOVs. The information described above has been documented in a report currently being reviewed by NRC.

Future Activities

From the lists of measurable parameters, key parameters will be selected for further study as part of the next phase. The bases for selection of key parameters include those identified with more frequent failure causes or the greatest number of different failure causes. Those parameters which can be trended to failure (such that criteria for maintenance prior to failure can be defined) will also be selected. The final basis for selection is that suitable, practical, cost-effective measuring techniques are either commercially available or could be readily developed for application to that component. To assist in the latter evaluation, a survey of the technologies of measurement applicable to trending the various parameters is currently underway. Techniques being surveyed include vibration monitoring, acoustic-emission monitoring, eddy-current testing, ultrasonic testing, remote infrared thermography, and thrust measuring devices. These will be considered along with the more conventional methods available for trending, including performance tests, dimensional checks, chemical analyses, etc.

Based on the selection of key parameters and measuring technologies, tests will be carried out, initially under controlled laboratory conditions and later in operating nuclear plants, which verify the applicability of the more promising methods to the trending of defects and component aging. The tests will determine selectivity and sensitivity, and will provide guidance as to the criteria needed with regard to continuing operation or carrying out suitable maintenance.

Surveillance and Diagnostics of Electrical Equipment Inside
Containment - Cable Monitoring Based on NPAR Strategy

S. Ahmed, G. J. Toman, and S. P. Carfagno

Franklin Research Center
20th and Race Streets, Philadelphia, PA   19103

ABSTRACT

This work addresses general concepts pertaining to inspection, sur-
veillance, and monitoring of electrical equipment inside containment, and
their application to electrical cables. The goal of condition monitoring
strategy is to identify potential failures in the incipient stage so that
preventive action can be taken before safety problems occur.

The application of condition monitoring to electrical cables located
inside of containment is discussed. The considerations that limit application
of test methods are described. Recommendations for practical approaches for
the implementation of a cable monitoring program and for development of
decision criteria are given. This paper presents an overview of the report
being prepared for the NPAR program.

1. INTRODUCTION

This presentation reports interim findings pertaining to initiating maintenance and replacement based on the results of inspection, surveillance, and condition monitoring of electrical equipment inside the containment of nuclear power plants. It is based on work performed as part of the Nuclear Plant Aging Research Program (NPAR) sponsored by NRC. The objective of this project is to develop interim recommendations, within the state of the art, for inspection, surveillance, and monitoring of aging effects for selected equipment. Further, criteria are to be established for the equipment of interest for decision making related to continued operation, maintenance, replacement, and repair. However, at this stage of the investigation, emphasis is placed on developing a framework to arrive at criteria and guidelines.

Section 2 provides an overview of various conceptual aspects of condition monitoring, including a basis for developing a strategy for surveillance, maintenance, and replacement; problem areas; and development of criteria for taking preventive measures. The status of cable condition monitoring (based on a literature review, experience, and communications with cable manufacturers and users) is documented in Section 3.

2. CONCEPTUAL ASPECTS OF CONDITION MONITORING

2.1 CONDITION MONITORING AS A STRATEGY FOR MAINTENANCE, REPAIR, AND REPLACEMENT

Condition monitoring of equipment may be defined as continuous or periodic observation and evaluation of critical parameters to assess the equipment's ability to continue to perform its specified safety functions during a period following the moment of observation. Observation may take the form of measurement or inspection. The specified functions of the equipment include those required in the event of applicable accidents as well as normal service. As used in this report, the term "condition monitoring" is distinguished from surveillance and diagnosis by its predictive feature. Condition monitoring is expected to reveal not only the functional state at the moment of observation, but also the ability of the equipment to remain capable of performing as specified for a period following the observation.

A simple picture of the ideal situation for the application of condition monitoring is given in Figure 2-1. The solid line represents the functional capability of the equipment, and the dashed lines represent parameters (or indicators) that have strong correlation to the functional capability or equipment degradation with time. An "acceptable" indicator for condition monitoring is one that shows a larger rate of change than that of the functional capability, thus providing a warning of impending functional degradation that may not yet be apparent. Conversely, if the rate of change of the indicator is slower than that of the function capability, then the indicator is not useful (labeled "unacceptable" in Figure 2-1). An indicator having a high rate of change relative to the rate of change of functional capability and good correlation with functional capability would be a good candidate for condition monitoring. Over a period of time, as shown in Figure 2-1, the functional capability may remain relatively constant and therefore may not provide sufficient evidence of equipment deterioration, whereas the condition monitoring indicator may indicate equipment deterioration and reveal an incipient failure condition.

Conceptually, a criterion may take the form of a statement such as: When the level of the functional indicator reaches the value A, preventive action B should be taken. For the purpose of illustration, consider an instrument cable (with all its connections) between an alarm in the control room and a
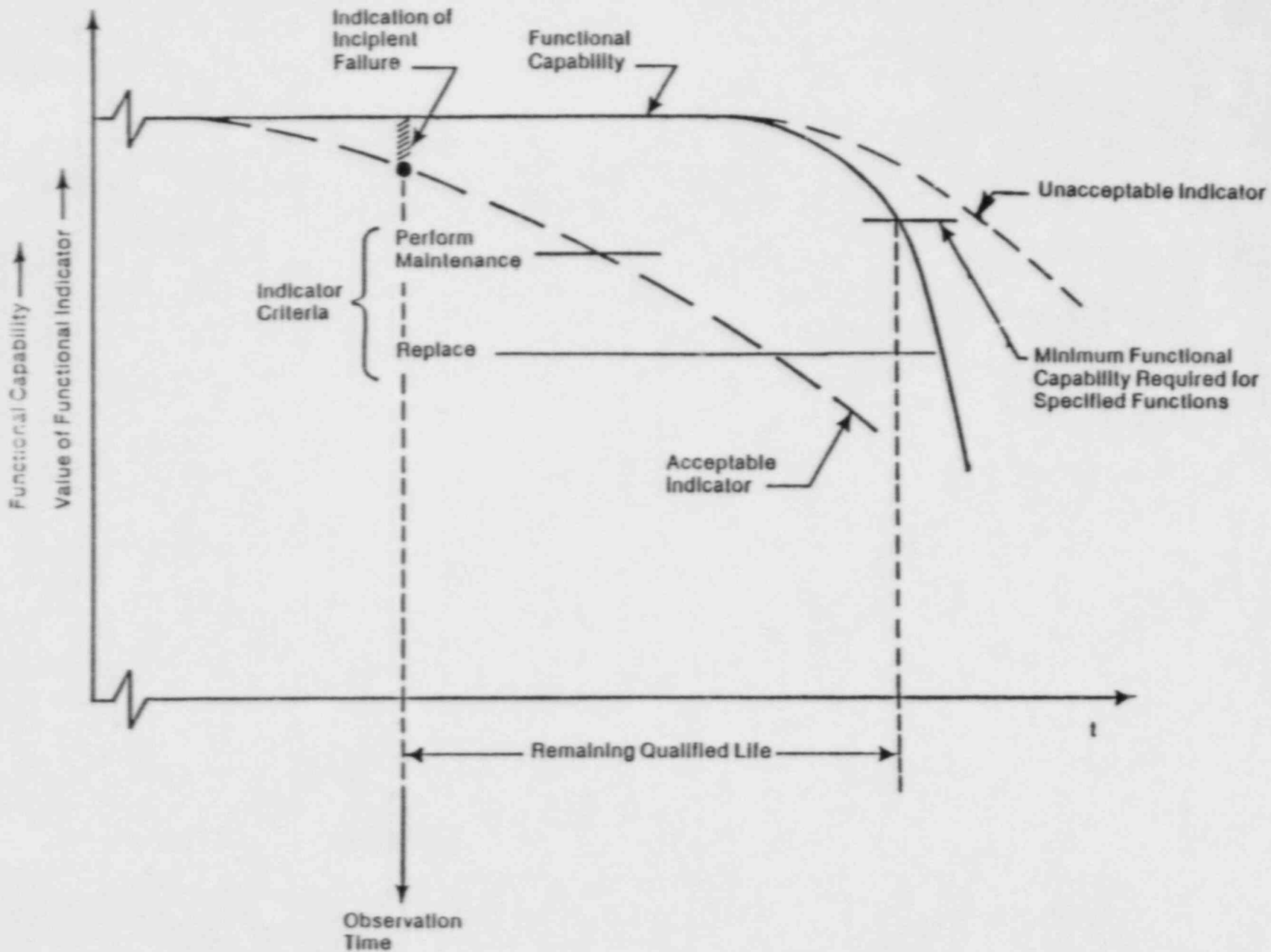
447

Figure 2-1. Use of Functional Indicators for Condition Monitoring

pressure transmitter in the containment of a nuclear power plant. Suppose it has been established that, when the leakage current in the cable measured at 500 Vdc exceeds 5 mA, the pressure transmitter signal may have excessive error should a LOCA occur 1 year after the observation. The condition monitoring criterion could take the following form: If the leakage current of the line measured at 500 Vdc exceeds 5 mA, the line must be examined within 1 year for defects and the appropriate corrective action must be taken. It may also be required that the frequency of monitoring be increased after the 5-mA warning level is reached.

2.2 FAILURE PATTERN AS A BASIS FOR CONDITION MONITORING, MAINTENANCE, AND REPLACEMENT STRATEGY

The previous section discussed the initiation of a maintenance, repair, and replacement action on the basis of condition monitoring results. At present, however, either sufficient data are not available or systematic evaluation of the data (data trending) has not been performed for much of the safety-related equipment, so that a maintenance, repair, and replacement strategy for the equipment of interest cannot easily be developed through condition monitoring. Another approach to arriving at such a strategy is to evaluate the statistical pattern of equipment failure over a period of time.

A knowledge of equipment failure patterns under normal service conditions is helpful in assessing the scheme of condition monitoring as well as surveillance, maintenance, or replacement logistics. Thus, the equipment failure pattern would indicate whether or not condition monitoring is necessary during the initial and intermediate periods of equipment life. The failure pattern would also indicate the frequency of inspection, preventive maintenance, and equipment replacement. It must be recognized that the determination of the frequency of such efforts must take the demands of accident service conditions into account. In other words, the frequency of surveillance and corrective actions must be adequate to provide reasonable assurance of satisfactory performance not only during a future period of normal service, but also during the usually more demanding conditions of an applicable accident occurring at the end of the period.

The failure patterns discussed here are statistical in nature, i.e., they indicate when the equipment will have a higher probability of failure during

449

operation. If significant statistical data are available for such failure predictions, then surveillance, periodic preventive maintenance, or replacement can be scheduled on the basis of failure trends. However, the statistically obtained failure trend does not itself indicate whether or not the aging or wearout degradation can be monitored. For example, nondestructive monitoring techniques may not be available for the parameter of interest for a particular device. However, the failure pattern of this device may show that the probability of failure increases significantly after a certain service life. In such cases, periodic replacement of the equipment, rather than condition monitoring, may be necessary.

Some of the failure patterns that have been observed for numerous components in the aircraft industry are shown in Figures 2-2, 2-3, and 2-4 [1]. However, an equipment item will not necessarily follow any one of these failure patterns.

Most components exhibit the failure pattern shown in Figure 2-2, in which a large number of failures occur at early stages of operation. Either continuous or periodic condition monitoring of the equipment may be necessary during the infant mortality period. For the stable period of equipment operation, periodic inspection and testing should be emphasized. The failure pattern shown in Figure 2-3 occurs when the failure rate is constant, which means the equipment failure will be random in nature. Scheduled maintenance or condition monitoring is not required for such equipment, but periodic surveillance may be required to ensure quick discovery of random failures. The failure pattern shown in Figure 2-4 is for equipment that is stable for a long period of time before it starts to exhibit wearout failures. For such equipment, condition monitoring should be performed periodically, but no preventive program is required until the equipment approaches the wearout region. The preventive maintenance can then mitigate aging of the equipment.

Condition monitoring may also be based on simple wearout or logarithmic (Arrhenius) degradation models [2]. Examples of the simple wear and logarithmic models are illustrated in Reference 2 for a pressure transmitter, where set point drift is considered the critical parameter to be monitored. In the example, a failure is considered to be a drift of 10% of the initial calibration (a calibration error of $\pm 2\%$ is considered, i.e., maximum acceptable drift is 8%). After an initial surveillance period t_1, the life of the
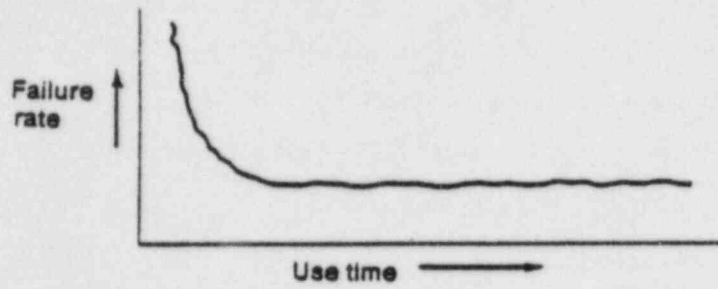
Figure 2-2.   Failure Pattern of Components with Initial High
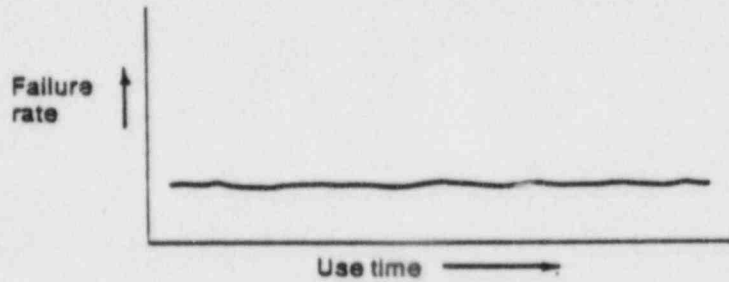Failure Rate Followed by Constant Failure Rate

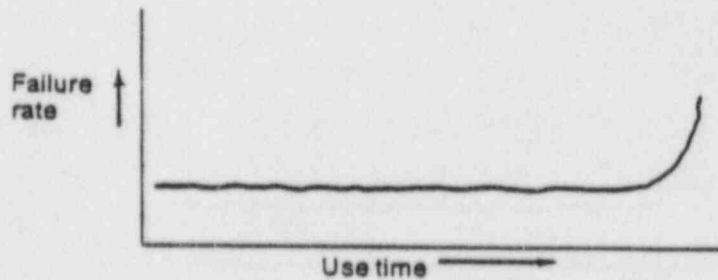Figure 2-3.   Failure Pattern of Components with Constant
Failure Rate

Figure 2-4.   Failure Pattern of Components Showing Wear
After Constant Failure Rate

451

transmitter can be reevaluated (from t_2 to t_3), using a simple wear or logarithmic model. On the basis of new evaluations, the initial surveillance period may be revised. A simple wearout model will provide a conservative (shorter) surveillance period than the logarithmic model.

The above examples of failure rate patterns relate to normal service conditions. Establishment of the frequency of inspection, maintenance, and replacement must include consideration of the effect of accident service stresses. Figure 2-5 shows the effect of normal and accident service stresses on accumulated deterioration. The accident service condition will cause stresses that are usually more severe than normal service stresses. Care must be taken in development of inspection, replacement, and maintenance intervals such that sufficient capability to withstand accident condition remains throughout each interval. The accumulation of normal stresses and possible accident stresses must be such that the equipment is not caused to significantly enter the wearout region (see Figure 2-4) where failure rates become exponential and the bulk of the equipment would be expected to fail.

2.3 APPROACHES FOR DEVELOPING INTERIM RECOMMENDATIONS FOR CONDITION MONITORING

Two basic approaches may be used to develop criteria for implementation of preventive action based on condition monitoring of equipment in nuclear power plants: (a) the absolute value approach and (b) the relative degradation approach. These may be used separately or in conjunction with each other. In the absolute value approach, the acceptable limits of the age-sensitive parameters are determined for each aging parameter from a review of applicable data, including information obtained from vendors, laboratory experiments, and power plant operation records and condition monitoring results as they are gathered. If the measured values of the parameters obtained by condition monitoring of an in-service equipment show degradation below these limit values, the equipment should be maintained or replaced. In the relative degradation approach, the significant age-sensitive parameters are monitored periodically, and the rate of degradation is evaluated with respect to time. If condition monitoring over a period of time reveals a relatively rapid and consistent rate of degradation, then there is a high probability of an early failure. A relatively large degradation of a condition monitoring parameter in a short period of time, therefore, warrants an early preventive action.
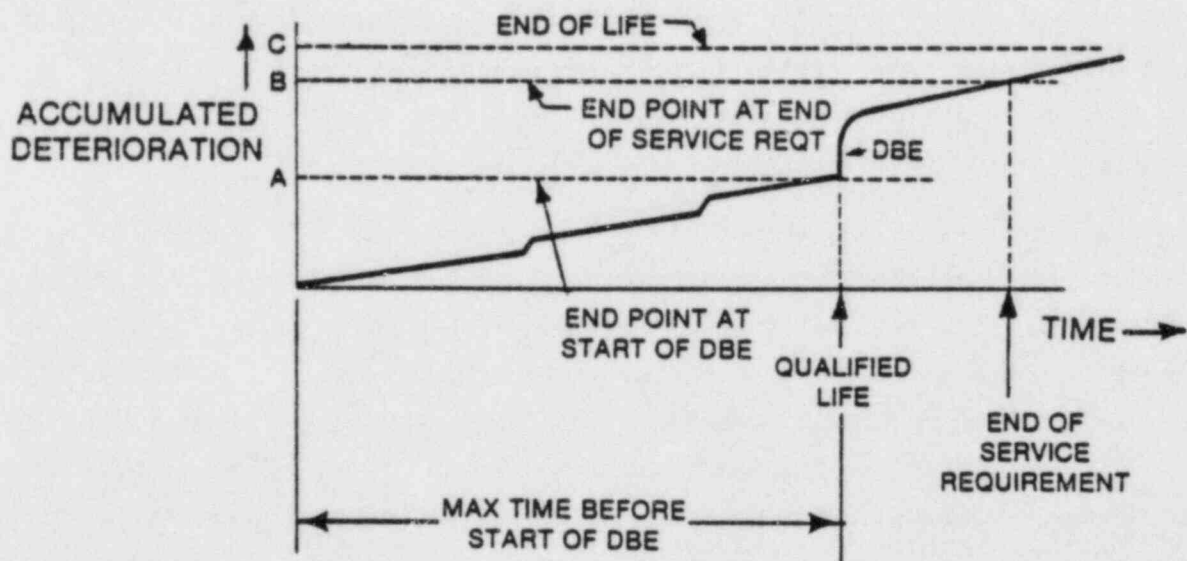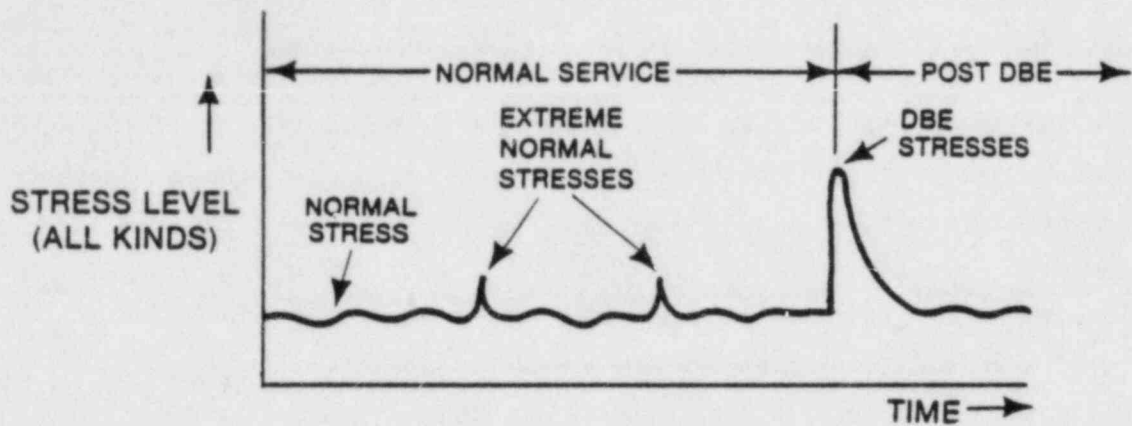
452

Figure 2-5. Accumulated Deterioration Related to Service and DBE Stresses
(Adapted from Figure 6-7, Ref. 3)

453

3. CONDITION MONITORING OF ELECTRICAL CABLES
LOCATED INSIDE CONTAINMENT

3.1 INTRODUCTION

The goals of condition monitoring are to predict the remaining useful life of equipment and to detect incipient failures so that preventive actions may be taken prior to actual failure. The question is "Why apply condition monitoring to cable?" Review of failure data from Licensee Event Reports indicates that very few cable failures have occurred by comparison to the number of cables in service. However, three prime reasons for condition monitoring exist: (1) cables are used in every active safety system; (2) failure rates may increase as cable nears the end of its installed life; and (3) cables inside containment may be subjected to accident environment stresses that will greatly change their accumulated stress level and affect their failure rate. Therefore, monitoring of cable deterioration levels and rates can provide information that will assure ability to function under both normal and accident conditions.

The evaluation of condition monitoring for cable entails determining the types of stresses that affect cable, the types of deterioration that may be expected, the means of detecting the deterioration, and the limitations on performing tests and monitoring.

The ideal situation for condition monitoring is to have one easily measured parameter that closely correlates with the continued capability to function. In addition, sufficient knowledge of the parameter would exist to allow decision criteria for preventive actions to be set. Unfortunately, the real situation is more complicated. Multiple parameters will have to be measured; not all of the tests are easily performed in the power plant, and only partial information for decision making is available at present.

3.2 CABLE TYPES

If only one type of cable and one type of environment existed in a plant, the situation would be simplified. However, four basic types of cable are used in many configurations. The general categories are: instrumentation cable, low voltage power cable, medium voltage power cable (4 to 15 kV), and

454

600 V control cable. In general, 4-kV power cable is not in safety-related service inside containment and 15-kV cable is used outside of containment in non-safety systems. The complexity of the cables ranges from those with a single stranded conductor with a single layer of extended insulation to those with multiple conductors, semi-conducting tapes, insulations, shields, fillers, and a jacket. Each type of cable has somewhat different aging characteristics since different materials are exposed to different stress levels.

3.3 STRESSES AND THEIR EFFECTS

The stresses affecting cables are thermal, radiological, electrical, mechanical, and chemical (including oxidation and moisture incursion). The levels of the stresses vary with the application (e.g., voltage stress) and the location of the cable inside of containment. The changes that these stresses may induce in the insulation are hardening or softening, deterioration of electrical properties such as conductivity and dielectric constant, and physical changes such as enlargement of voids and chaffing and cutting. These stresses may also cause the termination to deteriorate through insulation failure or corrosion.

3.4 TESTING

Many types of tests are possible for use on cable condition monitoring. These include insulation resistance, polarization index, step voltage, power factor, dissipation factor, partial discharge level, capacitance, time domain reflectometry, conductor and shield resistance, insulation tensile strength, and elongation, and dielectric withstand test. Not all of these apply to any one type of cable and some are destructive and cannot be performed on installed cables. Their correlation with continued ability to function under normal conditions is only partially defined. Their correlation to the ability to function during or following an accident is almost totally undefined.

3.5 LIMITATIONS ON TESTING

Limitations exist for both in-situ and laboratory evaluation of cable. For inside containment, access to the cable is a prime consideration. Testing requires the equipment to be out of service. Therefore, the testing will have to coincide with plant outages for refueling and maintenance. Disruption of

455

the cable circuit for testing is another concern. Improper restoration can cause significant safety problems. In addition, access points for testing of inside containment portions of the cable are frequently not available. For example, connections to most electrical penetrations are now made with insulated butt splices that are not readily broken and remade. Another problem is that many cables do not have an integral return path such as a shield. Insulation tests will be inconclusive for these cables since the cables will be insulated by surrounding cables or air. With regard to high voltage testing, care must be taken to prevent induced surges and flashovers to surrounding equipment and cables.

For destructive testing, further limitations exist. Samples of cables for such tests may not be readily available. Most spares have not been installed for testing purposes. Generally, they have been installed as replacement circuits or in the event that additional circuits are needed for modifications to the plant. Spare conductors may be in multiple conductor cable having other conductors in service. Removal of cable for tests also presents the possibility of dislodging or damaging surrounding cables. Only a few plants have installed spare cable specifically for testing purposes.

3.6 CURRENT PRACTICES

Condition monitoring is not being used on cable at present. However, some of the same tests that would be used to provide data for condition monitoring evaluation are being performed on certain cables. These tests include insulation resistance, polarization index, step voltage, and time domain reflectometry. In general, these tests are performed with the associated equipment connected to the cable. They are generally performed to provide present equipment status and the data are not used for predictive purposes. These tests are generally considered as good practice by the utilities that perform them and are not required by plant technical specifications.

3.7 RECOMMENDATIONS FOR DEVELOPMENT OF A CONDITION MONITORING PROGRAM

3.7.1 Testing Tactics

At present, continuous monitoring techniques are not available; therefore, any condition monitoring of cable will be limited to periodic

testing during refueling or maintenance outages. When condition monitoring programs are developed, the following should be taken into consideration. Disconnection of cable from the associated equipment for tests is costly and can present safety problems if the circuit is improperly restored. Therefore, as much testing as possible should be performed while the cable is connected to the associated equipment, providing the equipment is compatible with test voltages. For motors and most switches, this will be possible. Disconnections of cable segments for further tests would only be performed if a problem is detected. Electrical test access points outside of containment such as motor control centers and termination cabinets should be used. Disconnection of equipment should only be performed for those that cannot withstand test conditions. For cable applications having a larger quantity of similar circuits, testing should be performed on a selected group of samples rather than all circuits.

With regard to removal of samples for laboratory testing, the suggested initial interval between tests is 5 years with subsequent intervals based on the level of deterioration detected. The removal of samples should be performed in a manner that disturbs as little surrounding cable as possible. Care must be taken to assure that the sample is as representative as possible of the remainder of the installed cable with regard to materials and stress exposure. It is expected that initial attempts at condition monitoring will be applied to cables with the highest safety and operational importance.

3.7.2 Development of Decision Criteria

The key to condition monitoring is the means by which the test and inspection data are evaluated and used for decisions regarding the need for service, maintenance, or replacement. If decision criteria based on the rate or level of deterioration are not available, initiating preventive maintenance and replacement of cable based on condition monitoring will not be possible. At present, most decisions regarding cable replacement and repair are based on limited testing coupled with engineering judgment. Most of the experience that is the basis for the judgments relates to cable that would not be subject to accident environment situations.

A means of developing preliminary decision criteria would be to evaluate the properties of cable that had been subjected to accelerated aging during

457

qualification testing. Unfortunately, during qualification testing, the levels of deterioration reached before the cable was subjected to LOCA conditions were usually not determined. However, reperformance of aging simulations followed by parameter testing could provide this needed information. It must be recognized that each type of cable insulation will age somewhat differently, and such test results cannot be generalized. It must also be recognized that accelerated aging will not fully replicate actual aging. The values of cable parameters following accelerated aging would be useful only as a rough indicator of acceptable levels of deterioration. Subject to these reservations, if the installed cable displayed lower levels of deterioration than those displayed by qualification test specimens prior to LOCA testing and the rate of deterioration was slow enough, the cable would be considered acceptable for service during the next period up to the next surveillance. Modifications and refinements to these approximate criteria should be made as condition monitoring data are gathered and evaluated. If the cable is found to degrade in a manner different from that expected, further aging phenomena evaluation would be required. If the cable is found to degrade at a much slower rate than expected, the period between tests may be extended.

3.8 CONCLUSIONS

Condition monitoring of cable is a valuable tool that can help prevent failures under normal and accident environments. Further development of techniques for testing and data evaluation and development of decision criteria are necessary. Success of such a system requires implementation relatively early in the life of a power plant to allow recognition and tracking of deterioration trends. Particularly in its present state of development, application of condition monitoring can probably be justified only for the most critical cables, and the monitoring program should be designed as much to enhance the development of condition monitoring as to give approximate indications of cable deterioration.

4. REFERENCES

1. J. D. Patton, Jr., Preventive Maintenance, Instrumentation Society of America, Inc., New York, pp. 58-61, 1968

2. J. W. Wanless, "Condition Monitoring," Proceedings of the Workshop on Nuclear Power Plant Aging, NUREG/CP-0036, pp. 39-78, November 1982

3. S. P. Carfagno and R. J. Gibson, A Review of Equipment Aging Theory and Technology, Electric Power Research Institute, EPRI Report NP-1558, Palo Alto, CA, September 1980

4. Program Plan -- Nuclear Plant Aging Research for Operating Reactors Inspection, Surveillance and Maintenance
U.S. Nuclear Regulatory Commission ·
Revision 1 (Draft), July 1984

4. TITLE AND SUBTITLE (Add Volume No., if appropriate)	2. (Leave blank)
Proceedings of the Twelfth Water Reactor Safety Research Information Meeting	
	3. RECIPIENT'S ACCESSION NO.

7. AUTHOR(S)	5. DATE REPORT COMPLETED	
Compiled by: Stanley A. Szawlewicz, Consultant	MONTH December	YEAR 1984

9. PERFORMING ORGANIZATION NAME AND MAILING ADDRESS (Include Zip Code)	DATE REPORT ISSUED	
Office of Nuclear Regulatory Research	MONTH January	YEAR 1985
U. S. Nuclear Regulatory Commission	6. (Leave blank)	
Washington, DC 20555	8. (Leave blank)	

12. SPONSORING ORGANIZATION NAME AND MAILING ADDRESS (Include Zip Code)	10. PROJECT/TASK/WORK UNIT NO.
Same as Item 9.	11. CONTRACT NO.

13. TYPE OF REPORT	PERIOD COVERED (Inclusive dates)
Collection of Conference Papers	October 22-26, 1984

15. SUPPLEMENTARY NOTES	14. (Leave blank)

16. ABSTRACT (200 words or less)

The papers published in this six volume report were presented at the Twelfth Water Reactor Safety Research Information Meeting held at the National Bureau of Standards, Gaithersburg, Maryland during the week of October 22-26, 1984. The papers describe progress and results of programs in nuclear safety research conducted in this country and abroad. Foreign participation in the meeting included twenty-six different papers presented by researchers from seven European countries, Japan, and Canada.

17. KEY WORDS AND DOCUMENT ANALYSIS — 17a. DESCRIPTORS

17b. IDENTIFIERS/OPEN-ENDED TERMS

18. AVAILABILITY STATEMENT	19. SECURITY CLASS (This report)	21. NO. OF PAGES
Unlimited	Unclassified	465
	20. SECURITY CLASS (This page) Unclassified	22. PRICE S